# Drivers of cetacean diversity: Evidence from the past and present

Ellen Jane Coombs

Department of Genetics, Evolution, and Environment

University College London (UCL)

March 25th, 2021

Thesis submitted for the degree of Doctor of Philosophy (PhD)

I, Ellen Jane Coombs, confirm that the work presented in this thesis is my own. Where information has been derived from other sources, I confirm that this has been indicated in the thesis.

## Abstract

In just 8-12 million years, cetaceans (whales, dolphins, and porpoises) underwent profound changes in adaptive zone. Their evolution from land-dwellers to aquatic inhabitants is an exemplar of macroevolutionary change. However, there has been little study of evolutionary dynamics that span their entire 50-million-year history.

Using 3D geometric morphometrics and a rich dataset of 201 living and fossil species spanning Cetacea's evolutionary history, I quantify cranial morphology and investigate shifts in evolutionary rates and disparity. I find three key waves of diversification throughout cetacean evolution. The first is in archaeocete (early whales) evolution as cetaceans evolved rapidly to fill a largely vacant aquatic niche. The second, in the mysticetes (baleen whales) and odontocetes (toothed whales) which diverged ~39-36 Mya and followed unique evolutionary pathways, facilitated by key innovations: echolocation in odontocetes and filter-feeding in mysticetes. The third wave, in the Miocene, is mostly an odontocete signal (~18-10 Mya). Further, I find asymmetry related to echolocation in odontocetes is driven by the pressures of acoustically complex environments, and that multiple ecological factors influence skull shape.

I find climate fluctuations drive cranial evolution through deep-time. Importantly, ocean productivity drives evolutionary rates in mysticetes, whereas in odontocetes, these are driven by *rates* of temperature change. Finally, I switch from morphological to taxonomic diversity and investigate environmental and anthropogenic impacts on diversity in shallow-time, reinforcing the importance of long-term strandings data to monitor impacts.

My results highlight the idiosyncrasies of species responses to environmental and anthropogenic impacts. Differences in diversity between suborders reflects their different early innovations and resultant 'ecospace' occupation. Importantly, this work highlights the differences in drivers behind mysticete and odontocete evolutionary rates, particularly with regards to climate change. The different historical responses of extant suborders highlight a requirement for

separate, tailored conservation and mitigation of climate impacts for toothed and baleen whales.

## Impact statement

In this thesis I investigate cranial morphology in cetaceans (whales, dolphins, and porpoises) and address drivers behind their diversification through deep time using fossils, through to shallow time using strandings data. This is the most comprehensive investigation into cranial morphology in cetaceans to date, unsurpassed in its taxonomic sampling and quantification of morphology. It addresses questions of interest to evolutionary and developmental biologists, ecologists, and conservationists to build a picture of past and present influences of cranial morphology. This thesis has also produced the most detailed analyses to date of how ecology, allometry, phylogeny, global-scale change, and anthropogenic impacts influence diversity in cetaceans across their entire evolutionary history.

These results have helped assess the ecological limits and adaptations of cetaceans to biotic and abiotic changes in the past, and in future may help the development of more accurate models of evolution and a better understanding of impacts on cetacean diversification. This knowledge, from understanding the idiosyncrasies of how baleen whales respond to climate change compared to toothed whales, to highlighting stranding hotspots in UK and Irish waters, can be used to help mitigate the future impact of climate change and other anthropogenic impacts on cetaceans.

I have published two chapters from this thesis in internationally renowned journals. The chapters have been cited multiple times and the remaining chapters will be submitted for publication shortly. I have presented my work at twelve national and international conferences, twice as an invited speaker and at numerous public events at the Natural History Museum, London, including a panel event for 'Seven Worlds, One Planet' by the BBC's Natural History Unit. I have also been interviewed on UK television (ITV News) and German national radio as a whale specialist and have had news articles on my published research in The Conversation, iNews, National Geographic, MailOnline, and The Independent.

My cranial morphometric data set (200+) will be free to download from www.phenome10k.org. These skulls can be used by other researchers for further exploration into cetacean morphology, evolution, ecology, and much more. Finally, I have taught geometric morphometrics to students at UCL and Imperial College, built a teaching portfolio based on my PhD work, and gained an Associate Fellowship of the Higher Education Academy.

Cetaceans capture the imagination of scientists and the public, and I feel honoured to have had the opportunity to share my work with a variety of audiences. This thesis is an important contribution to our knowledge and understanding of the drivers and impacts on cetacean diversity. I use methods from a broad range of disciplines including palaeontology and neonatology to produce the most comprehensive research on cranial morphology and diversity across Cetacea to date. This research and the publications, conference talks, and collaborations that have disseminated from it will be a valuable contribution to cetacean science and the wider fields of evolutionary biology, morphometrics, and ecology. I have thoroughly enjoyed the public engagement and outreach that my research has offered me, and I strive to make this a significant part of my career.

## Acknowledgements

Doing this PhD has been an absolute privilege. I am so grateful to so many people who helped make it happen.

Lambert, thank you for welcoming me to RBINS and for your enthusiasm for my work. Felix Marx, it was great to meet you and to discuss whales. Ewan Fordyce, you made me so welcome in New Zealand, I am grateful for your guidance, time, and support – it was a pleasure to meet an inspiration. I hope our paths cross again. To Bobby Boessenecker, Morgan Churchill, Jonathan Geisler, and Brian Beatty, it has been a pleasure working with you all, thank you for your help.  To Philip Gingerich and Holly Smith, thank you for taking me under your wing in Peru, I learnt so much. To Oliver Hampe, it was lovely to have your company in Peru, thank you for your insight and discussion. To Alan Tennyson (MM), thank you for all the coffees and great chat! Rob Deaville, thank you for always being so kind, inspiring, and knowledgeable. To Rodolfo Salas-Gismondi (MUSM), Aldo Benites-Palomino (MUSM), Mario Urbina (MUSM), Kesler Randall and team (SDNHM), Tom A Deméré (SDNHM), Alan Tennyson (NMNZ – thank you for the coffee and chats!) Patricia Holroyd (UCMP), Ashley Poust (UCMP), Christine Mejia (UCMP). Meredith Rivin (UWBM), Greg Wilson (UWBM), Christian de Muizon (MNHN), Guillaume Billet (MNHN), Annelise Folie (RBINS), Daniele Ormezzano (MBGPT – thank you for making me feel so welcome), Piero Damarco (MPTAM), Chiara Sorbini (MSNTUP), Simone Farina (MSNTUP), Giovanni Bianucci, Carlo Sarti  (MGGCB), Roberto Barbieri (MGGCB), Nicholas Pyenson (USNM), Amanda Millhouse (USNM), Dieter Schreiber (SMNK), Dino Frey (SMNK), Björn Berning, Johannes Tuzar, Thomas Schossleitner (MB), Erin Maxwell (SMNS), Bill Simpson (FMNH), Matt Freidman, Adam Rountrey (FMNH), Samuel McLeod (LA), Amber Coste (OU), Daniel Brinkman (YPM), Jorge Vélez-Juarbe (LA), Vanessa Rhue (LA), Sam McLeod (LA), and so many others that I may have missed, I am so grateful to each and every one of you for your time.

To Dave Bohaska (USNM) thank you for helping me lift so many heavy skulls! You saved the day, and I enjoyed our whale chats. To Michael McGowen (USNM) thank you for welcoming me so warmly on my first day, and for all your help since, I look forward to working together in January 2022! Thank you to Thomas Guillerme, Jonathan Rio, and David Miller for helping me with my

code and funding applications. To Rosa, Walter, I am sorry I don't know your surnames but each of you was so helpful to me, thank you.

To my family, thank you for your endless support, love, and encouragement. How lucky I am to have you all, I am so grateful for your enthusiasm and for your faith in me.

Finally, to my husband, Ben. We've shared an office (our living room) in our tiny flat for a year whilst the pandemic has spread around the world. It's been tough and it's been challenging, but a real silver lining has been spending more time with you. I'm so grateful to you for always jumping in to support me no matter what. Regardless of the time of day, and no matter how busy you are. Cooking, finding solutions, mulling over ideas, building me up, cheering me on, you're always there. I am so grateful for your love and support. Ben, thank you for always pulling up a chair.

Qwe 'lhol mechen, this is for you.

# List of museum abbreviations

AMNH - American Museum of Natural History

CCNHM - College of Charleston Natural History Museum

ChM - Charleston Museum

FMNH - Field Museum Natural History

GSM - Georgia Southern Museum

GSP-UM - Geological Survey of Pakistan, University of Michigan

IRSNB/RBINS - Institute Royal des Sciences Naturelle's de Belgique

LACM - Natural History Museum of Los Angeles County

MB - Berlin Museum für Naturkunde

MBGPT - Museo Regionale di Storia Naturale di Torino

MLP - Museo de La Plata, Argentina

MM - Museum of New Zealand Te Papa Tongarewa

MNHN - Muséum national d'Histoire naturelle

MSNTUP - Museo di Storia Naturale e del Territorio, Università di Pisa

MSNUP - Museo di Storia Naturale di Pisa - Università di Pisa

MUSM - Museo de Historia Natural

NHMUK - Natural History Museum UK

NMNS-PV - National Museum of Nature and Science, Tsukuba

NMNZ - Museum of New Zealand, Te Papa Tongarewa

NMV - National Museum of Victoria

OL - Schlossmuseum - OÖ Landes-Kultur GmbH (EN)

OU - University of Otago

PVM - Museum of Paleontology, University of Michigan

SDNHM - San Diego Museum Natural History

SMNK PAL - Staatliches Museum für Naturkunde Karlsruhe

SMNS - Staatliches Museum für Naturkunde Stuttgart

UCMP - University of California Museum of Paleontology

USNM - National Museum of Natural History (Smithsonian)

UWBM - University of Washington Burke Museum

YPM - Yale Peabody Museum

# Table of Contents

# Table of Figures

*For Appendix figures see 'Table of Figures – Appendix'*

# Table of Tables

*For Appendix Tables see 'Table of Tables – Appendix'*

# Chapter one

## Introduction

*"Where great whales come sailing by,*

*Sail and sail, with unshut eye,*

*Round the world for ever and aye"*

- Matthew Arnold

## 1.1 General overview

For centuries, scientists have been inspired by key questions such as why some species survive and radiate, whilst others go extinct (Darwin, 1859). More recently, scientists have been asking questions about what will happen to organisms as the planet continues to warm and change due to human pressures (Pearson and Dawson, 2003; Bellard et al., 2012; Goswami et al., 2016). Global biodiversity patterns are the consequence of many historical and present spatial and temporal processes (Fritz et al., 2013). Therefore, to obtain a full understanding of this bigger picture we need to consider species' ecology, morphology, and adaptations both now and in the past using the fossil record. To investigate these influences on living and fossil animals at the larger scale, an integrated macroecological and macroevolutionary perspective is required (Fritz et al., 2013; Guillerme and Cooper, 2016).

In this thesis, I focus my research questions on cetaceans (whales, dolphins, and porpoises), the only fully aquatic mammals besides the sirenians (manatees and dugongs). Their distinctive anatomy and ecological adaptations make for 'the most peculiar and aberrant of mammals' – George Gaylord Simpson (Simpson, 1945). As far back as the 4th century BC, Aristotle marvelled at the fact that cetaceans breathe air, give birth to, and suckle live young, and provide parental care (Marx et al., 2016a). These charismatic mammals provide plentiful inspiration for the public and scientists alike. The scientific literature on cetaceans is extensive and broad, ranging from anthropogenic effects on ecology such as the impacts of whale watching on breeding behaviours in humpback whales (*Megaptera novaeangliae*) (Schaffar et al., 2009; Villagra et al., 2021), to bite force and diet specifics of individual species such as the fossil basilosaurids (Fahlke et al., 2013; Snively et al., 2015), through to macroevolutionary studies on diversity (Marx and Uhen, 2010; Marx and Fordyce 2015) and radiation (Steeman et al., 2009) through time. The latter area of study tends to focus on either baleen whales (mysticetes) (Marx and Uhen, 2010; Marx and Fordyce 2015) or on toothed whales (odontocetes) (Serio et al., 2019), bar some exceptions which look across both (Steeman et al., 2009; Slater et al., 2010) with increasing interest in molecular evolution and macroevolutionary patterns (McGowen et al., 2009;

McGowen et al., 2014). Numbers of publications on fossil whales have increased dramatically since the 1960s with around 50-60 publications each year in the 2010s (Marx et al., 2016a).

Today, the fate of cetaceans and their evolution is entangled with humans and our impacts on the planet. We have already caused the localised extinction of some populations such as the Atlantic population of the grey whale (*Eschrichtius robustus*) (Mead and Mitchell, 1984), and species extinctions of others including the Yangtze river dolphin (*Lipotes vexillifer*) (Turvey, 2008). At the time of writing, the population of Earth's smallest cetacean, the vaquita (*Phocoena sinus*) hovers at around 19 individuals (Gulland et al., 2020; Whibley, 2021). Information obtained from studies of evolutionary biology and the fossil record as well as more recent data on species distributions and diversity can help us to understand the ecology, adaptability, and distribution of living animals and importantly, can play a major role in their conservation (Jones and Safi, 2011).

In this introduction I first give an overview of cetaceans, their biology, adaptations, phylogeny, and evolution. I then discuss deep-time (geological time) and shallow-time (recent) impacts on cetaceans. I then discuss the whale cranium with a focus on its morphology, evolution, and drivers of morphology. I then outline the use, and drawbacks of using fossil data, and compare this to shallow time data. Finally, I conclude with my aims and objectives for this thesis and a chapter-by-chapter overview.

## 1.2. The subject: Why cetaceans?

In 2019, the International Monetary Fund placed a monetary value of $2 million on each great whale (Chami et al., 2019). This valuation was not based on goods such as meat or blubber or even tourism, but instead as a means of mitigating climate change. Microscopic phytoplankton contribute 50% of the oxygen in our atmosphere when they photosynthesise, and as they do so, they also sequester 37 billion metric tons of $CO_2$ annually (Chami et al., 2019). Whale faeces are rich in iron and nitrogen acting as a rich fertiliser, and wherever there are whales, there is a multiplier effect on these phytoplankton (Roman et al., 2014). Further, the vertical movement of whales in the water

column mixes these nutrients (Roman et al., 2014), and, once a whale dies, it will sequester 33 tons of $CO_2$ within its carcass. It is calculated that if whales were to return to their pre-whaling numbers, they would capture 1.7 billion tons of $CO_2$ annually (Chami et al., 2019). Furthermore, because cetaceans travel vast distances, they are exposed to multiple environmental pressures in diverse locations (Ramp et al., 2015); thus, their health offers an indication of the health of vast swathes of the environment year on year.

As well as being ecosystem engineers, whales occupy the top trophic position in the world's oceans. It is well established that large predators can critically alter food web structure and function, including direct effects on prey populations and indirect trophic cascades (Estes et al., 1998; Williams et al., 2004; Bowen and Lidgard, 2012; Riesch et al., 2012). Given that cetaceans are wide ranging, apex (top) predators, they integrate information from the bottom to the top of the food web and amplify trophic information across vast swathes of ocean habitat, offering a unique perspective into ocean functioning. There has therefore been increasing interest in developing methods of monitoring whales and improving methods for their conservation (Hunt et al., 2013).

Studying cetacean functional morphology, evolution, and ecology is important to better understanding ecosystem processes which could help manage changing marine environments now, and in the future (Bowen and Lidgard, 2012). This is especially important given that human impacts on whales have increased significantly over the past centuries and are predicted to continue to do so. Some of these threats include ship strikes, bycatch (the unintentional trapping of non-target species in commercial fishing nets), chemical and noise pollution, and climate change (Davidson et al., 2012; Hunt et al., 2013). There are many tools at our disposal to monitor cetaceans such as faecal sampling, respiratory sampling ('blow'), skin/blubber sampling, and photographic identification (Hunt et al., 2013). Unfortunately, despite the many benefits of studying cetaceans, there are logistical and operational challenges to studying large, mobile animals out at sea (Roman et al., 2014). Cetaceans can be difficult to locate in vast oceans, especially as they spend much of their lives submerged underwater and are often inconspicuous even at the surface. This

is where data from strandings, when a cetacean becomes grounded on land, (see 1.8.1) can be incredibly useful, particularly for long term monitoring of species assemblage and population declines (Pyenson, 2010; Gulland, 2006).

The benefits of researching cetaceans extend beyond the extant species. The study of the fossil record can help us understand the nature and adaptability of extinct species. Cetaceans are large and distinctive, and, because of that, their fossils are often easier to identify in deposits. Further, many parts of their skeleton, such as the dense inner and middle ear tend to preserve well, even in unfavourable conditions (Marx et al., 2016a) contributing towards their good fossil record. From an evolutionary perspective, cetaceans offer an exceptional opportunity to study ecological transitions and dramatic evolutionary transformations (Kelley and Pyenson, 2015; Pyenson, 2017). Cetaceans transitioned from being land-based, to wholly aquatic in just eight million years (Thewissen et al., 2009; Thewissen, 2014; Fordyce, 2018) (see 1.3). This transition is one of the most profound changes in adaptive zone captured in the fossil record (Thewissen, 2014). It showcases cetaceans as an exemplar of morphological and ecological change which, alongside their remarkably continuous fossil record, makes them ideal for macroevolutionary and palaeobiological studies (Thewissen and Bajpai, 2001). The cetaceans' move from a terrestrial to a wholly aquatic lifestyle engendered unique changes in anatomy, physiology, and behaviour (Gatesy et al., 2013). This move into a new adaptive zone gave rise to the largest, loudest, biggest brained, deepest diving, fastest swimming, longest migrating mammals on the planet. They evolved adaptations to hunt and navigate in murky waters (echolocation), and to filter feed (baleen). Thus, cetaceans provide a unique opportunity to study morphology and ecology through deep time to the present.

### 1.2.1 What is a whale?

There are around 95 extant species of cetaceans (McGowen et al., 2009; Jefferson et al., 2011; Marx and Fordyce, 2015) which comprises the whales, dolphins, and porpoises. Extant cetaceans are divided into two suborders, the Odontoceti (toothed whales) and the Mysticeti (baleen whales), which diverged *ca.* 39 million years ago (Steeman et al., 2009). Firstly, it is

worthwhile to consider the nomenclature describing this infraorder. Rather confusingly, the 'toothed whales' also includes all dolphins and porpoises, and the term 'whale' is today used as a loose description of *both* baleen whales and toothed whales. In the past the term whale tended to be associated with the larger baleen whales, such as the fin whale (*Balaenoptera physalus*) and the Sei whale (*Balaenoptera borealis*) but this is no longer the case. For example, beaked whales, are more closely related to dolphins and porpoises than they are to mysticetes. However, beaked whales do not sit within the family Delphinidae, which contains well-known dolphins such as bottlenose (*Tursiops truncatus*) and short-beaked common dolphins (*Delphinus delphis*) and instead sit within Ziphiidae. Furthermore, none of the 'river dolphins' sit within the family Delphinidae either, instead forming multiple distinct families: Iniidae, Platanistidae, Lipotidae, and Pontoporiidae (the last of which confusingly tends to inhabit coastal and saltwater estuaries rather than rivers) (Jefferson et al., 2011). The term 'whale' is often used as an umbrella term to encapsulate all cetaceans, tacitly including dolphins and porpoises, and I follow this terminology throughout this thesis, using 'whale' as an overarching term for all cetaceans. Mysticeti refers to the monophyletic clade encompassing the baleen whales, and extinct toothed mysticetes (i.e., early mysticetes which had teeth before baleen evolved – more below). Odontoceti refers to the toothed whales, a monophyletic clade which includes all extant cetaceans that do not have baleen, including whales which do not have any erupted teeth or any obvious dentition such as the suction feeding beaked whales. Finally, the archaeocetes, or ancient whales, form the cetacean stem group, and, in the earliest forms, do not resemble extant whales at all (more below); however, they are also included in the umbrella term 'whales'. I assign the mysticetes and the odontocetes as two separate suborders throughout as is commonly accepted for these groups. I also refer to the archaeocetes as a third suborder. However, although originally considered a formal suborder (Archaeoceti), the archaeocetes are a paraphyletic assemblage defined by retained plesiomorphic characters (Marx et al., 2016a). I use suborder as a loose term for ease to describe three separate groups of whales: the paraphyletic archaeocetes, the monophyletic mysticetes, and the monophyletic odontocetes.

### 1.2.2 Cetacean biology and adaptations

Cetaceans are the most taxonomically diverse aquatic mammal clade (Fordyce and Barnes, 1994), and inhabit most major ocean basins and some rivers (McGowen et al., 2009). Cetacea also contains the largest animals that have ever existed, with the largest being the extant blue whale (*Balaenoptera musculus)* (Fig. 1.1), which can reach 30 metres in length and can exceed 150,000 kg in weight (Nowak, 1999). In terms of body size, cetaceans span five orders of magnitude, from the vaquita (*Phocoena sinus)* (Fig. 1.1) weighing ~30-40 kg and measuring ~130cm (Gulland et al., 2020) to the balaenopterid behemoths. Generally, the extant mysticetes are bigger than the extant odontocetes, excluding the sperm whale (*Physeter macrocephalus*) and some of the larger beaked whales, with the smallest baleen whale, the pygmy right whale (*Caperea marginata*) still weighing a hefty 3,000 kg and measuring around 6.5 metres (Kemper, 2009). Several examples of this vast range in size and morphology are shown in Fig. 1.1.

[Figure on previous page]

**Fig. 1.1.** An example of some of the morphologies and scales of the cetacean skull. These skulls are 3D surface scans of skulls used throughout this study. 1. The largest mysticete and largest animal ever to exist, the extant blue whale *Balaenoptera musculus* (NHM 1892.3.1.1); 2. Miocene mysticete, *Diorocetus hiatus* (USNM 16783); 3. Extant Northern bottlenose whale, *Hyperoodon ampullatus* (NHM 1992.42); 4. The current earliest known mysticete, *Mystacodon selenensis* (MUSM 1917); 5. Middle Eocene protocetid, *Aegyptocetus tarfa* (MSNTUP I-15459); 6. Late Oligocene mysticete, *Aetiocetus cotylalveus* (USNM 25210); 7. Early Oligocene odontocete *Cotylocara macei* (CCNHM 101. 9); 8. Extant short-beaked common dolphin, *Delphinus delphis* (AMNH 75332); 9. The current earliest known cetacean, *Pakicetus attocki* (PVM 100148); 10. The current earliest known odontocete *Simocetus rayi* (USNM 256517); 11. The bizarre Pliocene odontocete, *Odobenocetops peruvianus* (SMNK PAL 2491); 12. The vaquita (*Phocoena sinus* (SDNHM 20697), the smallest extant cetacean. Note how the Miocene *Diorocetus* (2) and the extant *Balaenoptera* (1) have a similar morphology but very different size. The male *Hyperoodon* specimen (3) has massive maxillary crests, but the maxillary crests were not included (landmarked) in this study as I do not investigate sexual dimorphism.

Cetaceans display a wealth of different adaptations that allow them to live a fully aquatic existence. Most obviously, cetaceans have lost their external hind limbs (a vestigial pelvis is typical in mysticetes and common in odontocetes, most likely as an attachment point for muscles and reproductive organs; Adam, 2002; Gatesy et al., 2013). They have also evolved a hydrodynamic and streamlined fusiform body (Jefferson et al., 2011; Gatesy et al., 2013; Davis et al., 2019) (Fig 1.2). Many of the adaptations synonymous with being a whale are evolutionary losses: loss of external ears, loss of external hindlimbs, loss of full body hair, loss of teeth, and loss of olfaction in odontocetes (Gatesy et al., 2013; Marx et al., 2016a). Many of the acquisitions that whales have are unique among mammals: baleen, posteriorly positioned nares, dorsal fins, extreme retrograde (odontocetes) and prograde (mysticetes) telescoping in the skull, and pleated throat pouches (Gatesy et al., 2013; Davis et al., 2019). Further, cetaceans have evolved the ability to thermoregulate and osmoregulate in salt water, and some species can hunt

3km below the surface under immense ambient pressures in complete darkness. The cetacean navigation and detection system is also modified for a life aquatic. Odontocetes have evolved the ability to echolocate (using sound to detect prey and navigate in turbid waters), and mysticetes have evolved several mass feeding strategies such as lunge, and bulk feeding (Berta et al., 2016; Marx et al., 2016b). Both strategies were so successful that the mysticetes and odontocetes rapidly diversified, creating a gulf between the two suborders defined by these key adaptive characteristics.
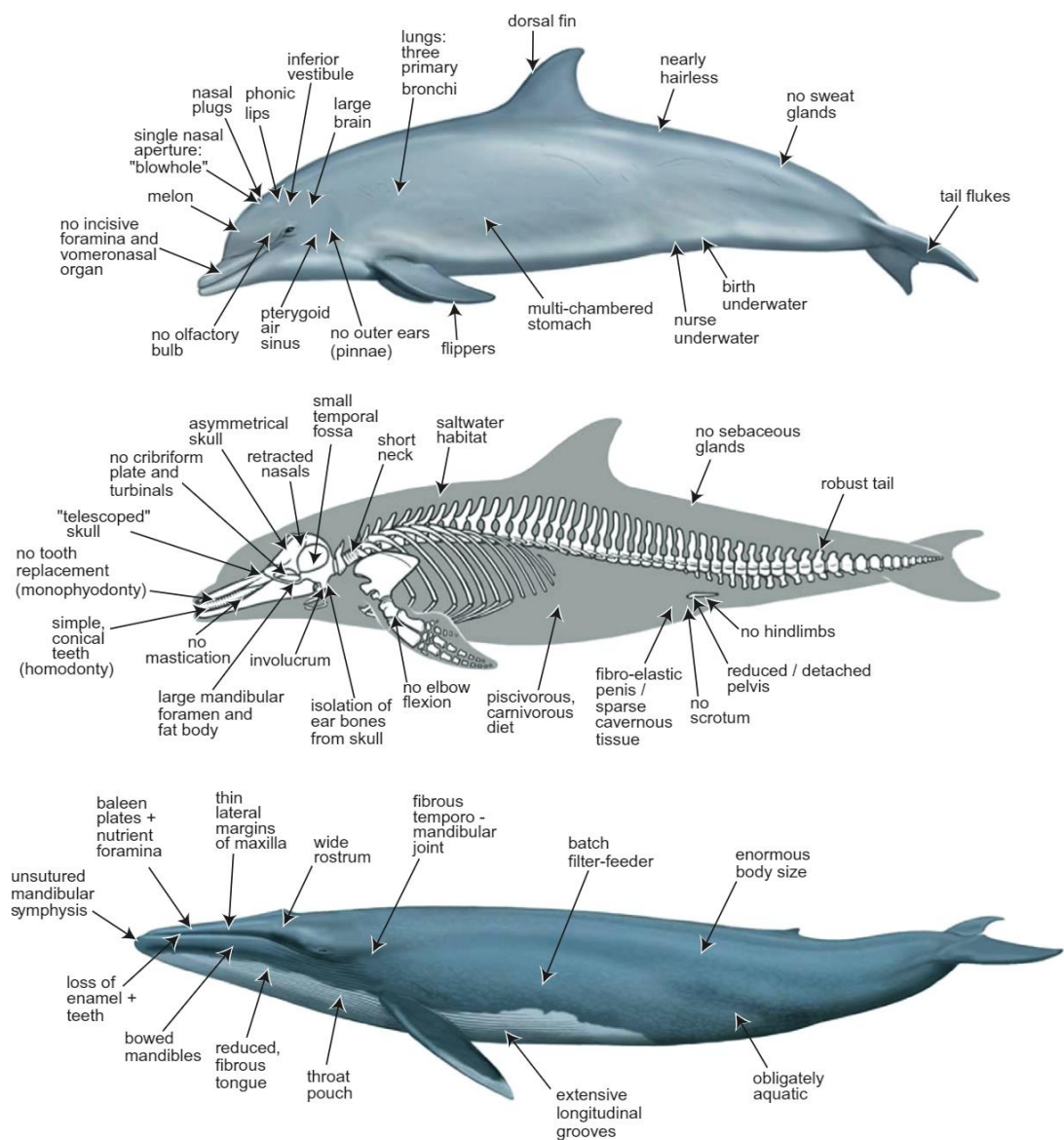
[Figure on previous page]

**Fig. 1.2.** Adaptations in modern cetaceans from Gatesy et al. (2013). Modern cetaceans represent a mixture of traits, many of which enable an obligately aquatic lifestyle. Some of the characteristic features of extant cetaceans are indicated in illustrations of the delphinid odontocete *Tursiops truncatus* (bottlenose dolphin), top and middle, and the balaenopterid mysticete *Balaenoptera musculus* (blue whale). Artwork is by Carl Buell. Source: Gatesy et al. (2013).

## 1.3 Cetacean evolution

Cetaceans originated approximately 55-54 Mya in the eastern Tethys sea (Bajpai and Gingerich, 1998). Hypotheses of Cetacea's origins have been discussed for centuries. In the 1880s, William Flower suggested that whales may have arisen from an archaic hoofed mammal due to the similarities in complex organs such as the stomach and in the development of young (Flower, 1883). Molecular and morphological findings indicate that Cetacea sits within Artiodactyla (i.e., even- toed-ungulates such as cows, pigs, deer, camels, and hippopotamuses) with hippopotamoids as the closest living relative was confirmed in the 1990s by DNA and protein analyses (Gatesy, 1998). As cetaceans are deeply nested within the artiodactyls, the term Cetartiodactyla is sometimes used with modern nomenclature further dividing the group into four subgroups, including the Whippomorpha (hippopotamids and whales) (Price et al., 2005; Marx et al., 2016a). Gingerich et al. (2001) found that Eocene archaeocetes bore astragali (ankle bones) similar to the highly derived ankle bones of artiodactyls (Fig. 1.3). The artiodactyl astragalus assumes a highly characteristic 'double-pulley' morphology unseen in any other mammal (Marx et al., 2016a), elucidating the relationship of whales to land-based mammals.

$\delta^{13}C$ and $\delta^{18}O$ from early cetacean bones and teeth indicate that the earliest cetaceans, the pakicetids (early to Middle Eocene) inhabited shallow, freshwater environments but were still mostly terrestrial (Clementz et al., 2006). The pakicetids lacked the aquatic adaptations which later Eocene cetaceans, such as the basilosaurids and dorudontids had. In the latter, these include shorter necks, a wrist and distal forearm flattened in the plane of the

hand; and tiny hind limbs (Thewissen et al., 2001). However, pakicetids do display some cetacean synapomorphies of the ear, with adaptations for underwater hearing (Thewissen et al., 1994). By 47.8-41.3 Mya, the 'walking whale', *Ambulocetus natans*, exhibited adaptations for both terrestrial and aquatic locomotion (Thewissen et al., 1994) (Fig. 1.3; 1.4). Although extant cetaceans do still have innominate pelvic bones, external hind limbs had disappeared by the end of the Eocene.
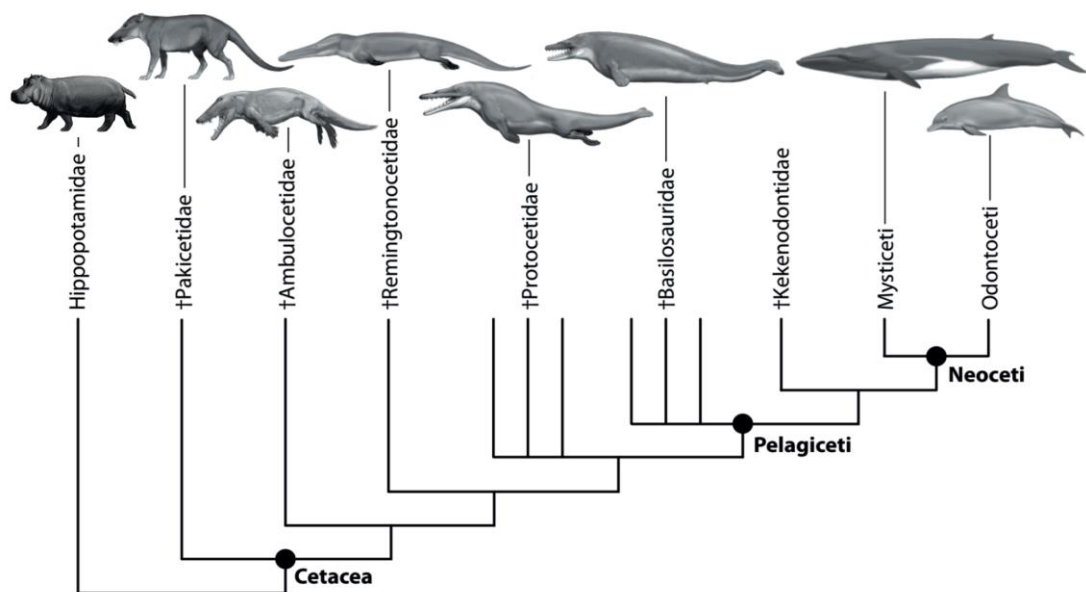


**Fig. 1.3.** Simplified phylogeny of archaeocetes (†) and their relation to the Neoceti. The basilosaurids and protocetids are likely paraphyletic. From Marx et al. (2016a).

Key aquatic adaptations in the protocetids and the basilosaurids, such as the ability to osmoregulate, emerged sometime after the cetacean ancestors migrated into the water. These adaptations facilitated a geographical move outside the Tethys sea into the Atlantic and Pacific oceans in the late Eocene (Clementz et al., 2006). The remingtonocetids, protocetids, and basilosaurids had higher $\delta^{18}O$ levels than pakicetids, indicating movement into marine environments, with the basilosaurids and protocetids (Fig. 1.4) exhibiting $\delta^{18}O$ levels almost identical to modern cetaceans (Clementz et al., 2006). Protocetidae (early Middle Eocene) and Basilosauridae (late Middle Eocene to Late Eocene) were among the lineage leading to modern mysticetes and

odontocetes (Slater et al., 2010; Marx and Fordyce, 2015) (Fig. 1.4). The basilosaurids and kekenodontids (the last of the archaeocetes) are part of the clade, Pelagiceti – the fully aquatic cetaceans which includes the mysticetes and odontocetes. We now know that the archaeocetes are a paraphyletic assemblage, which persisted (as the kekenodontids) until the Late Oligocene (ca 25 Mya), existing alongside their descendants, the Neoceti (Marx et al., 2016a).
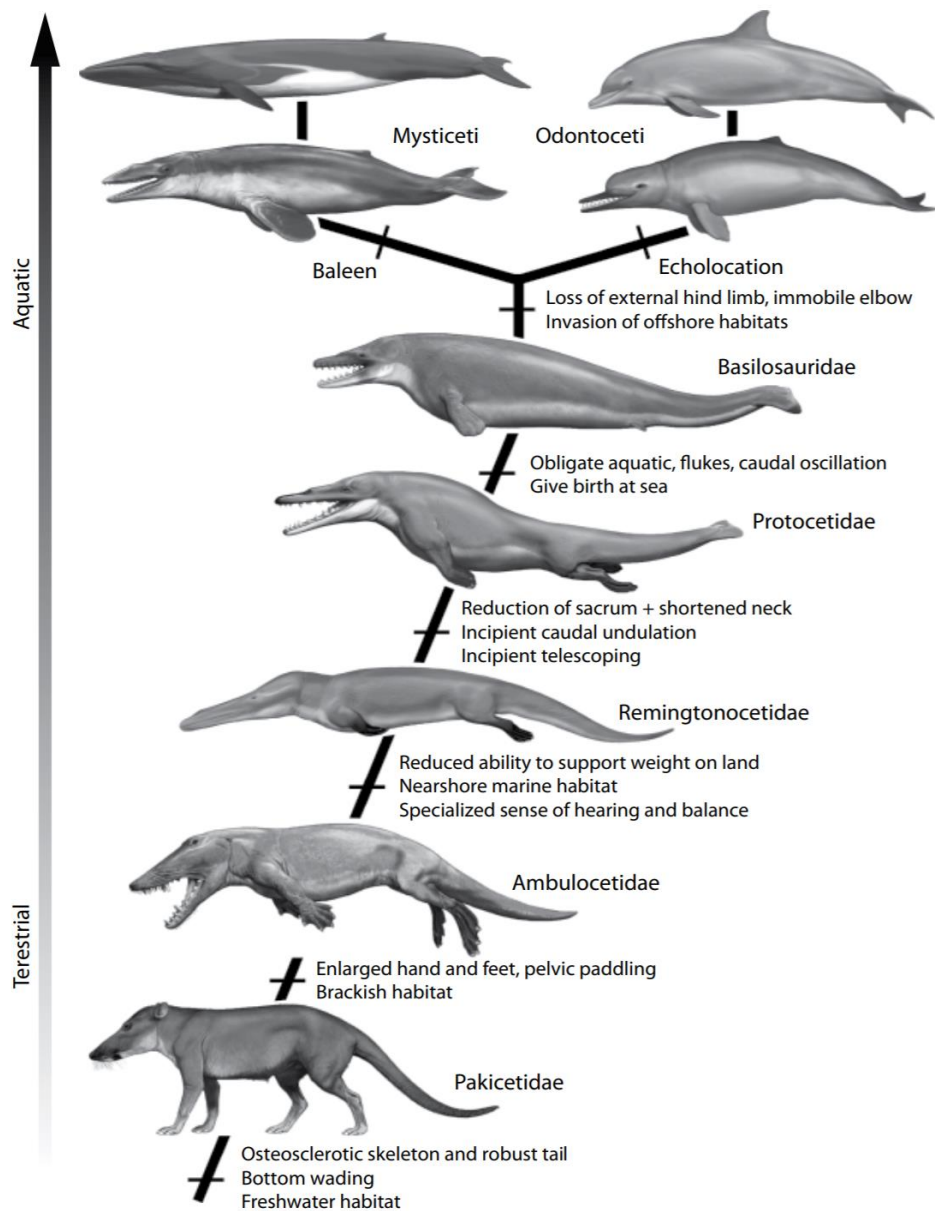


**Fig. 1.4.** Cetacean evolution from land to water. Overview of the transition from Pakicetidae, the terrestrial cetaceans (bottom) to the aquatic taxa of today (top). From Marx et al. (2016a).

Once cetaceans were fully aquatic, novel forms of feeding appeared. Around 33 Mya, some species had evolved ways to filter feed vast quantities of small prey, whilst others had evolved the ability to echolocate. Key families often referred to throughout this thesis are as follows: The Early-Middle Eocene is represented by the land-dwelling family Pakicetidae (Fig. 1.4; 1.5) through to semi-aquatic Ambulocetidae and Remingtonocetidae. The Pelagiceti (Fig. 1.5) are represented by the fully aquatic Basilosauridae of the Late Eocene through to the modern Neoceti. This includes representation of some early stem toothed mysticetes such as *Mystacodon selenensis*, Mammalodontidae and the Aetiocetidae of the Early-Mid Oligocene (Fig 1.5). Unfortunately, the Eomysticetidae (some of the first 'true' baleen whales) were not included in this study due to incompleteness of the material (see Chapter 6, section 6.3 for details). All four extant mysticete families are represented (Balaenidae, Neobalaenidae; Eschrichtiidae, and Balaenopteridae). The odontocetes are represented by early stem families; the Xenorophidae and the Simocetidae of the Early-Mid Oligocene and the 'Patriocetidae' (phylogenetic position is still being clarified) of the Late Oligocene. The more crownward odontocetes of the Miocene are represented by the Eurhinodelphinidae, Kentriodontidae, Albireonidae, Squalodelphinidae, Squalodontidae, and Allodelphinidae among other extinct families. All ten extant odontocete families are represented (Fig. 1.5). Fig. 1.5. shows the phylogeny from Lloyd and Slater (2020). This phylogeny is the most current phylogeny for Cetacea and is modified to represent my data set (with a few additions) in Chapters 2-4. A table of the families studied in this thesis is also provided (Table 1.1).
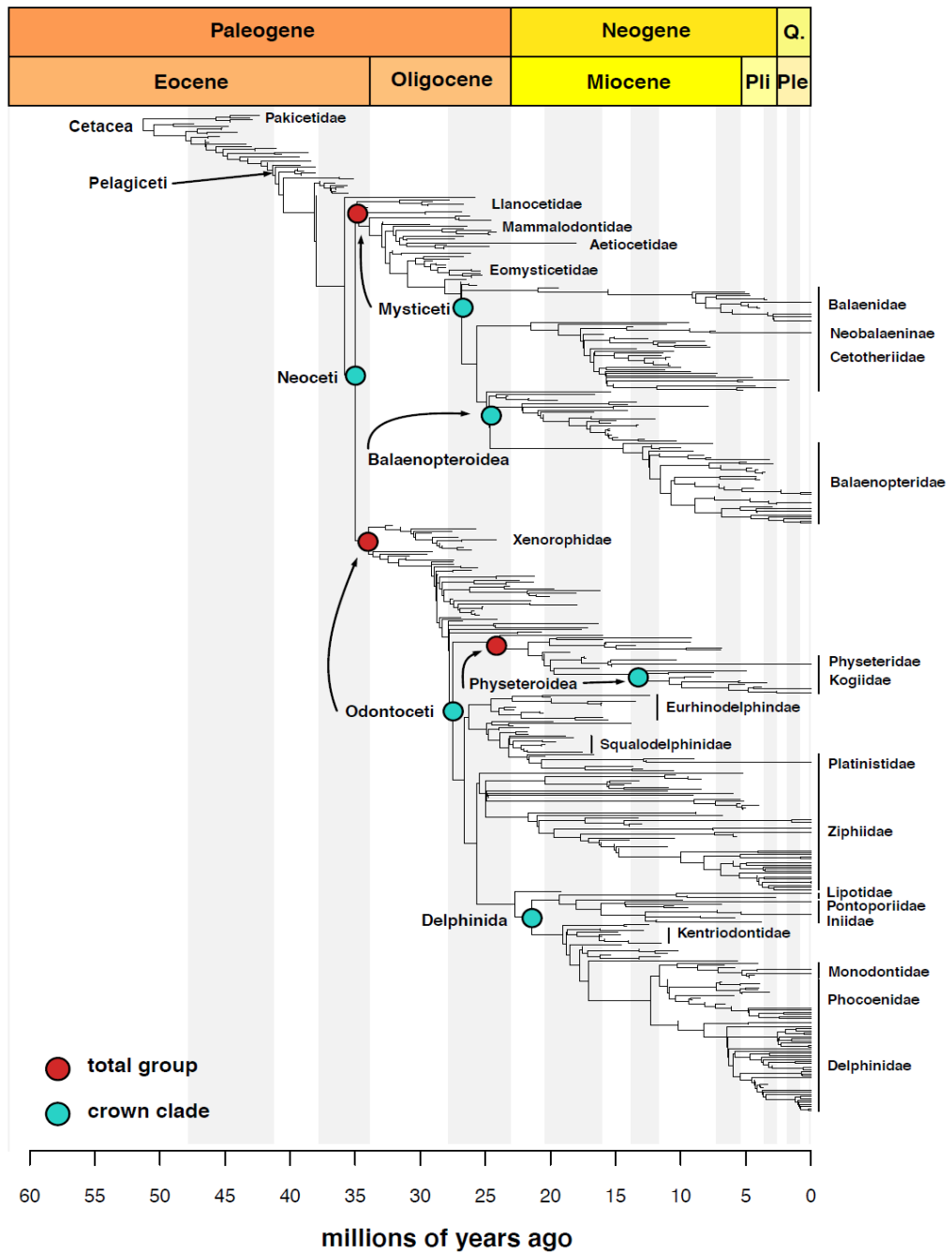
**Fig. 1.5.** Current up-to-date cetacean phylogeny from Lloyd and Slater (2020). Maximum a posteriori chronogram derived from simultaneous Bayesian inference of topology and branch lengths. The strict consensus metatree was derived from analysis of species–level Operational Taxonomic Units (OTUs) and was used as a topological constraint with stratigraphic ages for extinct taxa and Cytochrome B sequence data for extant taxa used to help resolve polytomies. Shaded bars correspond to marine stages. Source: Lloyd and Slater (2020).

**Table 1.1.** Stratigraphic ranges of major groups of cetaceans in age order from basal to crownward (Marx et al., 2016a). *Indicates those included in my research. Extant families are in bold. Note, these ranges are approximations based on current fossils and literature. For details on all specimens see Appendix 2 and 3.

| Family name | Assemblage (unofficially 'suborder') | Approximate stratigraphic range |
|---|---|---|
| Pakicetidae* | Archaeocete | Early Eocene (Ypresian) |
| Ambulocetidae* | Archaeocete | Middle Eocene (Lutetian) |
| Remingtonocetidae* | Archaeocete | Middle Eocene (Lutetian) |
| Protocetidae* | Archaeocete | Middle Eocene (Lutetian) – Late Eocene (Bartonian/Priabonian) |
| Basilosauridae* | Archaeocete | Middle Eocene (Lutetian) – Late Eocene (Bartonian/Priabonian) |
| Kekenodontidae* | Archaeocete | Early Oligocene (Rupelian) – Late Oligocene (Chattian) |
| Llanocetidae | Mysticete | Late Eocene (Priabonian) |
| Aetiocetidae* | Mysticete | Early Oligocene (Rupelian) – Late Oligocene (Chattian) + Miocene (?) |
| Charleston mysticetes | Mysticete | Early Oligocene (Rupelian) |
| Neobalaenidae* | Mysticete | Early Oligocene (Rupelian) |
| Eomysticetidae | Mysticete | Early Oligocene (Rupelian) – Late Oligocene (Chattian) + Miocene (?) |
| Mammalodontidae* | Mysticete | Late Oligocene (Chattian) |
| stem balaenopteroids | Mysticete | Late Oligocene (Chattian) + Miocene |
| **Balaenidae*** | Mysticete | Early Miocene (Burdigalian) – Quaternary |
| Aglaocetidae* | Mysticete | Early Miocene (Burdigalian) - Late Miocene (Tortonian) |
| **Balaenopteridae*** | Mysticete | Middle Miocene (Serravallian) – Quaternary |
| **Cetotheriidae*** | Mysticete | Middle Miocene (Serravallian) – Quaternary |
| Pelocetidae* | Mysticete | Middle Miocene (Serravallian) |
| **Eschrichtiidae*** | Mysticete | Late Miocene (Tortonian) – Quaternary |
| Tranatocetidae* | Mysticete | Late Miocene (Tortonian) |
| Simocetidae* | Odontocete | Early Oligocene (Rupelian) – Late Oligocene (Chattian) |
| Agorophiidae* | Odontocete | Early Oligocene (Rupelian) |
| Ashleycetidae | Odontocete | Early Oligocene (Rupelian) – Late Oligocene (Chattian) |
| Xenorophidae* | Odontocete | Early Oligocene (Rupelian) – Late Oligocene (Chattian) |
| Mirocetidae | Odontocete | Late Oligocene (Chattian) – Middle Miocene (Langhian) |
| Patriocetidae* | Odontocete | Late Oligocene (Chattian) – Late Miocene (Tortonian) |
| Waipatiidae* | Odontocete | Late Oligocene (Chattian) – Late Miocene (Tortonian) |
| **Physeteroidea*** (including Kogiidae) | Odontocete | Late Oligocene (Chattian) – Quaternary |
| Squalodontidae | Odontocete | Late Oligocene (Chattian) – Middle Miocene (Serravallian) |
| Eurhinodelphinidae* | Odontocete | Early Miocene (Aquitanian) – Middle Miocene (Serravallian) |
| Eoplatanistidae | Odontocete | Early Miocene (Aquitanian – Burdigalian) |
| Squalodelphinidae* | Odontocete | Early Miocene (Aquitanian) – Middle Miocene (Langhian) |
| **Platanistidae*** | Odontocete | Early Miocene (Aquitanian) – Quaternary |
| Allodelphinidae* | Odontocete | Early Miocene (Aquitanian) – Late Miocene (Tortonian) |
| **Ziphiidae*** | Odontocete | Early Miocene (Aquitanian) – Quaternary |
| Kentriodontinae* | Odontocete | Early Miocene (Aquitanian) – Late Miocene (Tortonian) |
| Lophocetinae* | Odontocete | Middle Miocene (Langhian) – Late Miocene (Tortonian) |

| Pithanodelphininae | Odontocete | Middle Miocene (Serravallian) – Late Miocene (Tortonian) |
|---|---|---|
| Albireonidae* | Odontocete | Late Miocene (Tortonian) – Quaternary (Gelasian) |
| Odobenocetopsidae* | Odontocete | Late Miocene (Tortonian) – Pliocene (Zanclean) |
| **Pontoporiidae*** | Odontocete | Late Miocene (Tortonian) – Quaternary |
| **Iniidae*** | Odontocete | Late Miocene (Tortonian) – Quaternary |
| **Phocoenidae*** | Odontocete | Late Miocene (Tortonian) – Quaternary |
| **Delphinidae*** | Odontocete | Late Miocene (Tortonian) – Quaternary |
| **Lipotidae*** | Odontocete | Late Miocene (Tortonian) – Quaternary |
| **Monodontidae*** | Odontocete | Late Miocene (Messinian) – Quaternary |

### *1.3.1. Macroevolutionary patterns in deep and shallow time*

Thanks to their remarkably continuous fossil record, cetaceans provide a good opportunity for studies of disparity (morphological diversity) and diversity through time. These previous studies have identified some key periods in cetacean evolution which are highlighted throughout this thesis. The Eocene-Oligocene boundary (*ca.* 34 Mya) marks a major transition in the diversification of cetaceans. Archaeocetes, except for the long surviving kekenodontids (which survived alongside the neocetes for another 10 million years), began to disappear, giving way to the mysticetes and odontocetes. Four of the five archaeocete families had already disappeared by the time the neocetes appeared, and it is likely that newly diverging toothed mysticetes continued the archaeocete strategy of ocean-going raptorial feeding (Marx et al., 2016a). It is unclear whether archaeocetes were outcompeted by the neocetes, but Marx et al. (2016a) suggest that the decline in the former, although profound, may not necessarily indicate a major replacement event.

It is unclear what caused this transition from the archaeocetes to the neocetes. Modern cetaceans are often described as an adaptive radiation which was either spurred on by an ecological opportunity created by the disappearance of the archaeocetes, or by the emergence of suborder-specific key innovations: baleen and echolocation (Slater et al., 2010). Slater et al. (2010) quantified phenotypic diversification and tempo of phenotypic evolution in cetaceans for the first time. Their study found that fluctuations in net diversifications (perhaps because of high extinction rate) may have erased any

signature of a proposed early burst early in the phylogeny (Slater et al., 2010). That study suggests that an adaptive radiation may have occurred and that a signature of the event may be retained within morphological traits, with a focus on size. Slater et al. (2010) concluded that changes in cetacean size are consistent with shifts in dietary strategy and that this has affected recent disparity. More recently, Lloyd and Slater (2020) have shown that the apparent pulse of increased cetacean diversification over the past 10 Ma is possibly not driven by increased speciation as previously thought but by reduced extinction rates. Lloyd and Slater (2020) highlight that this pattern is almost undetectable when using just extant species data but is long established in the fossil record.

It is presently unknown whether these hypothesised shifts occurring around the Eocene-Oligocene boundary are associated with competitive interactions, dietary shifts, the appearance of key adaptations (echolocation and baleen), or extrinsic factors such as climate change.

### 1.3.2 Deep time impacts on cetacean diversity – Climate and ocean restructuring

Palaeoclimate data are often used to consider how species adapted or evolved under past climate scenarios and perturbations. Studies such as Bown et al., (1994), Figueirido et al. (2012), Teplitsky and Millien (2013), and Clavel and Morlon (2017) consider the influence of abiotic factors, specifically climate, on body size in several clades. Figueirido et al. (2012) use $\delta^{18}O$ isotope values from Zachos et al., (2008), a commonly used proxy for palaeotemperatures. Older studies also considered palaeotemperature curves produced from $\delta^{18}O$ measurements of benthic and planktonic foraminifera (Wing et al., 1991; Bown et al., 1994). Clavel and Morlon (2017) use a temperature curve from Cramer et al. (2011), similar to the more widely used Zachos curve (Zachos et al., 2008), also derived from benthic foraminiferal $\delta^{18}O$ ratios (see 4.3.4 Palaeoclimate data for a detailed description of the data set). Cramer et al. (2011) account for fluctuations in sea water through time, which is important for highlighting periods of large-scale glaciations. Other commonly used palaeotemperature proxies include $TEX_{86}$, an organic paleothermometer measured by the distribution of isoprenoidal glycerol-dialkyl-glycerol-

tetraethers (GDGTs) in marine Archaea (Inglis et al., 2015) and Mg/Ca, which has some advantages over other palaeotemperature proxies and is often used to investigate changes in isotopic composition (Barker et al., 2005). Below I outline previous studies that consider palaeo proxies alongside cetacean evolution.

The Eocene-Oligocene boundary coincides (roughly) with a rapid drop in global temperatures, Antarctic glaciation, and the onset of the Antarctic Circumpolar Current (ACC), the dominant ocean current in the Southern hemisphere (Rintoul et al., 2001; Böning et al., 2008). The ACC appeared when South America and Antarctic separated, forming the Drake Passage, and is driven in part by vigorous mid-latitude winds (Böning et al., 2008). It provides an important heat and gas exchange surface between air and sea (Böning et al., 2008), and the circum-Antarctic cold-water currents positively influence phytoplankton productivity and circulation of nutrient rich waters (Lipps and Mitchell 1976; Kennett 1978; Fordyce 1980; Berger, 2007).

The onset of the ACC likely coincided with an increase in ocean productivity, and several studies attribute this ocean restructuring, at least partially, with the diversification of the Neoceti (Fordyce 1980; Berger, 2007; Marx and Fordyce, 2015; Marx et al., 2016a). Marx and Uhen (2010) suggest that the proliferation of large diatoms during the Late Eocene may have supported short food chains and large apex predators such as mysticetes (Marx and Uhen, 2010). Further, they suggest that the rise of diatoms may have facilitated the evolution of baleen. However, Pyenson (2017) argued that the link between diversification, mass filter feeding, and diatoms at this time is uncertain, as the timing of the onset of the ACC is still debated. Others concur that ACC of the Eocene-Oligocene was already deep enough to replicate modern mixing (Pfuhl and McCave, 2005), and therefore the immediate effects of the ACC are much debated (Marx et al., 2016a). Some studies, including Steeman et al. (2009), provide support for the potential link between neocete radiation and the onset of the ACC. In contrast to an adaptive radiation model, Steeman et al. (2009) found no support for a rapid burst in speciation. Instead, they found support for increased rates of diversification during periods of ocean restructuring, concluding that palaeoceanographic changes had the biggest influences on

cetacean radiations (Steeman et al., 2009). Rabosky et al. (2014) suggest that Cetacea underwent elevated rates of speciation followed by a steady decline which associated more so with an early adaptive radiation than one caused by ocean restructuring. Marx and Fordyce (2015) compiled a data matrix of 90 fossil and extant cetaceans, 86 of which were mysticetes, and scored them for morphological and molecular characteristics. They used climate data from Zachos et al. (2008) and total evidence dating and concluded that approximately 23 Mya evolutionary rates and disparity in the mysticetes fell and then became nearly constant. They suggest that this was the consequence of the ACC reaching its full strength (Marx and Fordyce, 2015). This study was conducted on mysticete rates and disparity only, to date no such study has been done across Cetacea.

Cetacean taxonomic diversity peaked again around the Mid-Miocene Climatic Optimum, a potential consequence of increased marine productivity and climate change (Marx and Uhen, 2010). Much of this peak is attributed to diversification in oceanic delphinids. However, it is unclear whether this is a consequence of ocean restructuring or innovations in delphinid evolution (Rabosky, 2014; Steeman et al., 2009) such as those shifts in dietary strategy and the effects of these shifts on size, as proposed by Slater et al. (2010), or perhaps even a reduction in extinction rates rather than in increased speciation – a pattern often seen in the fossil record (Lloyd and Slater, 2020). To date, most work on cetacean diversification has focused either on taxonomic diversity or univariate metrics, such as body size. No multivariate study has sampled across the whole of Cetacea nor quantified cetacean morphology using a morphometric approach to reconstruct the drivers of cetacean diversity, my thesis is the first to do so (see Chapters 3 and 4).

### 1.3.3 Shallow time impacts on cetacean diversity – human impacts

The fate of cetaceans is now intertwined with humans. Our activities regarding the atmosphere and oceans have a direct effect on the planet's biodiversity (Butchart et al., 2010; Jones and Safi, 2011). Human activities impact whales both indirectly via processes such as global warming and more directly through hunting, ship strike, and overfishing, to name just a few. In the past, humans

have mercilessly hunted whales almost to the brink of extinction (Roman et al., 2014). Between 1900 and 1999, 2.9 million whales were killed by the whaling industry, over two million of which were taken from the Southern Hemisphere, +270,000 from the North Atlantic, and +560,000 from the North Pacific (Rocha et al., 2014). Genetic analyses have shown that historic populations of fin whales (*Balaenoptera physalus*) and humpback whales (*Megaptera novaeangliae*) were between 6-20 times higher than they are today (Roman and Palumbi, 2003) and that baleen whale numbers crashed by at least 66% and as much as 90% during the twentieth century (Roman et al., 2014). Fortunately, in 1982, the International Whaling Commission announced that there should be a pause in whaling and an international moratorium was brought into effect in 1986 (Stoett, 1997). This is only a short time ago in the lifespan of some whales (Jefferson et al., 2011), and many populations of large baleen whales have still not recovered to their pre-whaling numbers (Rocha et al., 2014).

Due to their size, smaller cetaceans were not hunted in the same way that the baleen whales were, however, they are victim to other human impacts. The UK Cetacean Stranding Investigation Programme (CSIP) diagnosed that at least 17% of harbour porpoises (*Phocoena phocoena*), 43% of common dolphins (*Delphinus delphis*), and 36% of minke whales (*Balaenoptera acutorostrata)* recorded as strandings were killed in bycatch between 1990-2017 (Tindall et al., 2019). Every year 300,000 cetaceans are reportedly killed in bycatch, but this is likely a gross underestimate (Ross and Isaac, n.d). The list of human threats on cetaceans is extensive and includes but is not limited to toxins and pollutants (Hunt et al., 2013), overfishing and associated starvation (Leeney et al., 2008; Deaville et al., 2015), noise pollution (shipping and military sonar; Hunt et al., 2013), and global warming (Davidson et al., 2012). An overview of cetacean diversity in both shallow and deep time, the causes and consequences of past turnover events and current threats, is necessary for building a truly comprehensive picture of cetacean evolution.

### 1.3.4 Diversity through time - an interdisciplinary approach

Monitoring populations and cetacean numbers is crucial to understanding our impact on these animals. Monitoring programmes use sightings data (Evans and Hammond, 2004), strandings data (see Chapter 5 for details), and genetic data to monitor the health and resilience of populations. Thanks to monitoring and conservation programmes, in some localised cases, cetacean numbers are approaching pre-harvest levels (Roman et al., 2014). If this continues to be the case, we can expect to see a rise in the ecosystem benefits that healthy populations of whales bring (Roman et al., 2014). Likewise, we can also expect to see a rise in conflicts between human activities and cetaceans for example in bycatch and commercial fisheries (Roman et al., 2014). This is where field observations, strandings data, and an increased understanding of historical population dynamics are paramount to understanding patterns seen in the past and informing predictions for the future (Baker and Clapham, 2004; Roman et al., 2014).

Information provided by the fossil record and evolutionary biology plays an important role in understanding the ecology, distribution, and adaptability of extant species. Placing species in a phylogenetic context can help us to understand loss in genetic and morphological distinctiveness (Pyenson, 2009; Marx et al., 2016a) which is useful for targeting efforts for their protection (Marx et al., 2016a). It is challenging to answer questions on diversity and distribution for long extinct species; however, in many cases, fossils provide the only means of establishing what a species' original range was before humans interfered (Marx et al., 2016a). In this thesis I use a combination of methods from palaeontology and neontology to address questions on cetacean diversity through time, with a focus on the cetacean cranium.

## 1.4 The cranium

To answer questions on changes in morphological diversity through time, I focus on the cetacean cranium. The cranium (the skull minus the mandible) is a complex structure which serves diverse functional roles, from feeding, breathing, housing the brain, nervous system, and sensory structures, to

interacting with the environment. Because of these many functions, the skull is of particular interest to vertebrate palaeontologists as it can be used to infer diet and other aspects of paleoecology. The skull is the most informative part of the cetacean skeleton because of its inherent complexity and because most of the bones that comprise the skull have become simplified or modified in some way throughout cetacean evolution (Marx et al., 2016a). The developmental and functional complexities of the cranium make it ideal for investigating the complexities of asymmetry, patterns of trait evolution through time, and the evolution of different cranial regions. For these reasons, the focus of geometric morphometric studies is often biased towards the skull (Cardini et al., 2010; Goswami et al., 2012; Cardini and Polly, 2013; Santana and Lofgren, 2013; Santana, 2015; McCurry et al., 2017a; McCurry et al., 2017b; Felice and Goswami, 2018; Bardua et al., 2019b; Watanabe et al., 2019; Galatius et al., 2020) to name just a small fraction of examples for tetrapods.

### 1.4.1 The whale cranium

Cetaceans have undergone some of the most radical morphological changes of any animal on the planet. These massive changes evolved to adapt to a fully aquatic lifestyle (Fordyce and de Muizon, 2001) and cetaceans now show extremely divergent morphologies from their terrestrial artiodactyl relatives. Some of the biggest changes have occurred in the skull, particularly in the posterior shifting of the nasals (whereby they have moved from the tip of the snout as seen in terrestrial artiodactyls and archaeocetes to the top of the head seen in extant cetaceans) to accommodate easier breathing at the surface (Heyning and Mead 1990). In addition to this shifting of the nares, posterior displacement of the premaxilla and maxilla is seen across Cetacea. The cetacean skull varies in its appearance, from the brachycephalic, stubby face of the extant pygmy sperm whale (*Kogia breviceps*) (Fig. 1.6 (8)) and the bizarre walrus-like Pliocene *Odobenocetops* sp. to the extreme elongated dolichocephalic rostrum of *Schizodelphis morckhoviensis* (Fig. 1.6 (6)) and the extant Amazon river dolphin (*Inia geoffrensis*) (Fig. 1.6 (9)). The odontocetes are often considered to be the more variable of the extant suborders, with

crown mysticetes remaining generally consistent in their morphology across the clade with only some small fluctuations in asymmetry recorded through time (Fahlke and Hampe, 2015).



50 million years ago

Present
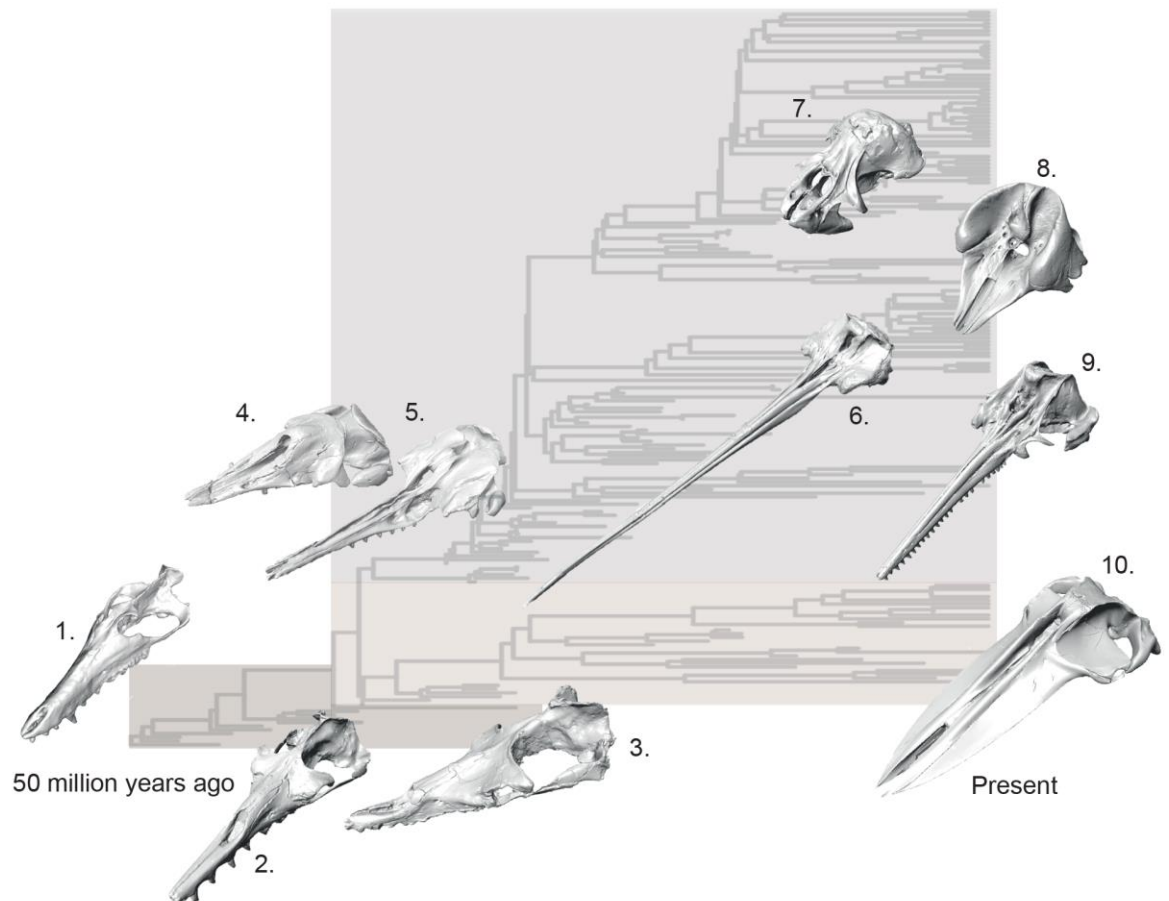
**Fig. 1.6.** Examples of skull morphology through time. Examples of skull morphology through time shown on the phylogeny used in this this thesis (adapted from Lloyd and Slater, 2020). The archaeocete part of the phylogeny (background*) is* highlighted in dark brown, mysticetes in light brown, and odontocetes in grey. 1. *Pakicetus attocki* PVM 100148 (Eocene archaeocete); 2. *Zygorhiza kochii* USNM 11962 (Eocene archaeocete); 3. *Mystacodon selenensis* MUSM 1917 (Eocene mysticete); 4. *Simocetus rayi* USNM 256517 (Oligocene odontocete); 5. *Echovenator sandersi* GSM 1098 (Oligocene odontocete); 6. *Schizodelphis morckhoviensis* USNM 13873 (Miocene odontocete); 7. *Odobenocetops peruvianus* SMNK PAL 2491 (Pliocene odontocete); 8. *Kogia breviceps* USNM 22015 (extant odontocete); 9. *Inia geoffrensis* AMNH 93415 (extant odontocete); 10. *Balaenoptera musculus* NHM 1892.3.1.1 (extant mysticete). Skulls not to scale.

The same cranial bones are retained across Cetacea; generally, there has been no loss or gain of bones across the clade, or throughout their evolution, bar a few exceptions. *Odobenocetops* lacks a ventral exposure of the maxilla on the palate (de Muizon, 1993; de Muizon and Domning, 2002). Instead, the maxillae are relegated to a small area on the side of the rostrum, and an elongated strip on the dorsal face (de Muizon and Domning, 2002). The kogiids are characterised by, among other features, the loss of both nasals (Huggenberger et al., 2017; Collareta et al., 2017; Benites-Palomino et al., 2019; Benites-Palomino et al., 2021).

### *1.4.2 The archaeocete cranium*

The cranium of early archaeocetes largely resembles that of terrestrial mammals and lacks most of the extreme modifications observed in later whales. The earliest archaeocetes, the pakicetids, had a narrow skull with close, dorsally oriented eyes (Nummela et al., 2006) that face sideways in the younger ambulocetids but are still located far dorsally. This may suggest that the early archaeocetes were ambush predators that spent much of their time submerged in shallow water (Thewissen, 2014; Marx et al., 2016a). Although very different to the skull of extant cetaceans, even the earliest pakicetids had the pachyosteosclerotic (thickened bone) tympanic bulla and anteroposterior

aligned shearing-adapted dentition which clearly marks them as cetaceans (Uhen, 2007). The younger archaeocetes, e.g., the basilosaurids, show some of the modifications associated with more modern cetaceans such as more posteriorly positioned nasals. None of the archaeocetes had telescoping, i.e., the posterior displacement and expansion of the maxilla and premaxilla (Churchill et al., 2018) which is associated with more crownward cetaceans.

One controversial feature observed in some archaeocetes is cranial asymmetry. Cranial asymmetry in cetaceans is associated with echolocation. The archaeocetes could not echolocate; however, some basilosaurids and protocetids show cranial asymmetry in the rostrum (Fahlke et al., 2011; Coombs et al., 2020). This asymmetry may be a consequence of fossil deformation (e.g., as in *Cynthiacetus peruvianus*) rather than biological, but it may also have some biological signal (Martínez-Cáceres and de Muizon, 2011; Martínez-Cáceres et al., 2017). Fahlke et al. (2011) suggested that asymmetry found in the archaeocete rostrum evolved to facilitate directional hearing.  An archaeocete skull is shown in Fig. 1.7.

DORSAL

VENTRAL



| | |
|---|---|
| basisphenoid | palate |
| basioccipital | parietal |
| frontal | premaxilla |
| jugal | pterygoid |
| mandibular process | supraoccipital |
| maxilla | squamosal (with zygomatic process) |
| nasal | |
| occipital condyles | |
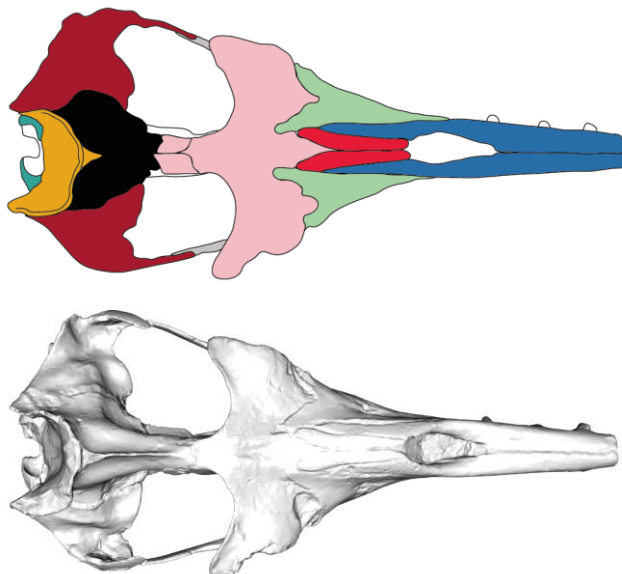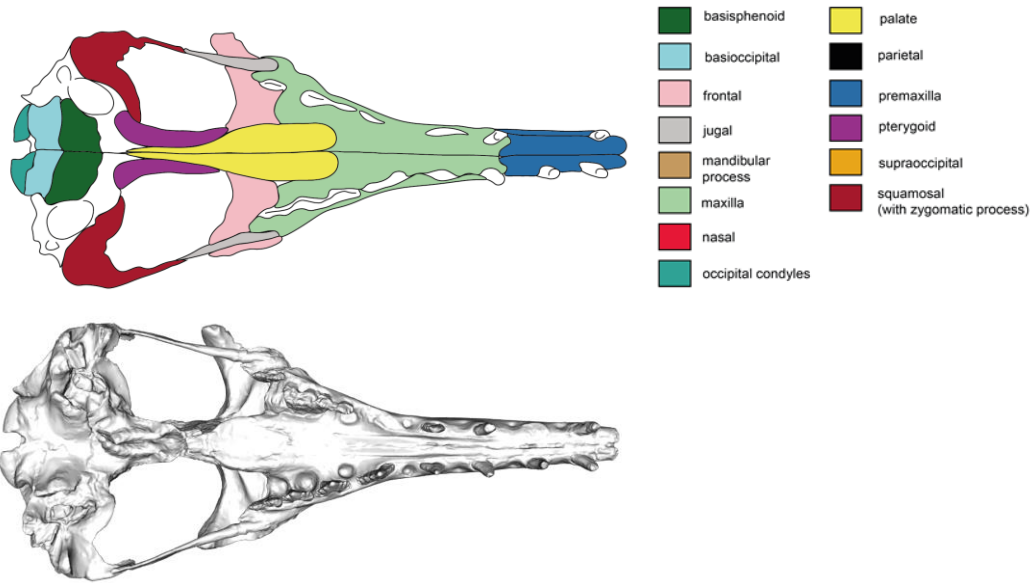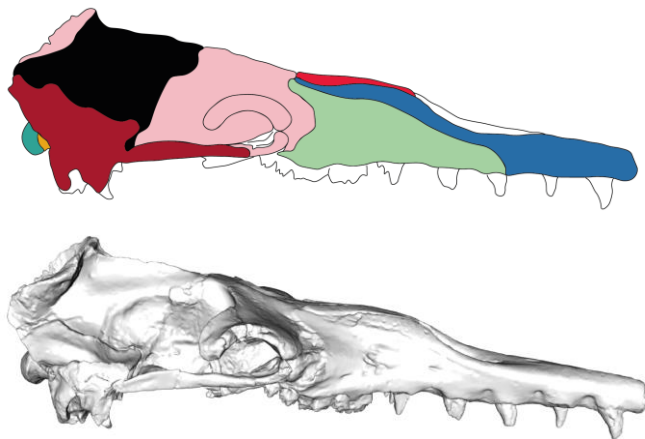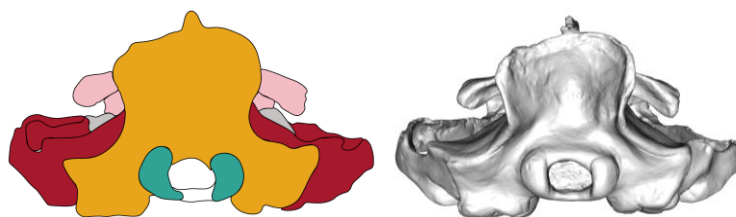
LATERAL



POSTERIOR



[Figure on this and previous page]

**Fig. 1.7.** The bones in the archaeocete skull. Each bone is colour coded (see key). Dorsal, ventral, lateral, and posterior views of bones are shown on the skull of the basilosaurid, *Zygorhiza kochii* (USNM 11962).

### 1.4.3 The mysticete cranium

One of the most obvious features of the mysticete cranium is the forward movement of the posterior cranial elements, referred to as prograde cranial telescoping (Miller, 1923; Churchill et al., 2018). Previous work has suggested that mysticetes have crania that are as bilaterally symmetrical as their terrestrial artiodactyl cousins (Fahlke and Hampe 2011), reflecting their lack of echolocating ability and specialisation towards a unique feeding strategy for mammals. The defining characteristic of extant mysticetes, and the 'true' toothless mysticetes, is the presence of baleen. Although not shown in Fig. 1.8 or landmarked in this thesis (no dentition is landmarked within this study), the presence of baleen influences the shape of the rest of the skull – for example driving selection for a larger, flatter palate and a more planar skull shape (Fig. 1.8), ideal for surface skimming and lunge feeding (Werth, 2000a). Baleen is keratinous sieve-like plates that hang from the upper jaw and allow mysticetes to strain vast quantities of zooplankton from the water. This innovative method of feeding was so successful that that, once fully adapted to filter feeding, the mysticetes rapidly diversified (Marx et al., 2016a). Further, the acquisition of vast quantities of prey became so effective that mysticetes were able grow to be the largest animals to have ever existed. A mysticete skull is shown in Fig. 1.8.

DORSAL



| | | | |
|---|---|---|---|
| 🟩 | basisphenoid | 🟨 | palate |
| 🟦 | basioccipital | ⬛ | parietal |
| 🟪 | frontal | 🟦 | premaxilla |
| ⬜ | jugal | 🟪 | pterygoid |
| 🟫 | mandibular process | 🟧 | supraoccipital |
| 🟩 | maxilla | 🟥 | squamosal (with zygomatic process) |
| 🟥 | nasal | | |
| 🟩 | occipital condyles | | |

VENTRAL

LATERAL



POSTERIOR



[Figure on this and previous page]

**Fig. 1.8.** The bones in the mysticete skull. Each bone is colour coded (see key). Dorsal, ventral, lateral, and posterior views of bones are shown on the skull of the balaenopterid, *Balaenoptera musculus* (NHM 1892.3.1.1).

### 1.4.4 The odontocete cranium

The odontocete cranium bears two dominant features: extensive posterior shifting of the anterior cranial bones (retrograde telescoping; Churchill et al., 2018) and extreme bilateral asymmetry. It is well known that many odontocetes show pronounced asymmetry in the nasals, premaxilla, and maxilla (Fig. 1.9) (Ness, 1967; Mead, 1975), adaptations which enable echolocation. The asymmetry in the skull is linked to the hypertrophied melon, phonic lips, nasal sacs, and other soft apparatus associated with high frequency sound production and echolocation (Cranford et al., 1996; Fahlke et al., 2011). The morphology of soft tissues (shifted sinistrally) is likely a consequence of the evolution of the underlying bony structures (Heyning and Mead, 1990). Echolocation is an extraordinary innovation, and its evolution and finesse has become a defining characteristic of the

odontocetes, as well as enabling them to diversify into a vast range of forms (Marx et al., 2016a). An odontocete skull is shown in Fig. 1.9.

DORSAL



| | | | |
|---|---|---|---|
| ■ basisphenoid | | ■ palate | |
| ■ basioccipital | | ■ parietal | |
| ■ frontal | | ■ premaxilla | |
| ■ jugal | | ■ pterygoid | |
| ■ mandibular process | | ■ supraoccipital | |
| ■ maxilla | | ■ squamosal (with zygomatic process) | |
| ■ nasal | | | |
| ■ occipital condyles | | | |

VENTRAL

LATERAL



POSTERIOR



| | basisphenoid | | palate |
|---|---|---|---|
| | basioccipital | | parietal |
| | frontal | | premaxilla |
| | jugal | | pterygoid |
| | mandibular process | | supraoccipital |
| | maxilla | | squamosal (with zygomatic process) |
| | nasal | | |
| | occipital condyles | | |

[Figure on this and previous page]

**Fig. 1.9.** The bones in the odontocete skull. Each bone is colour coded (see key). Dorsal, ventral, lateral, and posterior views of bones are shown on the skull of the delphinid, *Delphinus delphis* AMNH 75332.

## 1.5 Studying deep time morphological evolution

Morphology is a branch of biology concerned with the form and structure of organisms (part or whole), their composition, features, and related functions (Wake, 1991). Today, morphologists are generally interested in the structural integration of parts and their significance in organismal functioning, and the resultant limitations and possibilities for ecology and more widely, evolution (Kardong, 2019). Morphological analyses can focus on any scale of biological study, from proteins to cells, species, communities, lineages, and entire

clades. Macroevolutionary patterns of morphological variation, those observed above the species level, specifically focus on quantifying patterns across taxa and clades. In the context of this thesis, morphology is focused at and above the organismal level, including the constituent parts of the cranium, its shape and function, and its relevance for understanding an organism's position within an ecological community (Kardong, 2019). Specifically, I use quantitative methods to reconstruct the drivers of cetacean morphological evolution through deep time, with relevance for their future trajectory.

### 1.5.1 What drives the evolution of morphology?

Many factors influence the evolution of morphology. These include functional demands, biotic and abiotic factors, and phylogenetic history. Discerning which of these factors dominates or significantly contributes to the evolutionary patterns observed in a clade requires quantitative, comparative analysis. These factors can also influence different aspects of morphological evolution, from the specific aspects of morphological variation associated with certain biotic traits, to constraining or promoting morphological disparity and evolutionary rate, to determining evolutionary mode. The aspects are not necessarily aligned, with rate and disparity showing both concordant and discordant patterns in different clades and cranial modules (Goswami et al., 2010; Felice et al., 2018; Watanabe et al., 2019; Bon et al., 2020). All these aspects of morphological evolution are addressed in this thesis.

One of the most striking patterns that can reflect several of these factors is convergent evolution, whereby similar selection pressures in distantly related clades can result in similar morphologies. One such example, driven by the functional constraints of locomotion, is the morphological similarity between the extinct Mesozoic marine reptiles, ichthyosaurs, e.g., *Ichthyosaurus platyodon*, and the extant marine mammals, delphinids e.g., bottlenose dolphin (*Tursiops truncatus*) via a number of adaptations employed by multiple species in these clades (McGhee, 2011; Stayton, 2015). These adaptations include a fusiform body adapted for fast swimming and an elongate rostrum and homodont teeth used to catch fish (McGhee, 2011).

The opposite pattern of evolutionary conservatism, reflected as phenotypic constraint, also influences morphology in some clades. The mammalian cervical vertebra is a good example of morphology reflecting a conservative trait. First noted by Darwin (1868), extensive breeding and domestication have not altered the vertebra in the way it has produced a spectrum of cranial variation (Darwin, 1868; Drake and Klingenberg, 2010; Arnold et al., 2016). Importantly, some species of frog on different continents owe their morphological similarity to dispersal and evolutionary conservatism, rather than evolutionary convergence even over vast spatial and temporal scales (Moen et al., 2013). It is thus important to consider which taxa retain ancestral traits and resemble taxa due solely to recent shared ancestry.

Size can also constrain and influence shape. Cardini and Polly (2013) consider mammalian facial length and heterochrony. They conclude that growth of the face is linked to absolute size, which has implications and constraints on head shape. Further, a significant component in mammal facial variation is associated with their size diversity, which is orders of magnitude greater compared to other vertebrate groups (Cardini and Polly, 2013).

Habitat can also have a profound influence on morphology. Intraspecific studies of green anole lizards showed that animals living on broad, smoothed leaved foliage had shorter distal hindlimbs, longer forelimbs, larger toepads, and were more slender than those of the same species living only 30km away on more 'typical' continuous bush and shrub vegetation (Irschick et al., 2005). Habitat type can also promote faster rates of evolution in some species of labrid and haemulid fish (Price et al., 2011; 2013).

Diet also influences morphology (Santana et al., 2012; Law et al., 2019; Felice et al., 2019). In the vertebrate skull, cranial morphology is shaped by adaptive evolution for foraging and biomechanical performance required for the acquisition and processing of food (Santana et al., 2012). Santana et al. (2012) found that in phyllostomid bats, the most diverse mammalian dietary radiation, species that consume harder foods such as insect exoskeletons and hard fruits, have evolved skull shapes that allow for a more efficient bite force. In musteloids, although different diets also influence cranial shapes, species had

similar bite forces suggesting that other feeding performance metric and possibly even nonfeeding traits are important contributors to cranial evolution (Law et al., 2018). Patterns such as these are seen across the animal kingdom.

Another example, in this case driven by the functional ecological pressures of nocturnal hunting is enlarged eyes to increase retinal surfaces, as observed in nocturnal predators such as the great horned owl (*Bubo virginianus*) and the lesser bush baby (*Galago senegalensis*) (McGhee, 2011). Adaptations to the sensory system can also drive morphology, especially in the cranium which houses most of the sensory structures. In the odontocetes a key adaptation is the ability to echolocate. This has driven extensive change in the skull such as naso-facial asymmetry, which is unique to these echolocating whales (See 1.4.4). This in turn has helped develop an enormous brain, necessary for processing and interpreting acoustic data.

Developmental strategy has also been found to influence rates of morphological evolution. In salamanders, direct developers show the slowest rates of evolution and lowest disparity, and paedomorphic species show the highest rates and disparity in the cranium (Fabre et al., 2020), limbs (Fabre et al., 2014; Ledbetter and Bonett 2019), and vertebral column (Bonett et al., 2018). Developmental strategy in mammals has also been shown to influence integration in the skull. In marsupials, which are born at an altricial state, the crania, forelimb ontogeny, and oral apparatus are less disparate than placentals which are born at a relatively late stage of development (Goswami et al., 2016; Kelly and Sears, 2011). Presumably due to marsupial functional selection pressures of needing to climb to a pouch and suckle for extended periods. Conversely, cetaceans are highly precocial with long gestation and lactation periods (these vary between species and between the toothed whales and baleen whales), and typically give birth to just one offspring (Jefferson et al., 2011). Limited information is available on diversity in whale development, although some baleen whale foetuses do appear in whaling collections, studying reproduction in large, protected, mobile marine organisms is challenging.

There are many factors which influence skull morphology. Except for development and brain size, the impacts of echolocation and ecological factors such as diet and habitat are the primary factors accessible for living and fossil cetaceans and are considered further in this thesis.

### 1.5.2 How to quantify morphology

Understanding vertebrate morphology requires an appreciation of both diversity and breadth of shape, and constraints in shape (Webster and Webster, 1974). To better understand this, we must quantify morphology. The mammal skull is complex and capturing its shape often requires a 3D approach. Recent technological advances in 3D imaging have expanded these possibilities and enhanced the study of many diverse organisms (Adams et al., 2004; Zelditch et al., 2004; Mitteroecker and Gunz 2009). Throughout this thesis I employ a 3D imaging approach and geometric morphometrics (GMM) to capture a surface scan of the skull (Fig. 1.10).

Geometric morphometrics is an approach that quantifies shape using Cartesian coordinates that are placed on a surface of the structure of interest to represent its morphology (Adams et al., 2004; Zelditch et al., 2004; Adams et al., 2013). Morphometric studies can use 2D landmarks (x, y coordinates) on a 2D image (e.g., a photograph or single plane of a 3D scan), or linear measurements (Hedrick et al., 2015) or outline analysis if homologous landmarks are absent (Temple, 1992; Cardini, 2014). Technological advances in 3D imaging have increased the ability to generate comparative image data sets and use these to quantify morphology across a broad range of organisms (Bookstein et al., 1991; Rohlf and Marcus, 1993; Adams et al., 2004; Zelditch et al., 2004; Gunz et al., 2005; Adams et al., 2013; Bardua et al., 2019b). As a result, the use of 3D landmarks (x, y, z coordinates) digitised from 3D meshes are becoming more common.

Landmarks for both 2D and 3D analyses are chosen to capture clear, homologous points (Fig. 1.10). The two types of landmark used in this thesis are Type I (biological) and Type II (geometric) landmarks (Bookstein, 1991; Bookstein, 1997). Type I landmarks are defined locally, for example, on the

intersection between sutures whilst Type II landmarks are intermediate and usually placed on the process or maxima of a curvature or structure. Additionally, semi-landmarks (considered by some as Type III landmarks) can be added to capture even more morphometric data and estimate missing data in incomplete specimens (Gunz and Mitteroecker, 2013) (Fig. 1.10). Sliding of semi-landmarks minimizes differences in positions based on a criterion (generally bending energy or Procrustes distance) and puts them into geometric homologous positions (Adams and Otárola-Castillo, 2013). Sliding semi-landmark curves that define outlines and margins of bones represent an increase in the shape captured compared to using landmarks alone (Bookstein, 1997; Bardua et al., 2019a; Goswami et al 2019).
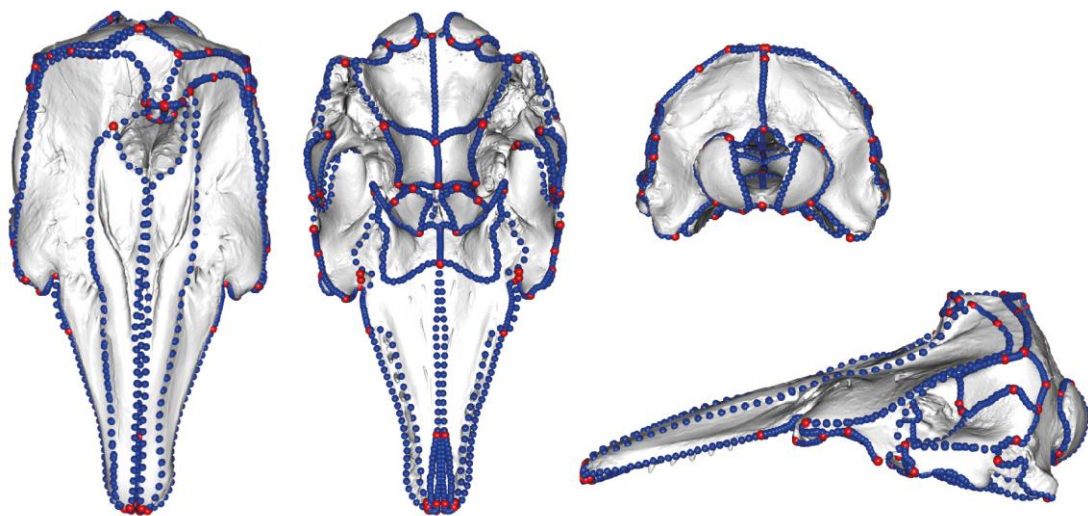


**Fig. 1.10.** Landmarks and curve sliding semi-landmark placement. From left to right, the skull is shown in dorsal, ventral, posterior (top) and lateral (bottom) view. The landmarks in red are type I and type II landmarks. The curves in blue define outlines and margins of bones. There are 123 landmarks and 124 curves on this specimen. Note the asymmetry in the naso-facial region of this odontocete (far left). Landmarks and curves shown on a beluga (*Delphinapterus leucas* USNM 305071) specimen.

Capturing shape can be challenging in highly diverse data sets or when structures have limited homologous landmarks such as smooth mandibles or limb bones. Landmarks alone can leave large sections of the morphology unsampled or under-sampled (Bardua et al., 2019a). This scenario is where sliding semi-landmarks are useful (Gunz and Mitteroecker 2013). Sliding semi-landmarks have been used successfully to quantify a vast array of organismal morphology, including beak shape (Cooney et al., 2017), forelimbs (Fabre et al., 2014), and cranial morphology (Bardua et al., 2019b, Felice et al., 2019). Developments have also been made in automated, pseudo-landmark, and landmark free methods (Boyer et al., 2011; Boyer et al., 2015) which have been used to quantify form, function, and ecological adaptation (Dickson and Pierce, 2019). The benefits of automated landmarks are that they greatly speed up data collection, reducing the time needed to manually place landmarks and removing issues of subjectivity in landmark placement (Boyer et al., 2011). However, there are downsides to using automated methods. Unlike semi-landmarks, automated landmarks do not retain correspondence between data points and thus make it difficult to partition landmarks into specific regions (Gonzalez et al., 2016). Landmarks and semi-landmarks have become a staple of geometric morphometrics and have been used to capture a wide range of morphologies such as the cranium (Gunz et al., 2009; Bardua et al., 2020; Bardua et al., 2019b; Felice et al., 2019), limbs (Fabre et al., 2014; Wölfer et al., 2019), wings (Schmieder et al., 2015), vertebrae (Randau and Goswami, 2017a, 2017b), and many more structures.

These advances in morphometrics, coupled with new tools for statistical analyses, have opened many new avenues of investigation in palaeobiology and neontology (Zelditch et al., 2012; Adams, 2014). Other advancements have been seen in computational power, open access databases (such as https://www.phenome10k.org/) and high resolution and three-dimensional imaging (Mitteroecker and Gunz, 2009; Lawling and Polly, 2010). These tools, in combination with a phylogenetic framework, allow for comprehensive analysis of morphological evolution through deep time.

### 1.5.3 Fossil specimens in morphological studies

Understanding the factors shaping morphological evolution requires a representative sample of a target group's diversity. While most analyses will focus entirely on extant diversity, most diversity and variation is actually extinct. Where fossils are concerned, we often investigate their functional morphology – the interpretation of function from morphology (Benton, 2005), because we cannot directly observe their behaviour, ecology, etc. Interpretations from the shape of the fossils themselves, for example the shape of a femoral head can provide us with information on rotation and hinging of the joint, from which we can infer movement (Benton, 2005). The same can be said of muscle scars from muscle attachments to indicate strength and size. A key component of fossilisation and our ability to interpret information from the fossil, thereafter, is taphonomy. Taphonomy is the burial and preservation of the fossil itself, and the processes that occur between the death of the organism and its appearance in the fossil record (Benton, 2005).

Whether a dead organism turns into a fossil is dependent on a wealth of factors including the composition of hard and soft tissues and the variable amounts of rock available that can be searched for fossils from different time periods (Uhen and Pyenson, 2007). Soft tissues do not preserve as well as hard tissues such a bone, which means there are few good examples of, for example, fossilised baleen. Once a cetacean has died and been deposited, abundant sediment in shallow and coastal waters can help fossilise the skeleton. The large weight of cetacean skeletons along with their robustness and durability can also help to preserve an articulated morphological record (Peters et al., 2009). While inclusion of fossils is not always possible for macroevolutionary studies of clades with poor fossil records, this is fortunately not the case with Cetacea. Where it is possible to include fossils, simulations and empirical analyses have demonstrated that fossil data greatly improves the accuracy of macroevolutionary reconstructions (Quental and Marshall, 2010; Slater et al., 2012; Finarelli and Goswami, 2013; Slater and Harmon, 2013). The importance of including fossils in macroevolutionary studies cannot be underestimated as researchers gain most power in understanding macroevolutionary data from both living and extinct taxa when they are

included together in the same phylogenetic framework (Slater and Harmon, 2013). The incorporation of fossil information dramatically improves the ability to distinguish between models of quantitative trait evolution (Slater et al., 2012) and improves ancestral state estimates compared to when deriving them using extant taxa alone (Slater et al., 2012).

Quantifying how biotic and abiotic factors affect morphology in extinct taxa further improves the accuracy of macroevolutionary analyses; however, involving fossils can introduce more complications than studies of extant taxa alone. Not only are fossils often incomplete, but we often must also infer ecology (palaeoecology) without observation. There are only a handful of fossils which preserve primary information on diet, for example, bite marks on *Dorudon* (basilosaurid archaeocete) skulls indicate that they were a prey item of the much larger *Basilosaurus isis* (basilosaurid archaeocete) (Snively et al., 2015). Further, juvenile *Dorudon* have even been found in the stomach contents of *Basilosaurus* (Voss et al., 2019). However, finds like this are rare and generally assumptions are made based on morphology and phylogenetic relatedness among species instead.

The assumptions behind interpreting ecology from morphology is that structures have evolved or adapted in a similar way to be efficient at a similar function (Benton, 2005). For example, we can infer that xenorophiids, one of the most basal odontocete families (Early Oligocene), could likely echolocate because of their cranial morphology: dense bone in the interorbital shield which may have reflected sounds forward, and a ventrally deflected rostrum which may also have reduced interference (Boessenecker et al., 2017). We can also infer feeding ecology based on morphology. For example, in the earliest transitional filter feeding whales, the Eomysticetidae (Late Oligocene), baleen is not actually preserved in the fossil, but due to the presence of lateral palatal foramina, a non-laterally deflected coronoid process, and an anteroposteriorly expanded palate, the authors infer that this animal had baleen in the posterior of the palate and likely skim fed on zooplankton (Boessenecker and Fordyce, 2015). The bones of fossil and extant specimens thus can reveal a great deal about their function and ecology.

Many studies of functional morphology link fossil forms to modern groups, whilst others infer details from the bones themselves, for example from processes or muscle scars which may offer insight into an animal's function and biomechanics (Benton, 2005). Sometimes it is more difficult to place fossil specimens if there are no living descendants or closely related relatives. *Odobenocetops*, a bizarre walrus-like whale from the Pliocene is one such example. This cetacean is known from one genus and has highly unusual modifications, such as binocular vision and the inferred loss of echolocation (the only odontocete that may not have been able to echolocate). Based on its morphology, it was placed within Delphinoidea (de Muizon et al., 2002). Even when specimens have no close relatives to draw information from, we can make functional assumptions based on the morphology, especially in the skull (Benton, 2005).

### 1.5.4 Bias and incompleteness of the fossil record

Beyond limited information on the biology and ecology of individual extinct species, discussed above, the fossil record itself introduces additional complications to macroevolutionary studies. Firstly, the fossil record is incomplete, with gaps caused by several factors. Taphonomy, the process of fossilisation, as previously discussed determines whether a dead animal fossilises, and leaves us with a record, or does not, and leaves us with gap. The factors affecting taphonomy vary greatly depending on sea level, climate, topography of tectonic plates, erosion, and many other factors (Marx et al., 2016a). Secondly, even if a specimen does fossilise, the chances it will be discovered vary greatly depending on its geographical or regional location (Marx et al., 2016a). Vegetation cover (e.g., dense cover in the Amazon rainforest), accessibility of rocks, human population, human willingness, ability, research effort, and finances or resources to excavate fossils all have an impact on creating hotspots of fossils in some regions and underrepresentation of fossils in others (Uhen and Pyenson, 2007; Marx et al., 2016a). For cetaceans, the discovery of fossil material is highest in Japan, Europe, New Zealand, and the United States. However, this does not necessarily mean that past cetacean diversity was highest in these regions, it

just suggests that the cetacean fossil record is subject to geographical, geological, and human biases that favour these regions (Marx et al., 2016a).

Despite these biases, and the incompleteness of the record, Slater and Harmon (2013) state that one cannot have a complete picture of macroevolution without considering fossil *and* extant relationships. See 1.5.3 for details on how simulations confirm that even a small amount of fossil taxa can more accurately recover most macroevolutionary patterns (Slater et al., 2012). Thus, the merger of the fields palaeontology and neontology can only benefit the understanding of macroevolutionary processes and patterns (Slater and Harmon, 2013). Here I use methods from both palaeontology and neontology to address macroevolutionary patterns in cetaceans.

## 1.6 Quantifying macroevolutionary patterns

Recent advances in statistical and morphometric methods have offered powerful new tools for macroevolutionary research, especially with regards to modelling evolutionary rates and disparity, as shown in this thesis (Chapters 2-4). As phylogenetic approaches proceed into the twenty-first century, a focus has been rightly placed on genome-scale data sets because of the nearly limitless supply of discrete systematic characters (Delsuc et al., 2005). Regardless, many neontologists realise that, moving forward, paleontological data is essential for phylogenetic analysis, divergence dating, estimation of diversification and extinction rates to quantify macroevolutionary patterns. Phylogenetic comparative methods (PCMs) have undergone rapid developments in the past few years and can be used to reconstruct the shared evolutionary history of taxa, map ancestral character states, map morphological evolution, and investigate the impacts of biotic and abiotic factors on macroevolutionary patterns (Pagel, 1999). These techniques can also be applied to standard statistical procedures such as MANOVAs and principal component analyses (PCA) (Revell et al., 2008; Clavel and Morlon, 2020).

There have also been recent advancements in statistical modelling for trait evolution using PCMs. Trait evolution can be modelled under different evolutionary scenarios; Brownian Motion (a 'random-walk' mode of evolution;

BM), Ornstein-Ulenbeck (a modification of the 'random-walk' process where evolution tends towards an optimum; OU), Early-Burst, or adaptive radiation (the rapid expansion of a diversifying clade as it fills a niche, for example; Yoder et al., 2010), and accelerated trend (an acceleration in rates, possibly driven by shorter generation times or mutualism between species). Furthermore, models can be run with a Markov Chan Monte Carlo (MCMC) algorithm which permits variable rates allowing the rate of change to vary through time (Plummer et al., 2006; Clavel et al., 2015).

A variety of tools are now available for quantifying evolutionary rates and disparity on a macroevolutionary scale. These tools include R packages such as 'dispRity', a tool measuring disparity from multidimensional matrices (Guillerme, 2018) and mvMORPH, a means for Fitting Evolutionary Models to Morphometric Data (Clavel et al., 2015). The recent development of packages like mvMORPH (Clavel et al., 2015) means that we can now fit multivariate models (such as BM, OU, Early-Burst) of continuous trait evolution to phylogenies and time-series (Clavel et al., 2015). We can also test for phylogenetic signal and quantify the rate and mode of evolutionary rates across a phylogeny and compute the likelihood of various evolutionary models to find a best model fit for our data. There are, however, currently few methods available that can handle multivariate data. I discuss the issues of multivariate data and high dimensionality in Chapters 3 and 4 with further details on limitations in Chapter 6.

## 1.7 The phylogenetic relationships among whales

The morphological data sets in this thesis are analysed under a phylogenetic comparative framework. This framework allows me to investigate morphological evolution whilst accounting for the shared evolutionary history of the species in my data set (Felsenstein, 1985; Benton 2005; Kardong, 2019). A published phylogeny (Lloyd and Slater, 2020) is used for Chapters 2-4 and is altered to include any additional species. The Lloyd and Slater (2020) phylogeny was chosen because not only does the resultant tree extend sampling from the ~90 extant species to over 500 living and extinct species, it also extends and applies recent meta-analytic approaches to synthesise

previously published phylogenies. Further, it brings together time-scaled phylogenetic hypotheses at the species-level, offering a robust and detailed inference of macroevolutionary dynamics. A phylogenetic framework is widely accepted as a critical requirement for addressing questions of diversity, phenotypic evolution, and biogeography (Lloyd and Slater, 2020; Adams, 2014), among many others. Phylogenies often combine morphological, molecular, and fossil data allowing us to view species in relation to one another in an evolutionary context. Furthermore, phylogenies allow us to assess species within context, for example their shared ancestry and historical influences on the evolution of characteristics (Dobson, 1985). The covariance between species imposed by the structure of a phylogenetic tree means that we must take the phylogeny, its patterns of divergence, branch lengths, and hierarchy into consideration when trying to understand the processes responsible for generating macroevolutionary patterns (Felsenstein, 1985; Harvey and Pagel, 1991; Lloyd and Slater, 2020).

Several recent studies of cetacean divergence and radiations have been based on molecular phylogenies (Steeman et al., 2009; Slater et al., 2010). Many phylogenies, albeit made using different approaches (supermatrix, supertree, metatree), agree that the divergence time of the neocetes (collectively the mysticetes and odontocetes) took place between around 39 and 36 Mya (Steeman et al., 2009; Slater et al., 2010; Marx et al., 2016a; Geisler, 2017), although this is regularly pushed back thanks to the discovery of archaic toothed mysticetes (Lambert et al., 2017a; Marx et al., 2019 a, b). There is currently no record of odontocetes older than ~ 33.9 million years (Fordyce, 2002), however the antiquity of the mysticetes suggests that a ghost linage of odontocetes also existed in the Late Eocene (Pyenson, 2017). This would further push back this divergence date. Most phylogenetic analyses fail to support a hypothesised sister group relationship between sperm whales (*Physeter macrocephalus*) and baleen whales (Milinkovitch et al., 1993, 1994) and instead reconstruct the physeteroids as the first of the major odontocete crown lineages to diverge (Marx et al., 2016a). Finally, there is unanimous agreement that an increase in cetacean diversification rates during the past 10 Ma were driven by the rapid speciation of the oceanic dolphins

(Delphinidae) (McGowen and Spaulding, 2009; Steeman et al., 2009; Slater et al., 2010; Rabosky and Goldberg, 2015).

There are some discrepancies between the topology and divergence estimates of some clades, or specifics of species positions within families depending on the data used (molecular or morphological) but generally, there is a consensus and stability in the cetacean phylogeny. In this thesis, I used a metatree phylogeny from Lloyd and Slater (2020) (Fig. 1.5). The metatree approach uses binary encoding of tree topologies to generate a matrix which can then be used for phylogenetic analysis (Lloyd and Slater, 2020). The tree samples from the ~90 extant species and 400+ extinct species allowing a robust inference of macroevolutionary dynamics (Lloyd and Slater, 2020). This recent metatree phylogeny from Lloyd and Slater (2020) (Fig. 1.5) which assembles a comprehensive set of phylogenies for extant and extinct cetaceans, allows me to include fossils spanning the full breadth of my macroevolutionary analyses. The phylogeny also includes many recently described South American taxa which I was also able to scan and include in my thesis, giving a much broader temporal and geographical breadth than other current cetacean phylogenies. The authors stress the importance of a palaeo-phylogenetic approach for studying macroevolutionary dynamics (Lloyd and Slater, 2020).

## 1.8. Shallow-time patterns in cetacean diversity and distributions

In the final section of my thesis, I shift from morphological to taxonomic diversity, and from deep to shallow time, analysing spatial and temporal patterns in cetacean strandings data (more below) to investigate shallow time changes in cetacean strandings, species composition, and correlates of strandings. This departure from the geometric morphometric approach in Chapters 2-4 provides the opportunity to explore a completely different data type, methods, and approach to investigate shifts in cetacean diversity at different temporal and spatial scales.

### 1.8.1 Cetacean stranding data

Cetacean strandings occur when cetaceans become grounded on a beach or in shallow water. Stranding events can consist of one individual or a whole pod. Mass strandings often make the media due to the huge numbers of individuals that strand, the rare opportunity to see cetaceans up close, and the emotions that accompany the event. For many inconspicuous, deep diving, or rare species, stranding data is the best record we have (Morin et al., 2017). In fact, the first and only data on many beaked whale species has been obtained from strandings data and subsequent collection of specimens for museums (Pitman, 2009; Lacsamana et al., 2015; Yamada et al., 2019).

Systematic cetacean stranding records have been kept by the Natural History Museum (NHM), London (UK) since 1913. The continuous data set records strandings around the UK coastline, and in most cases, includes the date of stranding and location. For most records, we have information on the species and whether the individual was a single incident, or part of a mass stranding. A Hawaiian data set investigated by Maldini et al. (2005) contains similar recorded information, e.g., date, location of stranding, species (when identifiable), but lacks the continuity and the detail of the UK data set. In 1990, the Cetacean Stranding Investigation Programme (CSIP) funded by the Department for Environment, Food, and Rural Affairs (DEFRA) took over the UK stranding programme. At the same time the Irish Whale and Dolphin Group (IWDG) was set up to record Irish cetacean strandings. These data sets are key data sources for assessing recent changes in cetacean taxonomic diversity because they (combined) provide over 100 years of valuable archive records (Pyenson, 2011; Coombs et al., 2019). Considering a long-term data set can allow for the separation of regular patterns from random events, and reduce the importance of small, atypical events (MacLeod et al., 2004). Using information from numerous stranding events and combined data sets, collected over a long period of time can counteract some limitations associated with using stranding data. However, due to the way the data are recorded, and the sets compiled, bias does need to be considered in any approach using strandings data. Excitingly, the final chapter of my thesis represents the first time these three data sets have ever been combined, creating a data set of

over 20,000 records. It is also the first time the NHM strandings (NHM, 2018) data has been investigated in its entirety.

### 1.8.2 Bias in strandings data

The NHM, CSIP, and IWDG strandings records provide a temporal and spatial approximation of species composition, diversity, and abundance of the species seen around UK and Irish coastlines. However, there are biases in how and when data were collected throughout the 102-year timeline (1913-2015). Each of these biases can have an impact on the number of records made for that year of period (Fig. 1.11). Cetaceans (and other marine mammals) can be notoriously difficult to study. They are wide ranging, deep diving and spend most of their lives submerged underwater (Evans and Hammond, 2004). Commonly used surveying techniques are often biased towards gregarious and conspicuous species that will approach boats such as short-beaked common dolphins (*Delphinus delphis*; Evans and Hammond 2004) as well as larger, more easily detected species, or those that live near the coastline. This is where strandings records can be incredibly useful, providing data on any cetacean that has washed ashore.

However, strandings data comes with its own limitations and caveats. Along with biases in the method, there are also biases in this data, mostly regarding collection effort. For example, sampling effort dropped during and after both world wars. This was due to several reasons: people were fearful of being too near to the beaches, especially on the south coast; inaccessibility to beaches due to training exercises and military occupation; or simply people being conscripted into helping the war effort and being occupied with the war (Klinowska 1985). Other influences that have affected strandings records throughout the twentieth century and into the twenty-first century are outlined in Fig. 1.11.

Further, there is a complex interaction between other factors such as drift, and deciphering whether stranding events along the north and west coasts of Britain, south and west coasts of Ireland may in part be due to the passive transport of carcasses by the North Atlantic drift (MacLeod et al., 2004). This

complicates interpreting whether stranding patterns are caused by a higher abundance and diversity of cetaceans for example in this same area, deep, prey rich waters off the west coasts and continental shelf support high abundance (Wall et al., 2009; Hammond et al., 2013), or whether other factors such as drift tides, current, winds (Peltier et al., 2012; Moore et al., 2020), migration routes or a combination of several factors influence high strandings numbers in these areas. Detectability of the carcass may also bias the data towards large cetacean species such as sperm whales (*Physeter macrocephalus*) or the baleen whales which are easier to detect on beaches, and less likely to be scavenged, damaged in stormy seas (Lawler et al., 2007), and otherwise rendered undetectable to the species level.

Finally, some whale species may have different blubber and/or gas compositions which would affect their buoyancy (Nowacek et al., 2001) and the chances of whether they will sink, float, or make landfall. Balaenids for example were nicknamed 'floaters' by whalers due to their thick blubber and their tendency to float after death (Reeves and Mitchell 1986; Kerr et al., 2014). Balaenopterids, on the other hand, have a thinner blubber layer and are less buoyant (Kerr et al., 2014). These factors are all incredibly complex to model. In Chapter 5 I investigate temporal and spatial trends in cetacean strandings using GAMs and attempt to address changes in sampling effort and sampling bias as an offset in my models (see Generalised Additive Models; GAMs)

1885: UK government examine claims of reducing fish stocks and habitat damage caused by steam powered boats[1]

1914-1918: WWI

1913: Natural History Museum (UK) starts to systematically record cetacean strandings

1939 – 1945: World War II, landings in fishing and whaling decrease

1950: Huge increase in post-war fishing and whaling effort. Increase in number of trawlers registered in England and Wales[2]

1982: The International Whaling Commission adopts a moratorium on commercial whaling

2013: European parliament votes for reform of the Common Fisheries Policy, including measures to protect endangered stocks and the ending of discards[6]

1971: UK signs the Accession Treaty of the Common Fisheries Policy (CFP)[3,4]

2009: Norway, Denmark, and Iceland pledge to increase whaling quota

1900          1950          1980          Present day

1889: Bottom trawl catches in England and Wales are first recorded[1]

1946: NATO increases in military testing in European waters. Submarine, military sonar, and torpedo use increase

1976: The EU extends its fishing waters from 12 miles to 200 miles of the coast[3,4]

1990: Cetacean Stranding Investigation Programme set up

2000s: Increase in pile-driving for offshore wind turbines[5]

[Figure on previous page]

**Fig. 1.11.** Influences on stranding data. A schematic of some events which may have impacted the UK stranding data. NB. This is not an exhaustive list and only considers the UK and surrounding area which may not be representative of factors incurred by farther ranging species. 1. Thurstan et al. (2010); 2. Holm (2016); 3. Common Fisheries Policy (n.d). 4. Jensen (1999); 5. Bailey et al. (2010); 6. European Commission, 2013.


### *1.8.3 Generalised Additive Models (GAMs)*

GAMs are commonly used in studies of spatiotemporal trends, distribution, and abundance. GAMs have been used to model abundance and seasonal fluctuations for many species including brown hares (*Lepus europaeus*) and mountain hares (*Lepus timidus*; Massimino et al., 2018), dung beetles (Scarabaeidae, Coleoptera; Gebert et al., 2019), marine mammals (both cetaceans and pinnipeds; Best et al., 2015), a whole wealth of large African fauna (Craigie et al., 2010), and many more. GAMs have been used to model seasonal and cyclic data including to investigate nonlinear relationships between humpback whale distribution and relative abundance and environmental variables (such as sea surface temperature, salinity, and chlorophyll abundance; Dalla-Rosa et al., 2012). GAMs are not dissimilar to Generalised linear models in that they use a link function. However, GAMs use this link function to establish relationships between a 'smoothed' function of the predictor and *multiple* explanatory variables (Guisan et al., 2002). Importantly, GAMs are substantially more flexible because relationships between dependent and independent variables are not assumed to be linear (Fig. 1.12; Wood, 2011; 2017). This means cyclical or seasonal data can be analysed using GAMs without losing any information on fluctuations, seasonality, or 'wobbliness' which might be lost by fitting a GLM (Fig. 1.12).
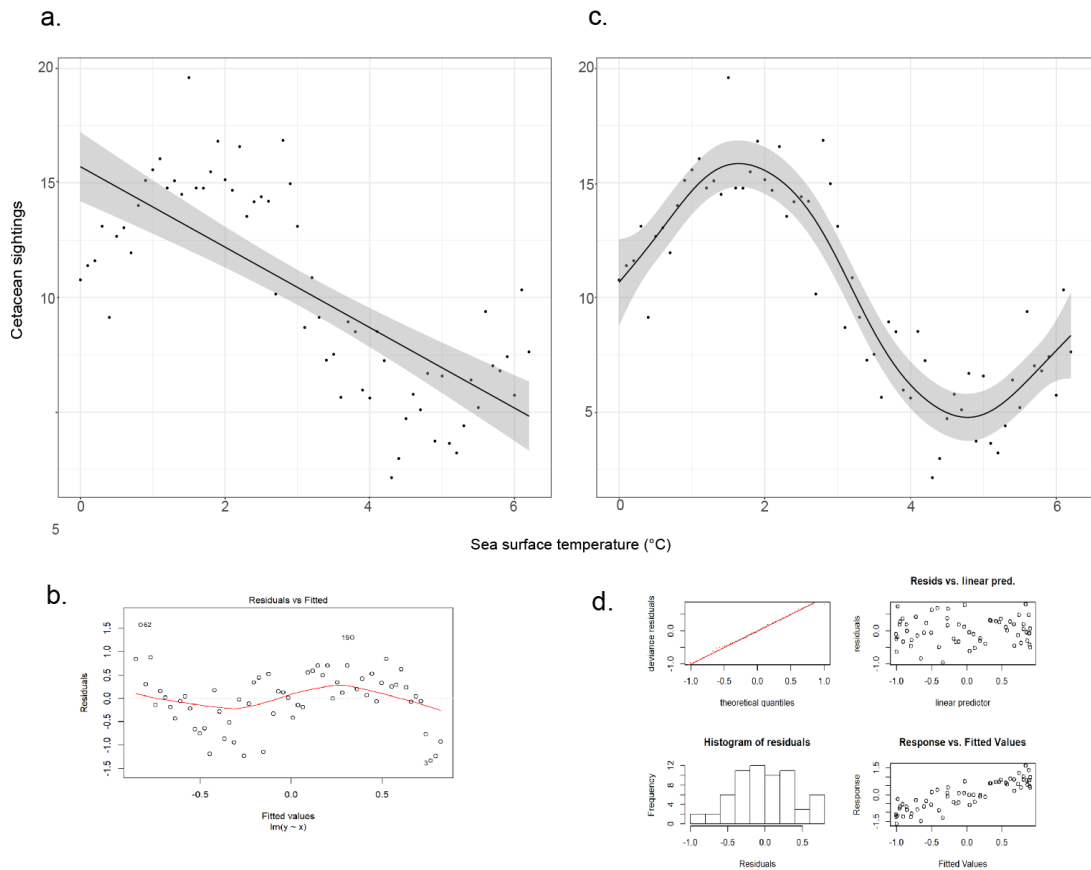
**Fig. 1.12.** An example of a normal linear model fit vs. a GAM fit. The linear model (a) fits the data sufficiently, but the residuals plot (b) is messy. The GAM (c) offers a better fit to the environmental data. It is essential to check the model diagnostics (d). The Q-Q plot (d, top left) shows the closest fit to a y=x line, here this shows a good model fit. The histogram of residuals (d, bottom left) also shows a normal distribution, suggesting that most of the residuals fall around the mean. The residuals vs. linear predictors plot (d, top right) shows that there is some heteroscedasticity in the data set i.e., there is an increase in the residuals with increasing values of the linear predictor. The response vs. fitted values show a normal distribution (d, bottom right). Data and code modified from http://environmentalcomputing.net/intro-to-gams/.

Finally, the use of GAMs in studies of abundance and ecosystem modelling have increased greatly in recent years. GAMs are a semi-parametric approach to predicting non-linear responses to a suite of predictor variables (Drexler and Ainsworth, 2013). In comparative studies, GAMs have often been shown to perform as well or better than other types of predictive models based on environmental conditions (Guisan et al., 2002; Drexler and Ainsworth, 2013)

## 1.9 Thesis overview

This thesis addresses the topic of cetacean diversity in three sections. Firstly, in Chapters 2 and 3, I investigate cranial morphology in the cetacean skull with a focus on quantifying asymmetry (Chapter 2), and modelling rates of evolution and disparity in the skull (Chapter 3). In Chapter 3, I also consider potential ecological influences on morphological variation in the cetacean cranium. The investigation into influences on cranial morphology is continued in Chapter 4 with a focus on the effects of past climate and ocean productivity on cetacean evolutionary rates. I use two data sets as proxies for past climate here: Cramer et al. (2015) and Westerhold et al. (2020), for a more robust approach and because of some discrepancies between the two data sets.

Throughout Chapters 2-4, I use landmarks and sliding semi-landmark curves to capture the morphology of individual bones in the cetacean skull. I subsample my semi-landmarks to reduce dimensionality and thus computational requirements while retaining sufficient coverage across the cetacean cranium (Watanabe et al., 2019; Felice and Goswami, 2018). Some studies use landmarks, semi-landmarks, and additionally surface semi-landmarks. However, curve semi-landmarks may be sufficient for shapes characterised by relatively conserved surface geometries between curves (Cooney et al., 2017; Bardua et al., 2019a). Goswami et al. (2019), showed that more than 90% of the shape signal is captured by curve data alone, relative to the full surface data set. For this reason, I decided to use landmarks and curve semi-landmarks but not surface points in my analyses. Although this reduced the amount of surface morphology captured in the data I collected, collecting semi-landmark data but not surface data takes significantly less time and meant I could achieve much greater taxonomic sampling and avoid dimensionality issues from having far more landmarks than specimens (Bardua et al., 2019a), as discussed further in Chapter 3.

Finally, I look at cetacean diversity in shallow time. In Chapter 5, I use strandings data to investigate spatial and temporal changes in strandings from 1913-2015. I combine three data sets for the first time and use them to investigate the potential trends in spatial and temporal patterns of strandings and environmental or anthropogenic predictors.

Across these chapters, I focus on the following five questions to bring together a study of cetacean diversity through deep time to the present:

1. When did cranial asymmetry first appear in cetacean evolution and how is this trait distributed across whales? What influences the evolution of this trait? (Chapter 2)

2. How do evolutionary rates and disparity vary across cetacean crania? (Chapter 3)

3. What are the primary aspects of variation across cetaceans and how do the following ecological factors influence the morphological evolution of the cetacean cranium? (Chapter 3)
   a. Dentition
   b. Diet
   c. Echolocation ability
   d. Feeding method
   e. Habitat

4. How does climate affect rates of cranial evolution? (Chapter 4)

5. How do the following environmental and anthropogenic factors influence the spatial and temporal patterns in cetacean strandings records in the more recent past? (Chapter 5)
   a. Fishing effort
   b. Geomagnetic fluctuations
   c. North Atlantic Oscillations
   d. Sea surface temperature
   e. Shipping traffic
   f. Storm events

### 1.9.1 Aims and objectives

The key aim of this thesis is to quantify cetacean diversity from past (deep time) to present (shallow time). This is done via a three-stepped approach; 1. Quantify cranial morphology, asymmetry, rates, and disparity across cetacean evolution (Chapters 2 and 3) 2. Quantify how ecological influences (biotic factors) and climate (abiotic factors) affect evolutionary rates and morphological diversity through time (Chapters 3 and 4). 3. Quantify the effects

of environmental and anthropogenic predictors on temporal and spatial cetacean strandings data over the past 100 + years (Chapter 5).

I used a variety of methodological approaches with these objectives:

1. Generate the largest 3D surface scan data set of cetacean crania to have ever been compiled, with near complete sampling of extant species
2. Sample the entirety of cetacean evolution with multiple specimens representing all 'suborders' (archaeocetes, mysticetes, odontocetes) and major clades (where possible) throughout their evolutionary history and phylogeny
3. Quantify asymmetry in the skull across Cetacea for the first time
4. Quantify evolutionary rates and disparity in the skull across Cetacea using morphological data for the first time
5. Collate existing information on cetacean ecology and then quantify the influence of ecology on cranial morphology
6. Model the influences of climate on rates of evolution across Cetacea by employing two widely used benthic foraminiferal $\delta^{18}O$ and $\delta^{13}C$ reference data sets
7. Combine the NHM, CSIP, and IWDG strandings data sets together for the first time to provide the longest continuous, systematic strandings data set in the world
8. Investigate spatial and temporal patterns in UK and Irish strandings data and model the effects of environmental and anthropogenic predictors on strandings

## 1.10 Chapter overviews

### 1.10.1 Chapter 2: Quantifying asymmetry in the cetacean skull.

Odontocetes (toothed whales) echolocate (navigate and feed using biosonar), which is reflected in their highly asymmetric crania. Some basilosaurids and protocetids (both members of the paraphyletic, basal archaeocete group) may have asymmetrical crania as well, whereas mysticetes have bilaterally

symmetrical skulls and no asymmetry in the naso-facial region because they do not echolocate. Previous studies have focused on either odontocete cranial shape and function, archaeocete asymmetry or mysticete symmetry with modern odontocetes for comparison, but none have looked at asymmetry across Cetacea and through their evolutionary history. It is also unclear when naso-facial asymmetry evolved during the transition from archaeocetes to modern whales. To answer these questions, I carried out a geometric morphometric analysis using a set of landmarks to quantify asymmetry in the skulls of 162 (78 fossil and 84 extant specimen) cetaceans. One skull was scanned per species that had suitable cranial representation. For species that had multiple suitable cranial representations (more in the Methods sections of Chapters 2 and 3), I selected only one skull to scan. This was so that I could compile a data set that covered the widest possible phylogenetic spread, rather than focusing on any intraspecific variation. I then tested alternative models to investigate where asymmetry may have arisen, and where changes in the rate are observed throughout cetacean evolution. This chapter has been published as: Ellen J. Coombs, Julien Clavel, Travis Park, Morgan Churchill, and Anjali Goswami. Wonky whales: the evolution of cranial asymmetry in cetaceans. BMC Biology volume 18, Article number: 86 (2020).

### 1.10.2 Chapter 3: Making waves: the rise and fall of cetacean evolutionary rates and disparity through their history

It is well known that the archaeocetes transitioned from a terrestrial lifestyle to a fully aquatic one within ~8-12 million years. The fossil record thereafter suggest that the two cetacean suborders diverged around ~39 million years ago. These two lineages still dominate the oceans today, armed with their key innovations: echolocation in the odontocetes and filter feeding in the mysticetes. In this chapter, I use geometric morphometrics (both landmarks and sliding semi-landmarks) to quantify skull shape from 201 specimens (113 fossils and 88 extant) spanning 50 million years of cetacean evolution. With these data, I first describe variation across whale crania and investigate ecological influences on their cranial morphology, focusing on dentition, diet, echolocation ability, feeding method, and habitat. Then, I reconstruct

evolutionary rates and disparity in the cetacean crania across their entire evolutionary history and assess how shifts in rates and disparity relate to the appearance of key innovations, the disappearance of the archaeocetes, and other evolutionary milestones.

### 1.10.3 Chapter 4: How does climate affect cetacean diversity – evidence from the past and present

I focused specifically on the influence of climate on cetacean morphological evolution, using the full cranial data set developed in Chapter 4. I use benthic foraminiferal $\delta^{18}O$ climate data and benthic foraminiferal $\delta^{13}C$ data to reconstruct palaeoclimatic and ocean productivity curves. I then tested alternative models for cetacean cranial evolution, from standard models, such as Brownian Motion, Early Burst, and accelerating rates, to novel environmental models where evolutionary rates track various proxies of climate and ocean productivity to establish whether these extrinsic factors are significant drivers of cetacean cranial evolution.

### 1.10.4 Chapter 5: Quantifying cetacean diversity in shallow time. What can 100 years of stranding records tell us?

As with other marine species, cetaceans can prove difficult to study as they are often wide-ranging and spend most of their lives submerged under water. Therefore, cetacean stranding records (where a whale, dolphin, or porpoise becomes beached) are a primary source of information for many cetacean species. This is particularly the case with rarer, more elusive, and less gregarious species. The Natural History Museum, London (NHM) has maintained a database of UK strandings since 1913, making it one of the longest, continuous, systematic cetacean stranding data sets in the world. In 1990, the NHM programme joined with the Cetacean Strandings Investigation Programme (CSIP) to record strandings in the UK. Despite records being available up to 2015, no comprehensive studies of temporal changes in cetacean strandings exist for this full period, i.e., from 1913-2015. In this chapter, I combine these data with that of the Irish Whale and Dolphin Group (IWDG) to obtain 100 years of strandings records. I assess spatio-temporal

patterns in the number of individuals stranding in the UK and Ireland and use Generalised additive Models (GAMs) to explore anthropogenic and environmental correlates of cetacean strandings. This chapter has been published as: Ellen J. Coombs, Rob Deaville, Richard C. Sabin, Louise Allan, Mick O'Connell, Simon Berrow, Brian Smith, Andrew Brownlow, Mariel Ten Doeschate, Rod Penrose, Ruth Williams, Matthew W. Perkins, Paul. D. Jepson, and Natalie Cooper. *What can cetacean stranding records tell us? A study of UK and Irish cetacean diversity over the past 100 years.* MARINE MAMMAL SCIENCE, 35(4): 1527–1555 (2019).

### 1.10.5 Chapter 6: Conclusions

In the final chapter of my thesis, I bring together results from the preceding chapters to produce a comprehensive picture of cetacean evolution and diversity through deep and shallow time. Specifically, I reconstruct the myriad of factors shaping the evolution of cetaceans throughout their history, with a focus on cranial rates and disparity. I then bridge scales of analysis and discuss temporal trends and the biotic and abiotic predictors of these patterns in both shallow and deep time. I finish by discussing the importance of these results for both evolutionary and conservation biology, discuss the limitations of these approaches, and suggest future directions this work could take.

**Chapter two**

**Wonky whales: The evolution of cranial asymmetry in cetaceans**

*'But as the colossal skull embraces so very large a proportion of the entire extent of the skeleton; as it is by far the most complicated part….you must not fail to carry it in your mind, or under your arm, as we proceed'*

Moby Dick – Herman Melville

## 2.1 Abstract

Unlike most mammals, toothed whale (Odontoceti) skulls lack symmetry in the nasal and facial (naso-facial) region. This asymmetry is hypothesised to relate to echolocation, which may have evolved in the earliest diverging odontocetes. Early cetaceans (whales, dolphins, and porpoises) such as archaeocetes, namely the protocetids and basilosaurids, have asymmetric rostra, but it is unclear when naso-facial asymmetry evolved during the transition from archaeocetes to modern whales. We used three-dimensional geometric morphometrics and phylogenetic comparative methods to reconstruct the evolution of asymmetry in the skulls of 162 living and extinct cetaceans over 50 million years.

In archaeocetes we found asymmetry is prevalent in the rostrum, but also in the squamosal, jugal, and orbit, possibly reflecting preservational deformation. Asymmetry in odontocetes is predominant in the naso-facial region. Mysticetes (baleen whales) show symmetry similar to terrestrial artiodactyls, such as bovines. The first significant shift in asymmetry occurred in the stem odontocete family Xenorophidae during the Early Oligocene. Further increases in asymmetry occur in the physeteroids in the Late Oligocene, Squalodelphinidae and Platanistidae in the Late Oligocene/Early Miocene and in the Monodontidae in the Late Miocene/Early Pliocene. Additional episodes of rapid change in odontocete skull asymmetry were found in the Mid-Late Oligocene, a period of rapid evolution and diversification. No high probability increases or jumps in asymmetry were found in mysticetes or archaeocetes. Unexpectedly, no increases in asymmetry were recovered within the highly asymmetric ziphiids, which may result from the extreme, asymmetric shape of premaxillary crests in these taxa not being captured by landmarks alone.

Early ancestors of living whales had little cranial asymmetry and likely were not able to echolocate. Archaeocetes display high levels of asymmetry in the rostrum, potentially related to directional hearing, which is lost in early neocetes - the taxon including the most recent common ancestor of living whales. Naso-facial asymmetry becomes a significant feature of Odontoceti skulls in the Early Oligocene, reaching its highest levels in extant taxa. Separate evolutionary regimes are reconstructed for odontocetes living in

acoustically complex environments, suggesting that these niches impose strong selective pressure on echolocation ability and thus increased cranial asymmetry.

**Keywords:** trait evolution, asymmetry, cetaceans, morphometrics, macroevolution

## 2.2 Background

Cetaceans (whales, dolphins, and porpoises) are the most taxonomically diverse aquatic mammal clade (Fordyce and Barnes, 1994), and inhabit most major ocean basins and some rivers (McGowen et al., 2009). Whales appear in the fossil record approximately 52.5 million years ago (Mya), with the two extant cetacean suborders, mysticetes (baleen whales) and odontocetes (toothed whales), diverging around 39 million years ago (Mya) (Marx and Fordyce, 2015). Mysticetes evolved large body sizes and specializations for bulk filter feeding whilst odontocetes evolved echolocation (biosonar) (Geisler et al., 2014; Churchill et al., 2016; Park et al., 2016) and employ various raptorial and/or suction feeding strategies (Hocking et al., 2017a; Hocking et al., 2017b). Cetaceans have undergone extensive morphological changes to adapt to a fully aquatic lifestyle (Fordyce and de Muizon, 2001; Uhen, 2007) and show extremely divergent morphologies compared to their terrestrial artiodactyl relatives. Some of the most striking changes have occurred in the skull, including the posterior displacement of the nares, maxilla, premaxilla, and a shortening of the nasals (Heyning and Mead, 1990; Klima, 1999; Churchill et al., 2018).

Odontocetes are well-known to have asymmetrical crania (Thompson, 1990, chapter 2), whereas mysticetes have bilaterally symmetrical skulls and no asymmetry in the naso-facial region (Fahlke et al., 2011; Fahlke and Hampe, 2015). Fahlke et al. (2011) hypothesised that basilosaurids and protocetids (early cetaceans belonging to the archaeocetes) also have cranial asymmetry thought to be linked to aquatic directional hearing with the most conspicuous asymmetry occurring in the rostrum (Fahlke et al., 2011; Fahlke and Hampe,

2015). Asymmetry in odontocetes is always unidirectional, with a posterior and sinistral shift in the bones, linked to the hypertrophied melon, phonic lips, and nasal sacs, all of which are associated with high-frequency sound production and echolocation (Cranford et al., 1996; Fahlke et al., 2011). Most of this asymmetry appears in the dorsal opening of the nares (Macleod et al., 2007; Fahlke and Hampe, 2015) and appears to be correlated with the degree of elevation in the cranial vertex Heyning and Mead, 1990). Species with high cranial vertices such as physeterids, kogiids, and ziphiids tend to have the most asymmetrical crania, likely because a functional component of asymmetry pertains to soft facial anatomy and consequently drives evolution of the underlying bony structures (Heyning and Mead, 1990).

Odontocete asymmetry is thought to have evolved as a result of an evolutionary hyperallometric investment into sound-producing structures to facilitate the production of high frequency vocalisations (Mead, 1975; Heyning, 1989; Heyning and Mead, 1990; Huggenburger et al., 2017; Jensen et al., 2018) but alternative explanations have been put forward. MacLeod et al. (2007) proposed that skull asymmetry is a by-product of the selection pressure for an asymmetrically positioned larynx, an aquatic adaptation which enables the swallowing of large prey underwater without mastication. However, this has been argued against because reduction of tooth size and loss of shearing occlusion started after asymmetry was well developed, suggesting that swallowing prey whole may not be the driver of asymmetry (Fahlke et al., 2011). Alternatively, cranial asymmetry in basilosaurids and protocetids is thought to be linked to aquatic directional hearing (Fahlke et al., 2011). The limited or lack of asymmetry in mysticetes, which do not echolocate and instead specialise in low and infrasonic frequencies (Ketten, 1997; Reidenburg and Laitman, 2007; Park et al., 2017) suggests directional cranial asymmetry is more likely related to echolocation than hearing (Fahlke et al., 2011).

Previous studies have focused on either odontocete cranial shape and function (Churchill et al., 2018), archaeocete asymmetry (Fahlke et al., 2011), or mysticete symmetry with modern odontocetes and archaeocetes for comparison (Fahlke and Hampe, 2015). There is, however, little resolution on how cranial asymmetry evolved during the transition from archaeocetes to

modern whales (Neoceti) (Fahlke et al., 2011) and little is known about archaeocete asymmetry and its relationship, if any, to that of odontocetes (Marx et al., 2016a). To assess when and how often asymmetry may have arisen, where and if it is present in the archaeocete skull, and how it relates to the evolution of echolocation, it is necessary to adopt a comparative approach by broadly sampling across living and extinct cetaceans. Here we use geometric morphometric techniques to quantify asymmetry in the skull across modern and fossil species of Cetacea. We then use these data to reconstruct the evolution of asymmetry across cetaceans and test for shifts (a change in the trait on the whole branch or clade) and jumps (a temporary or rapid change in the trait). Finally, we use these results to test potential factors associated with the evolution of asymmetry in specific cetacean clades, including presence or absence of echolocation, echolocation frequency, and inhabiting acoustically complex or high-pressure environments, such as shallow rivers, cluttered icy waters, and deep ocean.

## 2.3 Methods

### 2.3.1 Specimens

The data set comprises stem cetaceans (archaeocetes, n = 10), and both extant suborders: the baleen whales (mysticetes, n = 32) and toothed whales (odontocetes, n = 120). The final data set comprised 162 cetacean crania, of which 78 (48%) are extinct, ranging in age from 48.6 Mya to 2.59 Mya. Additionally, 10 terrestrial artiodactyls (representing 8 of the 10 Arctiodactyla families) were included to provide a baseline for symmetry, as cetaceans are nested within Artiodactyla. Specimen details (Appendix 2: Table S2.1) and museum abbreviations are provided in Appendix 2.

Specimens were selected to cover the widest possible phylogenetic spread, representing 39 families and 101 genera from the Eocene to the present. The Early-Middle Eocene is represented by the land-dwelling family Pakicetidae through to semi-aquatic Ambulocetidae and Remingtonocetidae.

The Pelagiceti are represented by the fully aquatic Basilosauridae of the Late Eocene through to the modern Neoceti. This includes representation of some early stem toothed mysticetes such as the Mammalodontidae and the Aetiocetidae. Three of the four extant mysticete families are represented. The odontocetes are represented by early stem families; the Xenorophidae and the Simocetidae of the Early-Mid Oligocene and the 'Patriocetidae' (phylogenetic position is still being clarified) of the Late Oligocene. The more crownward odontocetes of the Miocene are represented by the Eurhinodelphinidae, Kentriodontidae, Albireonidae, Squalodelphinidae, Squalodontidae, and Allodelphinidae among other extinct families. All ten extant odontocete families are represented. See Appendix 2: Table S2.1 for details.

As many extant and all fossil specimens lack information on sex, sexual dimorphism could not be considered. All specimens are adult except for one subadult, *Mesoplodon traversii*. Specimens were selected based on completeness, but some bones were broken (e.g., jugal) and were treated as missing data. 64 (~39%) of the specimens, including some extant specimens, had missing data concentrated in the pterygoid, palatine, jugal, squamosal, and tip of the rostrum. For this reason and because fossils often have a higher proportion of missing data, we also ran analyses without any fossils and without rostral landmarks. Specimens with obvious taphonomic or other deformation were excluded from further analysis (Appendix 2: Table S2.2). Excluded specimens include the basilosaurid *Cynthiacetus peruvianus* which shows sinistral torsion in the rostrum, although a potential natural feature in protocetids and basilosaurids (Fahlke et al., 2011; Fahlke and Hampe, 2015), it is suggested that rostral distortion in this particular specimen (MNHN.F. PRU 10) is at least partly the original morphology of the skull and potentially a result of some taphonomic distortion (Martínez-Cáceres et al., 2017). Inevitably, some fossil specimens have sections of reconstructed bone. Their inclusion in the study was based upon the extent and accuracy of the reconstruction and the unavailability of alternative specimens.

Skulls were scanned using a Creaform Go!SCAN 20, or Creaform Go!SCAN 50 depending on the size of the skull. Scans were cleaned, prepared, and merged in VXElements v.6.0 and exported in ply format before being further

cleaned and decimated in Geomagic Wrap software (3D Systems). Models were decimated down to 1,500,000 triangles, reducing computational demands without compromising on detail for further morphometric analyses. In many studies of morphology when the skull is incomplete, it is possible to digitally reconstruct bilateral elements by mirroring across the midline plane if preserved on one side (Gunz et al., 2009; Cardini et al., 2010; Gunz et al., 2013). However, due to the substantial asymmetry observed in many taxa in this study, mirroring a complete half of the skull was not possible (Fig. 2.1; Appendix 2: Fig. S2.1). For this reason, we limited mirroring to marginally damaged bones or easily mirrored missing bones only, where it was clear that mirroring would not mask any biological asymmetry, using the 'mirror' function in Geomagic Wrap (3D Systems).
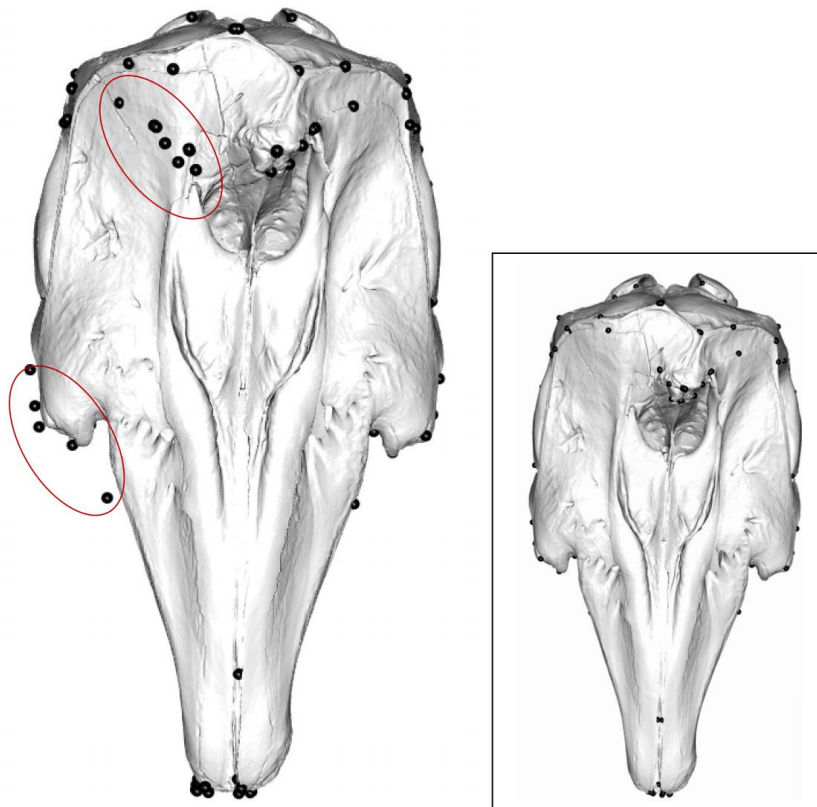
[Figure on previous page]

**Fig. 2.1.** An example of misaligned landmarks. Misalignment of mirrored landmarks when using the `mirrorfill` function on a specimen without bilateral symmetry. Landmarks mirrored in the geomorph package (Adams et al., 2019) on an asymmetric specimen. Note the incorrect mirroring of landmarks on the nasal and to a lesser extent on the posterior-ventral-lateral point of the maxilla (circled) in this specific specimen. Inset shows the same skull with the landmarks correctly placed. Specimen is *Delphinapterus leucas* USNM 305071.

### 2.3.2. Morphometric data collection

### 2.3.2.1 Manually placed landmarks (Fn)

We placed 123 anatomically defined landmarks over the surface of the skull in Stratovan Checkpoint (Stratovan, Davis, CA, USA) using the 'single point' option. We placed 57 landmarks on both the left-hand side (LHS) and right-hand side (RHS) of the skull, and 9 landmarks on the midline, totalling 123 landmarks covering both the dorsal and ventral sides of the skull (Fig. 2.2). Type I and II landmarks (Adams et al., 2019) were selected to comprehensively represent the full cranium (Fig. 2.2; Appendix 2: Table S2.2). 'Landmark 15' and the subsequent mirrored 'landmark 79' denote the back of the toothrow in most species. In some ziphiids e.g., *Mesoplodon carlhubbsi*, the teeth (or tusks) erupt midway along the mandible (Ellis and Mead, 2017) while other species present multiple pairs of tusks (Reid et al., 2003). In others (e.g., *Hyperoodon ampullatus*), teeth typically erupt as a single pair on the anterior mandible which often protrudes *beyond* the upper jaw (Ellis and Mead, 2017). Without the mandible, it is challenging to pinpoint the positioning of the back of the toothrow, and even then, the presence and number of teeth is negligible in some species. Further, these tusks only erupt in adult males. For these reasons, and to avoid simply estimating where the true tooth row may be, 'landmark 15' and 'landmark 79' in specimens with mandibular prognathism, absent, maxillary-only, or vestigial dentition (including all ziphiids, narwhals (*Monodon monoceros)* and sperm whales (*Physeter macrocephalus*)) were consistently placed on the proximal lateral maxilla

where the posterior end of a standard tooth row would be located (Appendix 2: Fig. S2.2).



a.                                              b.
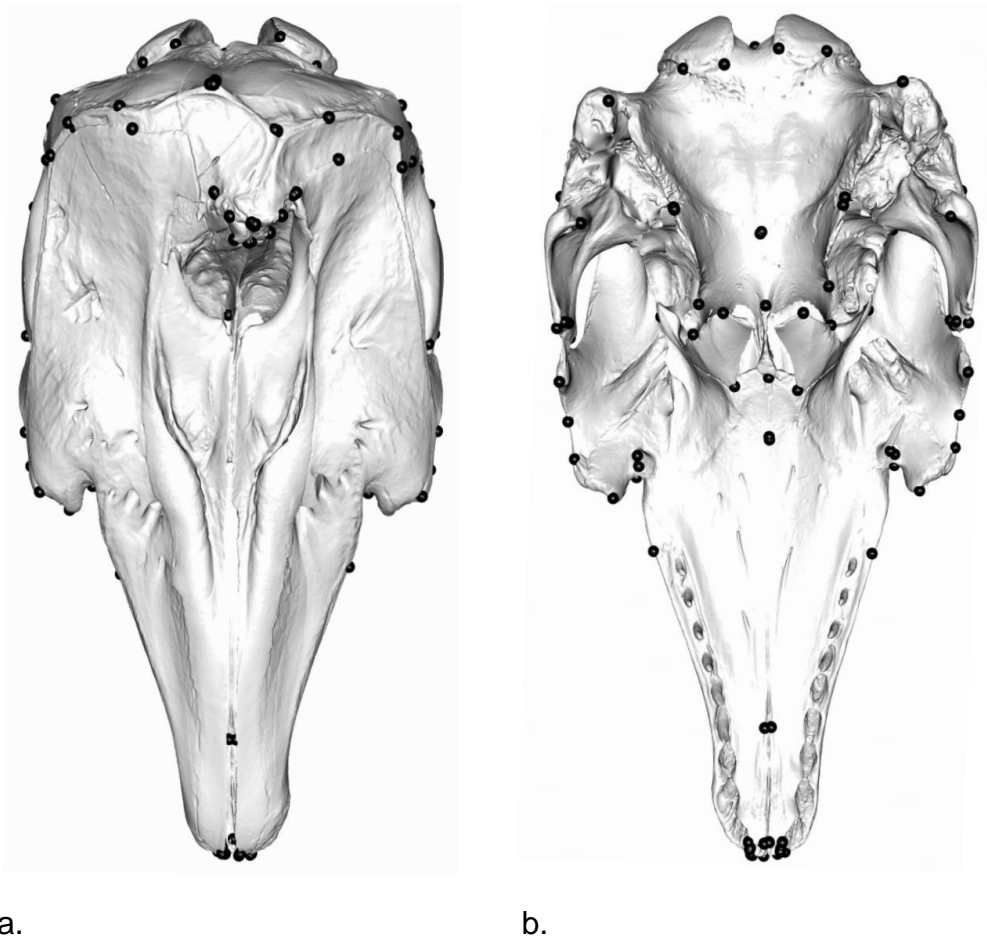
**Fig. 2.2.** 123 landmarks placed on the dorsal and ventral of the skull. a. dorsal, b. ventral. 9 landmarks were placed on the midline (for landmark details see Appendix 2: Table S2.2: 123 landmarks added to the entire surface of the skull). Specimen is *Delphinapterus leucas* USNM 305071.

As previously noted, some specimens have missing data. Geometric morphometric analyses and plotting functions implemented in geomorph v.3.1.0 require a full complement of landmarks (Adams et al., 2019). This complement can consist of actual landmarks and estimated positions for 'missing' landmarks. To estimate positions for missing landmarks, we placed

'missing' landmarks as close to the missing bone (areas that could not be digitally mirrored) as possible and then marked it as a 'missing landmark' in Checkpoint which automatically assigns a coordinate of –9999. We then used the `estimate.missing` function in `geomorph` and the 'TPS' (thin plate spline) method to estimate the location of landmarks on incomplete specimens. A reference specimen which has a complete complement of landmarks and sits close in the morphospace (to the incomplete specimen) is selected and the incomplete specimen is aligned against it using common landmarks (Gunz et al., 2009). In a TPS-based estimation missing landmarks are placed so that the overall bending energy between the reference and the incomplete specimen is smallest which creates a smooth deformation (Gunz et al., 2009). TPS was chosen over regression-based methods (i.e., 'Reg' in `geomorph`) because it performs better in simulations with missing data (Gunz et al., 2009).

### *2.3.3 Phylogeny*

Our study uses a phylogenetic framework to reconstruct macroevolutionary patterns of cranial asymmetry across Cetacea. To generate a tree that included all our sampled taxa, we used the time-calibrated phylogeny from Lloyd and Slater (2020). This 'genus tree' includes all species belonging to a genus that appear in a character matrix using taxonomic constraints to place taxa that lack data. We modified it as follows: First, we added several additional extant species (which were already represented to the genus level in the Lloyd and Slater (2020) phylogeny), with position based on recently published studies. We placed *Neophocaena asiaeorientalis* in the same genus as *Neophocaena phocaenoides* (Jefferson and Wang, 2011), *Sousa plumbea* + *Sousa teuszii* + *Sousa sahulensis* in the same genus as *Sousa chinensis* (Jefferson and Rosenbaum, 2014), *Orcaella heinsohni* in the same genus as *Orcaella brevirostris* (Beasley et al., 2005; Vilstrup, 2011); *Mesoplodon hotaula* in the genus *Mesoplodon* next to *Mesoplodon gingkodens* (Dalebout et al., 2014). Finally, we placed *Berardius minimus* in the genus *Berardius* next to *Berardius bairdii* and *Berardius arnuxii* following its recent description by Yamada et al. (2019). The following fossil species were directly swapped with their corresponding monophyletic congener as follows. We placed

*Balaneoptera sp.* (SDNHM 83695) as a sister taxon to *Balaenoptera siberi* (although not present in our sample), close to extant *Megaptera novaeangliae* as in Martin (2013), *Balaenoptera floridana* as a sister taxon to *Balaenoptera davidsonnii* (Demeré et al., 1986; Ekdale, 2016) (again, the latter species is not present in our sample), and *Orycterocetus crocodilinus* is placed in the physeterids according to Lambert et al. (2010). We placed *Globicephala sp.* as a sister taxon to *Globicephala etruriae* (Bianucci, 1996; Bianucci, 1998; Olson, 2008), and *Hemisyntrachelus cortesii* in the same genus as *Hemisyntrachelus oligodon* according to Post and Bosselaers (2005). We caution that Kentriodontidae is often considered a non-monophyletic 'waste-basket' for Late Oligocene and Miocene homodont odontocetes (Lambert et al., 2017b). Restrictions according to Peredo et al. (2018) leave *Tagicetus* and *Atocetus* (previously referred to as Kentriodontidae) outside of the family (Appendix 2: Table S2.1). The positioning of *Argyrocetus joaquinensis* is also unclear (Lambert et al., 2015). Two specimens (*Xenorophus* ChM PV7677 and Patriocetid or Waipatiid CCNHM 1078) were excluded from the analysis due to uncertainty in their position (Appendix 2: Table S2.3). For computational purposes, all polytomies in the tree were resolved by adding zero branch lengths using multi2di in ape v.5.0 (Paradis and Schliep, 2018) prior to downstream phylogenetic analyses.

### *2.3.4 Data analysis*

### *2.3.4.1 Quantifying asymmetry*

We generated mirrored landmarks for the right-hand side (RHS) of the skull and compared their positions to those of the original manually placed left-hand side (LHS) landmarks, measuring the amount of landmark displacement between the two. To do so, we used the 57 LHS landmarks and 9 midline landmarks (total = 66) (Appendix 2: Table S2.2) and mirrored the LHS landmarks onto the RHS using the `mirrorfill` function in the R package 'paleomorph' v.0.1.4 Lucas and Goswami (2017). Before carrying out further analyses, we superimposed the specimens to remove all non-shape elements

i.e., size (scaling), translation and rotation (positioning) from the data using Generalised Procrustes Analysis implemented in the `gpagen` function from the geomorph R package v.3.1.0 (Adams et al., 2019).

We used the R package 'landvR' v.0.4 (Guillerme and Weisbecker, 2019) to calculate the Euclidean distances between a reference specimen (the computer mirrored specimen) (*Rn*) and a focal specimen (the manually landmarked specimen) (*Fn*). Both *Rn* and *Fn* are defined by three coordinates (x, y, z). The landmark displacements were measured for each landmark individually using the spherical coordinates system which measures between the $n^{th}$ landmark of the *Fn* and the *Rn* specimens respectively (Guillerme and Weisbecker, 2019). This method provides 3 outputs from Guillerme and Weisbecker (2019):

- *ρ*, the Euclidean distance between *Fn* and *Rn*.
- *ϕ*, the azimuth angle formed by the projection of *Rn* on the equatorial plane *(f(x)=0)*.
- *θ* (when using 3D data only), the polar angle formed by the projection *Rn* on the polar plane *(f(y)=0)*.

We estimated differences between *Fn* and *Rn* in the spherical coordinates system using the `coordinates.difference` function in landvR and extracted the *ρ* (radius) for each landmark, for each specimen. This provides a measure of the Euclidean distance between a manually placed landmark which accurately represented the specimen's morphology (*Fn)*, and a computer mirrored landmark (*Rn)*. If the specimen is asymmetric, the computer mirrored landmark does not accurately reflect its morphology (Fig. 2.1).

The spherical coordinates system is preferable because it directly measures landmark displacement in any direction, and further, the values for each landmark displacement is discrete in space (i.e., independent from other landmarks) (Guillerme and Weisbecker, 2019). This is important because it allows identification of asymmetry which may occur in discrete parts of the skull e.g., the posterior nasal without blanket labelling all landmarks as 'asymmetric'. We obtained *ρ* for each of the 123 landmarks for each specimen,

including the terrestrial artiodactyls (21,156 radii values in total). The larger the radii (and consequently the larger the $\phi$ for a corresponding landmark) the more displacement between *Fn* and *Rn.* We interpret a higher $\rho$ as an indication of more asymmetry in the skull (see Fig. 2.3 for a visualisation of this). Higher displacement means that there is a greater difference between the placement of *Fn* and *Rn,* indicating asymmetry in those landmarks (Guillerme and Weisbecker, 2019). The closer the radius to 0, the more symmetrical the specimen as *Fn* hasn't displaced far from *Rn*. We took the averaged sum of radii for each landmark ($\bar{x}\rho_{land}$) to find the most asymmetrical landmarks and identify their location on the skull for each group (archaeocetes, odontocetes, mysticetes, and terrestrial artiodactyls) as well as an average total cranial asymmetry ($\bar{x}\rho$) for each group. We also took the sum radii for each of the individual specimens ($\Sigma\rho_{spec}$). We ran a principal components analysis (PCA) on the Procrustes aligned data using the 'factoextra' package v.1.0.7 (Kassambara and Mundt, 2017) in R to identify PC scores of maximum radii variation using the sum radii for each of the individual specimens ($\Sigma\rho_{spec}$). We then used overall asymmetry in each specimen ($\Sigma\rho_{spec}$) to reconstruct the evolution of cranial asymmetry.
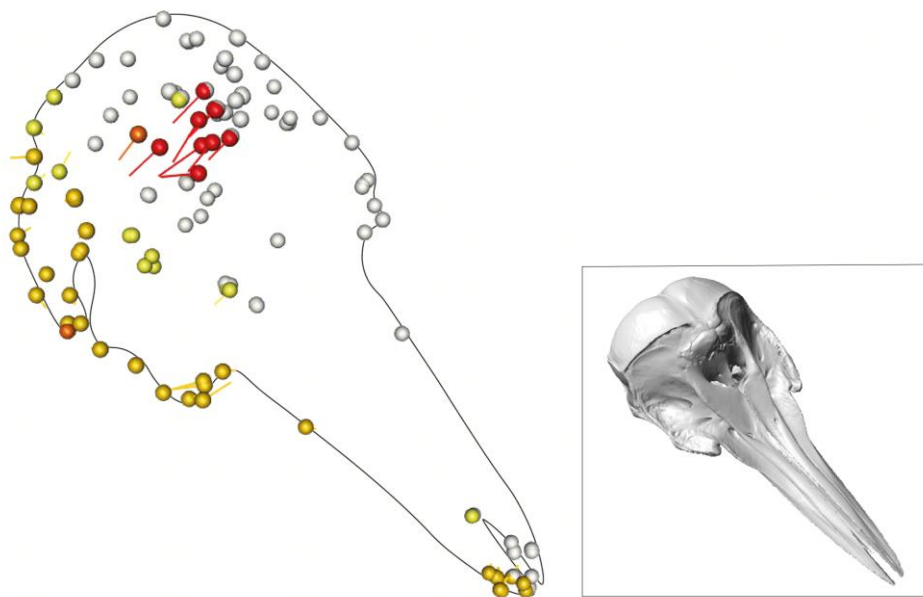
**Fig. 2.3.** Visualisation of p (radii) from landvR showing asymmetry in the dolphin skull. Landmarks are placed on a stylised outline of a dolphin skull. The 3D surface scan of a dolphin skull (inset) is shown for orientation and is *Lissodelphis borealis* USNM 550188. The white spheres on the `landvR` output show the fixed landmarks (1-66) on the left-hand side (LHS) of the skull (looking down on the skull with the rostrum pointing north). The landmarks on the right-hand side (RHS) of the skull vary in colour depending on how much difference there is between a computer mirrored landmark (which assumes the skull is bilaterally symmetrical) and a manually placed landmark (which accurately depicts asymmetry). The larger the difference between the computer mirrored landmark and the manually placed landmark, the hotter the colour. The highest amount of asymmetry is shown in red and dark orange, less asymmetry is shown in pale orange and yellow. Note the red landmarks on the nasal and posterior premaxilla of this odontocete. The tails coming from each of the landmarks show how much and in which direction the landmarks have moved from where the computer mirrored them, to where the landmarks sit when manually placed.

All models were run with cetacean data only (i.e., no terrestrial artiodactyls) and model fit was assessed using AIC. We also conducted the analyses after removing the rostrum (NR) as it may be more easily deformed through both taphonomic deformation and drying out in extant specimens. We also ran all models with a phylogeny that includes only taxa that appear in a character matrix from Lloyd and Slater (2020). We found no differences in the ordering of the best-fitting models with NR, nor with the phylogeny which only uses taxa that appear in the character matrix (see Appendix 2: Tables S2.4a-c; Figs S2.3-8); we thus focus the analyses on data including the rostral landmarks and the original 'genus tree'.

### 2.3.5 Modelling the evolution of cranial asymmetry

We assessed how asymmetry (the sum of radii for each species; $\Sigma\rho_{spec}$) has evolved across Cetacea using phylogenetic models of trait evolution. We investigated variation in rates of cranial asymmetry evolution using a relaxed Brownian Motion (BM) process with the `rjmcmc.bm` function implemented in the R package 'geiger' v.2.0.6.4 (Harmon et al., 2008; Eastman et al., 2011). This model uses a Bayesian framework with a reversible jump Markov Chain Monte Carlo (rjMCMC) algorithm to find the position and the amplitude of evolutionary rates changes and 'shifts' across the tree (Eastman et al., 2011). 'Jumps' indicate a temporary or rapid change in the trait.

We ran the rjMCMC chain for $10^6$ generations sampling each 10000 generations with the combined 'jump-rbm' class model (Eastman et al., 2011). We used the weakly informative Half-Cauchy distribution with scale parameter 25 (Gelman, 2006) as the prior density of the rate scalar and measurement error instead of the default exponential distribution and used default priors for the number of shifts (a Poisson distribution with mean equal to log(2) which places a 50% probability on a scenario with no shifts). For comparison and as a proposal mechanism for exploring the parameter space, we ran the same model with the 'rbm' class model and no jumps. We checked the effective sample size (ESS) and assessed convergence of the chains with Gelman and Rubin's diagnostics (Gelman and Rubin, 1992; Gelman, 2006) using the 'effectiveSize' and 'gelman.diag' functions implemented in the R package 'coda' (Plummer et al., 2006) (Appendix 2: Figs S2.9-13; Table S2.5).

### 2.3.6 Hypothesised evolutionary regimes for cranial asymmetry

Several state-dependent models were proposed as potential predictors for the level of asymmetry seen in the cetacean skull. For example, 'echolocation' (model: 'echo') (Table 2.1) is one model used to investigate whether the rate of evolution for skull asymmetry differs between species that can echolocate and those that cannot. We name two other models, the 'regime' model (model: 'regime') and the 'regime split' model (model: 'regime-split'). In these models

we test whether evolutionary changes in asymmetry in the cetacean cranium (the studied trait) can be associated with the states of another discrete trait. By 'regime' we mean a particular condition or process that may be underlying the observed patterns of cranial asymmetry. We further fitted a 'frequency echolocation' model (model: 'echo-freq') (Table 2.1; Appendix 2: Table S2.6). This study is not a specialist analysis of acoustics (nor behaviours affecting acoustics) in cetaceans, and we use these values to *indicate* potential drivers for the evolution of cranial asymmetry. We assigned species to several categories depending on how they predominantly produce sound (Table 2.1; Appendix 2: Table S2.6). We fitted our several state-dependent models with different variants of the BM and OU model (Table 2.2). The multiple models and different rates are summarized below.

[Table on next page]

**Table 2.1.** Models of asymmetry associated with other discrete traits. Models tested to assess whether evolutionary changes in asymmetry in the cetacean cranium are associated with the states of another discrete trait. The 'scenario' names the type of model fitted, for example the echolocation model is based on whether a cetacean can echolocate or not. The description and assumptions outline the conventions of the model.

| Scenario (model name) | Description | Model assumptions and references |
|---|---|---|
| Ancestral state reconstruction ('ancestral') | Species belong to one of three ancestral categories: 'archaeocete', 'odontocete', 'mysticete'. | The placing of species into 'archaeocete', 'odontocete', 'mysticete' was based on the literature and published fossil descriptions (Berta et al., 2014; Marx et al., 2016a). |
| 'Regime' model ('regime') | Assumes selective evolutionary regimes. Archaeocetes are assigned to 'regime1', mysticetes to 'regime2', and most odontocetes to 'regime3'.<br><br>The highly asymmetric monodontids, platanistids, and superfamily physeteroids are classified as a separate 'regime4'. | Regimes are based on a preliminary trait plot (see Results) which shows that the monodontids, platanistids, and superfamily physeteroids have a much higher trait value (sum radii for the individual specimen; $\Sigma\rho_{spec}$) ($\geq 0.42$, see Results) than other odontocetes and therefore may be evolving asymmetry under one different selective regime. |
| 'Regime-split' model ('regime-split') | As in the 'regime' model, archaeocetes are assigned to 'regime1', mysticetes to 'regime2', odontocetes in general to 'regime3', and the highly asymmetric odontocetes (monodontids, platanistids, and physeteroids) are | Each highly asymmetric group is evolving under its own separate selective regime; 1. monodontids, 2. platanistids, and 3. physeteroids. |

| | | |
|---|---|---|
| | in their own separate selective regimes. | |
| Echolocation model ('echo') | Species assigned to one of four groups depending on whether the species could echolocate.<br><br>Band0: cannot echolocate.<br><br>Band1: Not capable of echolocation, although reception of ultrasonic signals cannot be ruled out.<br><br>Band2: Early echolocation e.g., *Cotylocara macei* (Geisler et al., 2014) and *Echovenator* (Kyhn et al., 2009; Churchill et al., 2016)<br><br>Band3: Fully echolocating. | i. Although rudimentary, echolocation evolved very early in whale evolution, likely soon after odontocetes diverged from the ancestors of baleen whales (Berta et al., 2014).<br><br>ii. The ability to produce ultrasonic sounds, and therefore echolocate, has been inferred for almost all fossil odontocetes (Fordyce and de Muizon, 2001) although *Odobenocetops* likely had greatly reduced echolocation abilities (Lloyd and Slater, 2020).<br><br>iii. Mysticetes do not echolocate.<br><br>iv. All extant odontocetes echolocate (Racicot et al., 2019). |
| Echolocation-frequency model ('echo-freq') | Categorising by echolocation in the extant odontocetes and sound production in the extant mysticetes. | i. Data on frequency specifics is not available for fossils.<br><br>ii. Narrowband high-frequency (NBHF) cetaceans designated according to. Kastelein et al. (2002) and Khyn et al. (2009; 2013).<br><br>iii. The non-NBHF delphinids were assigned to broadband low frequency (BBLF) according to Turl et al. (1989) and Jensen et al. (2013). |

| | | iv. The sperm whale sits in its own category. The hypertrophied nasal structures and deep-diving behaviour produce a low-frequency multi-pulsed sound (Madsen et al., 2002). |
| | | |
| | | v. Ziphiids sit in their own category. They produce frequency-modulated buzz clicks (FM-buzz) (Johnson et al., 2008; Johnston et al., 2008; Baumann-Pickering, 2013a; Baumann-Pickering et al., 2013b). |
| | | |
| | | vi. Mysticetes do not echolocate and produce low-frequency sound (Clark, 1990; Reindenberg and Laitman, 2007) |
| | | |
| | | vii. The Monodontidae sit on their own category. They produce narrowband structured (NBS) pulses (Sjare and Smith, 1986; Turl, 1990; Racicot et al., 2018) |
| | | |
| | | See Appendix 2: Table S2.6 for further details. |

In addition, we evaluated the fit of 24 alternative models based on the states of a discrete character (Table 2.1) implemented in the 'mvMORPH' package in R (Clavel et al., 2015) using a maximum likelihood inference (Table 2.2). We used the 'fitDiscrete' function in the R package 'geiger' v.1.3-1 to fit various likelihood models for discrete character evolution. The model arguments tested were an 'equal-rates' model (ER) where all transitions occur at equal rates, a 'symmetric transitions are equal' model (SYM), and 'all rates different' model (ARD) where each rate is a separate parameter (Yang, 2006; Harmon et al., 2008). The ER model gave the best fit (Appendix 2: Table S2.7) (Yang, 2006; Harmon et al., 2008) and was thus used in all our alternative models using maximum-likelihood inference (Table 2.2).

The multiple models described above (Table 2.1) relax the assumption of a common dynamic for modelling the trait evolution by allowing the estimation of the model parameters that depend on the states of a discrete character. For these, we first had to 'paint' the evolutionary history (e.g., ancestral state) of the selective regime onto the tree. To do this we used write.simmap in the 'phytools' package v.0.6-99 (Revell, 2012). We ran these models under OUM (Ornstein-Uhlenbeck; OU) and BMM assumptions (Table 2.2). This includes iterations of these models for the data with the rostrum removed and with the phylogeny that includes only taxa that appear in a character matrix (Lloyd and Slater, 2020) (Appendix 2: Table S2.4b-c). All analyses were done in R v.3.5.0 (R Core Team, 2017).

[Table on next page]

**Table 2.2.** Evolutionary modes for changes in asymmetry. Models implemented using a maximum-likelihood inference to test evolutionary models for changes in asymmetry. Models test whether evolutionary changes in asymmetry (the studied trait) are associated with the states of another discrete trait. The model name is a combination of the model state and the model type and is used throughout the study for consistency. The state describes the model scenario. The model types are variations of an Ornstein-Uhlenbeck (OU) model of continuous trait evolution and a Brownian Motion (BM) model of continuous trait evolution (see description). All models were run using an 'equal-rates' (ER) likelihood model (Appendix 2: Table S2.7 - Likelihood model results (AIC) for each potential scenario for asymmetry in the cetacean cranium). For details on the model assumptions see **Table 2.1** - Models testing whether changes in cetacean cranial asymmetry are associated with other discrete traits.

| Model name | State | Model type | Description |
|---|---|---|---|
| **'OU-ancestral'** | ancestral state | OU | A classic Ornstein-Ulenbeck (OU) model |
| **'BM-ancestral'** | ancestral state | BM | A classic Brownian Motion (BM) model |
| **'BMtr-ancestral'** | ancestral state | BMtr | A classic BM model with an independent trend |
| **'BMsm-ancestral'** | ancestral state | BMsm | A classic BM model with no selective regime and which estimates separate phylogenetic means |
| **'BMM-ancestral', 'BMM-regime', 'BMM-regime-split', 'BMM-echo', BMM-echo-freq'** | ancestral state, regime, regime-split, echolocation, echolocation-frequency | BMM | A BM model with a selective regime |
| **'BMMtr-ancestral', 'BMMtr-regime', 'BMMtr-regime-split', 'BMMtr-echo', BMMtr-echo-freq'** | ancestral state, regime, regime-split, echolocation, echolocation-frequency | BMMtr | A BM model with a selective regime and an independent trend |
| **'BMMsm-ancestral', 'BMMsm-regime', 'BMMsm-regime-split', 'BMMsm-echo', BMMsm-echo-freq'** | ancestral state, regime, regime-split, echolocation, echolocation-frequency | BMMsm | A BM model with a selective regime which estimates separate phylogenetic means |

| | | | |
|---|---|---|---|
| **'OUM-ancestral', 'OUM-regime', 'OUM-regime-split', 'OUM-echo', OUM-echo-freq'** | ancestral state, regime, regime-split, echolocation, echolocation-frequency | OUM | An OU model with a selective regime |

Although the relaxed BM process described above is very flexible and allows the investigation of changes in evolutionary rates across the tree without strong *a priori*, it is however limited for assessing and interpreting changes in evolutionary modes. Moreover, recovered changes in rates might result from long term trends in the average asymmetry rather than actual changes in the pace of evolution. We considered multiple models including parameterizations of the BM and OU process (Table 2.2). Our models assume constant dynamics of trait evolution but a directional drift of the clade average value that might be interpreted as shifts in evolutionary rates in the relaxed BM model considered above. We also considered models with specific optimums (model "OUM" in '*mvOU*'), and ancestral states and/or rates (model "BMM" in '*mvBM*') in different parts of the tree. The more parameterized and refined models allow for testing of evolutionary changes in the studied trait and can be associated with the states of another discrete trait. In this study we consider different scenarios to assess whether the evolution of the skull asymmetry shows marked differences between the three major clades (archaeocetes, odontocetes, and mysticetes) and if it is related to the evolution of echolocation.

### 2.3.7 Analysis of variance

Lastly, we ran phylogenetically corrected ANOVAs (an ANOVA that takes into account relatedness (i.e., phylogenetic position) between species, so that this effect can be removed and/or analysed) on each of the different scenarios using the R package 'nlme' (v.3.1-137) (Pinheiro et al., 2020) and function 'gls' to test for correlations between the level of asymmetry seen in the skull and the potential scenarios (or regimes) hypothesised above (Table 2.1). 'gls' allows for a more flexible model with better power. Simulations were run using a 'Pagel's Lambda' ($\lambda$) correlation structure (corPagel) in the 'ape' package (Paradis and Schliep, 2018) which is derived from a Brownian Motion model by multiplying the covariances by $\lambda$. As we ran multiple models, we controlled for a false discovery rate using the Benjamini-Hochberg method (Benjamini and Hochburg, 1995; Benjamini and Yekutieli, 2001) (Appendix 2: Table S2.8).

The data sets generated and/or analysed during the current study are available in the Github repository:

https://github.com/EllenJCoombs/Asymmetry-evolution-cetaceans: (Coombs et al., 2020b).

## 2.4 Availability of data and materials

The data sets generated and/or analysed during the current study are available in the Github repository:

https://github.com/EllenJCoombs/Asymmetry-evolution-cetaceans.

All code and raw data are available to download, complete with MIT license. Please cite this paper when accessing the data or raw code.

## 2.5 List of abbreviations

AIC - Akaike information criterion

ANOVA - Analysis of variance

ARD – 'all rates different' model

BM - Brownian Motion

ER - 'equal-rates' model

FM-buzz - Frequency-modulated buzz clicks

*Fn* - manually placed landmark which accurately represented the specimen's morphology

Mya – Million years ago

NBHF - Narrowband high-frequency

NBS - narrowband structured

NR – no rostrum

OU – Ornstein-Uhlenbeck

$p$ – radius

rjMCMC - reversible jump Markov Chain Monte Carlo

*Rn* - computer mirrored landmark

SYM - 'symmetric transitions are equal' model

$\bar{x}\rho$ - average total cranial asymmetry for each group

$\bar{x}\rho_{land}$ - averaged sum of radii for landmark

$\Sigma\rho_{spec}$ - sum radii for each of the individual specimens

## 2.6 Results

### 2.6.1 Cranial asymmetry across cetaceans

Comparing the sum radii ($\Sigma\rho_{spec}$) for each specimen in our data set, we found that odontocetes, especially the monodontids, physeterids, and kogiids, are the most asymmetrical of the cetaceans (Table 2.3).
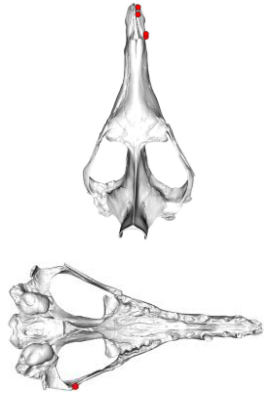
**Table 2.3.** Asymmetry in the cetacean skull. List of cetacean specimens with the highest sum radii across the cranium ($\Sigma\rho_{spec}$). $\rho$ is the radius value calculated as the Euclidean distance between the computer mirrored landmark and the manually placed landmark. The larger the value for $\rho$, the longer the radii for a corresponding landmark and the more it is displaced, indicating asymmetry between the two sides of the cranium.
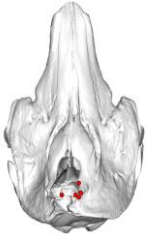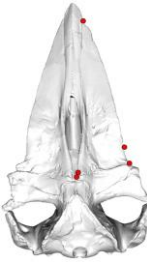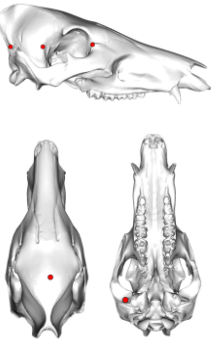
|  | species | family | suborder | sum radii ($\Sigma\rho_{spec}$) |
|---|---|---|---|---|
| 1 | *Monodon monoceros* USNM 267959 | Monodontidae | odontocete | 0.546 |
| 2 | *Orycterocetus crocodilinus* USNM 22926 | Physeteridae | odontocete | 0.518 |
| 3 | *Aulophyseter morricei* UCMP 81661 | Physeteridae | odontocete | 0.489 |
| 4 | *Kogia breviceps* USNM 22015 | Kogiidae | odontocete | 0.462 |
| 5 | *Kogia simus* NHMUK 1952.8.28.1 | Kogiidae | odontocete | 0.457 |
| 6 | *Physeter macrocephalus* NHM UK 2007.1 | Physeteridae | odontocete | 0.456 |
| 7 | *Delphinapterus leucas* USNM 305071 | Monodontidae | odontocete | 0.453 |
| 8 | *Platanista gangetica* USNM 172409 | Platanistidae | odontocete | 0.449 |
| 9 | *Globicephala melas* NMNZ MM001946 | Delphinidae | odontocete | 0.410 |
| 10 | *Pseudorca crassidens* USNM 11320 | Delphinidae | odontocete | 0.408 |

Of 172 specimens, the top 43 with the highest $\Sigma\rho_{spec}$ are odontocetes. The highest ranking mysticetes are a balaenopterid (MNNZ MM001630) ($\Sigma\rho_{spec}$ = 0.300), *Aglaocetus moreni* ($\Sigma\rho_{spec}$ = 0.298), and *Janjucetus hunderi* ($\Sigma\rho_{spec}$ = 0.295), ranked 47th, 50th, and 51st, respectively (Appendix 2: Table S2.1). The highest ranking archaeocetes are *Basilosaurus isis* ($\Sigma\rho_{spec}$ = 0.308) and *Zygorhiza kochii* ($\Sigma\rho_{spec}$ = 0.306) ranked 44th and 45th, respectively. The highest-ranking terrestrial artiodactyls do not appear until the 129th (*Capricornis sumatrensis*, $\Sigma\rho_{spec}$ = 0.205) and 139th (*Bos sp.*, $\Sigma\rho_{spec}$ = 0.195) positions. The mysticetes and terrestrial artiodactyls dominate the lower end of the ranking with eight of the last ten positions occupied by extant balaenids and balaenopterids and one fossil pelocetid (Appendix 2: Table S2.9). For the whole cetacean data set the most asymmetric landmarks are the nasals, the maxilla at the sutures with the nasals and premaxilla, and the posterior, dorsal premaxilla (Table 2.4). This distribution is heavily influenced by the odontocete sample (n = 120, 74% of cetacean specimens). For this reason, each cetacean suborder and the terrestrial artiodactyls were analysed separately. The mean total cranial radii for odontocetes is the highest of all groups at $\bar{x}\rho$ = 0.290 (Table 2.4). The most asymmetric landmarks for odontocetes are the dorsal and posterior-dorsal maxilla (suture with nasal and premaxilla), and nasals (Table 2.4). Terrestrial artiodactyls have the lowest overall asymmetry across the skull ($\bar{x}\rho$ = 0.171), followed closely by Mysticetes ($\bar{x}\rho$ = 0.191). Archaeocetes showed a moderately high level of asymmetry in the skull ($\bar{x}\rho$ = 0.251). Cetacean subgroups differ greatly in identity of the most asymmetric landmarks and magnitude of landmark asymmetry (Table 2.4). For example, the most asymmetric landmark in odontocetes is the dorsal medial maxilla (suture with nasal and premaxilla) with $\bar{x}\rho_{land}$ = 0.013, whereas the most asymmetric landmark in mysticetes is the posterior ventral lateral most point of the maxilla, with $\bar{x}\rho_{land}$ = 0.005 (Table 2.4). This difference is evident when comparing average landmark asymmetry across the groups (Fig. 2.4).

[Table on next page]

**Table 2.4.** Highest landmarks of asymmetry. List of the five landmarks with the greatest variation across the cranium for all cetaceans, archaeocetes, odontocetes, mysticetes, and terrestrial artiodactyls. $\rho$ is the radius value, calculated as the Euclidean distance between the computer-mirrored landmark and the manually placed landmark. The larger the value for $\rho$, the more it is displaced, indicating asymmetry between the two sides of the cranium. $\bar{x}\rho$ is the average of the total radii ($\sum\rho$) values across the skull for all the specimens in that group. $\bar{x}\rho_{land}$ is the average radii across all specimens in that group for that landmark. Each image shows the position of the five landmarks of greatest variation for each respective group. Skulls not to scale.

| Suborder | Average asymmetry in the skull ($\bar{x}\rho$) | 1st highest landmark of variation | | 2nd highest landmark of variation | | 3rd highest landmark of variation | | 4th highest landmark of variation | | 5th highest landmark of variation | | Specimen showing top 5 landmarks (red) |
|---|---|---|---|---|---|---|---|---|---|---|---|---|
| | | Landmark description | $\bar{x}\rho_{land}$ | Landmark description | $\bar{x}\rho_{land}$ | Landmark description | $\bar{x}\rho_{land}$ | Landmark description | $\bar{x}\rho_{land}$ | Landmark description | $\bar{x}\rho_{land}$ | |
| All cetaceans | 0.268 | **L74**: Dorsal medial maxilla (suture with nasal and premaxilla) | 0.010 | **L68**: Posterior lateral corner of nasal | 0.009 | **L71**: Posterior dorsal premaxilla | 0.009 | **L121**: Posterior point of nasal | 0.008 | **L67**: Left anterior lateral nasal | 0.007 | |
| Archaeocetes | 0.251 | **L72**: Anterior lateral ventral premaxilla | 0.007 | **L69**: Tip of rostrum, anterior dorsal side, anterior midline of tooth row | 0.007 | **L70**: Anterior dorsal premaxilla | 0.007 | **L82**: Jugal posterior ventral | 0.006 | **L73**: Anterior lateral ventral maxilla | 0.006 |  |

| Group | | L-A | | L-B | | L-C | | L-D | | L-E | | Image |
|---|---|---|---|---|---|---|---|---|---|---|---|---|
| **Odontocetes** | 0.290 | **L74:** Dorsal medial maxilla (suture with nasal and premaxilla) | 0.013 | **L68:** Posterior lateral corner of nasal | 0.011 | **L71:** Posterior dorsal premaxilla | 0.010 | **L121:** Posterior point of nasal | 0.009 | **L67:** Left anterior lateral nasal | 0.009 | |
| **Mysticetes** | 0.191 | **L78:** Posterior ventral lateral most point of maxilla (near orbit) | 0.005 | **L79:** Posterior tooth row lateral maxilla | 0.005 | **L72:** Anterior lateral ventral premaxilla | 0.005 | **L71:** Posterior dorsal premaxilla | 0.005 | **L122:** Anterior medial frontal | 0.005 | |
| **Terrestrial artiodactyls** | 0.171 | **L83:** Lateral posterior frontal (posterior lateral parietal suture) | 0.006 | **L87:** Anterior medial parietal | 0.005 | **L97:** Posterior lateral most point of the mandibular articular process | 0.005 | **L80:** Jugal anterior dorsal | 0.005 | **L98:** Lateral posterior squamosal (occipital suture) | 0.004 | |

104

The basilosaurid and protocetid archaeocetes show a high level of asymmetry, akin to the levels seen in fossil and extant odontocetes (Appendix 2: Table S2.9). The contribution of rostral landmarks to overall cranial asymmetry in these archaeocete families ranges from 13.8% in *Aegyptocetus tarfa* to 31.3% in *Artiocetus clavis.* The average amount of asymmetry concentrated in the rostrum is higher in archaeocetes (19.3%) (this includes the families Kekenodontidae, Pakicetidae, and Remingtonocetidae, which are not commonly associated with asymmetry) than in mysticetes (14.2%) and odontocetes (14.7%) (Appendix 2: Table S2.10-12.).



a.       b.       c.       d.
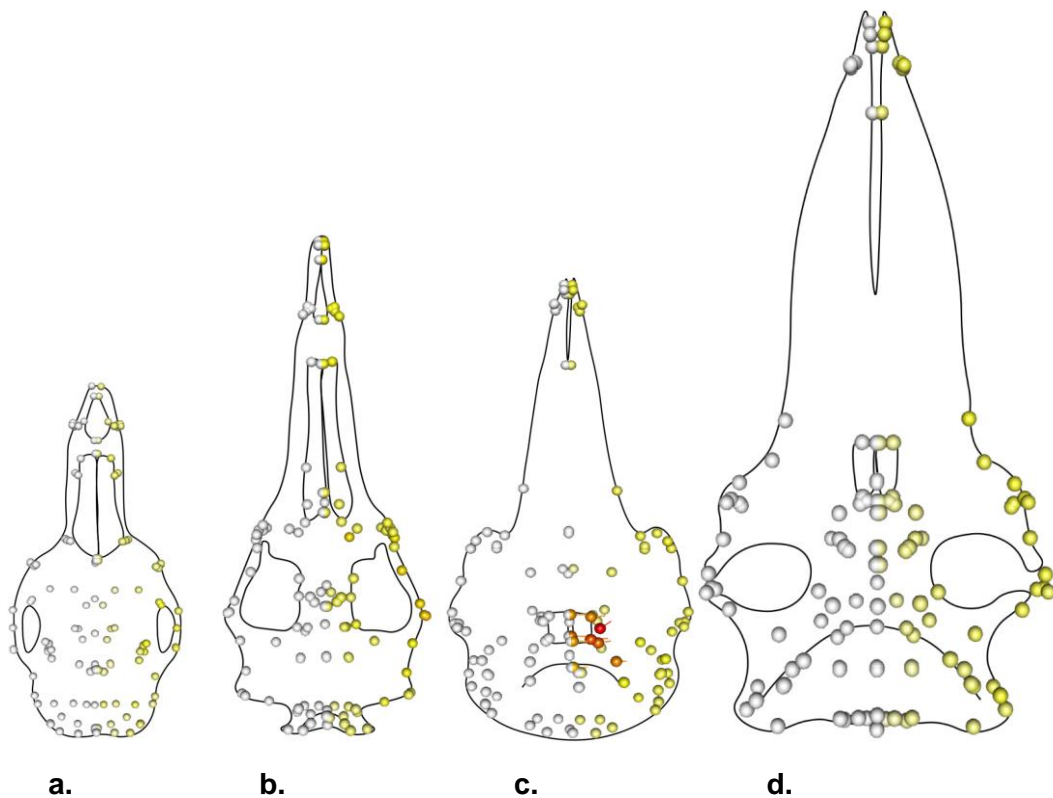
[Figure on previous page]

**Fig. 2.4.** Average radii per landmark ($\bar{x}\rho_{land}$) for each taxon group. Landmarks superimposed onto a stylised skull which represents an 'average specimen' for that group. From left to right: a) the average landmark radii ($\bar{x}\rho_{land}$) for terrestrial artiodactyls, b) the average landmark radii for archaeocetes, c) the average landmark radii for odontocetes, and d) the average landmark radii for mysticetes. Landmarks on skulls a) and d) consist of pale yellows indicating low asymmetry. The landmarks on skull b) are pale yellow, with darker yellows on the jugal, orbit, and rostrum indicating a higher level of asymmetry. Oranges and red landmarks in the nasal, posterior premaxilla, and posterior maxilla on skull c) (the odontocete) indicate a high level of asymmetry. Skulls not to scale.

As deformation during fossil preservation may create nonbiological asymmetry and previous studies suggest this may be concentrated in the rostrum of some fossil cetaceans, (Martínez-Cáceres and de Muizon., 2011; Fahlke and Hampe, 2015; Martínez-Cáceres et al., 2017), we also ran analyses without any fossils and without rostral landmarks. When fossils were removed there was a decrease in asymmetry in mysticetes ($\bar{x}\rho = 0.142$) (extant mysticetes: n = 12, 7% of the data set). In contrast, fossil odontocetes are more symmetrical than most extant odontocetes (Appendix 2: Table S2.9). For this reason, when fossil odontocetes were removed, the level of average asymmetry in the extant odontocete skull increased marginally ($\bar{x}\rho = 0.292$) (extant odontocetes: n = 72, 44% of the data set). Excluding rostral landmarks had the most impact on archaeocetes and mysticetes, as some of the highest levels of asymmetry in those clades are found in the rostral region (Table 2; Appendix 2: Tables S2.10-12). However, overall, removal of the rostral landmarks had only a minor effect on results (Appendix 2: Fig. S2.3-5, Table S2.4b). Principal components analysis of landmark asymmetries showed that odontocetes exhibit a wide range of patterns of cranial asymmetry (Fig. 2.5), and cranial shape (Appendix 2: Fig. S2.14). Mysticetes and terrestrial artiodactyls overlap in asymmetry morphospace, while archaeocetes have a higher level of asymmetry, similar to more moderately asymmetric odontocetes (Fig. 2.5). See Appendix 2: Fig. S2.15 for identification of each specimen in the morphospace.
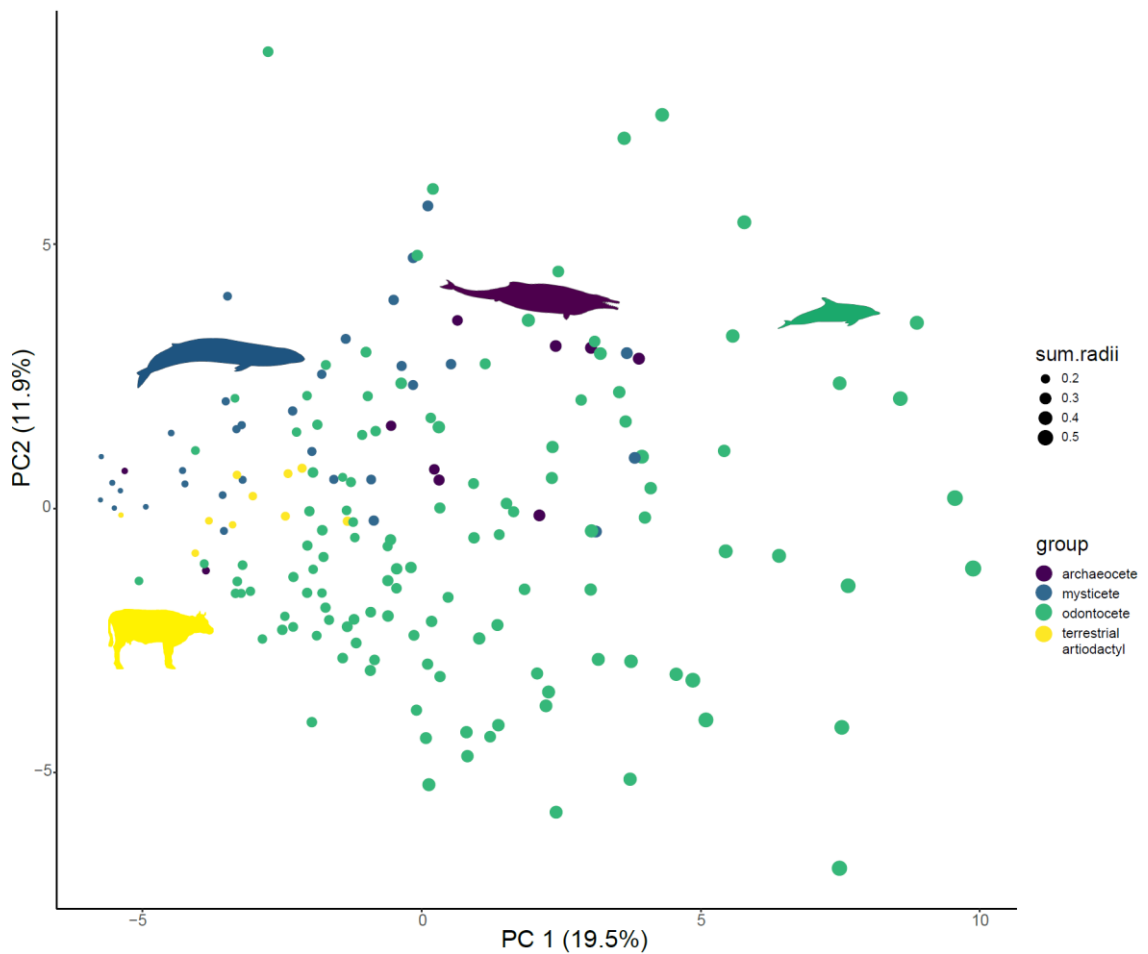
**Fig. 2.5.** Total cranial asymmetry in different taxa – a morphospace. Principal Components 1 and 2 for full data set (n = 172, including 10 terrestrial artiodactyls). Circle size reflects the sum radii ($\sum p_{spec}$) in the skull for each specimen, with larger circles indicating higher $\sum p_{spec}$. A morphospace labelled with a specimen key is provided in the Appendix 2: Fig. S2.15 - Principal Components plot with PC1 and PC2 plotted for each specimen. Silhouettes are from Phylopic with credit attributed to Chris Huh and used under the Creative Commons Licence (2020).

The basilosaurid and protocetid archaeocetes show a high amount of asymmetry ($\sum p_{spec}$) in the cranium (Fig. 2.6 (1)), similar to that observed in early odontocetes, such as xenorophids (Fig. 2.6 (4)). Asymmetry decreases towards the base of Neoceti, and mysticetes show the lowest level of cetacean asymmetry observed in the entire data set (Fig. 2.6 (2)), overlapping with terrestrial artiodactyls (Fig. 2.5). As expected, odontocetes show higher values of asymmetry but span nearly the full range of asymmetry morphospace (Fig. 2.5). The highest asymmetry is seen in the monodontids, platanistids, and physeteroids (Fig. 2.6 (6-8)). There are some exceptions within odontocetes, however, such as lower levels of asymmetry in the other extant river dolphins (*Inia*, *Pontoporia*, and *Lipotes*) (Huggenburger et al., 2010; Huggenburger et al., 2017). Lower asymmetry is also observed in the family Eurhinodelphinidae (Lambert, 2005), the extant phocoenids (Marx et al., 2016a; Racicot, 2018) and genus *Sousa* (Thompson, 1990) (Fig. 2.6 (5)).
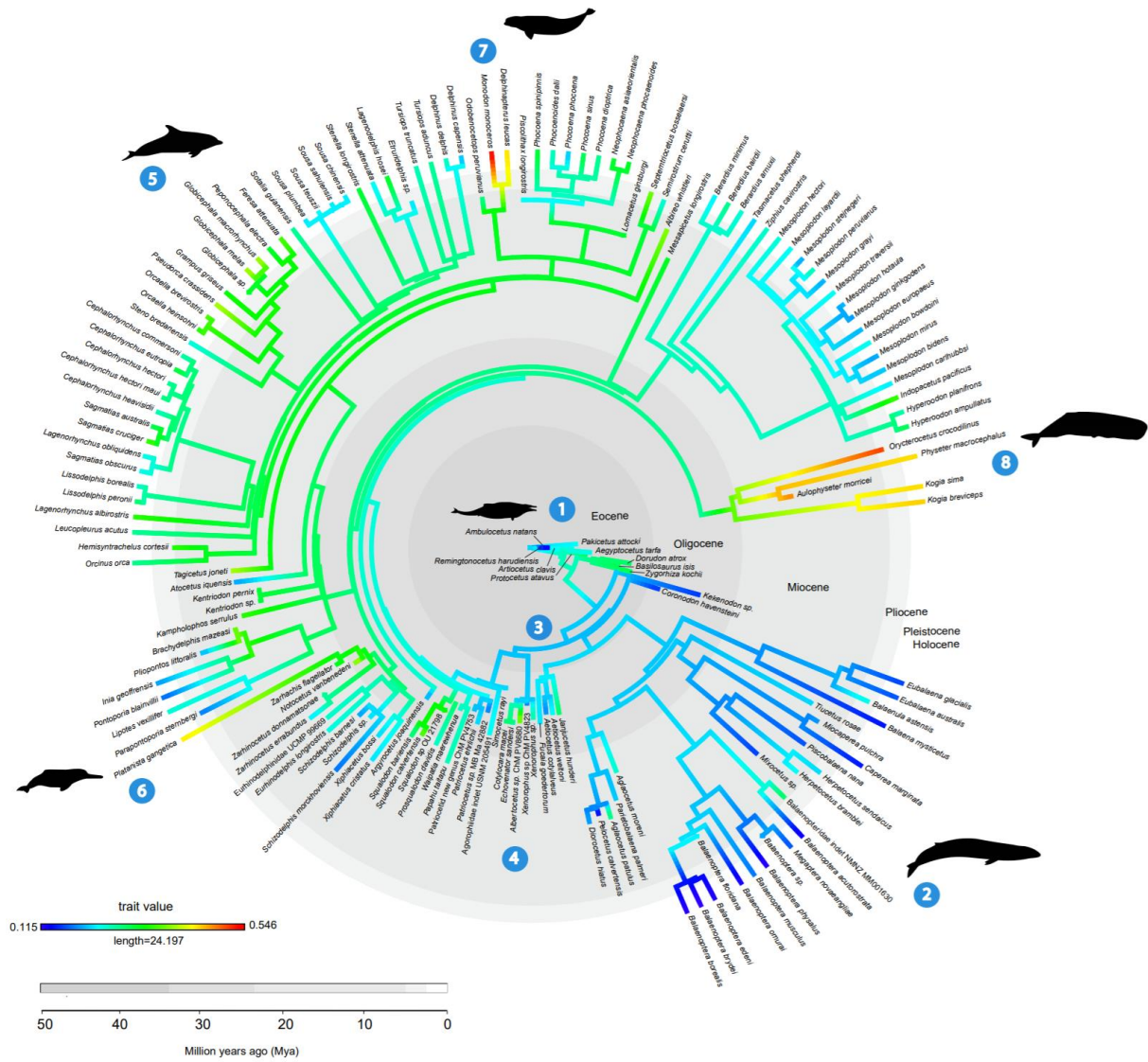
[Figure on previous page]

**Fig. 2.6.** Magnitude of cranial asymmetry across Cetacea. Time-calibrated phylogeny for sampled cetacean species indicating magnitude of cranial asymmetry ($\sum p_{spec}$). The labels highlight the following points: 1. archaeocetes; 2. mysticetes; 3. the origin of Neoceti (~39 Mya) (Marx et al., 2016a); 4. Early odontocetes including the xenorophids; 5. Odontocetes; 6. The highly asymmetrical *Platanista gangetica*; 7. The highly asymmetrical monodontids; and 8. The highly asymmetrical Physeteroidea. The full data set (n = 162) is used. Phylogeny based on Lloyd and Slater (2020). Silhouettes are from Phylopic with credit attributed to Chris Huh and used under the Creative Commons Licence (2020).

### *2.6.2 Evolutionary models of asymmetry*

Reconstructing shifts in the rate of asymmetry evolution supported three shifts with a probability > 0.375, with several additional shifts at lower probabilities (Fig. 2.7). There is a probability (0.375) of a shift in asymmetry occurring in the family Xenorophidae during the Early Oligocene (~30 Mya); this represents the first, large shift in asymmetry in the cetacean phylogeny (Fig. 2.7). Another shift occurs in the physeteroids (~23 Mya; probability = 0.750) and a later shift (probability = 0.625) is seen in the Late Miocene/Early Pliocene in the Monodontidae (Fig. 2.7). There are two smaller shifts (probability = 0.250) in the Squalodelphinidae and Platanistidae in the Late Oligocene/Early Miocene and later in the 'inioids'. There are no high probability shifts in asymmetry in the mysticete suborder, nor in the archaeocetes. Shifts with small (< 0.250) probabilities of occurrence are scattered throughout the phylogeny (Fig. 2.7), including one low probability shift at the root of Archaeoceti, but most shifts occur within the odontocetes. There is no measurable probability of a shift occurring in the archaeocete protocetids and basilosaurids. A slower or decreasing rate of asymmetry evolution is reconstructed within Mysticeti. Surprisingly, no shifts are reconstructed in the ziphiids, an odontocete family with bizarre asymmetrical premaxillary crests in most species (e.g., *Ziphius cavirostris*).
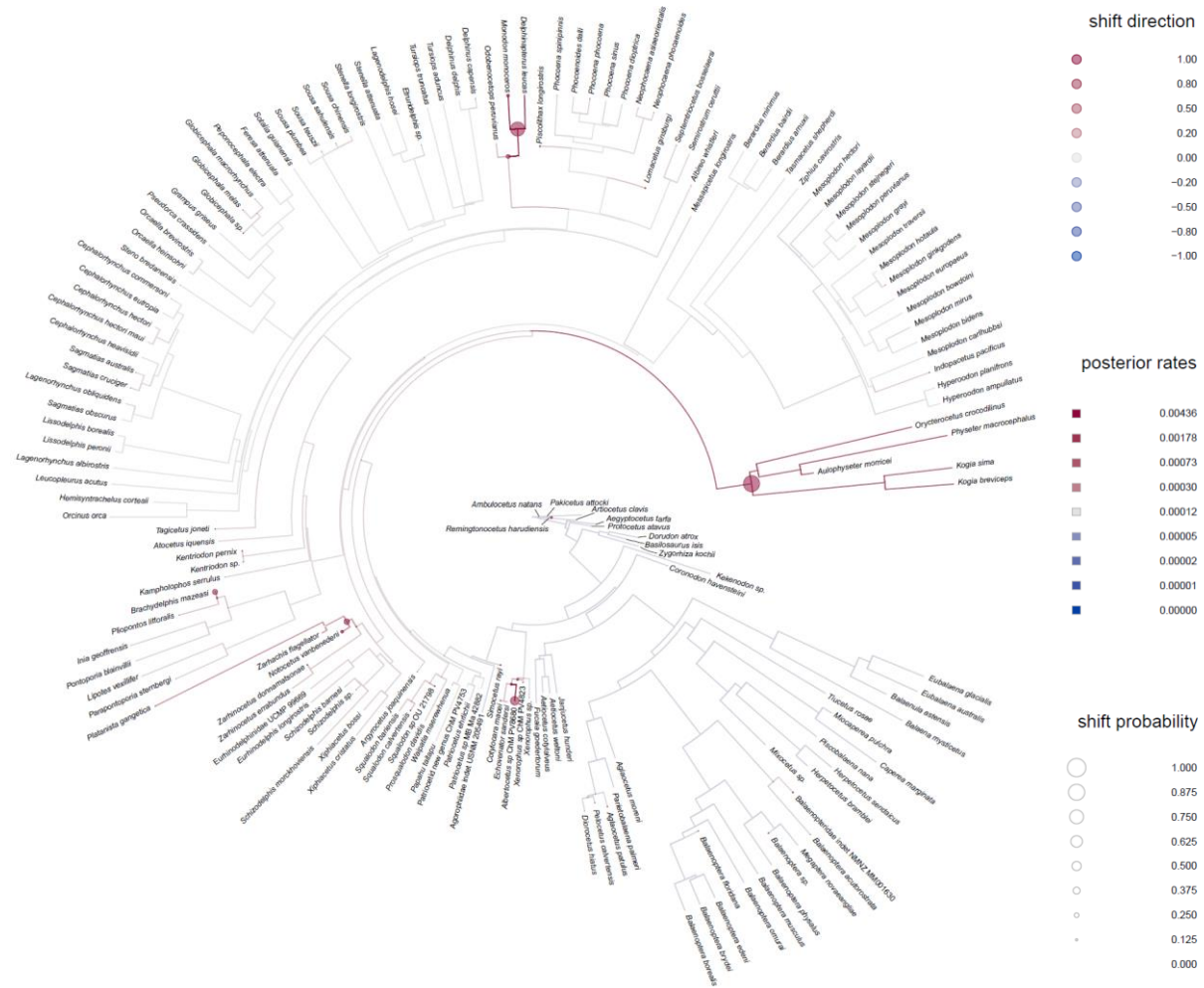
**Fig. 2.7.** Reconstructed probability of shifts in cetacean cranial asymmetry. Reconstructed probability along each branch of the phylogeny under the assumption of relaxed Brownian Motion with a Half-Cauchy distribution for the prior density of the rate scalar. Circles indicate a shift in the trait on either the branch or in the whole clade. The colour of the circle indicates the shift direction with red indicating forward shifts and blue indicating backwards shifts. The size of the circle indicates the probability of the shift occurring in that position in the clade with the largest circle (here, 0.750) indicating the highest probability of a shift occurring. The colour of the branch itself indicates posterior rates for that branch with red showing higher, increasing rates and blue showing lower, decreasing rates. The background rate is shown as grey. The asymmetry value is given as the sum of radii ($\sum p_{spec}$) per specimen. A trace of the chain is provided in Appendix 2: Fig. S2.13 - Gelman diagnostics for the two chains. Phylogeny based on Lloyd and Slater (2020).

We found a similar pattern for 'jumps' (a temporary or rapid change in the trait) (Fig. 2.8) as we did for 'shifts', with the addition of several jumps occurring in the Mid-Late Oligocene. The largest jumps (probability = 0.750) occur in the physeteroids and the monodontids. Smaller jump probabilities (0.625) occur in the Delphinidae, specifically in the subfamily Globicephalinae (e.g., *Globicephala* spp., *Pseudorca crassidens*) and Platanistidae and Squalodelphinidae and also at around probability = 0.40 in the xenorophids and the kentriodontids (Fig. 2.8). The traces of the chains for the two models (shifts and jumps) show that a successful burn-in occurs before 25% of the model iterations are run, justifying the use of the default value (Appendix 2: Fig. S2.9, S2.10 and Model diagnostics (Gelman and Rubin, 1992; Gelman, 2006; Plummer et al., 2006). All model diagnostics are provided in Appendix 2: Fig. S2.9-13; Table S2.5 and Model diagnostics section (Gelman and Rubin, 1992; Gelman, 2006; Plummer et al., 2006).
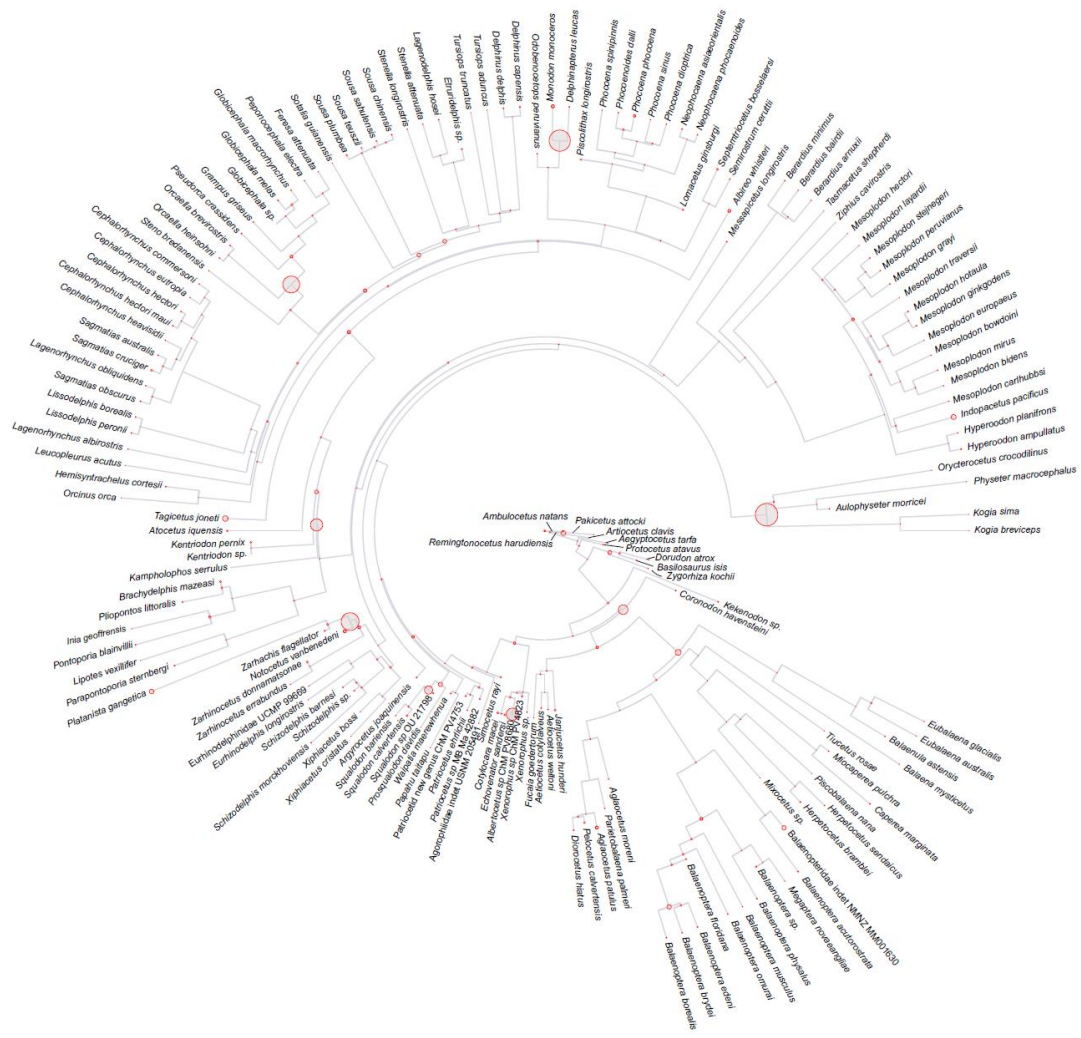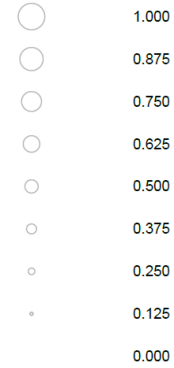
[Figure on previous page]

**Fig. 2.8.** Reconstructed probability of jumps in the rate of cetacean cranial asymmetry. The model also predicts the number of jumps which may have occurred. The size of the circle indicates the probability of the jump occurring in that position in the clade with the largest circle (here, 0.750) indicating the highest probability of a jump occurring. The colour of the circle indicates the number of inferred jumps, where dark red = 5 and pale red = 1. The asymmetry value is given as the sum of radii ($\sum p_{spec}$) per specimen. A trace of the chain is provided in Appendix 2: Fig. S2.13 - Gelman diagnostics for the two chains. Phylogeny based on Lloyd and Slater (2020).

### 2.6.3 Evolutionary models of influence on asymmetry

Inclusion or exclusion of the rostrum made no difference to the ordering of the 'goodness of fit' of the models (Table 2.5; Appendix 2: Table S4.5b (Lloyd and Slater, 2020). There was no difference in the ordering of the 'goodness of fit' of the top models when we ran all models with a phylogeny that includes only species that appear in a character matrix from Lloyd and Slater (2020) (Appendix 2: Fig. S2.6-8 Table S4.5c (Lloyd and Slater, 2020). For this reason, the results focus on the analyses which include the rostral landmarks and the original 'genus tree' phylogeny.

The best fit model for both data sets is the 'OUM-regime' (AIC = - 448) (Table 2.5), which is the model with a selective regime suggesting that the monodontids, physeteroids, and platanistids are evolving under a single different regime (Table 2.5; Appendix 2: Table S2.4a (Lloyd and Slater, 2020), under the assumption of Ornstein–Uhlenbeck (OU). The 'OUM-regime-split' model (the previously mentioned 'regime' model split into 4 separate 'regimes' i.e., one 'regime' (evolutionary state) for the monodontids, one for physeteroids, and one platanistids) also received strong support (AIC = - 445).

In both the 'OUM-regime' and 'OUM-regime-split' models, archaeocetes are placed into one regime, mysticetes in another, and the remaining odontocetes in a third. The third best fit model is the 'OUM-echo-freq' model (AIC = - 403)

(Table 2.5), again under an OU assumption, with species categorised by their predominant echolocation/sound group.

**Table 2.5.** Five best-fit evolutionary models for cranial asymmetry. Model ranked according to the Akaike Information Criteria (AIC). Models are detailed in Table 2.1 - Models testing whether changes in cetacean cranial asymmetry are associated with other discrete traits

| Model | Full landmark data set | | No rostrum | |
| --- | --- | --- | --- | --- |
| | Rank | Akaike Information Criteria (AIC) | Rank | Akaike Information Criteria (AIC) |
| 'OUM-regime' | 1 | -448 | 1 | -498 |
| 'OUM-regime-split' | 2 | -445 | 2 | -496 |
| 'OUM-echo-freq' | 3 | -403 | 3 | -449 |
| 'OUM-ancestral' | 4 | -379 | 4 | -424 |
| 'OUM-echo' | 5 | -373 | 5 | -422 |

Phylogenetic ANOVAs supported the 'OUM-regime', 'OUM-regime-split', and 'OUM-echo-freq' models as factors significantly associated with total cranial asymmetry ($\Sigma\rho_{spec}$) across cetaceans ($F = 26.97$, $p < 0.001$; $F = 15.78$, $p < 0.001$; $F = 5.83$, $p < 0.001$, respectively). Geological age, suborder, and presence/absence of echolocation were not significantly associated with cranial asymmetry ($F = 1.10$, $p = 0.36$; $F = 1.57$, $p = 0.21$; $F = 1.44$, $p = 0.23$, respectively). After correction for false discovery rate (using the Benjamini-Hochberg method (Benjamini and Hochberg, 1995; Benjamini and Yekutieli, 2001), the regime, regime-split, and echolocation frequency models remained significant ($p < 0.001$, $p < 0.01$, $p < 0.001$, respectively) (Appendix 2: Table S2.8; Benjamini and Hochberg, 1995; Benjamini and Yekutieli, 2001). Hereafter, results with the Benjamini-Hochberg correction are discussed.

## 2.7 Discussion

Our analyses of cranial asymmetry through the evolutionary history of whales suggests that the common ancestor of living whales (mysticetes and odontocetes) did not possess significant naso-facial asymmetry, and thus it is unlikely that echolocation was present at that stage of whale evolution or at any point in mysticete evolution. Cranial asymmetry is highest in crown odontocetes and first becomes a major feature of odontocete crania in the Early Oligocene, soon after their divergence from mysticetes. This period has previously been identified as one of unusually high diversity and evolution in neocete skull morphology (Fordyce, 1980; Berta et al., 2014; Churchill et al., 2018) alongside an explosive and rapid radiation of crown cetaceans (Fordyce, 1980; Slater et al., 2010; Boessenecker et al., 2017).

Rostral asymmetry is observed in some archaeocetes and is potentially related to directional hearing, possibly increased by deformation in some cases. Fahlke et al. (2011) suggest that *Artiocetus clavis* (GSP-UM 3458 - the same specimen as used in this study) was found palate-up with no evident compression or deformation, and further suggest that archaeocete asymmetry in the rostrum is consistent in direction. We found this same rostral asymmetry in this and other archaeocetes along with asymmetry in the jugal, orbit, and squamosal. This rostral asymmetry disappears in Neoceti and later arises in the naso-facial region in odontocetes. In archaeocetes, four of the ten most asymmetric landmarks ($\sum p_{land}$) were located in the rostrum (Table 2.4). This distribution could be inferred as torsion in the archaeocete rostrum as part of a complex of traits which led to directional hearing (Fahlke et al., 2011). This asymmetry then disappears during the transition from archaeocetes to early neocetes (Fig. 2.6; Appendix 2: Table S2.9). It is unclear whether this is due to an actual shift from a primitive form of aquatic directional hearing in specific archaeocetes (the basilosaurids and protocetids, as suggested by Fahlke et al. (2011) to a different regime (i.e., to high frequency sound production in the odontocetes, and low-frequency hearing in the mysticetes), or whether this is simply asymmetry unrelated to function in the rostrum as is reported for other mammals (e.g., dextral twist in the rostral region of some dogs (Howell, 1925) or even brought on by developmental and environmental

stressors (Willmore et al., 2005; Goswami et al., 2015). Further it could be related to specific feeding strategies such as bottom-feeding or other lateralized behaviours which can cause asymmetry related to increased muscle attachment or mechanical stress in the preferential side (Galatius, 2005; 2006). When looking at the primary landmarks displaying asymmetry in the basilosaurids and protocetids, there is no indication that these are dominated by rostral torsion more than in the other archaeocetes (Appendix 2: Table S2.10), and instead asymmetry appears to be spread in no particular pattern across the jugal, squamosal (which are possibly more susceptible to deformation), rostrum, and orbit for these families. Rostral asymmetry in the archaeocetes is at least partly caused by fossil distortion in some specimens (Martínez-Cáceres et al., 2011) but perhaps may also be biologically present in more archaeocete families than previously thought.

We found no high probability shifts (Fig. 2.7) in asymmetry occurring in the protocetids and basilosaurids, despite a rapid change from high asymmetry (found in the rostrum in these archaeocetes) to a more symmetrical skull in the early mysticetes such as *Coronodon havensteini* (Fig. 2.6). We did, however, find evidence for small temporary and rapid change (jumps) in asymmetry in the later archaeocetes (Fig. 2.8). Echolocation, telescoping, and ecological specialization rapidly evolved shortly after the divergence of Neoceti from Basilosauridae (Geisler et al., 2014; Boessenecker et al., 2017) and there may have been a rapid regime change from directional hearing occurring at the same time, possibly with associated asymmetry.

Asymmetry is lowest in basal mysticetes such as *Coronodon havensteini* and the aetiocetids and remains low in mysticetes from the Oligocene to present. There are no high probability shifts in asymmetry in the mysticetes. Rather, Mysticeti largely display a slower or decreasing rate of the trait. There are some increases in asymmetry observed in individual mysticetes, for example in Balaenopteridae indet (NMNZ MM00163) and *Aglaocetus moreni* (FMNH P13407), but this likely represents taphonomic distortion in the rostrum rather than biological asymmetry. Balaenopteridae indet NMNZ MM00163 especially has some distortion in the supraoccipital, postorbital process, lateral posterior squamosal, and the parietal which likely account for its high $\Sigma\rho_{spec.}$

Quantifying cranial asymmetry in living and extinct mysticetes allows reconsideration of the evolution of echolocation in this clade. The consensus is that cranial asymmetry in whales evolved due to the production of high frequency vocalisations (Mead, 1975; Heyning, 1989; Huggenberger et al., 2017). The consistent level of symmetry in the mysticetes corroborates the hypothesis that mysticetes never evolved sophisticated echolocation (Fitzgerald, 2006; Park et al., 2017) and also contradicts the hypothesis that this suborder secondarily lost their echolocation capabilities (Milinkovitch et al., 1995). Our analysis further suggests that echolocation was likely not present in the common ancestor of mysticetes and odontocetes (Fitzgerald, 2016; Park et al., 2017) but evolved early in the common ancestor of odontocetes shortly after they diverged from mysticetes (Geisler et al., 2014). As reported in Fahlke and Hampe (2015), mysticete crania are similar in magnitude of asymmetry to terrestrial artiodactyls (Table 2.4, Fig. 2.5). In mysticetes, the highest level of cranial asymmetry was found in the rostrum, likely due to deformation. In some extant specimens we observed that the tip of the rostrum has dried out and partly split apart. Even with drying-out and potential taphonomic deformation, the levels of asymmetry in mysticetes were lower than asymmetry seen in archaeocetes and much lower than that of odontocetes.

Cranial asymmetry first appears as a significant morphological trait in the Early Oligocene odontocetes Xenorophidae (Fig. 2.6; 2.7), suggesting that biosonar arose early in odontocete evolution. Odontocete asymmetry is overwhelmingly concentrated in the nasals including the posterior suture with the frontal, maxilla, and premaxilla. Most early odontocetes are less asymmetric (Fig. 2.6) compared to later extinct and modern forms (Thompson, 1990), bar a few exceptions. The extant La Plata dolphin (*Pontoporia blainvillei*), is one of few living odontocetes with cranial symmetry but asymmetric nasal sacs (Thompson, 1990), a trait it shares with other NBHF echolocators (Morisaka and Connor, 2007). It ranks here as the least asymmetric odontocete ($\sum p_{spec}$ = 0.179, Appendix 2: Table S2.9). Other extant odontocetes with low cranial asymmetry include *Sousa*, *Sotalia*, and *Steno* (Fig. 2.6) which have been suggested to converge in skull morphology with kentriodontids (Thompson,

1990), (Fig. 2.6). Phocoenids also exhibit a low level of cranial asymmetry (Fig. 2.6) (Marx et al., 2016a). This low asymmetry is likely tied to their relatively low peak-power biosonar (Jensen et al., 2018; Galatius et al., 2019). Further, many descriptions of eurhinodelphinids have suggested that their crania are only slightly asymmetric (Lambert, 2005; Benoit et al., 2011), as is supported here (Fig. 2.6). Thus, it should be considered that although some later fossil odontocetes had symmetrical skulls, they may have had asymmetrical nasal sacs as is observed in these extant species.

Macroevolutionary reconstruction of shifts and jumps in cranial asymmetry throughout cetacean evolution supported a high probability (probability = 0.375) of the first major positive shift in asymmetry occurring in xenorophids during the Early Oligocene (~30 Mya) (Fig. 2.6; Fig. 2.7). This result adds further evidence to the idea that xenorophids and other odontocetes iteratively evolved specialisations for the production of high frequency sounds necessary for echolocation (Geisler et al., 2014; Churchill et al., 2016; Park et al., 2016; Racicot et al., 2019). The distinct cranial morphology (and by inference, distinct soft tissue morphology) found in xenorophids (e.g., a deep rostral basin, a narrow premaxillary fossa, and a postnarial fossa), indicate a form of echolocation unique to the clade which interestingly, as it became more specialised, also became more asymmetrical, highlighting the importance of this trait for echolocation. The position of xenorophids as the earliest diverging clade within Odontoceti demonstrates that echolocation, telescoping, and ecological specialization rapidly evolved shortly after the extinction of the Basilosauridae (Churchill et al., 2016; Park et al., 2016; Boessenecker et al., 2017). Since then, cranial asymmetry has increased and remained generally high throughout the odontocete lineage (Fig. 2.6), bar a few exceptions.

Later shifts are observed in the physeteroids in the Late Oligocene (~23 Mya) and in the Squalodelphinidae (this increase in asymmetry is also recently mentioned in Bianucci et al. (2020)), and Platanistidae in the Late Oligocene/Early Miocene. The latter two families share marked asymmetry in the premaxillae with the right maxilla narrower than the left in dorsal view (Lambert et al., 2014). Further, asymmetry is recorded in the frontal and

maxillary crests of fossil platanistids such as *Zarhachis flagellator* (Lambert et al., 2014) although the supraorbital crests are not as developed as the extreme maxillary crests in the extant *Platanista gangetica* which is one of the most asymmetric of all odontocete skulls (Smith, 2002). There is also marked skull asymmetry in the distantly related squalodelphinid, *Notocetus vanbenedeni* which also sits within the superfamily; Platanistoidea (Lambert et al., 2014; Bianucci, 2020).

The best model fit, the 'regime' model ($p < 0.001$), assumes there is a distinct evolutionary regime for the most asymmetrical odontocete specimens (physeteroids, platanistids, and monodontids) indicating a single driver for their extreme asymmetry. We hypothesise that this 'regime' may be linked to the pressures which arise from inhabiting acoustically complex environmental niches. The physeteroids were the first of the major odontocete crown lineages to rapidly diverge and are easily recognisable due to a highly asymmetric facial region and supracranial basin (Marx et al., 2016a). Their large body size and hypertrophied nasal structures produce a low-frequency multi-pulsed sound (Madsen et al., 2002), which facilitates long range detection of prey (Jensen et al., 2018). This is highly advantageous when searching for patchy prey, especially as the physical properties of the water itself alter sound velocity and potentially constrain sensory morphology (Park et al., 2019).

*Platanista gangetica*, the sole modern survivor of Platanistidae sits alone amongst river dolphins for having a highly asymmetric cranium and echolocating at broadband low frequency (BBLF). The unique, autapomorphic bony maxillary crests of *Platanista* may help achieve a higher directionality than expected for a cetacean that clicks nearly an octave lower than similar sized odontocetes (Jensen et al., 2013), a feature that would be useful in the turbid, cluttered rivers they inhabit. Other species in this highly asymmetric model include both monodontids; belugas (*Delphinapterus leucas*) and the narwhal (*Monodon monoceros*). *Monodon* remains the most asymmetric skull in the sample, even when the rostrum is removed ($\Sigma\rho_{spec} = 0.472$) which rules out the possibility that the asymmetric tusk and residual teeth may be skewing the overall $\Sigma\rho_{spec}$ (see below for details). Their unique sound repertoire (narrowband structured, NBS) is ideal for projecting and receiving signals in

icy, shallow waters, where the animals can detect targets in high levels of ambient noise and backscatter (Turl and Penner, 1989) (Appendix 2: Table S2.8). Jumps detected in the delphinids all belong to the subfamily Globicephalinae (Fig. 2.8). In particular, the highly asymmetrical *Globicephala* (Table 2.3; Appendix 2: Table S2.9) has evolved a deep-dive pattern to target a deep-water niche occupied by large, calorific, and fast squid and its acoustic behaviour is more akin to deep divers than to oceanic delphinids (Aguilar Soto et al., 2008). The cochlea of *Globicephala* is also morphologically different to other delphinids (Park et al., 2019), which could also represent adaptation to the extreme acoustic environment of the deep ocean. Furthermore, studies suggest that *Pseudorca* (which also has a highly asymmetric cranium; Table 2.3) echolocates with different vertical and horizontal plane patterns to other delphinids (Au et al., 1995).

Surprisingly, no jumps or shifts are seen in the deep diving ziphiids (beaked whales), an odontocete family with bizarre asymmetrical premaxillary crests and an asymmetric prenarial basin (Appendix 2: Fig. S2.16). The asymmetry of the beaked whale skull is marked (Heyning, 1989; Baker, 2001; Rommel et al., 2005); so much so that the right premaxilla, premaxillary crest, premaxillary sac fossa, and the nasal bone are around 30% larger than those on the left (Rutherforde-Thorpe, 1938). Previous studies have suggested that the beaked whale genus *Berardius* (the most basal crown genus) shows the least bilateral asymmetry in the skull (Kasuya, 2009; Yamada et al., 2019), and we saw a similar result here. We attribute the underrepresentation of asymmetry in the ziphiid skull to the use of landmarks alone. Whilst detecting asymmetry in the *shifting* of the nasal, premaxilla, and maxilla to the left side of the skull, this method underrepresents the degree of asymmetry in the morphology of the bones themselves. The premaxilla is landmarked with points at the posterior dorsal premaxilla and the dorsal medial maxilla (suture with nasal and premaxilla) which accurately captures asymmetry in the positioning of the bone and its attachment but fails to capture the tapering of the highly asymmetric premaxillary crest itself (Appendix 2: Fig. S2.16). Future studies in this area should be done with curve sliding-semi landmarks and surface patches to more accurately capture the complex morphology (Bardua et al.,

2019a) of the premaxillary crests and premaxillary sac fossae in ziphiids which are not represented using fixed landmarks alone.

'Regime-split' was the second-best model fit which had a significant effect ($p$ < 0.01) on asymmetry in the cranium. This model suggests a different evolutionary regime for each of the most asymmetric groups. As above, it could be hypothesised that the highly asymmetric species live in unique, acoustically complex environments all of which have rather extreme specific environmental selection pressures. The reduction in the $p$-value after phylogenetic correction for the regime and regime-split models suggests that the factors influencing asymmetry may be shared by closely related taxa.

Frequency of echolocation (model: 'echo-freq') also had a significant effect ($p$ < 0.001) on the level of asymmetry in the cranium and was the third best model fit. Echolocation frequency has been widely suggested as a key driver of asymmetry in the cranium (Cranford, 1996; Fahlke et al., 2011) and soft tissues (Soldevilla et al., 2008). Although not the best model fit, we suggest that this relationship be investigated in more detail, for example with a more detailed analysis of species-specific echolocation frequencies and associated categories across Cetacea (Cranford, 1996). It is important to note that these methods assume a Brownian-motion model, which oversimplifies the actual evolutionary model underlying the evolution of asymmetry (shown here to be better described by an OU model).

We found no support for several other potential drivers for observed patterns of cranial asymmetry, independent of phylogeny. There is no significant effect of geologic age of the specimen (e.g., Eocene, Miocene, extant) on sum radii in the skull ($p = 0.36$). This result is likely because, despite odontocete crania becoming more asymmetrical in most extant families, mysticetes do not. There is no significant effect of 'suborder' ($p = 0.21$) on the total sum radii across the cranium. This is not surprising as there is generally a clear phylogenetic relatedness in whether a cetacean is symmetric (mysticete) or asymmetric (odontocete). Presence or absence of echolocation (model: 'echo') has no significant effect ($p = 0.23$) on the sum of radii in the cranium. Again, this is not surprising as there is a clear phylogenetic relatedness in whether a cetacean

can echolocate, i.e., the odontocete suborder, or not echolocate, i.e., the mysticete suborder.

There is a small chance that skulls used in this study may be more asymmetrical, i.e., deformed or distorted, than a standard skull of the species and therefore this is represented in the placed landmarks and the resulting $\sum p_{spec}$. Where possible, we chose skulls based on their overall quality and representation of the species. This was not possible for fossils which are often represented by one specimen, but deformed skulls were removed from the study so as not to falsely imply there is biological asymmetry in the skull when there is none. Further, the sex of the specimen may slightly alter the degree of asymmetry in the skull. Female false killer whales have a slightly more asymmetrical skull than males (Kitchener, 1990) and this may partially explain why the individual in this study appears to have a higher level of asymmetry than the other delphinids. However, the sex of this specimen (USNM 11320) is listed as unknown. It is important to note that adult male narwhal exhibit an extreme form of asymmetry in the tusk and vestigial teeth (Nweeia et al., 2009). The specimen in this study (USNM 267959) is female and therefore lacks a highly asymmetric tusk, however, the paired tusks embedded in the maxillae may still exhibit asymmetry (Nweeia et al., 2009) and may affect the overlying bone structure. This has not skewed the results seen here as the top 6 landmarks of asymmetry in the *Monodon* skull are in the nasals and posterior premaxilla and maxilla (i.e., not the rostrum or anterior maxilla where imbedded tusks reside). Further, no landmarks were placed on tusks or teeth (see Methods (2.3): Manually placed landmarks (*Fn*)), which ensures that extreme asymmetry seen in some tusked species for example, *Odobenocetops*, is not captured in this study. The 'skew' in *Globicephala* and monodontid skulls has also been attributed to some asymmetry in the attachment of the neck muscles (Ness, 1967); however, the asymmetry ($\Sigma\rho_{land}$) in eight landmarks associated with the condyle and posterior cranium do not differ between *Globicephala* and the monodontids compared to other closely related species (e.g., *Feresa attenuata* and *Peponocephala electra*).

Lastly, an argument against the hypothesis that echolocation drives asymmetry in the odontocete skull is that bats also echolocate and do not have

cranial asymmetry as the natural condition (Macleod et al., 2007). However, the extreme differences in the environments in which bats and cetaceans echolocate, as well as other ecological and morphological differences between the two clades complicates any meaningful comparison (Cranford et al., 2004). It should be noted that both odontocetes and bats share a remarkable convergence on narrow biosonar beams across species independent of body size (Jakobsen et al., 2013; Jensen et al., 2018), with the ability to do this in odontocetes likely a result of cranial asymmetry.

With the most widely supported explanation of asymmetry being sound production, our results support the hypothesis that craniofacial asymmetry (along with concavity in the facial area, hypertrophied naso-facial muscles, air sacs, melon, and premaxillary sac fossa (Marx et al., 2016a) arose in odontocetes to support high-frequency echolocation. Further, echolocating in complex environments continues to be a primary factor driving the evolution of asymmetry in the odontocete skull, as supported by the independent evolutionary regimes for the most asymmetric odontocetes.

## 2.8 Conclusions

Our study represents the first comprehensive analysis of cranial asymmetry spanning the evolutionary history of cetaceans.  We demonstrate that the common ancestor of living cetaceans had little cranial asymmetry and thus is unlikely to have possessed the ability to echolocate. Odontocetes display increasing cranial asymmetry from the Oligocene to present, reaching their highest levels in extant taxa. Separate evolutionary regimes are supported for three odontocete clades (monodontids, physeteroids, platanistids) that inhabit acoustically complex environments, suggesting that echolocation and cranial asymmetry are continuing to evolve under strong selection in these niches. Surprisingly, no increases in asymmetry were recovered within the highly asymmetric ziphiids. We attribute this to the extreme, asymmetric shape of the premaxillary crests and sac fossae in these taxa not being captured by landmarks alone.

Mysticetes have maintained a low level of cranial asymmetry since their origin and, if asymmetry reflects ultrasonic sound production ability, it is unlikely that

mysticetes were ever able to echolocate. Archaeocetes have a high level of asymmetry in the rostrum which could be linked to directional hearing, as reported by Fahlke et al. (2011), but this rostral asymmetry disappears in early neocetes as the dichotomous hearing abilities of the two suborders became established.

Modelling the evolution of cranial asymmetry across living and extinct cetaceans recovered the highest probabilities of shifts in the trait at three main points: first, in the extinct odontocete xenorophids in the Early-Mid Oligocene, then in the physeteroids (Late Oligocene), and finally in the monodontids in the Late Miocene/Early Pliocene. Smaller shifts were found in the Squalodelphinidae and Platanistidae. This was also true for 'jumps' in the trait, with an additional jump in a branch of the delphinids (namely the Globicephalinae e.g., pilot whales and false killer whales). Additional episodes of rapid change were found in the Mid-Late Oligocene, a period of rapid evolution in cranial asymmetry in odontocetes. These results support studies suggesting that biosonar, the signature adaptation of odontocetes, and associated asymmetry were acquired at or soon after the origin of this clade (Geisler et al., 2014; Park et al., 2016; Churchill et al., 2018; Racicot et al., 2019).

# Chapter three

# Making waves: the rise and fall of cetacean evolutionary rates and disparity throughout their history

*'On the whole, the most peculiar and aberrant of mammals'*

George Gaylord Simpson on cetaceans

(Simpson, 1945)

## 3.1 Abstract

In just 8-12 million years, cetaceans (whales, dolphins, and porpoises) underwent one of the most profound changes in adaptive zone observed in mammals. Their evolution from land-dwellers to highly successful aquatic inhabitants is an exemplar of morphological change. The whale skull has not only adapted to an aquatic lifestyle but also evolved innovative mass filter feeding in the mysticetes (baleen whales) and echolocation in the odontocetes (toothed whales). However, to date, there has been little study spanning cranial morphological evolution across Cetacea. In this chapter, I used three-dimensional geometric morphometrics to reconstruct evolutionary rates and disparity and to investigate ecological influences on morphology in the skulls of 201 living and extinct cetaceans.

I found that throughout Cetacea's evolutionary history, there have been three key waves of diversification in the skull. The first wave of diversification is seen in the early-mid archaeocetes (early whales) which have some of the some of the highest evolutionary rates seen in cetaceans, mostly attributed to changes in the maxilla, frontal, premaxilla, and nasal. The second wave of diversification occurs at the divergence of the mysticetes and odontocetes (neocetes) around ~39-36 Mya. An increase in rates and disparity following the divergence, and in the proceeding years throughout the Oligocene, suggest that there were functional constraints early on in cetacean evolution that were overcome by the neocetes. The third wave of diversification is seen in the Miocene and is mostly an odontocete signal (~18-10 Mya).

Across Cetacea, highest axes of shape variation are seen in the elongation of the rostrum and the positioning of the nares. Archaeocetes, mysticetes, and odontocetes occupy distinct areas of the morphospace likely driven by suborder-specific key innovations: echolocation in the odontocetes and baleen-filter feeding in the mysticetes. I found that diet and echolocation have the strongest influences on cranial morphology and that habitat, feeding method, and dentition have also shaped the morphology of the skull. Cetaceans with heterodont dentition, which includes the archaeocetes and early diverging neocetes have the highest rates while the later edentulous, filter-feeding baleen whales show some of the lowest evolutionary rates.

Disparity is lowest in the archaeocetes and high in the echolocating odontocetes, especially the suction feeders with reduced dentition such as the Ziphiids (beaked whales).

**Keywords:** morphology, evolutionary rates, diversity, ecology

## 3.2 Introduction

The evolution of cetaceans (whales, dolphins, and porpoises) involves arguably the most extreme transition of any mammal lineage (Marx et al., 2016a). From the four-legged landlubbers of ~50 million years ago to the fully aquatic behemoths we know today, cetaceans have evolved a wealth of different adaptations, including a hydrodynamic and streamline fusiform body (Jefferson et al., 2011). This transition to a fully aquatic lifestyle (Fordyce and de Muizon, 2001; Uhen, 2007) happened over an evolutionarily short 8-12 million years (Thewissen, 2014; Marx et al., 2016a). Early cetaceans (archaeocetes) diverged from their terrestrial artiodactyl relatives (e.g., bovids, camelids) in the early Eocene, approximately 53 million years ago (Mya), and by ~ 41 Mya, the first fully aquatic forms had already appeared (Marx et al., 2016a).

Quickly thereafter, by ~39 Mya, the Neoceti, the clade that comprises modern whales and dolphins (Marx et al., 2016a), diverged, forming the two modern suborders: the baleen whales (mysticetes) and the toothed whales (odontocetes) (Marx and Fordyce, 2015). These two lineages can be differentiated even in early fossil representatives as their evolutionary paths quickly diverged. Mysticetes later evolved large body sizes and specialisations such as baleen for several mass feeding strategies (Berta et al., 2016), while odontocetes evolved echolocation (biosonar) for navigation, hunting, and interaction with congeners (Geisler et al., 2014; Churchill et al., 2016; Park et al., 2016). These two vastly different strategies have resulted in distinctive adaptations of the skull (Marx et al., 2016a), which, due to its morphological and functional complexity, is highly informative for

understanding and reconstructing cetacean biology and evolution (Marx 2016a).

### 3.2.1 The major clades of living and extinct whales

### Archaeocetes - invasion of an aquatic niche

The archaeocetes, or ancient whales, are a paraphyletic assemblage (referred to here informally as a separate suborder) of stem cetaceans (Marx et al., 2016a) that bridge the transition from terrestrial ancestors to fully aquatic cetaceans (Bianucci and Gingerich, 2011). The pakicetids (*ca.* 53-47 Mya, Indo-Pakistan; Thewissen, 2014), the earliest archaeocetes, has nasals towards the tip of the snout (like terrestrial artiodactyls) (Clementz et al., 2006) and were capable of normal terrestrial locomotion. They had also already begun to adapt to an aquatic lifestyle, subsisting on freshwater prey (Clementz et al., 2006), and evolving pachyosteosclerotic tympanic bulla (surrounding the external part of the ear canal) that clearly identify them as cetacean (Uhen, 2007). By ~48 Mya, the next wave of archaeocetes, the protocetids, had already rapidly diversified and spread to North Africa and North America (Thewissen and Williams, 2001; Marx et al., 2016a). They were increasingly aquatic, with a weak sacrum indicating that their terrestrial abilities were limited (Gingerich et al., 1994). By the late Middle Eocene, one of the last radiations of archaeocetes, the basilosaurids, was fully aquatic and as widespread as New Zealand, South America, and Antarctica (Marx et al., 2016a). Within a short evolutionary window, cetaceans had undergone huge morphological and physiological changes to adapt to a fully aquatic lifestyle (Thewissen, 2014). The advent of the Neoceti saw further major transitional changes for Cetacea, which may have led to competition with and eventual decline of archaeocetes. By the Eocene-Oligocene boundary (~ 34 Mya), all but one archaeocete families (the kekenodontids), had disappeared.

### Arrival of the neocetes

The bones in the neocete skull are visibly shifted posteriorly compared to the earliest archaeocetes (Fahlke and Hampe, 2015), for which no overlapping of the frontals or maxillae has been documented (Fahlke et al., 2011). Although a posterior shifting of the *nasals* arose prior to the origin of the neocetes (Churchill et al., 2018) and can be seen in the later archaeocete basilosaurids, it is much more advanced in the crownward cetaceans. Even so, telescoping (so called because of the way the bones 'slide' over each other as does a collapsible telescope; Miller 1932; Churchill et al., 2018) is considered to be one of the defining characteristics that separates the neocetes from the archaeocetes (Berta et al., 2014; Roston and Roth, 2019). This shifting results in a foreshortening of the posterior skull and accommodates easier breathing at the water's surface (Heyning and Mead 1990; Klima 1999; Churchill et al., 2018), an important adaptation for an increasingly aquatic lifestyle. It is also thought that this retrograde cranial telescoping provides bracing and support for an elongated rostrum in the odontocetes (Miller, 1923) and later, prograde telescoping likely helped accommodate the evolution of mass filter-feeding and mass engulfment in the mysticetes (Berta et al., 2014).

### Mysticetes – baleen and mass filter feeding

Mysticetes first appeared in the latest Eocene (Marx et al., 2016a; Lambert et al., 2017a; Pyenson, 2017), and the evolution of the mysticetes is becoming increasingly well documented by the discovery of numerous transitional taxa, little differentiated from the archaeocetes (e.g., *Mystacodon* (Lambert et al., 2017a) and *Coronodon* (Marx and Fordyce, 2015; Geisler et al., 2017; Churchill et al., 2018). *Mystacodon selenensis* is currently the earliest known mysticete (36.4 Mya) (Lambert et al., 2017a) and already had several characteristics that define it as a mysticete (Lambert et al., 2017a), including a dorsoventrally flattened rostrum and a posterior extension of the palate. However, early mysticetes retained the ancestral toothed condition, and the dental formula of *Mystacodon* was much like that of basilosaurids (Lambert et al., 2017a). The broad-based flattened rostrum of toothed mysticetes appeared around 35 Mya (Fitzgerald, 2006). Marx et al. (2016b) suggest that a transition from raptorial to baleen filter feeding was mediated by suction

feeding in the aetiocetids, the most crownward of the toothed mysticetes. Peredo et al. (2017) suggest that the timing of the origin of baleen, although remaining obscure due to the fact that keratin does not fossilise well, is likely sometime between the latest Eocene (~ 34 Mya) to the latest Oligocene (~23 Mya). Tsai and Fordyce (2018) propose that the full transition from teeth to baleen probably occurred in the Early Oligocene. Fossil evidence suggests that the advent of baleen, or its precursor, coincided with an increase in marine primary productivity and ocean upwelling (Marx et al., 2016a; Marx et al., 2016b).

The wide, flat shape of the skull in extant balaenopterids (rorquals), and many extinct members of Cetotheriidae, Pelocetidae, Tranatocetidae (Miocene and Pliocene mysticetes all represented in this study) and others, facilitates easy intake of vast quantities of prey and water (Werth, 2000a). As noted above, mysticetes display extensive cranial telescoping which has also radically altered the skull. First observed in the late Early to Late Oligocene (Marx et al., 2016a), telescoping in mysticetes is dominated by a forward movement of the posterior cranial elements, referred to as prograde cranial telescoping (Miller, 1923; Churchill et al., 2018). Importantly, significant telescoping is not clearly evident in the mysticetes until the chaeomysticetes, or toothless 'true' mysticetes of the late Early-Late Oligocene (Marx et al., 2016a; Tsai and Fordyce, 2018), and it may be linked to the evolution of filter feeding (Berta et al., 2014), which was not present in the earliest diverging mysticetes. More crownward mysticetes are characterised by their unique mass filter and bulk feeding strategies. Feeding with baleen comes at high energetic cost but is evidently so successful that it has enabled extant mysticetes to be so competitively advantaged that they have reached the extreme maximum body size observed in mammals (Goldbogen et al., 2017).

### Odontocetes – echolocation

Unlike the early mysticetes which retained many archaeocete features in the clade's infancy, the odontocete's defining adaptation, echolocation, was present even in their earliest representatives (Geisler et al., 2014: Fordyce and Marx, 2018). However, the antiquity of the mysticetes does suggest that there

is likely a currently unknown Eocene odontocete lineage (Lambert et al., 2017a; Pyenson, 2017; Churchill et al., 2018) which could contain species more intermediate between the archaeocetes and odontocetes. *Simocetus rayi* is currently the oldest known odontocete (~ 33.9 Mya: Fordyce, 2002). Like other early odontocetes it retained a set of primitive features, the most obvious of which is heterodonty and relatively far anteriorly placed nasals (Fordyce, 2002). However, the skull structure and shifted positioning of cranial bones in *Simocetus* indicates that it may have had the same soft facial tissues that extant odontocetes have. Firstly, this sets the odontocetes apart from the archaeocetes and early mysticetes and secondly, bony rostral asymmetry is suggestive of soft tissue asymmetry (Mead, 1975) associated with the ability to produce high frequency sound (echolocate) (Fordyce, 2002).

The evolution of echolocation has resulted in odontocetes having one of the most radically altered skulls of any mammal. Interestingly, as with echolocation, retrograde cranial telescoping and asymmetry in the naso-facial region were already present to a modest degree in the earliest known odontocetes (Xenorophidae, Patriocetidae, *Simocetus*, *Agorophius*) (Churchill et al., 2018; Coombs et al., 2020) and asymmetry and echolocation are most likely synchronous with one another. These skull adaptations further set odontocetes apart from most other mammals which have bilateral symmetry in the skull. Throughout odontocete evolution, asymmetry has become more extreme in the crown cetaceans and is possibly linked to idiosyncrasies of specific ecological pressures (Coombs et al., 2020). Telescoping is also more extreme in the later diverging odontocetes and is dominated by the posterior expansion of anterior cranial elements (Miller, 1923) such as the frontals and maxillae (Churchill et al., 2018).

Although these features are present in the earliest representatives of the suborder, the early odontocetes *do* retain some archaeocete characteristics, such as heterodont dentition seen in the Early Oligocene Xenorophidae, Patriocetidae, and *Simocetus* (among many others). Thereafter, the Late Oligocene/Early Miocene squalodontids become moderately polydont but still evidently heterodont (Marx et al., 2016a). In crown cetaceans, dentition is either polydont in the (predominantly) raptorial feeders (e.g., delphinids) or

reduced or entirely absent in the suction feeders (e.g., monodontids, mesoplodonts). Not only do extant odontocetes showcase a diversity of feeding adaptations, they also show a diversity and range of cranial morphologies. Echolocation in the odontocetes, its evolution and advancement have likely been a key driver of this diversity (Marx et al., 2016a). For example, the Ganges river dolphin (*Platanista gangetica*) has autapomorphic bony maxillary crests which may help achieve a higher directionality when echolocating in turbid, murky rivers (Jensen et al., 2013). It also has a marked shift in echolocation frequencies and an extreme, elongated rostrum bearing numerous needle-like teeth to assist with raptorial snapping (Marx et al., 2016a). This is just one of many examples showing how adaptations to ecological conditions: water turbidity, prey type, have influenced cranial morphology in odontocetes.

### 3.2.2 Drivers of cetacean cranial evolution

Clearly, a functional requirement to breathe easily at the water's surface is a key driver in cetacean naso-facial morphology. In the odontocetes, cranial morphology is further influenced by the ability to echolocate, whilst in the mysticetes this is driven by functional requirements of the skull for suction and mass filter feeding. There are also other ecological drivers and constraints on whale skull morphology. A study investigating convergent evolution in crocodilian and cetacean skulls (McCurry et al., 2017a) suggests that the high convergence between dolichocephalic gharials and odontocetes might be due to directional selection from ecological factors such as habitat and diet (McCurry et al., 2017a). McCurry et al. (2017a) found that diet was more closely associated than habitat in elongate skulls with long mandibular symphyses (characteristics associated with river dolphins). The impact of diet and feeding strategy is also evident in the extremely broad, brachycephalic rostrum of the kogiids, adapted to produce high suction forces (McCurry et al., 2017a), suggesting that that there are trade-offs between skull morphology and function. Skulls must be able to handle forces associated with catching prey in their upper size limits but must also be streamlined and hydrodynamic (McCurry et al., 2017a). Studies have suggested that these trade-offs may

explain why there is so much variation in the rostra of marine tetrapods (Busbey,1995; McHenry et al., 2006; McCurry et al., 2017a).

Within odontocetes, there is considerable variation in rostrum form, from elongation and narrowing of the rostra in raptorial predators of small prey (e.g., *Delphinus*), toward wider skulls with downward-orientated rostra in suction feeders (e.g., *Globicephala*), and shorter, broader skulls and enlarged temporal fossae in species such as the orca which handle larger prey (*Orcinus orca*) (Galatius et al., 2020). This variation reflects an identified relationship between prey size and odontocete skull shape (McCurry et al., 2017b, Galatius et al., 2020). In comparison, far less work has focused on the ecological influences on cranial shape in mysticetes. The size of the skull is thought to differentiate between rorquals that feed on small fish or krill, with smaller, more agile balaenids such as minke whales (*Balaenoptera acutorostrata*) tending to select faster moving small fish over slow, dense krill patches (Murase et al., 2007; Goldbogen et al., 2010). Much work has been done investigating engulfment capacity (Goldbogen et al., 2010), drag and kinematic diversity (Goldbogen et al., 2007; Cade et al., 2016; Goldbogen et al., 2017) and other such feeding mechanism functioning in extant rorquals, but little work has considered ecological influences.

Previous work on mysticete and all neocete diversity has suggested that bursts of evolution follow the origination of the major clades, coincident with Cenozoic ocean restructuring which in turn affected climate, ocean circulation, and ocean productivity (Steeman et al., 2009; Marx and Uhen, 2010; Marx and Fordyce, 2015). Additional work has been done regarding the radiation of modern neocetes, suggesting that morphological evolution - specifically body size, can retain a signature of early niche filling despite evidence for secondary radiations (Slater et al., 2010). Further studies suggest that cetacean evolution in general may follow a pattern of rapid niche filling (Lipps and Mitchell, 1976) and later, an explosive radiation of crown cetaceans during the Oligocene (Slater et al., 2010; Pyenson, 2017).

To date, work on cetacean macroevolution has largely focused on one or the other suborders, or on radiations and diversification in the neocetes (Steeman

et al., 2009: Marx and Uhen, 2010). These studies of cetacean diversity have used body size metrics (e.g., average female body length in Slater et al. (2010)) molecular data (Steeman et al., 2009), or whole-body discrete morphological and molecular characters (Marx and Fordyce, 2015) but not multivariate morphometric data, nor with a focus on the cranium. The skull is the most informative part of the cetacean skeleton because of its inherent complexity and because most of the bones that comprise the skull have become modified in some way throughout cetacean evolution (Marx et al., 2016a). Furthermore, the cranium is a complex structure which serves diverse functional roles, from feeding, breathing, housing the brain, nervous system, and sensory structures, to interacting with the environment. However, there has not yet been a comprehensive analysis of the macroevolution of the cetacean skull or the relative influences of diet, habitat, and other factors on its evolution. Furthermore, there has been no study of evolutionary rates and disparity (morphological diversity) throughout their entire evolutionary history.

Here I reconstruct the drivers of shape variation, disparity, and evolutionary rate in the cetacean cranium throughout their evolutionary history for the first time. I present the largest 3D scan data set ever gathered for Cetacea, spanning their evolutionary history from the Eocene to Recent with 88 living species (representing ~ 95% of extant cetacean species; Jefferson et al., 2011) and 113 fossil species. From these scans I extract 3D geometric morphometric data and use these to quantify morphology, disparity, and evolutionary rate of the cetacean cranium in unprecedented detail to address the following questions:

First, how do cranial evolutionary rates and disparity vary throughout cetacean evolutionary history? Second, do cranial evolutionary rates and disparity vary between the suborders, both in the whole skull and in individual bones? Third, do dentition (tooth type), diet, feeding method, prey detection (i.e., the ability to echolocate), and habitat influence skull shape, rates, or disparity?

### 3.3 Methods

#### 3.3.1 Specimens

My data set comprises stem cetaceans (archaeocetes, n = 11), and both extant suborders: baleen whales (mysticetes, n = 33) and toothed whales (odontocetes, n = 157). The final data set includes 201 cetacean crania, of which 113 (56%) are extinct, ranging in age from 48.6 Mya to 2.59 Mya. I selected specimens to cover the widest possible phylogenetic spread, representing 41 families, 122 genera, and ~95% of extant species from the Eocene to the present (Appendix 3, Table S3.1).

Due to the use of 3D geometric morphometric data covering the entire cranium, sampling was limited by specimen completeness and preservation. Inclusion of fossil specimens was determined by the extent of deformation and missing data. 87 (43%) of the specimens, including some extant specimens, had missing data, which was concentrated in the pterygoid, palate, jugal, squamosal, and tip of the rostrum (this had minimal impact on data collection as was dealt with accordingly, see 'Missing bones'). Where possible, we chose skulls based on their overall quality and representation of the species. This was not possible for fossils which are often represented by one specimen. Deformed skulls were removed from the study (Appendix 3, Table S3.2). Sexual dimorphism was not considered in this study as many fossils lack data on sex. Specimens with sex data were selected based on completeness of the skull and skull availability. All specimens are adults except for *Mesoplodon traversii* (NMNZ TMP012996) which is a sub-adult.

I scanned skulls using a Creaform Go!SCAN 20 or Creaform Go!SCAN 50 handheld surface scanner, depending on the size of the skull. Scans were initially cleaned, merged, and exported in ply format using VXElements v.6.0, and further cleaned and decimated in Geomagic Wrap software (3D Systems). I decimated models down to 1,500,000 triangles, reducing computational demands, while retaining sufficient detail for morphometric analysis. In many morphometrics studies, it is possible to digitally reconstruct bilateral elements by mirroring across the midline plane if the skull (or object) is preserved on one side (Gunz et al., 2009; Gunz and Mitteroecker, 2013; Cardini et al., 2014).

Due to a natural asymmetry occurring in the archaeocete and odontocete skull (Fahlke et al., 2011; Coombs et al., 2020), I limited mirroring to marginally damaged bones or easily mirrored missing bones only, where it was clear that mirroring would not mask asymmetric morphology. Elements were mirrored using the 'mirror' function in Geomagic Wrap (3D Systems).

### 3.3.2 Morphometric data collection

I placed 123 landmarks and 124 curve sliding semi-landmarks over the surface of every skull in Stratovan Checkpoint (Stratovan, Davis, CA, USA). I used the 'single point' option to add fixed landmarks, and the 'curve' option to add semi-landmark curves (Appendix 3, Fig S3.1). Landmarks were defined by Type I (biology) and Type II (geometry) (Bookstein, 1991; Bookstein, 1997) and were chosen to capture clear definitions e.g., tripartite sutures. Sliding semi-landmark curves (hereafter also termed 'curves') define key structures such as the margins of bones and anatomical ridges, representing a significant increase in shape capture compared to landmark-only data sets (Bookstein, 1997; Bardua et al., 2019a). Sliding semi-landmarks have been used successfully to quantify a vast array of organismal morphology, including beak shape (Cooney et al., 2017) and cranial morphology (Bardua et al., 2019b, Felice et al., 2020). Their use expands the quantification of shape to include the morphology of outlines (e.g., bone margins) and ridges (Cooney et al., 2017; Bardua et al., 2019b). Dentition was not landmarked. The sliding semi-landmark curve and landmark configuration for this data set is detailed in Appendix 3 Table S3.3; S3.4 and Fig. S3.1; S3.2; S3.3.

Archaeocetes have prevalent asymmetry in the rostrum and in the squamosal, jugal, and orbit, and although some of this may represent preservational deformation, it is likely that a significant amount of it is biological (Fahlke et al., 2011; Coombs et al., 2020). Asymmetry in odontocetes is predominant in the naso-facial region, whilst mysticetes show a high degree of symmetry, similar to terrestrial artiodactyls (Fahlke and Hampe, 2015). Due to these differences in asymmetry among suborders, I modified my landmarking protocol for bilaterally symmetrical skulls vs. asymmetric skulls. The differences in methodology regarding asymmetry (or lack thereof) between the suborders

required manually placing some landmarks and curves in asymmetrical taxa that could be mirrored in symmetrical taxa, as detailed below. However, the resulting data set is identical in terms of landmarks and curves across all suborders, allowing unified analyses across the whole of Cetacea (Fig. 3.1).

### *Placing landmarks on bilaterally symmetrical skulls*

A separate protocol was devised for the bilaterally symmetrical mysticetes (Fig. S3.2). I placed 57 landmarks on the left-hand side (LHS) of the skull and nine landmarks on the midline. I placed 60 sliding semi-landmark curves on the sutures between bones on the LHS of the skull and four curves on the midline. These curves and landmarks were then mirrored (using the midline landmarks and curves as an anchor) using the `mirrorfill` function in the R package 'paleomorph' v.0.1.4 (Appendix 3, Fig. S3.1; S3.2).

### *Placing landmarks on asymmetric skulls*

A separate protocol was required for the archaeocetes and odontocetes (the latter in particular) due to their significant bilateral asymmetry. Simply mirroring all sliding semi-landmark curves would misrepresent the asymmetric morphology of the skull (Coombs et al., 2020). I used the results from Chapter 2 (Coombs et al., 2020) to determine which of the bones in the skull were asymmetric and thus requiring manual landmarking and which were equivalently symmetrical to terrestrial taxa and could be reliably placed by mirroring bilaterally symmetric landmarks across the skull midline. I placed 57 landmarks on the LHS of the skull and nine landmarks on the midline. I mirrored 33 landmarks to symmetrical bones on the right-hand side (RHS) of the skull and I manually placed 24 landmarks on asymmetric bones on the RHS of the skull, totalling the same number of landmarks as in the mysticetes. I manually placed 60 curves on the sutures between bones on the LHS of the skull and four curves on the midline (Fig S3.3). I manually placed 21 curves on asymmetrical bones on the RHS, mostly concentrated in the nasals, dorsal premaxilla, dorsal maxilla, orbit and rostrum, and the rest were mirrored from the LHS (Fig. S3.3).

DORSAL



VENTRAL

POSTERIOR



basisphenoid

basioccipital

frontal

jugal

mandibular process

maxilla

nasal

occipital condyles

palate

parietal

premaxilla

pterygoid

supraoccipital

squamosal (with zygomatic process)
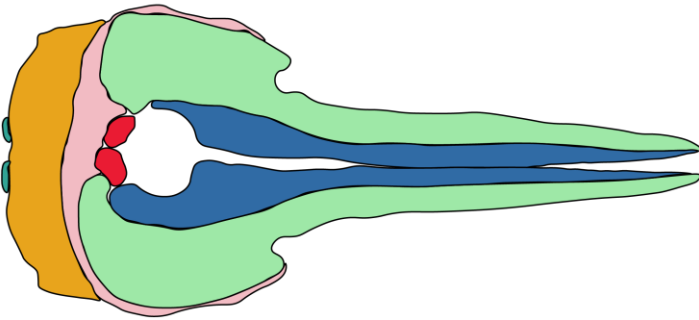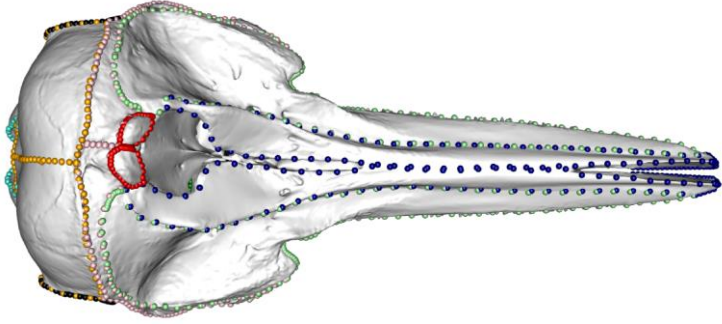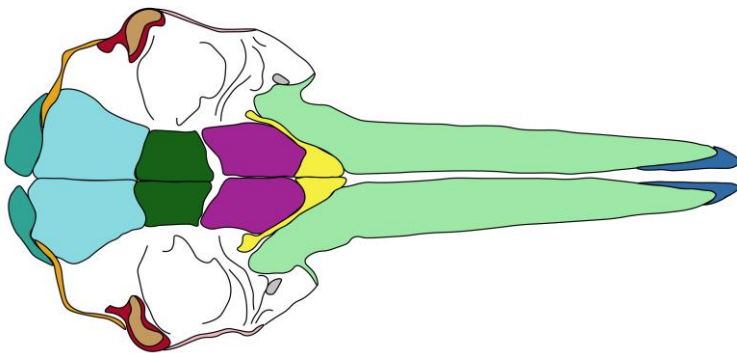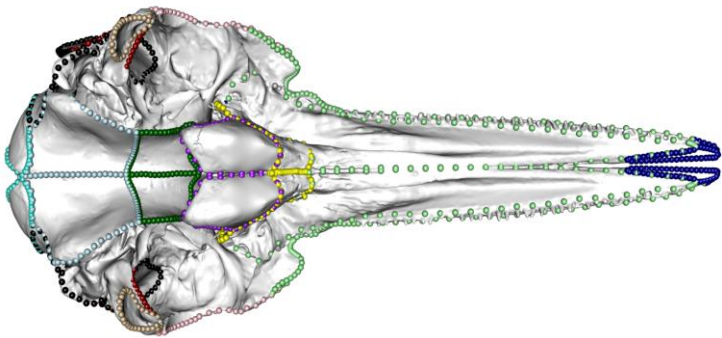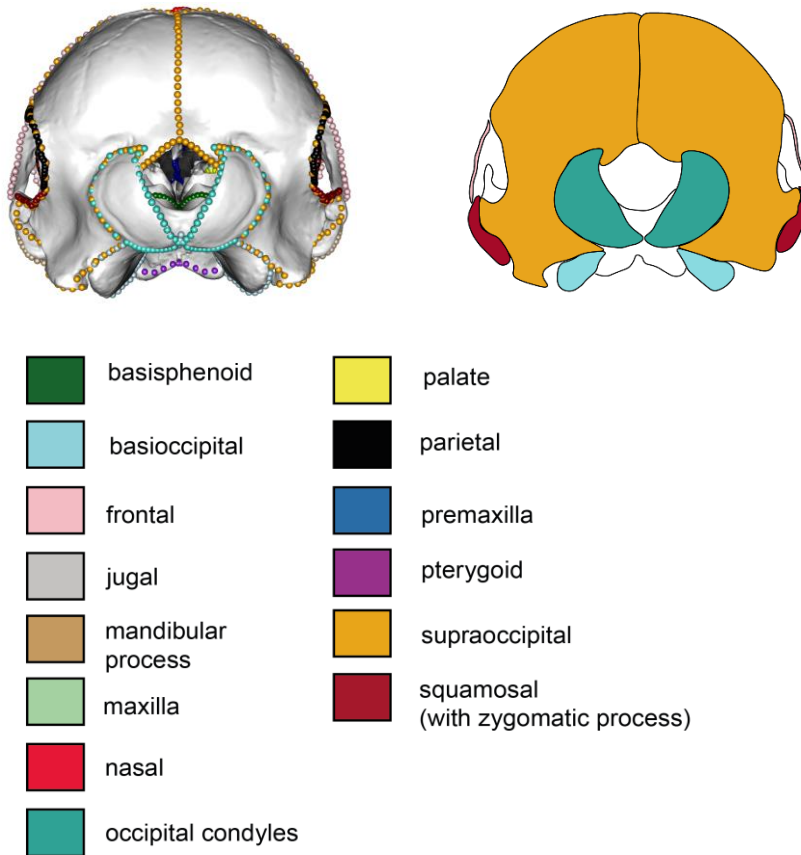
[Figure on this and previous page]

**Fig. 3.1.** Landmark and curve configuration for the cetacean skull. Landmarks and curves are shown on *Delphinus delphis* AMNH 75332. Dorsal (top), ventral (middle), posterior (bottom). Coloured bones match the colours of the landmarks and semi-landmark curves to help illustrate placement.

### *Resampling and sliding*

Due to the manual placement of semi-landmarks in Stratovan Checkpoint, there are not always the same number of points in each curve across specimens, and the points are not evenly spaced along the curve. I resampled semi-landmark curves to a consistent number with even spacing along each curve across specimens. I set semi-landmark numbers to appropriately capture curve shape across the full range of skull shapes (Table S3.4), for example to provide suitable sampling of the most dolichocephalic rostra, but to not oversample the most brachycephalic rostra (Table S3.4; Fig. S3.4).

Resampling also helped to reduce computational requirements during analyses. I then slid resampled semi-landmarks along tangents to minimize thin-plate spline bending energy between specimens and the mean shape, resulting in semi-landmark positions that are geometrically homologous across specimens (Gunz et al., 2005; Bardua et al., 2019a). Following sliding, all morphometric data were subjected to Procrustes superimposition to remove shape variation associated with differences in orientation (both rotation and translation) and isometric size (Rohlf and Slice 1990).

### Missing and variably present bones

Geometric morphometric analyses and plotting functions implemented in geomorph v.3.1.0 (Adams et al., 2019) require a full complement of landmarks (Adams et al., 2019). This complement can consist of actual landmarks and estimated positions for 'missing' landmarks. I dealt with missing bones in the following way:

### Missing bones

This refers to bones that should be present but have subsequently broken off or been damaged and could not be reliably digitally reconstructed or mirrored. To estimate positions for landmarks on missing bones, I placed 'missing' landmarks as close to the missing structure as possible and then marked it as a 'missing landmark' in Checkpoint, which automatically assigns a coordinate of $-9999$.

I then used the `fixLMtps` command from the R package 'Morpho' (Schlager, 2017) to estimate missing landmarks by mapping weighted averages from three similar, complete configurations onto the missing specimen. Missing landmarks are estimated for missing bones by deforming a sample average or a weighted estimate of the three skull configurations most similar to that with the missing element (Schlager, 2013; Schlager, 2017). Estimated landmarks are then added to the deficient configuration (Schlager, 2017). The deformation is performed by a thin-plate-spline interpolation calculated by the available landmarks (Bookstein, 1991; Schlager, 2017).

### Variably present bones

Cetaceans, despite huge variability and change in skull shape across their evolution and within extant suborders, retain all the bones of typical mammals with just a few exceptions. In *Odobenocetops*, a bizarre walrus-like whale from the Pliocene of Peru, the maxilla does not extend ventrally, and thus must be allocated as 'absent' in ventral view. Further, the nasals are absent in Kogiidae (Velez-Juarbe et al., 2015; Collareta et al., 2017; Benites-Palomino et al., 2019), represented here by fossil species *Aprixokogia kelloggi*, *Koristocetus pescei* (Collareta et al., 2017), *Scaphokogia totajpe* and extant species *Kogia simus* and *Kogia breviceps.* These absent bones were coded as such for these specimens by placing all relevant landmarks and semi-landmarks onto a single "zero-area" point, adjacent to its position in other taxa, following the method described by Bardua et al. (2019a).

### 3.3.3 Size

I extracted log centroid size of the cranium from shape data during Procrustes superimposition and used it as a proxy of overall size (Appendix 3, Table S3.5).

### 3.3.4 Ecology

Given the breadth of species in this data set, as well as inevitable uncertainties on ecology and life history for many rarer species, and the need for a minimum of five species in each bin for statistical analyses, we used relatively broad categories to capture diet and habitat. I focused on ecological categories relevant to cranial functions, including feeding and sensory structures, as follows:

### Dentition

I divided dentition into four categories: homodont, heterodont, reduced, and edentulous (baleen). I used data from the primary literature, as well as categories established in previous studies (Hocking et al., 2017a, b; Berta and Lanzetti 2020) (Appendix 3, Table S3.1).

*Diet*

I divided diet into five categories: 'fish', 'benthic invertebrates + fish', 'cephalopods + fish', 'tetrapods +fish', and 'zooplankton + fish'. In the latter four categories, fish make up a substantial, but minority component of the diet whereas the first prey item forms the majority of the diet. I used data from the primary literature, as well as categories established in previous studies (Hocking et al., 2017a, b; Berta and Lanzetti 2020) (Appendix 3, Table S3.1).

*Echolocation ability*

Echolocation is a known key driver of morphology in the odontocete cranium (Cranford et al., 1996; Fahlke et al., 2011; Coombs et al., 2020). I split echolocation ability into two categories: band1, all non-echolocating cetaceans (archaeocetes and mysticetes), and band2, echolocating cetaceans (all odontocetes apart from *Odobenocetops*; de Muizon et al., 2002; Marx et al., 2016a). I assigned species to categories depending on whether they are known to echolocate or not, based on data from the primary literature (Appendix 3, Table S3.1). I scored fossils based on species-specific reconstructions in the literature. Although finer categories are possible, they bring substantial uncertainty in scoring, particularly with fossil data.

*Feeding method*

I divided feeding method into three categories: biting, suction, and filter feeding. I used data from the primary literature for extant taxa, as well as reconstructions for fossil taxa from published studies (predominately Hocking et al. (2017a, b) and Berta and Lanzetti (2020), see Appendix 3, Table S3.1 for individual references). As with the other traits, complex behaviours associated with feeding are difficult or impossible to establish for fossils and thus finer categories are not considered in this study. Where possible specimens were categorised by feeding method and diet based on Hocking et al. (2017a, b) which does consider dietary behaviour and handling of prey. Hocking et al. (2017a, b) rely entirely on model experimental and observational data to build their framework. This is beneficial because it allows behaviour that does not fossilise to be included and allows inferences from the fossil record to be tested (Hocking et al., 2017a, b).

***Habitat***

I divided habitat into four categories: riverine (freshwater), coastal, coastal-pelagic, and pelagic. I used data from the primary literature, as well as categories established in previous studies (Berta and Lanzetti 2020) (Appendix 3, Table S3.1). Data for fossil taxa were taken from the literature (predominantly Berta and Lanzetti (2020)), details can be found in Appendix 3, Table S3.1.

### 3.3.5 Phylogeny

My study uses a phylogenetic framework to reconstruct macroevolutionary patterns across Cetacea. I used the same tree with the same modifications as in Chapter 2 (adapted from Lloyd and Slater (2020)) and added the following specimens: *Hemisyntrachelus oligodon* (SMNK-PAL 3841) was placed is the same genus as *Hemisyntrachelus cortesii* (Post and Bosselaers, 2005), MUSM 605 and MUSM were ascribed to the subfamily, Lophocetinae as sister taxon to *Macrokentriodon* (Molina et al., 2018). *Yaquinacetus* sp. (USNM 214705) was placed in the Squaloziphiidae as in Lambert et al. (2018), near to the Chilcacetus clade which includes *Chilcacetus cavirhinus* (MUSM 1401) (also in this study). Finally, I placed *Scaphokogia totajpe* in the same genus as *Scaphokogia cochlearis* as in Benites-Palomino et al. (2019) (Appendix 3; Fig. S3.5).

### 3.3.6 Data analyses

***Morphology of the skull***

I ran a principal component analyses (hereafter, PCA) on the Procrustes-transformed morphometric data to assess the primary aspects of shape variation and morphospace occupation for the cranium. A PCA is a method often used in geometric morphometric analyses to reduce the dimensionality of large data sets by transforming a large set of variables, via a series of ordinations, into a smaller one that still contains most of the morphometric information. I conducted a PCA using the `gm.prcomp` function in the R package 'geomorph' v.3.3.1 (Adams et al., 2020).

Morphologies representing the extreme shapes along the principal component (PC) axes were generated to visualise shape variation. I corrected data for phylogeny by conducting a phylogenetic principal component analyses to visualise shape variation after accounting for phylogenetic non-independence. Phylogenetic PC scores (hereafter, pPC scores) representing 95% of the total variation were extracted and used in further analyses where data dimensionality prevented use of Procrustes coordinates for the full data set. I calculated pPC scores using the 'phyl.pca' function in the R package 'phytools' v.0.7-70 (Revell, 2012). In highly dimensional data sets like this one (where resampled specimens still had 2028 coordinates over each skull surface), reducing the data to its principal components (PCs) means that simulations can be run on a reduced set of axes, reducing computational demands (Clavel and Morlon, 2020). Using pPC scores, although less ideal than considering all traits, is a better alternative than distance approaches which cannot accommodate departures from Brownian motion (Clavel and Morlon, 2020). Raw pPCscores for all cetaceans, and separately for archaeocetes, mysticetes, and odontocetes are shown in Appendix 3; Table S3.6; S3.7; S3.8; S3.9.

### *Allometry*

I used the procD.lm function in geomorph to investigate whether allometry (size-related shape variation) was a significant aspect of overall variation in skull shape across Cetacea.

### *Patterns of Cranial Evolution*

### *Rates of cetacean cranial evolution through time*

I investigated branch-specific evolutionary rates and rates through time using BayesTraitsV3 (http://www.evolution.rdg.ac.uk/). I ran analyses for the entire skull and for individual bones, using (pPC) scores that represent 95% of the shape variation for the relevant structure (Appendix 3, Table S3.6). I ran models under several assumptions to find the best model fit. These models were a Brownian Motion model (BM), a kappa model (a measure of punctuated evolution), a delta model (indicating an increase or decrease in the rate of evolution through time such as an 'early-burst' model), a lambda model (a

measure of phylogenetic signal in which the shared history of taxa drives trait distribution at the tips (Pagel 1997; 1999), and an Ornstein-Ulenbeck model. I also ran all models with variable rates making a total of 10 models.

I ran the following analyses with each of the above model assumptions. I ran a reversible-jump Markov Chan Monte Carlo (MCMC) algorithm which permitted fitting of both single and variable rates models. The latter allows the rate of change to vary through time, automatically detecting shifts in rates of evolution. I ran several chains and assessed for convergence of the chains by first visually assessing the trace plots and then checking the effective sample size (ESS) with Gelman and Rubin's diagnostics (Gelman and Rubin, 1992; Gelman, 2006), using the 'effectiveSize' and 'gelman.diag' functions implemented in the R package 'coda' v.0.19-4 (Plummer, 2006). If the runs had not converged successfully, longer MCMC chains were run. I ran each model for 100-500 million iterations. Convergence was achieved using 200 million iterations and a burn-in of 20 million, sampling every 20,000 iterations for the whole skull data set and all bones. A stepping-stone sampler was used to estimate marginal likelihood for each model (Xie et al., 2011), setting 500 stones to each run for 5000 iterations, with results processed using BTProcessR (Ferguson-Gow, 2020).

The best model fit was the lambda model with variable rates (lambda_var) (Venditti et al., 2011) which was chosen by comparing the marginal likelihoods of each of the models using the Bayes Factor and the 'BTprocessR' package in R (Ferguson-Gow, 2020) (Appendix 3, Fig. S3.6, Table S3.10). Trace plots and Gelman and Rubin diagnostics are shown for the lambda_var model (Appendix 3, Fig. S3.7; Table S3.11).

I processed outputs from the lambda model with variable rates using BTRTools (Ferguson-Gow, 2020) and combined them with a tree topology using the R package 'treeio' (Wang et al., 2020). Rate shifts with posterior probabilities > 0.6 and branch-specific rates were visualised for the best supported model. I estimated the average evolutionary rates through time for the whole cranium across Cetacea, and for each suborder, and for each cranial bone across Cetacea and for each suborder. These were visualised

using the `rttplotter` function and the `mytreebybranch` function from Felice (2021). Finally, mean log rates per family were also plotted using the `rjpp` output from BayesTraits. Several specimens are categorised as '*incertae sedis*' as they have not yet been formally assigned to a family and thus, they were not included in the plots showing family rates (Appendix 3; Table S3.1).

Finally, I used the output from the BTRTools to build density plots to compare evolutionary rates between suborders and families using methods from Felice (2021).

### *Evolutionary Rate by Clade*

I calculated the rate of morphological evolution in each bone in the skull for each of the suborders, again using pPC scores that represented 95% of the shape variation for the whole cranium. I used stochastic character mapping and the '`make.simmap`' function with an 'ARD' model in phytools to reconstruct ancestral state and transition histories across a sample of 100 simulated trees. Simmap sampling works by running simulations and then averaging the results at the nodes to obtain ancestral states, allowing for a more robust model which considers multiple possible outcomes of reconstructed history and provides information on uncertainty. I then used the '`paintAllTree`' function, soon to be added to the R package 'mvMORPH' (Clavel et al., 2015) to reconstruct the marginal ancestral state reconstructions from the sample of simulated trees. I summarised the evolutionary histories on all the simmap trees to obtain one reconstructed ancestral history on which I then fitted my morphometric data models. I applied the state-specific Brownian Motion (BMM) model in the '`mvgls`' function in mvMORPH v.1.1.4 (Clavel et al., 2015) with the option '`error = TRUE`' to mitigate sources of evolutionary rates inflation, including departures from Brownian Motion. This flexible approach also assesses model fit by jointly estimating the contribution of measurement error and any intra-specific variation (Bardua et al., 2021: in review).

### Disparity by Clade

I calculated disparity (Procrustes variance) for each of the bones and for the whole skull for each of the suborders and for Cetacea as a whole using the 'morphol.disparity' function geomorph (Adams et al., 2020). To directly compare across bones, I scaled total disparity by the number of landmarks and semi-landmarks for each bone.

To further illustrate disparity in the skull, I used the R package 'landvR' v.0.4 (Guillerme and Weisbecker, 2019) to calculate the Procrustes distance from the mean skull shape for a selection of key families. I plotted these results so that landmark colours are proportional to the Procrustes distances from the mean shape of all Cetacea, allowing clear indication of regions of high disparity for each clade. Families were chosen to represent early, middle, and late (including all extant mysticetes and odontocetes) members of each suborder. The final skulls represent the mean disparity of each selected family and the Procrustes distance from the mean shape for all Cetacea.

### Influences on cranial shape

After modelling rates of evolution and disparity through time, I tested whether rates of morphological evolution were correlated with ecological factors using phylogenetic MANOVAs (pMANOVAs) in mvMORPH (Clavel et al., 2015). As most of the ecological variables predominately related to diet, I first ran Chi-squared tests ($\chi^2$) to ascertain whether two variables are related or independent from one another and to inform which, if any, models with interactions to test. I found that there was a strong relationship between all variables except for echolocation ability and habitat ($\chi^2 = 8.509$, p = 0.484). Due to these relationships between dentition, diet, feeding method, and echolocation, I did not run pMANOVAs with interactions. As there was no clear relatedness between echolocation ability and habitat, I ran a pMANOVA with interactions for these variables and found that there was no strong effect of an interaction between them on skull shape ($F = 1.6009$, $p = 0.09$).

I then ran Type II pMANOVAs using the pPC scores explaining 95% of the total variation, with centroid size, dentition, diet, feeding method, echolocation ability, and habitat as the predictors. Applying the mvgls and manova.gls commands. I fitted multivariate phylogenetic models with Pagel's lambda using penalised likelihood. The significance of each predictor was assessed with Pillai's statistic and 1000 permutations. This flexible approach accommodates departures from single rate Brownian Motion models and thus is preferred over the approach implemented in geomorph. I corrected all p-values for false discovery rate using Benjamini-Hochberg correction (Benjamini and Hochberg, 1995; Benjamini and Yekutieli, 2001).

### *Disparity and Evolutionary Rate by Ecology*

I used the approaches described above for 'Disparity by Clade' and 'Evolutionary Rate by Clade' to calculate disparity and evolutionary rates for each ecological regime for dentition, diet, feeding method, echolocation ability, and habitat, in geomorph and mvMORPH, respectively.

All analyses were done in R v.3.5.0 (R Core Team, 2017).

## 3.4 Results

### *3.4.1 Morphology of the skull*

39 PC scores were necessary to capture 95% of the variation in skull shape across Cetacea (Appendix 3, Table S3.6). Between four and 30 pPC scores were required to represent the bones and skulls across the different suborders (Appendix 3, Table S3.6; S3.7; S3.8; S3.9; S3.12).

Archaeocetes, mysticetes, and odontocetes occupy distinct areas of the morphospace on PC1 and 2 (Fig. 3.2), with early members of each extant clade bridging these regions. PC1 accounts for 41.6% of skull shape variation and is dominated by shape change in the length of the rostrum. The negative end of PC1 represents the brachycephalic faces of suction-feeding species such as the Pliocene *Odobenocetops,* extant kogiids, and other snub-faced

species such as *Orcaella* sp., as well as some phocoenids. The positive end of PC1 is occupied by dolichocephalic, long snouted fish-eating species such as the extinct eurhinodelphinids and extant river dolphins.

PC2 accounts for 24.9% of total shape variation and predominantly reflects changes in the positioning of the nares. The negative end of PC2 is represented by early archaeocetes such as *Pakicetus* and *Ambulocetus* which have anteriorly positioned nares, with Eocene and Oligocene specimens occupying more intermediate positions on this axis. The positive end of PC2 is occupied by later Miocene and extant odontocetes which have nasals positioned high on the head. The mysticetes occupy the middle region of PC2, reflecting a contribution from the forward movement of posterior cranial elements (prograde cranial telescoping). See Appendix 3, Fig. S3.8 for a morphospace with phylogenetic relationships and Appendix 3, Fig. S3.9 for a morphospace with species names.
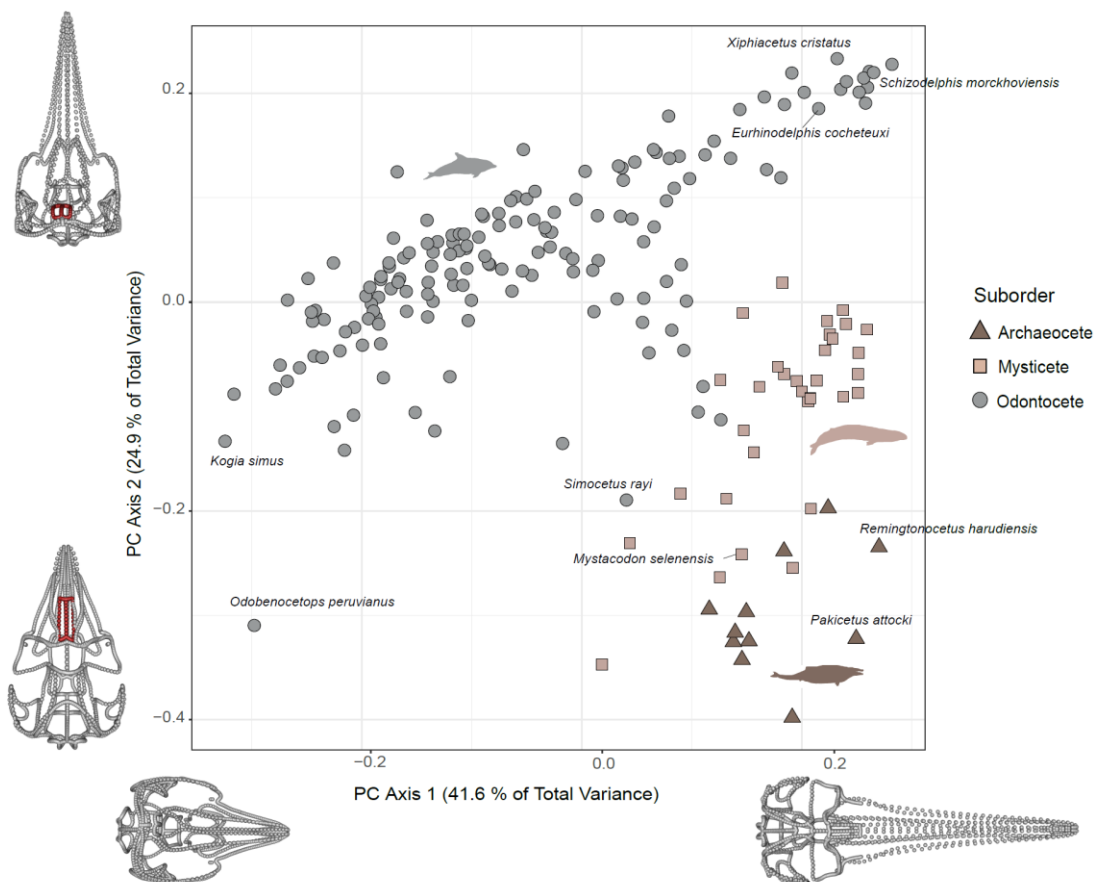
**Fig. 3.2.** Cetacean skulls in a morphospace. Morphospace of all 201 specimens using the entire landmark and curve semi-landmark data set. Skull shapes represent the positive and negative extremes along PC1 (41.6%) and PC2 (24.9%). Specimens that represent the extreme morphologies along each axis are highlighted. Note how the earliest odontocete in the data set (*Simocetus rayi*: Early Oligocene) and the earliest mysticete (*Mystacodon selenensis*: Late Eocene) occupy a position intermediate between the archaeocetes and the early odontocetes and mysticetes, respectively. Further, note the clustering of Eocene and Oligocene specimens in the morphospace and the clustering of morphologically similar Miocene and extant specimens, particularly in the mysticetes. For morphospaces of PC1 through PC4, see Appendix 3, Fig. S3.10-S3.12. For a morphospace labelled with species names, see Appendix 3, Fig. S3.9.

Odontocetes occupy the largest region of morphospace on these axes, spanning the full range of PC1, in comparison to the other subclades. Extant odontocetes define the upper left quadrant of the PC1-PC2 morphospace, which characterises a mid-length rostrum, a bulbous cranium, and nares that have moved posteriorly on the skull. Miocene odontocetes such as the extremely dolichocephalic Eurhinodelphinidae and Allodelphinidae dominate the upper right quadrant with their exceptionally elongated rostrums and posterior nasals (Fig 3.2). The middle region of the morphospace is occupied by Oligocene odontocetes, which bridge the regions occupied by archaeocetes and later Miocene and extant odontocetes. These Oligocene odontocetes in the centre of the morphospace include squalodontids, patriocetids, and early diverging xenorophids which have nares positioned slightly more anteriorly and still retain basal features such as heterodonty (Boessenecker et al., 2017).

Mysticetes occupy the positive end of PC1 and an intermediate position on PC2, a region defined by the characteristic elongating of the mysticete rostrum and the prograde telescoping of the mysticete nares. There is a clear division among mysticetes of different ages. The Eocene *Mystacodon selenensis*, which is not only the oldest mysticete in this data set but is also the oldest

known neocete (Lambert et al., 2017a; Geisler, 2017), sits proximal to the Eocene archaeocetes, while Oligocene mysticetes bridge the space between archaeocetes and modern baleen whales. One specimen of note is *Caperea marginata*, an extant mysticete and sole living representative of the family Cetotheriidae which displays a morphology that is highly unique among living mysticetes (Fordyce and Marx, 2013). *Caperea* sits closer in the morphospace to extinct forms such as *Miocaperea pulchra*, a fossil pygmy right whale from the Miocene (Bisconti, 2012), than it does to most extant mysticetes. The nares are further posteriorly positioned in the mysticetes than in their archaeocete ancestors which occupy the lower right quadrant of the morphospace, reflecting their long rostra and anteriorly placed nasals. It is noteworthy that extinct toothed mysticetes and archaeocetes overlap substantially in this cranial morphospace.

When individual bones were analysed separately, the number of PCs required to explain 95% of the variation ranged from four (basisphenoid) to 22 (maxilla). For most elements, especially the maxilla, *Odobenocetops peruvianus* is the most differentiated from other cetaceans in the bone-specific morphospaces (Appendix 3, Fig. S3.13-S3.26). Cetaceans are least differentiated in the basioccipital and basisphenoid morphospaces although *Odobenocetops* is again the most distinct (Appendix 3, Fig. S3.13 and S3.14). For the nasal, which contributes substantially to variation seen across the entire cranium, *Pakicetus attocki* and *Physeter macrocephalus* are the more distinct specimens, although in different ways (Appendix 3, Fig. S3.19). Bone-specific morphospaces are provided in Appendix 3, Fig. S3.13-S3.26). Fig. 3.3 shows positive (+) and negative (-) shape extremes for each bone. Note the variation in shapes in the maxilla (mint green: dorsal and ventral view), premaxilla (navy blue: dorsal and ventral view), and nasal (red: dorsal view) compared to the more conservative shape variation observed for the basioccipital (light blue: ventral view), basisphenoid (dark green: ventral view), and the occipital condyles (teal: posterior view) (Fig. 3.3).

DORSAL

Max + Max - Premax - Premax +

Nas - Nas +

Fron + Fron -

VENTRAL

Premax - Premax - Max +

Pal + Pal - Max -

Pteryg + Pteryg -

Bsphn + Bsphn -

Mandp + Mandp -

Bsocc + Bsocc +

LATERAL

Fron + (lateral view) Par - Par +

Fron - (lateral view)

zygo-squa zygo-squa -

POSTERIOR

Supocc + Supocc -

Occip + Occip -

153

| | | |
|---|---|---|
| ■ basisphenoid | ■ palate |
| ■ basioccipital | ■ parietal |
| ■ frontal | ■ premaxilla |
| ■ jugal | ■ pterygoid |
| ■ mandibular process | ■ supraoccipital |
| ■ maxilla | ■ squamosal (with zygomatic process) |
| ■ nasal | |
| ■ occipital condyles | |

[Figure on previous page]

**Fig. 3.3.** Shape variation per bone in the cetacean skull. Exploded view of positive (+) and negative (-) shape extremes for each cranial element (see Fig. 3.1 for the bone outlines). Positions of landmarks and semi-landmarks (coloured by bone) are shown on *Delphinus delphis* (AMNH 75332) in dorsal, ventral, lateral, and posterior view. Extreme shapes were generated from PCAs for each bone; thus, axis direction is arbitrary. The frontal (light pink) is shown in both dorsal and lateral view for clarity. bsocc = basioccipital, bsphn = basisphenoid, fron = frontal, mandp = mandibular process, max = maxilla, nas = nasal, occip = occipital condyles, pal = palate, par = parietal, premax = premaxilla, pteryg = pterygoid, supocc = supraoccipital, zygo-squa = zygomatic (including squamosal).

### *Allometry*

Allometry (or shape related to size) is a significant albeit relatively small contributor to skull shape variation (p < 0.001, $r^2$ = 0.15, F = 35.70).

### 3.4.2 Patterns of cranial evolution

I modelled the rate of evolution for the whole skull (Fig. 3.4; Fig. 3.6) and for separate bones (Fig. 3.5; Fig. 3.6 (1. a-d)). I also modelled rates of evolution for the different suborders (Fig. 3.6 (1. b-d); Fig. 3.7), and families (Fig. 3.8). The minimum plotted posterior probability for rate shifts was set to a threshold of 0.6 as determined by the count and log mean rate of the data. Convergence diagnostics are provided in Appendix 3, Table.S3.11; Fig. S3.7. A variable-rates Lambda model (Lambda_var) had the best model fit for the entire skull and for all individual skull bones (Appendix 3, Table. S3.10 and Fig. S3.6). Lambda was estimated as 0.69 for the whole skull. As a lambda equal to one is equivalent to a Brownian Motion model, lambda below one suggests departure from Brownian Motion, with more evolution occurring on terminal branches than expected from the phylogeny.

**Whole skull rates**

156
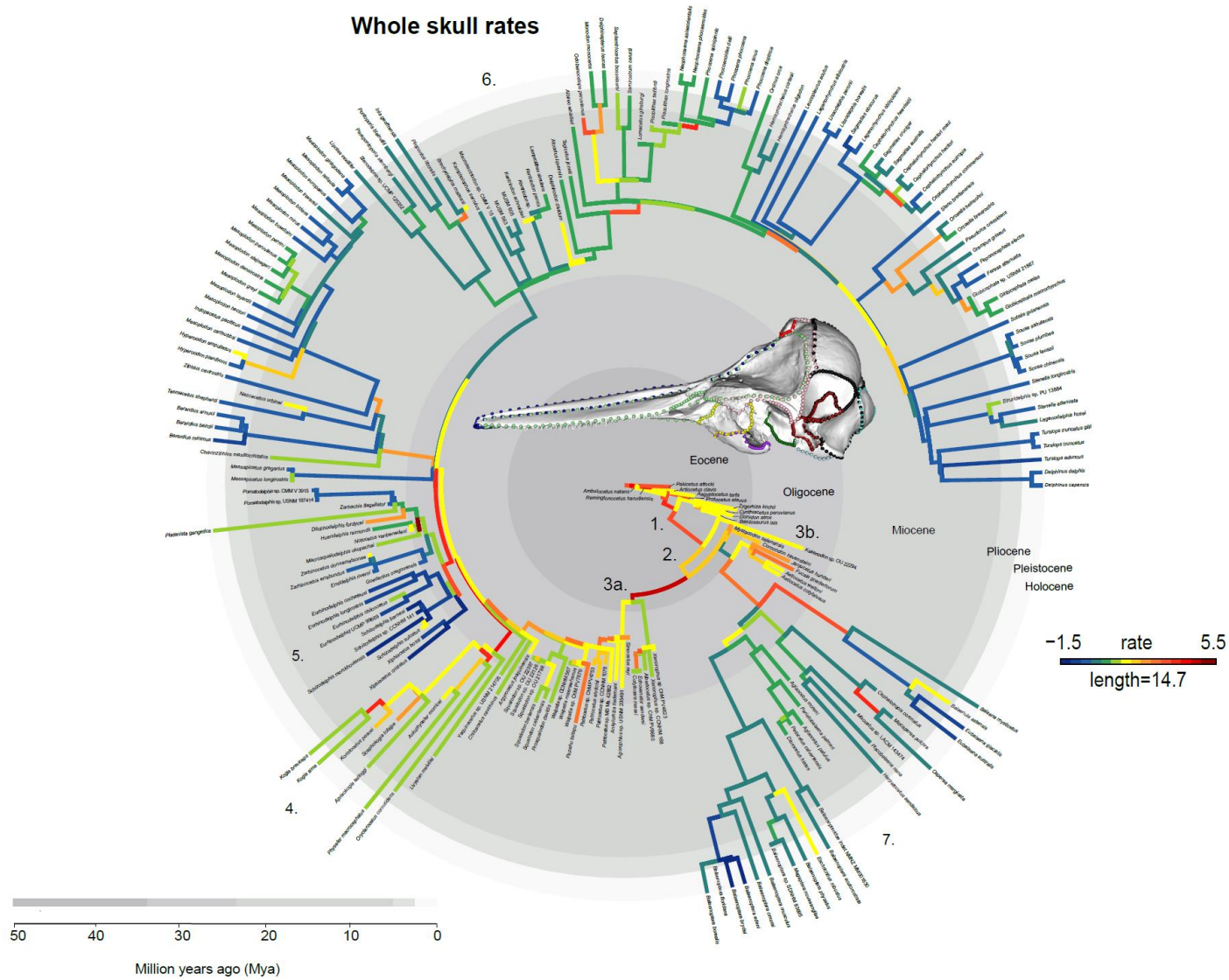
[Figure on previous page]

**Fig. 3.4.** Branch-specific rates of cranial evolution for Cetacea. Rates modelled using a variable-rates Lambda model of evolution. Numbers indicate: 1. archaeocetes; 2. the origin of Neoceti (~39-36 Mya); 3a. early diverging odontocetes; 3b. early diverging mysticetes; 4. Physeteroidea: 5. Eurhinodelphinidae; 6. extant odontocetes; and 7. extant mysticetes. A negative rate of evolution indicates a slowing down in the rate of trait change.

The highest rates are observed within the archaeocetes (Fig. 3.7), throughout the Mid Eocene and, and then at the end of the Eocene (~39-36 Mya), with the origin of Neoceti (Fig. 3.4). I observe high evolutionary rates in the newly diverging odontocetes (Fig. 3.4 (3a)) and mysticetes (Fig.3.4 (3b)) of the Late Eocene (mysticetes only) and early Oligocene. Thereafter, high rates of evolution are observed in the odontocete superfamily Physeteroidea (Fig. 3.4 (4)), which includes the kogiids (Fig. 3.8), and in the early divergence of the eurhinodelphinids from the Allodelphinidae, Squalodelphinidae, and Platanistidae. Rates rapidly slow down within the eurhinodelphinids in the Mid-Late Miocene (Fig. 3.4 (5)).

frontal rates

−2.1  rate  3.4
length=14.7

maxilla rates

−2.8  rate  4
length=14.7

nasal rates

−1.8  rate  3.4
length=14.7

premaxilla rates

−2.8  rate  3.7
length=14.7

basioccipital
rates

−3  rate  1.6
length=14.7

basisphenoid
rates

−2.7  trait value  2
length=14.7
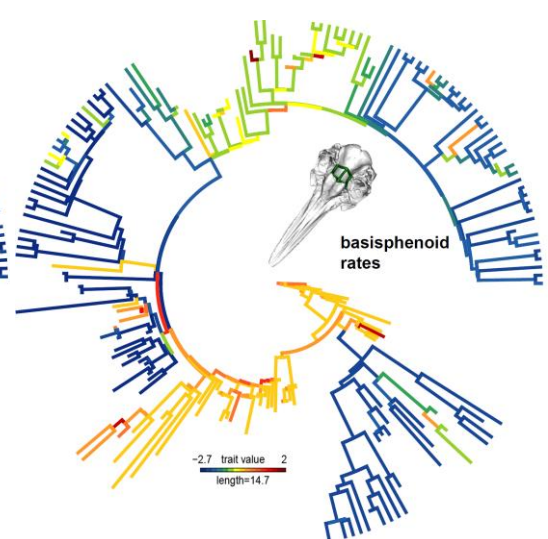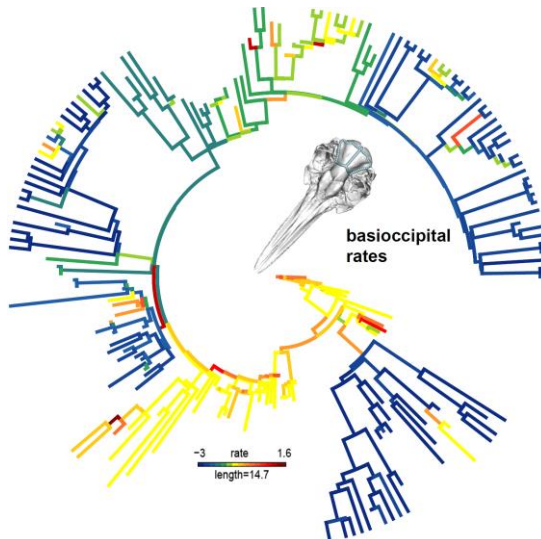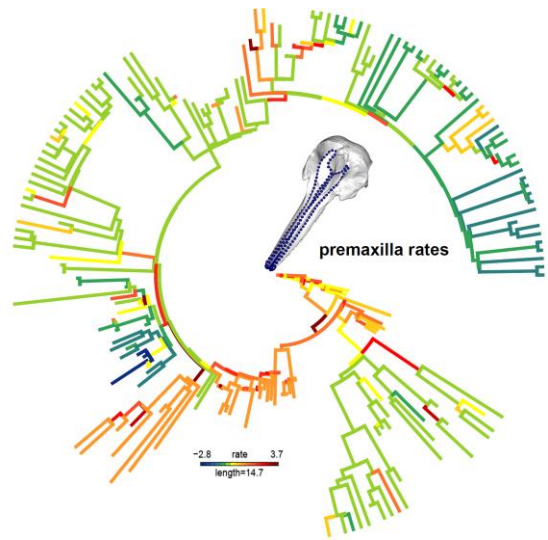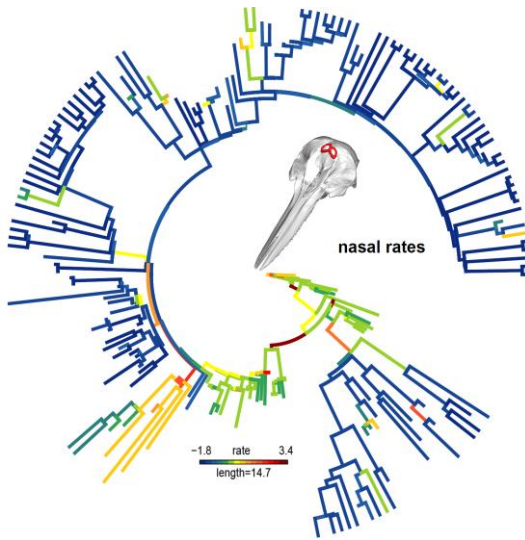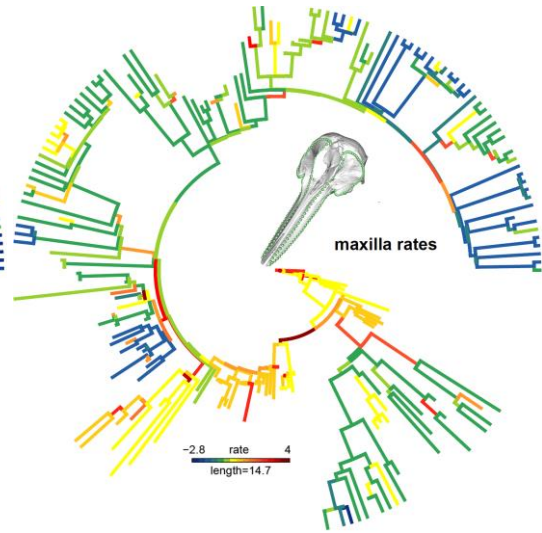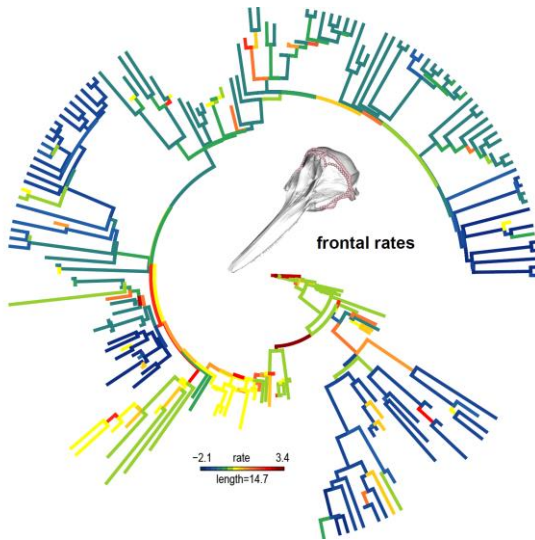
**Fig. 3.5.** Estimated rates of cranial evolution per bone - phylogeny. Rates shown on a time-calibrated phylogeny of Cetacea using a variable-rates Lambda model of evolution. Rates are calculated for individual bones. Reds and oranges show higher evolutionary rates, greens and blues show lower evolutionary rates. Top left to bottom right: frontal, maxilla, nasal, premaxilla, basioccipital, basisphenoid. The positioning of the landmarks for each respective bone is shown on the mesh in the centre of the phylogeny. Note the deep red colour of the branch in the frontal, maxilla, and nasal of the early diverging odontocetes.

### 3.4.3 Rates of cetacean cranial evolution through time

Across Cetacea, there are three key peaks in the rate of evolution in separate bones. These peaks are seen in the Late Eocene, the Mid-Late Oligocene and to a lesser extent in the Mid-Miocene (Fig 3.5; 3.6 (1)). Unsurprisingly, the nasal shows high rates of evolution, particularly in the Mid-Late Eocene. The archaeocetes show a peak in maxilla, premaxilla, and nasal rates in the Mid-Eocene (Fig. 3.6 (1.b)). The flatline in the data thereafter is due to there only being one archaeocete in the data set (*Kekenodon*) which lived into the Late Oligocene. The mysticetes show a peak in the evolutionary rates of several bones towards the end of the Eocene after the two suborders had diverged with a further peak in the Late Oligocene (Fig. 3.6 (1.c)). Thereafter, rates remain conservative. Note the deep red colour (high rates) of the branch leading to the earliest diverging odontocetes for the frontal, maxilla, and nasal in Fig. 3.5. As well as high rates in their early divergence, the odontocetes show several peaks in evolutionary rate (mostly in the maxilla, frontal, and nasal) in the Mid-Late Oligocene (Fig. 3.6 (1.d)) with smaller peaks in the Miocene.

1.

Bone

basioccipital
basisphenoid
frontal
jugal
mandibular process
maxilla
nasal
occipital condyles
palate
parietal
premaxilla
pterygoid
supraoccipital
squamosal
(with zygomatic process)

160

Evolutionary rate

**2.**

Records of earliest 'true' baleen
~ 27.5 Mya (Tsai and Fordyce,
2017)

Earliest mysticete in data set:
*Mystacodon selenensis*
~ 36.4 - 33.9 Mya

Earliest archaeocete in
data set:
*Pakicetus atrox*
~ 48.6 Mya

Earliest records of
echolocation ~ 33.9 Mya
(Fordyce, 2002)

Earliest odontocete in
data set: *Simocetus rayi*
~ 32.3-30.5 Mya

Eocene          Oligocene          Miocene          Pliocene    Pleistocene Holocene

Time from present (million years ago)
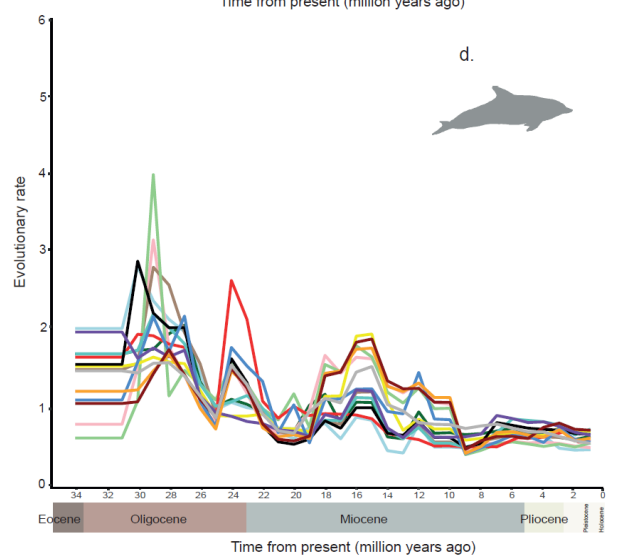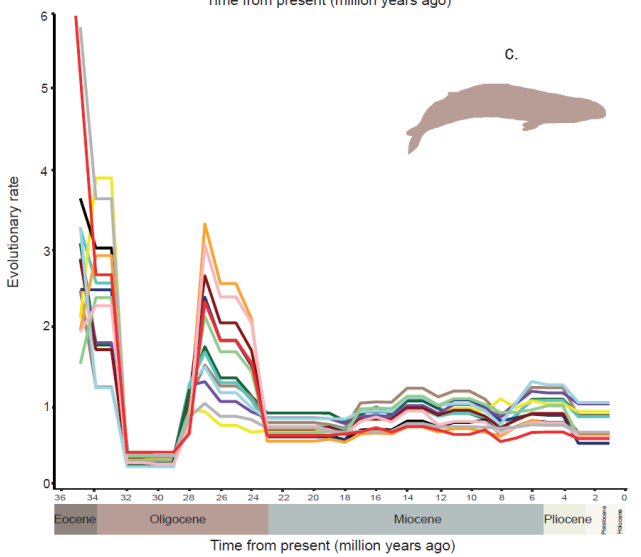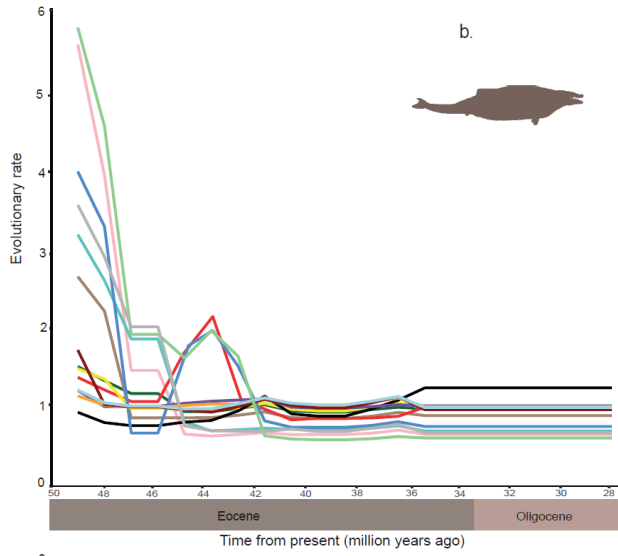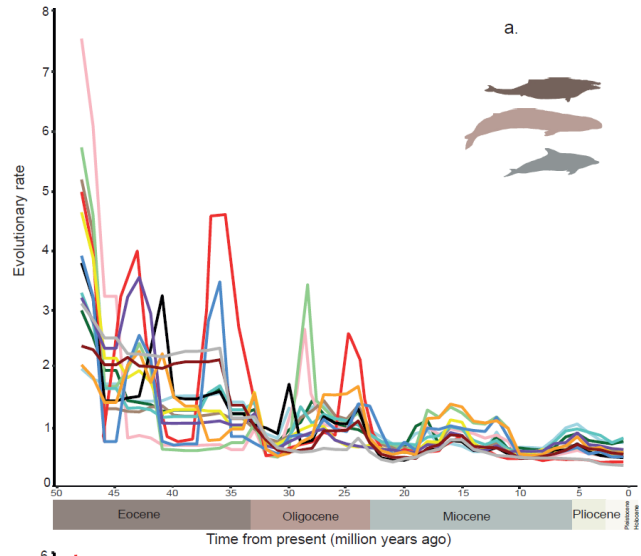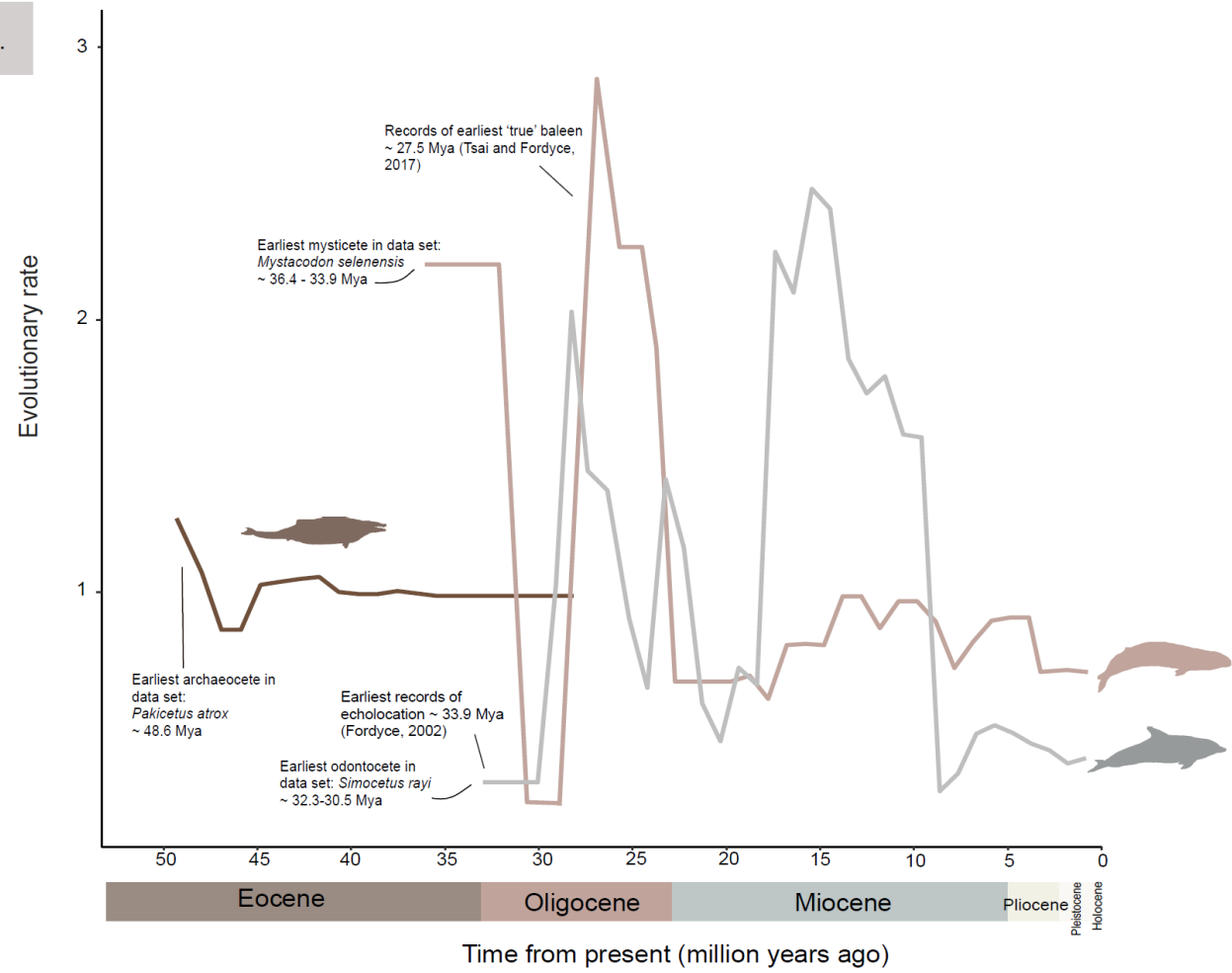
[Figure on previous page]

**Fig. 3.6.** Evolutionary rates per bone and across the skull for Cetacea and each suborder. Models run under the assumption of a Lambda model with variable rates of evolution. The y-axis shows evolutionary rate, the x-axis shows time from present (million years ago). **1.** Evolutionary rates per bone. **a.** evolutionary rate per bone for all cetaceans in this data set, **b.** evolutionary rate per bone for archaeocetes, **c.** evolutionary rate per bone for mysticetes, **d.** evolutionary rate per bone for odontocetes. Note that Cetacea (a) are represented on a different scale to the suborders (b-d). This was so that details in the suborder plots, which were lost on a larger scale, could be easily viewed. **2.** Average evolutionary rates across the whole skull for archaeocetes (dark brown), mysticetes (light brown), and odontocetes (grey).

### 3.4.4 Evolutionary Rate by Clade

A pairwise *t-test* with Bonferroni correction (Dunn, 1961) showed a significant difference between archaeocete and mysticete evolutionary rates ($p < 0.001$), archaeocete and odontocete rates ($p < 0.001$), and mysticete and odontocete rates ($p < 0.001$) (Fig. 3.7). Note the high rates in *Odobenocetops* (Fig. 3.8), a cetacean morphologically unlike any other in my data set. The family Odobenocetopsidae also accounts for the highest evolutionary (log mean) rates in odontocetes, followed by the early diverging Xenorophidae, Simocetidae, and later the kogiids (Fig. 3.8). General mid to high rates are observed in the patriocetids and waipatiids of the Oligocene, with the lowest rates seen in the later Eurhinodelphinidae, Lipotidae, and Iniidae (Fig. 3.8). The highest rates in the mysticetes are seen in the early diverging Mystacodontidae and Mammalodontidae, followed by Aetiocetidae, the last of the toothed mysticetes. The lowest rates are seen in the Balaenopteridae (Fig. 3.8). The highest rates in the archaeocetes are in Ambulocetidae, Remingtonocetidae, and Protocetidae (note that the high rates to the right of the density peak in this family are obscured by Remingtonocetidae). The lowest rates are seen in the Kekenodontidae (Fig. 3.8).
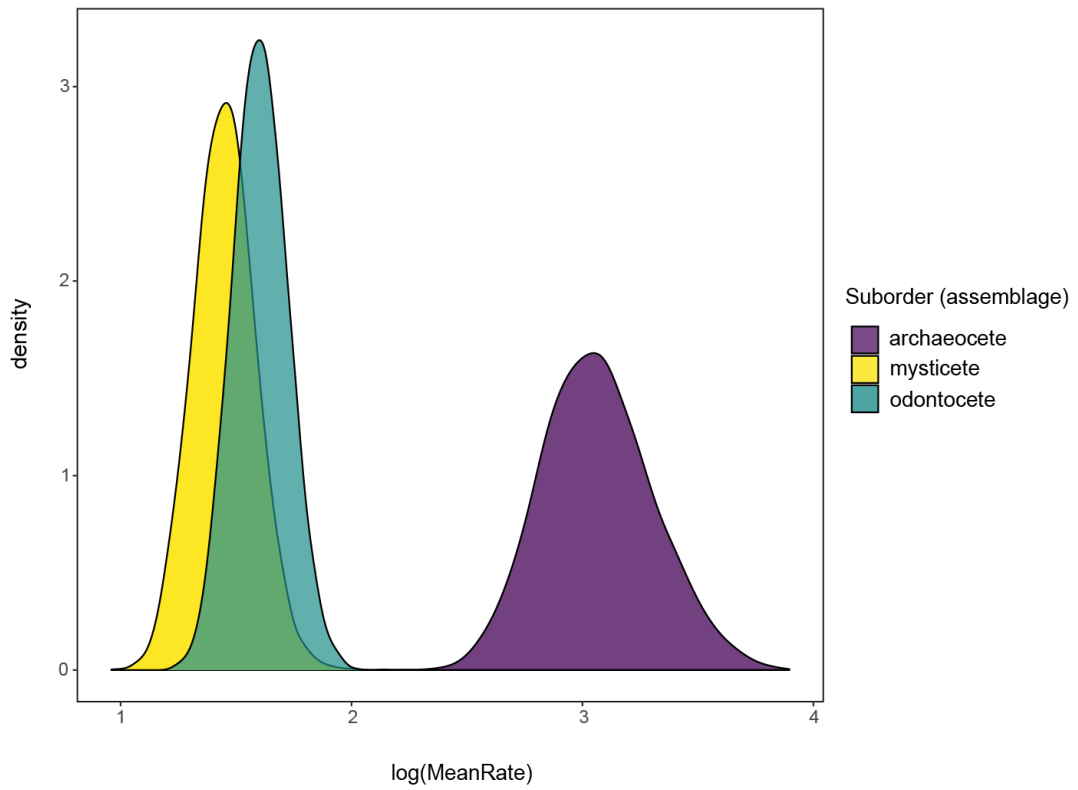
**Fig. 3.7.** Mean log rates and the density of specimens per suborder. Rates were obtained from the `rjpp` output from BayesTraits (http://www.evolution.rdg.ac.uk/) based on pPC scores that explain 95% of skull shape variation.
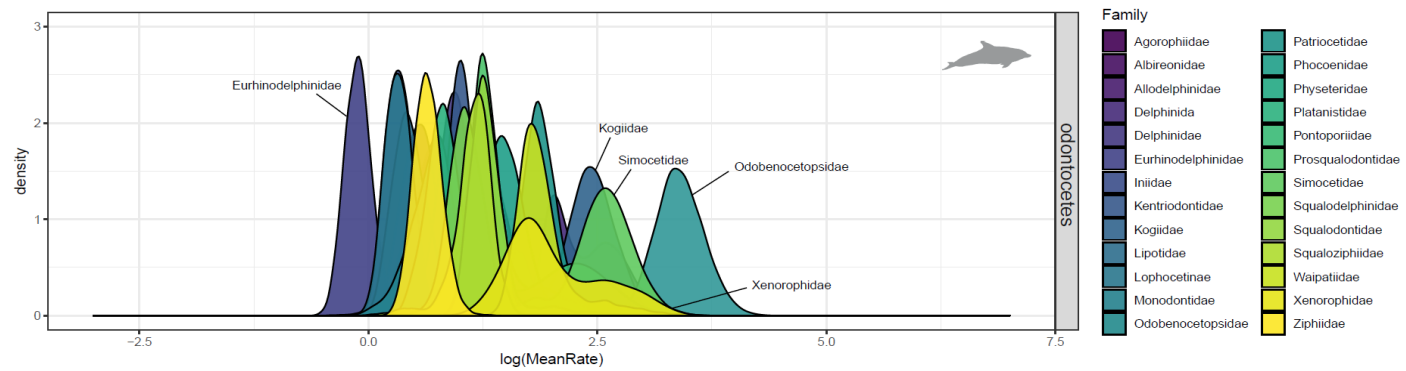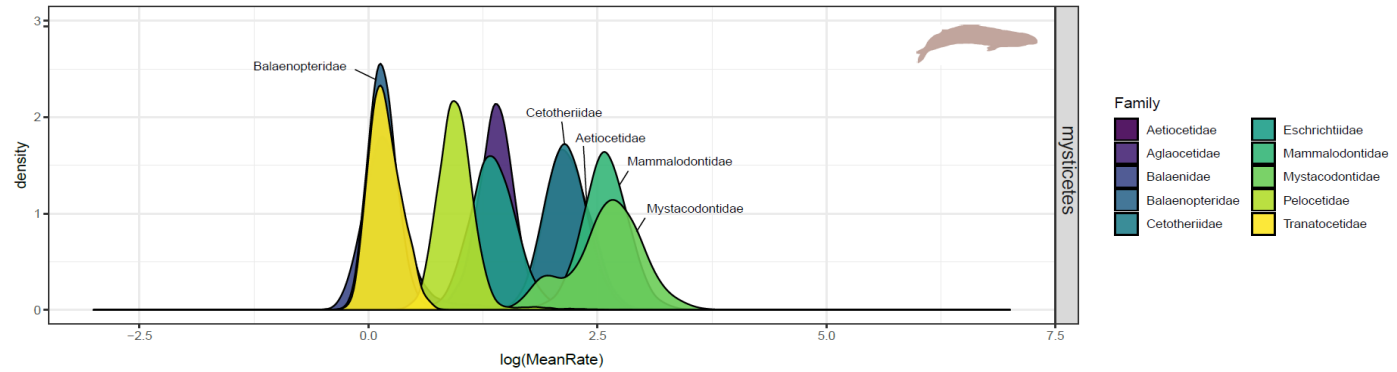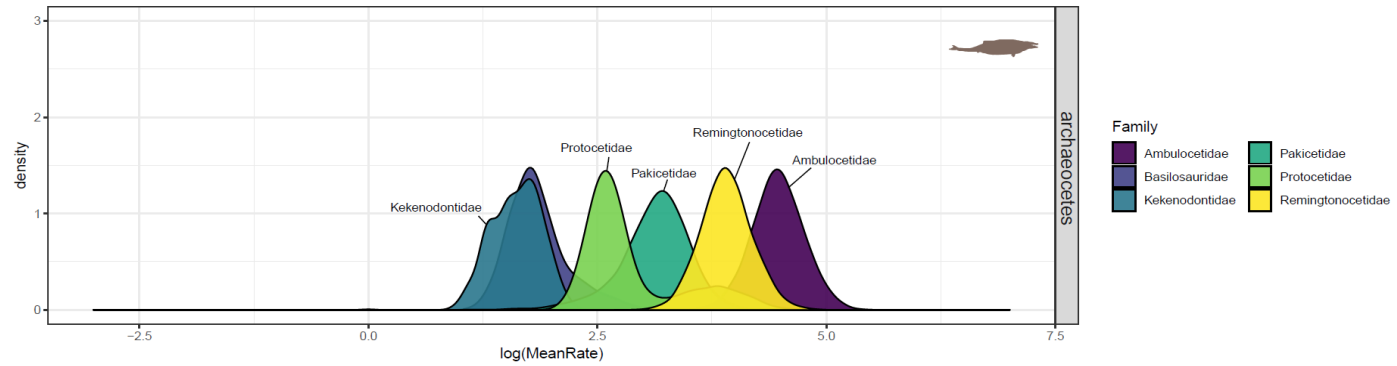
[Figure on previous page]

**Fig. 3.8.** Distribution of log mean rates of skull evolution for each family within the three suborders. Rates were obtained from the `rjpp` output from BayesTraits (http://www.evolution.rdg.ac.uk/) based on pPC scores that explain 95% of skull shape variation.

In addition, I quantified rates of evolution per suborder and per bone in mvMORPH using the state-specific Brownian Motion (BMM) model in the 'mvgls' function. I found that archaeocetes have the highest rates of evolution ($\sigma^2_{mult} = 123.02$), followed by odontocetes ($\sigma^2_{mult} = 16.87$) and mysticetes ($\sigma^2_{mult} = 15.91$) (Fig. 3.7; 3.9) Across the skull, the highest evolutionary rates were seen in the archaeocete skull, with the highest rates in the maxilla and nasal ($\sigma^2_{mult} = 53.64$ and 52.44, respectively) (Fig. 3.9; Appendix 3, Table S3.14). Although evolving at a lower rate than the archaeocetes, the highest rates in odontocetes were seen in the nasal ($\sigma^2_{mult} = 16.14$) and in the mysticetes in the maxilla ($\sigma^2_{mult} = 14.60$). Mysticetes have the lowest rates across all bones except the maxilla, jugal, mandibular process, and zygomatic (with squamosal).
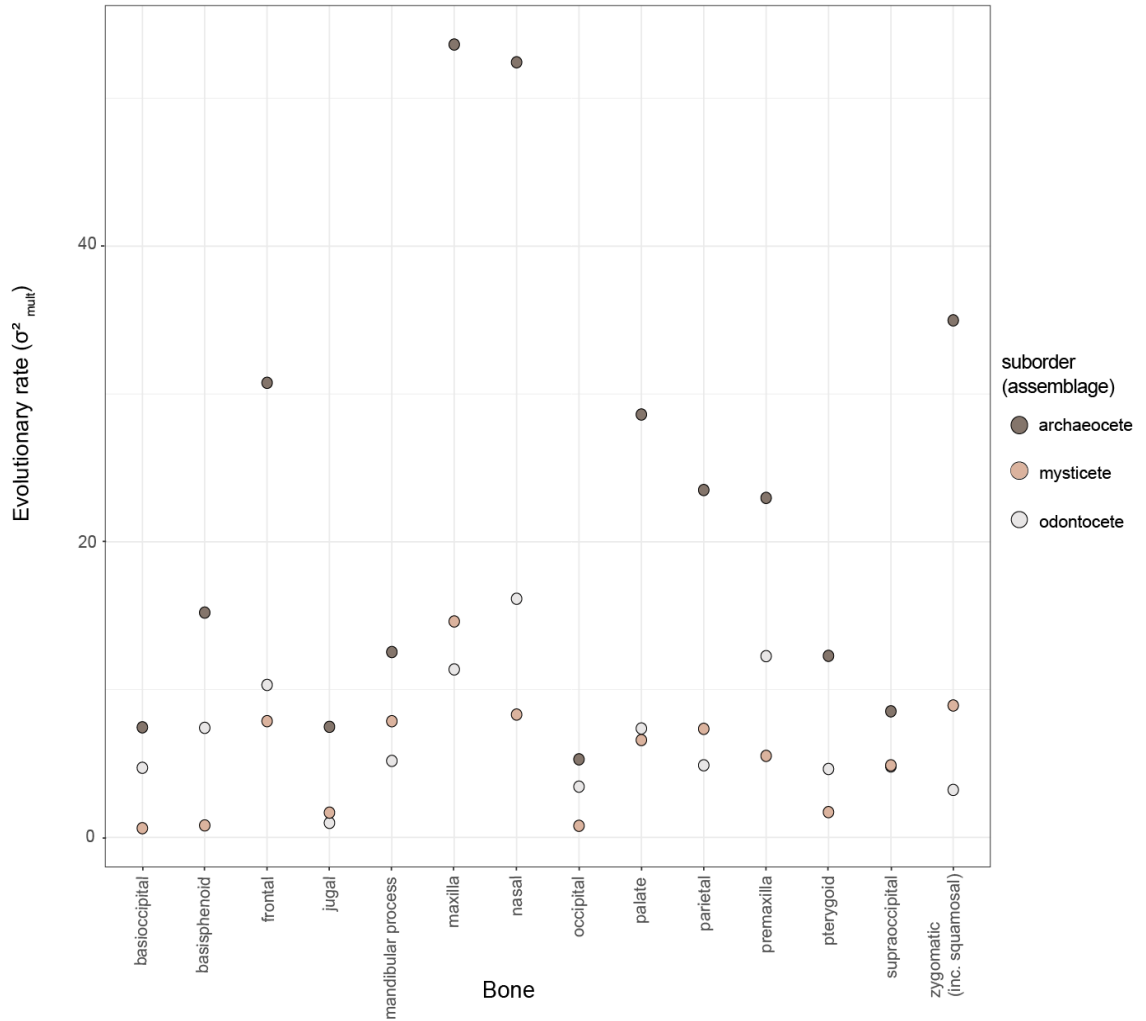
**Fig. 3.9.** Evolutionary rates ($\sigma^2_{mult}$) per bone, per suborder (assemblage). Archaeocetes (dark brown), mysticetes (orange), and odontocetes (light grey).

### 3.4.5 Disparity by Clade

Although the archaeocetes have the highest rates of evolution across the skull (most of which is attributed to the maxilla, frontal, premaxilla, and nasal (Fig. 3.6 (1.b)), they have the lowest disparity across the skull (measured as Procrustes variance; $pv$) ($pv = 1.68 \times 10^{-2}$). Disparity across the mysticetes and odontocete skull is higher: $pv = 5.84 \times 10^{-2}$, $pv = 6.75 \times 10^{-2}$, respectively. The archaeocete maxilla is the most disparate of the skull bones in this early whale assemblage ($pv = 3.27 \times 10^{-3}$) but the level of disparity is much lower

than that seen in the mysticete and odontocete maxilla ($pv$ = 1.36 x 10$^{-2}$; 1.60 x 10$^{-2.}$, respectively) (Fig. 3.10; Appendix 3, Table S3.15). The highest disparity is seen in the naso-facial region of the odontocetes and the mysticetes (Fig. 3.10). The maxilla shows the highest disparity, followed by the premaxilla, and frontal in both suborders (Fig. 3.3; 3.10; Appendix 3, Table S3.15). The lowest disparity is found in the ventral and posterior regions of the skull in the occipital condyles, basioccipital, and basisphenoid across Cetacea (Fig. 3.10). This low disparity is also reflected in the minimum and maximum shapes of these bones, which are relatively conservative in total shape range (Fig. 3.3).
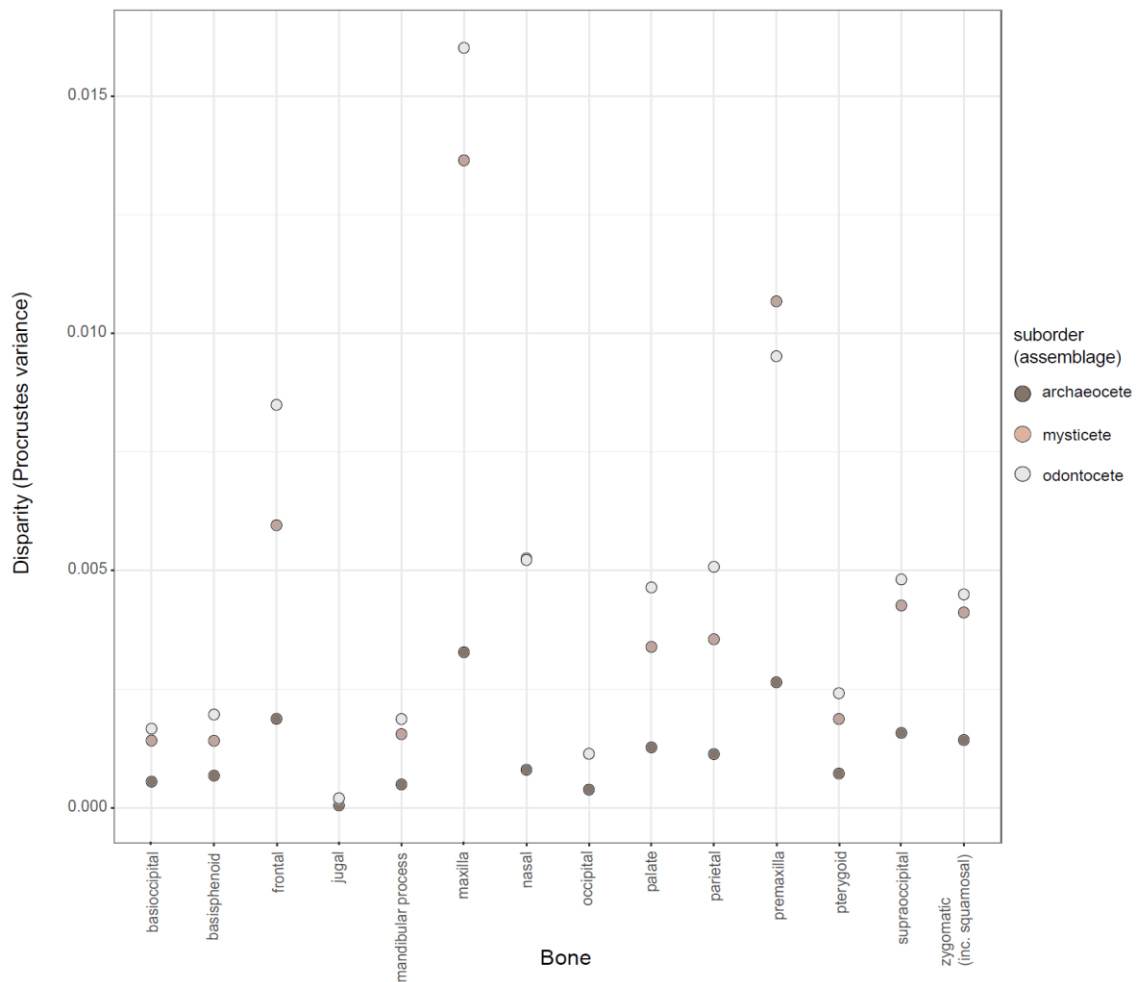


**Fig. 3.10.** Disparity (Procrustes variance) per bone, per suborder (assemblage). Archaeocetes (dark brown), mysticetes (orange), and odontocetes (light grey).

To further visualise the distribution of disparity across the skull, I calculated the distance from the mean skull shape for all landmarks and curve semi-landmarks in some key families. The hotter colours show a higher Procrustes distance, or greater variation from the average skull shape (Fig. 3.11). When compared to the average cetacean skull shape, the predominant differences Pakicetidae, Basilosauridae, and Protocetidae are concentrated in the positioning of the nares. In the mysticetes, hotter colours in the nares indicate high Procrustes distances between early mysticetes, such as the mammalodontids and aetiocetids, and the mean skull shape. Later across mysticetes, the highest Procrustes distances (disparity) in the rostrum is seen along the whole length of the premaxilla and maxilla from the antorbital and lateral processes to the tip of the rostrum. The early odontocetes (represented by Xenorophidae, Patriocetidae, and Squalodontidae) do not show marked deviation from the mean shape, but in later odontocetes, there is high family-specific variation from the mean skull shape (Fig. 3.11). *Odobenocetops* (Fig. 3.2; Appendix 3, Fig. S.13-S.26) exhibits a large amount of phenotypic variation from the mean skull shape, illustrated by the hot colours (reds, oranges) over most of the skull (Fig. 3.11). In the Eurhinodelphinids and some extant river dolphin families (Lipotidae, Iniidae, Platanistidae, but not Pontoporiidae), variation from the mean specimen is highest in the rostrum, which is highly elongated in these families but not in some pontoporiids such as *Brachydelphis mazeasi*. Generally, in odontocetes, high variation from the mean in extant families is concentrated in the naso-facial region and is particularly high in the delphinids and monodontids (Fig. 3.11).
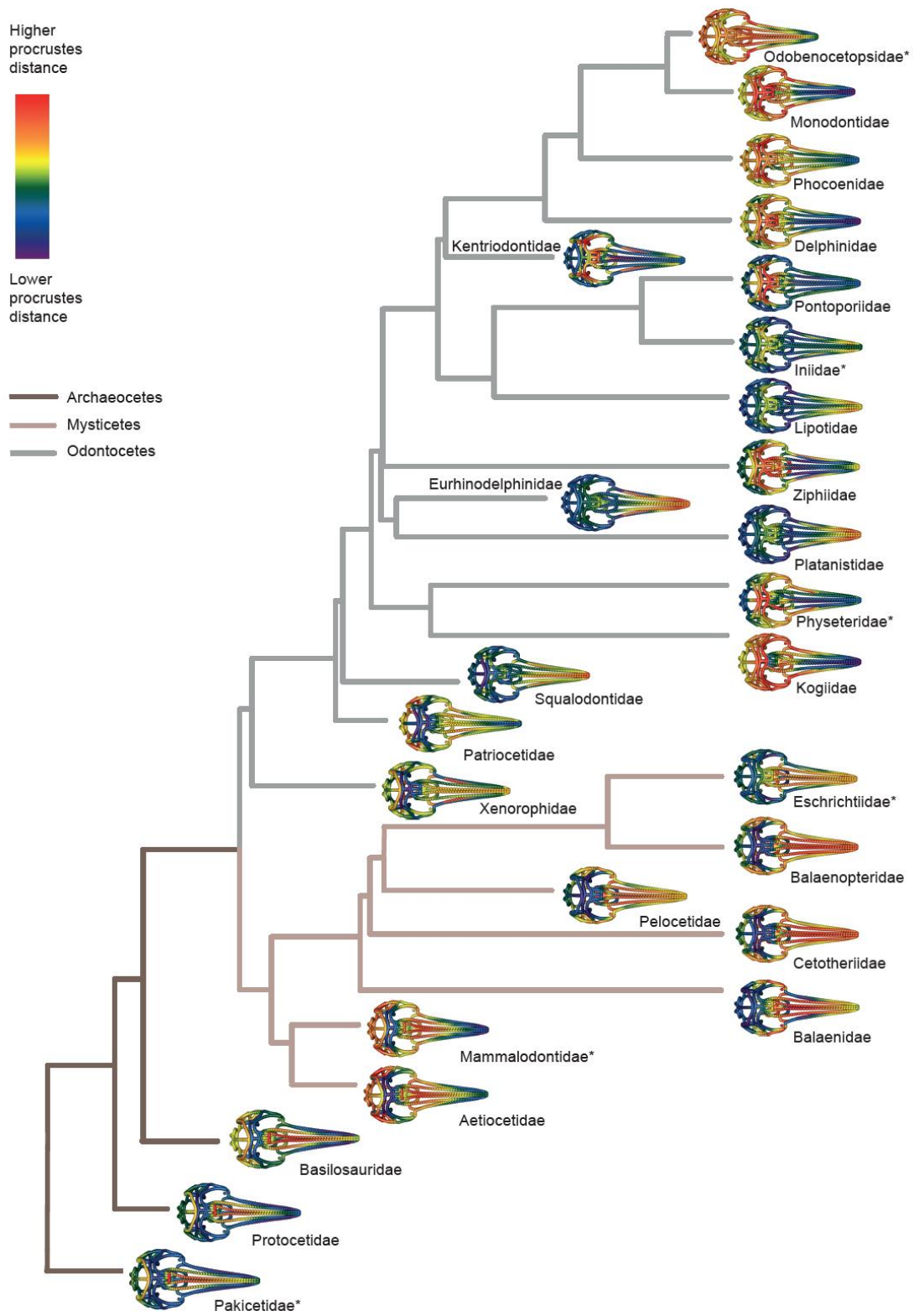
[Figure on previous page]

**Fig. 3.11.** Disparity across the skull in cetacean families. Each depicted cranium displays the difference between mean skull shape for that family compared to the mean skull shape for Cetacea, with hotter colours indicating greater Procrustes distance (greater difference) in landmark positions. *Indicates families represented by only one specimen in this dataset.

### 3.4.6 Disparity and Evolutionary Rate by Ecology

#### pMANOVAs

Phylogenetic MANOVAs of pPC scores that represented 95% of the shape variation for the whole cranium supported all ecological categories: dentition, main diet component, echolocation ability, feeding method, and habitat as showing a significant effect on skull shape. After correction for false discovery rate using the Benjamini-Hochberg method (Benjamini and Hochberg, 1995; Benjamini and Yekutieli, 2001), diet (effect size (es) = 4.51, $p < 0.001$), echolocation (es = 4.18, $p < 0.001$), dentition (es = 3.29, $p < 0.001$), size (es = 2.98, $p < 0.001$), feeding (es = 2.63, $p < 0.008$), and habitat (es = 2.11, $p < 0.02$) have a significant effect on skull shape. I then looked at the effects of these ecological variables on rate of evolution in each of the bones (Fig. 3.12 (a-e)).

#### Evolutionary rates by ecological category

When separated by dentition, heterodont cetaceans have the highest evolutionary rate of any group ($\sigma^2_{mult}$ = 109.95) (Appendix 3: Section 1 - Ecological rates). Further, heterodont whales have the highest rate of evolution across every bone in the skull (Fig. 3.12 (a)). Generally, the lowest evolutionary rates per bone belong to the 'reduced' dentition feeders and the baleen feeders with the exception of the maxilla, mandibular process, and zygomatic (including squamosal) in the baleen whales which have the second highest rates of any group ($\sigma^2_{mult}$ = 13.04; 6.38; 5.78, respectively), although these are far behind rates per bone seen in heterodont whales (Fig. 3.12 (a): Appendix 3, Table S3.16).

When separated by dietary factor, the highest evolutionary rates ($\sigma^2_{mult}$) are seen in cetaceans that feed predominantly on benthic invertebrates + fish ($\sigma^2_{mult}$ = 131.98), and the lowest evolutionary rates are seen in cetaceans that feed on zooplankton + fish ($\sigma^2_{mult}$ = 11.82) (Appendix 3: Section 1 - Ecological rates). A similar pattern is also seen when individual bones are analysed separately (Fig. 3.12 (b)). Compared to other dietary categories, cetaceans that feed on benthic invertebrates + fish have high rates of evolution in the nasal, parietal, premaxilla, and maxilla ($\sigma^2_{mult}$ = 53.40; 51.17; 45.70; 42.98, respectively). There are also high evolutionary rates in the nasal of species that feed on tetrapods + fish ($\sigma^2_{mult}$ = 50.82). The lowest evolutionary rates per bone generally belong to zooplankton + fish feeders and cephalopod + fish feeders, with piscivores commonly having intermediate rates (Fig. 3.12 (b); Appendix 3, Table S3.17).

When separated by echolocation ability, evolutionary rates are generally higher in cetaceans that cannot echolocate (archaeocetes, mysticetes, and the odontocete, *Odobenocetops*: band1) (Appendix 3: Section 1 - Ecological rates), with some exceptions. Rates are highest in the maxilla ($\sigma^2_{mult}$ = 22.43) and nasal ($\sigma^2_{mult}$ = 20.25) of non-echolocating, band1 cetaceans and also highest in the maxilla ($\sigma^2_{mult}$ = 10.30) and nasal ($\sigma^2_{mult}$ = 16.51) of band2 cetaceans (all echolocating odontocetes) (Fig. 3.12 (c), Appendix 3, Table S3.18). The high rates in band1 are reflecting the signal of high evolutionary rates seen in archaeocetes and early mysticetes.

When separated by feeding category, suction feeders (including but not exclusively) early mysticetes (e.g., the aetiocetids), most members of Physeteroidea (e.g., kogiids), Ziphiids (beaked whales), and monodontids (narwhals and belugas) have the highest evolutionary rates ($\sigma^2_{mult}$ = 44.15) (Appendix 3: Section 1 - Ecological rates). Filter feeders, which are all baleen-baring mysticetes and all Miocene or younger in age (in this study), generally have the lowest evolutionary rates across the skull ($\sigma^2_{mult}$ = 9.96) and in individual bones (Fig. S12 (d); Appendix 3, Table S3.19).

When separated by habitat, the highest rates across the skull are seen in cetaceans that live in coastal ($\sigma^2_{mult}$ = 29.74) and coastal-pelagic ($\sigma^2_{mult}$ =

27.78) environments, with the lowest rates seen in freshwater (riverine) inhabitants ($\sigma^2_{mult}$ = 0.49) (Appendix 3: Section 1 - Ecological rates). Similar patterns are seen in results for individual bones, with some of the highest rates of evolution in the nasal (the highest at $\sigma^2_{mult}$ = 31.64 in coastal cetaceans), frontal, premaxilla, and maxilla of coastal and coastal-pelagic inhabitants (Fig. 3.12 (d); Appendix 3, Table S3.20) and the lowest rates in the riverine taxa.
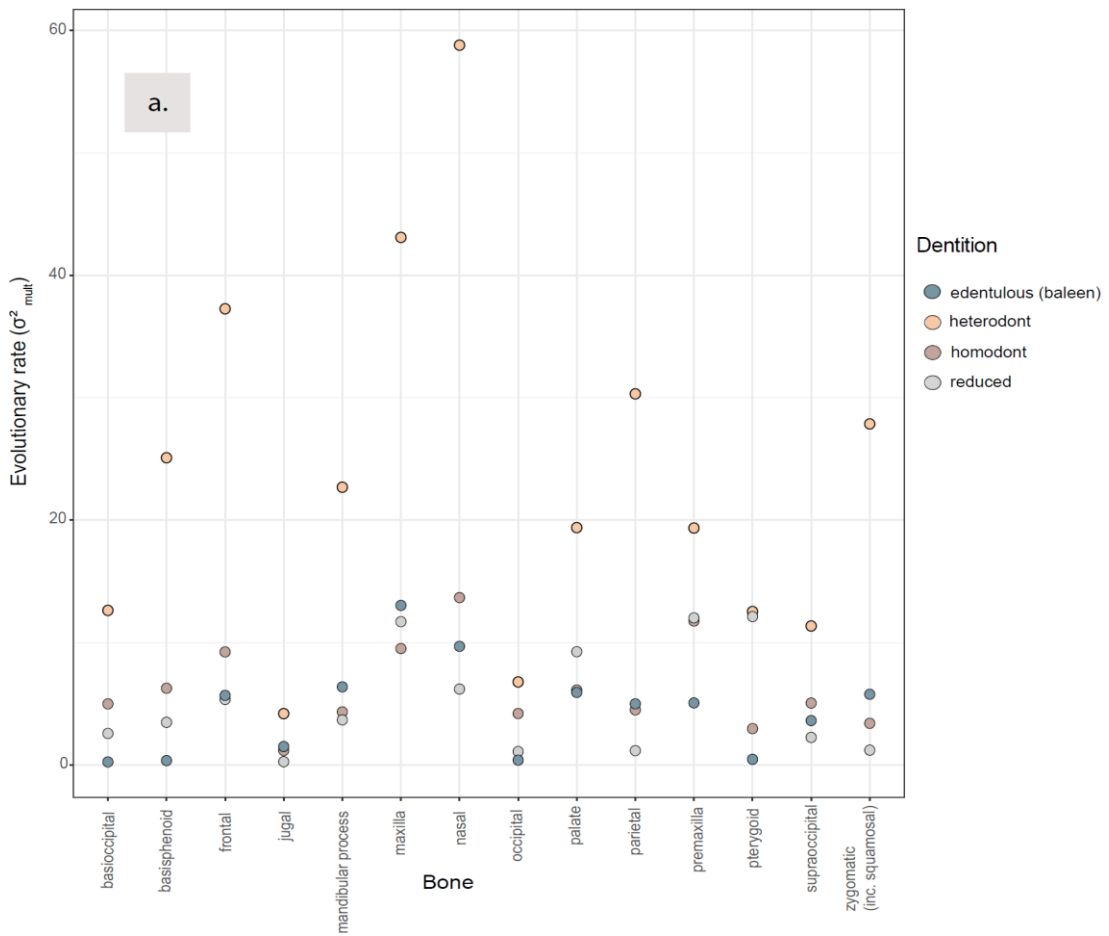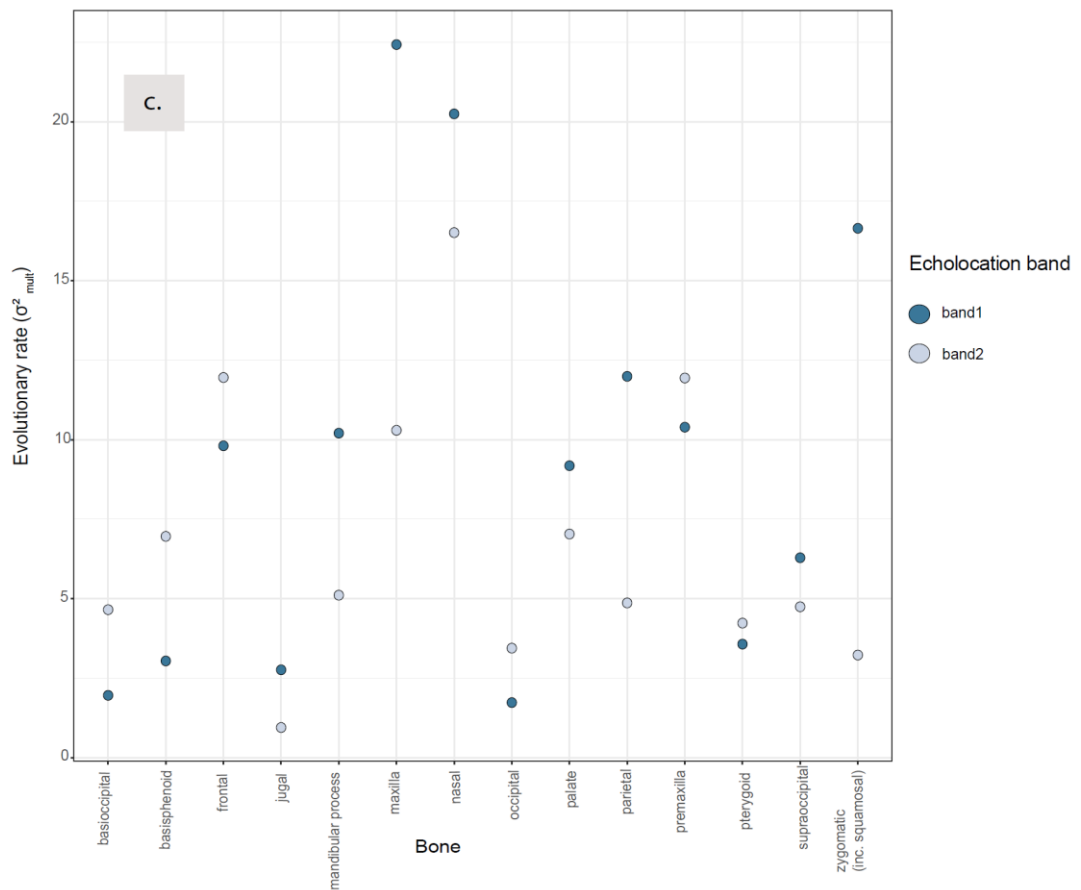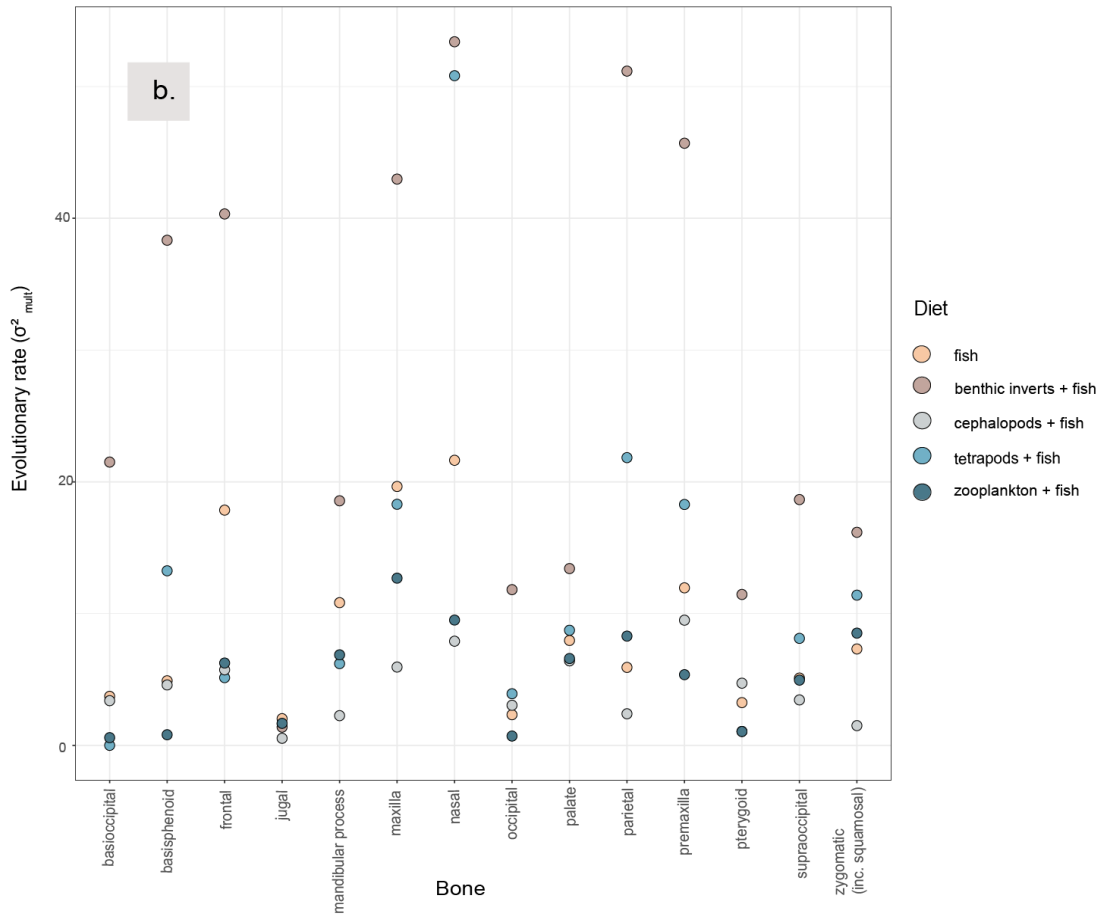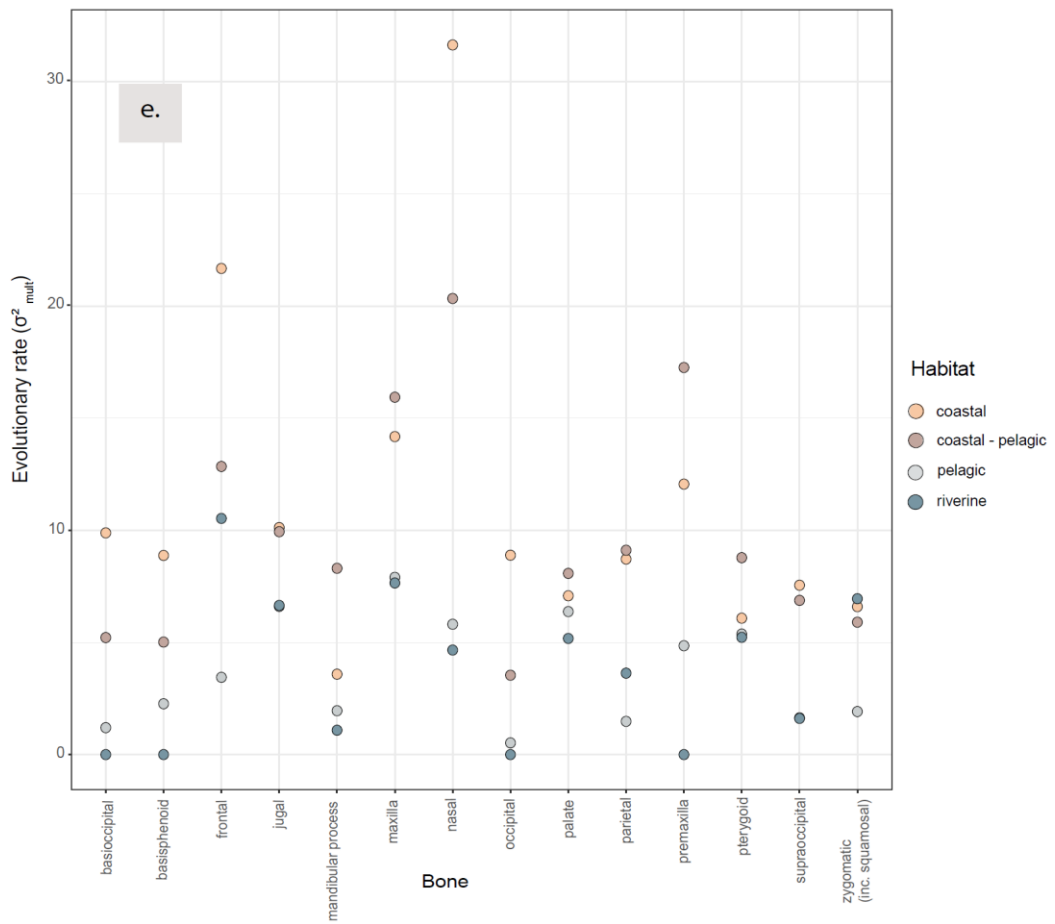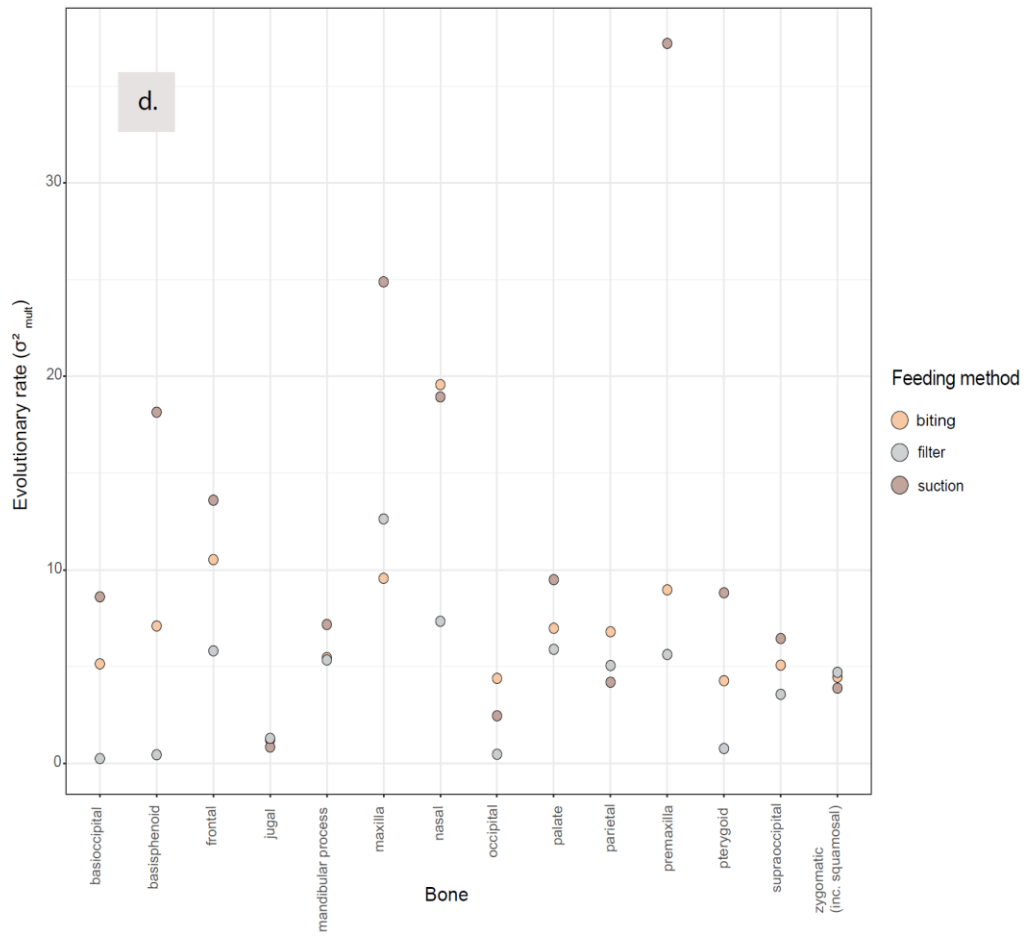
[Figure on previous page]

**Fig. 3.12 (a-e).** Evolutionary rates per bone per ecological factor. Rates calculated using the whole cetacean data set. a. Dentition categories: edentulous (baleen), heterodont, homodont, reduced. b. Diet categories: fish, benthic invertebrates + fish, cephalopods + fish, tetrapods + fish, zooplankton + fish. c. Echolocation ability: Band1: Not capable of echolocation (archaeocetes and mysticetes), Band2: Fully echolocating (all odontocetes except Odobenocetops). d. Feeding method: biting, filter, suction. e. Habitat type: coastal, coastal-pelagic, pelagic, riverine. Raw data can be found in Appendix 3, Table S3.16-20).

*Disparity by ecological category*

Across all cetaceans, disparity is highest in the maxilla, premaxilla, frontal, and nasal and lowest in the jugal, and posterior (occipital condyles) and ventral (basioccipital and basisphenoid) (Fig. 3.10). The highest disparity is seen in across the bones of cetaceans with reduced dentition (Fig. 3.13 (a); Appendix, Table S3.21), such as the beaked whales (Ziphiids), all of which are suction feeders that feed on cephalopods + fish. Suction feeders have the lowest disparity (of all feeders) in the posterior and ventral of the skull and high disparity is concentrated in the face and other parts of the skull (Fig, 3.13 (d); Appendix 3, Table S3.24). Generally, the lowest disparity is seen across the bones of the filter feeders, that is the mysticete whales from the Miocene to the present day (Fig. 3.13 (d)). When separated by dietary factor, there is no group that is consistently more disparate across the whole skull (Appendix 3: Section 2 - Ecological disparity); however, when considering separate bones, it is clearer to see that feeders on zooplankton + fish generally have some of the lowest levels of disparity across bones (Fig. 3.13 (b); Appendix 3, Table S3.22). Echolocating cetaceans (solely the odontocetes) have the highest disparity across each bone, with lower disparity seen in taxa that do not echolocate (the archaeocetes and mysticetes) (Fig. 3.13 (c): Appendix 3, Table S3.23). Finally, when categorised by habitat, some of the highest disparity is observed in the skulls of pelagic cetaceans, which includes all mesoplodonts and some oceanic dolphins. The lowest disparity is seen in the

bones of the skull of riverine cetaceans, which comprises the 3 extant freshwater species in this study (*Inia geoffrensis*, *Lipotes vexillifer*, and *Platanista gangetica*).
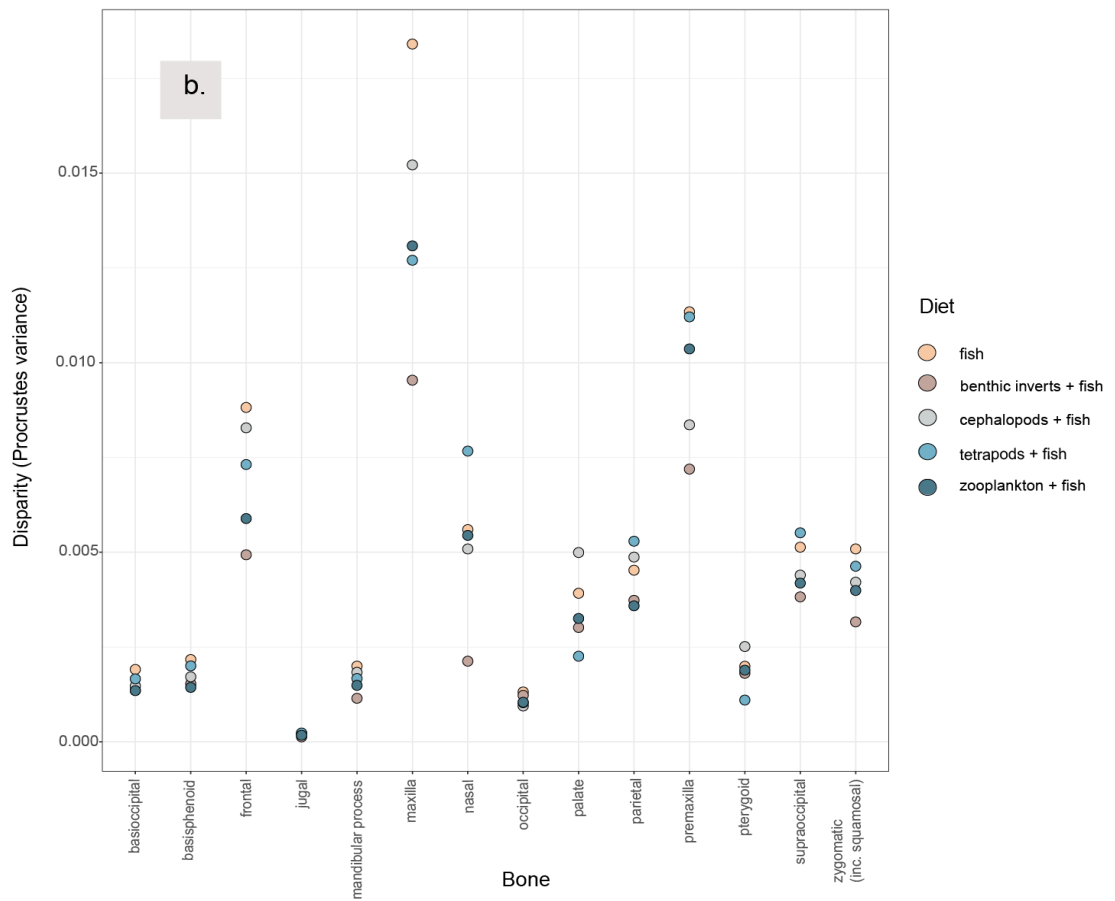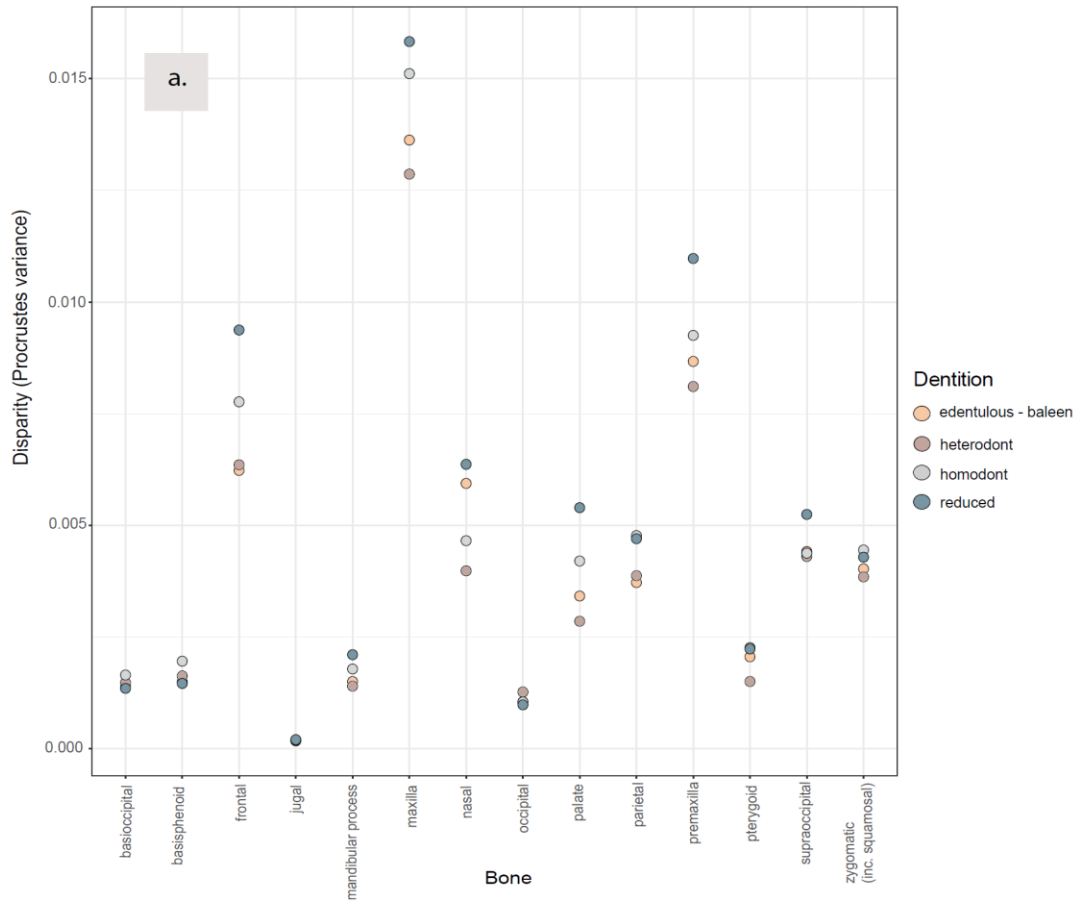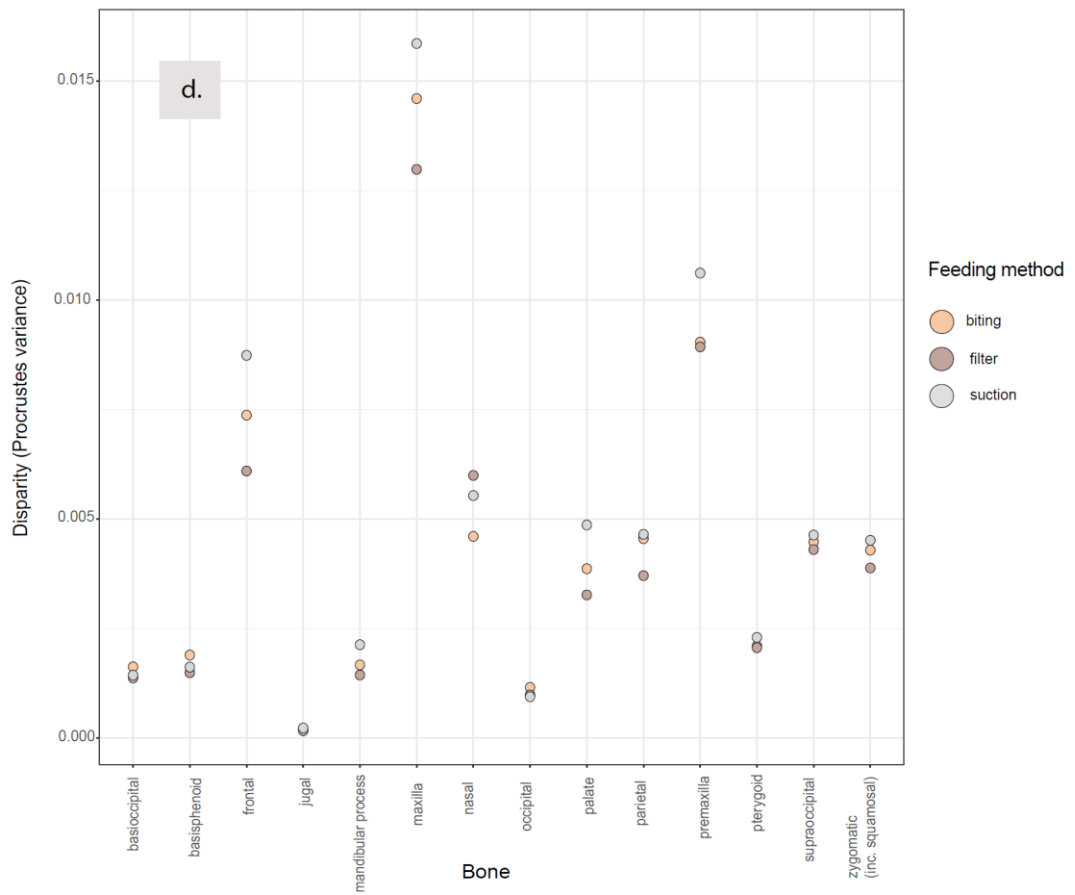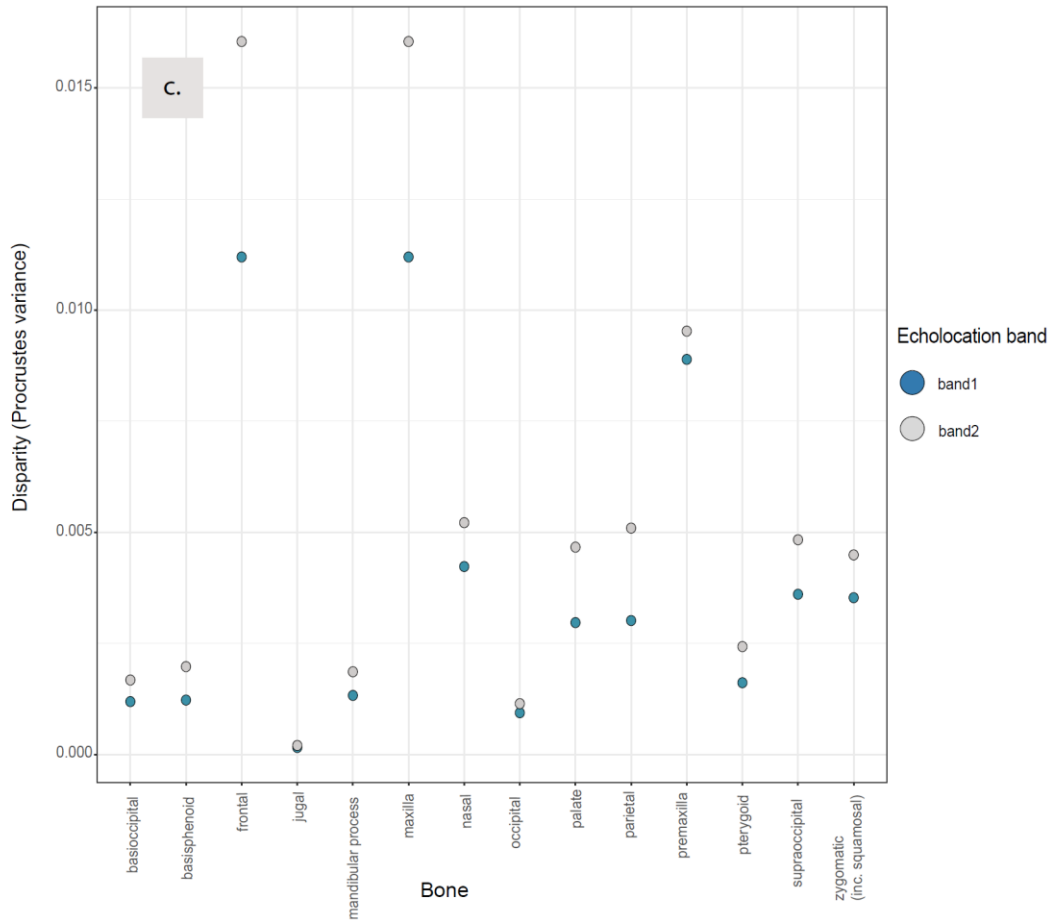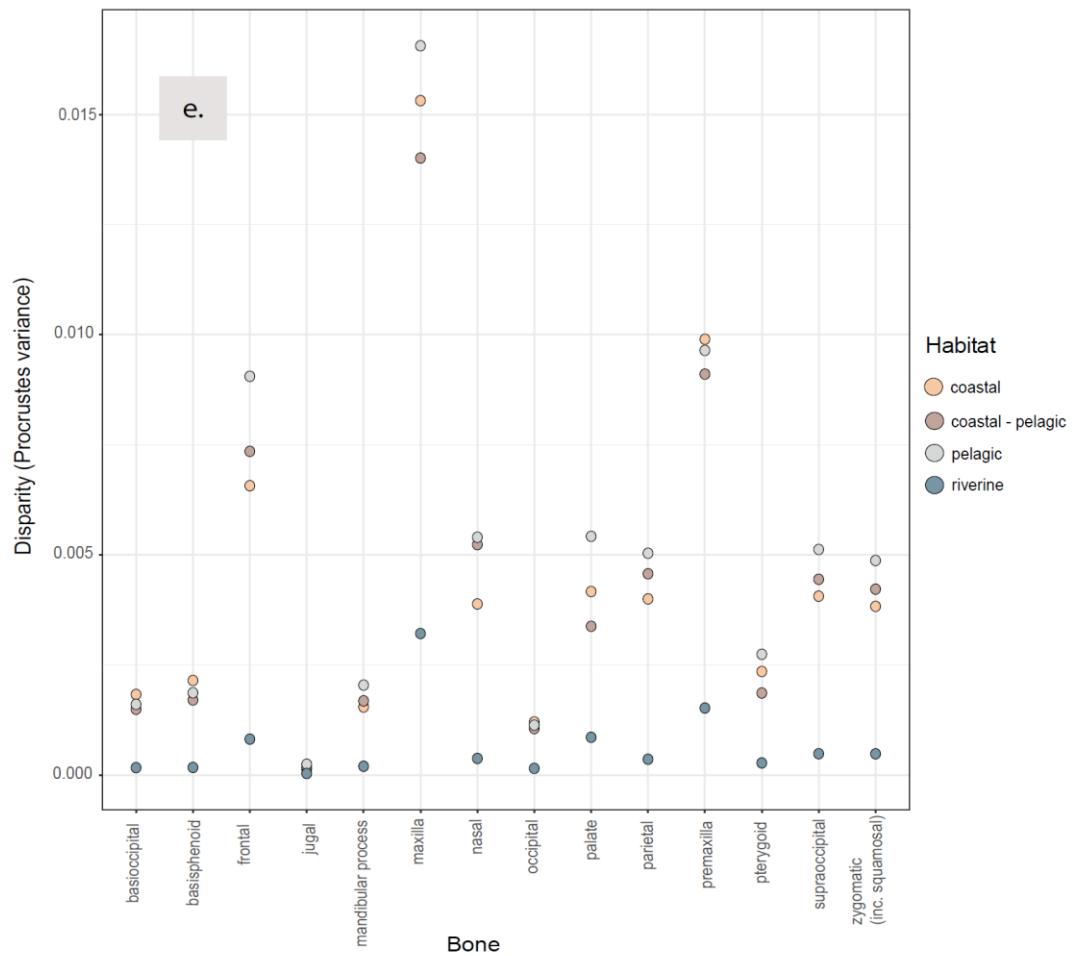
[Figure on this and previous pages]

**Fig. 3.13 (a-e).** Disparity (Procrustes variance) per bone per ecological factor. Disparity calculated for the whole cetacean data set. a. Dentition categories: edentulous (baleen), heterodont, homodont, reduced. b. Diet categories: fish, benthic invertebrates + fish, cephalopods + fish, tetrapods + fish, zooplankton + fish. c. Echolocation ability: Band1: Not capable of echolocation (archaeocetes and mysticetes), Band2: Fully echolocating (all odontocetes except *Odobenocetops*). d. Feeding method: biting, filter, suction. e. Habitat type: coastal, coastal-pelagic, pelagic, riverine. Raw data can be found in Appendix 3, Table S3. 21-25.

## 3.5 Discussion

Cetaceans transitioned from being land-based, to wholly aquatic in just eight million years (Thewissen, 2014). This transition is one of the most profound changes in adaptive zone captured in the fossil record (Thewissen et al., 2001) and showcases cetaceans as an exemplar of morphological and ecological change. This initial transition, followed by a divergence between the suborders and later radiations, led to an extraordinary diversity of forms from river dolphins to the mighty blue whale. Here, I collected and analysed the first morphometric data set to quantify cetacean cranial morphology throughout their entire evolutionary history, spanning ~47.8 million years to reconstruct the processes and factors that drove this diversity. Using high-dimensional landmark data to comprehensively represent the entire cranium, I reconstructed the drivers of shape variation, disparity, and evolutionary rate, demonstrating several major patterns in cetacean cranial evolution: 1) the evolution of the whale cranium is characterized by three major waves of diversification, with the fastest evolutionary rates observed in the archaeocetes, during the initial radiation of whales; 2) each cetacean 'suborder' occupies a distinct region of cranial morphospace, with fossil specimens bridging the gap between archaeocetes and the modern mysticetes and odontocetes; 3) diet and echolocation have the strongest effects on cetacean skull variation and evolution.

### 3.5.1 Three waves of cetacean diversification

Throughout their evolutionary history, there have been three key waves of diversification in the cetacean skull. The first and most prominent evolutionary wave in the cetacean skull is seen in the early archaeocetes (~ 47.8-42 Mya). It has been suggested that the archaeocetes evolved rapidly, radiating in the Eocene, likely responding to ecological opportunities, and filling a vacated marine niche (Lipps and Mitchell, 1976). The archaeocetes transitioned from land-based to freshwater, to coastal, to fully marine within a short 8-12 million years (Thewissen, 2014; Marx et al., 2016a). Slater and Friscia (2019) suggest that early bursts restricted to traits are often associated with higher level niches, such as macrohabitat use or dietary strategy, as may be the case here.

Evolutionary diversification following an 'early-burst' process, i.e., acceleration early in the history of a clade (facilitated by available niche space) is well known in many taxa such as squamates (Pincheira-Donoso et al., 2015), birds (Cooney et al., 2017), and perhaps most famously Theria (mammals including the eutherians and the metatherians) in the Middle to Late Jurassic (Close et al., 2015). As well as ecological opportunities such as high productivity at the time (Lipps and Mitchell, 1976), it is possible that the archaeocete early burst of evolution was facilitated by a sparsity of competition. The pinnipeds (seals and sea lions) (which also feed raptorially and occupy a similar niche) did not appear in the fossil record until 27-25 Mya (Late Oligocene) (Berta, 2018), long after the archaeocetes began to enter the water (~53 Mya). The last archaeocetes, the kekenodontids, possibly only overlapped with the pinnipeds for a short time, but it is unclear if they competed.

Empirical evidence suggests that maximum morphological disparity tends to be established early in the evolutionary history of many diverse clades (e.g., brachiopods, birds, cichlid fish, crinoids, among many others) (Foote, 1999; Smith and Bunje, 1999; López-Fernández, 2013; Cooney et al., 2017; Arbour et al., 2019). Interestingly, despite showing the highest evolutionary rates, the archaeocetes show some of the lowest levels of cranial disparity. Although these animals evolved rapidly to adapt to an aquatic lifestyle, the assemblage retained many plesiomorphic characteristics such as heterodont dentition, no cranial telescoping, and tooth replacement throughout their existence (Marx et al., 2016a). Even so, archaeocete evolutionary rates dominate those seen across Cetacea and define a rapid, first wave of diversification. This is not only seen in the whole skull (Fig. 3.4; 3.7), but also in individual cranial bones (Fig. 3.6 (1)). Unsurprisingly, the nasal, which shifted posteriorly prior to the origin of the neocetes (Churchill et al., 2018), shows high evolutionary rates, particularly in the Mid-Late Eocene when the nares were moving from the tip of the snout to the top of the head before later settling into the functional implications of the two suborders (Berta et al., 2014). Consequently, extremely high rates are seen in the archaeocete maxilla, premaxilla, and frontal (Fig. 3.6 (1.b)). There is a slowing down in evolutionary rates in the archaeocete skull (both whole skull and separate bones) at ~42 Mya. Although it is

challenging to conclude whether this slowdown in evolutionary rates and eventual disappearance of the archaeocetes was driven by abiotic factors such as climate or by biotic factors such as competition, it is clear that towards the Mid-Late Eocene, the neocetes had appeared, were rapidly diverging, and the second wave of cetacean cranial diversification was well under way.

Around ~39 Mya the neocetes (mysticetes and odontocetes) diverged (Marx et al., 2016a). The archaeocete to neocete transition is the second major wave of cetacean diversification. I find that the initial divergence of the neocetes is followed by a period of high evolutionary rates, in both new suborders, which continues into the Mid-Late Oligocene as the suborders diversified, evolving rapidly to occupy their distinct niches. Evolutionary rates and disparity in the mysticetes are highest at their origin (Mystacodontidae, Mammalodontidae (Fig 3.8)). The earliest diverging mysticete, *Mystacodon selenensis* (Late Eocene (36.4 Ma); Lambert et al., 2017a; de Muizon et al., 2017), which lived alongside later archaeocetes such as *Kekenodon*, retained many basilosaurid-like features such as a narrow rostrum. However, it also has a telescoped vertex, and more posteriorly placed nares (Muizon et al., 2017) seen in later mysticetes. Thereafter, morphologies associated with more crownward mysticetes start appearing, including an elongated rostral portion of the maxilla with a broad-based rostrum as in *Janjucetus hunderi* (Early Oligocene; Fitzgerald, 2006; Fitzgerald, 2010), and later, a broader platyrostral skull, and maxillae with thin lateral edges (Fitzgerald, 2006; Fitzgerald, 2010).

High evolutionary rates are seen in the nasal, maxilla, and premaxilla of the early Oligocene neocetes (Fig 3.5; Fig 3.6 (1)) shortly after the divergence. It is well known that the earliest diverging odontocetes (Early Oligocene) possessed some of the greatest facial morphological diversity associated with telescoping of the bones (Churchill et al., 2018). These high rates reflect advances in echolocation, telescoping, and ecological specialisation which rapidly evolved after the disappearance of the Basilosauridae (Churchill et al., 2016; Park et al., 2016; Boessenecker et al., 2017).

High evolutionary rates persist until the Late Oligocene/Early Miocene in both suborders with specific transitional morphologies found in the early neocetes,

accounting for some of these higher rates. These include the transition from an elongate rostrum seen in *Mystacodon*, to the broad-based rostrum of mysticetes such as *Janjucetus hunderi* (Fitzgerald, 2006) and the elongation and flattening of the rostrum in the aetiocetids (Mid-Late Oligocene) (Fitzgerald, 2006; Marx et al., 2016a). Of the suborders, including the archaeocetes, mysticetes have the lowest rates across all bones except the maxilla, jugal, mandibular process, zygomatic (with squamosal), and the parietal, all of which underwent rapid change in the early divergence of the mysticetes. The bones especially associated with jaw functioning (mandibular process, jugal, and zygomatic (with squamosal)) show some of the highest evolutionary rates for mysticetes. These bones endured a massive functional change from raptorial feeding in the early toothed mysticetes to filter feeding in the crownward mysticetes (El Adli et al., 2014; Boessenecker and Fordyce, 2015).

Interestingly, at this time, the remaining archaeocete family, the kekenodontids, were evolving at a lower rate than the toothed mysticetes and odontocetes they lived alongside (the kekenodontids have the lowest evolutionary rates of any of the archaeocetes). Archaeocetes at the time were a minor component of the cetacean faunal assemblage, which was increasingly dominated by a variety of rapidly diversifying neocetes (Fitzgerald, 2006; Geisler et al., 2014). This does not necessarily indicate a replacement event of the last surviving archaeocetes by the toothed mysticetes, after all, some early mysticetes employed similar raptorial feeding strategies and archaic mysticetes likely inherited a functional dentition and the ability to suction feed from their archaeocete ancestors (Werth 2000a, Marx et al., 2016b). Further, neither had the advantage of echolocation (Barnes and Sanders, 1996). However, due to a foreshortened rostrum and fibrocartilaginous mandibular symphysis, early mysticete mammalodontids (such as *Janjucetus*) did have the advantage of refined suction abilities (Fitzgerald, 2006) and may have benefited from this.

Towards the end of the Oligocene/Early Miocene toothed mysticetes may have been outcompeted by echolocating odontocetes which had the advantage of refined biosonar, and also by early filter feeding mysticetes (such as the

eomysticetids; Boessenecker and Fordyce, 2017), which, with baleen now in place, were advantaged by their filtering methods and associated behaviours (Marx et al., 2016b). The disappearance of the toothed mysticetes came not long after the last archaeocetes, which disappeared ~26 Mya. Thereafter, baleen-assisted mysticetes successfully filled an ecospace that was increasingly disparate from odontocetes (Marx et al., 2019a). High evolutionary rates generally persist in the odontocetes throughout the Oligocene. As the earliest known odontocetes already possessed traits associated with this suborder (retrograde telescoping, asymmetry, and associated echolocation), high cranial rates of evolution in the Oligocene may reflect these early advantages as echolocation abilities continued to refine and evolve, further setting the odontocetes apart from other cetaceans.

An increase in rates and disparity following the archaeocete to neocete transition could suggest that there were functional constraints early on in cetacean evolution which were overcome at or around the divergence of the Mysticeti and Odontoceti. After the initial high evolutionary rates seen at the divergence, another peak in evolutionary rates in the skull and individual bones (namely the supraoccipital and frontal) is observed in the mysticetes at ~30-24 Mya, and in the odontocetes (namely the maxilla and frontal) between ~30-26 Mya and again from ~24-22 Mya in the nasal and premaxilla especially. In the mysticetes these high rates are especially evident in toothed suction feeders, the Aetiocetidae. An almost identical pattern in mysticete evolutionary rates and disparity was seen in Marx and Fordyce (2015), who also found evidence for an early adaptive radiation (36–30 Mya), followed by a shift towards bulk filter-feeding (30–23 Mya). Marx and Fordyce (2015) used a morphological and molecular matrix as a measure of diversity and attributed the coincidence of increasing rates with global cooling, eutrophication in the Southern Ocean, and the progression of the Antarctic Circumpolar Current (ACC).

Finally, regarding this second wave, Steeman et al. (2009) used molecular data and also found that palaeoceanographic modifications and subsequent alterations to circulation patterns and temperature influenced the dynamics of radiations in modern cetaceans (Steeman et al., 2009). Although Steeman et

al. (2009) attributed an increase in radiation to palaeoceanographic events happening ~35-31 Mya, I see an increase in rates later, which could be attributed to the later intensification of the ACC, and other knock-on effects (e.g., climate, productivity) of this earlier ocean restructuring. Steeman et al. (2009) further suggest that there was a second radiation influenced by ocean dynamics in the Miocene (9-4 Mya). I also find evidence for increased evolutionary rates in the cetacean cranium during the Miocene.

The third wave of diversification in the cranium is seen in the Miocene and appears to predominantly be an odontocete signal. In the mysticetes, most filter feeders, except for the aetiocetids and *Kekenodon* (both toothed filter feeders, although there is contention over whether aetiocetids had insipient baleen or not; Deméré et al., 2008; Deméré and Berta, 2008), are Miocene or younger in age. Unfortunately, there are no Chaeomysticeti (toothless 'true' mysticetes) in this study due to incompleteness of New Zealand material and constraints for accessing Japanese collections. Hereafter, barring high rates in the early divergence of the Balaenidae (right whales (*Eubalaena*) and the bow head whale (*Balaena mysticetus*)) and the cetotheriids, evolutionary rates and disparity remain conservative across Mysticeti. The Balaenidae especially evolved highly specialised skim feeding and associated morphology (Werth and Potvin, 2016; Rommel et al., 2009) which may account for high rates seen early in the divergence of this clade. Conservative rates thereafter may be a consequence of achieving an optimal morphology for their functional niche (i.e., filter feeding). Since then, various successful feeding methods have evolved (Werth 2000a; Hocking et al., 2017a; Goldbogen and Madsen, 2018) which have enabled baleen whales to exploit rich food resources and become the largest animals that have ever existed. A transition to a gigantic body size is suggested to be a relatively recent occurrence (a clade-wide shift in the Plio-Pleistocene; Slater et al., 2017), but the recent discovery of a gigantic, toothed raptorial and suction feeding Eocene mysticete (*Llanocetus denticrenatus: ~ 34 Mya* and unfortunately too incomplete to include in this study) suggests that gigantism evolved before the emergence of filter feeding in some whales (Fordyce and Marx, 2018). However, although gigantic compared to other early mysticetes *Llanocetus* (~ 8m in length) was small in comparison to

baleen whales today (the largest blue whales can reach 30m; Jefferson et al., 2011). Later, it appears that the general mysticete skull plan, and associated disparity, has not changed to a great extent (other than by size) since the Latest Oligocene (Marx and Fordyce, 2015). This is evident in the clustering of specimens in the shape space from Miocene to present (Fig. 3.2).

Boessenecker et al. (2017) found that diversity in odontocete rostral length likely peaked in the Early Miocene (20-16 Mya). I also found high variation in odontocete maxillary and premaxillary rates around this time, for example in the Physeteroidea, the first of the major odontocete crown lineages to rapidly diverge, in the Early Miocene (Fig 3.4). This is possibly due to a shortening in rostrum length associated with the ability to produce higher forces needed for suction feeding (Norris and Møhl, 1983; Werth, 2006) a specialist strategy observed in many species in this superfamily. However, these high rates are also detected in the nasal across Physeteroidea and could be associated with shifts in advancing echolocation and associated cranial asymmetry at this time, as discussed in Coombs et al. (2020) and Chapter 2. Throughout the Miocene, higher rates are mostly attributed to the Physeteroidea. Thereafter, there is a general reduction in evolutionary rates across Odontoceti, bar a few individuals and clades. This likely indicates that unlike in the mysticetes, the odontocetes had smaller secondary radiations. In a disparity-through-time analysis, using body size data as a measure of disparity, Slater et al. (2010) found evidence for a secondary radiation between 11 and 6 Mya, when members of the Delphinidae (e.g., *Grampus*, *Globicephala*) transitioned to cephalopod specialisation, an adaptation which generally had already occurred in older odontocete clades (Physeteridae, Kogiidae, and Ziphiidae) (Slater et al., 2010). I see several small peaks in odontocete rates from 18-9 Mya. These peaks are likely driven by the Delphinidae, which show an explosive radiation with rich diversity between ~15-10 Mya (Steeman et al., 2009; McGowen, 2009; McGowen et al., 2011, 2019; Galatius et al., 2020).

### 3.5.2 The distribution and drivers of cetacean cranial shape

These three waves of evolution in cetacean cranial history not only highlight key transitional periods for the clade, but also showcases the distinct evolutionary differences between the suborders. With this key information in mind, it is fitting that the suborders occupy such distinct areas of the morphospace (Fig. 3.2). Importantly, the transitional periods, and associated transitional taxa, occupy the gaps between suborders. This is highlighted by intermediate morphologies such as the early diverging odontocetes and mysticetes: *Simocetus rayi* (~ 33.9 Mya) (Fordyce, 2002) and *Mystacodon selenensis* (37.2 to 33.9 Mya) (Lambert et al., 2017a) which are the current, oldest known odontocete and mysticete, respectively.

There is also a clear separation in the age of specimens in the morphospace, with Eocene archaeocetes and Oligoene neocetes occupying the bottom right of the morphospace which is defined by morphologies with long snouts and anteriorly placed nasals. The Miocene and extant mysticetes occupy the same shape space, except for the pygmy right whales (Neobalaenidae) *Caperea marginata* (extant) and *Miocaperea pulchra* (Late Miocene). Both are members of the family Cetotheriidae (thought extinct until *Caperea* was reclassified) (Fordyce and Marx, 2013), and they have a unique cranial architecture, distinguished from other mysticetes by a large, more anteriorly thrusted occipital shield (Barnes and McLeod, 1984). I find lower evolutionary rates in the mysticetes from the Late Oligocene onwards (Fig. 3.4; Fig. 3.6), with the exception of an increase in rates seen in the early divergence of the Neobalaenidae (Late Miocene) (Fig. 3.4), which have the most disparate skulls of any living and recently extinct mysticetes (Marx et al., 2016a). These high rates could be attributed to the sparse Neobalaenidae fossil record which might account for long-term morphological stasis before the *Miocaperea – Caperea* lineage and, in turn, a punctuated equilibrium (Tsai and Fordyce, 2015).

The Oligocene odontocetes occupy the intermediate shape space between the archaeocetes and extant odontocetes – species in this shape space include the (then) newly diverging xenorophids, patriocetids, waipatiids, and

later the squalodontids. These families all display early telescoping, more posteriorly placed nasals, and the advent of asymmetry in the naso-facial region, a consequence of asymmetry in the overlying soft tissues which relates to the ability to echolocate (Heyning and Mead, 1990; Boessenecker et al., 2017; Coombs et al., 2020). This makes for a unique morphology disparate from the newly diverging mysticetes which sit closer in the morphospace to the archaeocetes, both of which employed similar raptorial feeding methods. The boundary between the archaeocete-neocete transition is becoming increasingly blurred by specimens with potential temporal overlap (toothed Eocene mysticetes especially). However, the fossil record of the mysticetes strongly suggests that a ghost lineage of Eocene odontocetes also exists (Pyenson, 2017; Churchill et al., 2018) which would likely further bridge the morphospace between archaeocetes and odontocetes. Finally, the odontocetes occupy a much broader range of the morphospace. Echolocation in the odontocetes, both its evolution and refinement become a defining characteristic of this suborder, as well as enabling them to diversify into a vast range of forms (Marx et al., 2016a). Conversely, the morphology of the later mysticetes is likely constrained by the functional and morphological requirements of the dominant feeding strategies associated with an edentulous-baleen condition.

### 3.5.3 Ecological influences on cranial morphology

Considering the potential opportunities and constraints that these key innovations may impose on cranial morphology, I investigated the influence of echolocation, dentition, and feeding method, as well as several other factors: diet, habitat, and size. I found that all factors had a significant effect on skull morphology. Firstly, I investigated the influence of allometry, or size, on skull shape. Allometry explains around ~ 15% of skull shape variation across Cetacea. This is broadly in keeping with allometric effects seen in other mammals, for example, 18.6% and 16.5% in male and female antelope (Cetarctiodactyla: Antilopinae and Cephalophinae) (Cardini and Polly, 2013) and ~ 13% in pinnipeds (Randau et al., 2019). Cetaceans vary in size by orders of magnitude, from the one metre long vaquita (*Phocoena sinus*) to the

30-metre-long blue whale (*Balaenoptera musculus*), and thus it is not surprising that allometry is a significant component of variation in skull shape.

Of the ecological factors, I found that diet and echolocation have the strongest effects on cetacean skull variation and evolution. The link between prey size, diet type, and feeding method with odontocete skull shape has previously been established (McCurry et al., 2017a; McCurry et al., 2017b; Galatius et al., 2020). As in Galatius et al. (2020), there is a clustering in the morphospace of brachycephalic species such as the kogiids, *Globicephala* sp, *Orcaella* sp, and many Phocoenids. When looking at feeding method, some of the highest per-bone rates are seen in the suction feeders (Fig 3.12(d)) which includes the aetiocetids, the last of the toothed mysticetes. Many of these high rates are concentrated in the naso-facial region (the premaxilla especially, maxilla, nasal, and frontal) and most likely reflect a signal seen in the suction feeding (bar the raptorial *Livyatan melvillei*) superfamily Physeteroidea and the suction feeding Monodontidae (Fig. 3.5). Members of both families have heightened facial asymmetry (Coombs et al., 2020; Benites-Palomino et al., 2021) in the premaxilla, maxilla, and nasals (although the kogiids lack nasals, Benites-Palomino et al., 2021). I found the lowest evolutionary rates per bone (bar the maxilla and zygomatic (including squamosal)) in species that filter feed – all edentulous mysticetes with baleen (Fig. 3.12 (d)), reflective of that constant and conservative rate of evolution seen in the Miocene mysticetes and crownward, as previously discussed. Foraging strategy has been highlighted as a major evolutionary driver of diversification in the delphinid skull shape (Galatius et al., 2020), and this is also suggested for Odontoceti in general (Boessenecker et al., 2017; McCurry et al., 2017a, Noris and Møhl, 1983). With this considered, these results should be caveated firstly with the complexity of categorising cetaceans into feeding methods. It could be argued that *all* delphinid species (the majority of all bar *Globicephala* and *Grampus* are categorised as biting (raptorial) feeders here) in fact rely on some combination of raptorial *and* suction feeding (Galatius et al., 2020). Secondly, this is especially difficult when categories do not include behavioural frameworks (for details see Hocking et al., 2017a; 2017b) which are often complex in cetaceans. Killer whales (*Orcinus orca*) for example are classed as

raptorial feeders here, but some ecomorphs of orca feed almost exclusively by suction feeding stunned herring and mackerel (Werth 2000b). Further, the large cheek teeth of *Mystacodon selenensis* suggest a raptorial feeding strategy with assisted suction feeding (Lambert et al., 2017a) making it difficult to assign to one category or the other. Finally, skulls were selected as accurate representatives of the species, however, there may be some slight individual variation that may play a role in the skull morphology and results.

Galatius et al. (2020) and McCurry et al. (2017a), both using morphometric data, also found an association between prey size and skull shape in odontocetes, especially when suction feeding taxa are excluded (McCurry et al., 2017a). Galatius et al., (2020) found that feeding mode and prey size are primary drivers of the evolution of dolphin skull shapes. Here, diet also has a significant effect on skull shape with all mysticetes (zooplankton feeders + fish) exhibiting some of the lowest evolutionary rates per bone (Fig. 3.12 (b)), reflective of that more constant and conservative rate of evolution previously discussed. Additionally, this group also has some of the lowest disparity across the skull and consists entirely of filter and suction feeding mysticetes and one archaeocete; the Late Oligocene *Kekenodon* which likely fed raptorially *and* via filtration (Marx et al., 2016a).

Most archaeocetes in this study (pakicetids, protocetids, ambulocetids, and remingtonocetids), as well as many early odontocetes (xenorophids, patriocetids, simocetids) fed on benthic invertebrates + fish as a key component of their diet (Fahlke et al., 2013). As discussed, the archaeocetes and the early diverging odontocetes have some of the highest rates of cranial evolution, and it is thus not surprising that when categorised by diet, highest rates are seen in this dietary category (Fig. 3.12 (b)). Further, the archaeocetes and early neocetes had heterodont dentition. The heterodont cetaceans are diverse and temporally wide ranging. It includes all archaeocetes and early diverging odontocetes and mysticetes (for example *Coronodon havensteini*: Early Oligocene; Geisler et al., 2017) as well as the last heterodont cetaceans (squalodonts of the Late Oligocene – Mid Miocene) and the toothed mysticetes (including the last toothed mysticetes such as the incipiently homodont Aetiocetidae (Rivin, 2010). High evolutionary rates in the

nasal are seen in 'tetrapod + fish' feeders. This includes the basilosaurids which showed marked retrograde movement of the nares, the Oligocene *Ankylorhiza tiedemani*, the first large macrophagous odontocete which reoccupied the niche vacated by basilosaurids (Boessenecker et al., 2020), and the Miocene *Livyatan melvillei* another macrophagous odontocete analogous with modern killer whales (Lambert et al., 2010). Finally, it includes the killer whale and false killer whale (*Pseudorca crassidens*), the latter of which particularly shows high asymmetry in the nares (Coombs et al., 2020) possibly associated with a unique echolocation plane pattern, different to other delphinids (Au et al., 1995). Finally, regarding diet and feeding method, this study does not consider the morphology of the mandible and as such misses information on jaw size and functioning, which of course play a key component in feeding method (Geisler et al., 2017) and diet (McCurry et al., 2017b).

When categorised by echolocation ability, cetaceans that cannot echolocate (archaeocetes and mysticetes; band1) generally show higher rates of evolution in the skull. This result is likely representative of the high evolutionary rates seen in the archaeocetes and the early mysticetes such as *Mystacodon*. Some exceptions are the premaxilla and frontal which show higher rates of evolution in the echolocating odontocetes. Premaxillary rates are particularly high in the early divergence of this suborder and again in the early diverging Physeteroidea (Mid-Late Oligocene). These are likely due to changes occurring in the face to accommodate echolocation as seen in Chapter 2. Despite high evolutionary rates, disparity is lowest in the band1 cetaceans, except for the anomalous and highly disparate only non-echolocating odontocete, *Odobenocetops*.

Regardless of ecological category, disparity is consistently highest in the maxilla, premaxilla, frontal, and nasal. The cetacean face and nasals have been modified more so than in any other mammalian group (Berta et al., 2014). Odontocetes generally have the highest disparity in the skull (Fig. 3.5; 3.10), this is unsurprising as odontocetes exhibit an exceptional diversity in skull shape with rostra that range from brachycephalic (e.g., *Odobenocetops* and *Kogia* sp) to grossly elongate in dolichophallic species such as *Schizodelphis morckhoviensis.* Fish eating odontocetes generally have the most disparate

bones in the skull, but this is closely contested by 'cephalopod + fish' feeders and 'tetrapod + fish' feeders. Fish eaters include the Late Oligocene heterodont squalodontids and waipatiids through to the highly disparate Eurhinodelphinidae. The 'cephalopod + fish' feeders include the Physeteroidea, mesoplodonts, and many extant delphinids. As suggested by Slater et al. (2010), a recent shift to a cephalopod diet in delphinids may explain an increase in body size disparity and there may be a concurrent shift in cranial disparity then also.

Suction feeding cetaceans show some of the highest disparity in the skull. Specimens here range from the broad-based rostrum of early mysticetes through to the elongate rostra of mesoplodonts. Norris and Møhl (1983) related blunt rostra and reduced dentition with suction feeding and this is the case in *Odobenocetops*, kogiids, and the narwhal among others. However, there may be a relaxation on these constraints in morphology when coupled with increased size (McCurry et al., 2017a). In fact, large body size appears to have been selected for in squid-feeding taxa such as ziphiids and sperm whales (*Physeter macrocephalus*) (Slater et al., 2010). Large suction feeders such as the ziphiids take in vast quantities of water, generating adequate suction forces and thus may not require the shortened rostral morphology of some smaller suction feeding taxa (McCurry et al., 2017a). Hence there is greater disparity in this feeding category than functional constraints might suggest.

Unlike Galatius et al. (2020), I found a clear relationship between skull morphology and habitat type, although Galatius et al. (2020) did focus primarily on the delphinid skull and stated that it is very probable that adaptations for specific habitats do occur in that particular family as in other clades such as the subfamily Lissodelphininae (Galatius and Goodall, 2016). The lowest disparity and also some of the lower rates are seen in the bones of the skull of riverine cetaceans, which comprises the three extant freshwater species in this study (*Inia geoffrensis*, *Lipotes vexillifer*, and *Platanista gangetica*). The living river dolphins are the last survivors of their respective families. Possibly marooned in freshwater environments following a reduction in sea levels in the later Miocene, the river dolphins have been largely sheltered from intense competitive pressure from the oceanic delphinoids, which may have caused a

decline in their marine cousins (Cassens et al., 2000; Marx et al., 2016a). Finally, convergent morphologies in unrelated river dolphin lineages may suggest that these cetaceans have successfully adapted to their freshwater niches (Page and Cooper, 2017) and this coupled with functional constraints of the environment may result in low evolutionary rates. It should be noted that habitat can be difficult to ascertain in cetaceans. Many species migrate vast distances, traversing many different environments following migrating food sources or avoiding predation and it is challenging to assign them to one habitat type.

Finally, it should also be noted that ecological data for fossils (palaeoecology) is inferred without observation, as is often standard in studies of this kind. For cetaceans, there are only a handful of fossils which preserve primary information on diet, for example, juvenile *Dorudon* have been found in the stomach contents of *Basilosaurus* (Voss et al., 2019) and further, bite marks on *Dorudon* skulls also indicate that they were a prey item of the much larger basilosaurids (Fahlke et al., 2012). Information like this is rare and generally assumptions are made based on morphology and phylogenetic relatedness among species instead, as is the case for fossils in this study.

I have highlighted variation in evolutionary rates and disparity across the cetacean skull, between the archaeocete assemblage and the two neocete suborders with a focus on ecological influences. It is difficult to conclude whether these patterns happened as a result of direct competition between taxa, or equally whether they were driven by external abiotic and biotic factors. Simpson (1953) argues that a major feature of the fossil record, and correspondingly of the history of life, is that we can often infer succession and replacement of one group of organisms by another, especially when taxa are alike enough that there is a certain relation between expansion of one phylum and contraction of the other (Simpson, 1953). To investigate potential evolutionary drivers such as competition we need an estimate of past biological diversity, which is fortunately well represented in the cetacean fossil record. Competitive interaction may rule in local populations, but differential response to mass extinctions (unlikely to be a matter of conventional competition) likely set the relative histories of large groups through geological

time (Gould and Calloway, 1980). There is still generally too little information to tell us whether turnover events happened as a direct result of competition (Marx et al., 2016a), and we can only hypothesise in the absence of primary evidence.

Further, it is also important to note that, although these results may point towards an early adaptive radiation, most testing of such hypotheses require both disparity and diversity data (Slater et al., 2010), the latter of which is not included here. Although it is difficult to infer ecological interactions with incomplete and uneven data (namely fossils), the benefits of using fossil taxa to reconstruct evolutionary rates and, where possible, interpret ecological data to account for other potential drivers of evolution outweighs the omission of fossil data from such studies. Finally, several other factors likely influence cranial morphology in cetaceans which were not covered in this study. For example, encephalization, or brain size and its effect on cranial morphology linked to echolocation (and the processing of acoustic data), thermoregulation, and complex social structure – the latter two of which are almost impossible to study in fossil Cetacea. Perhaps more importantly, temperature has not been considered. Thermoregulation for example could explain the lack of longirostrine delphinids in polar waters (Galatius et al., 2020), but on a greater scale, climate is also likely to have influenced skull shape as it has been shown to influence radiations in the modern whales, and diversity and disparity in mysticetes. The topic of climate and its influence on cetacean cranial evolution is the focus of the next chapter of this thesis.

## 3.6 Conclusions

Early archaeocetes (~ 48 Mya) show some of the highest evolutionary rates of all cetaceans, a rapid burst in evolution that sees high rates over the whole skull and for individual bones, particularly in the frontal, maxilla, and nasal. Archaeocetes evolved quickly to fill a previously vacated niche and adapted to an aquatic lifestyle, with rates slowing down ~ 42 Mya. However, disparity across the archaeocete skull is the lowest of any of the suborders. Around 39 Mya when the neocetes diverged, there was a continuation of high evolutionary rates into the early diverging mysticetes such as *Fucaia*

*goedertorum* and *Janjucetus hunderi*. These high rates continue into the Mid-Late Oligocene, particularly early in the divergence of the balaenids and eubalaenids. Disparity is also highest in the early diverging mysticetes, as the suborder adapted to a variety of different feeding strategies. By the end of the Oligocene, evolutionary rates in the mysticete skull were slowing down (bar a couple of exceptions in the Neobalaenidae and the Balaenidae) before settling into a more constant and conservative rate of evolution. Thereafter, there is little change in the mysticete occupation of cranial morphospace from the Miocene to the present. Archaeocetes disappeared in the Late Oligocene, perhaps outcompeted by the increasingly successful suction feeding (leading to filter feeding) mysticetes and the echolocating odontocetes.

The early diverging odontocetes also show some of the highest evolutionary rates in the suborder and this continues throughout the Late Oligocene with a further peak in rates in the Miocene. Both the mysticetes, and to a greater extent, the odontocetes, show higher disparity in the skull than the archaeocetes. This could suggest that the key innovations that define these suborders, filter feeding in the mysticetes, and echolocation in the odontocetes, catalysed higher disparity in these newly diverging suborders. Alternatively, it could suggest that there were functional constraints early on in cetacean evolution that were overcome at or around the divergence of the Mysticeti and Odontoceti.

Archaeocetes persisted alongside the neocetes until the Late Oligocene, occupying a similar niche to toothed mysticetes such as the raptorial *Janjucetus*. The toothed mysticetes increasingly began to diversify but ultimately disappeared shortly after the last archaeocetes. Their extinction was perhaps facilitated by competition with the echolocating odontocetes; however, there is no direct evidence supporting this hypothesis. The fully-fledged filter-feeding mysticetes continued to diversify whilst the odontocetes successfully occupied both raptorial and suction feeding niches with the advantage of echolocation. Mysticetes appear to have undergone an adaptive radiation followed by relative evolutionary stability, whilst the odontocetes also followed a similar pathway but with the addition of secondary radiations later in the Miocene and thereafter. It is unclear whether this is a direct result of

competition, with early innovation opening separate evolutionary pathways of success for the neocetes, or whether external factors such as environmental change played a part as ecological factors are shown to here. High evolutionary rates in the early diverging mysticetes and odontocetes, accompanied by high disparity, could be linked to the opportunities presented by global cooling and changes associated with the strengthening of the Antarctic Circumpolar Current (ACC) such as increased ocean productivity. However, more work needs to be done assessing the impact of climate and abiotic factors on diversification and morphology of the cetacean skull.

The highest axes of variation in the cetacean skull are seen in the elongation of the rostrum, and the positioning of the nares, from anteriorly placed in ancestral species, to posteriorly placed in more crownward species. Archaeocetes, mysticetes, and odontocetes occupy distinct areas of the morphospace. Shape space between the suborders is occupied by intermediate morphologies such as the later archaeocetes and the early diverging neocetes. The odontocetes occupy a vast range of the shape space. Echolocation in the odontocetes, its evolution, and development has enabled these toothed cetaceans to diversify into a vast range of forms. Conversely, the mysticetes, especially more crownward taxa, occupy a much smaller range of the shape space likely constrained by the functional and morphological requirements of filter feeding with baleen.

Dentition, diet, echolocation ability, feeding method, and habitat all have a significant effect on cranial morphology in cetaceans. Generally, baleen filter feeders have the lowest evolutionary rates, with low disparity, and a stabilized morphology after the end of the Oligocene. This is likely due to all mysticetes thereafter being constrained to a small but very successful niche of baleen filter feeding allowing them to reach gargantuan body sizes. Among dietary categories, the highest rates are seen in the 'benthic invertebrate + fish' feeders which is dominated by the heterodont archaeocetes and the early heterodont odontocetes and earliest toothed (heterodont) mysticetes, all of which had high rates of evolution, as discussed. This work highlights the impact of key innovations (baleen and echolocation) and their role in driving skull shape evolution. Further it shows that cranial shape evolution is also

influenced by ecology, especially diet and echolocation. Finally, that changes in skull rates and disparity may have been driven by larger environmental change such as the strengthening of the ACC and resultant changes to climate and ocean productivity as is evident in studies which consider molecular, morphological character, and genus-level diversity data. More work is required to determine the impacts of large-scale environmental change on the cetacean cranium.

**Chapter four**

**How does climate affect cetacean diversity? Evidence from the past and present**

*"They say the sea is cold, but the sea contains the hottest blood of all"*

D.H. Lawrence, 'Whales Weep Not!'

## 4.1 Abstract

Current climate change is already having a profound impact on biodiversity, and this effect is only predicted to get worse under future scenarios. Despite these concerns, climatic influence on dynamics at the macroevolutionary level are still poorly understood. Although many studies have involved climate as a driver of cetacean evolution, no studies to date have quantitatively assessed how past climate change and other shifts in ocean ecosystems has influenced the morphological evolution of whales. Here, I used 3D geometric morphometric data for 201 specimens spanning the 50-million-year evolutionary history of whales to establish whether temperature and ocean productivity are significant drivers of cetacean cranial evolution. To do so, I ran novel evolutionary models where rates of cranial evolution track climate and ocean productivity, using $\delta^{18}O$ and $\delta^{13}C$ as proxies. I further compared the fit of these environmental models to that of standard evolutionary models, such as Brownian Motion and Early Burst.

My results support the hypothesis that both climate fluctuations and ocean productivity drive cetacean cranial evolution through deep time. Models where evolutionary rates track various climate and ocean productivity outperformed standard models such as Brownian Motion in neocetes. However, I found that evolutionary rates of the archaeocetes (ancient whales), mysticetes (baleen whales), and odontocetes (toothed whales) are all impacted in different ways and to varying degrees by temperatures and ocean productivity. Both an Early Burst mode of evolution *and* fluctuations associated with ocean productivity were supported as best fit models for archaeocete evolution. Mysticete rates of evolution are predominately driven by fluctuating levels of ocean productivity, whereas odontocete evolutionary rates have been driven by the *rate* of temperature change, as opposed to temperature itself or changes in temperature.

My results clearly demonstrate that temperature and associated ocean productivity have driven evolutionary rates in cetaceans throughout their history from the Early Eocene to the present day. These fluctuations are likely driven by palaeoceanographic changes and the subsequent impacts of ocean restructuring on temperature and productivity. The different historical

responses observed for the extant suborders highlights a requirement for separate, tailored conservation and mitigation of climate impacts for toothed whales and baleen whales.

**Keywords:** cetaceans, climate, diversity, ocean productivity

## 4.2 Introduction

Large-scale environmental change has been the driver behind many dramatic faunal extinctions and radiations. The end-Cretaceous extinction at ~ 66 Ma is the most famous example, but plentiful other examples exist such as the end-Permian (~252 Mya) which saw > 90% of marine species lost amid a deluge of warming, anoxia, and acidification (Bond and Grasby, 2017). Today, the fate of cetaceans and their evolution is entangled with humans and our impacts on the planet. There is unequivocal evidence that climate change is occurring (IPCC, 2007), and anthropogenic warming could, and already is, causing abrupt and often irreversible impacts on biodiversity (Simmonds and Elliot, 2009).

As a result, scientists have paid increasing attention to questions concerning species response as the planet continues to warm and change (Pearson and Dawson, 2003; Bellard et al., 2012; Goswami et al., 2016). Global biodiversity patterns are the consequence of many historical spatial and temporal processes (Ricklefs, 2004; Fritz et al., 2013) and to obtain a full understanding of this bigger picture, we need to consider species' ecology, morphology, and adaptations both now and in the past, using the fossil record. George Gaylord Simpson hypothesised that much biological diversity originated during adaptive radiations (Simpson, 1953), an idea that places biotic interactions at the centre of phenotypic evolution (Simpson, 1953; Clavel and Morlon, 2017). However, there is a widespread alternative view that environmental, abiotic factors play an equal or even larger role in evolutionary processes (Benton, 2009; Erwin, 2009) Commonly referred to as the 'Court Jester hypothesis' (Barnosky, 2001; Benton, 2009) this idea states that abiotic influences such as climate, function as a major driving force behind the processes of evolution (Barnosky, 2001). The Court Jester hypothesis is provided as contrast to the

'Red Queen hypothesis' (Van Valen, 1973; Benton, 2009) which focuses on the influences of biotic interactions on evolution such as co-evolution of species to mutually drive each other to adapt (Benton, 2009). The dichotomy between the two hypotheses is suggested to really be a dichotomy of scale, rather than one hypothesis dominating the other, with evolution at the macro scale more likely driven by abiotic factors than biotic factors (Barnosky, 2001). While the influence of abiotic factors, specifically climate, has been considered for several clades using body size (Figueirido et al., 2012; Teplitsky and Millien, 2013; Clavel and Morlon, 2017), the influence on dynamics of complex or multivariate aspects of morphology at the macroevolutionary level are still poorly understood Figueirido et al., 2012).

Cetaceans (whales, dolphins, and porpoises) have a remarkably continuous fossil record, ideal for investigating the impacts of biotic and abiotic factors throughout their evolution on a macroevolutionary scale. Furthermore, cetaceans travel vast distances, occupying the top trophic position (as apex predators) in the world's oceans, which offers insight into wider ocean health and functioning (Ramp et al., 2015). Quantifying the impact of abiotic factors such as climate change on cetaceans thus has important implications for understanding how ongoing physical environmental change may affect their future evolution, as well as that of the broader marine ecosystem.

Previous work on taxonomic diversity, disparity, and body size has suggested that cetacean evolution is defined by a series of key events. From their initial invasion of the aquatic niche approximately 53 million years ago (hereafter Mya), archaeocetes (stem whales) transitioned from a terrestrial to fully aquatic lifestyle within 8-12 million years (Thewissen, 2014; Marx et al., 2016a), supported by the high rates of cranial evolution for archaeocetes estimated in Chapter 3. It is hypothesised that the archaeocetes evolved rapidly to occupy a vacant aquatic niche, facilitated by ocean upwelling and an increase in productivity during the Eocene (Lipps and Mitchell, 1976). Then, around 39 Mya, Cetacea split into two extant suborders, the mysticetes (baleen whales), and the odontocetes (toothed whales) which are collectively known as the neocetes, while the archaeocetes persisted for another 10 million years or so and then disappeared.

Reasons for the disappearance of the archaeocetes are debated, but it has been suggested that there were functional constraints early on in cetacean evolution that were overcome after the divergence of the neocetes (Chapter 3). Marx and Fordyce (2015) scored morphological and molecular characters for 90 taxa (86 representing mysticetes) and found high rates of evolution in the early divergence of the clade, possibly suggestive of an adaptive radiation as hypothesised by Lipps and Mitchell (1976), followed by relative evolutionary stability. Lipps and Mitchell (1976) base their model on the trophic requirements of marine mammals and the favourable oceanographic conditions needed to fulfil those requirements. A similar pattern is observed in the neocetes by Slater et al. (2010) who used body size data as a measure of disparity and found that some of the highest rates in this suborder are seen early in the divergence of the clade – suggestive of an adaptive radiation (Slater et al., 2010). In Chapter 3, I modelled evolutionary rates and disparity in the cetacean cranium and also found evidence for high evolutionary rates in the early diverging neocetes. In addition, increased evolutionary rates in the odontocetes in the Mid-Late Miocene, also found in Chapter 3, are likewise highlighted by Slater et al. (2010) and by Steeman et al. (2009).

It has long been hypothesised that the evolution of modern cetaceans has been influenced by global temperature changes (Fordyce 1980; Flower and Kennett, 1994; Fordyce, 2001; Steeman et al., 2009), ocean upwelling, and fluctuations in primary productivity (Lipps and Mitchell, 1976; Berger 2007; Marx and Uhen, 2010). Cetaceans are apex predators, and to support these apex predators, marine ecosystems must be productive, with energy transmitted efficiently through the food chain (Eddy et al., 2021). Lipps and Mitchell (1976) hypothesised a trophic model for adaptive radiations in the cetaceans, with an initial invasion into the adaptive zone (in the archaeocetes) driven by a response to upwelling and ocean productivity. They further suggest that the neocetes also evolved rapidly and radiated because of upwelling and productivity, dependent on trophic resources (Lipps and Mitchell, 1976). More recently, Marx and Uhen (2010) used diatom and nannoplankton species diversity as a measure of ocean productivity and concluded that cetacean palaeodiversity can be explained by diatom diversity alongside variations in

climate (Marx and Uhen, 2010). Using a comprehensive genus-level cetacean diversity data set, the study supported the hypothesis that the onset of the Antarctic Circumpolar Current (ACC) may have triggered the radiation of modern whales due to an increase in nutrient circulation and availability in the upper layers of the Southern Ocean (Fordyce, 1980; Berger, 2007; Marx and Uhen 2010). Using a morphological data set of 89 extant cetacean species and three outgroup taxa Steeman et al. (2009) also found support for increased diversification during periods of physical restructuring in the oceans, implying that palaeoceanographic modifications affect cetaceans directly through changes in geographic range (opening and closing of seaways) and alterations to circulation patterns which influence climate (Fordyce, 2001; Hampe and Baszio, 2010). Furthermore, studies of extant cetaceans have suggested that climate change and temperature-dependent factors such as prey abundance and range changes have had substantial effects on cetacean taxonomic diversity (Whitehead et al., 2008).

Previous studies have highlighted the impacts of ocean restructuring, subsequent climate change, and nutrient upwelling separately for the mysticetes (Marx and Fordyce, 2015), and collectively for the neocetes (Berger, 2007; Steeman et al., 2009; Marx and Uhen, 2010), but not for Cetacea as a whole. Others highlight the importance of a tropic model driving adaptive radiation and extinctions in cetaceans (Lipps and Mitchell, 1976); however, this has not been fully tested. These studies all use different metrics for diversity; Steeman et al. (2009) use molecular data to model neocete radiations. In comparison, Marx and Fordyce (2015) scored morphological and molecular characters for 90 taxa (86 representing mysticetes) to derive phylogenetically informed estimates of taxonomic and morphological diversity. Finally, Marx and Uhen (2010), as noted above, use a genus-level cetacean diversity data set to investigate whether ocean productivity triggered the radiation of the neocetes. These studies also use several different proxies against which to measure cetacean diversity. Marx and Uhen (2010) use diatom diversity whilst Marx and Fordyce (2015) use carbon and oxygen stable isotope data from Zachos et al. (2008) as a proxy for palaeotemperature.

However, the influence of complex interactions between biotic and abiotic factors on cetacean morphology at the macroevolutionary level are still poorly understood (Figueirido et al., 2012). We know that many factors such as temperature and ocean productivity are inherently related and should be considered simultaneously. Ocean cooling generally has a positive effect on productivity (Behrenfeld et al., 2006). Cooler surface waters mix better than warmer waters, facilitating the upwelling of deep-water nutrients to the euphotic zone. This causes an increase in phytoplankton growth (increased productivity and carbon uptake) shown by a negative carbon isotope ($\delta^{13}C$) shift in palaeo records (Steeman et al., 2009). As well as temperature, productivity is also driven by physical ocean restructuring, atmospheric dust deposition, the solar cycle (i.e., fluctuations in light availability and intensity) (Behrenfeld et al., 2006), ocean chemistry (e.g., nutrients), and biology (e.g., grazer abundance) (Deppeler and Davidson, 2017). For these reasons, and unlike previous studies, we look at both carbon and oxygen isotope ratios as proxies for productivity and temperature, respectively (See 4.3.4).

Further, unlike previous measures of cetacean diversity, I focus on a cranial morphology data set. The cranium (the skull minus the mandible) is a complex structure and the most informative part of the cetacean skeleton (Marx et al., 2016a). The skull provides many functions and is of particular interest to biologists and palaeontologists alike, wishing to infer aspects of ecology (palaeoecology in fossils) such as feeding, breathing, brain functioning, nervous system, and sensory functions (Rommel et al., 2009). Most of the bones in the skull have been modified in some way throughout cetacean evolution and this, coupled with the remarkably complete cetacean fossil record makes them an ideal candidate for macroevolutionary studies.

The complexity of the skull and its constituent parts justifies a multivariate approach. Multivariate data allow for the investigation of several aspects of phenotypic evolution in a way that univariate data simply cannot (Revell and Collar 2009; Clavel et al., 2015; Caetano and Harmon 2017; Clavel et al., 2019). Phenomic evolution is multivariate and complex by nature, and basic traits are influenced by different developmental constraints and effects (Felsenstein, 1985; Clavel et al., 2015). Thus, multivariate analyses should be

chosen over univariate ones where possible to best represent complex structures of multiple covarying traits (Clavel et al., 2015).

Here I present the first study to model the impacts of climate and ocean productivity on the tempo of cetacean morphological evolution throughout their entire 50-million-year history. My results summarise the impacts of abiotic and biotic factors throughout cetacean evolution and, importantly, highlight a requirement for separate, tailored conservation and mitigation of climate impacts for toothed whales and baleen whales.

## 4.3 Methods

### 4.3.1 Morphometric data

My analyses use the cranial morphometric data set described in Chapter 3. The final morphological data set comprises 201 cetacean crania, of which 113 (56%) are extinct, ranging in age from 48.6 Mya to 2.59 Mya. Specimens were selected to cover the widest possible phylogenetic, temporal, and spatial range (where possible), representing 41 families and 122 genera from the Eocene to the present. 123 landmarks and 124 semi-landmark curves were placed over the surface of each skull, as described in Chapter 3 (Appendix 3, Table S3.3; S3.4, Figs. S3.1 – S3.3).

### 4.3.2 Phylogeny

My study uses a phylogenetic framework to model potential drivers in evolutionary rates across Cetacea. To generate a tree that included all our sampled taxa, I modified the time-calibrated phylogeny from Lloyd and Slater (2020) to sample only the taxa used in this study. This is the same phylogenetic framework as used in Chapter 3.

### 4.3.3 pPCscores

A main drawback of working with multivariate dimensions is the exponential growth of computational time (Felsenstein, 1985; Freckleton, 2012; Clavel et

al., 2015). In highly dimensional data sets like this one (where resampled specimens still had 2028 coordinates over each skull surface and reducing dimensionality by using only one side of the skull is impossible due to natural asymmetry; Chapter 2), reducing the data to its principal components (PCs) means that simulations can be successfully run on a reduced set of axes (Clavel and Morlon, 2020). Using pPC scores, although less ideal than considering all traits, is a better alternative than distance approaches (Clavel and Morlon, 2020). This approach gave satisfactory results when used in the R package 'mvMORPH' (Chapter 3) and is used again here. In order to minimize data loss from the use of principal axes of variation rather than raw data, I inputted phylogenetic principal component (pPC) scores that represented 95% of the shape variation for the whole cranium (Appendix 3, Table S3.6-S3.9). pPC scores were calculated using the 'phyl.pca' function in the R package phytools v.0.7-70 (Revell, 2012). 39 pPC scores were required to represent 95% of shape variation in the crania for Cetacea.

Following from the work undertaken in Chapter 3, it is evident that the cetacean suborders (used loosely here to indicate the two extant suborders as well as the paraphyletic stem whales, archaeocetes) evolved at different rates throughout their evolutionary history. For this reason, I ran analyses both on the full cetacean data set and for the separate suborders. Between 8 and 30 pPC scores were required to capture 95% of variation in each of the three suborders (Appendix 3, Table S3.12, 'Whole skull'). Models were also run using the landmark data (excluding curves) for comparison (Appendix 4, Table S4.1), but as landmarks do not capture several interesting aspects of morphology, such as vaults and processes and fail to characterize the shape between landmarks (Bardua et al., 2019a; Chapter 2), I focus on the results using pPC scores.

### 4.3.4 Palaeoclimate data

I used palaeotemperature data from Cramer et al. (2011) and Westerhold et al. (2020) (Fig. 4.1) which spans 66 million years. Firstly, the Cramer et al. (2011) data are particularly useful in studies of marine megafauna because the data are split into different ocean basins, from which a LOESS smoothed

long-term value is taken. This is important because the final data set consists of records from different ocean basins rather than just one locality, providing a global picture of ocean hetero- or homogeneity in $\delta^{18}O$ fluctuations. Similarly, to Zachos et al. (2008), the Cramer et al. (2011) curve is derived from benthic foraminiferal $\delta^{18}O$ isotope ratios. Additionally, Cramer et al. (2011) is useful in that it combines benthic oxygen isotope data ($\delta^{18}O$) with benthic Mg/Ca data (which provides temperature without the ice component) and sea-level data (which can be used as a global ice indicator) (Cramer et al., 2011). Contrary to the commonly used Zachos et al. (2008) curve, the Cramer et al. (2011) curve accounts for fluctuations in sea water (sw) ($\delta^{18}O_{sw}$) through time which is also important for measuring large-scale glaciations and changing sea levels (Clavel and Morlon, 2017). The other advantage is that Cramer et al. (2011) uses oxygen isotope data separated by ocean basin (there is increasing heterogeneity across ocean basins during the Cenozoic) (Fordyce, 2001). Hereafter, the Cramer et al. (2011) data set is referred to as $\delta^{18}O_{Cr.}$

Secondly, I also ran models using the Westerhold et al. (2020) palaeoclimate data set. This was done for several reasons. One, Westerhold et al. (2020) present an astronomically (the response of Earth's climate system to orbital forcing) dated, continuous composite of benthic foraminifer isotope records ($\delta^{13}C$ and $\delta^{18}O$). Two, these newly generated benthic stable isotope data span the middle to Late Eocene and Late Miocene to fill intervals inadequately covered by existing records with an estimated chronologic accuracy of ±100 thousand years (Westerhold et al., 2020). The data set also covers multiple ocean basins with higher signal-to-noise ratio than any previous compilation (Westerhold et al., 2020). This data set is an updated version of the commonly used Zachos et al. (2008) compilation. Finally, the data set also includes $\delta^{13}C$ (Fig. 4.2) which can be used as a proxy for ocean productivity. One marker of the fertility of sub-surface waters (i.e., nutrients available) is the carbon isotope ratio ($^{13}C/^{12}C$, expressed as $\delta^{13}C$) (Wefer et al., 1999). $\delta^{13}C$ ratios in sediments, assumed to have originated from production within the water column, are often used as a proxy for planktonic carbon and past environmental changes such as ecosystem productivity (Schelske & Hodell, 1991; Shemesh et al., 1993; Gu et al., 1999; Chen et al., 2015), and that is

their use within this study. Note that *positive* $\delta^{13}C$ shifts indicate enhanced productivity. Ocean productivity is reflected in the flux of carbon into the sediment (Wefer et al., 1999). Hereafter, the Westerhold et al. (2020) data sets are referred to as $\delta^{18}O_W$ and $\delta^{13}C_W$.

**Deep sea δ¹⁸O reconstructed ocean temperatures**
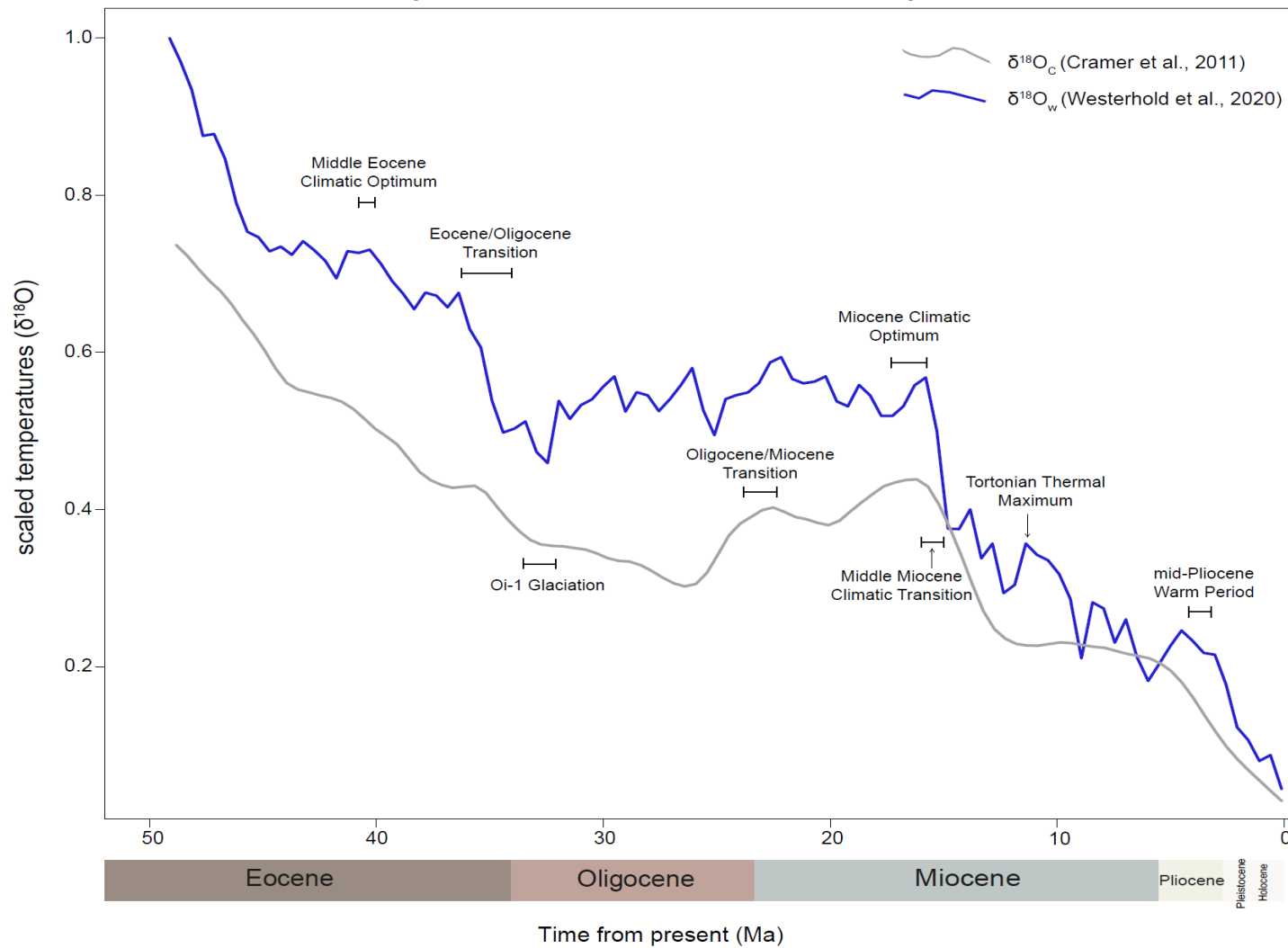
**Fig. 4.1.** Cenozoic Global Reference benthic foraminifer oxygen isotope data. Data spans the last 48.6 million years. Data are mostly generated by using benthic foraminifera tests of the taxa *Cibicidoides* and *Nuttallides* extracted from carbonate-rich deep-sea sediments drilled during Ocean Drilling Program (ODP) and Integrated Ocean Drilling Program (IODP) expeditions. Data are from Cramer et al. (2011) (grey) and Westerhold et al. (2020) (blue) and are scaled here. Oi-1 is the first major glacial period in the Oligocene. Key past climatic events have been added.



Deep sea δ¹³C reconstructed ocean productivity
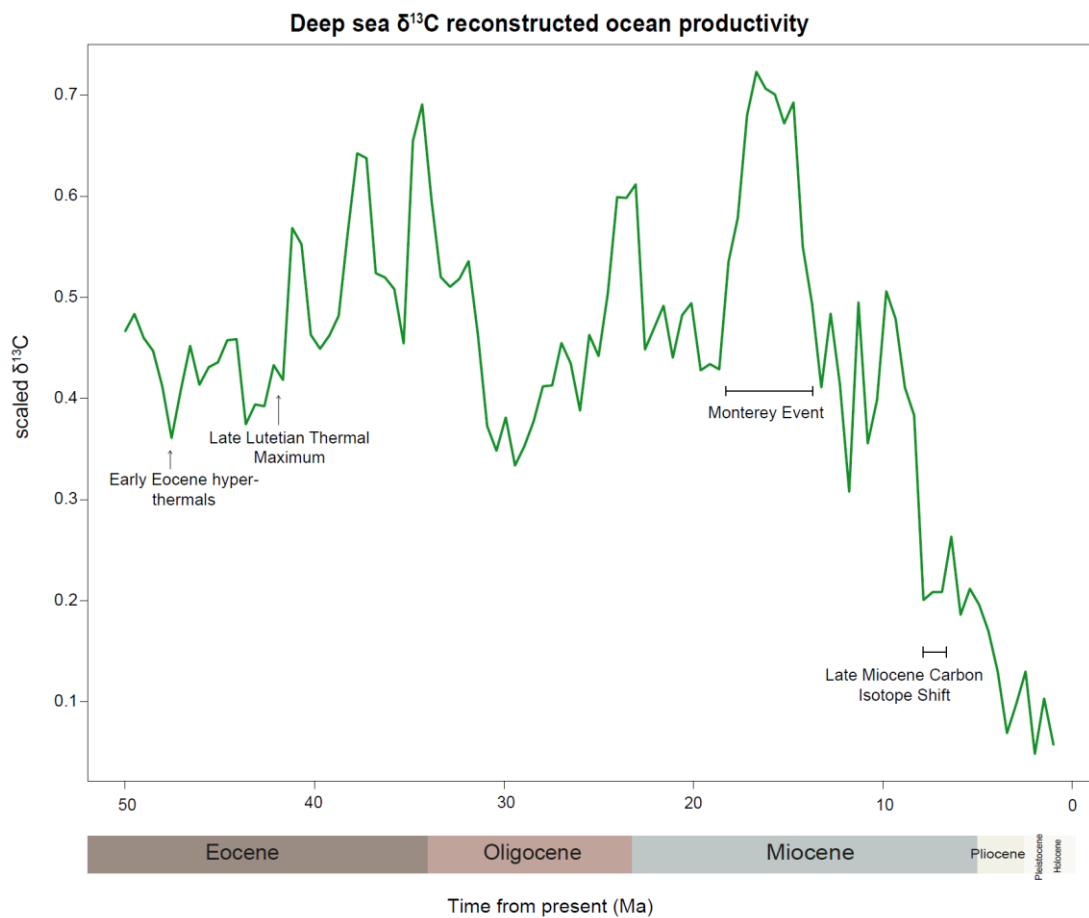
**Fig. 4.2.** Cenozoic Global Reference benthic foraminifer carbon isotope data. Data spans the last 48.6 million years. Data are mostly generated by using benthic foraminifera tests of the taxa *Cibicidoides* and *Nuttallides* extracted from carbonate-rich deep-sea sediments drilled during Ocean Drilling Program (ODP) and Integrated Ocean Drilling Program (IODP) expeditions. Data are from and Westerhold et al. (2020) and are scaled here. The Monterey Event refers to a long-lasting positive carbon excursion (Vincent and Berger, 1985). Note that *positive* $\delta^{13}C_W$ shifts indicate enhanced productivity.

### 4.3.5 Analyses

#### Climate and evolutionary models

I computed both the detrended and the derivative curve for the various models (see below). To do this I made a continuous function by extrapolating the curve with a spline and scaling it between 0 and 1. Scaling the data often makes it easier to choose starting values for the optimiser. The temperature function is then plotted over the same range as the cetacean phylogeny (i.e., 50-0 Mya). Evolutionary rates were determined from multivariate, morphometric data (see 4.3.3 pPCscores) by measuring the amount of phenotypic difference between species scaled to the amount of time since they diverged. As we calculated this for multivariate traits across a large phylogeny, we needed a matrix that describes the phylogenetic relationships as well as the differences in form. Models were run using the R packages mvMORPH v.1.1.4 (Clavel et al., 2015) and RPANDA v.1.9 (Morlon et al., 2016).

I ran three standard evolutionary models and ten novel climate models to test alternative drivers for cetacean cranial evolution. The standard models were Brownian Motion (BM), Early Burst (EB), and accelerating rates (AC). The novel climate models are detailed in Table 4.1 and Appendix 4; Fig. S4.1-6. The models vary in their use of the environmental parameters and the interactions among variables. For example, between a detrended variable and its trend which can be the climate variable, the detrended climate variable (removing any general Cenozoic trend, i.e., change in climate variable), or the derivative of the detrended climate variable (i.e., rate of change in the climate variable). I ran 31 models for each cranial data set (this includes running nine climate models using all three climate data sets (n = 27), three standard evolutionary models, and one climate combined model; Table 4.1). These 31 models were run for four cranial data sets (all Cetacea, archaeocetes, mysticetes, odontocetes), in total I ran 124 models. I did not run models with an Ornstein–Uhlenbeck assumption of evolutionary mode for several reasons: 1. The commands that run the other models (BM, EB, AC, and environmental models) cannot run OU with non-ultrametric trees and multivariate data at present. 2. In Chapter 3, a single rates OU model produced the worst fit model

for Cetacea (Appendix 3, Table S3.10), and 3. A single-rate OU model is the only model of that type that can currently be run with multivariate data in mvMORPH, and most packages at present. Given the incredible morphological difference between archaeocetes, baleen whales, and toothed whales (Chapter 3), it is unrealistic to assume that they are evolving towards one single optimum.

As in Clavel et al. (2019), I used the penalised likelihood to compare Generalised information criterion (GIC) to identify the best model fit (Table 4.2). The GIC is an extension of the Akaike information criterion (AIC) for comparing maximum likelihood estimators (or M-estimators, Konishi and Kitagawa, 2008). When the models are not nested, for example, if they have the same number of parameters, they can potentially obtain the same GIC, which can be difficult to interpret. Here, when there are multiple best fit models supported by similar GIC scores, I discuss models that have a GIC score within 2 of the best fit model.

Output from the models (and associated plots) have different scales because the model is calculated as: rates(t)*$\mathbf{R}$ where rates(t) is the overall rate change and $\mathbf{R}$ is the matrix of evolutionary covariance. Hence, one can either increase 'rates(t)' and decrease $\mathbf{R}$ or vice versa to obtain the same result. This does not change the likelihood (this is invariant) and the recovered trend is the same, meaning that the scale of evolutionary rates (as in the y-axis of several figures shown below) is arbitrary.

Finally, best-fit models (based on GIC value) were checked for convergence (and any peculiarities in the curve) using a simple diagnostic check - the 'opt' function in mvMORPH (Clavel et al., 2015). For each of the models discussed, convergence = 0, interpreted as no model issues.

[Table on next page]

**Table 4.1.** Standard evolution and novel climate models used in this study. The first 3 models are standard evolution models. BM is Brownian Motion, EB is Early Burst, and AC is accelerating rates. Traits (Y) are the morphometric cranial data. Model name, as referred to throughout this study, model components, and description of the model are provided. As throughout $\delta^{18}O_{Cr}$ is the Cramer et al. (2011) temperature data, $\delta^{18}O_W$ is the Westerhold et al. (2020) temperature data, and $\delta^{13}C_W$ is the Westerhold et al. (2020) carbon data. Curve = data from $\delta^{18}O_{Cr}$ or $\delta^{18}O_W$ or $\delta^{13}C_W$. All climate models also use the traits data (Y). Plots of the detrended and derivative curve are in Appendix 4, Fig S4.1-6.

| Model name | Components | Description and information |
| --- | --- | --- |
| BM | Traits (Y) | Brownian motion model of trait evolution. The traits (Y) evolve at a constant rate through time |
| EB | Traits (Y) | Assuming an Early Burst model of adaptive radiation |
| AC | Traits (Y) | Assuming an accelerating rate of evolution |
| Clim_combined | curve 1 is $\delta^{18}O_W$, curve 2 is $\delta^{13}C_W$ | Rates can follow the combining (additive) effects of the two curves with beta_1 controlling the first curve and beta_2 the second |
| Clim1 | raw curve | The rates follow the curve. The $\beta$ parameter controls the strength and the direction of the relationship with the climatic curve |
| Clim2 | detrended curve + trend | The rates follow the detrended curve. The $\beta$ parameter controls the strength and the direction of the relationship with the climatic curve.<br><br>Rate changes depend on the detrended environmental function and the trend, but with no interaction between them. |
| Clim3 | Detrended curve + trend + interaction | The rates follow the detrended curve + interaction with trend. The β parameter controls the strength and the direction of the relationship with the climatic curve.<br><br>Rate changes depend on the detrended environmental function and the trend, but with an interaction between them. |
| Clim4 | Detrended curve + time | The rates follow the detrended curve + time. The β parameter controls the strength and the direction of the relationship with the climatic curve Observing the change in the rate of fluctuation.<br><br>Rate changes depend on the detrended environmental function and the trend, but with *no* interaction between them. |
| Clim5 | Detrended curve + raw curve + trend | The rates follow the detrended curve + raw curve + trend. The β parameter controls the strength and the |

| | | direction of the relationship with the climatic curve observing the change in the rate of fluctuation. Rate changes depend on the detrended environmental function and the raw curve and the trend, but with *no* interaction between any of them. |
|---|---|---|
| Clim6 | Derivative curve | The rates follow the derivative curve. The β parameter controls the strength and the direction of the relationship with the climatic curve Observing the change in the rate of fluctuation. Rates depend on the derivative of the environmental curve (rate of change) only. |
| Clim7 | Detrended curve + derivative curve + trend | The rates follow the detrended curve + derivative curve + trend. The β parameter controls the strength and the direction of the relationship with the climatic curve observing the change in the rate of fluctuation. Rate changes depend on the detrended environmental function and derivative of the environmental function and the trend, but with *no* interaction between them. |
| Clim8 | Detrended curve + derivative curve + trend + interactions of detrended and derivative curve | As fitenv7 but with interactions. Rate changes depend on the detrended environmental function and derivative of the environmental function and the trend, with an interaction between the detrended and derivative curves. |
| Clim9 | Detrended curve + derivative curve (no trend) | The rates follow the detrended curve + derivative interaction but no overall trend. Rate changes depend on the detrended environmental function and derivative of the environmental function with an interaction between them (no trend involved) |

*Time bin analysis*

Rates of evolution were also plotted in a time bin analysis, independent of evolutionary models, for all Cetacea. This allows direct comparison of the reconstructed rates from the best fit evolutionary models against observed rates to qualitatively assess the fit of the best supported model. The time bin analyses were run in RPANDA v.1.9 (Morlon et al., 2016) by inserting the root age of the tree (e.g., max(nodeHeights(phy))) and specifying time bins. Time bins were chosen to best represent the raw, expected rates of cetacean evolution throughout the required period with no interaction with any climate or productivity data. All analyses were done in R v.3.5.0 (R Core Team, 2017).

## 4.4 Results

### 4.4.1 Cetacea

Novel environmental models where evolutionary rates track climate and ocean productivity consistently outperformed standard models such as Brownian Motion across all cetaceans (Table 4.2). Across all cetaceans, the top six models are extremely similar in GIC score and all involved the $\delta^{18}O_W$ data set (Table 4.2). Models run using temperature data provide a better model fit than those using ocean productivity data ($\delta^{13}C_W$). The best fit models were the 'Clim2' and 'Clim3' models followed by 'Clim5' (Fig. 4.3). After these top six models, there is a gap in GIC scores of ~9, and the next best fit models are also 'Clim3' but using the $\delta^{18}O_{Cr}$ data set (Appendix 4, Fig. S4.7) 'Clim2' and 'Clim3' are simple climate models that track temperature with no interaction or trend. The best model fit using $\delta^{13}C_W$ data was 'Clim7' a more complex model which tracked rates of $\delta^{13}C$ change (Appendix 4, Fig. S4.8). This model was ranked 8 of the 31 tested models. Results are in Table 4.2. A table with all ranked model results is available in Appendix 4, Table S4.2.

[Table on next page]

**Table 4.2.** Results for models fitted to cetacean evolutionary rates data. Top results (including the climate data used) for each model are shown. I ran 31 models, a combination of standard evolutionary models (Brownian Motion, (BM), Early-Burst (EB), and accelerating rates (AC)) and novel climate models using 3 different climate/productivity proxies. These are then ranked. The best fit model for Cetacea and each suborder is in bold. GIC scores within 2 points of the best model fit are in black, models with GIC scores > 2 of the best fit model are greyed out. The cells are coloured according to which of the climate data sets was used: $\delta^{18}O_{Cr}$ results are shown in grey, $\delta^{18}O_W$ in blue, $\delta^{13}C_W$ in green, and the combined model ($\delta^{18}O_W/ \delta^{13}C_W$) in orange. Cells coloured white are standard evolutionary models. Model is the type of model fitted to the evolutionary rates data (Table 4.1); rank is the model rank according to the GIC (generalised information criterion) score. Log-likelihood is is a measure of goodness of fit for the model. For example, the top fit 'Clim 7' model for Cetacea was a model using $\delta^{18}O_W$ data (coloured blue) and this model ranked 4/31. All model descriptions are in (Table 4.1).

| Model | Cetaceans | | | Archaeocetes | | | Mysticetes | | | Odontocetes | | |
|---|---|---|---|---|---|---|---|---|---|---|---|---|
| | Rank | GIC | LL | Rank | GIC | LL | Rank | GIC | LL | Rank | GIC | LL |
| BM | 31 | 66452.14 | -32655.34 | 27 | 917.60 | - 449.14 | 29 | 5463.24 | -2680.62 | 31 | 40542.44 | -19930.87 |
| EB | 16 | 65836.59 | -32374.81 | 3 | 909.63 | - 445.81 | 24 | 5443.44 | -2668.91 | 15 | 40406.42 | -19863.72 |
| AC | 17 | 65836.66 | -32374.9 | 11 | 911.65 | - 445.81 | 18 | 5309.32 | -2607.66 | 16 | 40409.41 | -19863.71 |
| Clim1 | 23 | 66053.98 | -32479.51 | 22 | 914.58 | - 446.62 | 23 | 5432.90 | -2667.48 | 25 | 40474.68 | -19898.52 |
| Clim2 | **1** | **65800.37** | **-32351.27** | **1** | **908.83** | **- 444.76** | **1** | **5300.38** | **-2598.81** | 4 | 40395.78 | -19856.8 |
| Clim3 | 2 | 65801.34 | -32351.33 | 2 | 908.93 | - 444.20 | 2 | 5302.41 | -2598.75 | 8 | 40401.39 | -19859.05 |
| Clim4 | 5 | 65802.77 | -32351.46 | 8 | 910.85 | - 444.79 | 3 | 5302.47 | -2598.87 | 5 | 40395.81 | -19856.81 |
| Clim5 | 3 | 65802.39 | -32351.25 | 7 | 910.84 | - 444.76 | 5 | 5302.95 | -2598.98 | 7 | 40397.75 | -19856.78 |
| Clim6 | 29 | 66368.65 | -32614.04 | 26 | 917.60 | - 448.51 | 28 | 5462.32 | -2679.45 | 23 | 40430.84 | -19870.69 |
| Clim7 | 4 | 65802.6 | -32350.92 | 4 | 909.68 | - 444.05 | 6 | 5302.98 | -2599.00 | **1** | **40394.02** | **-19852.83** |
| Clim8 | 6 | 65803.86 | -32349.02 | 15 | 912.75 | - 444.65 | 10 | 5304.98 | -2599.01 | 2 | 40394.48 | -19852.37 |
| Clim9 | 24 | 66113.34 | -32483.83 | 12 | 912.46 | - 445.63 | 21 | 5358.59 | -2633.23 | 19 | 40413.04 | -19862.12 |
| Clim_combined | 21 | 65976.05 | -32440.19 | 14 | 912.72 | - 445.82 | 19 | 5310.06 | -2606.50 | 24 | 40436.81 | -19875.85 |

For all Cetacea, 'Clim5' provides a very similar model fit to 'Clim2' and 'Clim3' (Table 4.2; Fig. 4.3), but unlike these models, the climatic curve in 'Clim5' observes the change in the *rate* of temperature fluctuation rather than tracking temperature or change in temperature itself. Full model results are provided in Appendix 4, Table S4.2.

Reconstructed evolutionary rates for the top three best fit models for all Cetacea display a general decline through time after an initial large peak in rates ~45 Mya. Further, smaller peaks in evolutionary rates are seen just before the Middle Eocene Climatic Optimum (MECO) at ~ 42 Mya and then at ~38 Mya. Similar patterns in evolutionary rates are seen when modelling the $\delta^{18}O_{Cr}$ data (Appendix 4, Fig. S4.7). Rates remain high but follow a general decline (bar the peaks mentioned) throughout the Mid-Late Eocene (Fig. 4.3(a)). There is a sharp uptick in rates just after the Eocene-Oligocene Transition (EOT), around 33 Mya, peaking at around 32 Mya before declining throughout the Oligocene and into the Miocene. Throughout the Miocene there are several small increases in evolutionary rates, but generally rates remain low (Fig. 4.3(a)). A time bin analysis shows expected cetacean evolutionary rates, when considered with no climate interaction (Fig. 4.3(b)). The observed rates from the climate driven models (Fig. 4.3(a)) match those obtained from the expected cetacean rates with peaks in the Early-Middle Eocene, the EOT, and smaller peaks in the Miocene (Fig. 4.3(b)).

a.

b.
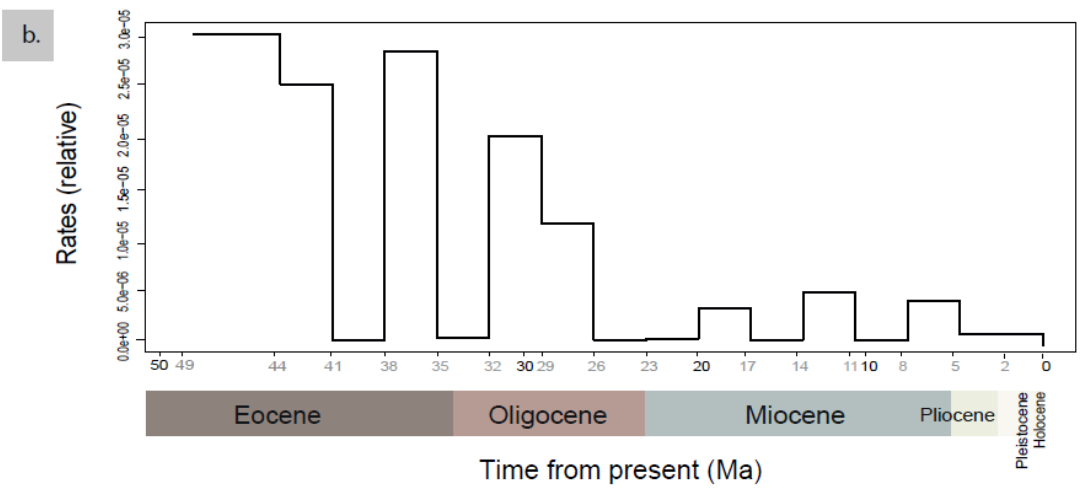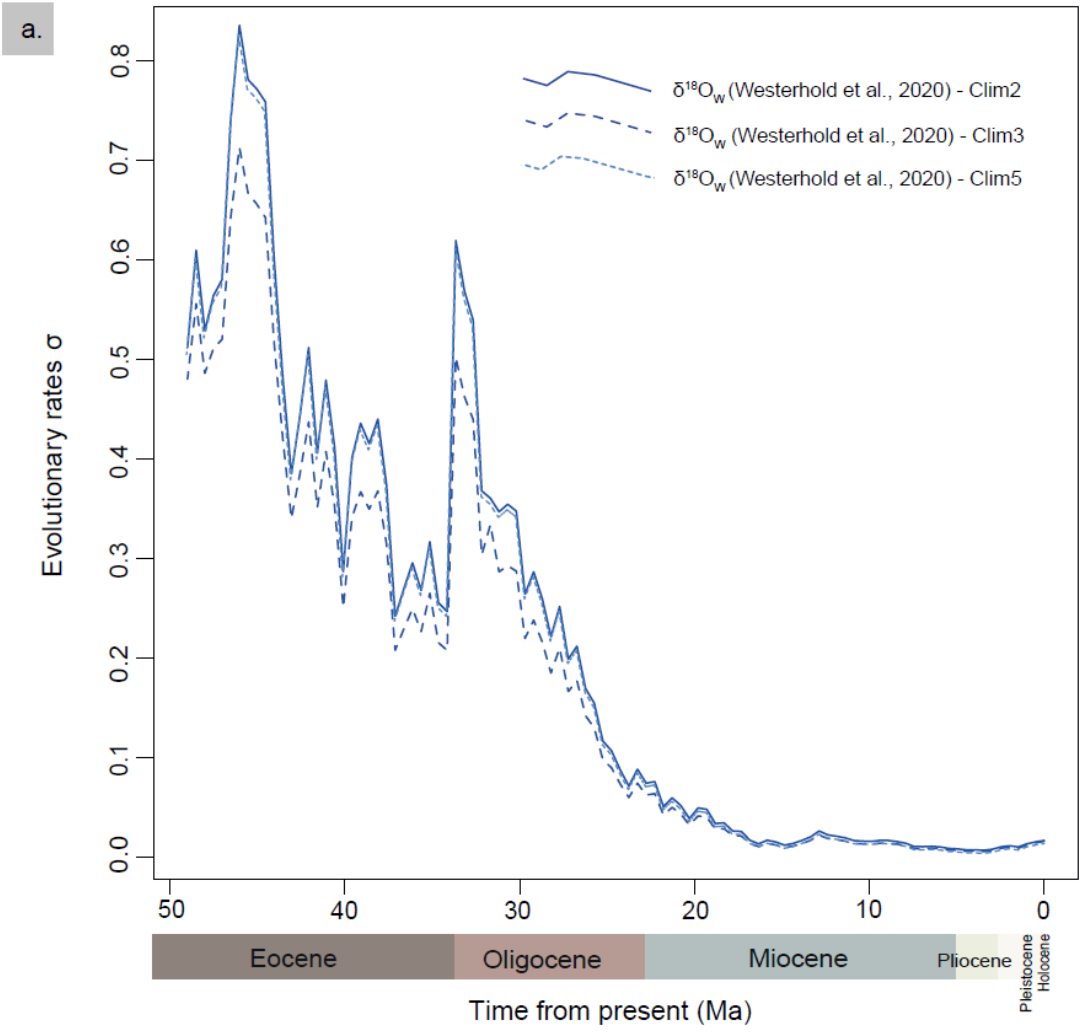
[Figure on previous page]

**Fig. 4.3.** Reconstructed evolutionary rates for Cetacea under the 'Clim2', 'Clim3', and 'Clim5' models. a) Rates modelled using deep sea $\delta^{18}O_W$ reconstructed ocean temperatures. b) Estimated rates of evolution plotted in a time bin analysis, independent of any evolutionary model. Numbers on x-axis are highlighted black to match up with (a). Greyed numbers show time-bins i.e., every 3 years in this case. The observed rates produced from the best fit models (a) are considered against the expected rates results. i.e., independent of any evolutionary model (b) to assess for model fit. Scale on the y-axis is arbitrary (see Methods, 4.3).

### 4.4.2 Archaeocetes

As there are only 11 archaeocetes in the data set, these results should be interpreted with caution.  The top seven models all return very similar GIC scores (difference in GIC score of ~ 2) and support a range of models. The top two best fit models are 'Clim2' and 'Clim3' and track $\delta^{13}C_W$ (Fig. 4.4; 4.5), followed closely by an Early Burst model (Table 4.1, Fig. 4.6). Two of the top seven models involve $\delta^{18}O_{Cr}$, while four, including the top two best fit models, track $\delta^{13}C_W$. A time bin analysis shows expected archaeocete evolutionary rates, when considered with no climate interaction (Fig. 4.4(b)). The observed rates from the climate driven models (Fig. 4.4(a)) match those obtained from the expected archaeocete rates with peaks in the Early Eocene and again at ~ 40 Mya (Fig. 4.4(b)).

a.

b.
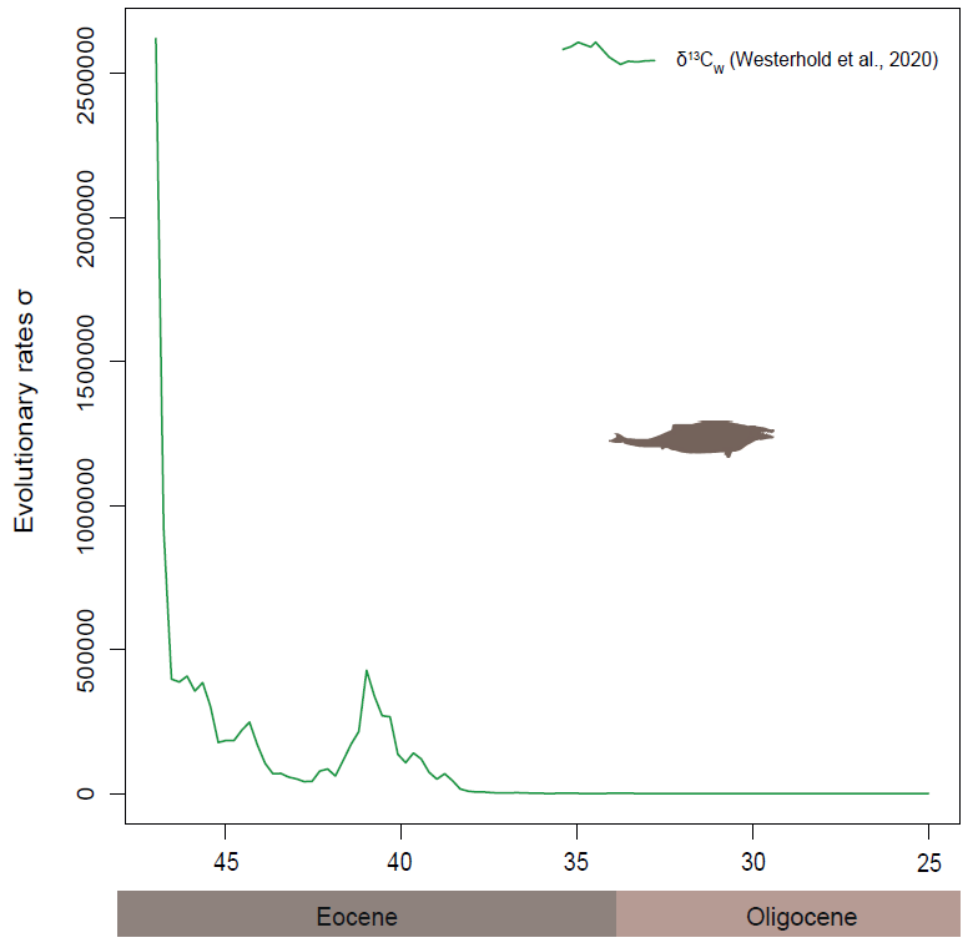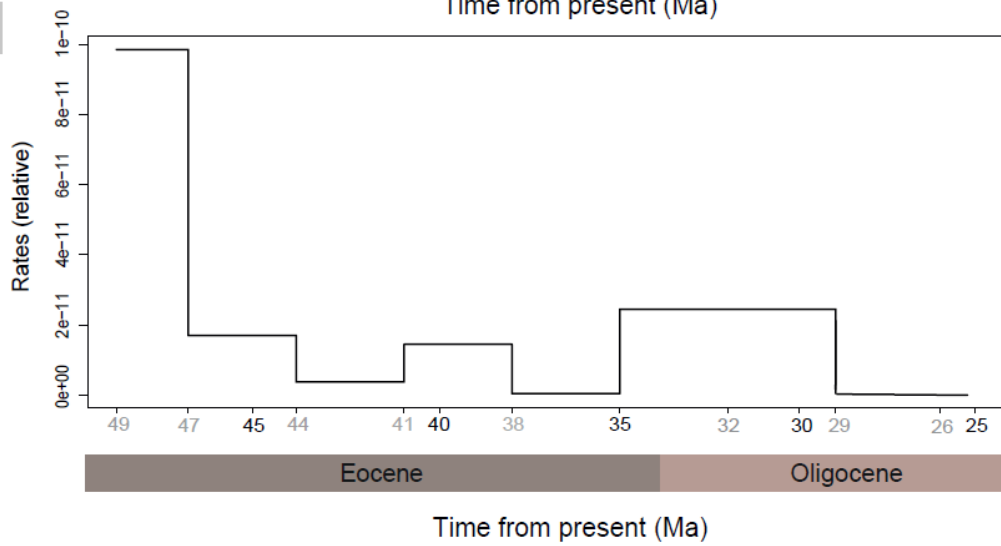
**Fig. 4.4.** Reconstructed evolutionary rates for archaeocetes under the 'Clim2' model. a) Rates modelled using deep sea $\delta^{13}C_W$ reconstructed ocean productivity. b) Estimated rates of evolution plotted in a time bin analysis, independent of any evolutionary model. Numbers on x-axis are highlighted black to match up with (a). Greyed numbers show time-bins i.e., every 3 years in this case. The observed rates produced from the best fit models (a) are considered against the expected rates results i.e., independent of any evolutionary model (b) to assess for model fit. Scale on the y-axis is arbitrary (see Methods 4.3).
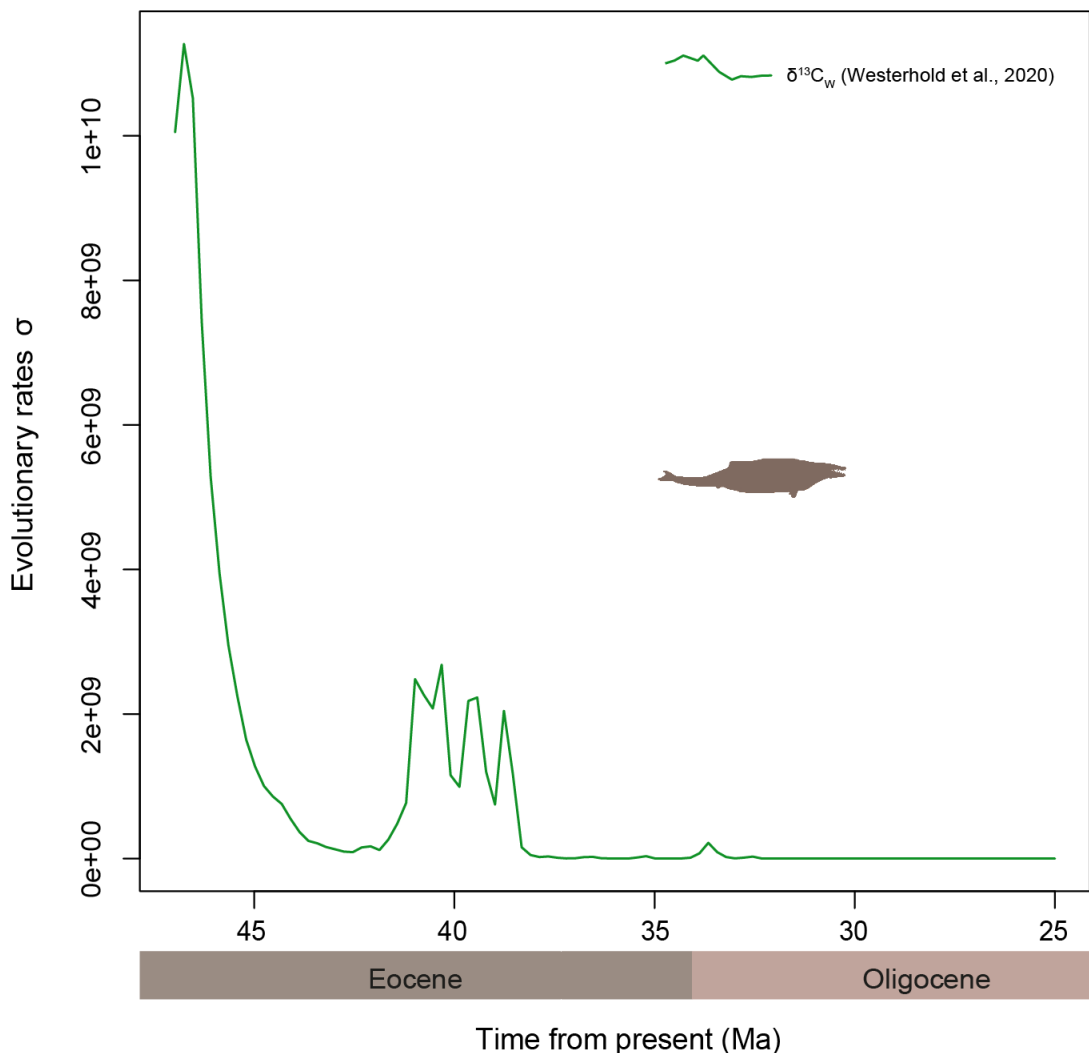


**Fig. 4.5.** Reconstructed evolutionary rates for archaeocetes under the 'Clim3' model. Rates modelled using deep sea $\delta^{13}C_W$ reconstructed ocean productivity. Scale on the y-axis is arbitrary (see Methods, 4.3).

Archaeocete evolutionary rates are characterised by high rates during the early to Mid-Eocene (Fig 4.4; 4.5; 4.6). Following a decline in rates after this initial radiation, I see an increase in evolutionary rates in the late Middle Eocene, around 42-38 Mya with a decrease in rates at ~40 Mya, in both models, around the time of the MECO (Fig 4.4(a); 4.5). Low rates of evolution are estimated from the late Eocene through the Oligocene, at the end of which the archaeocetes disappear from the fossil record (Fig 4.4(a); 4.5).
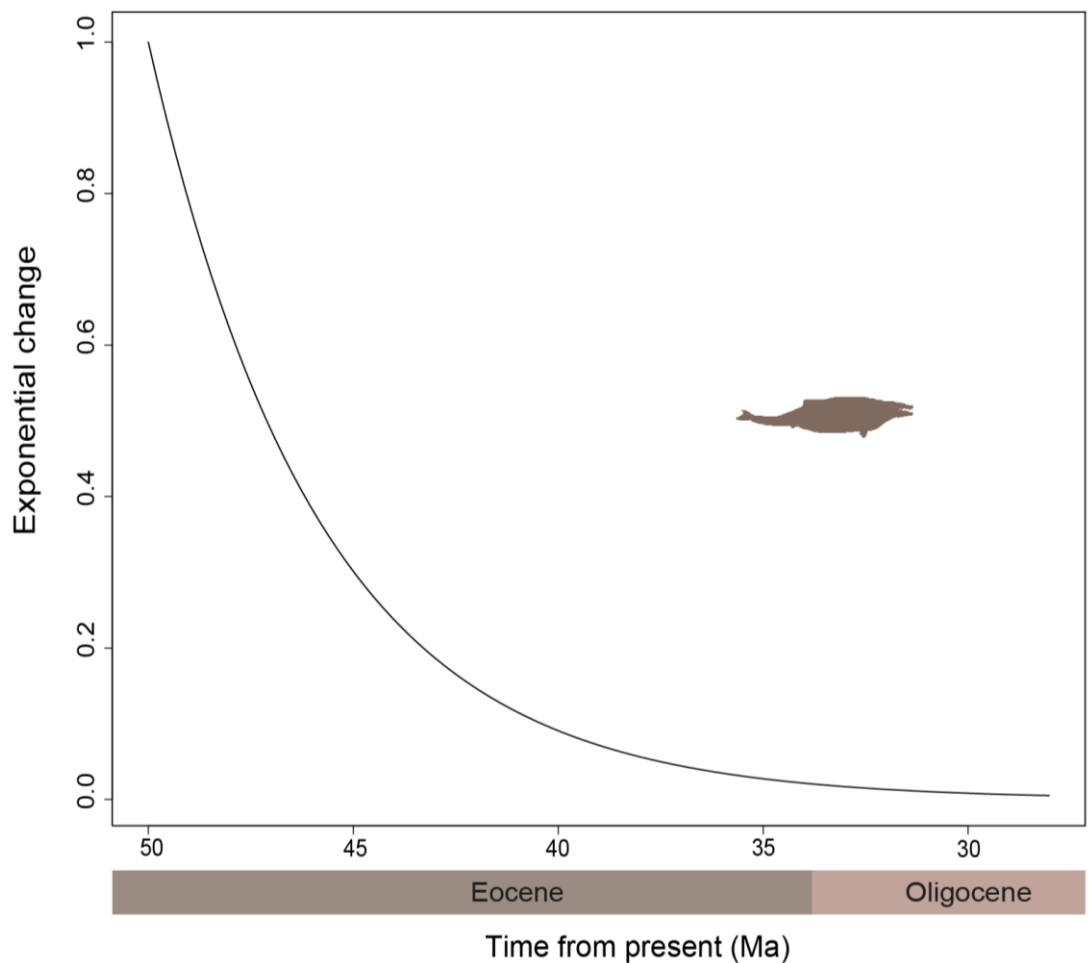


**Fig. 4.6.** Exponential change in the archaeocete Early Burst model parameter.

### 4.4.3 Mysticetes

The best fit model for mysticete rates of evolution is 'Clim2' with the $\delta^{13}C_W$ data which predominately tracks changes in ocean productivity (Table 4.2; Fig.4.7). No other model is within GIC < 2 of this model, though six are ranked between GIC 2-3 thereafter. Of those, four other models involve $\delta^{13}C_W$, while two are $\delta^{18}O_{Cr}$ (Appendix 4; Table S4.2). Reconstructed rates of evolution for mysticetes are high in the Late Eocene and reach a peak at ~ 30 Mya, in the Early-Mid Oligocene (Fig. 4.7). A time bin analysis shows expected mysticete evolutionary rates, when considered with no climate interaction (Fig. 4.7(b)). The observed rates from the climate driven models (Fig. 4.7(a)) match those obtained from the expected mysticete rates with peaks in the Late Eocene and Mid-Late Oligocene (Fig. 4.7(b)).

a.

b.
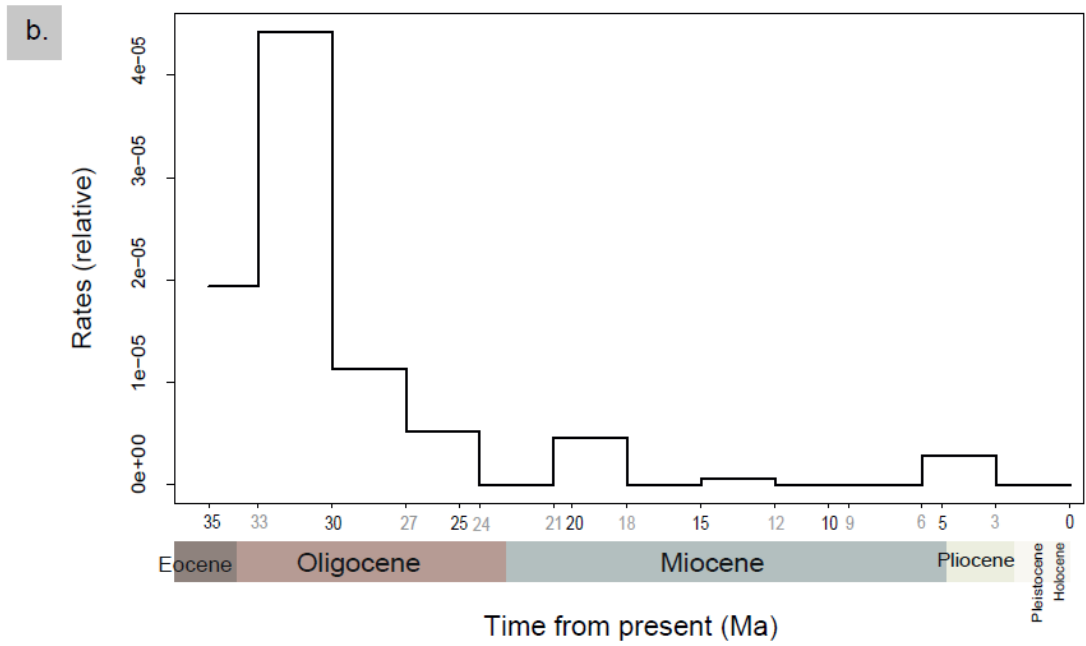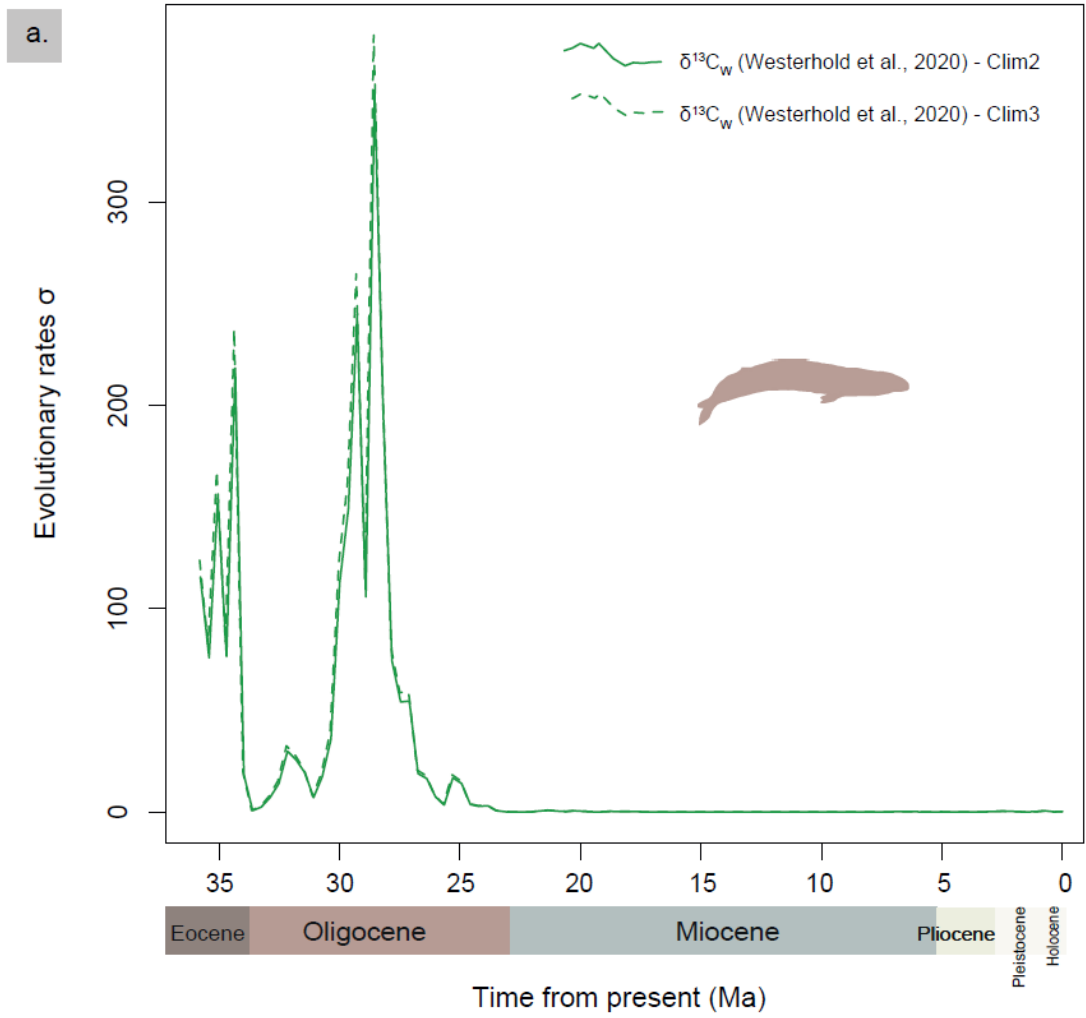
[Figure on previous page]

**Fig. 4.7.** Reconstructed evolutionary rates for mysticetes under the 'Clim2' and 'Clim3' models. a) Rates modelled using deep sea $\delta^{13}C_W$ reconstructed ocean productivity. b) Estimated rates of evolution plotted in a time bin analysis, independent of any evolutionary model. Numbers on x-axis are highlighted black to match up with (a). Greyed numbers show time-bins i.e., every 3 years in this case. The observed rates produced from the best fit models (a) are considered against the expected rates results i.e., independent of any evolutionary model (b) to assess for model fit. Scale on the y-axis is arbitrary (see Methods, 4.3).

From around 25-23 Mya through to the present, mysticete evolutionary rates slow down (Fig. 4.7; 4.8). The same pattern is seen when modelling most of the other top 7 models, including the 'Clim2' model with $\delta^{18}O_{Cr}$ (Fig. 4.8), which is the 4th best fit model. The one exception to this pattern is the third-best model fit, 'Clim4' with $\delta^{13}C_W$ data (Table 4.2, Fig. 4.9), reconstructs additional peaks in rates in the Pliocene to present. 'Clim4' fits a detrended environmental function with overall time, but with no interactions.
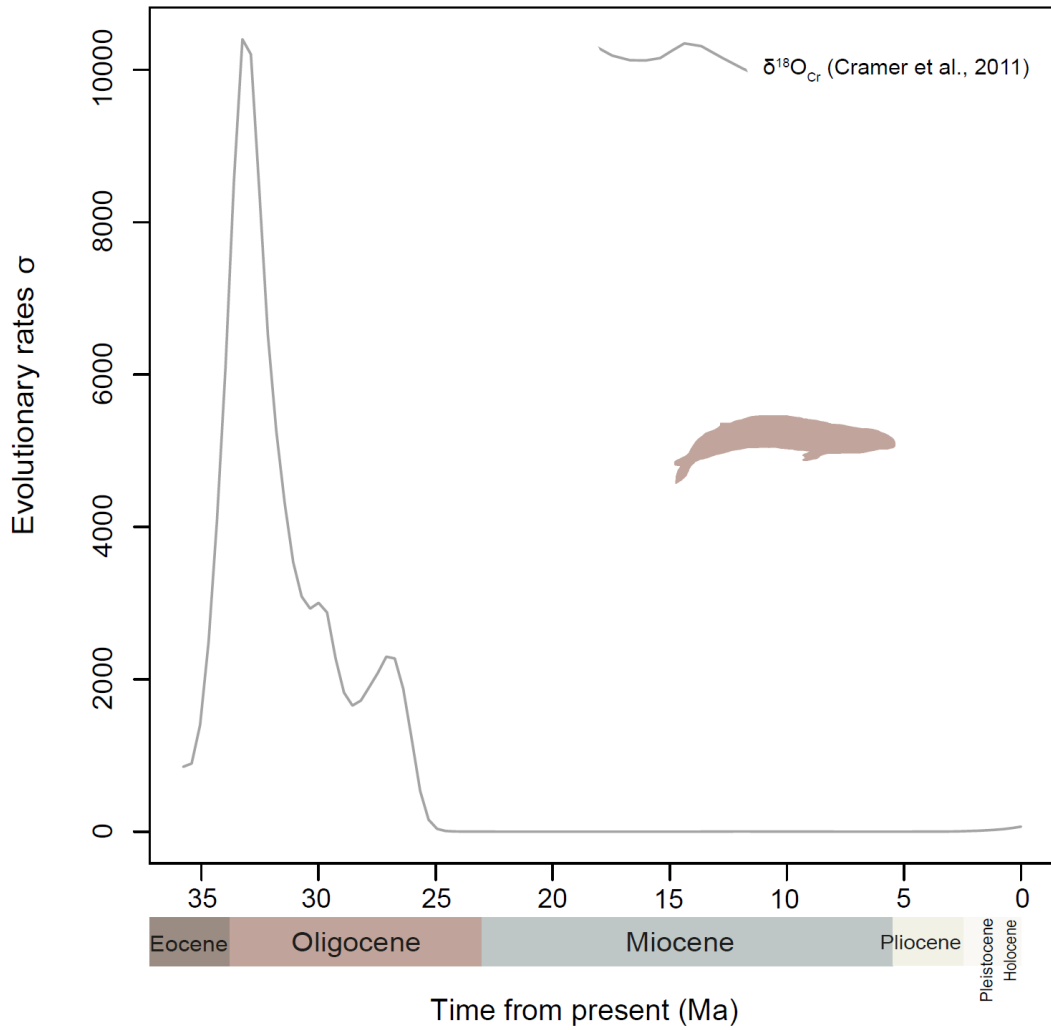
**Fig. 4.8.** Reconstructed evolutionary rates for mysticetes under the 'Clim2' model. Rates modelled using deep sea $\delta^{18}O_{Cr}$ reconstructed ocean temperatures. Scale on the y-axis is arbitrary (see Methods, 4.3).
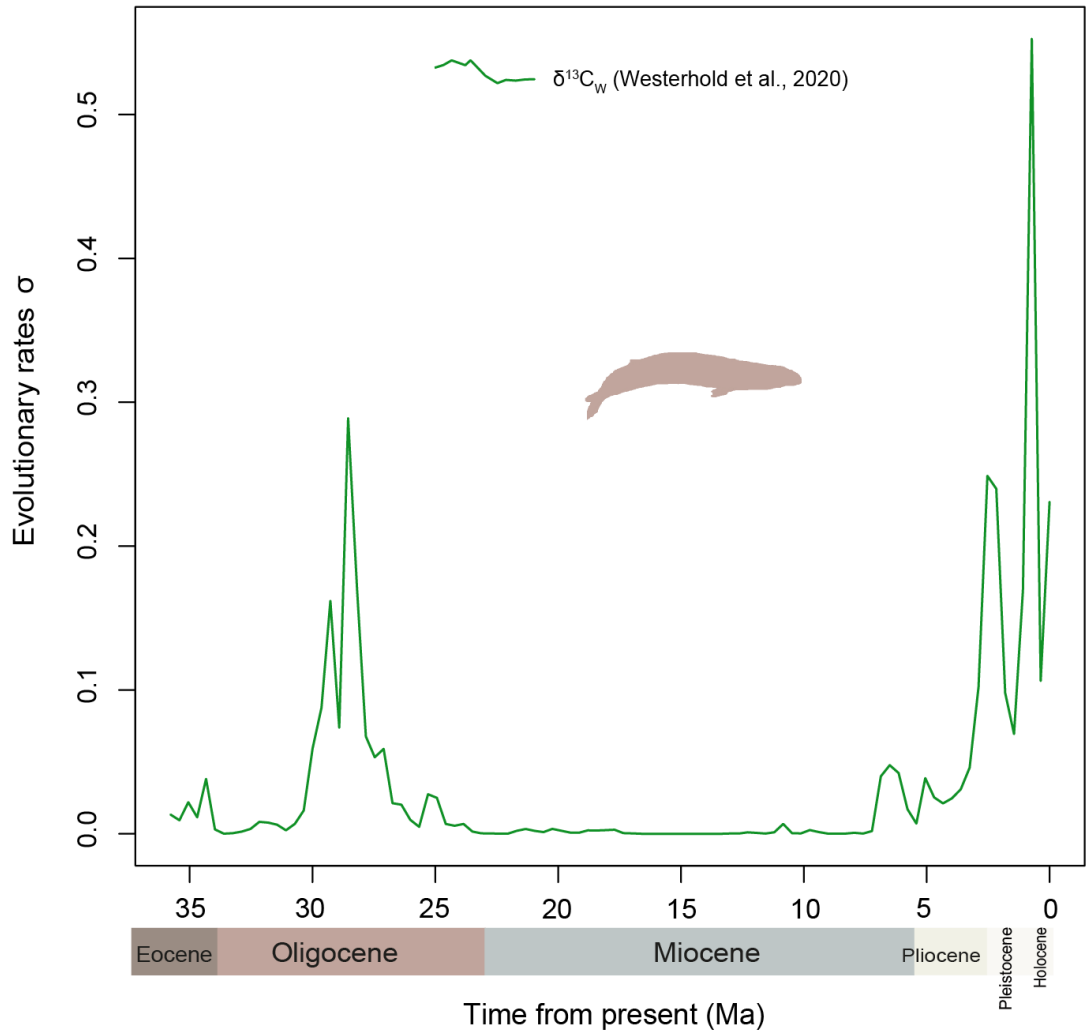
**Fig. 4.9.** Reconstructed evolutionary rates for mysticetes under the 'Clim4' model. Rates modelled using deep sea $\delta^{13}C_W$ reconstructed ocean productivity. Scale on the y-axis is arbitrary ((see Methods 4.3).

### 4.4.4 Odontocetes

Complex environmental models based on temperature were best supported for odontocetes. The top three best fit models are within GIC < 1 of each other and all involve the 'Clim7' or 'Clim8' models with one of the two $\delta^{18}O$ data sets. The $\delta^{18}O_{Cr}$ data provided the best model fit (Table 4.2, Fig. 4.10, Appendix 4, Table S4.2) with the $\delta^{18}O_W$ offering an almost identical model fit under 'Clim7' and 'Clim8' (Table 4.2; Fig.4.11). In these two models, rate of evolution tracks palaeotemperature, with rate of temperature changes interacting with absolute temperatures, see Appendix 4, Table S4.2 for the differences between the models. A time bin analysis shows expected odontocete evolutionary rates, when considered with no climate interaction (Fig. 4.10(b)). The observed rates from the climate driven models (Fig. 4.10(a)) match those obtained from the expected odontocete rates. The odontocetes show several peaks in evolutionary rate throughout the past ~ 36 million years. The highest rates are observed in the latest Eocene to Early Oligocene and again later in the Oligocene, with a further increase in evolutionary rates after the Middle Miocene and throughout the Pliocene (Fig. 4.10).

a.



b.
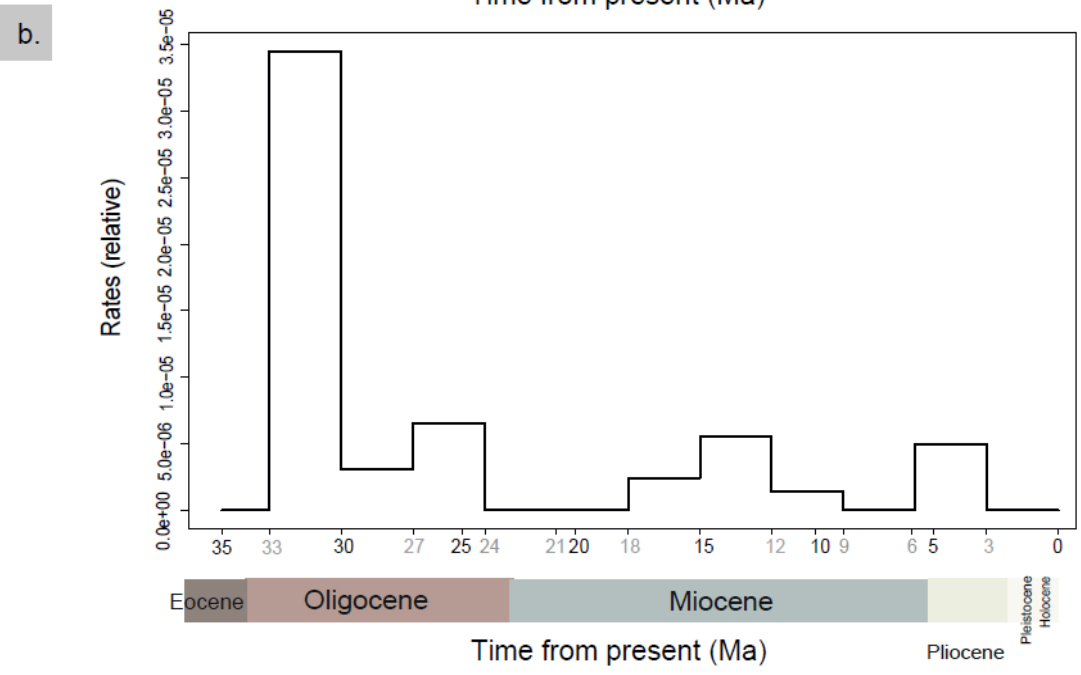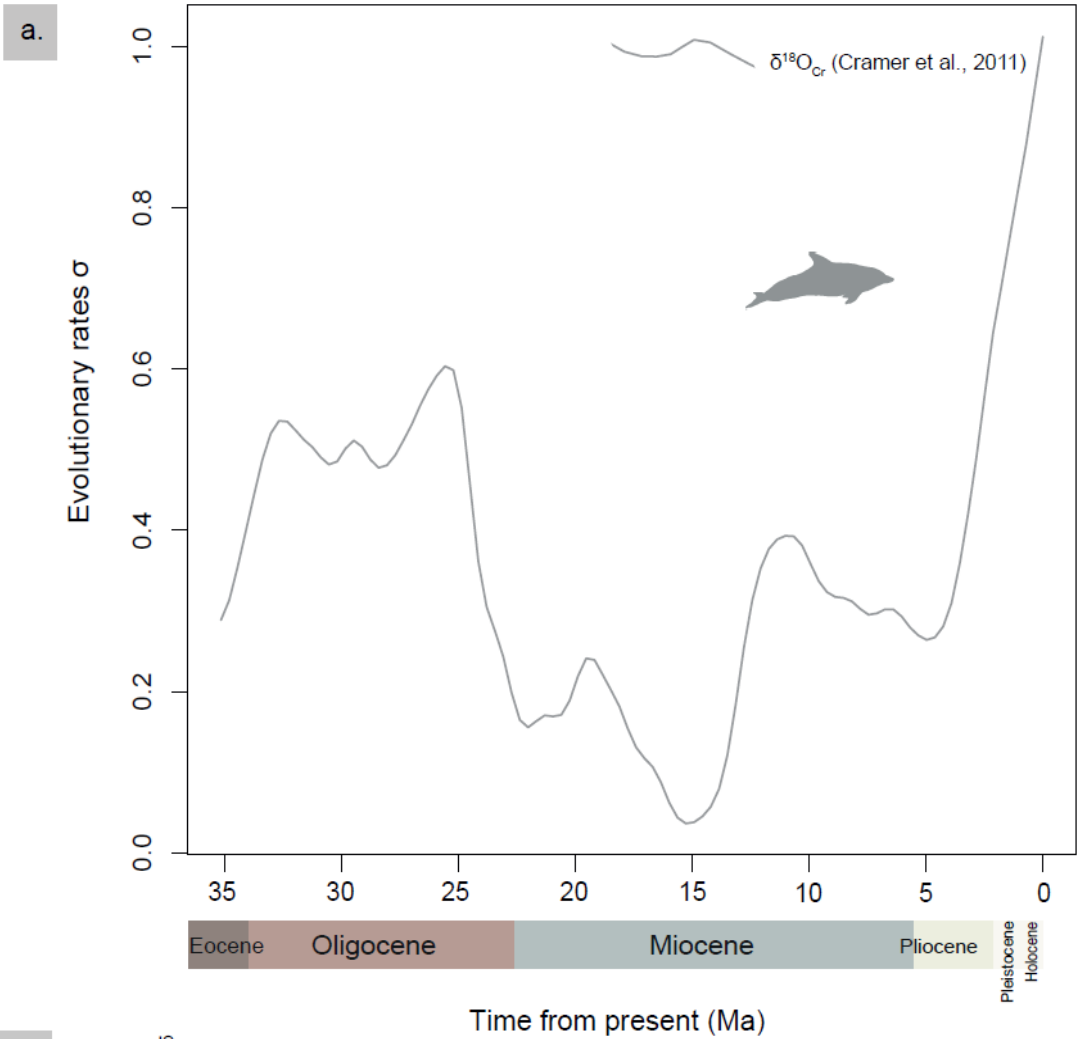
[Figure on previous page]

**Fig. 4.10.** Reconstructed evolutionary rates for odontocetes under the 'Clim7' model. a) Rates modelled using deep sea $\delta^{18}O_{Cr}$ reconstructed ocean temperatures. b) Estimated rates of evolution plotted in a time bin analysis, independent of any evolutionary model. Numbers on x-axis are highlighted black to match up with (a). Greyed numbers show time-bins i.e., every 3 years in this case. The observed rates produced from the best fit models (a) are considered against the expected rates results i.e., independent of any evolutionary model (b) to assess for model fit. Scale on the y-axis is arbitrary (see Methods, 4.3).
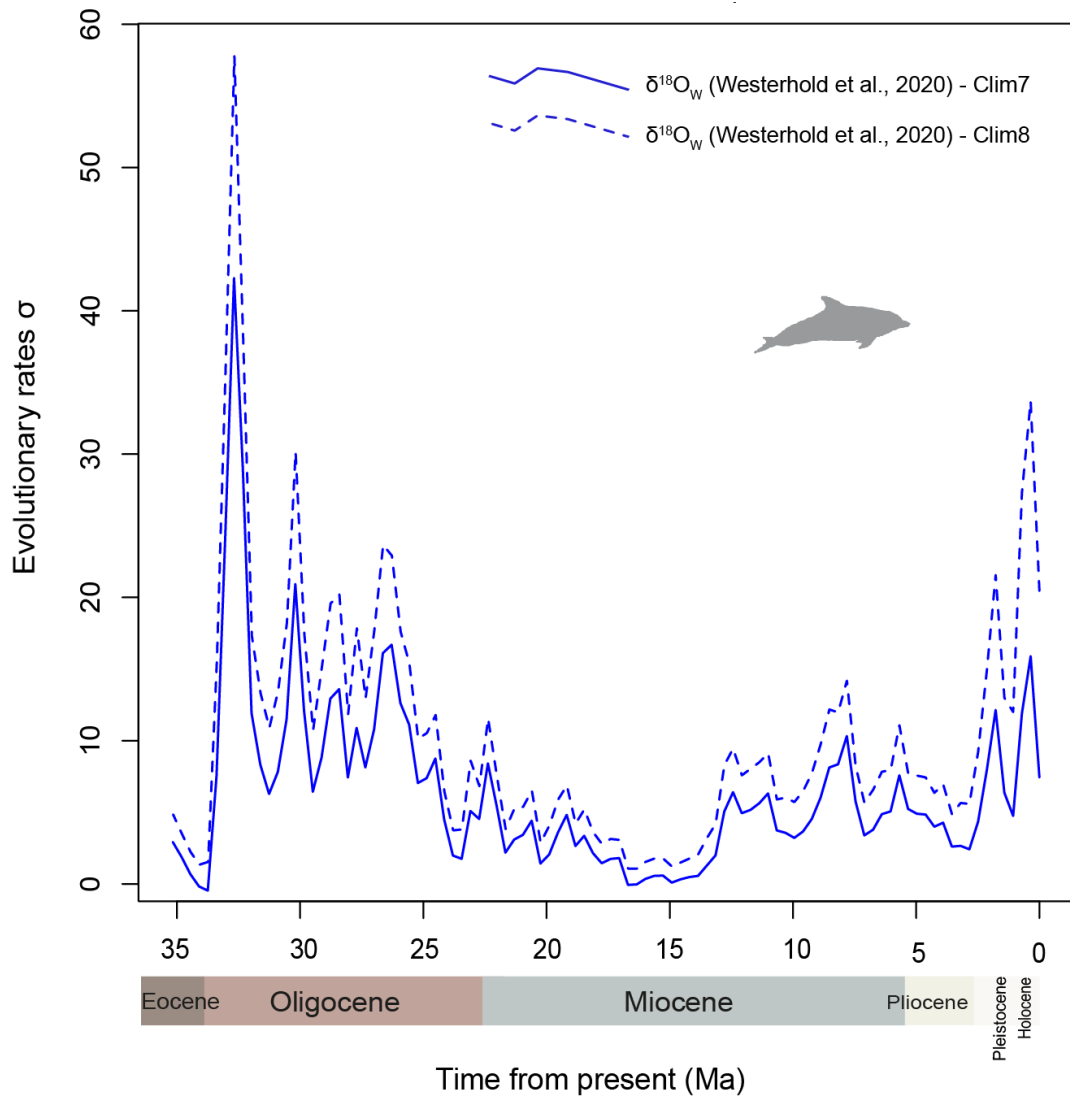
**Fig. 4.11.** Reconstructed evolutionary rates for odontocetes under the 'Clim7' and 'Clim8' models. Rates modelled using deep sea $\delta^{18}O_W$ reconstructed ocean temperatures. Scale on the y-axis is arbitrary (see Methods 4.3).

Models fitted with $\delta^{13}C_W$ generally offer a poorer model fit for the odontocetes. The top model fit using the $\delta^{13}C_W$ was a 'Clim7' model, which was ranked 13 out of 31, with difference in GIC of 11.2 from the best fit model. Reconstructed rates under this suggests multiple peaks in odontocete evolutionary rates, with the most prominent in the Mid-Oligocene and Late Miocene (Appendix 4, Fig. S4.9). For ease of comparison, the single best fit model fit for each suborder, and for all Cetacea, is shown in Figure 4.12. Note the differences in patterns of evolutionary rates for each of the suborders.

a.

δ¹⁸O$_w$ (Westerhold et al., 2020) - Clim2

Evolutionary rates σ

Time from present (Ma)

Eocene | Oligocene | Miocene | Pliocene | Pleistocene Holocene

b.

δ¹³C$_w$ (Westerhold et al., 2020) - Clim2

Evolutionary rates σ

Only kekenodontids remain

Time from present (Ma)

Eocene | Oligocene | Miocene | Pliocene | Pleistocene Holocene

c.

δ¹³C$_w$ (Westerhold et al., 2020) - Clim2

Evolutionary rates σ

Records of earliest 'true' baleen ~ 27.5 Mya

Earliest mysticete in data set: *Mystacodon selenensis* ~ 36.4 - 33.9 Mya

Time from present (Ma)

Eocene | Oligocene | Miocene | Pliocene | Pleistocene Holocene

d.

δ¹⁸O$_{cr}$ (Cramer et al., 2011) - Clim7

Evolutionary rates σ

Earliest records of echolocation ~ 33.9 Mya

Earliest odontocete in data set: *Simocetus rayi* ~ 33.9 - 28.4 Mya

Time from present (Ma)

Eocene | Oligocene | Miocene | Pliocene | Pleistocene Holocene

234

[Figure on previous page]

**Fig. 4.12.** Best fit climate model for Cetacea, archaeocetes, mysticetes, and odontocetes. Evolutionary rates are shown for Cetacea (a), archaeocetes (b), mysticetes (c), and odontocetes (d). Note the different climate data sets: $\delta^{18}O_W$ (blue), $\delta^{18}O_{Cr}$ (grey), and $\delta^{13}C_W$ (green). Some key evolutionary events are added. Note that the scale on the y-axis is arbitrary and not comparable across analyses (see Methods, 4.3).

## 4.5 Discussion

The influence of abiotic factors, specifically climate, has been considered for several clades using body size (Bown et al., 1994; Figueirido et al., 2012; Teplitsky and Millien, 2013; Clavel and Morlon, 2017). Clavel and Morlon (2017) found that across birds and mammals, the rate of body size evolution is driven by past climate and that evolutionary rates are higher during periods of cold, rather than warm, climates in most groups. They suggest that temperature influences evolutionary rates by modifying selective pressures (Clavel and Morlon, 2017). Figueirido et al., (2012) found that diversity patterns in chronofaunas can be correlated with a stacked deep-sea benthic foraminiferal oxygen isotope ($\delta^{18}O$) curve (from Zachos et al., 2008) which suggests climate forcing of faunal dynamics over a large macroevolutionary timescale. Teplitsky and Millien (2013) reviewed the literature on body size changes and climate fluctuations and found that size decreases could be due to non-adaptive plasticity in response to changing environmental conditions. They concluded that more studies are needed before further conclusions can be drawn about the underlying causes regarding body size and responses to a warming climate (Teplitsky and Millien, 2013). Fewer studies consider the impacts of ocean productivity on evolutionary rates other than those already discussed for cetaceans and others which consider mollusk diversity (Rex et al., 2005) and other marine invertebrates (and even then, these generally consider diversity rather than evolutionary rates). Further, the influence on dynamics of complex or multivariate aspects of morphology at the

macroevolutionary level are still poorly understood (Figueirido et al., 2012) making the results outlined here unique.

My analysis demonstrates that climate drives rates of cranial evolution across cetaceans and has done so throughout their 50-million-year evolutionary history. Importantly, I find that the evolutionary rates of archaeocetes, mysticetes, and odontocetes are impacted in different ways and to varying degrees by temperatures and ocean productivity. Climate models consistently outperformed Brownian motion and Early Burst models for all groups bar the archaeocetes. This result not only has implications for understanding the drivers behind major turnover events, but also highlights a requirement for tailored conservation and mitigation of current and future climate change for toothed whales and baleen whales.

The best-fit models for all Cetacea are simple climate models that show that evolutionary rates track the rise and fall of global temperature, as opposed to the rate of change in temperature. It is unclear why the $\delta^{18}O_W$ data provides a better model fit here than the $\delta^{18}O_{Cr}$, but the former does cover multiple ocean basins with higher signal-to-noise ratio than any previous compilation and this could provide a better model fit for globally dispersed, marine taxa. Considering the reconstructed rates of evolution for all Cetacea in light of the subordinal analyses, it is clear which clades are driving different aspects of the whole-clade pattern. The first peak in evolutionary rates (~ 45 Mya) is solely the signature of the archaeocetes, the first and only cetaceans around at that time. The archaeocetes evolved rapidly to occupy vacated aquatic niches and new ecological opportunities (Lipps and Mitchell, 1976), and were fully aquatic within 8-12 million years (Thewissen, 2014; Marx et al., 2016a). In this classic model of adaptive radiation, a clade experiences an ecological opportunity (here, progression into the marine zone from a terrestrial one), and then undergoes an 'early burst' of rapid trait evolution and speciation (Simpson, 1953; Ingram et al., 2012). Simpson (1944) hypothesised that shifts of adaptive zone would be simple and direct and would involve very high 'tachytelic' rates of evolution throughout the transitions (Simpson, 1944), and this appears to be the case in the early archaeocetes. As well as for the Early Burst model, there was an equivalent level of support for a simple model with

236

evolutionary rates driven by fluctuations in $\delta^{13}C$ as a proxy for ocean productivity. Interestingly, the similar model fits for the Early Burst and ocean productivity models for archaeocetes offers strong support for the original hypothesis of Lipps and Mitchell (1976), which proposed the archaeocetes adapted to the aquatic realm and diversified rapidly, likely responding to upwelling intensity and concomitant primary and secondary productivity (Lipps and Mitchell, 1976).

The initial rapid rates of evolution in the archaeocetes slow down throughout the Eocene with a further peak around ~ 42 Mya. By the end of the Lutetian (~ 41.7 Mya), the protocetids had dispersed outside Indo-Pakistan (their origin being the shores of the Tethys Sea) as far as western Africa and North America (Gingerich et al., 2001; Gingerich and Cappetta, 2014). By the Mid-Late Eocene, the archaeocetes (by now, all basilosaurids and possibly early kekenodontids) were fully-aquatic, had achieved a global distribution, and were directly reliant on ocean productivity, unlike during the clade's infancy, when the pakicetids and ambulocetids likely still inhabited freshwater environments (Marx et al., 2016a; Clementz et al., 2006). This peak in rates of archaeocete cranial evolution (~ 42 Mya) is consistent with an increase in productivity, where abundant, low-oxygen tolerant planktonic foraminiferal assemblages suggest increased nutrient input and surface ocean productivity in response to the environmental perturbation just before the Middle Eocene Climatic Optimum (MECO) (Luciani et al., 2010). The MECO itself (~ 40 Mya) saw a 4°C increase in surface and deep-water temperatures and a subsequent downturn in productivity (*positive* $\delta^{13}C_W$ shift, Fig. 4.2) (Boscolo-Galazzo et al., 2014; Westerhold et al., 2020). Thereafter, archaeocete evolutionary rates are low, represented by the only remaining family, the kekenodontids, from ~ 36-27 Mya. Around this same time, Cetacea was undergoing a major transition – from archaeocetes to neocetes.

The neocetes began diverging ~39 Mya, a schism that saw the mysticete and odontocetes follow distinct evolutionary pathways later supported by their unique key innovations – baleen in the mysticetes and echolocation in the odontocetes. Previous studies have estimated high evolutionary rates using a variety of methods: average adult female body length as the disparity measure

for neocetes in Slater et al. (2010) and a cladistic biogeographical analysis using taxon–area cladograms to find support for an adaptive radiation (cladogenesis) in mysticetes (specifically aetiocetids) (Hernandez Cisneros and Velez-Juarbe, 2021). Although using a variety of methods, these studies were supportive of an adaptive radiation in the neocetes (Lipps and Mitchell, 1976; Hernandez Cisneros and Velez-Juarbe, 2021; Chapter 3). However, in contradiction to this hypothesis, Steeman et al. (2009) assessed the tempo of linage accumulation through time in the neocetes and found no support for an "Early Burst" model. My results support this latter interpretation, as despite a burst in high evolutionary rates observed during the early divergence of the neocetes, climate models far outperformed an EB model for both neocete clades.

Rates of evolution in the mysticete cranium are predominately driven by fluctuating levels of ocean productivity ($\delta^{13}$C). Firstly, during the early divergence of the mysticetes as new methods of feeding were rapidly evolving, there is a peak in evolutionary rates coincident with high levels of productivity (Fig. 4.2). Then, during the Mid-Late Oligocene (~30-25 Mya), there is a second, larger increase in evolutionary rates and a concurrent increase in ocean productivity (positive $\delta^{13}$C) (Fig. 4.2). At this time, toothed mysticetes lived alongside the earliest known 'true' baleen whales, suggesting the transition from teeth to baleen-bearing occurred in the Early Oligocene (Tsai and Fordyce, 2018). It is possible that filter-feeding mysticetes were better equipped to successfully exploit high ocean productivity in upwelling regions, seen around ~30 Mya. Mysticetes with baleen (living alongside toothed mysticetes and archaeocetes) may have been at an advantage to exploit high ocean productivity, utilizing these resources and evolving feeding mechanisms and behaviours adapted to their prey (Marx et al., 2016a; Hernandez Cisneros and Velez-Juarbe, 2021). By the Late Oligocene, mysticetes display a variety of jaw forms, function, and development of baleen implying a wide range of raptorial, suction, and filter feeding behaviours (Marx et al., 2016a; Tsai and Fordyce, 2017). The archaeocetes disappeared by the end of the Oligocene and the toothed mysticetes shortly thereafter (possibly persisting into the Early

Miocene), while the chaeomysticetes (toothless 'true' mysticetes) flourished and continued to diversify (Marx et al., 2016a).

The evolutionary rates of the odontocetes, like their baleen cousins, are driven by climate fluctuations. However, unlike the mysticetes, the best model fit for the odontocetes is a more complex model suggesting that odontocete evolutionary rates are driven by the *rate* of temperature ($\delta^{18}O_W$) change rather than simply by fluctuations in temperature. These differences between the best fit models driving morphological evolution in the two extant suborders likely reflects their vastly different early key innovations and resultant 'ecospace' occupation, e.g., feeding and prey types. Even the earliest known odontocetes could echolocate (Geisler et al., 2014: Fordyce and Marx, 2018; Fordyce, 2018). This key adaptation, possibly influenced by interspecific competition, meant that odontocetes were able to utilize resources other than those in the euphotic zone, such as deep-water cephalopods and grazers predating vertically migrating prey (Lipps and Mitchell, 1976; Berger et al., 2007). This unique adaptation which enabled the exploitation of unique resources, and still does in extant species, likely bolstered high rates of evolution early in the clade's divergence. Conversely, the filter-feeding mysticetes are dependent on short food chains where energy is transmitted efficiently (Eddy et al., 2021) – namely high-density prey which aggregates in euphotic and surface waters.

These key innovations have also had a profound influence on skull shape. High evolutionary rates in the archaeocete cranium are coupled with low disparity, possibly indicating functional constraints early on in whale cranial evolution (Chapter 3). This changes after the divergence of the neocetes (~39 Mya). In the early diverging mysticetes and odontocetes, I found high evolutionary rates and increasing levels of disparity in the mysticete and odontocete skull (Chapter 3). These high rates coupled with high disparity may be a consequence of a rapid evolution towards a variety of feeding strategies in the toothed mysticetes, such as suction feeding and maybe even incipient filter-feeding and a refining and further development of echolocation in the odontocetes (Chapter 3). Cranial variation in rates and disparity between the two neocete subclades highlights the dichotomy between toothed,

echolocating whales and baleen whales as they continue to evolve to occupy their disparate ecospaces.

High evolutionary rates and diversification using morphological and molecular character scorings (Marx and Fordyce, 2015), radiation of the neocetes using molecular data to quantify the tempo of lineage accumulation (Steeman et al., 2009), and diversity using a comprehensive genus-level cetacean diversity data set (Marx and Uhen, 2010) all suggest that patterns in cetacean evolution (the mysticetes in Marx and Fordyce, 2015) are attributable to changes to ocean restructuring and resultant fluctuations in primary productivity. Particularly high rates are seen around the Eocene-Oligocene Boundary (EOB) and in the transitionary period (EOT) thereafter which are attributed to periods of palaeoceanographic changes, the main being the opening of the Southern Ocean via the Drake Passage and the Tasman Seaway (e.g., Scher and Martin 2006; Steeman et al., 2009).

Though the timing of the Drake Passage opening is controversial, this opening facilitated deep oceanic mixing that developed the Antarctic Circumpolar Current (ACC), driving increases in productivity (Kennett, 1978; Berger, 2007; Marx and Fordyce, 2015). Furthermore, Antarctic ice-sheet development (termed the Oi-1 glaciation, the first major glacial period in the Oligocene; Westerhold et al., 2020), and a lowering of sea levels by ~50 m (Miller et al., 2008, 2020), may have enhanced ocean eutrophication by the exposure and transfer of nutrient rich sediments on the continental shelf into the ocean. Marx and Uhen (2010) suggested that it was an increase in diatom diversity, driven by an upwelling of nutrients and silica, which provided an ecosystem robust enough to support the energetic requirements of these apex marine predators. The physical opening of sea ways also created more heterogeneous oceans (e.g., complexity in temperature regimes, water masses, current systems) (Fordyce, 2001), opening the passage for a truly global and circumpolar distribution in the neocetes (Fordyce, 2001; Marx et al., 2016a). However, Pyenson (2017) argues that these opportunities are not sufficient to explain the selection pressures of echolocation and mass (bulk) filter feeding at this time. It is also important to note that bulk filter-feeding and echolocation did not evolve until between four and ten million years after the advent of the ACC

(Pyenson, 2017), with echolocation evolving before baleen-filter feeding. However, the timing of the onset of the ACC is contested (Hill et al., 2013; Berger, 2007), but generally considered to have been under gradual development by the EOB, with Southern Ocean water circulation underway by 33.9 Mya (Hassold et al., 2009). I find high rates of evolution in both the mysticetes and odontocetes from 30-25 Mya; at this time the ACC was well established and strengthening. By this time baleen filter-feeding had evolved (Boessenecker and Fordyce, 2015; Tsai and Fordyce, 2018), and echolocation (present in the oldest known diverging odontocetes) was likely highly developed (Marx et al., 2016a).

Steeman et al. (2009) also attributed changes in cetacean lineage accumulation during the Miocene (~13-4 Mya) to periods of palaeoceanographic restructuring. My results suggest that this pattern does not apply to all cetaceans. Rather, only the odontocetes show fluctuations in evolutionary rates for the cranium throughout the Miocene, with mysticetes showing low rates throughout this interval. Following the Miocene Climatic Optimum, ~ 15 Mya (You et al., 2009), the Mid Miocene Climatic Transition (MMCT; Fig. 4.1) (~14.8-12.9 Mya) was a period of cooling, ice growth, ocean productivity, and enhanced deep-water circulation (Flower and Kennett, 1994; Westerhold et al., 2020). Major ocean restructuring at the time included the closure of the eastern Tethys sea (~ 13-11.6 Mya) (Torfstein and Steinberg, 2020), restriction and closure of the Central American seaway (~ 14-4.2 Mya) (Molnar, 2008), and restriction of the Indo-Pacific seaway (~ 12-5 Mya) (Kuhnt et al., 2014). This combination of planetary cooling and geographic shifts drove thermohaline circulation and enhanced phosphate deposition which saw a surge in ocean productivity: the Late Miocene Carbon Isotope Shift of 7.6-6.3 Mya (Zachos et al., 2001; Westerhold et al., 2020). Slater et al. (2010), using female body length as a measure of disparity, also found evidence for a secondary odontocete radiation and elevated levels of subclade disparity between 11 and 6 Mya, after the MMCT (the primary being the divergence of the neocetes), into areas of niche space not previously occupied, driven by a dietary shift. Furthermore, the Delphinidae show an explosive radiation that evolved in a short time span between ~15-10 Mya as quantified by

investigating diversity, measured using molecular data (McGowen et al., 2009; Steeman et al., 2009; McGowen, 2011; 2019) and skull morphology, quantified with 48 cranial landmarks (Galatius et al., 2020).

Low mysticete evolutionary rates during peaks of productivity throughout the Miocene is perhaps surprising. Coincident with the Miocene Climatic Optimum is the Monterey positive carbon isotope ($\delta^{13}C$) excursion (Woodruff and Savin, 1991; Holbourn et al., 2007). The classic interpretation of the Monterey Hypothesis proposes that long-term cooling increased the latitudinal gradient, invigorating upwelling, which led to increased organic carbon burial rates, lowering atmospheric $CO_2$ (Sosdian et al., 2020). During this time oceans became more depleted in $^{12}C$ relative to $^{13}C$ than any time in the past 50 Ma (Sosdian et al., 2020). This direct impact on productivity may have influenced the low evolutionary rates I see in the mysticetes. Fordyce (2001) suggested that one might expect that the evolution of large cetacean species (namely the mysticetes) be influenced by larger scale geological changes due to their wider distribution, whilst smaller species (namely the odontocetes, but also the remaining toothed mysticetes of the Early Miocene) were susceptible to smaller changes such as the opening or isolation of smaller ocean basins or the loss of shallow, continental shelf margins (Marx et al., 2019a). Marx et al. (2019) highlight the Miocene as a mysticete 'dark age', with a sparse fossil record, compared to the odontocetes. They attribute this to environmental change occurring around the Oligocene-Miocene boundary, such as a drop in sea levels and ocean productivity, which facilitated the decline of endemic coastal assemblages (usually the smaller bodied toothed mysticetes) (Marx et al. (2019a). Larger bodied filter feeders persisted offshore, facilitated by baleen feeding and reappeared near the shores later in the Miocene, highlighting the importance that habitat occupancy has on mysticete turnover (Marx et al., 2019a). This pattern of low mysticete rates throughout the Miocene may alternatively be a simple case of mysticetes fully filling their ecological niche around ~25 Mya, and, because of that successful early diversification, baleen-assisted filter feeding became dominant (Marx and Fordyce, 2015) and has remained largely unchanged since the Late Oligocene/Early Miocene (Werth, 2000a) as I find is the case in Miocene-to-

present mysticete skull morphology (Chapter 3). As a result, their evolutionary rates have also remained low ever since (Marx and Fordyce, 2015; Chapter 3). Finally, a drop in evolutionary rates in mysticetes in the Early Miocene may also be correlated with a drop in diatom diversity, which would be particularly impactful on cetaceans reliant on these small prey (Marx and Uhen, 2010; Bianucci et al., 2018).

Finally, low evolutionary rates remain consistent in the mysticetes from the Miocene to the present day. High evolutionary rates in the odontocetes throughout the Pliocene could be consistent with palaeoceanographicic and climatic changes occurring at this time followed by further general cooling and ice-growth trends to the present (Zachos et al., 2001). Rapid speciation in the delphinids could also reflect a diversity of ecological niche exploitation, facilitated by sophisticated echolocation, as well as other competitive advantages such as large brain sizes and sociality (LeDuc et al., 2002; Steeman et al., 2009). Steeman et al. (2009) use molecular data to attribute later speciation in the delphinids to the adaptation of geographically concentrated prey in the later Miocene, and with intensification of ocean circulation during the Plio-Pleistocene (Steeman et al., 2009) and towards the present day.

These results demonstrate that climate change and associated ocean productivity have driven evolutionary rates in cetaceans throughout their history from the Early Eocene to the present day. Furthermore, that there are different drivers behind archaeocete, mysticete, and odontocete evolutionary rates. My research highlights the idiosyncrasies of suborder responses to environmental perturbations, reinforcing the message that targeted conservation and management at a level more defined than the 'cetacean' level, for example at the genus or species level and the very least a tailored conservation approach for mysticetes and odontocetes, is a conservation requirement going forward. This is significant for the two extant suborders because not only have their evolutionary rates been driven and influenced by differing aspects of climate change in the past, but this could also have implications for how they respond to climate change in the future. Temperature amplification in the surface ocean is projected to impact primary and

secondary production (Richardson and Schoeman, 2004) due to increased stratification, diminished vertical mixing and nutrient exchange (Sarmiento et al., 2004; Behrenfeld et al., 2006). Anecdotal evidence suggests that recent warming in Nova Scotia has resulted in an *increase* in herring and humpback whale (*Megaptera novaeangliae*) numbers (Askin et al., 2017). Others have suggested that a decrease in polar ice, and thus an increase in well-lit waters, mixed by winds blowing over open, ice-free oceans has fueled a plankton bloom (Moore, 2016). Specifically, humpback, fin, and minke whales (*Megaptera novaeangliae*, *Balaenoptera physalus*, and *Balaenoptera acutorostrata*) are now regularly reported in the Pacific Arctic, exploiting these productive waters (Moore, 2016). However, these positive cases are thought to be short lived, and models have predicted that declines in prey abundance could lead to local population extinctions by 2100 (Tulloch et al., 2019). For the mysticetes whose evolutionary rates are driven by ocean productivity, conservation and management might take the form of furthering our knowledge of ocean productivity projections, for example the effects of warming oceans on phytoplankton blooms to better understand how this will affect large baleen whales, their migration to productive feeding grounds, and food availability. Conservation efforts should also focus on protecting key feeding grounds.

For the odontocetes, whose evolutionary rates are driven by the rate of temperature change, conservation efforts could focus on mitigating this as a key avenue. Loss of ice coverage and snow melt in shallow coastal and estuarine habitats pose a threat to Arctic species, particularly belugas (*Delphinapterus leucas*) and narwhals (*Monodon monoceros*) which rely on the pack ice for food and shelter (Simmonds and Elliot, 2009). Furthermore, there is concern that reduced ice will result in an increase in human oil exploration and shipping traffic (Mcleish 2013), which is detrimental to all cetaceans in the area. The effects of warming are already being observed. In Scotland, between 1992 and 2003, the relative stranding frequency of white-beaked dolphins (*Lagenorhynchus albirostris*), a cold-water species, declined, whilst records of common dolphins (*Delphinus delphis*), a warmer water species, increased (MacLeod et al., 2005).

Anthropogenic climate change poses a real and abrupt threat to cetaceans, especially those with a limited habitat range, such as the small, coastal porpoises, or those for which sea ice is an important habitat for them or their prey (Simmonds and Elliot, 2009). Further, changes in weather patterns, water temperatures, and ocean acidification associated with climate change is already affecting cetaceans through the availability, locality, and abundance of their prey (Simmonds and Elliot, 2009). Climate change could also influence reproduction; female sperm whales have shown lower rates of conception during periods of unusual warmth (Whitehead, 1997) and fluctuating rates of reproductive success in humpback whales (*Megaptera novaeangliae*) have been linked to recent climate anomalies (Cartwright et al., 2019). Many cetaceans may time breeding to coincide with maximum abundance of suitable prey. A mismatch in this timing (phenotypic mismatching), brought on by climate fluctuations will likely affect cetaceans that travel long distances between breeding and feeding grounds (Simmonds and Elliot, 2009). Finally, climate change has the potential to increase heat stress, pathogen development, and disease transmission in terrestrial and marine biota (Harvell et al., 2002).

Future climate scenarios outlined by the Intergovernmental Panel on Climate Change (IPCC) suggest that at greater depth, warming is projected to be most pronounced in the Southern Ocean (Collins et al., 2013). The Southern Ocean has been, and is, a major driver in ocean nutrient cycling and resultant cetacean diversity, likely triggering the radiation of modern whales (Fordyce, 1980; Berger, 2007; Marx and Uhen 2010). Changes to temperature and nutrient cycling in this locality could be catastrophic for cetaceans and other marine life. The IPCC suggests that best estimates of ocean warming in the top one hundred meters are about 0.6°C to 2.0°C, and about 0.3°C to 0.6°C at a depth of about 1 km by the end of this century (Collins et al., 2013), these depths are primary feeding grounds for cetaceans – especially odontocetes which hunt throughout the water column, even at great depths. Ocean warming and changes in primary production since the 20th century are related to changes in productivity of many fish stocks with high confidence in decreased net productivity (Bindoff et al., 2019) which ultimately impacts other

marine fauna. The IPCC predicts that net primary productivity will very likely decline by 4–11% (Blindoff et al., 2019) and highlights concerns regarding changes, fluctuations, and unpredictability in ocean primary productivity, upwelling, nutrient transport, and temperature (Collins et al., 2013; Blindoff et al., 2019). Further, shifts in distribution of marine species from phytoplankton to marine mammals have been observed across all ocean regions (Poloczanska et al., 2016), with range shifts in the epipelagic region strongly correlated with ocean temperature change (Poloczanska et al., 2016) – the key driver of odontocete evolutionary rates in my models. My models show that evolutionary rates in cetaceans are driven by associated climate change and ocean productivity making these future scenarios a very real threat to cetacean diversity.

Finally, it should be noted that the models in this study use benthic foraminifera as a proxy for ocean productivity. Although a commonly used proxy, benthic foraminifera are reflective of lower-level oceanic conditions. Future studies should consider other proxies of productivity such as diatom and nannofossil diversity. Further, it is increasingly recognised in conservation and ecosystem management that ecology needs a palaeontological perspective (Louys et al., 2012) and this should be a priority for studies of this type. Although it is unclear how and if species will adapt to climate change in the future and to what extent they will be able to respond to climate pressures, this work shows that different aspects of environmental change have affected cetacean evolution in the past and provides critical new understanding for more accurately predicting their future responses. By looking at the fossil record we can assess the ecological limits and adaptations of cetaceans to past climate changes and use this knowledge in our arsenal to help protect them in the future.

## 4.6 Conclusions

This study is the first comprehensive analysis of the impact of Cenozoic climate change on the morphological evolution of cetaceans. I find that changes in climate and climate-related variables better explain variation in rates of cranial evolution than do standard evolutionary models; however, the key variables differ across cetacean suborders. The stem whales,

archaeocetes, showed similar levels of support for an Early Burst model and a model driven by ocean productivity. This period of cetacean evolution, immediately following their invasion into the aquatic realm from around ~53 Mya, is characterised by the fastest rates seen across Cetacea (Chapter 3), with a peak in evolutionary rates around ~42 Mya that is best explained by $\delta^{13}C$ fluctuations. By this time, archaeocete families were fully aquatic and fully reliant on ocean productivity. Like the archaeocetes, rates of evolution for the mysticete cranium are also driven by fluctuations in $\delta^{13}C$, whereas odontocete evolutionary rates track the rate of temperature change. Despite high rates of evolution in the early diverging neocetes, climate models consistently outperform standard EB, BM, or accelerating rates models for both suborders.

Peaks in both mysticete and odontocete evolutionary rates coincide with massive ocean restructuring. At the Eocene-Oligocene Boundary, the opening of the Drake Passage and intensification of Southern Ocean currents appears to have driven high rates of cranial evolution in both suborders. Ocean restructuring during the Miocene, although more localised than in the Oligocene, likely also impacted rates and dispersion, particularly in the odontocetes. At this same time, the oceanic delphinids were undergoing an explosive radiation which likely represents most of the signal seen in Cetacea during this period. Evolutionary rates in the mysticetes and odontocetes are driven by different aspects of climate change, and this has clear implications for their evolution under future climate scenarios. It highlights the idiosyncrasies of suborder responses to environmental perturbations, reinforcing the message that targeted conservation and management at a level more defined than the 'cetacean' level, at the very least tailored to the suborder level, is a conservation requirement going forward. For the mysticetes whose evolutionary rates are driven by ocean productivity, conservation efforts should focus on protecting key feeding grounds, furthering our knowledge of ocean productivity under different climate scenarios, and mitigating climate change. For the odontocetes, whose evolutionary rates are driven by the *rate* of temperature change, conservation efforts should focus on mitigating this as a key avenue of protection. For both suborders, applying additional protections to species that are most vulnerable e.g., those at the

polar extremes or those with niche and specialist diets, both examples of animals more vulnerable to perturbations, should be a priority.

**Chapter five**

**What can cetacean stranding records tell us? A study of UK and Irish cetacean diversity over the past 100 years**

*This paper is dedicated to the memory of my friend Joanna Toole who worked tirelessly to improve ocean health and conservation and to reduce the impacts of bycatch on marine species. Jo left this planet far too soon, but her work and legacy will benefit wildlife well into the future.*

https://joannatoolefoundation.org/

## 5.1 Abstract

There are many factors that may explain why cetaceans (whales, dolphins, and porpoises) strand. Around the UK and Ireland, over 20,000 stranding records have been collected since 1913, resulting in one of the longest, continuous, systematic stranding data sets in the world. We use this data set to investigate temporal and spatial trends in cetacean strandings and use Generalised additive models (GAMs) to investigate correlates of strandings. We find a dramatic increase in strandings since the 1980s, most likely due to increases in recording effort, and the formation of formal strandings networks. We found no correlation between the numbers of cetaceans stranding each year and several potential environmental and anthropogenic predictors: storms, geomagnetic activity, North Atlantic Oscillations, sea-surface temperature, and fishing catch. We suggest that this is because the scale of change in the variables is too coarse to detect any potential correlations. It may also highlight the idiosyncratic nature of species' responses to external pressures, and further the need to investigate other potential correlates of strandings, such as bycatch and military sonar. Long-term cetacean stranding data provide vital information on past and present diversity for common, rare, and inconspicuous species. This study underlines the importance of continued support for stranding networks.

**Keywords:** cetaceans, strandings, diversity, generalised additive models, macroecology

## 5.2 Introduction

Cetaceans (whales, dolphins, and porpoises) are major components of oceanic ecosystems (Roman et al., 2014). They are top predators and their distributions can provide an indication of prey abundance and wider ocean health (Friedlaender et al., 2006; Burek et al., 2008; Roman et al., 2014). Unfortunately, many cetacean species are threatened (Reeves et al., 2003; IUCN SSC, 2018) and are vulnerable to anthropogenic impacts, such as incidental entanglement in fishing gear (bycatch), ship strikes, hunting, chemical or noise pollution, and environmental changes across their ranges (Parsons et al., 2013; Ramp et al., 2015). It is therefore important to monitor cetaceans to determine the impacts of these pressures on their abundance and behavior (Bejder et al., 2006). As with other marine species, cetaceans can prove difficult to study as they are often wide-ranging and spend most of their lives submerged under water (Evans and Hammond, 2004). Frequently employed monitoring techniques, such as surveying from boats, are not only expensive and time consuming, but are often biased towards conspicuous species or those that respond positively to boat presence, such as bottlenose dolphins (*Tursiops truncatus*) and short-beaked common dolphins (*Delphinus delphis*; Evans and Hammond, 2004). One approach to these constraints is to use strandings data, i.e., records of cetaceans that have washed ashore.

Stranding records are the primary source of information for many elusive species, such as beaked whales (Ziphiidae; Morin et al., 2017) and can provide an indication of relative abundance and richness in extant cetacean communities (Evans and Hammond, 2004; Maldini et al., 2005; Pyenson, 2011). Globally, there are several long-term, regional stranding data sets: the northwest Pacific USA, e.g., Norman et al. (2004) who reported 904 records, concluding that most reports are made in summer time when sampling effort is higher; Hawaii, e.g., Maldini et al. (2005); who documented 202 odontocete strandings; the Netherlands, e.g., Murphy et al., (2006) who have ~10,000 strandings records to date, the majority of which are harbour porpoises; and Australia, e.g., Evans et al. (2005), who analyzed 639 stranding events comprising 39 taxonomic groups. The Australian data set only has 21 records gathered prior to 1960 (Lloyd and Ross, 2015), while the Hawaiian and North

American data sets have limited accuracy prior to the 1960s and 70s when systematic recording of strandings became more standardized (Pyenson, 2010). The Dutch data set has systematic records dating back to at least the 1920s (Murphy et al., 2006), with some records dating back hundreds of years. Similarly, the Irish Whale and Dolphin Group (IWDG) stranding records date back to the 18th Century. Although globally there are several long-term stranding data sets the majority of them are not systematic, nor as long-term as the one we present here. The Natural History Museum, London (NHM) has maintained a database of UK strandings since 1913, making it one of the longest, continuous, systematic cetacean stranding data sets in the world (NHM, 2018). The program became part of the Cetacean Strandings Investigation Programme (CSIP) in 1990, which continues to record cetacean strandings in the UK to the present day and investigates the causes of strandings through systematic postmortem examinations, under contract to the UK government (CSIP, 2019). The IWDG has been systematically recording strandings since 1990 (IWDG, 2019).

Despite records being available up to 2015, no comprehensive studies of temporal changes in cetacean strandings exist for this full period, i.e., from 1913-2015. The unique characteristics of this data set are ideal for investigating trends and inter-annual variability in cetacean strandings alongside anthropogenic and/or environmental changes.

### 5.2.1 Potential correlates of strandings

Many studies have investigated possible causes of cetacean strandings. Strandings may be triggered by geomagnetic storms affecting the orientation of cetaceans that navigate by these means (Vanselow et al., 2017). Other (i.e., meteorological) storms may exhaust, displace, or physically injure cetaceans, increasing the risk of disorientation and stranding (Mignucci-Giannoni et al., 2000; Bogomolni et al., 2010; Schumann et al., 2013). Fluctuations in the North Atlantic Oscillation (NAO) can lead to storms and wind and sea surface temperature (SST) changes, that may in turn influence prey abundance and distributions (Hurrell, 1995; Pierce et al., 2007) that can alter cetacean distributions and lead to strandings (Simmonds and Eliott, 2009; Schumann et

al., 2013). Anthropogenic impacts such as military sonar can cause cetaceans to surface quickly resulting in fatal decompression sickness (Jepson et al., 2003). Further, direct physical contact with ships (i.e., ship strike) (Laist et al., 2001) has also been attributed to deaths in a number of stranding records. Starvation is a known cause of death recorded in stranding necropsies (Leeney et al., 2008; Deaville et al., 2015), which may be linked to overfishing. Other effects of human fishing efforts e.g., bycatch, are well documented (Read et al., 2017). Entanglement in fisheries nets, and other commercial debris (Leeney et al., 2008; Deaville et al., 2015) causes either immediate asphyxiation (often the case in smaller cetaceans) or exaggerated energy expenditure from the drag of nets, often leading to emaciation and asphyxiation (Moore and van Der Hoop, 2012). Pollution and plastic contamination have also been attributed to cetacean death and subsequent stranding (Simmonds, 2012).

Our overall objective is to explore broad-scale patterns and correlates of cetacean strandings through time. Combining all three data sets for the first time, we present over 100 years of data, and show spatio-temporal patterns in the number of individuals stranding in the UK and Ireland. We also used Generalised additive Models (GAMs) to explore correlates of strandings.

## 5.3 Methods

### 5.3.1 Study area

All stranding records were recorded from UK and Irish coastlines between 49°N and 61°N, and 11°W and 3°E. The predominant ocean current in this region is the North Atlantic drift, which travels eastwards with prevailing winds towards the western UK and Ireland. Further, there are powerful currents associated with submarine canyons to the extreme southwest of the UK, near the edge of the continental shelf. Bed stress (disturbance to the sea floor by tidal currents) is lowest in the more sheltered, shallower waters of the Irish sea, English Channel, and the southern North Sea, near East Anglia (Connor et al., 2006). The UK continental shelf includes parts of the North Sea, Irish Sea, English Channel, and North Atlantic, and is under 200 m deep around most of the UK. This continental shelf slopes down into a deep-sea zone off the west coast of Ireland (Connor et al., 2006).

### 5.3.2 Strandings data sets

During the early 20<sup>th</sup> century most UK stranding reports were sent to the NHM by HM Coastguard. Information was collected *via* standardized forms that showed the basic data requirements. Members of the public also submitted reports *via* the coastguard. As photography became more widely used, more reports to the NHM were supported by images. With the development of Wildlife Trusts around the UK, wardens, officers, and rangers became key reporters of strandings. When CSIP and the IWGD were set up in 1990, wider publicity was given to the work on strandings, raising public awareness and understanding. Reporting strandings *via* online forms, telephone, and social media became common practice and is still used today. Many reported strandings are attended by the CSIP and IWDG teams.

We used stranding data from the NHM, CSIP and IWDG to investigate temporal and spatial patterns of cetacean strandings around the UK and Ireland. In the present study, a stranding is defined as any individual found beached or washed up onto land (beaches, mudflats, sandbanks *etc.*) either alive or dead, and also includes a small number of records where the individual was re-floated. All three data sets contain information on the stranded species, the date it was discovered, the latitude and longitude of the stranding location, and whether the animal was alive or dead on discovery. For some specimens, the NHM and CSIP data sets also have information on whether the individual stranded alone or with others of the same species (a mass stranding, i.e.*,* more than one individual, excluding mother-calf pairs), the decomposition condition of the carcass, sex, and body length. The NHM data set contains 4,311 UK and Irish stranding records from 1913-1989 (NHM, 2018). The CSIP data set contains 13,084 UK, and seven Irish stranding records from 1990-2015 (CSIP, 2018), and the IWDG data set contains 2,973 Irish cetacean records for the period 1913-2015 (IWDG, 2018). We combined the data sets and removed 220 duplicate records found in both the NHM and IWDG data sets.

Before analyses, we cleaned the data by removing any records where species were listed as 'unknown', 'unknown cetacean', or similar. Around 13% of records, most of which were historical, were assigned as 'unknown' and

removed from the study. Then we removed any species that are rarely seen in UK waters, defined using Reid et al. (2003) and OBIS-SEAMAP (Halpin et al., 2009); Appendix 5: Table S5.1; S5.2). These are likely to represent one-off events that will not contribute to general patterns, or may be misidentifications, especially in the historical data. These species were: narwhal (*Monodon monoceros*), beluga (*Delphinapterus leucas*), dwarf sperm whale (*Kogia sima*), Blainville's beaked whale (*Mesoplodon densirostris*), Gervais' beaked whale (*Mesoplodon europaeus*), Fraser's dolphin (*Lagenodelphis hosei*), and melon-headed whale (*Peponocephala electra*) and combined only accounted for 11 records. Where possible, we converted grid references and detailed location descriptions into latitudes and longitudes for records that did not have this information. We sense-checked all anomalous strandings, such as those with localities far inland, and removed any that were not near a viable water source. Lastly, we standardized the date formats and scientific names across the combined data set, using YYYY-MM-DD for dates and the taxonomy of Reid et al. (2003) for scientific names.

### 5.3.3 Correlates of strandings through time

We plotted changes in the total number of stranded individuals through time for all species combined, for each species separately, and for mysticetes (baleen whales) and odontocetes (toothed whales). Next, we explored the spatio-temporal patterns in strandings for all species combined, and for mysticetes and odontocetes separately, across the UK and Ireland at 25-year intervals and decadal intervals (Fig. S5.3).

We considered drivers of changes in strandings through time. We fitted models of numbers of individuals stranded against various predictor variables thought to correlate with cetacean strandings (Table 5.1, Fig. 5.1). We included the following predictors because they have been reported to potentially influence strandings, and because we could collate data for them on a yearly basis for the UK and Ireland for the full-time span of our data set (1913-2015) (Appendix 5: Data Collection). **(1) Geomagnetic activity.** Some cetaceans, such as sperm whales (*Physeter macrocephalus*) may use Earth's geomagnetic fields for navigation (Kirschvink et al., 1986; Kremers et al., 2014; Vanselow et al.,

2017), thus changes in geomagnetic activity, e.g*.,* solar storms, may affect their navigation and increase the likelihood of strandings (Vanselow et al*.,* 2017). **(2) Sea surface temperature (SST)**. Changes in SST (°C) can affect prey abundance, resulting in net movements of cetaceans as they follow their prey (Pierce et al., 2007, Simmonds and Eliott, 2009), which could result in changes in cetacean distribution and therefore the spatial distribution of strandings. **(3) Storm events.** Storm conditions, hurricane events and associated oceanographic disturbances may increase strandings (Mignucci-Giannoni et al., 2000; MacLeod et al., 2004; Bogomolni et al., 2010) as individuals suffer from exhaustion, disorientation, or direct physical injury. Further, these impacts can also affect food sources (Lawler et al., 2007; Evans et al., 2005), which may alter cetacean distributions and therefore the likelihood of strandings. **(4) North Atlantic Oscillations (NAO).** Fluctuations in the NAO can affect prey distribution and abundance via associated wind and temperature changes (Hurrell, 1995; Pierce et al., 2007). Low NAO indexes have been associated with physiological stress in North Atlantic right whales (*Eubalaena glacialis*). Note that although NAO and storms, and NAO and SST are related, they are not strongly correlated ($r^2 < 0.16$ and $r^2 < 0.001$ respectively; Appendix 5; Environmental variables). Therefore, we included all three variables. **(5) Fishing catch.** Over-fishing can have a direct impact on cetaceans due to a reduction of their prey (Evans, 1990; Weir et al., 2007), causing starvation, or a shift in cetacean distribution as they search for prey elsewhere. Further, discarded or fixed fishing nets and creel lines are partly responsible for cetacean mortality as bycatch (Leeney et al., 2008). Note that ideally, we would have included sonar use, bycatch, and chemical pollution, but none of these variables were available for every year in our data set (i.e*.,* 1913 - 2015), particularly for the historical data. We ran a model that included a proxy for shipping traffic, but these data were only available for 1950-2015 (Appendix 5; Shipping model). Sources and units of the main model data set are in Table 5.1.

[Table on next page]

**Table 5.1.** Predictor variables thought to correlate with cetacean strandings. Units, data type, and source of raw data are shown. SST is sea surface temperature. NAO is North Atlantic Oscillation. Human population data are used as an offset in our models. Details on how each of these variables were sourced and calculated can be found in the Appendix 5: Data analysis.

| Variable (units) | Data | Sources |
|---|---|---|
| **Storm events (count/year)** | Storm events over 47 knots | Lamb and Frydendahl (1991) Met Office, UK

Multiple sources: https://github.com/EllenJCoombs/strandings-project |
| **Geomagnetic activity (K - index)** | The K-index is used to characterize the magnitude of geomagnetic storms. The range is 0–9, with 1 being calm and 5 or more indicating a geomagnetic storm

Three-hourly readings obtained from:
1913 - 1925: Greenwich
1926 - 1939: Abinger
1940 - 1956: Abinger, Eskdalemuir and Lerwick
1957 - 2015: Hartland, Eskdalemuir and Lerwick

A mean maximum yearly K-index reading was used in the model | British Geological Survey |
| **Sea surface temperature (°C)** | Maximum yearly SST from 14 UK and Irish locations (Appendix 5; Fig. S5.1). A mean maximum yearly reading was used in the model (Appendix 5; Fig. S5.2). | Met Office: HadISST |
| **North Atlantic Oscillation (mb)** | Yearly readings

The NAO is based on the difference in normalized sea level pressure (SLP) between Stykkisholmur/Reykjavik, Iceland, and Lisbon, Portugal. | University Corporation for Atmospheric Research |

| | | |
|---|---|---|
| **Yearly fishing catch (1000 tonnes)** | Total yearly catch (1000 tonnes) data of ~ 58 fish species in UK and Ireland. Combined data sets for England and Wales, Scotland, Northern Ireland, and Ireland to get a yearly total. | International Council for the Exploration of the Sea (ICES) |
| **UK and Ireland yearly human population** | 1913-1922 are figures for England, Wales, and Scotland; from 1922, onwards Northern Ireland is included | Office of National statistics (ONS) |
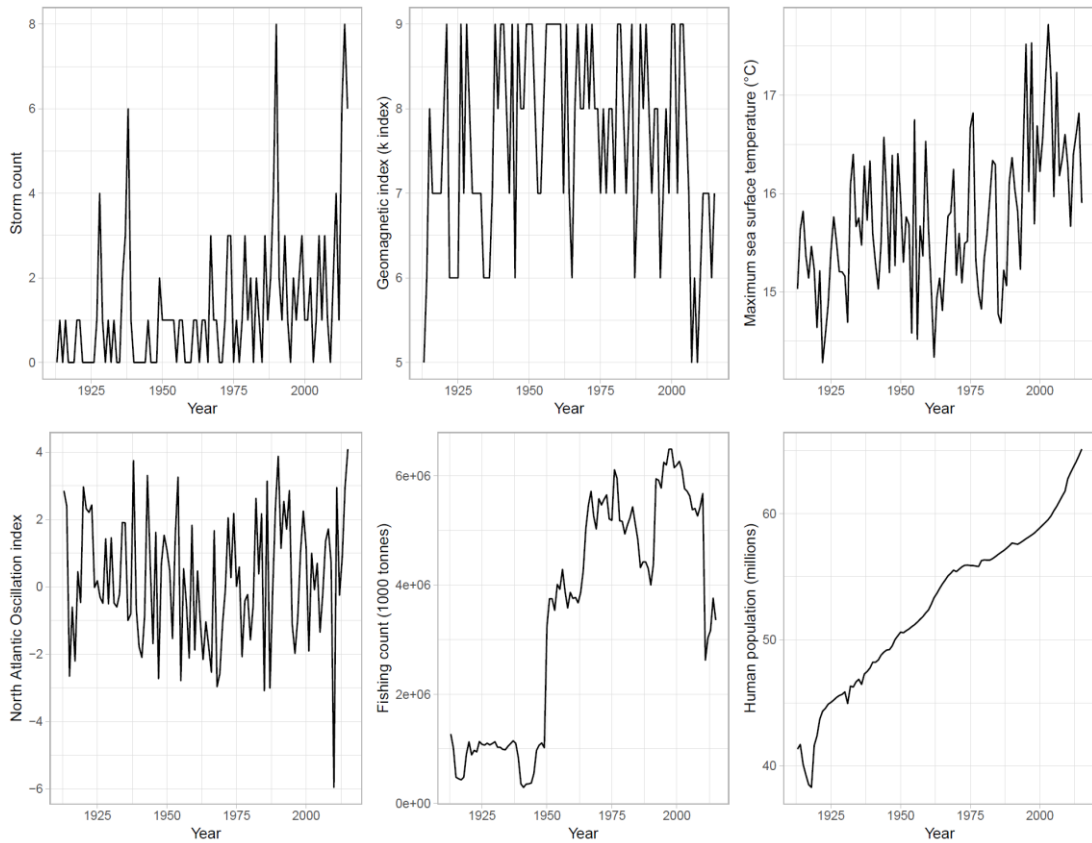
**Fig. 5.1.** Predictor variables thought to correlate with cetacean strandings. From top left to bottom right: storm count, geomagnetic index (k-index), maximum sea surface temperature (°C), North Atlantic Oscillation index, Fishing count (1,000 tons), and human population (millions). All variables show data for the UK and Ireland, apart from geomagnetic index and human population which show data for the UK only due to availability. All data are shown from 1913 – 2015. Details on how the data were obtained is in Table 5.1 and the Appendix 5, Data collection. Extra details on each of the variables are in the Appendix 5; Data collection

### 5.3.4 Generalised additive models (GAMs)

We modelled the effects of our predictors on the number of cetacean individuals stranded using GAMs. GAMs allow for smooth relationships between multiple explanatory variables and the response variable (Wood, 2017). Like Generalised linear models (GLMs), GAMs use a link function. GAMs use this link function to establish a relationship between a 'smoothed' function of the predictor variable(s) and the mean of the response variable (Guisan et al., 2002). A GAM is substantially more flexible because the relationships between independent and dependent variables are not assumed to be linear (Wood, 2017). Our initial data exploration found that relationships between the individual predictors and the number of individuals stranded were nonlinear.

We modelled the total number of stranded individuals as a sum of smooth functions of covariates in a GAM framework (1). In an attempt to account for changes in the potential for detection of stranded cetaceans through time we included yearly UK population size based on the assumption that as population size increases, or activity in an area increases, it is more likely that strandings will be observed and reported (Norman et al., 2004, Maldini et al., 2005, Pyenson, 2011, McGovern et al., 2016). Stranding studies highlight the importance of considering population growth as a proxy for observer effort (Maldini et al., 2005, Pyenson, 2011). However, it is often difficult to obtain accurate population estimates over the time frame of these stranding databases or in regions where populations have varied considerably (e.g., the Hawaiian Islands, Maldini et al., 2005)., we used yearly UK human population size (Table 5.1) as an offset in the model. To further investigate the impacts of sampling effort, we ran two case study models that look at differences in population between the populated southern UK, and the less populated northern UK (Appendix 5; Regional study 1 & 2). Smooths were modelled using a thin plate spline basis with shrinkage (Marra and Wood, 2011), which allowed terms to be removed from the model (i.e., their effect size shrunk to zero) during fitting, thus terms were selected during model fitting. As we wanted to model species-specific effects, we included a factor-smooth

interaction between year of stranding and species; this term fitted a smooth of time for each species but allowed common smooths to be fitted for the other covariates. An advantage of this approach is that the per-species smooths are estimated as deviations from a base-level smooth, so some information is shared between species. We fitted models with the following candidate response count distributions: Poisson, quasi-Poisson, negative binomial, and Tweedie. We used standard residual checks for GAMs (Q-Q plot, histogram of residuals, residuals *vs.* linear predictors, response *vs.* fitted values) to decide between response distributions and assess model fit. We report the results using the negative binomial distribution as this was the best fit for the data (Appendix 5: GAM candidate response distributions) when investigating each of the different response distributions (Appendix 5: Fig. S5.7-S5.10). The total number of stranded individuals was modelled as a sum of smooth functions of the $k$ explanatory variables $z_{tk}$ using a GAM with the general formulation:

(1)

$$s_{t,\ species} = exp\left[\log(p_t) + \beta_0 + \sum_{k=1}^{K} f_k\left(z_{tk}\right) + f_{t,\ species}\left(t, species\right)\right]$$

Where $s \sim$ negative binomial ($\theta$), $s$ is the number of stranded individuals, $t$ is year, $species$ is the cetacean species in the stranding data set, $p$ is an offset of human population size, $\beta_0$ is the intercept and $f_k$ are smooths of the $k$ explanatory variables are smooths of the K explanatory variables. The explanatory variables for inclusion in the models were smooth functions of year, with the additional species smooth as mentioned and shown in (1), and storm events, geomagnetic activity, sea surface temperature, North Atlantic oscillation, and fishing catch.

We fitted models using Restricted Maximum Likelihood (REML) in the R 'mgcv' package version 1.8.17 (Wood, 2011). REML was preferable because when models contain highly correlated covariates, REML finds an optimal degree of smoothing (Reiss and Ogden 2009). In a GAM, k is the maximum complexity

of the basis used to represent the smooth term. If the k value is high enough, we can be sure that there is enough flexibility in the model. We can find out if k is high enough by increasing the k value and refitting the original model (Appendix 5: Setting the k parameter). After refitting the model and analyzing the GAM output, we set the k parameter for storm events and geomagnetic activity to k = 7 and k = 4, respectively. The k parameter did not need to be set for NAO, SST, or fishing catch because these terms had more unique covariate combinations than the specified maximum degrees of freedom. To avoid fitting overly complex models, the maximum basis size for the smooth terms were limited to these values. Finally, we plotted the residuals by covariate (Appendix 5; GAM model checking) to confirm the goodness of our model fit. These plots showed low variation in the covariate residuals suggesting that the model is a good fit (Fig. S5.11).

We removed 'rare' and 'unknown' records from the final model to account for possible misidentifications in the stranding record. These records were also removed because of the effect one or two records could have on skewing the species smooth. We also ran a GAM with all 'rare' and 'unknown' records included (2,664 records) to investigate the effect of these additional strandings.

### 5.3.5 Sensitivity analyses

There are many ways to subdivide the data set, and many possible sources of error. Therefore, we ran a series of additional analyses on subsets of the data, or different arrangements of the data, to identify any obvious issues. These are described briefly below; for more details see Appendix 5.

### Species identification models

We ran the model with all stranding records at genus-level to account for possible misidentification at the species-level, particularly in the historical data. Because species identifications by dedicated strandings networks are likely to be more reliable than those in the historic data, we also ran a model using CSIP and IWDG stranding records only (1990 – 2015).

### Ship strike models

To investigate ship strike effects on strandings we ran a model that included a proxy for shipping traffic around the UK. These data were only available from 1950-2015; therefore, the other predictors and the response were constrained accordingly, and shipping was not included in the full model. Note that we use shipping traffic as a proxy for ship strikes because direct ship strike data was not available historically, and even those data available mainly focus on mysticetes or are geographically restricted.

### Stranding events models

In the main model the response is all individual stranding records, with each and every cetacean in a mass stranding recorded by species, location, and date. Cetaceans that mass strand are generally pelagic odontocetes (Jepson et al., 2013), and we felt it was important to assess the effects of correlates on these mass strandings. We therefore also fitted a model with the number of stranding events as the response (with a single mass stranding event recorded as a '1' for all individuals of the same species at that location and date) to investigate whether the correlates had a different effect on single and mass strandings, and to see whether our results were reflecting a signal of multiple mass strandings of pelagic odontocetes.

### Species specific models

47% of the data set were harbour porpoise (*Phocoena phocoena*) records, as these small cetaceans are widespread and abundant in UK and Irish waters (Fig. S5.4). To ensure that our results were not merely reflecting a signal in the harbour porpoise data we repeated our analyses after removing this species from the data set, and then for the harbour porpoise data separately. For completeness we also fitted models for all other species with over 100 stranding records in the data set (we excluded five species with fewer than 100 strandings records; sei whale (*Balaenoptera borealis*), blue whale (*Balaenoptera musculus*), pygmy sperm whale (*Kogia breviceps*), humpback whale (*Megaptera novaeangliae*), and True's beaked whale (*Mesoplodon mirus*), because they had insufficient data to fit the models.

### Suborder models

The cetaceans were split by suborder (i.e., Mysticeti or Odontoceti) to investigate whether the predictors affected the numbers of strandings differently in each suborder. The two suborders are generally different ecologically (e.g*.,* diet specialization and larger body size in the mysticetes), and it has been suggested that only some genera (e.g*., Delphinus, Grampus*, and *Ziphius*; Kirschvink et al., 1986), of which all are odontocetes, use geomagnetic features to navigate, with Balaenoptera (a mysticete), to a lesser extent (Kirschvink et al., 1986). We therefore investigated the differences in this and the other correlates of strandings for the two suborders.

### Habitat models

We ran a model with a smooth of habitat (i.e*.,* oceanic, coastal, or both) (Table S5.2) rather than a species smooth because some of the predictors e.g*.,* storms, may have had more of an effect on species in certain habitats. For example, shallow water species, such as porpoises, may be more likely to strand due to severe weather as they are less able to escape from storm impacts (Lawler et al., 2007; Schumann et al., 2013). Species habitat data were from Reid et al. (2003).

### Regional models

Finally, we ran two regional models for strandings from; 1. the south west coast of the UK where cetacean stranding records and human population have increased, and 2. the north west cost of the UK where cetacean stranding records have increased, but human population has decreased. These models were run to assess the possible effects that using one standard UK human population size may have had in the original model and to see if correlates of strandings were different in different regions of the UK and Ireland. The same predictors were used in these models but were constrained to 1991-2015 as county-level human population data are only available for this time period in the UK.

All data required to reproduce our analyses are available from the NHM Data Portal (data.nhm.ac.uk, Coombs et al*.,* 2018). We performed all data cleaning,

data exploration, plotting and analyses in R version 3.4.0 (R Core Team, 2017). A fully reproducible workflow is available on GitHub (https://github.com/EllenJCoombs/cetacean-strandings-project) and Coombs et al. (2019).

## 5.4 Results

### 5.4.1 Data exploration

Temporal and spatial patterns in the strandings data

A total of 17,491 strandings comprising 21 species were recorded. The data set contains 786 mysticete records from five species, and 16,705 odontocete records from 16 species. Temporal patterns in strandings varied across and within species (Fig. 5.2; 5.3).

[Figure on previous page]

**Fig. 5.2.** Temporal stranding patterns of each species from 1913-2015. The y-axis shows total stranding count per year, the x-axis shows the year. Note that y-axis scales are different for different species. Rare and 'unknown' records are not represented.
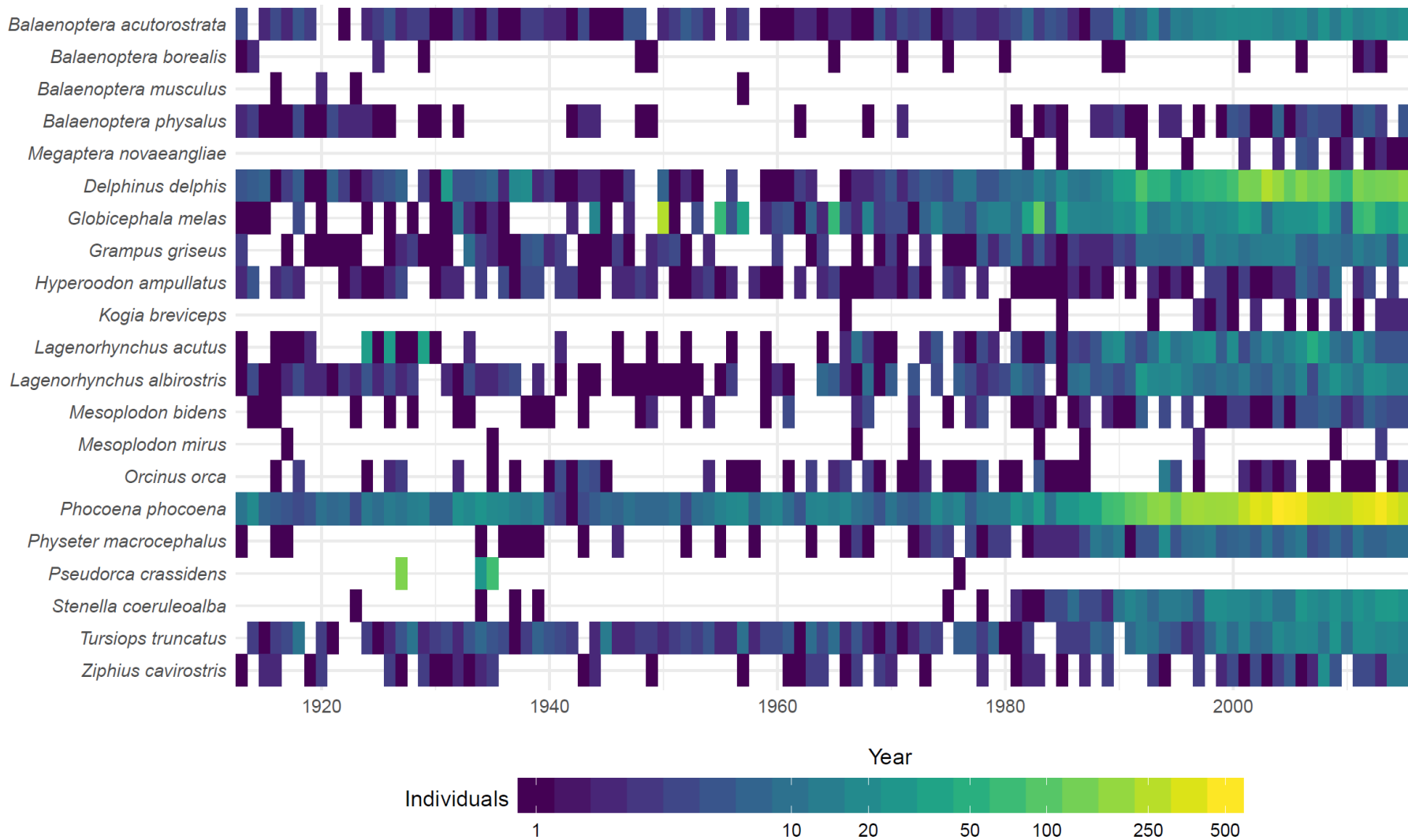
[Figure on previous page]

**Fig. 5.3.** Stranding events of cetacean species in UK and Irish waters from 1913-2015. The x-axis shows the years 1913-2015 with individual tiles representing one year. The y-axis shows the species found in the UK and Irish stranding records. The first five species are mysticetes (baleen whales), and the rest of the species are odontocetes (toothed whales). The coloured boxes show the number of individuals that stranded each year. Dark blue shows one to a few individuals, yellow shows more than 200 individuals. Rare and 'unknown' records are not represented.

Some species e.g., blue whales and false killer whales (Pseudorca crassidens), stranded in the earlier parts of the time series but then disappear from the strandings record (Fig. 5.3). Conversely, some species appear for the first time in the latter half of the century. For example, the first humpback whale stranding record was in 1982 and the first pygmy sperm whale (*Kogia breviceps*) stranding record was in 1966 (Fig. 5.2; 5.3). Species such as northern bottlenose whales (*Hyperoodon ampullatus*) and Cuvier's beaked whales (*Ziphius cavirostris*) have stranded consistently throughout the century, with an increase in records towards the present day.

Overall, cetacean strandings records have increased over the past century, with a rapid rise from the late 1980s to the present (Fig. 5.4). There were several prominent spikes in stranding numbers before the 1990s (Fig. 5.4) caused by mass strandings. In 1927, there was a mass stranding of 150 false killer whales, with further mass strandings of this species in 1934 and 1935, the largest being 41 individuals. In 1950 there were two long-finned pilot whale (*Globicephala melas*) mass strandings (totaling 245 individuals; Fig. 5.2; 5.4), with further mass strandings of this species in 1983. All these mass strandings occurred in Scotland, which accounts for the high numbers in that region from 1926-1950 (Fig. 5.4).

The most frequently stranded species were harbour porpoise (*Phocoena phocoena*; $n$ = 8,265; 47% of all stranding records), short-beaked common dolphin (*Delphinus delphis*; $n$ = 3,110; 18% of all stranding records) and long-finned pilot whale (*Globicephala melas*; $n$ = 1,606; 9% of all stranding records) (Fig. 5.2; 5.3). Mysticete strandings were much less frequent (Fig. 5.4) and

accounted for around 4% of total strandings records. Mysticete strandings showed an overall decline throughout the century until the 1980s. Generally stranding records of all odontocetes increased throughout the 1990s to the present. The exceptions were false killer whale, as previously mentioned, and killer whale (*Orcinus orca*) that stranded intermittently in low numbers, with one mass stranding event (*n* = 11) in 1994 in Scotland. 1990 was the first year that mysticete stranding records reached double figures. There was an increase in mysticete strandings after 1987 and throughout the 1990s to the present. Minke whales *(Balaenoptera acutorostrata)* accounted for 79% of all mysticete strandings and also accounted for the majority of the post-1990 rise in mysticete strandings.

Mysticete records remained low throughout the 1950s and 60s (Fig. 5.4). There was a slight decline in the number of odontocete stranding records during the early period of WWII, but there are other years throughout the period that reported lower numbers of odontocete strandings. The CSIP and IWDG programs began in 1990, after which there was an increase in stranding records for both mysticetes and odontocetes (Fig.5.3; 5.4).
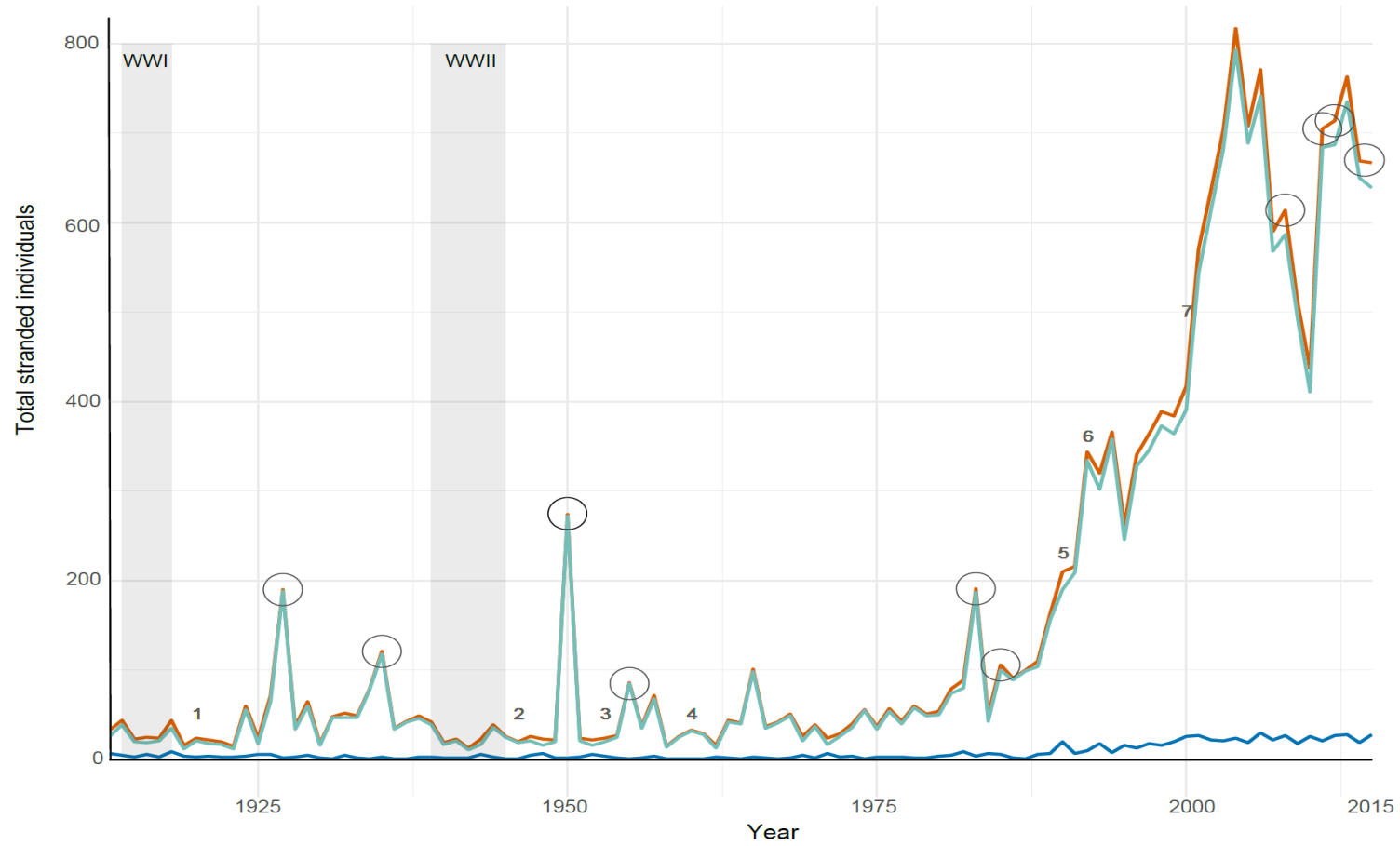
1. 1920s: Sonar use in French and UK waters
2. 1946: NATO military testing in European waters: submarine, sonar, & torpedo testing increase
3. 1950s: Increase in post–war fishing & whaling effort
4. 1960s: Increase in use of polychlorinated biphenyls (PCBs) and other chemical pollutants
5. 1985/86 season: Moratorium on whaling comes into effect
6. 1990: The CSIP and IWDG programmes start
7. 2000s: Increase in pile–driving for offshore wind turbines

[Figure on previous page]

**Fig. 5.4.** Temporal variation in cetacean strandings records for all species. Records for odontocetes (toothed whales), and mysticetes (baleen whales) in the waters around the UK and Ireland from 1913-2015. 1913 is when the NHM started to record cetacean strandings. The plot shows strandings through time for all species (orange), odontocetes (blue), and mysticetes (green). The y-axis shows total number of individuals that stranded each year. Key anthropogenic events are labelled with numbers, with the corresponding text below the plot. Key periods are shaded in light grey. WWI is World War I, WWII is World War II, CSIP is the Cetacean Stranding Investigation Programme, IWDG is the Irish Whale and Dolphin Group. The circles highlight years with mass strandings of > 20 individuals.

Columns: 1913–1925, 1926–1950, 1951–1975, 1976–2000, 2001–2015

Rows: All, Mysticete, Odontocete

274
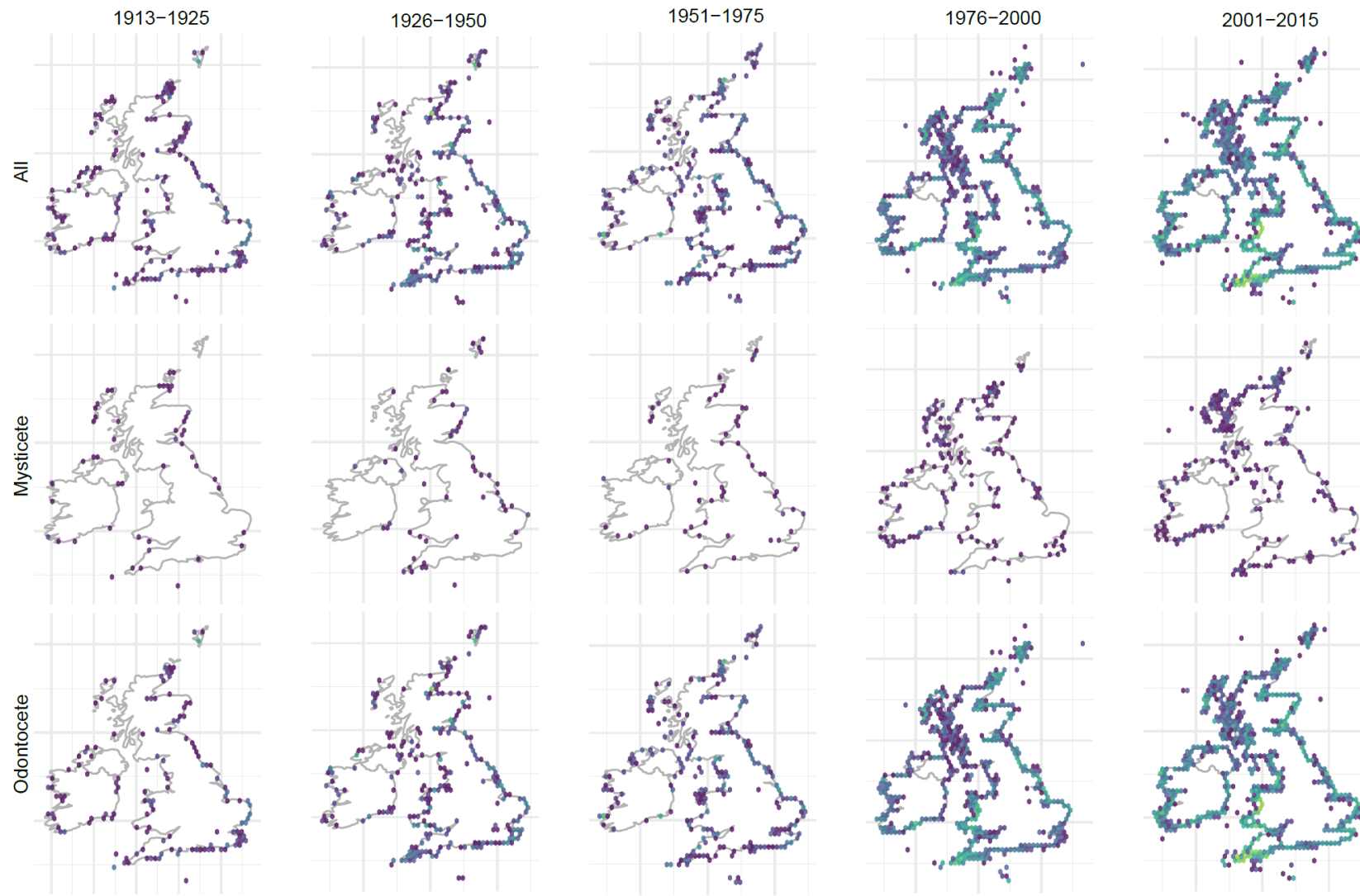
[Figure on previous page]

**Fig. 5.5.** Temporal and spatial variation in cetacean stranding records for all species. Records for odontocetes (toothed whales), and mysticetes (baleen whales) in the waters around the UK and Ireland from 1913-2015 at 25-year intervals. Low numbers of strandings are shown as dark blue, higher numbers of strandings shown in light green, the highest numbers of strandings are shown in yellow.


Most strandings were of odontocetes, therefore the plot for odontocetes and all species combined show a similar pattern (Fig. 5.4). Most strandings occurred around the south coast of England and the west coasts of Ireland and Scotland (Fig. 5.5; S5.6).  This pattern was particularly evident in common dolphin and harbour porpoise strandings (Fig. S5.4; S5.5). Stranding hotspots in southern and southwest England were first documented from 1926-1950 (Fig. 5.5). Over the next 25 years (1951-1975) there was an increase in stranding records around northern England. Over the next few decades (1976-2000) stranding density increased along the northeast and north of Scotland (Fig.5. 5).  From the 1990s, stranding records can be observed around most of the coastline concomitant with the advent of the modern stranding programs. Mysticete strandings increased around southwest England, southwest and western Ireland, and western Scotland in the last few decades (2001-2015; Fig. 5.5). East Anglia, Wales, and eastern Ireland have fewer records for mysticete strandings compared to other parts of the UK and Ireland (Fig. 5.5).

***Correlates of strandings through time***

We found significant effects for NAO, SST, and fish catch ($P < 0.05$, $P < 0.001$, $P = 0.02$, respectively) suggesting the smooth of these variables were significantly different from "no effect" (Table 5.2). However, the estimated degrees of freedom (EDF) were very low (i.e., less than, or not much greater than 1) indicating that the number of individuals that strand was not strongly influenced by any of our predictor variables apart from year of stranding (Table 5.2, Fig. 5.6). The factor smooth term s(Year, Species) has an EDF of 103 (Table 2; deviance explained = 84.5%, $n = 2,163$). The results of the GAMs

were qualitatively similar when we included all 'rare' and 'unknown' records, except fishing catch had an EDF a little higher than 1 (EDF = 4.04) (Table S5.4; S5.15, Fig. S5.15).

**Table 5.2.** Correlates of strandings outputs. Generalised additive model (GAM) outputs from a model of correlates of strandings for the UK and Ireland, from 1913-2015. s() are smooths of the explanatory variables. 'Storms' refer to the storm count for each year, 'Max_K_Index' is the geomagnetic reading (where the K-index is used to characterize the magnitude of geomagnetic storms), 'Max_SST' is the yearly maximum sea surface temperature (°C), 'NAO_index' is the North Atlantic Oscillation which is the difference in normalized sea level pressure (SLP) between Stykkisholmur/Reykjavik, Iceland, and Lisbon, Portugal, 'Fish_catch' is annual fish catch (1,000 tons) for the UK and Ireland, 'Year' is the years 1913-2015, 'Species' are the 21 cetacean species that make up the data set. This table shows the estimated degrees of freedom (EDF) for each of the different predictor variables. The *P*-values show whether the smooth of that variable is significantly different from "no effect", i.e., if we estimated the smooth as a flat line at zero. k shows the maximum basis complexity

| Correlates as modelled | EDF | *P*-value | k value |
|---|---|---|---|
| s(Storms) | < 0.001 | 0.94 | 6.0 |
| s(Max_K_index) | < 0.001 | 0.79 | 4.0 |
| s(Max_SST) | 2.40 | < 0.001 | 9.0 |
| s(NAO_index) | 0.92 | < 0.05 | 9.0 |
| s(Fish_catch) | 0.79 | 0.02 | 9.0 |
| s(Year, Species) | 103 | < 0.001 | 210 |
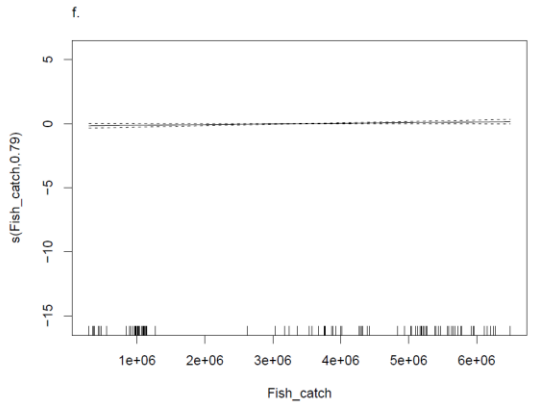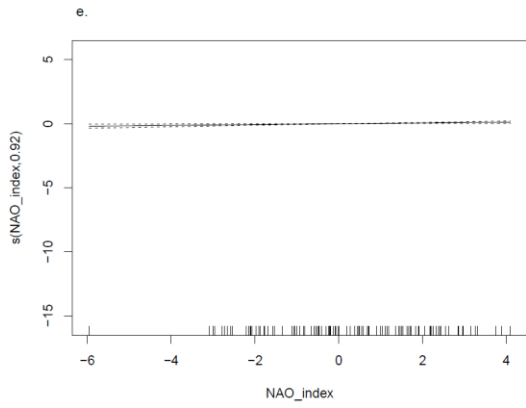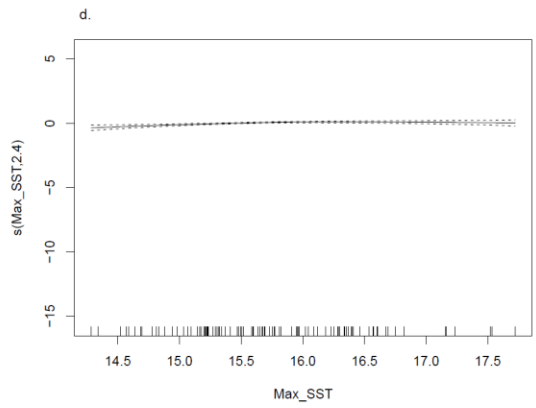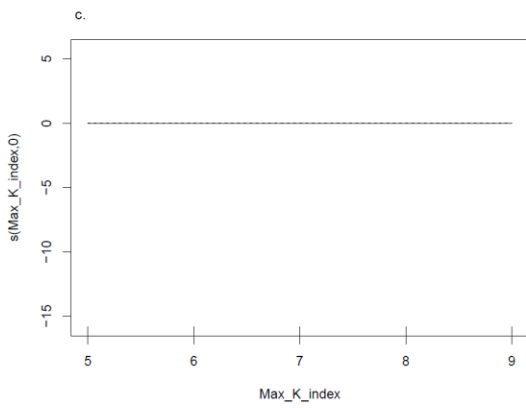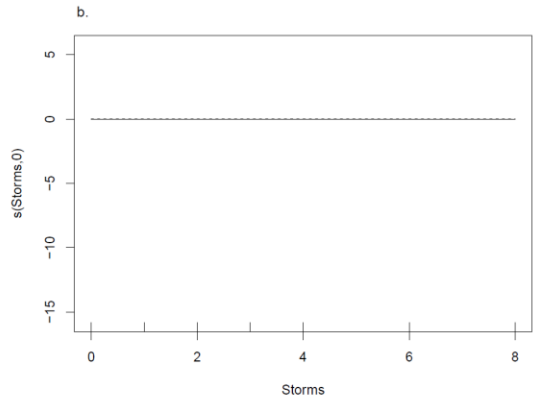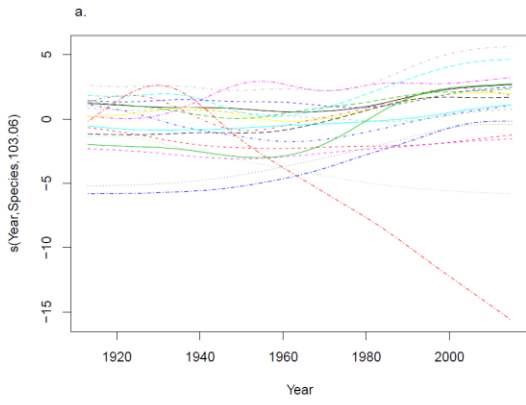
**Fig. 5.6.** Generalised additive Model (GAM) summary plots for stranding variables. Variables included in the final model of correlates of cetacean strandings; a) Year, species smooth (s(Year, Species), b) storm events s(Storms), c) geomagnetic index, s(Max_K_index), d) maximum sea surface temperatures, s(Max_SST), e) North Atlantic Oscillation index, s(NAO_index), f) annual fishing catch, s(Fish_catch). X-axis shows the values for that variable (i.e., the year 1913-2015 (a), storm counts (b), maximum k-index value (c), maximum sea surface temperature (°C) (d), NAO index value (e), and fishing catch (1,000 tons) (f)). The y-axis shows the smooth and the estimated degrees of freedom (EDF) (e.g*.,* s(Max_SST, 2.4)). These EDF values are also reported in Table 5.2. Modelled using the negative binomial response count distribution. The model has a deviance explained of 84.5%, $n = 2163$.

### 5.4.2 Sensitivity analyses

We found significant *P*-values for some variables in our sensitivity analyses (see below for details) suggesting the smooth of these variables were significantly different from "no effect". However, the EDFs for all variables (with a few exceptions; see below) were low, indicating that across all sensitivity analyses the number of individuals that strand was not strongly influenced by any of our predictor variables, except year of stranding, i.e., our results were qualitatively identical to those for the full model described above. This was true across all sensitivity analyses (Tables S5.4; S5.5; S5.7-S5.12; S5.15 and Fig. S5.15; S5.16; S5.18-S5.23); therefore, we only report the differences below. All results are compiled in Table S5.15.

### Species identification models

In the genus-level models we found significant effects for SST, NAO index, and fishing catch ($P < 0.001$, $P = 0.01$, $P = 0.01$, respectively) (Table S5.5, Fig. S5.16). For the CSIP and IWDG (1990 – 2015) data we found significant *P*-values for storms, NAO, fishing catch, and shipping traffic (Table 5.3, Fig. S5.17).

### Species specific models

When we removed harbour porpoises from the data set, we found significant effects for SST, NAO, and fishing catch ($P < 0.001$, $P = 0.001$, $P = 0.07$, respectively) (Table S5.7, Fig. S5.18) and showed that the original model was not merely reflecting a signal in the harbour porpoise data. When we modelled harbour porpoise only, we found a significant *P*-value for SST *($P < 0.01$)* but no influence of any of the other predictor variables (Table S5.8, Fig. S5.19). When modelling each species separately, we found no influence of any of the predictor variables (Table 5.4).

### Ship strike models

We found significant *P*-values for all of the variables; storms ($P < 0.005$), geomagnetic k-index ($P < 0.01$), SST *($P < 0.01$)*, NAO ($P < 0.01$), fishing catch ($P < 0.001$), and shipping traffic ($P < 0.001$) (Table S5.9, Fig. S5.20), however, all variables (except fishing catch) had low EDFs (Table S5.9). The EDF for fishing catch was 5.57, but the relationship was not particularly "wiggly" meaning we can

also interpret this as having little effect on the number of stranded individuals (Wood, 2017).

### Stranding events models

Our model with the number of stranding events as the response (with a single mass stranding event recorded as a '1') had a significant $P$-value for maximum SST, NAO, and fishing catch ($P = 0.005$, $P < 0.001$, $P = 0.04$, respectively) (Table S5.10, Fig. S5.21) but EDFs were low. The correlates did not have a different effect on single and mass strandings. Further, our results were not merely reflecting a signal from multiple mass strandings of pelagic odontocetes.

### Suborder models

We found a significant effect for maximum SST, and fishing catch ($P < 0.005$, $P < 0.001$, respectively) (Table S5.11, Fig. S5.22) but otherwise the models for odontocetes and mysticetes were qualitatively similar to those for the full data set.

### Habitat models

We found significant effects for maximum SST, and fishing catch ($P = 0.001$, $P < 0.001$, respectively) but overall, the results were the same as in the models without a habitat smooth (Table S5.12, Fig. S5.23).

### Regional models

The two regional models had different EDFs, with higher EDFs found in the southwest (region 1) model (Table 5.3). We found significant $P$-values for all the variables except for maximum k-index and maximum SST in both models (Table S5.13, S5.14). The region 1 model had an EDF of 6.62 for NAO but the relationship was not particularly "wiggly". We therefore interpret this as having little effect on the number of stranded individuals (Wood, 2017). Apart from year of stranding, the EDFs for the other variables were still too low to be fully conclusive (Table 5.3, Fig. S5.24; S5.25).

**Table 5.3.** Generalised additive model (GAM) outputs from additional models. '1990s model' is correlates of stranding GAM using only CSIP and IWDG stranding data (1990 – 2015). 'Regional model 1' is correlates of stranding GAM using data from the south west of the UK. 'Regional model 2' is correlates of stranding GAM using data from the north west of the UK. s() are smooths of the explanatory variables. 'Storms' refer to the storm count for each year, 'Max_K_Index' is the geomagnetic reading (where the K-index is used to characterize the magnitude of geomagnetic storms), 'Max_SST' is the yearly maximum sea surface temperature (°C), 'NAO_index' is the North Atlantic Oscillation which is the difference in normalized sea level pressure (SLP) between Stykkisholmur/Reykjavik, Iceland, and Lisbon, Portugal, 'Fish_catch' is annual fish catch (1,000 tons) for the UK and Ireland, 'Year' is the years 1990-2015 in the 1990s model, and 1991-2015 in the Regional models. 'Ships_tons' is the combined yearly weight of ships over 500 tons in the UK, as a proxy for ship strike. 'Species' are the cetacean species that make up the strandings data set. This table shows the estimated degrees of freedom (EDF) for each of the different variables. The *P*-values show whether the smooth of that variable is significantly different from "no effect", i.e*.,* if we estimated the smooth as a flat line at zero.

| Correlates as modelled | 1990s model | Regional model 1 | Regional model 2 |
|---|---|---|---|
| s(Storms) | 0.79* | 0.93* | 0.81* |
| s(Max_K_index) | 0.38 | < 0.001 | 0.12 |
| s(Max_SST) | < 0.001 | < 0.001 | < 0.001 |
| s(NAO_index) | 1.36** | 6.62** | 1.11** |
| s(Fish_catch) | 0.79* | 3.95** | 2.38** |
| S(Ships_tons) | 1.13** | 4.40** | 1.07** |
| s(Year, Species) | 43.0** | 40.1** | 25.5** |

*P < 0.05; **P < 0.01

[Table on next page]

**Table 5.4.** Generalised additive model (GAM) outputs for stranding models. GAM outputs from a model of correlates of cetacean strandings for the UK and Ireland, from 1913-2015 for each individual species. s() are smooths of the explanatory variables. 'Storms' refer to the storm count for each year, 'Geomagnetic k-index' is the geomagnetic reading (where the K-index is used to characterize the magnitude of geomagnetic storms), 'Maximum SST' is the yearly mean maximum sea surface temperature (°C), 'NAO index' is the North Atlantic Oscillation which is the difference in normalized sea level pressure (SLP) between Stykkisholmur/Reykjavik, Iceland, and Lisbon, Portugal, Fishing catch' is annual fish catch from the UK and Ireland (1,000 tons), 'Year' is the years 1913-2015, 'Species' are the 16 cetacean species which had 100 or more strandings in the data set. Rarer species were removed because they had insufficient data to fit the models. This table shows the estimated degrees of freedom (EDF) for each of the different predictor variables. The P-values show whether the smooth of that variable is significantly different from "no effect", i.e., if we estimated the smooth as a flat line at zero. k shows the maximum basis complexity.

| | Year | | | Storms | | | Geomagnetic k-index | | | Maximum SST (°C) | | | NAO index | | | Fishing catch | | |
|---|---|---|---|---|---|---|---|---|---|---|---|---|---|---|---|---|---|---|
| Species | EDF | *P*-value | k | EDF | *P*-value | k | EDF | *P*-value | k | EDF | *P*-value | k | EDF | *P*-value | k | EDF | *P*-value | k |
| *Balaenoptera acutorostrata* | 4.98 | < 0.001 | 9 | 0.51 | 0.14 | 4 | 0.23 | 0.25 | 3 | 0.71 | 0.06 | 9 | < 0.001 | 0.96 | 9 | 0.79 | 0.02 | 9 |
| *Balaenoptera physalus* | 3.57 | < 0.001 | 9 | 0.94 | < 0.005 | 4 | 0.58 | 0.13 | 3 | < 0.001 | 0.58 | 9 | 0.93 | < 0.005 | 9 | 0.79 | 0.02 | 9 |
| *Delphinus delphis* | 7.03 | < 0.001 | 9 | 0.58 | 0.11 | 4 | 0.87 | 0.02 | 3 | < 0.005 | 0.48 | 9 | 0.13 | 0.30 | 9 | 0.84 | 0.01 | 9 |
| *Globicephala melas* | < 0.001 | 0.93 | 9 | < 0.001 | 0.86 | 4 | < 0.001 | 1.00 | 3 | 1.02 | < 0.001 | 9 | < 0.001 | 0.76 | 9 | 0.67 | < 0.001 | 9 |
| *Grampus griseus* | 56.3 | < 0.001 | 9 | < 0.001 | 0.53 | 4 | 0.84 | 0.02 | 3 | < 0.001 | 0.56 | 9 | <0.001 | 0.18 | 9 | 0.66 | 0.05 | 9 |
| *Hyperoodon ampullatus* | < 0.001 | 0.95 | 9 | 0.36 | 0.22 | 4 | 1.03 | < 0.001 | 3 | < 0.001 | 0.33 | 9 | < 0.001 | 0.43 | 9 | < 0.001 | 0.59 | 9 |
| *Lagenorhynchus acutus* | 7.21 | < 0.001 | 9 | 0.50 | 0.16 | 4 | < 0.001 | 0.21 | 3 | < 0.001 | 0.91 | 9 | < 0.001 | 0.60 | 9 | < 0.001 | 0.59 | 9 |
| *Lagenorhynchus albirostris* | 3.70 | < 0.001 | 9 | < 0.001 | 0.57 | 4 | 0.14 | 0.28 | 3 | < 0.001 | 0.77 | 9 | < 0.001 | 0.82 | 9 | 0.61 | 0.08 | 9 |
| *Mesoplodon bidens* | 1.20 | < 0.001 | 9 | < 0.001 | 0.46 | 4 | < 0.001 | 0.66 | 3 | < 0.001 | 0.54 | 9 | < 0.001 | 0.09 | 9 | < 0.001 | 0.40 | 9 |
| *Orcinus orca* | 0.64 | 0.10 | 9 | 0.75 | 0.05 | 4 | < 0.001 | 0.47 | 3 | < 0.001 | 0.38 | 9 | < 0.001 | 0.80 | 9 | < 0.001 | 0.76 | 9 |
| *Phocoena phocoena* | 8.27 | < 0.001 | 9 | 0.74 | 0.05 | 4 | < 0.005 | 0.67 | 3 | 0.89 | 0.01 | 9 | 0.04 | 0.32 | 9 | 0.39 | 0.19 | 9 |
| *Physeter macrocephalus* | 4.19 | < 0.001 | 9 | 0.71 | 0.05 | 4 | < 0.001 | 0.80 | 3 | < 0.001 | 0.44 | 9 | < 0.005 | 0.31 | 9 | < 0.001 | 0.75 | 9 |
| *Pseudorca crassidens* | 1.04 | 0.05 | 9 | < 0.001 | 0.88 | 4 | < 0.001 | 0.46 | 3 | 0.99 | 0.07 | 9 | < 0.001 | 0.76 | 9 | < 0.001 | 0.93 | 9 |
| *Stenella coeruleoalba* | 5.45 | < 0.001 | 9 | < 0.001 | 0.89 | 4 | < 0.001 | 0.83 | 3 | < 0.001 | 0.75 | 9 | 0.76 | 0.05 | 9 | 0.18 | 0.24 | 9 |
| *Tursiops truncatus* | 3.54 | 0.001 | 9 | < 0.001 | 0.92 | 4 | < 0.001 | 0.90 | 3 | < 0.001 | 0.77 | 9 | < 0.001 | 0.79 | 9 | < 0.001 | 0.79 | 9 |
| *Ziphius cavirostris* | 2.70 | 0.001 | 9 | < 0.001 | 0.95 | 4 | < 0.001 | 1.00 | 3 | < 0.001 | 1.00 | 9 | < 0.001 | 0.45 | 9 | < 0.001 | 0.76 | 9 |

## 5.5 Discussion

We looked at 17,491 UK and Irish cetacean stranding records from 1913-2015 from the Natural History Museum (NHM), the Cetacean Stranding Investigation Programme (CSIP), and the Irish Whale and Dolphin Group (IWDG). We found that stranding numbers increased throughout the century, with hotspots along the southern and western coast of the UK and Ireland. We investigated several potential environmental and anthropogenic predictors: storms, geomagnetic activity, North Atlantic Oscillations, sea-surface temperature, and fishing catch. Except for year of stranding, we found no significant correlation between the numbers of cetaceans stranding each year and these potential predictors.

### 5.5.1 Temporal and spatial patterns in the strandings data

We found that temporal and spatial variation in cetacean strandings has occurred over the last 100 years (from 1913-2015) on the shores of the UK and Ireland. Generally, cetacean strandings have increased throughout the century.

A reduction in mysticete strandings in the 1950s is likely to be related to a substantial increase in post-WWII commercial whaling that affected North Atlantic stocks (Braham, 1984; Amundsen et al*.,* 1995), reducing the number of individuals available to strand. Mysticete stranding numbers increase after 1987, the year after the International Whaling Commission moratorium on whaling came into effect.

Stranding events along the north and west coasts of Britain, south and west coasts of Ireland (McGovern et al*.,* 2016), and around the English Channel, Irish Sea, and Sea of the Hebrides may in part be due to the passive transport of carcasses by the North Atlantic drift (MacLeod et al*.,* 2004). Further, these areas support a higher abundance and diversity of cetaceans, particularly the deep, prey rich waters off the west coasts and continental shelf (Evans, 1980, Wall et al*.,* 2009, Hammond et al*.,* 2013). Many cetaceans including fin and sperm whales migrate along the west coasts of Ireland and Scotland (Evans, 1980) and are therefore more likely to strand in these regions.

Studies have highlighted the impacts of bycatch and entanglement as a cause of strandings (Leeney et al*.,* 2008; Parsons et al*.,* 2010; Deaville and Jepson 2011; Prado et al*.,* 2016). Strandings of harbour porpoise and common dolphin were particularly frequent around Cornwall and the southwest coast of England (Leeney et al*.,* 2008; Deaville et al*.,* 2015) and the Isles of Scilly (Sabin et al*.,* 2005). This spatial pattern has been attributed to entanglement in bycatch and intense fishing pressures off the southwest coast, one of the most heavily fished regions of the UK (Leeney et al*.,* 2008; Deaville et al*.,* 2015). Incidences of bycatch and entanglement in fishing gear for smaller cetacean species are generally higher in these regions (Leeney et al*.,* 2008; Deaville and Jepson, 2011; Deaville et al*.,* 2015). Despite an increase in bycatch monitoring and recording effort through initiatives such as the Agreement on the Conservation of Small Cetaceans of the Baltic, North East Atlantic, Irish, and North Seas (ASCOBANS), monitoring of cetacean bycatch in the majority of fisheries and areas is still insufficient (Read et al*.,* 2017). Entanglement in fishing gear also affects larger species and there has been a documented rise in the number of humpback whales caught in static creel lines in Scottish waters (Ryan et al*.,* 2016). Entanglement was the cause of fatality in half of all baleen whales examined at necropsy in Scotland (Northridge et al*.,* 2010), which may help explain high mysticete stranding rates in this region or reflect higher densities of these species in this region. It is also important to note that the proximity of the Atlantic shelf-edge to the Scottish islands, coupled with the influence of the Gulf Stream, make this a particularly rich area for migrating and feeding mysticetes (Evans, 1980; Pollock et al*.,* 2000).

### 5.5.2 Correlates of strandings through time

To further investigate spatial and temporal variation, we examined several possible correlates of strandings: storm events, geomagnetic fluctuations, North Atlantic Oscillation (NAO), maximum sea surface temperature (SST), and fishing catch data. However, none of these potential predictors explained the variation in cetacean strandings once we accounted for time. We suggest that this is because the scale of change in the variables is too coarse to detect any potential correlations. Due to the availability of human population data

(used as a proxy for sampling effort in our models) we were constrained to examining correlates at yearly intervals. Similar results and criticisms arose from the CSIP and IWDG (1990-2015) data only model, despite this model suffering less from the biases inherent in historical data. Further, the genus-level model and the model with 'rare' and 'unknown' records showed qualitatively similar results most likely due to the coarse, yearly constraints of the models. Below we discuss each correlate in turn.

### *Storms*

We found no significant indication of storms as a correlate for strandings records. Storm events have been reported to have a greater effect on smaller, shallow water species (Lawler et al*.,* 2007, Schumann et al*.,* 2013). However, we found no such effect in any of our 16 species-specific models, including our harbour porpoise only model, nor in our suborder model despite odontocetes generally having a smaller body size. Further, we found no effect of storms on strandings in our habitat model, despite storms potentially affecting shallow, coastal water species to a greater extent (Lawler et al*.,* 2007). We suggest that these effects may be population, location, or season-specific. Further, carcasses of offshore species may be blown onshore during storm events making species-specific and habitat-specific impacts harder to identify; consistent data on carcass condition would be required to analyze this. Stormy weather can increase the chances of mass stranding events in some species, sometimes with multiple species stranding together (Bogomolni et al*.,* 2010, Schumann et al*.,* 2013), however, we found no effect of storms when we included mass strandings as multiple events (i.e*.,* each species in that location, on that date is a single record). Again, it is likely that the scale of change in our variables is too coarse to model these effects.

### *Geomagnetic fluctuations*

We found no significant indication of geomagnetic fluctuations as a correlate for strandings. Geomagnetic fluctuations may increase the likelihood of stranding in some species, e.g*.,* sperm whales (Smeenk, 1997; Pierce et al*.,* 2007; Vanselow et al*.,* 2017). Only some genera (e.g*., Delphinus*, *Grampus,* and *Ziphius*; Kirschvink et al*.,* 1986) likely use geomagnetic features to

navigate, with others to a lesser extent (e.g*., Balaenoptera*; Kirschvink et al*.,* 1986), however, this was not detected in our species-specific models, nor in our suborder model. It should be noted that many of these studies focus on one species in one ocean basin e.g*.,* the effect of geomagnetic activity on sperm whales stranding in the North Sea (Vanselow et al*.,* 2017) and that these regional and species-specific definitions were not investigated in our macroecological study. We did not find a correlation between geomagnetic fluctuations and strandings in our regional models, perhaps because these effects are population, or season specific.

### North Atlantic Oscillation (NAO)

In contrast to other studies (Pierce et al*.,* 2007, Truchon et al*.,* 2013), we found only a slight effect of NAO on the number of stranding events in our main model. However, this was so small that it was inconclusive. Previously, positive NAO indices have been positively correlated with high stranding frequencies for seasonal migratory cetaceans (such as minke whales) in the Atlantic (Truchon et al*.,* 2013). Further, incidences of sperm whale strandings in the North Sea are higher during warm periods (associated with the NAO and higher SST), a likely reflection on changes in distribution of their prey (Robinson et al*.,* 2005, Pierce et al*.,* 2007). Again, this may be because many of these previous studies focus on one species, in a specific geographical region (e.g*.,* the North Sea only (Smeenk, 1997; Pierce et al*.,* 2007; Vanselow et al*.,* 2017), and show regional, and seasonal definitions that are not detected in our wider macroecological study.

### Sea surface temperature (SST)

We found only a slight correlation between SST and stranding records in our main model. The EDF was so low, that this is not a conclusive correlate of strandings. Studies that have investigated SST and cetacean strandings are species, and region specific. For example, in western Scotland, the relative frequency of strandings of white-beaked dolphins, a colder water species, have declined whilst strandings of common dolphins, a warmer water species, have increased (MacLeod et al*.,* 2005). We found no such species-specific effects. We also found no effects of SST on strandings in our regional models

(southwest UK and northwest UK). The effects of an increase in SST may be particularly profound in species that are constrained to shelf-waters and are unable to retreat to deeper, oceanic waters (MacLeod et al*., 2009). However, we saw no such effect of SST in our habitat model. Again, it is likely that the scale of change in our variables is too coarse to model these effects, and further, that seasonal definitions are not investigated in our model.

### *Fishing catch*

We found only a small correlation between stranding events and fishing catch. It is well known that over-fishing can directly impact cetaceans by reducing their prey (Evans, 1990; Weir et al*., 2007), which can lead to starvation, or a shift in cetacean distribution as they search for prey elsewhere. Starvation is a common cause of death recorded in stranding reports (Kirkwood et al*., 1997; Deaville and Jepson, 2011; Deaville et al*., 2015), with many cases ascertaining that no other disease processes could explain the animal's poor nutritional status (Jepson, 2005; Deaville and Jepson, 2011). We found a correlation between fishing catch and strandings in the southwest regional model, the habitat model, and the model with all 'rare' and unknown records included, although these correlations are too small to be conclusive. Future studies should investigate the effects of fishing catch at a finer seasonal, and regional scale, and importantly, in conjunction with bycatch data.

### *Model criticisms*

Our models may have failed to fully explain the variation in cetacean strandings because we did not include other possible predictors such as reported bycatch numbers, or sonar use. Other causes of death, and of strandings include infections from bacteria and other pathogens, impacts of legacy chemical contaminants, particularly in top predators such as killer whales and false killer whales which have seen a decline in stranding records, physical trauma from boat strikes, in addition to interspecific aggression, and starvation (Sabin et al*., 2005; Deaville and Jepson, 2011; Jepson et al*., 2016, Law et al*., 2012). Other studies have shown that beaked whales and pilot whales are particularly sensitive to sound pollution from ship sonar and military exercises, causing fatal gas bubble lesions from rapid ascents (Jepson et al*.,

2003; McGeady et al*., *2016; Harris et al*., *2017). However, responses varied between, and within, individuals and populations (Harris et al*., *2017). We were unable to include these variables because data were not available for the full period of our stranding data set at a yearly resolution. In addition, they have been addressed elsewhere through the work of the current UK strandings program (e.g*., *Deaville and Jepson, 2011; Jepson et al*., *2016).

Our results may be confounded by the way we performed our analyses. First, we were unable to account, in a satisfactory way, for sampling effort, instead using yearly UK population size as a proxy. This is problematic as it cannot account for social and attitudinal changes over the 103-year period that are likely to have had an impact on reporting effort. In addition, we used a population measure for the whole UK, which shows that apart from the years 1916-1918 (i.e*., *WWI), the human population rose every year (Appendix 5: Human population data). A total UK population count misrepresents some rural counties that have seen population fluctuations (for example Anglesey, Wales) or declines (for example Argyll and Inverclyde, Scotland, and Donegal, Ireland). Our two regional models, one for the southwest of England where human population has increased over the century, and one for the northwest of Scotland where human population has decreased over the century, were designed to account for this, but we did not find much variation in our results. A better model would incorporate monthly human population data for each county with a coastline, for the period 1913-2015, and therefore represent changing sampling effort in that region over the century. This would also allow us to model the other variables at monthly intervals. We could not incorporate these data because county-level population data dating back to 1913 is only available decadally in UK and Irish Census data, and county (and country) boundaries have changed in this time. Further, fluctuations in stranding records may be attributable to uneven observer effort caused by specific events, for example reduced effort during and after both world wars (Klinowska 1985).

We also highlight that the spatio-temporal difference between the death of the animal and its discovery may affect stranding records, but that this is too

variable to model. This includes factors such as initial location of the animal at the time of death, buoyancy of the carcass/species, and proximity of the carcass to strong currents, all of which determine where and if the animal washes up.

### *Sampling effort*

It is most likely that the increase in stranding records throughout the 1980s to the present was due to an increase in observer effort (Leeney et al*., 2008; Deaville and Jepson, 2011; Pyenson, 2011) and dedicated recording effort from the CSIP and the IWDG from 1990 onwards. It may also be the result of an increase in interest and reporting (O'Connell and Berrow, 2007), and knowledge of the public (Norman et al*., 2004; Leeney et al*., 2008). An increase in stranding records from the late 1980s onwards was also reported from southeast Australia (Evans et al*., 2005), the northwest Pacific in the USA (Norman et al*., 2004), and from the Hawaiian Islands (Maldini et al*., 2005). These increases are also associated with an increase in observer effort, and the formation of formal strandings networks. We see this pattern in the UK and Irish stranding data.

Overall, we found numerous potential drivers of cetacean stranding events, but that the causes of strandings often remain undetermined (Dolman et al., 2010). Cetaceans in UK and Irish waters are facing numerous challenges such as reductions in prey stocks, increases in chemical and noise pollution, and bycatch/entanglement (Parsons et al., 2010; Deaville and Jepson, 2011). It is likely that the number of stranded cetaceans will continue to rise as reporting effort and public interest in cetaceans continue to increase, and further, as environmental, and anthropogenic pressures on cetaceans persist or perhaps as some populations increase in numbers following conservation efforts as has been reported from some sightings data (Stevick et al., 2003; Brower et al., 2018). Brower et al., (2018) highlight the importance of considering the impacts of survey (sampling) effort on records, especially when considering a broad temporal scale, as is considered here. We suggest that future studies continue to consider anthropogenic and environmental threats that are likely to affect the numbers of cetaceans that strand as well as incorporating the effects of sampling effort and population recovery where possible.

Long-term strandings data provides vital information on past and present cetacean diversity and distribution for common, rare, and inconspicuous species, highlighting the importance of stranding programs. Such data on cetaceans can provide an indication of wider ecosystem health (Friedlaender et al., 2006; Roman et al., 2014) making these an important data source to consider when informing conservation decisions.

# Chapter six

# Conclusions

*'I can see no difficulty in a race of bears being rendered, by natural selection, more and more aquatic in their structure and habits, with larger and larger mouths, 'til a creature was produced as monstrous as a whale.'*

Charles Darwin - 'On the Origin of Species By Means of Natural Selection'

## 6.1 Broader context

Cetaceans have undergone extensive morphological changes to adapt to a fully aquatic lifestyle (Fordyce and de Muizon, 2001; Uhen, 2007). Because of this, they show extremely divergent morphologies compared to their terrestrial artiodactyl relatives. Some of the most striking changes have occurred in the skull and include the posterior displacement of the nares, maxilla, premaxilla, and a shortening of the nasals (Heyning and Mead, 1990; Klima, 1999; Churchill et al., 2018). These extreme adaptations coupled with a remarkably continuous fossil record make cetaceans a prime candidate for macroevolutionary studies. In this thesis I quantify morphology, and investigate shifts in asymmetry (Chapter 2), evolutionary rates, and disparity in the cetacean skull over their entire 50-million-year evolutionary history (Chapters 2-4). I then investigate several possible influences on cranial morphology, including ecological factors such as echolocation ability and feeding method (Chapter 3) and separately, larger scale macroevolutionary change: palaeoclimate and ocean productivity (Chapter 4). In the final chapter of my thesis (Chapter 5), I shift from morphological to taxonomic diversity, and from deep to shallow time, analysing 102 years of spatial and temporal patterns in $20^{th}$ and $21^{st}$ century strandings data. I use methods from palaeontology and neontology to build a comprehensive picture of cetacean diversity through time. Like other historical data, the fossil record and strandings data provide an important insight into the ecological limits and evolutionary responses of cetaceans and should continue to be used and studied to help address future conservation and management. Here I bring together results from the preceding chapters and produce a comprehensive picture of cetacean diversity through time.

In this chapter, I bring together results from the preceding chapters to produce a comprehensive picture of cetacean evolution and diversity through deep and shallow time. I finish by discussing the importance of these results for both evolutionary and conservation biology, discuss the limitations of this work, and suggest future directions this work could take.

## 6.2 Key findings

### *6.2.1 A quantification of asymmetry in the whale skull*

The cetacean skull has undergone a variety of complex changes, while adapting to the pressures of aquatic life. These morphological changes include the posterior shifting of the nares, seen in the archaeocetes before the divergence of the neocetes, which facilitated easier breathing at the water's surface and catalysed huge change in the naso-facial region of cetaceans (Chapter 2 and 3). From the very divergence of the neocetes (~39 Mya), the differences between the two suborders are clear. It is well known that the odontocetes have asymmetric crania, likely because asymmetry in the soft facial anatomy (the melon and phonic lips employed in echolocation) consequently drives evolution of the underlying bony structures (Heyning and Mead, 1990). However, until now no work had been done regarding when and how often asymmetry may have arisen throughout cetacean evolution. The objectives for Chapter 2 were two-fold. Firstly, to quantify the evolution of cranial asymmetry in cetaceans and secondly to use these results to build a landmarking protocol that would accurately capture morphology in the cranium, including the asymmetry and telescoping unique to cetaceans. This protocol was required to accurately capture skull morphology and then model evolutionary rates and disparity in the skull in Chapters 3 and 4.

Once I had quantified the amount of asymmetry in the skull, I ran evolutionary models on univariate trait data: the measure of asymmetry obtained for each skull. I found that the early ancestors of living whales (the archaeocetes) had little naso-facial asymmetry and thus it was unlikely that they could echolocate. Asymmetry in the archaeocete skull is highest in the rostrum, orbit, and squamosal, and is potentially related to directional hearing. Asymmetry in the odontocetes, which diverged later, is highest in the naso-facial region. It is unclear whether this shift from rostral to facial asymmetry is due to an actual shift from a primitive form of aquatic directional hearing in specific archaeocetes (the basilosaurids and protocetids, as suggested by Fahlke et al. (2011)) to a different regime (i.e., to high frequency sound

production in the odontocetes, and low-frequency hearing in the mysticetes). Further, it is unclear how much of the asymmetry seen in the archaeocete rostrum is preservational deformation. Regardless, this specific pattern of asymmetry then disappears during the transition from archaeocetes to early neocetes. Naso-facial asymmetry is a significant feature in the earliest diverging odontocetes, evident in skulls in the Early Oligocene and, as with telescoping, it reaches its highest levels in more crownward taxa (Churchill et al., 2018). I confirmed that the mysticetes (baleen whales) show symmetry similar to terrestrial artiodactyls, such as bovines, and that asymmetry has never been a significant aspect of mysticete skull morphology, even in the earliest diverging members of the subclade, arguing against echolocation ability in the early mysticetes. In the odontocetes, I found that the first significant shift in asymmetry occurred in the stem odontocete family Xenorophidae during the Early Oligocene. Further increases in asymmetry occur in the physeteroids in the Late Oligocene, Squalodelphinidae and Platanistidae in the Late Oligocene/Early Miocene and in the Monodontidae in the Late Miocene/Early Pliocene. Additional episodes of rapid change in odontocete skull asymmetry were found in the Mid-Late Oligocene, highlighting the Oligocene as a period of rapid evolution of asymmetry. No high probability increases or jumps in asymmetry were found in mysticetes or archaeocetes.

Unexpectedly, no increases in asymmetry were recovered within the highly asymmetric ziphiids, which may result from the extreme, asymmetric shape of premaxillary crests and premaxillary sac fossae in these taxa not being captured by landmarks alone (as opposed to a combination of landmarks and semi-landmark curves). I cover this in more detail in 6.4.1. Ultimately, this led to me devising a landmarking protocol that included semi-landmark curves to define outlines and margins of bones and capture more shape data than just landmarks. This protocol was used in Chapter 3 and 4. Finally in Chapter 2, I reconstructed separate evolutionary regimes for odontocetes with the highest cranial asymmetry and found that they all live in acoustically complex or high-pressure environments, such as shallow rivers, cluttered icy waters, and deep

ocean. I found that these niches impose strong selective pressure on echolocation ability and thus increased cranial asymmetry.

### 6.2.2 A comprehensive analysis of evolutionary rates and disparity throughout cetacean history

Once I had quantified evolutionary shifts and jumps in a single trait (asymmetry) using univariate data (Chapter 2), I moved to quantifying evolutionary rates and disparity across the whole skull. I used the results from Chapter 2 (Coombs et al., 2020) to determine which of the bones in the skull were asymmetric and thus required manual landmarking of both the left and right sides of the skull to accurately capture this morphology. In Chapter 3, I used three-dimensional geometric morphometrics to reconstruct the drivers of shape variation, disparity, and evolutionary rates in the cetacean cranium (across the whole skull and in individual bones) throughout their evolutionary history for the first time.

Using this rich, multivariate data set, I found that throughout Cetacea's evolutionary history, there have been three key waves of diversification in the skull. Early archaeocetes (~ 48 Mya) show some of the highest evolutionary rates of all cetaceans, including a rapid burst in evolution that sees high rates over the whole skull and for individual bones, particularly in the frontal, maxilla, and nasal, likely associated with rapid backwards movement of the nares. The second wave of diversification occurs at the divergence of the neocetes around ~39-36 Mya. An increase in rates and disparity following the divergence, and in the proceeding years throughout the Oligocene, suggests that there were functional constraints in the archaeocete cranium that were overcome by the neocetes. Specific transitional morphologies found in the early neocetes account for some of these higher cranial evolutionary rates and disparities as the two suborders rapidly diverged.

The third wave of diversification is seen in the Miocene and is mostly an odontocete signal (~18-10 Mya). Interestingly, the timing of higher evolutionary rates in odontocetes coincided with higher probabilities of shifts and jumps in asymmetry: in the Early Oligocene in the early diverging odontocetes, in the

Late Oligocene/Early Miocene in the physeteroids, and again in the Late Miocene/Early Pliocene (Chapter 2, Chapter 3), which suggests that echolocation in odontocetes (synonymous with asymmetry) is a key driving force behind skull evolution in this suborder. In contrast, the mysticetes, which do not exhibit cranial asymmetry, diverged down a different evolutionary pathway with their own distinct morphology driven by the evolution and development of the ability to mass filter feed (Chapter 3). Evolutionary rates and disparity in the mysticetes are high in the early divergence of the suborder and peak again during the Mid-Late Oligocene. Thereafter, evolutionary rates in this suborder drop as baleen-assisted mysticetes successfully filled their ecospace and become increasingly disparate from the odontocetes (Marx et al., 2019a; Chapter 3).

I found that the suborders occupy distinct areas of the morphospace, with extreme axes of variation seen in the elongation of the rostrum and the positioning of the nares (Chapter 3). Echolocation, and its associated morphology, set the earliest odontocetes apart from the earliest mysticetes, which instead were rapidly evolving a range of different feeding ecologies of their own. The odontocetes occupy a broader range of the morphospace, which is likely driven by the ability to echolocate, a defining characteristic of this suborder. This also enables them to diversify into a vast range of forms (Marx et al., 2016a). Conversely, the morphology of the later mysticetes was likely constrained by the functional and morphological requirements of the dominant feeding strategies associated with an edentulous-baleen condition.

### 6.2.3 An in-depth analysis of ecological influences on cranial morphology

Cranial shape is driven by suborder-specific influences on diversification: echolocation in the odontocetes and baleen-filter feeding in the mysticetes (Chapter 3). To explore these ecologies further, I looked at the influence of dentition (e.g., baleen), diet (e.g., zooplankton), feeding method (e.g., filter feeding), and habitat (e.g., pelagic) on cranial morphology. In Chapter 2, the best fit model for explaining why some odontocetes have more exaggerated

asymmetry than others was a model that highlighted the impact of habitat, specifically high-pressure environments such as turbid, shallow rivers and their strong selective pressure on the ability to echolocate (and thus influence asymmetric in the skull). I therefore wanted to investigate ecological influences on cranial morphology across the skull. As in Chapter 2, I found that echolocation ability and habitat had a significant effect on skull shape. Further, I found that dentition, diet, and feeding method have also shaped the morphology of the skull (Chapter 3). Again, these results highlighted the key differences between odontocetes and mysticetes with regards to their unique adaptations and subsequent niche occupation. For example, some of the highest evolutionary rates were found in heterodont cetaceans which includes the archaeocetes, odontocetes, and early toothed mysticetes which lived during the Eocene and Oligocene – periods highlighted for high evolutionary rates in the cetacean cranium. Whilst some of the lowest evolutionary rates were found in the mysticetes which a) are edentulous (have baleen), b) filter feed, and c) feed on zooplankton. 'True' baleen evolved around 27.5 Mya (Tsai and Fordyce, 2018), and the toothed mysticetes disappeared early in the Miocene, after which only filter feeding mysticetes remain, occupying a small but very successful niche of baleen filter feeding allowing them to reach gargantuan body sizes. This occupation likely accounts for the low evolutionary rates seen in mysticetes thereafter (Chapter 3).

In Chapter 3 I identified three key waves in cetacean evolutionary rates and disparity in the cranium. I showed that a cetacean's ecology has an impact on skull morphology, specifically its ability to echolocate, its dentition (for example edentulous, filter feeding with baleen), its diet, and feeding method. However, evolutionary influences on morphology are complex and are often driven by a complicated suite of factors. George Gaylord Simpson hypothesised that much biological diversity originated during adaptive radiations and placed biotic interactions at the centre of phenotypic evolution (Simpson, 1953). A widespread alternative view suggests that environmental, abiotic factors play an equal or even larger role in evolutionary processes (Benton, 2009; Erwin, 2009). Commonly referred to as the 'court jester hypothesis' (Barnosky, 2001; Benton, 2009) this hypothesis states that abiotic influences such as climate,

function as a major driving force behind the processes of evolution (Barnosky, 2001). The differences between the two hypotheses is likely one of scale, with evolution at the macro scale more likely driven by abiotic factors than biotic factors (Barnosky, 2001). The impacts of abiotic factors, specifically climate, on complex or multivariate aspects of morphology at the macroevolutionary level are still poorly understood. Several studies suggest that changes in cetacean diversity and radiation (these studies consider molecular, morphological character, and genus-level diversity data) are driven by larger environmental change such as the opening of the Drake Passage (opening of the Southern Ocean), strengthening of the Antarctic Circumpolar Current, and resultant changes to climate and ocean processes. In Chapter 4, I tackle the challenge of quantifying these hypothesised impacts of large-scale environmental change on the cetacean cranium.

### *6.2.4 The impact of climate on cetacean cranial evolution*

In Chapter 4, I use the same rich morphological data set and landmark and semi-landmark data, as used in Chapter 3, to establish whether temperature and ocean productivity are significant drivers of cetacean cranial evolution. This study is the first comprehensive analysis of the impact of Cenozoic climate change on the morphological evolution of cetaceans. My results support the hypothesis that climate fluctuations and ocean productivity drive cetacean cranial evolution through deep time. Interestingly, climate models consistently outperformed Brownian motion and Early Burst models for all groups bar the archaeocetes. Importantly, mysticete rates of evolution are predominantly driven by fluctuating levels of ocean productivity, whereas odontocete evolutionary rates are driven by the *rate* of temperature change, as opposed to temperature itself or changes in temperature. My results clearly demonstrate that climate change and associated ocean productivity have driven evolutionary rates in cetaceans throughout their history from the Early Eocene to the present day. I show that peaks in neocete evolutionary rates coincide with massive ocean restructuring at the Eocene-Oligocene Boundary and during the Miocene, although more localised than in the Oligocene, likely also impacted rates and dispersion, particularly in the odontocetes. In the Early

Miocene, I found increased evolutionary rates in the naso-facial bones (Chapter 4) and an increase in naso-facial asymmetry (Chapter 2) in the Physeteroidea which could be associated with a shift to a cephalopod diet – an easy prey item when hunting is facilitated by advanced echolocation (Chapter 2). Later in the Mid-Miocene, I found increased evolutionary rates in the odontocetes which is likely a delphinid signal. A recent shift to a cephalopod diet in the delphinids may explain an increase in body size disparity (Slater et al., 2010) and a concurrent shift in cranial disparity then also. This peak in oceanic delphinid diversity in the Miocene is also a potential consequence of increased marine productivity and climate change (Marx and Uhen, 2010; Chapter 4).

Coupled with my results from Chapter 3, which highlighted the importance of echolocation and baleen in driving skull morphology in the neocetes, it is possible that filter-feeding mysticetes were better equipped to successfully exploit high ocean productivity in upwelling regions from around ~30 Mya. The differences observed between the best fit models driving morphological evolution in the two extant suborders likely reflects their vastly different early key innovations and resultant 'ecospace' occupation, e.g., feeding and prey types. That evolutionary rates in the mysticetes and odontocetes are driven by different aspects of climate change has clear implications for their evolution under future climate scenarios. Rates of evolution are likely a combination of the Court Jester and Red Queen hypotheses with abiotic and biotic factors playing a part as shown in Chapters 3 and 4. My results clearly demonstrate that climate change and associated ocean productivity have driven evolutionary rates in cetaceans throughout their history from the Early Eocene to the present day, with the differences between the groups reflecting their different ecological strategies. The different evolutionary responses to past climate change observed for the neocetes highlights a requirement for separate, tailored conservation and mitigation of climate impacts for toothed whales and baleen whales. This is especially true as current climate change is already having a profound impact on biodiversity, and this effect is only predicted to get worse under future scenarios.

### 6.2.5 An overview of ecological and anthropogenic influences on cetacean diversity

Unfortunately, the fate of cetaceans is now intertwined with humans and our activities regarding the atmosphere and oceans has a direct effect on the planet's biodiversity (Butchart et al., 2010; Jones and Safi, 2011). A complete study of cetacean diversity through time must consider shallow time impacts of human activities on whales both indirectly via processes such as global warming and more directly through hunting, ship strike, and overfishing, to name just a few. In my final chapter, I make a departure from the geometric morphometric approach (Chapters 2-4) and explore a completely different data type. I use strandings data (when cetaceans become grounded on a beach or in shallow water) to bridge scales of analysis, departing from larger evolutionary scales and instead exploring environmental and anthropogenic predictors of cetacean diversity in shallow time.

In Chapter 5, I combined cetacean strandings data from the Natural History Museum (NHM), Cetacean Stranding Investigation Programme (CSIP), and the Irish Whale and Dolphin Group (IWDG), building a data set of 17,491 records and 102 years of UK and Irish strandings data. Combining these data sets resulted in one of the longest, continuous, systematic stranding data sets in the world offering a unique opportunity to investigate what has happened to cetacean records in the recent past and present. My overall objective was to explore broad-scale patterns and correlation of cetacean strandings through time. Combining all three data sets for the first time, I presented more than 100 years of data, and showed spatio-temporal patterns in the number of individuals stranding in the UK and Ireland. Importantly, I looked at a variety of potential correlates of strandings including environmental (such as storm data) and anthropogenic factors (such as fishing catch data). Firstly, I found a dramatic increase in strandings since the 1980s, most likely due to increases in recording effort and the formation of formal strandings networks (CSIP and IWDG were both officially formed in 1990). I also found strandings hotspots along the southern and western coast of the UK and Ireland. This may in part be due to the passive transport of carcasses by the North Atlantic drift (MacLeod et al., 2004). Further, these areas support a higher abundance and

diversity of cetaceans, particularly the deep, prey rich waters off the west coasts and continental shelf (Evans, 1980, Wall et al., 2009, Hammond et al., 2013). Many cetaceans including fin and sperm whales migrate along the west coasts of Ireland and Scotland (Evans, 1980) and are therefore more likely to strand in these regions.

I looked at the following potential environmental and anthropogenic predictors: storms, geomagnetic activity, North Atlantic Oscillations, sea-surface temperature, and fishing catch, as well as an additional shipping traffic model. I found no correlation between the numbers of cetaceans stranding each year and any of the potential environmental and anthropogenic predictors. This is possibly because the scale of change in the variables is too coarse to detect any potential correlations. As in Chapter 4, it may also reflect the idiosyncratic nature of species' responses to external pressures. This provides further support for targeted conservation and management at a level more defined than the 'cetacean' level, for example at the genus or species level and the very least a tailored conservation approach for mysticetes and odontocetes.

### 6.2.6. Implications for conservation

There is a growing body of literature substantiating the fidelity of palaeontological data on a variety of spatial and temporal scales and the potential insights that the fossil record can provide into the current biodiversity crisis (Louys et al., 2012; Tyler and Schneider, 2018). This approach offers a temporal scope and historic perspective that is often lacking in studies with short time spans, such as modern ecological assessments, which may fail to consider deep-time perturbations and past impacts on ecology (Tyler and Schneider, 2018). Fossils can document response and recovery brought on by past global crises, and this concert of historical and present-day ecology, as shown in my thesis, has the potential to positively inform conservation efforts (Louys et al., 2012; Tyler and Schneider, 2018).

There are many studies that employ this approach, for example, subfossil baleen whale samples have been used to map habitat and range expansion in bowhead whales (*Balaena mysticetus*) throughout Late Pleistocene climate

change (Foote et al., 2013). Further, a different study which looked at grey whale (*Eschrichtius robustus*), subfossil records showed that the Pleistocene glacial maxima may have created multiple, weak genetic bottlenecks for this species but that the population would have been sufficient to survive the loss of major benthic feeding areas (i.e., the majority of the Bering Shelf) during glacial maxima (Pyenson and Lindberg, 2011). These studies have implications for conservation including extensions and provisions for protecting the habitats that these species rely on. Polly et al., (2011) suggest that functional morphological traits can form a common denominator for studying interactions between species and climate across taxa and ecosystems and across space and through time (Polly et al., 2010). These results can be used to inform habitat modelling and species occurrence maps (to name just two examples) using palaeontological and other historical data as evidence to test whether realised habitats are coincident with potential habitats under realised and potential climate scenarios (Polly et al., 2010). Studies which do not consider historical data can call into question the baselines used in modern-day marine mammal conservation and management debates (Alter et la., 2007; Pyenson and Lindberg, 2011).

My research covers a much greater temporal scale than these examples, providing a unique insight into the impacts of 50 million years of climate and ocean fluctuations on extinct and extant cetaceans. I use a combination of methods from palaeontology and neontology to address questions on cetacean macroevolution and macroecology through time, with a focus on the cetacean cranium and strandings data. Monitoring cetacean populations, both in deep time and shallow time, is crucial to our understanding of these animals. Information provided by both the monitoring of extant species (here, via strandings records) and from the fossil record play an important role in understanding the ecology, distribution, and adaptability of species both now and in the past and better informs those baselines used in modern-day conservation. Further, placing species in a phylogenetic context can help us to understand loss in genetic and morphological distinctiveness (Pyenson, 2009; Marx et al., 2016a) which is useful for targeting efforts for their protection (Marx et al., 2016a). I show that evolutionary responses to past climate change

(Chapter 4) highlight a need for tailored conservation and mitigation of climate impacts for odontocetes and mysticetes, separately. Coupled with shallow time strandings data, we build a bigger picture of past abiotic and biotic influences on cetacean diversity with present and ongoing environmental and anthropogenic threats. Finally, in a similar vein, long-term strandings data provides vital information on past and present cetacean diversity and distribution for common, rare, and inconspicuous species, this time on a different temporal and spatial scale. It also highlights the importance of stranding programmes (and requirements for future UK and Irish Government investment and continued support) for informing conservation. Such data on cetaceans can provide an indication of wider ecosystem health (Friedlaender et al. 2006, Roman et al. 2014) making these important data sources to consider when informing conservation decisions. As with the deep-time data, my research highlights the idiosyncrasies of species-specific responses to environmental perturbations, reinforcing the 'bigger picture' message that targeted conservation and management at a level more defined than the 'cetacean' level, for example at the genus or species level and at the very least a tailored conservation approach for mysticetes and odontocetes, is a conservation requirement going forward. Finally, it is increasingly recognised in conservation and ecosystem management that ecology needs a palaeontological perspective (Louys et al., 2012) and this should be a priority for studies of this type.

## 6.3 Limitations

As with every study, I had to make decisions on which analyses to focus on and which to cut due to both time and computational constraints. Regarding time constraints, the key adjustment I made was to not study intraspecific variation. Furthermore, due to time constraints, resources, and specimen availability, I was not able to collect data in Japan. This would have provided me with data on the Eomysticetidae – or 'dawn mysticetes' which are among the oldest of the chaeomysticetes – the 'true' toothless mysticetes from the Early-Late Oligocene (Marx et al., 2016a). I did not have the time or resources to study *Yamatocetus canaliculatus* (KMNH VP 000,017) (Japan) (Okazaki, 2012) and eomysticetid specimens I observed in New Zealand were too

distorted and incomplete to include in this thesis. I also did not look at sexual dimorphism in the cranium. This is often very difficult, if not impossible, to decipher for fossils and many of my extant specimens lacked data on sex too.

One of the main issues I came across when using large multivariate data sets was their high dimensionality. Multidimensional data require increased computational time, higher memory requirements, and the number of parameters needed to fit models increases non-linearly (Clavel et al., 2015; Clavel et al., 2019). Large multivariate data sets such as my landmark data introduce both statistical and analytical challenges as the number of variables or trait dimensions ($p$) (here landmarks) far exceed the number of specimens ($n$) (Clavel et al., 2019). Multivariate data such as 3D landmarks and curve semi-landmarks have three dimensions (x, y, z), which means the number of variables can quickly escalate. As the number of trait dimensions increase, parametric methods such as MANOVAs can lose statistical power (Collyer et al., 2015) and can even fail altogether when $p > n$. This happens because the inverse of the covariance matrix (required to run such tests) cannot be calculated when $p > n$. Conversely, reducing the number of variables also has its problems as organisms are multidimensional and therefore reducing variables severely impedes representative morphological quantification (Collyer et al., 2015).

In chapters 2-4 I use an R package called 'geomorph'. Adams et al. (2014) developed geomorph for many standard analyses of geometric morphometric data, including to compare evolutionary rates across clades, measure phylogenetic signal, and perform regression analyses for multidimensional data. The phylogenetic comparative methods implemented in geomorph assume a Brownian Motion (BM) model (Clavel et al., 2019) and are not flexible enough to consider other models. Some methods implemented in geomorph, e.g., phylogenetic regressions, also suffer from low statistical performances, particularly when data depart from the BM assumption (Goolsby, 2016; Clavel et al., 2019). To address the issue of high dimensionality without losing detail on morphology, I made two main changes in Chapters 3 and 4 where high dimensionality was an issue for me, even when using a Dell PowerEdge C6420 (48x) and R940xa (1x) supercomputing

cluster. Firstly, I stepped away from some of the more traditional methods such as calculating evolutionary rates in geomorph (which assumes a BM mode of evolution) and instead used mvMORPH and RPANDA (Clavel et al., 2015; Morlon et al., 2016), which can accommodate departures from BM in phylogenetic regressions and explicitly incorporate other models in rate analyses. Secondly, in Chapter 3 and Chapter 4, I reduced the dimensionality of my data by reducing the data to its phylogenetic principal components (PCs). Importantly, it should be noted that pPC analyses also assume a BM mode of evolution. My model analyses (Chapter 3) show support for a lambda model, with lambda closer to 1 than to 0 (0.69, Chapter 3). Given that there are only two options for ordination at present, specifically doing it with or without a BM-based phylogenetic transformation, and given that lambda is close to 1, using the BM assumption here is better than not doing it at all. More importantly, this impact is strongest where studies only use a few pPC axes in their downstream analyses, which is extremely common and should be avoided. I used pPC axes that captured 95% of the total variance in my data set, which means that the rotation of the axes should have little impact on my results. I also ran my analyses on the landmark only and full data sets as well, with results largely consistent. The pPC scores approach is a compromise between using the full data set (computationally intensive) and excluding all the information in the curves, which is not ideal as shown in Chapter 2.

Finally, when investigating the influence of ecological traits on my high-dimensional cranial data, I used a phylogenetic MANOVA (pMANOVA) with error, which accounts for interspecific variation and departures from BM, which have been shown to perform better than phylogenetic regressions as implemented in 'geomorph' when the underlying model is not BM (Adams 2014b). This is particularly important as a lambda model consistently outperformed BM for my cetacean cranial data set. More details are provided in the relevant chapters.

Regarding the strandings data set, due to the requirement for CSIP to submit their own annual reports to the Department for Environment, Food and Rural Affairs (DEFRA), I was only provided with data up to 2015. This inevitably means ~4 years of strandings data were not included in my models. This is

especially important because the quality and quantity of strandings reports appear to increase in more recent years, likely a result of increased sampling effort (discussed further in Chapter 5). I also had issues with data availability for some predictors such as shipping data which is only available for 1950-2015 rather than the entire 102-year strandings data span. Data availability also had implications for the exclusion of some predictors such as the effects of bycatch for which data was only released from 2012-present from DEFRA and military sonar data which has been shown to influence stranding numbers (Jepson et al., 2003). Due to confidentiality, I was not allowed access to Ministry of Defence military sonar data. Ideally, I would have included sonar use, bycatch, and chemical pollution, but none of these variables were available for every year in our data set (i.e., 1913–2015), particularly for the earlier part of the 20th century.

## 6.4 Future directions

### 6.4.1 Asymmetry and semi-landmark curves

The work undertaken in this thesis has highlighted some key gaps in the literature that could not be addressed in this thesis due to time and resource constraints. Firstly, regarding cetacean asymmetry (Chapter 2), I would like to run the analyses with both landmark and curve data as sliding semi-landmark curves are used to define outlines and margins of bones, representing an increase in the shape captured compared to using landmarks alone (Bookstein, 1997; Bardua et al., 2019; Goswami et al 2019). I predict that this would help capture shape data, particularly in the curvature of the premaxillary crests and premaxillary sac fossae of the beaked whales. It would enable me to also test whether asymmetry in this clade which spend considerable time hunting in deep waters – much like *Physeter* and the kogiids (to a lesser extent), have also got extreme asymmetry and an associated acoustic repertoire (echolocation) to facilitate hunting in such extreme environments If time permitted, I would rerun the asymmetry analyses with all curve data collected for Chapter 3 and 4, and I would also explore another area of future research looking at modularity in the cetacean skull.

### 6.4.2 Modularity

The theory behind modularity is that structures (for example, bones in the skull), can be divided up into subsets of associated (integrated) traits that may evolve in a coordinated way. Within this network of modules can have strong or weak intra-module integration and this can affect the rate at which modules evolve as a unit and alongside other modules. There have been many studies of modularity in tetrapods including in the caecilian skull (Bardua et al., 2019b; Marshall et al., 2019), archosaur skull (Felice et al., 2019), mammal cranium (Goswami, 2007; Churchill et al., 2019 (see Klingenberg (2013) for a review of studies concerning modularity in the mammal skull)), and nasal modularity in bats (Santana and Lofgren, 2013), to name just a few. Modularity in the cetacean has been analysed in the vertebral column in living and fossil whales to better understand the evolutionary location of the transition from terrestrial to neocete modularity (Buchholtz, 2007). Churchill et al. (2019) used a 10 module and 5 module hypothesis to quantify modularity in the common dolphin (*Delphinus delphis*) skull. Morphological changes in the skull related to the evolution of echolocation, and the loss of mastication best explained the novel modules (Churchill et al., 2019). Future research could use this approach and methodology, combined with a taxonomically broader morphometric data set to analyse modularity across Cetacea. It would be interesting to see how the archaeocetes and neocetes differ in their modularity with a focus on the evolution of echolocation and baleen filter-feeding.

### 6.4.3 Post cranial evolution

Often in cetacean fossils, the skull has become disarticulated from the body as it is one of the heaviest parts, it can detach from the carcass, fall away, and sink before any full skeleton burial and fossilisation can take place (Marx et al., 2016a). The result is that many cetacean fossils and extant material lack cranial material. Of course, specimens lacking cranial material were not used in this thesis, but studies of isolated post-cranial material could open up the study to many more specimens. Future studies could investigate evolutionary rates and trait integration across postcranial bones in cetaceans as an interesting comparison to the work done in this thesis. Most studies of the

cetacean post-cranial skeleton concern locomotion in living and extinct specimens (Buchholtz, 1998; Buchholtz, 2001), and modularity as previously mentioned (Buchholtz, 2007).

### 6.4.4 Intraspecific variation

My thesis is predominantly concerned with rates of evolution and disparity at the macroevolutionary level. However, the study of morphology at the intraspecific (static) level can help reveal genetic variation across the skull. Extreme environmental change can often result in developmental abnormalities, especially when incurred during growth (Badyaev et al., 2005). Furthermore, intraspecific morphology can then be compared to the evolutionary level to better understand where these relationships are maintained across species and have perhaps formed a persistent constraint on evolution. Marshall et al. (2019) investigated this in the caecilian crania and found congruent patterns across the crania of two species, both of which were consistent with patterns recovered at a macroevolutionary level (Marshall et al., 2019; Bardua et al., 2019b). Studies of intraspecific morphology can provide a gateway to study morphology at the ontogenetic level which could help reveal how modularity and integration changes throughout development. Further, intraspecific studies can provide an opportunity to study sexual dimorphism, for example female false killer whales have a slightly more asymmetrical skull than males (Kitchener, 1990) and would be interesting to quantify the extent of morphological differences between males and females. Of course, most intraspecific studies could only be carried out on extant cetaceans due to specimen availability, however the remarkable cetacean fossil record does present some examples of multi-specimen fossils such as *Piscobalaena nana*, *Basilosaurus Isis*, and *Atocetus iquensis* to name a few.

### 6.4.5 Mandible morphology and trade-offs

On several occasions, the results of Chapter 3 pinpointed the importance of considering the mandible in studies that quantify the ecological influences on cranial morphology in the skull. For example, dentition, diet, and feeding method are all directly driven by mandible morphology and function. The

mandible in toothed whales has two key functions; 1. to process food (eat) and 2. to receive incoming sounds (hear). As both functions place demands on form, there is likely a 'trade-off' between these two antagonists. To date, little work has been done on the trade-off between these two functions in toothed whales. Future studies could quantify the relationships and trade-offs between mandible morphology, prey, and echolocation across toothed whales, on a macroevolutionary scale. This could also provide a platform for an intraspecific study, investigating whether mandible morphology, echolocation, and hearing are driven by prey type within a single species; the killer whale, on a microevolutionary scale. The overarching aim would be quantifying the link between morphology, feeding, and sensory function across all toothed whales, which has not been done before.

## 6.5 Conclusions

This study is the first comprehensive analysis of diversity across the cetacean cranium, spanning their evolutionary history. I employed methods from palaeontology and neontology to quantify diversity using two very distinct data sets, a three-dimensional morphometric data set spanning the entirety of cetacean evolution, made up of 56% fossil material and representing ~95% of extant species and as well as a combination of 3 UK and Irish strandings data sets combining 17,491 records and 102 years of data, resulting in the longest, continuous, systematic strandings data set in use. Firstly, I captured cranial shape in unprecedented detail using advanced methods of 3D scanning and morphometrics that permit the comparison of extremely disparate shapes. I used these data to build the first comprehensive analysis of cranial asymmetry spanning the evolutionary history of cetaceans. This highlighted key morphological differences between the suborders, and specifically between the neocetes, even in their early divergence. I then used these results to inform a landmarking and curve semi-landmark protocol for asymmetric (odontocete and archaeocete) and bilaterally symmetric (mysticete) skulls. I used this to quantify cetacean cranial morphology throughout their entire evolutionary history, spanning 47.8 million years to reconstruct the processes and factors that drove this diversity for the first time. This study pinpointed key periods of high evolutionary rates and disparity in the diversification of the cetacean skull

driven in part by the morphological and ecological impacts of key innovations such as echolocation in the odontocetes and mass filter-feeding. I found that habitat, diet, feeding method, and detention also influenced cranial morphology. These patterns in evolution and disparity led me to model abiotic factors: climate and ocean productivity. This was the first study to quantify the impact of Cenozoic climate change on the morphological evolution of cetaceans.

Finally, I used the strandings data set to measure the effects of environmental and anthropogenic impacts on cetacean stranding. This completed the investigation in cetacean diversity from deep to shallow time, bridging scales of analyses, and highlighting the drivers of cetacean diversity throughout their evolution. This work should serve as a useful resource for future researchers interested in morphology, univariate, and multivariate trait evolution, and more specifically, influences on cranial morphology in cetaceans. Importantly, differences in how the suborders have responded to past climate change, and more recently, species-specific responses to environmental and anthropogenic impacts have important implications for tailored future management and conservation. By combining data on extant cetaceans with data from the fossil record we can assess the ecological limits and adaptations of cetaceans to pressures in the past, both deep time and more recently, and use this knowledge to help protect them in the future.

# References

Adam P (2002) Pelvic anatomy W.F. Perrin, B. Würsig, J.G.M. Thewissen (Eds.), Encyclopedia of Marine Mammals, Academic Press, San Diego, CA pp. 894-897

Adams D (2014). Quantifying and comparing phylogenetic evolutionary rates for shape and other high-dimensional phenotypic data. *Syst. Biol.* 63:166–177.

Adams D and Otárola-Castillo E. (2013). Geomorph: an R package for the collection and analysis of geometric morphometric shape data. *Methods Ecol. Evol.* 4:393–399.

Adams D, Collyer M and Kaliontzopoulou A (2020). 'Geomorph: Software for geometric morphometric analyses. R package version 3.2.1.' Available https://cran.r-project.org/package=geomorph.

Adams D, Collyer M and Kaliontzopoulou A. 'Geomorph: Software for geometric morphometric analyses. R package version 3.1.0'. Available at: https://cran.r-project.org/package=geomorph. 2019.

Adams D, Rohlf F and Slice D. (2013). A field comes of age: geometric morphometrics in the 21st century. Hystrix, *Ital. J. Mammal.* 24:7–14.

Adams, D, Rohlf F and Slice D. (2004). Geometric morphometrics: ten years of progress following the 'revolution.' *Ital. J. Zool.* 71:5–16.

Aguilar Soto N, Johnson M, Madsen P, Díaz F, Domínguez I, Brito, A and Tyack P (2008). Cheetahs of the deep sea: deep foraging sprints in short-finned pilot whales off Tenerife (Canary Islands). *Journal of Animal Ecology.* 77: 936-947.

Alter SE, Rynes E, Palumbi SR (2007). DNA evidence for historic population size and past ecosystem impacts of gray whales. Proc Natl Acad Sci U S A 104: 15162–15167.

Amundsen E, Bjorndal T and Conrad J. (1995). Open access harvesting of the Northeast Atlantic minke whale. *Environmental & Resource Economics*, 6:167–185.

Arbour JH, Curtis AA and Santana SE (2019) Signatures of echolocation and dietary ecology in the adaptive evolution of skull shape in bats. *Nat Commun* **10,** 2036

Arnold P, Forterre F, Lang J and Fischer M. (2016). Morphological disparity, conservatism, and integration in the canine lower cervical spine: Insights into mammalian neck function and regionalization. *Mammalian Biology*, *81*(2), 153–162.

Askin N, Belanger M and Wittnich C. (2017). Humpback Whale Expansion and Climate Change-Evidence of Foraging Into New Habitats. *Journal of Marine Animals and Their Ecology*: 9(1): 13-17

Au W, Pawloski J and Nachtigall P (1995) Echolocation signals and transmission beam pattern of a false killer whale (*Pseudorca crassidens*). *Journal of the Acoustical Society of America*. 98(1): 51–59.

Bailey H, Senior B, Simmons D, Rusin J, Picken G and Thompson P (2010). Assessing underwater noise levels during pile-driving at an offshore windfarm and its potential effects on marine mammals. *Marine Pollution Bulletin, 60*(6), 888–897.

Bajpai S and Gingerich P (1998). A New Eocene Archaeocete (Mammalia, Cetacea) from India and the Time of Origin of Whales. *Proceedings of the National Academy of Sciences of the United States of America*, 95(26), 15464–15468.

Baker A. (2001) Status, Relationships, And Distribution of Mesoplodon Bowdoini Andrews, 1908 (Cetacea: Ziphiidae). *Marine Mammal Science.* 17(3): 473–493.

Baker C and Clapham P (2004). Modelling the past and future of whales and whaling. In *Trends in Ecology and Evolution* (Vol. 19, Issue 7, pp. 365–371).

Bardua C, Fabre A, Bon M, Das K, Stanley E, Blackburn D and Goswami A. (2020). Evolutionary integration of the frog cranium. *Evolution,* 74, 1200–1215

Bardua C, Fabre AC, Clavel J, Bon M, Das K, Stanley E, Blackburn D, Goswami A. (2021). Size, microhabitat, and loss of larval feeding drive cranial diversification in frogs. Nature Communications, in press.

Bardua C, Felice R, Watanabe A, Fabre A and Goswami A. (2019a). A Practical Guide to Sliding and Surface Semi landmarks in Morphometric Analyses, *Integrative Organismal Biology.* 1(1): 1-34

Bardua C, Wilkinson M, Gower D, Sherratt E, Goswami A (2019b). Morphological evolution and modularity of the caecilian skull. *BMC Evol. Biol.* 19(30):1-23.

Barker S, Cacho I, Benway H and Tachikawa K (2005). Planktonic foraminiferal Mg/Ca as a proxy for past oceanic temperatures: a methodological overview and data compilation for the Last Glacial Maximum. Quaternary Science Reviews, Multiproxy Approach for the Reconstruction of the Glacial Ocean surface 24, 821–834.

Barnes L and McLeod S. (1984). The fossil record and phyletic relationships of gray whales. In *The gray whale Eschrichtius robustus* (eds Jones ML, Swartz SJ, Leatherwood S.), pp. 3–32 New York, NY: Academic Press

Barnes L and Sanders A (1996). The transition from archaeocetes to mysticetes: Late Oligocene toothed mysticetes from near Charleston, South Carolina. In: *Sixth North American Paleontological Convention Abstracts of Papers*, J. E. Repetski, ed., p. 24, Paleontol. Soc., Washington, D.C., Special Publication No. 8.

Barnosky A (2001). Distinguishing the effects of the Red Queen and Court Jester on Miocene mammal evolution in the Northern Rocky Mountains. In *Journal of Vertebrate Paleontology*, 21(1).

Baumann-Pickering S, Simonis A and Wiggins S. (2013a) Aleutian Islands beaked whale echolocation signals. *Marine Mammal Science*, 29(1): 221–227

Baumann-Pickering S. (2013b) Baird's beaked whale echolocation signals. *The Journal of the Acoustical Society of America. Acoustical Society of America (ASA)*, 133(6): 4321–4331.

Beasley I, Robertson K and Arnold P. (2005) Description Of A New Dolphin, The Australian Snubfin Dolphin *Orcaella Heinsohni* Sp. N. (Cetacea, Delphinidae). *Marine Mammal Science*, 21(3): 365–400.

Behrenfeld, M., O'Malley, R., Siegel, D. et al. Climate-driven trends in contemporary ocean productivity. Nature 444, 752–755 (2006).

Bejder L, Samuels A, Whitehead H, Gales N, Mann J, Connor R, Heithaus M, Watson-Capps J, Flaherty C and Krutzen M (2006). Decline in relative abundance of bottlenose dolphins exposed to long-term disturbance. *Conservation Biology*, 20(6):1791–1798.

Bellard C, Bertelsmeier C, Leadley P, Thuiller W and Courchamp F. (2012). Impacts of climate change on the future of biodiversity. In *Ecology Letters* (Vol. 15, Issue 4, pp. 365–377).

Benites-Palomino A, Vélez-Juarbe J, Collareta A, Ochoa D, Altamirano A., Carré M, Laime, M, Urbina, M and Salas-Gismondi R. (2021). Nasal compartmentalization in Kogiidae (Cetacea, Physeteroidea): insights from a new late Miocene dwarf sperm whale from the Pisco Formation. *Papers in Palaeontology*, spp2.1351.

Benites-Palomino A, Vélez-Juarbe J, Salas-Gismondi R and Urbina M. (2019). Scaphokogia totajpe, sp. nov., a new bulky-faced pygmy sperm whale (Kogiidae) from the late Miocene of Peru. *Journal of Vertebrate Paleontology*, *39*(6).

Benites-Palomino A, Vélez-Juarbe J, Salas-Gismondi R and Urbina M. (2019). Scaphokogia totajpe, sp. nov., a new bulky-faced pygmy sperm whale (Kogiidae) from the late Miocene of Peru. *Journal of Vertebrate Paleontology*, *39*(6): 18

Benjamini Y and Hochberg Y (1995) Controlling the False Discovery Rate: A Practical and Powerful Approach to Multiple Testing. *Journal of the Royal Statistical Society: Series B (Methodological)*. Wiley. 1995;57(1):289–300.

Benjamini Y and Yekutieli D (2001) The control of the false discovery rate in multiple testing under dependency. *Annals of Statistics*, 29(4): 1165–1188.

Benoit J, Adnet S, Welcomme J and Fabre P. (2011) New skull of *Schizodelphis sulcatus* Gervais, 1861 (Mammalia, Odontoceti, Eurhinodelphinidae) from the Lower Miocene of Pignan (Hérault, France) and its implications for systematics of Eurhinodelphinidae. *Geobios*, 44(4): 323–334.

Benton M (2005). *Vertebrate Palaeontology* (3rd ed). Wiley-Blackwell, pp472.

Benton M (2009). The Red Queen and the Court Jester: Species diversity and the role of biotic and abiotic factors through time. In *Science* (Vol. 323, Issue 5915, pp. 728–732). American Association for the Advancement of Science.

Berger W (2007) Cenozoic cooling, Antarctic nutrient pump, and the evolution of whales. Deep-Sea Res. II Top. Stud. *Oceanogr.* 54,2399–2421.

Berta A (2018). Pinniped Evolution. In *Encyclopedia of Marine Mammals* (pp. 712–722).

Berta A and Lanzetti A (2020). Feeding in marine mammals: An integration of evolution and ecology through time. *Palaeontologia Electronica*, 23(2):40.

Berta A, Ekdale E and Cranford T (2014). Review of the cetacean nose: form, function, and evolution. *Anat Rec,* 297:2205–2215.

Berta A, Lanzetti A, Ekdale E and Deméré T (2016). From Teeth to Baleen and Raptorial to Bulk Filter Feeding in Mysticete Cetaceans: The Role of Paleontological,

Genetic, and Geochemical Data in Feeding Evolution and Ecology. *Integrative and Comparative Biology*, *56*(6), 1271–1284.

Berta A, Sumich J and Kovacs K (2005) Marine Mammals: Evolutionary Biology.

Best B, Fox C, Williams R, Halpin P and Paquet P (2015). 'WBI Studies Repository WBI Studies Repository 2015 Updated Marine Mammal Distribution and Abundance Estimates Updated Marine Mammal Distribution and Abundance Estimates in British Columbia in British Columbia'. Available at: https://www.wellbeingintlstudiesrepository.org/popdhab

Bianucci G (1996) The Odontoceti (Mammalia, cetacea) from Italian Pliocene. Systematics and Phylogenesis of Delphinidae. *Palaeontograpbia Ital*, 83: 73-167

Bianucci G (2020) Extensive Diversity and Disparity of the Early Miocene Platanistoids (Cetacea, Odontoceti) in the Southeastern Pacific (Chilcatay Formation, Peru). *Life*, 10(3), 27.

Bianucci G and Gingerich P (2011). *Aegyptocetus tarfa*, n. gen. et sp. (Mammalia, Cetacea), from the middle Eocene of Egypt: clinorhynchy, olfaction, and hearing in a protocetid whale View supplementary material Eocene of Egypt: clinorhynchy, olfaction, and hearing in a protocetid whale. *Journal of Vertebrate Paleontology*, *31*(6), 1173–1188.

Bianucci G, Collareta A, Bosio G, Landini W, Gariboldi K, Gioncada A, Lambert O, Malinverno E, de Muizon C, Varas-Malca R, Villa I, Coletti G, Urbina M and Di Celma C. (2018). Taphonomy and palaeoecology of the lower Miocene marine vertebrate assemblage of Ullujaya (Chilcatay Formation, East Pisco Basin, southern Peru). *Palaeogeography, Palaeoclimatology, Palaeoecology*, *511*, 256–279.

Bianucci G, Sarti G, Catanzariti R and Santini U (1998) Middle pliocene cetaceans from Monte Voltraio (Tuscany, Italy). Biostratigraphical, paleoecological and paleoclimatic observations', *Rivista Italiana di Paleontologia e Stratigrafia*, 104(1):123–130

Bindoff NL, Cheung WWL, Kairo JG, Arístegui J, Guinder VA et al., (2019): Changing Ocean, Marine Ecosystems, and Dependent Communities. In: IPCC Special Report on the Ocean and Cryosphere in a Changing Climate

Bisconti M (2012). Comparative osteology and phylogenetic relationships of *Miocaperea pulchra*, the first fossil pygmy right whale genus and species (Cetacea, Mysticeti, Neobalaenidae). *Zoological Journal of the Linnean Society*, *166*(4), 876–911.

Boessenecker R and Fordyce R (2015). Anatomy, feeding ecology, and ontogeny of a transitional baleen whale: a new genus and species of Eomysticetidae (Mammalia: Cetacea) from the Oligocene of New Zealand. *PeerJ* 3:1129

Boessenecker R and Fordyce R (2017). Cosmopolitanism and Miocene survival of Eomysticetidae (Cetacea: Mysticeti) revealed by new fossils from New Zealand. *New Zealand Journal of Geology and Geophysics*, *60*(2), 145–157.

Boessenecker R, Churchill M, Buchholtz E, Beatty B and Geisler J (2020). Convergent Evolution of Swimming Adaptations in Modern Whales Revealed by a

Large Macrophagous Dolphin from the Oligocene of South Carolina. *Current Biology*, *30*(16), 3267-3273.

Boessenecker R, Fraser D, Churchill M and Geisler J (2017) A toothless dwarf dolphin (Odontoceti: Xenorophidae) points to explosive feeding diversification of modern whales (Neoceti). *Proc. R. Soc. B*; 284: 20170531.

Bogomolni A, Pugliares K, Sharp S, Patchett K, Harry C, LaRocque J, Touhey K, Moore M (2010). Mortality trends of stranded marine mammals on Cape Cod and southeastern massachusetts, USA, 2000 to 2006. *Diseases of Aquatic Organisms*, 88(2):143–155.

Bon M, Bardua C, Goswami A and Fabre A (2020) Cranial integration in the fire salamander, *Salamandra salamandra* (Caudata: Salamandridae). *Biological Journal of the Linnean Society*, 130 (1):178-194.

Bond D and Grasby S (2017) On the causes of mass extinctions. Palaeogeogr. Palaeoclimatol. Palaeoecol., 478 (2017):3-29

Bonett RM, Phillips JG, Ledbetter NM, Martin SD, Lehman L. 2018 Rapid phenotypic evolution following shifts in life cycle complexity. Proc. R. Soc. B 285: 20172304.

Böning C, Dispert A, Visbeck M, Rintoul S and Schwarzkopf F (2008). The response of the Antarctic Circumpolar Current to recent climate change. *Nature Geoscience*, *1*(12), 864–869.

Bookstein F (1991) *Morphometric tools for landmark data: geometry and biology. Cambridge*. Cambridge University Press.

Bookstein F (1997). Landmark methods for forms without landmarks: localizing group differences in outline shape. *Medical Image Analysis* 1:225–243.

Boscolo-Galazzo F, Thomas E, Pagani M, Warren C, Luciani V and Giusberti L (2014). The middle Eocene climatic optimum (MECO): A multiproxy record of paleoceanographic changes in the southeast Atlantic (ODP Site 1263, Walvis Ridge). *Paleoceanography*, *29*(12): 1143–1161.

Bowen W and Lidgard D (2012) Marine mammal culling programs: Review of effects on predator and prey populations. *Mammal Rev.* 43:207–220.

Bown TM, Holroyd PA, Rose KD. 1994. Mammal extinctions, body size, and paleotemperature. Proc. Natl. Acad. Sci. USA 91:10403–6

Boyer D, Lipman Y, Clair E, Puente J, Patel B, Funkhouser T, Jernvall J and Daubechies I. (2011). Algorithms to automatically quantify the geometric similarity of anatomical surfaces. *Proceedings of the National Academy of Sciences USA* 108: 18221-1

Boyer D, Puente J, Gladman J, Glynn C, Mukherjee S, Yapuncich G and Daubechies I. (2015). A New Fully Automated Approach for Aligning and Comparing Shapes. *The Anatomical Record*, *298*(1):249–276.fisher

Braham H (1984). The status of endangered whales: An overview. *Marine Fisheries Review*, 46:2-6.

Brower, AA, Clarke, JT and Ferguson, MC. (2018). Increased sightings of subarctic cetaceans in the eastern Chukchi Sea, 2008-2016: population recovery, response to climate change, or increased survey effort? Polar Biology, 1, 3.

Buchholtz E (1998). Implications of Vertebral Morphology for Locomotor Evolution in Early Cetacea. In *The Emergence of Whales*: 325–351.

Buchholtz E (2001). Vertebral osteology and swimming style in living and fossil whales (Order: Cetacea). In *Journal of Zoology* 253(2):175–190.

Buchholtz E (2007). Modular evolution of the Cetacean vertebral column. *Evolution & Development*, *9*(3):278–289.

Burek K, Gulland F, and O'Hara T (2008). Effects of climate change on Arctic marine mammal health. *Ecological Applications,* 18:126–134.

Busbey A (1995) *The structural consequences of skull flattening in crocodilians*, pp. 173 – 192. Cambridge, UK: Cambridge University Press.

Butchart S, Walpole M, Collen B, Van Strien A, Scharlemann J, Almond R (2010) Global biodiversity: indicators of recent declines. *Science*, 328(5982):1164–1168.

Cade D, Friedlaender A, Calambokidis J and Goldbogen J (2016) Kinematic diversity in rorqual whale feeding mechanisms. *Curr. Biol.* 26, 2617–2624

Caetano D and Harmon L. (2017). Ratematrix: an R package for studying evolutionary integration among several traits on phylogenetic trees. *Methods Ecol. Evol.*

Cardini A and Polly D (2013). Larger mammals have longer faces because of size-related constraints on skull form. *Nature Communications*, *4*(1):1–7.

Cardini A, Felizola Diniz Filho J, Polly D, Elton S (201) Biogeographic analysis using geometric morphometrics: Clines in skull size and shape in a widespread African arboreal monkey, in *Lecture Notes in Earth Sciences*:191–217.

Cardini A. (2014) Missing the third dimension in geometric morphometrics: How to assess if 2D images really are a good proxy for 3D structures? *Hystrix* 25:73–81.

Cartwright R, Venema A, Hernandez V, Wyels C, Cesere J, Cesere D. (2019) Fluctuating reproductive rates in Hawaii's humpback whales, *Megaptera novaeangliae*, reflect recent climate anomalies in the North Pacific. *R. Soc. open sci.* 6:181463.

Cassens I, Vicario S, Waddell V, Balchowsky H, Van Belle D, Ding W, Fan Cm Mohan R, Simoes-Lopes P, Bastida R, Meyer A, Stanhope M, Millinkovitch M (2000) Independent adaptation to riverine habitats allowed survival of ancient cetacean lineages. *Proc. Natl Acad. Sci. USA* 97, 11343– 11 347.

Cermeño, P., Benton, M.J., Paz, Ó. *et al.* (2017) Trophic and tectonic limits to the global increase of marine invertebrate diversity. *Sci Rep* **7,** 15969 (2017).

Cetacean Stranding Investigation Programme (CSIP) (2019) 'UK Cetacean Strandings Investigation Programme' Available at: www.ukstrandings.org

Chami R, Cosimano T, Fullenkamp C, and Oztosun S. (2019). 'Nature's Solution to climate change. A strategy to protect whales can limit greenhouse gases and global warming'.

Chen R, Sharma S, Bank T, Soeder D and Eastman H. (2015). Comparison of isotopic and geochemical characteristics of sediments from a gas- and liquids-prone wells in Marcellus Shale from Appalachian Basin, West Virginia. *Applied Geochemistry*, *60*, 59–71.

Churchill M, Geisler J, Beatty B and Goswami A. Evolution of cranial telescoping in echolocating whales (Cetacea: Odontoceti), Evolution. *Society for the Study of Evolution.* 2018; 72(5), 1092–1108.

Churchill M, Martínez-Cáceres M, de Muizon C, Mnieckowski J and Geisler J. The Origin of High-Frequency Hearing in Whales. *Current Biology. Cell Press.* 2016; 26(16), 2144–2149.

Clark C (1990) Acoustic Behavior of Mysticete Whales, in *Sensory Abilities of Cetaceans.* Springer US:571–583.

Clavel J and Morlon H. (2017). Accelerated body size evolution during cold climatic periods in the Cenozoic. *Proceedings of the National Academy of Sciences of the United States of America*, *114*(16), 4183–4188.

Clavel J and Morlon H. (2020). Reliable Phylogenetic Regressions for Multivariate Comparative Data: Illustration with the MANOVA and Application to the Effect of Diet on Mandible Morphology in Phyllostomid Bats. *Systematic Biology*, *69*(5), 927–943.

Clavel J, Aristide L, Morlon H. (2019). A penalized likelihood framework for high-dimensional phylogenetic comparative methods and an application to new-world monkeys brain evolution. *Syst Biol* 68:93–116.

Clavel J, Escarguel G and Merceron G (2015) mvMORPH: An R package for fitting multivariate evolutionary models to morphometric data. *Methods in Ecology and Evolution.* Edited by Poisot T. 6(11): 1311–1319.

Clementz M, Goswami A, Gingerich P and Koch P (2006). Isotopic records from early whales and sea cows: contrasting patterns of ecological transition. *Journal of Vertebrate Paleontology*, *26*(2), 355–370.

Close RA, Friedman M, Lloyd GT, Benson RBJ (2015). Evidence for a Mid-Jurassic adaptive radiation in mammals. Curr. Biol., 25, pp. 1-6

Collareta A, Lambert O, de Muizon C, Urbina M and Bianucci G. (2017). *Koristocetus pescei* gen. et sp. nov., a diminutive sperm whale (Cetacea: Odontoceti: Kogiidae) from the late Miocene of Peru. *Fossil Record, 20*, 259–278.

Collins M, Knutti R, Arblaster J, Dufresne J-L, Fichefet T et al., (2013): Long-term Climate Change: Projections, Commitments and Irreversibility. In: Climate Change 2013: The Physical Science Basis. Contribution of Working Group I to the Fifth Assessment Report of the Intergovernmental Panel on Climate Change [Stocker, T.F., D. Qin, G.-K. Plattner, M. Tignor, S.K. Allen, J. Boschung, A. Nauels, Y. Xia, V. Bex and P.M. Midgley (eds.)]. Cambridge University. Press, Cambridge, United Kingdom and New York, NY, USA.

Collyer M, Sekora D and Adams D. (2015). A method for analysis of phenotypic change for phenotypes described by high-dimensional data. *Heredity*. 115:357–365.

Colwell R, Mao C, Chang J. (2004). Interpolating, Extrapolating, and Comparing Incidence-Based Species Accumulation Curves. *Ecology* 85, 2717–2727.

Common Fisheries Policy (CFP) (n.d) 'Fisheries'. Available at: https://ec.europa.eu/fisheries/cfp_en

Connor D, Gilliand P, Golding N, and Robinson P. (2006). 'UKSeaMap: the mapping of seabed and water column features of UK seas' Available at: http://www.jncc.gov.uk/page-3918

Coombs E, Clavel J, Park T, Churchill M and Goswami A (2020) Wonky whales: The evolution of cranial asymmetry in cetaceans. BMC Biology, 18(86: 1-24

Coombs E, Clavel J, Park T, Churchill M and Goswami A (2020b). Github release for publication: https://github.com/EllenJCoombs/Asymmetry-evolution-cetaceans. DOI: 10.5281/zenodo.3893943

Coombs E, Deaville R, Sabin R, (2019). GitHub: ellenjcoombs/cetacean-stranding-project: release for publication. DOI: 10.5281/zenodo.2613807

Coombs E, Deaville R, Sabin R, Allan L, O'Connell M, Berrow S, Smith B, Brownlow A, Doeschate M, Penrose R, Williams R, Perkins M, Jepson P and Cooper N. (2019). What can cetacean stranding records tell us? A study of UK and Irish cetacean diversity over the past 100 years. *Marine Mammal Science* 35:1527-1555.

Cooney C, Bright J, Capp A, Chira A, Hughes E, Moody C, Nouri L, Varley Z, and Thomas G (2017). Mega-evolutionary dynamics of the adaptive radiation of birds. *Nature*. 542:344–347.

Craigie I, Baillie J, Balmford A, Carbone C, Collen B, Green R and Hutton J (2010). Large mammal population declines in Africa's protected areas. *Biological Conservation*, *143*(9), 2221–2228.

Cramer B, Miller K, Barrett P and Wright J (2011). Late Cretaceous-Neogene trends in deep ocean temperature and continental ice volume: Reconciling records of benthic foraminiferal geochemistry (d 18 O and Mg/Ca) with sea level history. *J. Geophys. Res*, *116*, 12023.

Cramer B, Toggweiler J, Wright J, Katz M, and Miller K (2009), Ocean overturning since the Late Cretaceous: Inferences from a new benthic foraminiferal isotope compilation, *Paleoceanography*, 24, PA4216.

Cranford T and Amundin M. (2004) Biosonar pulse production in Odontocetes: The state of our knowledge. In *Echolocation in Bats and Dolphins* (ed. J. Thomas, C. F. Moss and M. Vater). Chicago: University of Chigaco Press: 27-35.

Cranford T, Amundin M and Norris K (1996). Functional morphology and homology in the odontocete nasal complex: Implications for sound generation. *Journal of Morphology:*228(3): 223–285.

Creative Commons (2020). 'Attribution-ShareAlike 3.0 Unported (CC BY-SA 3.0)'. Available at: https://creativecommons.org/licenses/by-sa/3.0/* [March 2020].

Dalebout M, Bake S, Steel D, Thompson K, Robertson K, Chivers S, Perrin W, Goonatilake M (2014). Resurrection of *Mesoplodon hotaula* (*Deraniyagala*) 1963: A new species of beaked whale in the tropical Indo-Pacific, *Marine Mammal Science*; 30(3):1081–1108.

Dalla-Rosa L, Ford J and Trites A (2012). Distribution and relative abundance of humpback whales in relation to environmental variables in coastal British Columbia and adjacent waters. *Continental Shelf Research*, *36*, 89–104.

Darwin C (1859). *The Origin of Species.* London, John Murray.

Darwin C (1868) *The variation of animals and plants under domestication.* London: John Murray (1st edn), second issue. Volume 1.

Davidson A, Boyer A, Kim H, Pompa-Mansilla S, Hamilton M, Costa D, Ceballos G, Brown J (2012) Drivers and hotspots of extinction risk in marine mammals. *Proc Natl Acad Sci USA* 109: 3395–3400.

Davis R (2019). Marine mammals: Adaptations for an aquatic life. Berlin: Springer-Verlag.

De Muizon C (1993). *Odobenocetops peruvianus*, una remarcable convergencia de adaptación alimentaria. *Bulletin de l'Institut Français d'Études Andines* 22: 671–683.

De Muizon C and Domning D. (2002). The anatomy of *Odobenocetops* (Delphinoidea, Mammalia), the walrus-like dolphin from the Pliocene of Peru and its palaeobiological implications. *Zoological Journal of the Linnean Society*, *134*(4), 423–452.

Deaville R and Jepson P (compilers) (2011). 'UK Cetacean Strandings Investigation Programme Final report for the period 1st January 2005-31st December 2010'.

Deaville R, Jepson P and Perkins M (2015). 'Cetacean Stranding Investigation Programme Annual Report for the period 1st January – 31st December 2015'.

Delsuc F, Brinkmann F, and Philippe H (2005). Phylogenomics and the reconstruction of the tree of life. *Nat. Rev. Genet.* 6:361–375.

Demeré T (1986) The Fossil Whale, Balaenoptera Davidsonii (Cope 1872), With A Review Of Other Neogene Species Of Balaenoptera (Cetacea: Mysticeti), *Marine Mammal Science.* 2(4):277–298.

Deméré T and Berta A. (2008). 'Skull anatomy of the Oligocene toothed mysticete *Aetioceus weltoni* (Mammalia; Cetacea): implications for mysticete evolution and functional anatomy'.

Deméré T, McGowen M, Berta A and Gatesy J (2008). Morphological and Molecular Evidence for a Stepwise Evolutionary Transition from Teeth to Baleen in Mysticete Whales. *Systematic Biology*, 57(1), 15–37.

Deppeler SL and Davidson AT, 2017, Southern Ocean phytoplankton in a changing Dickson B and Pierce S (2019). Functional performance of turtle humerus shape across an ecological adaptive landscape. *Evolution*, 73(6): 1265–1277.

Dobson F (1985). The Use of Phylogeny in Behavior and Ecology. *Evolution, 39*(6), 1384-1388.

Dolman S, Pinn E, Reid R, Barley J, Deaville R, Jepson P, O'Connell M, Berrow S, Penrose R, Tevick P, Calderan S, Robinson K, Brownell R and Simmonds M (2010). A note on the unprecedented strandings of 56 deep-diving whales along the UK and Irish coast. *Marine Biodiversity Records*, 3:16.

Drake A and Klingenberg C (2010). Large-scale diversification of skull shape in domestic dogs: disparity and modularity. *Am. Nat.* 175 (3):289-301

Drexler M and Ainsworth C (2013). Generalized Additive Models Used to Predict Species Abundance in the Gulf of Mexico: An Ecosystem Modeling Tool. *PLoS ONE*, *8*(5), e64458.

Dunn O (1961) Multiple Comparisons among Means, *Journal of the American Statistical Association*, 56:293, 52-64

Earth and Planetary Science Letters, 235 (2005), pp. 715-728

Eastman J, Alfaro M, Joyce P, Hipp A and Harmon L (2011). A Novel Comparative Method For Identifying Shifts In The Rate Of Character Evolution On Trees. *Evolution*;65: 3578-3589.

Eddy T, Bernhardt J, Blanchard J, Cheung W., Colléter M, du Pontavice H, Fulton E, Gascuel D, Kearney K, Petrik C, Roy T, Rykaczewski R, Selden R, Stock C, Wabnitz, C and Watson R (2021). Energy Flow Through Marine Ecosystems: Confronting Transfer European Efficiency. In *Trends in Ecology and Evolution*, 36(1):76–86.

Ekdale E (2016) Morphological variation among the inner ears of extinct and extant baleen whales (Cetacea: Mysticeti), *Journal of Morphology*, 277(12):1599–1615.

El Adli J, Deméré T and Boessenecker R (2014). *Herpetocetus morrowi* (Cetacea: Mysticeti), a new species of diminutive baleen whale from the Upper Pliocene (Piacenzian) of California, USA, with observations on the evolution and relationships of the Cetotheriidae. *Zoological Journal of the Linnean Society* 170:400-466.

Ellis R and Mead J (2017). *Beaked Whales: A Complete Guide to Their Biology and Conservation*. Johns Hopkins University Press.

Erwin D (2009) Climate as a driver of evolutionary change. *Curr Biol* 19:575–583.

Estes J, Tinker M, Williams T and Doak D (1998). Killer whale predation on sea otters linking oceanic and nearshore ecosystems. *Science* 282, 473–476.

Evans K. Thresher R, Warneke R, Bradshaw C, Pook M, Thiele D and Hindell M (2005). Periodic variability in cetacean strandings: links to large-scale climate events. *Biology Letters*, 1:147–150.

Evans P (1980). Cetaceans in British waters. *Mammal Review*, 10:1–52.

Evans P (1990). European cetaceans and seabirds in an oceanographic context. *Lutra*, 33:95–125.

Evans P and Hammond P (2004). Monitoring cetaceans in European waters. *Mammal Review,* 34:131–156.

Fabre A, Bardua C, Bon M, Clavel J, Felice R, Streicher J, Bonnel J, Stanley E, Blackburn D and Goswami A. (2020). Metamorphosis shapes cranial diversity and rate of evolution in salamanders. *Nature Ecology and Evolution*, *4*(8), 1129–1140.

Fabre A, Goswami A., Peigné S and Cornette, R. (2014). Morphological integration in the forelimb of musteloid carnivorans. *Journal of Anatomy*, *225*(1), 19–30.

Fahlke J and Hampe O. (2015) Cranial symmetry in baleen whales (Cetacea, Mysticeti) and the occurrence of cranial asymmetry throughout cetacean evolution. *Science of Nature.* Springer Verlag; 102(9).

Fahlke J, Bastl K, Semprebon G and Gingerich P (2013). Paleoecology of archaeocete whales throughout the Eocene: Dietary adaptations revealed by microwear analysis. *Palaeogeography, Palaeoclimatology, Palaeoecology*, *386*, 690–701.

Fahlke J, Gingerich P, Welsh R and Wood A (2011) Cranial asymmetry in Eocene archaeocete whales and the evolution of directional hearing in water', *Proceedings of the National Academy of Sciences of the United States of America,* 108(35): 14545–14548.

Felice R (2020). hot.dots: Calculate per-landmark rates and plot them. R package version 0.0.0.9000. Available at: https://github.com/rnfelice/hot.dots

Felice R (2021) Macroevo plots in R. Available at: https://github.com/rnfelice/macroevo.plots/tree/master/R

Felice R and Goswami A (2018). Developmental origins of mosaic evolution in the avian cranium. *Proc Natl Acad Sci USA* 115:555–60.

Felice R and Goswami A, (2018) Developmental origins of mosaic evolution in the avian cranium. Proc. Natl. Acad. Sci. U.S.A. 115, 555–560

Felice R, Tobias J, Pigot A, Goswami A (2019) Dietary niche and the evolution of cranial morphology in birds. *Proc. R. Soc.* B 286, 20182677.

Felice R, Watanabe A, Cuff A, Hanson M, Bhullar B, Rayfield E, et al. (2020), Decelerated dinosaur skull evolution with the origin of birds. *PLoS Biology*, 18 Article e3000801

Felsenstein J (1985). Phylogenies and the comparative method. *The American Naturalist.* 125: pp. 1–15.

Ferguson-Gow H (2020). BTprocessR: A set of tools to help with the interpretation and analysis of the output of BayesTraits MCMC analyses.

Figueirido B, Janis C, Pérez-Claros J, De Renzi M, Palmqvist P (2012) Cenozoic climate change influences mammalian evolutionary dynamics. *Proc Natl Acad Sci USA* 109(3):722–727

Finarelli J and Goswami A (2013). Potential pitfalls of reconstructing deep time evolutionary history with only extant data, a case study using the canidae (mammalia, carnivora). *Evolution*, *67*(12), 3678–3685.

Fitzgerald E (2006) A bizarre new toothed mysticete (Cetacea) from Australia and the early evolution of baleen whales. *Proceedings of the Royal Society B: Biological Sciences. Royal Society*; 273(1604): 2955–2963.

Fitzgerald E (2010). The morphology and systematics of *Mammalodon colliveri* (Cetacea: Mysticeti), a toothed mysticete from the Oligocene of Australia, *Zoological Journal of the Linnean Society*, *158*, 367–476.

Flower B and Kennett J. (1994). The middle Miocene climatic transition: East Antarctic ice sheet development, deep ocean circulation and global carbon cycling. *Palaeogeography, Palaeoclimatology, Palaeoecology*, *108*(3–4), 537–555.

Flower W (1883). On whales, past and present, and their probable origin. *Nature* 28:199–202; 226–230.

Foote A, Kaschner K, Schultze S. et al., (2013) Ancient DNA reveals that bowhead whale lineages survived Late Pleistocene climate change and habitat shifts. Nat Commun 4, 1677 (2013).

Foote, M (1999) Paleontological Society morphological diversity in the evolutionary radiation of Paleozoic and post-Paleozoic crinoids. *Palaeobiology* **25**, 1–115.

Fordyce R (1980) Whale evolution and Oligocene Southern Ocean environments. *Palaeogeography, Palaeoclimatology, Palaeoecology*; 31:319–336.

Fordyce R (2002) *Simocetus rayi* (Odontoceti: Simocetidae) (new species, new genus, new family), a bizarre new archaic Oligocene dolphin from the eastern North Pacific. Smithson. *Contrib, Paleobiol*, 93:185-222)

Fordyce R (2018). Cetacean Evolution. In *Encyclopedia of Marine Mammals* (pp. 180–185).

Fordyce R and Barnes L. (1994) The Evolutionary History of Whales and Dolphins. *Annu. Rev. Earth Planet. Sci*; 22, 419–455.

Fordyce R and de Muizon C (2001) Evolutionary history of cetaceans: a review, in *Secondary adaptation of tetrapods to life in water*;169–233.

Fordyce R and Marx F (2013). The pygmy right whale *Caperea marginata*: The last of the cetotheres. *Proceedings of the Royal Society B: Biological Sciences*, *280*(1753).

Fordyce R and Marx F (2018). Gigantism Precedes Filter Feeding in Baleen Whale Evolution. *Current Biology*, *28*(10), 1670-1676.e2.

Fordyce, R & de Muizon C. (2001). Evolutionary history of cetaceans: A review.

Freckleton R (2012) Fast likelihood calculations for comparative analyses. *Methods in Ecology and Evolution,* 3:940–947.

Friedlaender A, Halpin P, Qian S (2006). Whale distribution in relation to prey abundance and oceanographic processes in shelf waters of the Western Antarctic Peninsula. *Marine Ecology Progress Series*, 317:297–310.

Fritz S, Schnitzler J, Eronen J, Hof C, Böhning-Gaese K., Graham, C (2013). Diversity in time and space: wanted dead and alive. *Trends in Ecology & Evolution* 28:509–516.

Galatius A (2006). Taxonomy of dolphins Delphinus and Tursiops spp. View project Marine mammal management in light of eco-tourism View project Bilateral Directional Asymmetry of the Appendicular Skeleton of the White-Beaked Dolphin (*Lagenorhynchus albirostris*).

Galatius A and Goodall R (2016). Skull shapes of the Lissodelphininae: radiation, adaptation and asymmetry. *J. Morphol*, 277:776–785.

Galatius A, Olsen M, Steeman M, Racicot R (2019) Raising your voice: Evolution of narrow-band high-frequency signals in toothed whales (Odontoceti). *Biological Journal of the Linnean Society. Oxford Academic*. 126(2): 213–224

Galatius A, Racicot R, McGowen M, Olsen M (2020). Evolution and diversification of delphinid skull shapes. *iScience23*: 101543.

Galatius A. and Jespersen Å (2005). Bilateral Directional Asymmetry Of The Appendicular Skeleton Of The Harbor Porpoise (*Phocoena Phocoena*). Marine Mammal Science, 21(3), 401–410.

Gatesy J (1998). Molecular evidence for the phylogenetic affinities of Cetacea; pp. 63–112 in J. G. M. Thewissen (ed.), *The Emergence of Whales*. Plenum Press, New York.

Gatesy J, Geisler J, Chang J, Buell C, Berta A, Meredith R, Springer M, McGowen M (). A phylogenetic blueprint for a modern whale. Molecular Phylogenetics and Evolution, 66(2): 479-506)

Gebert F, Steffan-Dewenter I, Moretto P and Peters M (2020). Climate rather than dung resources predict dung beetle abundance and diversity along elevational and land use gradients on Mt. Kilimanjaro. *Journal of Biogeography, 47*: 371–381.

Geisler J (2017). Evolution: Hearing and Feeding in Fossil Whales. In *Current Biology*, 27(12):596–598)

Geisler J, Boessenecker R, Brown M and Beatty B (2017). The Origin of Filter Feeding in Whales. *Current Biology, 27*(13), 2036-2042.

Geisler J, Colbert M and Carew J (2014) A new fossil species supports an early origin for toothed whale echolocation. *Nature. Nature Publishing Group*, 508(7496), 383–386.

Gelman A (2006). Prior distributions for variance parameters in hierarchical models (Comment on Article by Browne and Draper). *Bayesian Analysis,* 515–534.

Gelman A and Rubin D (1992). Inference from iterative simulation using multiple sequences', Statistical Science. *Institute of Mathematical Statistics,* 7(4): 457–472.

Gingerich P (1994). The whales of Tethys. *Nat Hist* 94:6–88.

Gingerich P and Cappetta H. (2014). A new archaeocete and other marine mammals (Cetacea and Sirenia) from lower middle Eocene phosphate deposits of Togo. *Journal of Paleontology, 88*(1), 109–129.

Gingerich P, Haq Mu N, Zalmout I, Khan I and Malkani M (2001). Origin of whales from early artiodactyls: hands and feet of Eocene Protocetidae from Pakistan. *Science,* 293(5538), 2239–2242.

Goldbogen J and Madsen P (2018). The evolution of foraging capacity and gigantism in cetaceans. *Journal of Experimental Biology*, 221:166033.

Goldbogen J, Cade D, Calambokidis J, Friedlaender A, Potvin J, Segre P and Werth A. (2017). How Baleen Whales Feed: The Biomechanics of Engulfment and Filtration. *Annual Review of Marine Science*, 9(1), 367–386.

Goldbogen J, Potvin J and Shadwick R (2010). Skull and buccal cavity allometry increase mass-specific engulfment capacity in fin whales. *Proceedings of the Royal Society B: Biological Sciences*, 277(1683), 861–868.

Goldbogen J, Pyenson N, Shadwick R (2007). Big gulps require high drag for fin whale lunge feeding. *Marine Ecology Progress Series:* 349: 289-301.

Gonzalez P, Barbeito-Andrés J, D'Addona L, Bernal V, and Perez S (2016). Technical note: performance of semi and fully automated approaches for registration of 3D surface coordinates in geometric morphometric studies. *Am. J. Phys. Anthropol.* 160:169–178.

Goolsby E (2016). Likelihood-based parameter estimation for high-dimensional phylogenetic comparative models: overcoming the limitations of "distance-based" methods. *Syst. Biol.* 65: 852–870.

Goswami A (2007) Cranial modularity and sequence heterochrony in mammals. *Evol. Dev.*9: 290 –298.

Goswami A, Binder W, Meachen J, O'Keefe F (2015). The fossil record of phenotypic integration and modularity: A deep-time perspective on developmental and evolutionary dynamics. *Proceedings of the National Academy of Sciences of the United States of America. National Academy of Sciences*;112(16):4891–4896.

Goswami A, Mannion P, Benton M (2016). Radiation and extinction: investigating clade dynamics in deep time. *Biol. J. Linn. Soc.* 118, 6–12.

Goswami A, Watanabe R, Felice C, Bardua A, Fabre C, and Polly P (2019). High-Density Morphometric Analysis of Shape and Integration: The Good, the Bad, and the Not-Really-a-Problem. *Integrative and Comparative Biology* 59:669–683.

Goswami A., Polly P, Mock O, and Sánchez-Villagra M. (2012). Shape, variance and integration during craniogenesis: contrasting marsupial and placental mammals, *Journal of Evolutionary Biology,* 25(5):1-11

Gould SJ., and Calloway CB. 1980. Clams and brachiopods-ships that pass in the night. Paleobiology 6(4):383-396.

Gu B, Alexander V and Schell D (1999). Seasonal and interannual variability of plankton carbon isotope ratios in a subarctic lake. *Freshwater Biology*, *42*(3), 417–426.

Guillerme T (2018). DispRity: A modular R package for measuring disparity. *Methods in Ecology and Evolution*, 9(7), 1755-1763.

Guillerme T, Cooper N (2016). Effects of missing data on topological inference using a Total Evidence approach. *Molecular Phylogenetics and Evolution* 94, Part A, 146–158.

Guillerme, T and Weisbecker V (2019) landvR: Tools for measuring landmark position variation. Zenodo.

Guisan A, Edwards T, and Hastie T (2002). Generalized linear and generalized additive models in studies of species distributions: setting the scene. *Ecological Modelling*, 157: 89–100.

Guisan A, Edwards T, Hastie T (2002) Generalized linear and generalized additive models in studies of species distributions: setting the scene. *Ecol Modell* 157: 89–100

Gulland F (2006). Review of the Marine Mammal Unusual Mortality Event Response Program of the National Marine Fisheries Service. NOAA Tech. Memo. NMFS-OPR-33. 37

Gulland F, Danil K, Bolton J, Ylitalo G, Okrucky R, Rebolledo F, Alexander-Beloch C, Brownell R, Mesnick S, Lefebvre K, Smith C, Thomas P and Rojas-Bracho L (2020). Vaquitas (Phocoena sinus) continue to die from bycatch not pollutants. *Veterinary Record*, *187*(7), 51.

Gunz P and Mitteroecker P (2013) Semilandmarks: A method for quantifying curves and surfaces. *Hystrix*, 24(1) 103-9

Gunz P, Mitteroecker P, and Bookstein F (2005). Chapter three: semilandmarks in three dimensions. Pp. 73–98 in D. E. Slice, ed. *Modern Morphometrics in Physical Anthropology*. Kluwer Academic/Plenum, New York.

Gunz P, Mitteroecker P, Neubauer S, Weber G (2009) Principles for the virtual reconstruction of hominin crania. *Journal of Human Evolution. Academic Press.* 57(1):48–62.

Halpin P, Read A and Fujioka E (2009). OBIS-SEAMAP: The world data center for marine mammal, sea bird, and sea turtle distributions. *Oceanography*, 22:104-115.

Hammond P, MacLeod K, Berggren P (2013). Cetacean abundance and distribution in European Atlantic shelf waters to inform conservation and management. *Biological Conservation,* 164:107–122.

Hampe O and Baszio S (2010). Relative warps meet cladistics: A contribution to the phylogenetic relationships of baleen whales based on landmark analyses of mysticete crania. *Bulletin of Geosciences*, *85*(2),199–218.

Harmon L, Weir J, Brock C and Glor R (2008). GEIGER: investigating evolutionary radiations. *Bioinformatics*, 24(1):129–131.

Harris C, Thomas L, Falcone E (2018). Marine mammals and sonar: Dose-response studies, the risk-disturbance hypothesis and the role of exposure context. *Journal of Applied Ecology,* 55(1):396–404.

Harvell C, Mitchell C, Ward J, Altizer S, Dobson A, Ostfeld R and Samuel M (2002) Climate warming and disease risks for terrestrial and marine biota. *Science* 296, 2159–2162

Harvey P and Pagel M (1991). The *Comparative Method in Evolutionary Biology*. 835 vol. 239. Oxford University Press, Oxford.

Hassold N, Rea D, Van der Pluijm B, and Parés J (2009), A physical record of the Antarctic Circumpolar Current: Late Miocene to recent slowing of abyssal circulation, *Palaeogeogr. Palaeoclimatol. Palaeoecol.,* 275, 28–36

Hedrick BP, Manning PL, Lynch ER, Cordero SA, Dodson P. 2015. The geometry of taking flight: Limb morphometrics in Cretaceous theropods. Journal of Morphology 276: 152–166.

Hernández Cisneros A and Velez-Juarbe J. (2021). Palaeobiogeography of the North Pacific toothed mysticetes (Cetacea, Aetiocetidae): a key to Oligocene cetacean distributional patterns. *Palaeontology*, *64*(1), 51–61.

Heyning J (1989) Comparative facial anatomy of beaked whales (Ziphiidae) and a systematic revision among the families of extant Odontoceti. *Contributions in Science,* Natural History Museum of Los Angeles County, 405: 1–64

Heyning J and Mead J (1990) Evolution of the Nasal Anatomy of Cetaceans, in *Sensory Abilities of Cetaceans*. Springer US, 67–79.

Hill D, Haywood A, Valdes P, Francis J, Lunt D, Wade B, Bowman V (2013) Paleogeographic controls on the onset of the Antarctic circumpolar current. *Geophys. Res. Lett.* 40, 5199–5294

Hocking D, Marx F, Park T, Fitzgerald E and Evans A (2017b). Reply to comment by Kienle (2017b). *Proceedings of the Royal Society B: Biological Sciences.* 284(1863):1836.

Hocking D, Marx F, Park T, Fitzgerald, E and Evans A (2017a). A behavioural framework for the evolution of feeding in predatory aquatic mammals. *Proceedings of the Royal Society B: Biological Sciences*. 284(1850), p.20162750.

Holbourn A, Kuhnt W, Schulz M, Flores J and Andersen N. (2007). Orbitally-paced climate evolution during the middle Miocene "Monterey" carbon-isotope excursion. *Earth and Planetary Science Letters*, *261*(3–4), 534–550.

Holm P. (2016). World War II and the "Great Acceleration" of North Atlantic Fisheries. *Global Environment*, *5*(10), 66–91.

Howell A (1925). Asymmetry in the skulls of mammals. *Proceedings of the United States National Museum*. 67(2599):1–18.

Huggenberger S, Leidenberger S and Oelschläger HHA. Asymmetry of the nasofacial skull in toothed whales (Odontoceti). Journal of Zoology. 2017; 302(1): 15–23.

Huggenberger S, Vogl TJ and Oelschlager HHA. 2010. Epicranial complex of the La Plata dolphin (Pontoporia blainvillei): Topographical and functional implications. Marine Mammal Science 26:471–481.

Hunt K, Moore M, Rolland R, Kellar N, Hall A, Kershaw J, Raverty S, Davis C, Yeates L, Fauquier D, Rowles T and Kraus S (2013). Overcoming the challenges of studying conservation physiology in large whales: a review of available methods. *Conservation Physiology*, *1*(1)

Hurrell J (1995). Decadal Trends in the North Atlantic Oscillation: Regional Temperatures and Precipitation. *Science*, 269:676–679.

Inglis GN, Farnsworth A, Lunt D, Foster GL, Hollis CJ et al. (2015). Descent toward the Icehouse: Eocene sea surface cooling inferred from GDGT distributions. Paleoceanography 30, 2014PA002723.

Ingram T, Harmon L and Shurin J (2012). When should we expect early bursts of trait evolution in comparative data? Predictions from an evolutionary food web model. *J. Evol. Biol.*, 25, 1902–1910.

IPPC (2007) Summary for Policymakers. In*: Climate Change 2007: The Physical Science Basis. Contribution of Working Group I to the Fourth Assessment Report of the Intergovernmental Panel on Climate Change*. Solomon S., Qin D.M., Manning Z., Chen M., Marquis K.B., Avery T., Tignor M., and Miller H.L. (eds.) Cambridge University Press, Cambridge, United Kingdom and New York, NY, USA.

Irish Whale and Dolphin Group (IWDG) (2019). 'IWDG' Available at: http://www.iwdg.ie/

Irschick D, Carlisle E, Elstrott J, Ramos M, Buckley C., Vanhooydonck B, Meyers J and Herrel A. (2005). A comparison of habitat use, morphology, clinging performance and escape behaviour among two divergent green anole lizard (Anolis carolinensis) populations. *Biological Journal of the Linnean Society*, *85*(2), 223–234.

IUCN SSC (2018). 'IUCN' Available at: http://www.iucn-csg.org/

Jakobsen L, Ratcliffe J, and Surlykke A (2013) Convergent acoustic field of view in echolocating bats. *Nature*: 493.

Jefferson T and Rosenbaum H (2014) Taxonomic revision of the humpback dolphins (Sousa spp.), and description of a new species from Australia', *Marine Mammal Science*, 30(4):1494–1541.

Jefferson T and Wang J (2011) Revision of the taxonomy of finless porpoises (genus Neophocaena): The existence of two species. *Journal of Marine Animals and Their Ecology*. 4(1):3–16.

Jefferson T, Webber M and Pitman R (2011). Marine Mammals of the World: A Comprehensive Guide to Their Identification. Academic Press.

Jensen C (1999). *A Critical Review of the Common Fisheries Policy 1.*

Jensen F, Johnson M, Ladegaard M, Wisniewska D and Madsen P (2018). Narrow acoustic field of view drives frequency scaling in toothed whale biosonar. *Current Biology*, 28(23): 3878-3885.

Jensen F, Rocco A, Mansur R, Smith B, Janik V and Madsen P (2013). Clicking in shallow rivers: short-range echolocation of Irrawaddy and Ganges River dolphins in a shallow, acoustically complex habitat. *PLoS ONE*. 8(4), e59284.

Jepson P (2005). Cetacean Strandings Investigation and Co-ordination in the UK. Final report to the Department for Environment, Food and Rural Affairs.

Jepson P, Arbelo M, Deaville R (2003). Gas-bubble lesions in stranded cetaceans. *Nature,* 425(6958):575–576.

Jepson P, Deaville R, and Acevedo-Whitehouse K (2013) What Caused the UK's Largest Common Dolphin (*Delphinus delphis*) Mass Stranding Event? *PLoS ONE 8*(4): e60953.

Jepson P, Deaville R, and Barber J (2016). PCB pollution continues to impact populations of orcas and other dolphins in European waters. *Scientific Reports,* 6:18573.

Johnson M, Hickmott L, Aguilar Soto N and Madsen P (2008) Echolocation behaviour adapted to prey in foraging Blainville's beaked whale (*Mesoplodon densirostris*). *Proceedings of the Royal Society B: Biological Sciences.* 275(1631):133–139.

Johnston D, McDonald M, Polovina J and Domokos R (2008). Temporal patterns in the acoustic signals of beaked whales at Cross Seamount', *Biology Letters.* 4(2): 208–211.

Jones K and Safi K (2011). Ecology and evolution of mammalian biodiversity. *Philosophical Transactions of the Royal Society B: Biological Sciences*, *366*(1577), 2451–2461.

Kardong K (2019). *Vertebrates: Comparative Anatomy, Function, Evolution*, (8th ed). McGraw-Hill

Kassambara A and Mundt. F (2017). Factoextra: Extract and Visualize the Results of Multivariate Data Analyses. R package version 1.0.5.999. Available at: http://www.sthda.com/english/rpkgs/factoextra

Kastelein R, Bunskoek P, Hagedoorn M and Au W (2002). Audiogram of a harbor porpoise (*Phocoena phocoena*) measured with narrow-band frequency-modulated signals. *The Journal of the Acoustical Society of America.* 112(1): 334–344.

Kasuya T (2009) Giant Beaked Whales: Berardius bairdii and B. arnuxii, in *Encyclopedia of Marine Mammals.* Elsevier Ltd. 498–500.

Kelley N, Pyenson N. (2015), Evolutionary innovation and ecology in marine tetrapods from the Triassic to the Anthropocene. Science, 348 p. aaa3716

Kelly E Sears K (2011). Reduced integration in marsupial limbs and the implications for mammalian evolution. *Biol J Linn Soc*, 102: 22–36.

Kemper C (2009). Pygmy right whale Caperea marginata. Pages 939–941 in W. F. Perrin, B. Wursig and J. G. M. Thewissen, eds. *Encyclopaedia of marine mammals* (2nd edn). Academic Press, San Diego, CA.

Kennett J (1978). The development of planktonic biogeography in the southern ocean during the Cenozoic. *Marine Micropaleontology* 3, 301–345. DOI 10.1016/0377-8398(78)90017-8

Kerr G, Nousek-Mcgregor A., Miller C, Moore, M and Nowacek, D (2014). Effects of Body Condition on Buoyancy in Endangered North Atlantic Right Whales. *Physiological and Biochemical Zoology*, *87*(1), 160–171.

Ketten D (1997) Structure and function in whale ears. *Bioacoustics.* 8(1–2): 103–135

Kirkwood J, Bennett J, Jepson P, Kuiken T, Simpson V, and Baker J. (1997). Entanglement in fishing gear and other causes of death in cetaceans stranded on the coasts of England and Wales. *The Veterinary Record*, 141(4):94.

Kirschvink J, Dizon A and Westphal A. (1986). Evidence from Strandings for Geomagnetic Sensitivity in Cetaceans. *Journal of Experimental Biology*, 120(1):1–24.

Kitchener D, Ross G and Caputi N (1990) Variation in skull and external morphology in the False Killer Whale, *Pseudorca crassidens*, from Australia, Scotland and South Africa. *Mammalia.* 54(1):119–136.

Klima M (1999) Development of the cetacean nasal skull. *Advances in anatomy, embryology, and cell biology.* 149, 1–143.

Klinowska M (1985). Cetacean Live Stranding Sites Relate to Geomagnetic Topography. *Aquatic Mammals* 1:27–32.

Konishi S Kitagawa G. (2008). *Information Criteria and Statistical Modeling.* Springer New York.

Kremers D, López Marulanda J, Hausberger M, and Lemasson A (2014). Behavioural evidence of magnetoreception in dolphins: detection of experimental magnetic fields. *Naturwissenschaften,* 101(11):907–911.

Kuhnt W, Holbourn A, Hall R, Zuvela M, Käse R, Cliff P (2004) Neogene history of the Indonesian throughflow, Continent-ocean interactions within East Asian marginal seas, Washington (DC) *American Geophysical Union*: 1-22)

Kyhn L, Tougaard J, Beedholm K, Jensen F, Ashe E, Williams R and Madsen P (2013). Clicking in a killer whale habitat: narrow-band, high-frequency biosonar clicks of harbour porpoise (*Phocoena phocoena*) and Dall's porpoise (*Phocoenoides dalli*). *PLoS ONE.* 8(5), e63763.

Kyhn L, Tougaard J, Jensen F, Wahlberg M (2009) Feeding at a high pitch: Source parameters of narrow band, high-frequency clicks from echolocating off-shore hourglass dolphins and coastal Hector's dolphins. *The Journal of the Acoustical Society of America. Acoustical Society of America (ASA).* 125(3): 1783–1791.

Lacsamana J, Ventolero M, Blatchley D and Santos M (2015). First record of a rare beaked whale *Mesoplodon hotaula* in the Philippines. *Marine Biodiversity Records, 8.*

Ladegaard, M. Jensen F, de Freitas M (2015). Amazon river dolphins (*Inia geoffrensis*) use a high-frequency short-range biosonar', *Journal of Experimental Biology.* 218(19): 3091–3101.

Laist D, Knowlton A, Mead J, Collet A, and Podesta M (2001). Collisions between ships and whales. *Marine Mammal Science,* 17(1):35–75.

Lamb H and Frydendahl K (1991). Historic storms of the North Sea, British Isles, and Northwest Europe. *International Journal of Climatology* (Vol. 12). Cambridge University Press.

Lambert O (2005) Phylogenetic affinities of the long-snouted dolphin Eurhinodelphis (Cetacea, Odontoceti) from the Miocene of Antwerp, Belgium. *Palaeontology.* 48(3): 653–679.

Lambert O, Bianucci G, and Urbina M (2014) *Huaridelphis raimondii*, a new early Miocene Squalodelphinidae (Cetacea, Odontoceti) from the Chilcatay Formation, Peru. *Journal of Vertebrate Paleontology.* 34:987–1004.

Lambert O, Bianucci G, Post K, De Muizon C, Salas-Gismondi R, Urbina M and Reumer J. (2010). The giant bite of a new raptorial sperm whale from the Miocene epoch of Peru. *Nature*, *466*(7302), 105–108.

Lambert O, Bianucci G, Urbina M, and Geisler J (2017b). A new inioid (Cetacea, Odontoceti, Delphinida) from the Miocene of Peru and the origin of modern dolphin and porpoise families. *Zoological Journal of the Linnean Society.*179:919-946.

Lambert O, de Muizon C and Bianucci G (2015) A new archaic homodont toothed whale (Mammalia, Cetacea, Odontoceti) from the early Miocene of Peru. *Geodiversitas.* 37:79-108.

Lambert O, Godfrey S and Fitzgerald E (2018). *Yaquinacetus meadi*, a new latest Oligocene–early Miocene dolphin (Cetacea, Odontoceti, Squaloziphiidae, fam. nov.) from the Nye Mudstone (Oregon, U.S.A.). *Journal of Vertebrate Paleontology, 38*(6).

Lambert O, Martinez-Cáceras M, Bianucci G, Di Celma C, Salas-Gismondi R, Steurbaut E, Urbina M and de Muizon C. (2017a). Earliest mysticete from the late Eocene of Peru sheds new light on the origin of baleen whales. Curr. Biol. 27 pp. 1535-1541

Law C, Duran E, Hung N, Richards E, Santillan I and Mehta R (2018). Effects of diet on cranial morphology and biting ability in musteloid mammals. *Journal of Evolutionary Biology*, *31*(12), 1918–1931.

Law R, Barry J and Barber J (2012). Contaminants in cetaceans from UK waters: Status as assessed within the Cetacean Strandings Investigation Programme from 1990 to 2008. *Marine Pollution Bulletin*, 64(7):1485–1494.

Lawing A, and Polly P (2010). Geometric morphometrics: Recent applications to the study of evolution and development, *Journal of Zoology*, 280(1):1-7

Lawler I, Parra G and Noad M (2007). Vulnerability of marine mammals in the Great Barrier Reef to climate change (Chapter 16, Part II: Species and species groups). In *Climate Change and the Great Barrier Reef: A Vulnerability Assessment*. Townsville: Great Barrier Reef Marine Park Authority. Chapter 16.

Ledbetter N and Bonett R (2019) Terrestriality constrains salamander limb diversification: implications for the evolution of pentadactyly. *J. Evol. Biol.* 32, 642–652.

LeDuc R (2002) Delphinids, overview. In: Perrin W.F., Würsig B., Thewissen J.G.M., editors. *Encyclopedia of Marine Mammals. Academic Press*:242–246.

Leeney R, Amies R, Broderick A, Witt M, Loveridge J, Doyle J, and Godley B (2008). Spatio-temporal analysis of cetacean strandings and bycatch in a UK fisheries hotspot. *Biodiversity and Conservation,* 17(10):2323–2338.

Lipps J and Mitchell E (1976). Trophic model for the adaptive radiations and extinctions of pelagic marine mammals. *Paleobiology* 2(3), 147–155.

Lloyd G and Slater G (2020). A Total-Group Phylogenetic Metatree of Cetacea and the Importance of Fossil Data in Diversification Analyses, *Systematic Biology.*

Lloyd H and Ross G (2015). Long-term trends in cetacean incidents in New South Wales, Australia. *Australian Zoologist*, 37(4):492–500.

López-Fernández H, Arbour JH., Winemiller KO and Honeycutt RL. Testing for ancient adaptive radiations in Neotropical cichlid fishes. Evolution 67, 1321–1337 (2013).

Louys J, Wilkinson DM, Bishop LC (2012). Ecology needs a paleontological perspective. In: Louys J (ed) Paleontology in ecology and conservation. Springer, New York, pp 23–38

Lucas T and Goswami A (2017). paleomorph: geometric morphometric tools for paleobiology. R package version 0.1.4. Available at: https://CRAN.R-project.org/package=paleomorph

Luciani V, Giusberti L, Agnini C, Fornaciari E, D Rio et al. (2010) Ecological and evolutionary response of Tethyan planktonic foraminifera to the middle Eocene climatic optimum (MECO) from the Alano section (NE Italy), Palaeogeography, Palaeoclimatology, Palaeoecology, Volume 292, Issues 1–2, 2010, Pages 82-95.

MacLeod C (2009). Global climate change, range changes and potential implications for the conservation of marine cetaceans: a review and synthesis. *Endangered Species Research*, 7(2):125–136

Macleod C, Reidenberg J, Weller M, Santos M et al. (2007) Breaking symmetry: The marine environment, prey size, and the evolution of asymmetry in cetacean skulls. *The Anatomical Record: Advances in Integrative Anatomy and Evolutionary Biology.* John Wiley & Sons, Ltd.; 290(6): 539–545.

MacLeod CD, Santos MB, Lopes A. & Pierce GJ. (2006) Relative prey size consumption in toothed whales: implications for prey selection and level of specialisation. Mar. Ecol. Prog. Ser. 326, 295–307.

MacLeod, C, Pierce G, and Santos M. (2004). Geographic and temporal variations in strandings of beaked whales (Ziphiidae) on the coasts of the UK and the Republic of Ireland from 1800-2002. *Journal of Cetacean Research and Management*, 6(1):79–86.

MacLeod, C., Bannon S, Pierce G, Schweder C, Learmonth J, Herman J, and Reid J. (2005). Climate change and the cetacean community of north-west Scotland. *Biological Conservation*, 124(4):477–483.

Madsen P, Payne R, Kristiansen N and Wahlberg M (2002). Sperm whale sound production studied with ultrasound time/depth-recording tags. *The Journal of Experimental Biology.* 205: 1899–1906

Maldini D, Mazzuca L, and Atkinson S. (2005). Odontocete Stranding Patterns in the Main Hawaiian Islands (1937-2002): How Do They Compare with Live Animal Surveys? *Pacific Science*, 59(1):55–67.

Marra G, and Wood S. (2011). Practical variable selection for generalized additive models. *Computational Statistics and Data Analysis*, 55(7):2372–2387.

Marshall A, Bardua C, Gower D, Wilkinson M, Sherratt E and Goswami A. (2019). High-density three-dimensional morphometric analyses support conserved static (intraspecific) modularity in caecilian (Amphibia: Gymnophiona) crania. *Biological Journal of the Linnean Society,* 126(4), 721–742.

Martin J (2013) From Finbacks to Humpbacks: Investigation of The Evolutionary History Of Balaenopteridae, MSc. Dissertation. San Diego State University.

Martínez-Cáceres M and de Muizon C (2011) A new basilosaurid (Cetacea, Pelagiceti) from the Late Eocene to Early Oligocene Otuma Formation of Peru, Comptes Rendus - *Palevol.* No longer published by Elsevier; 10(7): 517–526.

Martínez-Cáceres M, Lambert O and de Muizon C (2017) The anatomy and phylogenetic affinities of Cynthiacetus peruvianus, a large Dorudon-like basilosaurid (Cetacea, Mammalia) from the late Eocene of Peru. *Geodiversitas. Museum National d'Histoire Naturelle*. 39(1): 7–163.

Marx F and Fordyce R (2015). Baleen boom and bust: a synthesis of mysticete phylogeny, diversity and disparity. *Royal Society Open Science* 2.; 140434.

Marx F and Uhen M (2010). Climate, Critters, and Cetaceans: Cenozoic Drivers of the Evolution of Modern Whales. *Science*, *327*(5968), 993–996.

Marx F, Buono M, Evans A, Fordyce R, Reguero M and Hocking D (2019b). Gigantic mysticete predators roamed the Eocene Southern Ocean. *Antarctic Science*, *31*(2), 98–104.

Marx F, Fitzgerald, E., & Fordyce R. (2019a). Like phoenix from the ashes: How modern baleen whales arose from a fossil "dark age." In *Acta Palaeontologica Polonica* (Vol. 64, Issue 2, pp. 231–238).

Marx F, Lambert O and Uhen M. (2016a) Major Steps in the Evolution of Cetaceans, in: *Cetacean Paleobiology*;157–197.

Marx F, Hocking D, Park T, Ziegler T, Evans, A and Fitzgerald E. (2016b). Suction feeding preceded filtering in baleen whale evolution. In *Memoirs of Museum Victoria* (Vol. 75).

Massimino D, Harris S, and Gillings S. (2018). Evaluating spatiotemporal trends in terrestrial mammal abundance using data collected during bird surveys. *Biological Conservation*, *226*, 153–167.

McCurry M, Evans A, Fitzgerald E, Adams J, Clausen P and McHenry C (2017a). The remarkable convergence of skull shape in crocodilians and toothed whales. *Proc. R. Soc. B* 284, 20162348.

McCurry M, Evans A, Fitzgerald E, McHenry C, Bevitt J and Pyenson N (2019) The repeated evolution of dental apicobasal ridges in aquatic-feeding mammals and reptiles, *Biological Journal of the Linnean Society*,127(2):245–259

McCurry M, Fitzgerald E, Evans A, Adams J, Mchenry C (2017b) Skull shape reflects prey size niche in toothed whales. Biol. J. Linn. Soc., 121:936-946.

McGeady R, McMahon B and Berrow S. (2016) The effects of seismic surveying and environmental variables on deep diving odontocete stranding rates along Ireland's coast. *Proceedings of Meetings on Acoustics*, 27(1):040006.

McGhee G (2011) *Convergent evolution: limited forms most beautiful*. The MIT Press, Cambridge, Massachusetts.

McGovern B, Culloch R, O'Conell M and Berrow S. (2016) Temporal and spatial trends in stranding records of cetaceans on the Irish coast, 2002–2014. *Journal of the Marine Biological Association of the United Kingdom*.

McGowen M (2011). Toward the resolution of an explosive radiation-a multilocus phylogeny of oceanic dolphins (Delphinidae) *Mol. Phylogenet. Evol.,* 60, pp. 345-357

McGowen M, Gatesy J and Wildman D (2014). Molecular evolution tracks macroevolutionary transitions in Cetacea. In *Trends in Ecology and Evolution* (Vol. 29, Issue 6, pp. 336–346).

McGowen M, Spaulding M and Gatesy J (2009). Divergence date estimation and a comprehensive molecular tree of extant cetaceans. *Molecular Phylogenetics and Evolution*, *53*(3), 891–906.

McGowen M, Spaulding M, Gatesy J (2009) Divergence date estimation and a comprehensive molecular tree of extant cetaceans. *Mol. Phylogenet. Evol.*; 53, 891–906.

McGowen M, Tsagkogeorga G, Àlvarez-Carretero S, dos Reis M, Struebig M, Deaville R, Jepson P, Jarman S, Polanowski A and Morin P (2019). Phylogenomic resolution of the cetacean tree of life using target sequence capture. *Syst. Biol*:1-24.

McHenry C, Clausen P, Daniel W, Meers M and Pendharkar A (2006) Biomechanics of the rostrum in crocodilians: a comparative analysis using finite element modeling. *Anat. Rec. A* 288, 827– 849.

McLeish T (2013). *Narwhals: Arctic Whales in a Melting World*. Seattle: University of Washington Press

Mead J (1975) Anatomy of the External Nasal Passages and Facial Complex in the Delphinidae (Mammalia: Cetacea), *Smithsonian Contributions to Zoology* (207): 1–35.

Mead J (1975) Anatomy of the external nasal passages and facial complex in the Delphinidae (Mammalia: Cetacea). *Smithson. Contrib. Zool.* 207:1–35.

Mead J and Mitchell E (1984). "Atlantic gray whales". In Jones ML, Swartz SL, Leatherwood S (eds.) *The Gray Whale*. London: Academic Press. pp. 33–53.

Mignucci-Giannoni A, Toyos-González M, Pérez-Padilla J, Rodríguez-López M and Overing J (2000). Mass stranding of pygmy killer whales (*Feresa attenuata*) in the British Virgin Islands. *Journal of the Marine Biological Association of the United Kingdom,* 80(4):759–760.

Milinkovitch M (1995) Molecular phylogeny of cetaceans prompts revision of morphological transformations. *Trends Ecol. Evol.*;10, 328–334.

Miller G (1923). The telescoping of the cetacean skull. *Smithsonian Miscellaneous Collections* 76:1–71.

Miller KG, Browning JV, Schmelz WJ, Kopp RE, Mountain GS and Wright JD. (2020). Cenozoic sea-level and cryospheric evolution from deep-sea geochemical and continental margin records: Science Advances, 6(20), eaaz1346.

Miller KG, Wright JD, Katz ME, Browning JV, Cramer BS, Wade BS, and Mizintseva SF (2008). A view of Antarctic ice-sheet evolution from sea-level and deep-sea isotope changes during the Late Cretaceous – Cenozoic, in Antarctica: A Keystone in a Changing World—Proceedings of the 10th International Symposium on Antarctic Earth Sciences, edited by A. Cooper et al., pp. 55 – 70, Natl. Acad., Washington, D. C.

Mitteroecker P and Gunz P (2009). Advances in Geometric morphometrics. *Evolutionary Biology.* 36:235–247.

Moen D, Irschick D and Wiens J (2013). Evolutionary conservatism and convergence both lead to striking similarity in ecology, morphology and performance across continents in frogs. *Proc. R. Soc. B* 280: 20132156.

Molina M, Urbina Schmitt M, Chacaltana Budiel C, and Medina L (2018). Los Delfines Lophocetinae (Mammalia: Cetacea: Kentriodontidae) De La Formación Pisco De Cerro Yesera De Amara, Ocucaje, Ica.

Molnar P (2008) Closing of the Central American seaway and the ice age: a critical review. *Paleoceanography* 23: 2201.

Moore M, and Van Der Hoop J (2012) The Painful Side of Trap and Fixed Net Fisheries: Chronic Entanglement of Large Whales. *Journal of Marine Biology*, Volume 2012, Article ID 230653.

Moore M, Mitchell G, Rowles T and Early G (2020) Dead Cetacean? Beach, Bloat, Float, Sink. In *Frontiers in Marine Science* (Vol. 7). Frontiers Media S.A.

Moore S (2016) Is it "boom times" for baleen whales in the Pacific Arctic region? In *Biology Letters* (12)9 Royal Society of London.

Moors-Murphy H (2015) Patterning in northern bottlenose whale (hyperoodon ampullatus) click trains. *Canadian Acoustics - Acoustique Canadienne*; 48–49.

Morin P, Baker S, Brewer R, Burdin A, Dalebout M, Dines J and Wade P (2017) Genetic structure of the beaked whale genus Berardius in the North Pacific, with genetic evidence for a new species. *Marine Mammal Science,* 33(1):96–111.

Morisaka T and Connor R (2007) Predation by killer whales (*Orcinus orca*) and the evolution of whistle loss and narrow-band high frequency clicks in odontocetes. *Journal of Evolutionary Biology*; 20(4): 1439–1458.

Morlon H, Lewitus E, Condamine F, Manceau M, Clavel J and Drury J (2016). "RPANDA: an R package for macroevolutionary analyses on phylogenetic trees." *Methods in Ecology and Evolution*, 7: 589-597. R package version 1.4,

Murase H, Tamura T, Kiwada H, Fujise Y, Watanabe H, Ohizumi H, Yonezaki S, Okamura H and Kawahara S (2007) Prey selection of common minke (*Balaenoptera*

*acutorostrata*) and Bryde's (*Balaenoptera edeni*) whales in the western North Pacific in 2000 and 2001. *Fish. Oceanogr* (16): 186 –201.

Murphy S, Herman J, Pierce G, Rogan E and Kitchener A (2006) Taxonomic Status and Geographical Cranial Variation of Common Dolphins (*Delphinus*) In the Eastern North Atlantic. *Marine Mammal Science*, 22(3):573–599.

Natural History Museum (2018) 'Dataset: Historical UK cetacean strandings dataset' (1913-1989) Natural History Museum Data Portal. Available at: data.nhm.ac.uk.

Ness A (1967) A Measure of Asymmetry of the Skulls of Odontocete Whales. *Journal of Zoology.* 153:209-221.

Norman A, Bowlby C, Brancato M, Calambokidis J, Duffield D and Gearin P (2004). Cetacean strandings in Oregon and Washington between 1930 and 2002. *Journal of Cetacean Research Management*, 6(1):87–99.

Norris K and Møhl B (1983) Can odontocetes debilitate prey with sound? *American Naturalis*t 122:85–104.

Northridge S, Cargill A, Coram A, Mandleberg L, Calderan S, Reid B and Wirz M (2010). 'Entanglement of minke whales in Scottish waters; an investigation into occurrence, causes and mitigation. Sea Mammal Research Unit. Final Report to Scottish Government' CR/2007/49.

Nowacek D, Johnson M, Tyack P, Shorter K, McLellan W and Pabst D (2001). Buoyant balaenids: The ups and downs of buoyancy in right whales. *Proceedings of the Royal Society B: Biological Sciences*, *268*(1478), 1811–1816.

Nowak R (1999). *Walker's Mammals of the World* (6th edn), Johns Hopkins Univ. Press.

Nummela S, Hussain T, Thewissen J and Taseer Hussain S (2006). Cranial anatomy of Pakicetidae (Cetacea, Mammalia). *Journal of Vertebrate Paleontology*, *26*(3), 746–759.

Nweeia M, Nutarak C, Eichmiller F and Eidelman N (2009) Considerations Of Anatomy, Morphology, Evolution, and Function for Narwhal Dentition, in Smithsonian at the poles: *Contributions to International Polar Year Science*. 2009;223–240.

O'Connell M and Berrow S (2007) Records from the Irish Whale and Dolphin Group for 2006. *The Irish Naturalists' Journal*, 28(11):459–466.

Okazaki Y (2012) A new mysticete from the upper Oligocene Ashiya Group, Kyushu, Japan and its significance to mysticete evolution. *Bulletin of the Kitakyushu Museum of Natural History and Human History Series A (Natural History)* 10:129-152.

Olson P (2008) Pilot whale Globicephala melas and *G. muerorhynchus* in *Encyclopedia of Marine Mammals*. Perrin W, Wursig B and Thewissen J (eds.). Academic Press (2nd edn). ISBN 0-12-551340-2.; 847–52.

Page CE and Cooper N (2017). Morphological convergence in 'river dolphin' skulls. PeerJ, 5, e4090

Pagel M (1997) Inferring evolutionary processes from phylogenies. *Zoologica Scripta* 26: 331-348.

Pagel M (1999). Inferring the historical patterns of biological evolution. *Nature* 401: 877.

Paradis E and Schliep K (2018) Ape 5.0: an environment for modern phylogenetics and evolutionary analyses in R. *Bioinformatics.* 1;35(3): 526-528.

Park T, Evans A, Gallagher S and Fitzgerald E (2017) Low-frequency hearing preceded the evolution of giant body size and filter feeding in baleen whales. *Proc. R. Soc. B.* 284: 20162528.

Park T, Fitzgerald E and Evans A (2016) Ultrasonic hearing and echolocation in the earliest toothed whales. *Biology Letters. Royal Society of London.* 12: 20160060.

Park T, Mennecart B, Costeur L, Grohé, C and Cooper N (2019) Convergent evolution in toothed whale cochleae', *BMC Evolutionary Biology.* BioMed Central Ltd. 19(1): 1–11.

Parsons E, Clark J, and Simmonds M (2010). The conservation of British cetaceans: A review of the threats and protection afforded to whales, dolphins, and porpoises in UK waters, part 2. *Journal of International Wildlife Law and Policy*, 13(2):99–175.

Pearson R and Dawson T (2003). Predicting the Impacts of Climate Change on the Distribution of Species: Are Bioclimate Envelope Models Useful? *Global Ecology and Biogeography* (12): 361-371

Peltier H, Dabin W, Daniel P, Van Canneyt O, Dorémus G, Huon M and Ridoux V (2012). The significance of stranding data as indicators of cetacean populations at sea: Modelling the drift of cetacean carcasses. *Ecological Indicators*, *18*, 278–290.

Peredo C, Pyenson N and Boersma A (2017). Decoupling Tooth Loss from the Evolution of Baleen in Whales. *Frontiers in Marine Science*, *4*(MAR), 67.

Peredo C, Uhen M and Nelson M (2018) A new kentriodontid (Cetacea: Odontoceti) from the early Miocene Astoria Formation and a revision of the stem delphinidan family Kentriodontidae. *Journal of Vertebrate Paleontology*: e1411357.

Peters S, Antar M, Zalmout I and Gingerich P (2009). Sequence stratigraphic control on preservation of late Eocene whales and other vertebrates at Wadi Al-Hitan, Egypt. *Palaios*, *24*(5–6), 290–302.

Pfuhl H and McCave I (2009). Evidence for late Oligocene establishment of the Antarctic Circumpolar Current, *Earth and Planetary Science Letters*, 235(3-4):715-728

Pierce G, Santos M, Smeenk C, Saveliev A and Zuur A. (2007). Historical trends in the incidence of strandings of sperm whales (*Physeter macrocephalus*) on North Sea coasts: An association with positive temperature anomalies. *Fisheries Research*, 87(2–3):219–228.

Pincheira-Donoso D, Harvey LP and Ruta M (2015). What defines an adaptive radiation? Macroevolutionary diversification dynamics of an exceptionally species-rich continental lizard radiation. BMC Evol Biol 15, 153.

Pinheiro J, Bates D, DebRoy S, Sarkar D (2020) R Core Team. nlme: Linear and Nonlinear Mixed Effects Models. R package version 3.1-147, https://CRAN.R-project.org/package=nlme.

Pitman R (2009) Mesoplodont Whales: (*Mesoplodon* spp.). In *Encyclopedia of Marine Mammals*: 721–726).

Plummer M, Best N, Cowles K and Vines K (2006) CODA: convergence diagnosis and output analysis for MCMC. *R News.*; 6:7–1

Pollock C, Mavor R, Weir C, Reid A, White R, Tasker M, Webb A, and Reid J (2000) The distribution of seabirds and marine mammals in the Atlantic Frontier, north and west of Scotland. *Joint Nature Conservation Committee* (JNCC).

Poloczanska ES, Burrows MT, Brown CJ, Garcia Molinos J et al., (2016) Responses of marine organisms to climate change across oceans. Front Mater Sci 3:62.

Post K and Bosselaers M (2005) Late Pliocene occurrence of Hemisyntrachelus (Odontoceti, Delphinidae) in the southern North Sea – *DEINSEA*.; 11: 29-45.

Prado J, Mattos P, Silva K, and Secchi E (2016) Long-term seasonal and interannual patterns of marine mammal strandings in subtropical western South Atlantic. *PLoS ONE,* 11(1).

Price S, Holzman R, Near T and Wainwright P (2011). Coral reefs promote the evolution of morphological diversity and ecological novelty in labrid fishes. *Ecology Letters*, *14*(5), 462–469.

Price S, Tavera J, Near T and Wainwright P (2013). Elevated Rates Of Morphological And Functional Diversification In Reef-dwelling Haemulid Fishes. *Evolution*, *67*(2), 417–428.

Price SA, Bininda-Emonds ORP, Gittleman JL (2005) A complete phylogeny of the whales, dolphins and even-toed hoofed mammals (Cetartiodactyla). Biol. Rev., 80 (2005), pp. 1-29

Pyenson N (2009) Requiem for Lipotes: an evolutionary perspective on marine mammal extinction. *Mar Mammal Sci* 25:714—724.

Pyenson N (2010) Carcasses on the coastline: measuring the ecological fidelity of the cetacean stranding record in the eastern North Pacific Ocean. *Paleobiology*, 36(3): 453–480.

Pyenson N (2011) The high fidelity of the cetacean stranding record: insights into measuring diversity by integrating taphonomy and macroecology. *Proceedings: Biological Sciences*, 278(1724):3608–3616.

Pyenson N (2017) The ecological rise of whales chronicled by the fossil record. *Current Biology* 27: 558–564.

Pyenson ND and Lindberg DR (2011) What happened to gray whales during the Pleistocene? The ecological impact of sea-level change on benthic feeding areas in the North Pacific Ocean. PLoS ONE 6

Quental T and Marshall C (2010). Diversity dynamics: Molecular phylogenies need the fossil record. *Trends in Ecology and Evolution*, *25*(8), 434–441.

R Core Team (2017). R: A language and environment for statistical computing. R Foundation for Statistical Computing, Vienna, Austria. Available at: https://www.R-project.org/.

Rabosky D (2014) Automatic Detection of Key Innovations, Rate Shifts, and Diversity-Dependence on Phylogenetic Trees. *PLoS ONE* 9, e89543.

Rabosky D and Goldberg E (2015) Model Inadequacy and Mistaken Inferences of Trait-Dependent Speciation. *Systematic Biology* 64:340–355

Racicot R (2018) Dolphins, Porpoises, and Monodontids, *Evolution in Encyclopedia of Marine Mammals*. Elsevier; 271–274.

Racicot R, Boessenecker R, Darroch S, Geisler J (2019) Evidence for convergent evolution of ultrasonic hearing in toothed whales (Cetacea: Odontoceti). *Biol. Lett.;*15: 20190083.

Racicot R, Darroch S and Kohno N (2018) Neuroanatomy and inner ear labyrinths of the narwhal, *Monodon monoceros*, and beluga, *Delphinapterus leucas* (Cetacea: Monodontidae). *Journal of Anatomy*. Blackwell Publishing Ltd.

Ramp C, Delarue J, Palsbøll P, Sears R, and Hammond P (2015). Adapting to a Warmer Ocean Seasonal Shift of Baleen Whale Movements over Three Decades. *PLoS ONE*, 10(3): e0121374.

Randau M and Goswami A (2017a) Morphological modularity in the vertebral column of Felidae (Mammalia, Carnivora). *BMC Evolutionary Biology*, *17*(1), 133.

Randau M and Goswami A (2017b) *Unravelling intravertebral integration, modularity and disparity in Felidae (Mammalia); Unravelling intravertebral integration, modularity and disparity in Felidae (Mammalia)*

Randau M, Sanfelice D and Goswami A (2019). Shifts in cranial integration associated with ecological specialization in pinnipeds (Mammalia, Carnivora). *R. Soc. Open Sci.* 6:190201–24

Read F, Evans P, and Dolman S (2017). Cetacean Bycatch Monitoring and Mitigation under EC Regulation 812/2004 in the Northeast Atlantic, North Sea and Baltic Sea from 2006 to 2014. *Whale and Dolphin Conservation.*

Reeves R and Mitchell E (1986). The Long Island, New York, right whale fishery: 1650-1924. *Rep. int. Whal. Commn* (special issue) 10:201-20.

Reeves R, Smith B, Crespo E, and di Sciara G (2003). Dolphins, whales, and porpoises: 2003–2010 conservation action plan for the world's cetaceans. *IUCN Species Survival Commission* (Vol. 658).

Reid J, Evans P and Northridge S (2003). Atlas of Cetacean Distribution in Northwest European Waters. *Joint Nature Conservation Committee*, Peterborough, UK.

Reidenberg J and Laitman J (2007). Discovery of a low frequency sound source in Mysticeti (baleen whales): Anatomical establishment of a vocal fold homolog. *Anatomical Record.* 290(6): 745–759.

Reiss P and Todd Ogden R (2009). Smoothing parameter selection for a class of semiparametric linear models. *Journal of the Royal Statistical Society. Series B: Statistical Methodology,* 71(2):505–523.

Revell L (2012) Phytools: An R package for phylogenetic comparative biology (and other things). *Methods in Ecology and Evolution.* 3(2): 217–223.

Revell L and Collar D (2009) Phylogenetic analysis of the evolutionary correlation using likelihood. *Evolution,* 63:1090–1100.

Revell L, Harmon L and Collar D (2008). Phylogenetic Signal, Evolutionary Process, and Rate, <u>*Systematic Biology*</u> 57(4):591-601.

Rex MA, Crame, JA, Stuart CT and Clarke A. (2005) Largescale biogeographic patterns in marine mollusks: A confluence of history and productivity? Ecology, 86, 2288–2297.

Ricklefs R (2006). Global variation in the diversification rate of passerine birds. *Ecology* 87, 2468–2478.

Riesch R, Barrett–Lennard L, Ellis G, Ford J and Deecke V (2012). Cultural traditions and the evolution of reproductive isolation: ecological speciation in killer whales? *Biological Journal of the Linnean Society.* 106(1):1–17.

Rintoul S, Hughes C and Olbers D (2001) in *Ocean Circulation Climate* (eds Siedler, G., Church J and Gould J.) 271–302.

Robinson R, Learmouth J, Hutson A, Macleod C, Sparks T, Leech D, Pierce G, Rehfisch M and Humphrey Q (2005) Climate change and migratory species. *BTO Research Report* 414.

Rocha R, Clapham P and Ivashchenko Y (2015). Emptying the Oceans: A Summary of Industrial Whaling Catches in the 20th Century. <u>*Marine Fisheries Review*</u> 76(4):37-48.

Rohlf F and Marcus L (1993). A revolution in morphometrics. *Trends Ecol. Evol.* 8:129–132.

Rohlf F and Slice D (1990). Extensions of the Procrustes method for the optimal superimposition of landmarks. *Syst. Zool.* 39:40–59.

Roman J, Estes J, Morissette L, Smith C, Costa D, McCarthy J, Nation J, Nicol S, Pershing A and Smetacek K (2014). Whales as marine ecosystem engineers. *Frontiers in Ecology and the Environment* 12(7): 377-385.

Roman J, Palumbi S (2003). Whales before whaling in the North Atlantic. *Science.* 25;301(5632):508-10.

Rommel S, Costidis A, Fernandez A and Jepson P (2005) Elements of beaked whale anatomy and diving physiology and some hypothetical causes of sonar-related stranding. *Journal of Cetacean Research and Management.* 7(3):189.

Rommel S, Pabst D and McLellan W. (2009). Skull Anatomy. In *Encyclopedia of Marine Mammals* (1033–1047).

Ross A. and Isaac S. (n.d.). *The Net Effect? A review of cetacean bycatch in pelagic trawls and other fisheries in the north-east Atlantic A WDCS report for Greenpeace*.

Roston R and Roth V (2019). Cetacean Skull Telescoping Brings Evolution of Cranial Sutures into Focus. *Anat Rec*, *302*: 1055–1073.

Rutherforde-Thorpe M (1938) Notes on the osteology of a beaked whale. *Journal of Mammology.*19(3): 354–362

Ryan C, Leaper R and Evans P (2016). Entanglement: an emerging threat to humpback whales in Scottish waters. *International Whaling Commission.*

Sabin R, Spurrier C, Chimonides P, Jepson P, Deaville R, Reid R, Patterson I, Penrose R, Law R (2005). Cetaceans strandings investigation and co-ordination in the UK for the period 1st January 2000 - 31st December 2004. Consultancy Report to the Department for Environment, Food and Rural Affairs.

Santana S (2015). Quantifying the effect of gape and morphology on bite force: biomechanical modeling and in vivo measurements in bats. *Funct. Ecol.* 30, 557–565.

Santana S and Lofgren S (2013). Does nasal echolocation influence the modularity of the mammal skull? *J Evol Biol.* Nov;26(11):2520-6.

Santana S, Grosse I and Dumont E (2012). Dietary Hardness, Loading Behavior, And The Evolution Of Skull Form In Bats. *Evolution*, *66*(8), 2587–2598.

Sarmiento JL, Gruber N, Brzezinski MA, and Dunne JP (2004), High-latitude controls of thermocline nutrients and low latitude biological productivity, Nature, 427, 56 – 60.

Schaffar A, Madon B, Garrigue C and Constantine R (2009) Avoidance of whale watching boats by humpback whales in their main breeding ground in New Caledonia. Doc SC/61/WW6. *Scientific Committee of the International Whaling Commission*, Madeira.

Schelske C and Hodell D (1991) Recent changes in productivity and climate of Lake Ontario detected by isotopic analysis of sediments. *Limnology and Oceanography*, 36: 961-975.

Scher H and Martin E (2006). Timing and climatic consequences of the opening of Drake Passage, *Science,* 312: 428-430.

Schlager S (2013). Morpho: calculations and visualizations related to geometric morphometrics. R package v. 0.23.3. Available at: http://CRAN.R-project.org/package = Morpho.

Schlager S (2017). Morpho and Rvcg - Shape Analysis in R. Pp. 217–256 in G. Zheng, S. Li, and G. Szekely, eds. *Statistical Shape and Deformation Analysis*. Academic Press

Schmieder D, Benítez H, Borissov I and Fruciano C (2015). Bat Species Comparisons Based on External Morphology: A Test of Traditional versus Geometric Morphometric Approaches. *PLoS ONE*, *10*(5), e0127043.

Schumann N, Gales N, Harcourt R, and Arnold J (n.d). Impacts of climate change on Australian marine mammals. *Australian Journal of Zoology,* 61(2): 146–159.

Serio C, Castiglione S and Mondanaro A. (n.d.). Macroevolution of Toothed Whales Exceptional Relative Brain Size RRphylo-Phylogenetic Ridge Regression Methods for Comparative Studies View project EcoPast: methods and tools for deep-time macroecology of fossil species View project.

Shemesh A, Macko S, Charles C and Rau G (1993) Isotope evidence for reduced productivity in the glacial Southern Ocean. *Science,* 262: 407-410.

Simmonds M (2012) Cetaceans and Marine Debris: The Great Unknown. *Journal of Marine Biology*, 2012:1–8.

Simmonds M and Eliott W (2009). Climate change and cetaceans: Concerns and recent developments. *Journal of the Marine Biological Association of the United Kingdom*, 89(1):203–210.

Simpson G (1944) *Tempo and mode in evolution.* Reprint, 1984, Columbia University Press, New York.

Simpson G (1945) The principles of classification and a classification of mammals [Monograph]. *Bulletin of the American Museum of Natural History*, 85, 1–350. Available at: http://hdl.handle.net/2246/1104

Simpson G (1953) *The Major Features of Evolution*, Columbia Univ Press, New York.

Sjare B and Smith T (1986) The vocal repertoire of white whales, Delphinapterus leucas, summering in the Cunningham Inlet, Northwest Territories. *Can. J. Zoo*l. 64: 407-415.

Slater G and Harmon L (2013). Unifying fossils and phylogenies for comparative analyses of diversification and trait evolution. *Methods in Ecology and Evolution*, *4*(8), 699–702.

Slater G, Goldbogen J and Pyenson N (2017). Independent evolution of baleen whale gigantism linked to Plio-Pleistocene ocean dynamics. *Proceedings of the Royal Society B: Biological Sciences*, *284*(1855).

Slater G, Harmon L and Alfaro M (2012). Integrating Fossils With Molecular Phylogenies Improves Inference Of Trait Evolution. *Evolution*, *66*(12), 3931–3944.

Slater G, Price S, Santini F and Alfaro M (2010). Diversity versus disparity and the radiation of modern cetaceans', in *Proceedings of the Royal Society B: Biological Sciences*. 3097–3104.

Slater GJ and Friscia AR. (2019) Hierarchy in adaptive radiation: A case study using the Carnivora (Mammalia). Evolution. 2019;0. pmid:30690704

Smeenk C (1997). Strandings of sperm whales (*Physeter macrocephalus*) in the North Sea: history and patterns. *Bulletin De L'institut Royal Des Sciences Naturelles De Belgique:* 15–28.

Smith B (2002). In *Encyclopaedia of Marine Mammals*, Perrin W, Wursig B, Thewissen J. (eds). Academic Press: San Diego. 1208–1213.

Smith L and Bunje PM (1999) Morphological diversity of inarticulate brachiopods through the Phanerozoic. Palaeobiology 25, 396–408.

Snively E, Fahlke J and Welsh R. (2015). Bone-Breaking Bite Force of *Basilosaurus isis* (Mammalia, Cetacea) from the Late Eocene of Egypt Estimated by Finite Element Analysis. *PLoS ONE*, *10*(2), e0118380.

Soldevilla M, Henderson E, Campbell G, Wiggins S and Hildebrand J (2008). Classification of Risso's and Pacific white-sided dolphins using spectral properties of echolocation clicks. *The Journal of the Acoustical Society of America.*;124(1):609–624.

Sosdian S, Babila T, Greenop R., Foster G and Lear C (2020). Ocean Carbon Storage across the middle Miocene: A new interpretation for the Monterey Event. *Nature Communications,* 11: 134.

Stayton C (2015). The definition, recognition, and interpretation of convergent evolution, and two new measures for quantifying and assessing the significance of convergence. *Evolution*, *69*(8), 2140–2153.

Steeman M, Hebsgaard M, Fordyce R, Ho S, Rabosky D, Nielsen R, Rahbek C, Glenner H, Sørensen M and Willerslev E (2009). Radiation of Extant Cetaceans Driven by Restructuring of the Oceans. *Syst. Biol*, *58*(6), 573–585.

Stevick PT, Allen J, Clapham PJ, Friday N, Katona, SK, Larsen F, Lien J et al., (2003). North Atlantic Humpback Whale Abundance And Rate Of Increase Four Decades After Protection From Whaling. Marine Ecology Progress Series 258:263-273.

Stoett P (1997) The International Politics of Whaling. Vancouver, BC: UBC

Sugimatsu H, Kojima J, Tamaki U and Bahl R (2014) Advanced technique for automatic detection and discrimination of a click train with short interclick intervals from the clicks of Ganges river dolphins (*Platanista gangetica gangetica*) recorded by a passive acoustic monitoring system using hydrophone arrays. *Marine Technology Society Journal. Marine Technology Society Inc,* 48(3): 167–181

Temple J (1992). The progress of quantitative methods in palaeontology. *Palaeontology.* 35:475–484.

Teplitsky C and Millien V (2014). Climate warming and Bergmann's rule through time: is there any evidence? *Evolutionary Applications*, *7*(1), 156–168.

Thewissen J (2014) *The Walking Whales, from Land to Water in Eight Million Years. Berkeley*: University of California Press.

Thewissen J and Bajpai S (2001). The cast of Eocene cetaceans. In *BioScience*, 51: 12.

Thewissen J and Williams E (2002). The Early Radiations Of Cetacea (Mammalia): Evolutionary Pattern and Developmental Correlations. *Annu. Rev. Ecol. Syst*, *33*, 73–90.

Thewissen J, Cooper L, Georges J and Bajpai S (2009). From land to water: the origin of whales, dolphins and porpoises. *Evo Edu Outreach* 2: 272-288.

Thewissen J, Hussain S and Arif M (1994). Fossil Evidence for the Origin of Aquatic Locomotion in Archaeocete Whales. *Science,* 263(5144), 210–212.

Thewissen J, Williams E, Roe L and Hussain S (2001). Skeletons of terrestrial cetaceans and the relationship of whales to artiodactyls. *Nature,* 413(6853): 277.

Thompson P (1990). The bottlenose dolphin. *Trends in Ecology & Evolution*. Edited by Leatherwood S and Reeves R. Elsevier Science. 1990; 5(11): 390.

Thurstan R, Brockington, S and Roberts C (2010). The effects of 118 years of industrial fishing on UK bottom trawl fisheries. *Nature Communications*, *1*(2), 1–6.

Tindall C, Hetherington S, Bell C, Deaville R, Barker J, Borrow K, Oakley M, Bendall V and Engelhard G (Eds) (2019). *Hauling Up Solutions: Reducing Cetacean Bycatch in UK Fisheries*. Final Workshop Report: 31.

Torfstein A, Steinberg J (2020). The Oligo–Miocene closure of the Tethys Ocean and evolution of the proto-Mediterranean Sea. *Sci Rep* 10**,** 13817.

Truchon M, Measures V, L'Hérault  Brêthes J, Galbraith P, Harvey M, Lessard S, Starr M, Lecomte N (2013). Marine Mammal Strandings and Environmental Changes: A 15-Year Study in the St. Lawrence Ecosystem. *PLoS ONE,* 8(3): e59311.

Tsai C and Fordyce R (2015). Ancestor-descendant relationships in evolution: origin of the extant pygmy right whale. *Caperea marginata. Biol Lett.* 11:20140875.

Tsai C and Fordyce R (2018). A new archaic baleen whale, *Toipahautea waitaki* (Early late Oligocene, New Zealand) and the origins of crown mysticeti. *Royal Society Open Science*, *5*(4).

Tulloch V, Plagányi É, Brown C, Richardson A and Matear R. (2019). Future recovery of baleen whales is imperilled by climate change. *Global Change Biology*, *25*(4), 1263–1281.

Turl C (1990) Echolocation abilities of the beluga, A review and comparison with the bottlenose dolphin Tursiops truncatus. Advances in research of the Beluga whale, Delphinapterus leucas.

Turl C and Penner R (1989). Differences in echolocation click patterns of the beluga (*Delphinapterus leucas*) and the bottlenose dolphin (*Tursiops truncatus*)', *Journal of the Acoustical Society of America.* 1989; 86(2):497–502.

Turvey S (2008). *Witness to extinction: How we failed to save the Yangtze River dolphin*. Oxford University Press, Oxford, UK.

Tyler CL and Schneider CL. (2018) An Overview of Conservation Paleobiology. In: Tyler C., Schneider C. (eds) Marine Conservation Paleobiology. Topics in Geobiology, vol 47. Springer, Cham.

Uhen M (2007) Evolution of marine mammals: Back to the sea after 300 million years, The Anatomical Record: Advances in Integrative Anatomy and Evolutionary Biology. John Wiley & Sons, Ltd. 2007; 290(6), p. 514–522.

Uhen M and Pyenson N (2007). Diversity estimates, biases, and historiographic effects: resolving cetacean diversity in the Tertiary. *Palaeontologia Electronica*, *10*(2), 754.

Van Valen L (1973). A new evolutionary law. *Evolutionary Theory* 1:1–30.

Vanselow K, Jacobsen S, Hall C and Garthe S (2018). Solar storms may trigger sperm whale strandings: Explanation approaches for multiple strandings in the North Sea in 2016. *International Journal of Astrobiology*, 17(4): 336-344.

Velez-Juarbe J, Wood A, De Gracia C, Hendy A (2015). Evolutionary patterns among living and fossil kogiid sperm whales: evidence from the Neogene of Central America. *PLoS ONE* 10:e0123909.

Venditti C, Meade A, Pagel M (2011) Multiple routes to mammalian diversity. *Nature* 479: 393–396.

Villagra D, García-Cegarra A., Gallardo D and Pacheco A  (2021) Energetic Effects of Whale-Watching Boats on Humpback Whales on a Breeding Ground. *Frontiers in Marine Science*, *7*, 1208.

Vilstrup J, Ho S, Foote A, Morin P, Kreb D, Krutzen M, Parra G, Robertson K, de Stephanis R, Verborgh P, Willerslev E, Orlando L, Gilbert M (2011) Mitogenomic phylogenetic analyses of the Delphinidae with an emphasis on the Globicephalinae. *BMC Evol Biol.* 2011;11, 65.

Vincent E and Berger W (1985) Carbon dioxide and polar cooling in the Miocene: The Monterey hypothesis, in The Carbon Cycle and Atmospheric CO2: Natural Variations Archean to Present, *Geophys. Monogr. Ser.*, vol. 32, edited by Sundquist E and Broecker W, pp. 455–468.

Voss M, Antar M, Zalmout I and Gingerich P (2019). Stomach contents of the archaeocete Basilosaurus isis: Apex predator in oceans of the late Eocene. *PLOS ONE*, *14*(1), e0209021.

Wake M (1991), 'Morphology, the Study of Form and Function, in Modem Evolutionary Biology', *Oxford Surveys in Evolutionary Biology* 8 289-346.

Walker M, Dennis T and Kirschvink J (2002) The magnetic sense and its use in long-distance navigation by animals. *Current Opinion in Neurobiology*: 735-744

Wall D, O'kelly I, Whooley P and Tyndall P (2009) New records of blue whales (Balaenoptera musculus) with evidence of possible feeding behaviour from the continental shelf slopes to the west of Ireland. *Marine Biodiversity Records*, 2, e128.

Wang L, Lam T, Xu S, Dai Z, Zhou L, Feng T, Guo P, Dunn C, Jones B, Bradley T, Zhu H, Guan Y, Jiang Y, Yu G (2020) "Treeio: an R package for phylogenetic tree input and output with richly annotated and associated data." *Molecular Biology and Evolution,* 37, 599-603.

Watanabe A, Fabre A, Felice R, Maisano J, Müller J, Herrel A and Goswami A (2019) Ecomorphological diversification in squamates from conserved pattern of cranial integration. *National Acad Sciences*, *116*, 14688–14697.

Webster D and Webster M (1974) *Comparative Vertebrate Morphology*: 126-47. New York, London: Academic Press.

Wefer G, Berger W, Bijma J and Fischer G (1999) Clues to Ocean History: a Brief Overview of Proxies. In *Use of Proxies in Paleoceanography* (pp. 1–68).

Weir C, Stockin K and Pierce G (2007) Spatial and temporal trends in the distribution of harbour porpoises, white-beaked dolphins and minke whales off Aberdeenshire (UK), north-western North Sea. J*ournal of the Marine Biological Association of the United Kingdom*, 87(1):327–338.

Werth (2006) Mandibular and dental variation and the evolution of suction feeding in Odontoceti. *J. Mammal.* 2006; 87:579–588.

Werth A (2000a) Feeding in marine mammals; pp. 487-526 in Schwenk, K. (ed.), *Feeding: Form, Function and Evolution in Tetrapods*. Pubisher, San Diego

Werth A (2000b) A kinematic study of suction feeding and associated behavior in the long-finned pilot whale, Globicephala melas. *Mar. Mammal Sci.*16:299–314.

Werth A and Potvin J (2016) Baleen hydrodynamics and morphology of cross-flow filtration in balaenid whale suspension feeding. *PLoS ONE* 11:e0150106.

Westerhold T, Marwan N, Drury A, Liebrand D, Agnini C, Anagnostou E, Barnet J, Bohaty S, De Vleeschouwer D, Florindo F, Frederichs T, Hodell D, Holbourn A, Kroon D, Lauretano V, Littler K, Lourens L, Lyle  M, Pälike H, Röhl U, Tian J, Wilkens R,

Whibley A (2021). Genome insights give cause for optimism in the ongoing battle to save the vaquita. *Molecular Ecology Resources,* 1755-0998.13345.

Whitehead H (1997) Sea surface temperature and the abundance of sperm whale calves off the Galapagos Islands: implications for the effects of global warming. *Report of the International Whaling Commission* 47, 941–944.

Whitehead H, McGill B and Worm B (2008) Diversity of deep-water cetaceans in relation to temperature: implications for ocean warming. *Ecol. Lett.* 11, 1198–1207

Whittaker R (1972). Evolution and Measurement of Species Diversity. *Taxon* 21, 213–251

Williams T, Estes J, Doak D and Springer A (2004). Killer appetites: Assessing the role of predators in ecological communities. *Ecology* 85, 3373–3384.

Willmore K, Klingenberg C and Hallgrímsson B (2005). The relationship between fluctuating asymmetry and environmental variance in rhesus macaque skulls. *Evolution. Society for the Study of Evolution.* 59(4): 898–909.

Wilson P and Zachos J (2020) An astronomically dated record of Earth's climate and its predictability over the last 66 million years, *Science*, 369, 1383–1387.

Wing SL, Bown TM and Obradovich JD. (1991) Geology 19, 1189-1192.

Wölfer J, Amson P, Arnold L, Botton-Divet A, Fabre A, van Heteren H, and Nyakatura J (2019). Femoral morphology of sciuromorph rodents in light of scaling and locomotor ecology. *J. Anat.* 234: 731-747.

Wood S (2011). Fast stable restricted maximum likelihood and marginal likelihood estimation of semiparametric generalized linear models. *Journal of the Royal Statistical Society: Series B (Statistical Methodology),* 73(1):3–36.

Wood S (2017). *Generalized Additive Models: An Introduction with R. CRC Texts in Statistical Science* (2nd edn).

Woodruff F and Savin SM (1991). Mid-Miocene iso- tope stratigraphy in the deep sea: high resolution correlations, paleoclimatic cycles, and sediment preservation, Paleoceanography, 6, 755-806, 1991.

Xie W, Lewis P, Fan Y, Kuo L and Chen M (2011). Improving marginal likelihood estimation for bayesian phylogenetic model selection. *Syst. Biol.* 60:150–160.

Yamada T, Kitamura S, Abe S, Tajima Y, Matsuda A, Mead J, Matsuishi T (2019). Description of a new species of beaked whale (*Berardius*) found in the North Pacific. *Sci Rep* 9. 2019; 12723.

Yang Z (2006). *Computational Molecular Evolution.* Oxford University Press: Oxford.

Yoder J, Clancey E, Des Roches S, Eastman J, Gentry L, Godsoe W, Hagey T, Jochimsen J, Oswald B, Robertson J, Sarver B, Schenk J, Spear S and Harmon L (2010). Ecological opportunity and the origin of adaptive radiations. *J. Evol. Biol.* 23: 1581– 1596.

You Y, Huber M, Müller R, Poulsen C and Ribbe J (2009). Simulation of the Middle Miocene Climate Optimum. *Geophysical Research Letters*, *36*(4), L04702.

Zachos J, Dickens G and Zeebe R (2008). An early Cenozoic perspective on greenhouse warming and carbon-cycle dynamics. *Nature* 451, 279–283.

Zachos J, Pagani M, Sloan L, Thomas E, Billups K (2001). Trends, rhythms, and aberrations in global climate 65 Ma to present, *Science,* 2001, 292: 686-693)

Zelditch M, Swiderski D and Sheets H (2012). *Geometric Morphometrics for Biologists: A Primer* (2nd edn). Academic Press: 488.

Zelditch M, Swiderski D, Sheets H, and Fin W (2004). *Geometric morphometrics for biologists: a primer*. Elsevier, Amsterdam:44.

# Appendices

Please note, **there is no appendix to accompany Chapter 1, Introduction**. Every other appendix accompanies the chapter with the same number.

# Table of Figures – Appendix

# Table of Tables - Appendix

Appendix 2

# Chapter 2 Appendix

[Table on next page]

**Table S2.1.** List of specimens used in the study. *Denotes terrestrial artiodactyls. Data on the specimen and ID, species, suborder, family, and geologic age are given. +Name in brackets denotes genus name given in phylogeny.

| | Specimen | Species | Group | Family | Geologic age |
|---|---|---|---|---|---|
| 1 | *Aegyptocetus tarfa* MSNTUP I-15459 | *Aegyptocetus tarfa* | Archaeocete | Protocetidae | Eocene |
| 2 | *Aetiocetus cotylalveus* USNM 25210 | *Aetiocetus cotylalveus* | Mysticete | Aetiocetidae | Oligocene |
| 3 | *Aetiocetus weltoni* UCMP 122900 | *Aetiocetus weltoni* | Mysticete | Aetiocetidae | Oligocene |
| 4 | *Aglaocetus patulus* USNM 23690 | *Aglaocetus patulus* | Mysticete | Aglaocetidae | Miocene |
| 5 | *Aglaocetus moreni* FMNH P13407 | *Aglaocetus moreni* | Mysticete | Aglaocetidae | Miocene |
| 6 | Agorophiid *sp* USNM 205491 | Agorophiid *sp* | Odontocete | Agorophiidae | Oligocene |
| 7 | *Albertocetus* ChM PV8680 | *Albertocetus sp* | Odontocete | Xenorophidae | Oligocene |
| 8 | *Albireo whistleri* UCR 14589 | *Albireo whistleri* | Odontocete | Albireonidae | Miocene |
| 9 | *Ambulocetus natans* MSNUP I-16826 | *Ambulocetus natans* | Archaeocete | Ambulocetidae | Eocene |
| 10 | *Argyrocetus joaquinensis* USNM 11996 | *Argyrocetus joaquinensis* | Odontocete | Unclear | Miocene |
| 11 | *Artiocetus clavis* GSP-UM 3458 | *Artiocetus clavis* | Archaeocete | Protocetidae | Eocene |
| 12 | *Atocetus iquensis* MNHN.F.PPI. 113 | *Atocetus iquensis* | Odontocete | Delphinida | Miocene |
| 13 | *Aulophyseter morricei* UCMP 81661 | *Aulophyseter morricei* | Odontocete | Physeteridae | Miocene |
| 14 | *Balaena mysticetus* NHMUK 1986.1.16 | *Balaena mysticetus* | Mysticete | Balaenidae | Extant |
| 15 | *Balaenoptera acutorostrata* NHMUK 1965.11.2.1 | *Balaenoptera acutorostrata* | Mysticete | Balaenopteridae | Extant |
| 16 | *Balaenoptera borealis* NHMUK 1934.5.25.1 | *Balaenoptera borealis* | Mysticete | Balaenopteridae | Extant |
| 17 | *Balaenoptera brydei* USNM 572922 | *Balaenoptera brydei* | Mysticete | Balaenopteridae | Extant |
| 18 | *Balaenoptera sp* SDNHM 83695 | *Balaenoptera sp* | Mysticete | Balaenopteridae | Pliocene |
| 19 | *Balaenoptera edeni* NHMUK 1920.12.31.1 | *Balaenoptera edeni* | Mysticete | Balaenopteridae | Extant |
| 20 | *Balaenoptera floridana* USNM 529244 | *Balaenoptera floridana* | Mysticete | Balaenopteridae | Pliocene |
| 21 | *Balaenoptera musculus* NHMUK 1892.3.1.1 | *Balaenoptera musculus* | Mysticete | Balaenopteridae | Extant |
| 22 | *Balaenoptera omurai* NN – data: https://www.cityu.edu.hk/lib/about/event/tk_brown/ | *Balaenoptera omurai* | Mysticete | Balaenopteridae | Extant |
| 23 | *Balaenoptera physalus* NHMUK 1862.2.7.181 | *Balaenoptera physalus* | Mysticete | Balaenopteridae | Extant |
| 24 | Balaenopteridae NMNZ MM001630 | *Balaenopteridae* | Mysticete | Balaenopteridae | Miocene |
| 25 | *Balaenula astensis* MSNUP I-12555 | *Balaenula astensis* | Mysticete | Balaenidae | Pliocene |
| 26 | *Basilosaurus isis* SMNS 11787 | *Basilosaurus isis* | Archaeocete | Basilosauridae | Eocene |
| 27 | *Berardius arnuxii* NHMUK 1935.10.23.1 | *Berardius arnuxii* | Odontocete | Ziphiidae | Extant |
| 28 | *Berardius bairdii* NHMUK 1954.9.21.1 | *Berardius bairdii* | Odontocete | Ziphiidae | Extant |
| 29 | *Berardius minimus* USNM 276366 | *Berardius bairdii* | Odontocete | Ziphiidae | Extant |
| 30 | \**Bos sp* NHMUK 1981.984 | *Bos sp* | Terrestrial artiodactyl | Bovidae | Extant |
| 31 | *Brachydelphis mazeasi* MNHN.F.PPI. 266 | *Brachydelphis mazeasi* | Odontocete | Pontoporiidae | Miocene |
| 32 | \**Camelus dromedarius* NHMUK NN | *Camelus dromedarius* | Terrestrial artiodactyl | Camelidae | Extant |
| 33 | *Caperea marginata* NHMUK 1876.2.16.1 | *Caperea marginata* | Mysticete | Cetotheriidae | Extant |
| 34 | \**Capricornis sumatrensis* NHMUK 24.5.29.1 | *Capricornis sumatrensis* | Terrestrial artiodactyl | Bovidae | Extant |
| 35 | *Cephalorhynchus commersonii* USNM 252568 | *Cephalorhynchus commersonii* | Odontocete | Delphinidae | Extant |
| 36 | *Cephalorhynchus eutropia* NHMUK 1881.8.17.1 | *Cephalorhynchus eutropia* | Odontocete | Delphinidae | Extant |
| 37 | *Cephalorhynchus heavisidii* NHMUK 1948.7.27.1 | *Cephalorhynchus heavisidii* | Odontocete | Delphinidae | Extant |
| 38 | *Cephalorhynchus hectori maui* NMNZ MM002607 | *Cephalorhynchus hectori maui* | Odontocete | Delphinidae | Extant |

| 39 | *Cephalorhynchus hectori* NMNZ MM002288 | *Cephalorhynchus hectori* | Odontocete | Delphinidae | Extant |
|----|------|------|------|------|------|
| 40 | \**Cervus elaphus* NHMUK 2005.16 | *Cervus elaphus* | Terrestrial artiodactyl | Cervidae | Extant |
| 41 | \**Choeropsis liberiensis* NHMUK 1967.3.20.1 | *Choeropsis liberiensis* | Terrestrial artiodactyl | Hippopotamidae | Extant |
| 42 | *Chonecetus goedertorum* LACM 131146 (⁺*Fucaia*) | *Chonecetus goedertorum* | Mysticete | Aetiocetidae | Oligocene |
| 43 | *Coronodon havensteini* CCNHM 108 | *Coronodon havensteini* | Mysticete | Aetiocetidae | Oligocene |
| 44 | *Cotylocara macei* CCNHM 101 | *Cotylocara macei* | Odontocete | Xenorophidae | Oligocene |
| 45 | *Delphinapterus leucas* USNM 305071 | *Delphinapterus leucas* | Odontocete | Monodontidae | Extant |
| 46 | *Delphinus capensis* NHMUK 1981.7.11 | *Delphinus capensis* | Odontocete | Delphinidae | Extant |
| 47 | *Delphinus delphis* AMNH 75332 | *Delphinus delphis* | Odontocete | Delphinidae | Extant |
| 48 | *Diorocetus hiatus* USNM 16783 | *Diorocetus hiatus* | Mysticete | Pelocetidae | Miocene |
| 49 | *Dorudon atrox* PV M 100149 cast | *Dorudon atrox* | Archaeocete | Basilosauridae | Eocene |
| 50 | *Echovenator sandersi* GSM 1098 | *Echovenator sandersi* | Odontocete | Xenorophidae | Oligocene |
| 51 | *Etruridelphis sp* MGPT PU 13884 | *Etruridelphis sp* | Odontocete | Delphinidae | Pliocene |
| 52 | *Eubalaena australis* NHMUK 1873.3.3 | *Eubalaena australis* | Mysticete | Balaenidae | Extant |
| 53 | *Eubalaena glacialis* MSNUP NN | *Eubalaena glacialis* | Mysticete | Balaenidae | Extant |
| 54 | Eurhinodelphinidae UCMP 99669 | *Eurhinodelphinidae* | Odontocete | Eurhinodelphinidae | Miocene |
| 55 | *Eurhinodelphis longirostris* USNM 244404 | *Eurhinodelphis longirostris* | Odontocete | Eurhinodelphinidae | Miocene |
| 56 | *Feresa attenuata* USNM 504916 | *Feresa attenuata* | Odontocete | Delphinidae | Extant |
| 57 | \**Giraffa camelopardalis* NHMUK NN | *Giraffa camelopardalis* | Terrestrial artiodactyl | Giraffidae | Extant |
| 58 | *Globicephala sp* USNM 21867 | *Globicephala sp* | Odontocete | Delphinidae | Pleistocene |
| 59 | *Globicephala macrorhynchus* NHMUK 1912.10.27 | *Globicephala macrorhynchus* | Odontocete | Delphinidae | Extant |
| 60 | *Globicephala melas* NMNZ MM001946 | *Globicephala melas* | Odontocete | Delphinidae | Extant |
| 61 | *Grampus griseus* USNM 571602 | *Grampus griseus* | Odontocete | Delphinidae | Extant |
| 62 | *Hemisyntrachelus cortesii* MBGPT NN cast | *Hemisyntrachelus cortesii* | Odontocete | Delphinidae | Pliocene |
| 63 | *Herpetocetus bramblei* UCMP 219111 | *Herpetocetus bramblei* | Mysticete | Cetotheriidae | Pliocene |
| 64 | *Herpetocetus sendaicus* NMNS-PV 19540 cast | *Herpetocetus sendaicus* | Mysticete | Cetotheriidae | Pliocene |
| 65 | \**Hydropotes inemis* NHMUK 1551c | *Hydropotes inemis* | Terrestrial artiodactyl | Cervidae | Extant |
| 66 | *Hyperoodon ampullatus* NHMUK 1992.42 | *Hyperoodon ampullatus* | Odontocete | Ziphiidae | Extant |
| 67 | *Hyperoodon planifrons* NHMUK 1952.9.30.1 | *Hyperoodon planifrons* | Odontocete | Ziphiidae | Extant |
| 68 | *Indopacetus pacificus* USNM 593534 | *Indopacetus pacificus* | Odontocete | Ziphiidae | Extant |
| 69 | *Inia geoffrensis* AMNH 93415 | *Inia geoffrensis* | Odontocete | Iniidae | Extant |
| 70 | *Janjucetus hunderi* NMV P216929 | *Janjucetus hunderi* | Mysticete | Mammalodontidae | Oligocene |
| 71 | *Kampholophus serrulus* UMCP 36045 | *Kampholophus serrulus* | Odontocete | Kentriodontidae | Miocene |
| 72 | *Kekenodon sp* OU 22294 | *Kekenodon sp* | Archaeocete | Kekenodontidae | Oligocene |
| 73 | *Kentriodon pernix* USNM 10670 | *Kentriodon pernix* | Odontocete | Kentriodontidae | Miocene |
| 74 | *Kentriodon sp* NN | *Kentriodon sp* | Odontocete | Kentriodontidae | Miocene |
| 75 | *Kogia breviceps* USNM 22015 | *Kogia breviceps* | Odontocete | Kogiidae | Extant |
| 76 | *Kogia simus* NHMUK.1952.8.28.1 | *Kogia simus* | Odontocete | Kogiidae | Extant |
| 77 | *Lagenodelphis hosei* USNM 571619 | *Lagenodelphis hosei* | Odontocete | Delphinidae | Extant |
| 78 | *Lagenorhynchus acutus* USNM 504196 (⁺*Leucopleurus*) | *Lagenorhynchus acutus* | Odontocete | Delphinidae | Extant |

| | | | | | |
|---|---|---|---|---|---|
| | | (*Leucopleurus*) | | | |
| 79 | *Lagenorhynchus albirostris* AMNH 37162 | *Lagenorhynchus albirostris* | Odontocete | Delphinidae | Extant |
| 80 | *Lagenorhynchus australis* 1944.11.30.1 (*Sagmatias*) | *Lagenorhynchus australis* (*Sagmatias*) | Odontocete | Delphinidae | Extant |
| 81 | *Lagenorhynchus cruciger* NHMUK 1960.8.24.1 (*Sagmatias*) | *Lagenorhynchus cruciger* (*Sagmatias*) | Odontocete | Delphinidae | Extant |
| 82 | *Lagenorhynchus obliquidens* NHMUK 1992.83 | *Lagenorhynchus obliquidens* | Odontocete | Delphinidae | Extant |
| 83 | *Lagenorhynchus obscurus* NHMUK 1846.3.11.8 (*Sagmatias*) | *Lagenorhynchus obscurus* (*Sagmatias*) | Odontocete | Delphinidae | Extant |
| 84 | *Lipotes vexillifer* AMNH 57333 | *Lipotes vexillifer* | Odontocete | Lipotidae | Extant |
| 85 | *Lissodelphis borealis* USNM 550188 | *Lissodelphis borealis* | Odontocete | Delphinidae | Extant |
| 86 | *Lissodelphis peronii* NMNZ MM002116 | *Lissodelphis peronii* | Odontocete | Delphinidae | Extant |
| 87 | *Lomacetus ginsburgi* MNHN.F.PPI.104 | *Lomacetus ginsburgi* | Odontocete | Phocoenidae | Miocene |
| 88 | *Megaptera novaeangliae* GERM.792a (NHMUK) | *Megaptera novaeangliae* | Mysticete | Balaenopteridae | Extant |
| 89 | *Mesoplodon bidens* USNM 593438 | *Mesoplodon bidens* | Odontocete | Ziphiidae | Extant |
| 90 | *Mesoplodon bowdoini* NMNZ MM001900 | *Mesoplodon bowdoini* | Odontocete | Ziphiidae | Extant |
| 91 | *Mesoplodon carlhubbsi* USNM 504128 | *Mesoplodon carlhubbsi* | Odontocete | Ziphiidae | Extant |
| 92 | *Mesoplodon europaeus* USNM 571665 | *Mesoplodon europaeus* | Odontocete | Ziphiidae | Extant |
| 93 | *Mesoplodon ginkgodens* USNM 298237 | *Mesoplodon ginkgodens* | Odontocete | Ziphiidae | Extant |
| 94 | *Mesoplodon grayi* USNM 49880 | *Mesoplodon grayi* | Odontocete | Ziphiidae | Extant |
| 95 | *Mesoplodon hectori* NHMUK 1949.8.19.1 | *Mesoplodon hectori* | Odontocete | Ziphiidae | Extant |
| 96 | *Mesoplodon hotaula* USNM 593426 | *Mesoplodon hotaula* | Odontocete | Ziphiidae | Extant |
| 97 | *Mesoplodon layardii* USNM 550150 | *Mesoplodon layardii* | Odontocete | Ziphiidae | Extant |
| 98 | *Mesoplodon mirus* USNM 504612 | *Mesoplodon mirus* | Odontocete | Ziphiidae | Extant |
| 99 | *Mesoplodon peruvianus* USNM 571258 | *Mesoplodon peruvianus* | Odontocete | Ziphiidae | Extant |
| 100 | *Mesoplodon stejnegeri* USNM 504330 | *Mesoplodon stejnegeri* | Odontocete | Ziphiidae | Extant |
| 101 | *Mesoplodon traversii (juvenile)* NMNZ TMP012996 | *Mesoplodon traversii (juvenile)* | Odontocete | Ziphiidae | Extant |
| 102 | *Messapicetus longirostris* MSNUP NN | *Messapicetus longirostris* | Odontocete | Ziphiidae | Miocene |
| 103 | *Miocaperea pulchra* SMNS 46978 | *Miocaperea pulchra* | Mysticete | Cetotheriidae | Miocene |
| 104 | *Mixocetus sp* LACM 143474 | *Mixocetus sp* | Mysticete | Tranatocetidae | Miocene |
| 105 | *Monodon monoceros* USNM 267959 | *Monodon monoceros* | Odontocete | Monodontidae | Extant |
| 106 | *Neophocaena asiaeorientalis* USNM 240001 | *Neophocaena asiaeorientalis* | Odontocete | Phocoenidae | Extant |
| 107 | *Neophocaena phocaenoides* NHMUK 1903.9.12.3 | *Neophocaena phocaenoides* | Odontocete | Phocoenidae | Extant |
| 108 | *Notocetus vanbenedeni* MLP 55 | *Notocetus vanbenedeni* | Odontocete | Squalodelphinidae | Miocene |
| 109 | *Odobenocetops peruvianus* SMNK PAL 2491 | *Odobenocetops peruvianus* | Odontocete | Odobenocetopsidae | Pliocene |
| 110 | *Orcaella brevirostris* NHMUK.1883.11.20.2 | *Orcaella brevirostris* | Odontocete | Delphinidae | Extant |
| 111 | *Orcaella heinsohni* USNM 284430 | *Orcaella heinsohni* | Odontocete | Delphinidae | Extant |
| 112 | *Orcinus orca* USNM 11980 | *Orcinus orca* | Odontocete | Delphinidae | Extant |
| 113 | *Orycterocetus crocodilinus* USNM 22926 | *Orycterocetus crocodilinus* | Odontocete | Physeteridae | Miocene |
| 114 | *Pakicetus attocki* PV M 100148 cast | *Pakicetus attocki* | Archaeocete | Pakicetidae | Eocene |

| 115 | *Papahu taitapu* OU 22066 | *Papahu taitapu* | Odontocete | Waipatiidae | Miocene |
|---|---|---|---|---|---|
| 116 | *Parapontoporia sternbergi* SDNHM  75060 | *Parapontoporia sternbergi* | Odontocete | Lipotidae | Pliocene |
| 117 | *Parietobalaena palmeri* USNM 24883 | *Parietobalaena palmeri* | Mysticete | Pelocetidae | Miocene |
| 118 | Patriocetid *sp* new genus ChM PV4753 | Patriocetid | Odontocete | Patriocetidae | Oligocene |
| 119 | *Patriocetus ehrlichii* OL1999-3 Cet. 4 | *Patriocetus ehrlichii* | Odontocete | Patriocetidae | Oligocene |
| 120 | *Patriocetus sp* MB Ma. 42882 | *Patriocetus sp* | Odontocete | Patriocetidae | Oligocene |
| 121 | *Pelocetus calvertensis* USNM 11976 | *Pelocetus calvertensis* | Mysticete | Pelocetidae | Miocene |
| 122 | *Peponocephala electra* USNM 504511 | *Peponocephala electra* | Odontocete | Delphinidae | Extant |
| 123 | *Phocoena dioptrica* NHMUK 1939.9.30.1 | *Phocoena dioptrica* | Odontocete | Phocoenidae | Extant |
| 124 | *Phocoena phocoena* AMNH 212161 | *Phocoena phocoena* | Odontocete | Phocoenidae | Extant |
| 125 | *Phocoena sinus* SDNHM 20697 | *Phocoena sinus* | Odontocete | Phocoenidae | Extant |
| 126 | *Phocoena spinipinnis* NHMUK 1900.5.7.29 | *Phocoena spinipinnis* | Odontocete | Phocoenidae | Extant |
| 127 | *Phocoenoides dalli* USNM 276062 | *Phocoenoides dalli* | Odontocete | Phocoenidae | Extant |
| 128 | *Physeter macrocephalus* NHMUK 2007.1 | *Physeter macrocephalus* | Odontocete | Physeteridae | Extant |
| 129 | *Piscobalaena nana* MNHN 1618 cast | *Piscobalaena nana* | Mysticete | Cetotheriidae | Miocene |
| 130 | *Piscolithax longirostris* SAS 933 | *Piscolithax longirostris* | Odontocete | Phocoenidae | Miocene |
| 131 | *Platanista gangetica* USNM 172409 | *Platanista gangetica* | Odontocete | Platanistidae | Extant |
| 132 | *Pliopontos littoralis* SAS 193 | *Pliopontos littoralis* | Odontocete | Pontoporiidae | Pliocene |
| 133 | *Pontoporia blainvillei* USNM 482727 | *Pontoporia blainvillei* | Odontocete | Pontoporiidae | Extant |
| 134 | *Prosqualodon davidis* USNM 467596 | *Prosqualodon davidis* | Odontocete | Prosqualodontidae | Oligocene |
| 135 | *Protocetus atavus* SMNS 11084 | *Protocetus atavus* | Archaeocete | Protocetidae | Eocene |
| 136 | *Pseudorca crassidens* USNM 11320 | *Pseudorca crassidens* | Odontocete | Delphinidae | Extant |
| 137 | *Remingtonocetus harudiensis* USNM PAL 559313 | *Remingtonocetus harudiensis* | Archaeocete | Remingtonocetidae | Eocene |
| 138 | *\*Saiga tatarica* NHMUK 1961.5.30.1 | *Saiga tatarica* | Terrestrial artiodactyl | Bovidae | Extant |
| 139 | *Schizodelphis barnesi* MNHN AMN 19 | *Schizodelphis barnesi* | Odontocete | Eurhinodelphinidae | Miocene |
| 140 | *Schizodelphis morckhoviensis* USNM 13873 | *Schizodelphis morckhoviensis* | Odontocete | Eurhinodelphinidae | Miocene |
| 141 | *Schizodelphis sp* CCNHM 141 | *Schizodelphis sp* | Odontocete | Eurhinodelphinidae | Miocene |
| 142 | *Semirostrum cerutti*  SDNHM  65276 | *Semirostrum cerutti* | Odontocete | Phocoenidae | Pliocene |
| 143 | *Septemtriocetus bosselaersi* IRSNB M.1928 | *Septemtriocetus bosselaersi* | Odontocete | Phocoenidae | Pliocene |
| 144 | *Shark tooth Squalodon sp* OU 21798 | *Squalodon sp* | Odontocete | Squalodontidae | Oligocene |
| 145 | *Simocetus rayi* USNM 256517 | *Simocetus rayi* | Odontocete | Simocetidae | Oligocene |
| 146 | *Sotalia guianensis* USNM 571558 | *Sotalia guianensis* | Odontocete | Delphinidae | Extant |
| 147 | *Sousa chinensis* NHMUK 1992.97 | *Sousa chinensis* | Odontocete | Delphinidae | Extant |
| 148 | *Sousa plumbea* USNM 550941 | *Sousa plumbea* | Odontocete | Delphinidae | Extant |
| 149 | *Sousa sahulensis* NHMUK 1992.92 | *Sousa sahulensis* | Odontocete | Delphinidae | Extant |
| 150 | *Sousa teuszii* NHMUK 1992.138 | *Sousa teuszii* | Odontocete | Delphinidae | Extant |
| 151 | *Squalodon bariensis* IRSNB 2372 | *Squalodon bariensis* | Odontocete | Squalodontidae | Miocene |
| 152 | *Squalodon calvertensis* NMNZ MM001996 | *Squalodon calvertensis* | Odontocete | Squalodontidae | Miocene |
| 153 | *Stenella attenuata* NHMUK 1966.11.18.5 | *Stenella attenuata* | Odontocete | Delphinidae | Extant |
| 154 | *Stenella longirostris* USNM 395270 | *Stenella longirostris* | Odontocete | Delphinidae | Extant |
| 155 | *Steno bredanensis* USNM 572789 | *Steno bredanensis* | Odontocete | Delphinidae | Extant |

| 156 | *Tagicetus joneti* IRSNB M. 1892 | *Tagicetus joneti* | Odontocete | Delphinida | Miocene |
|-----|-----|-----|-----|-----|-----|
| 157 | *Tasmacetus shepherdi* USNM 484878 | *Tasmacetus shepherdi* | Odontocete | Ziphiidae | Extant |
| 158 | *\*Tayassu pecari labiatus* NHMUK 47.4.6.8 | *Tayassu pecari labiatus* | Terrestrial artiodactyl | Tayassuidae | Extant |
| 159 | *Tiucetus rosae* MNHN.F. PPI261 | *Tiucetus rosae* | Mysticete | Cetotheriidae | Miocene |
| 160 | *\*Tragulus kanchil* NHMUK 9.1.5.850 | *Tragulus kanchil* | Terrestrial artiodactyl | Tragulidae | Extant |
| 161 | *Tursiops aduncus* NHMUK 1882.1.2.3 | *Tursiops aduncus* | Odontocete | Delphinidae | Extant |
| 162 | *Tursiops truncatus* SDNHM 23798 | *Tursiops truncatus* | Odontocete | Delphinidae | Extant |
| 163 | *Waipatia maerewhenua* OU 22095 | *Waipatia maerewhenua* | Odontocete | Waipatiidae | Oligocene |
| 164 | *Xenorophus sp* ChM PV4823 | *Xenorophus sp* | Odontocete | Xenorophidae | Oligocene |
| 165 | *Xenorophus sp* Yap CCNHM 168 | *Xenorophus sp* | Odontocete | Xenorophidae | Oligocene |
| 166 | *Xiphiacetus bossi* USNM 8842 | *Xiphiacetus bossi* | Odontocete | Eurhinodelphinidae | Miocene |
| 167 | *Xiphiacetus cristatus* USNM 21363 | *Xiphiacetus cristatus* | Odontocete | Eurhinodelphinidae | Miocene |
| 168 | *Zarhachis flagellator* USNM 10911 | *Zarhachis flagellator* | Odontocete | Platanistidae | Miocene |
| 169 | *Zarhinocetus donnamatsonae* UCMP 86139 | *Zarhinocetus* | Odontocete | Allodelphinidae | Miocene |
| 170 | *Zarhinocetus errabundus* LACM 149588 | *Zarhinocetus* | Odontocete | Allodelphinidae | Miocene |
| 171 | *Ziphius cavirostris* NHMUK 2006.15 | *Ziphius cavirostris* | Odontocete | Ziphiidae | Extant |
| 172 | *Zygorhiza kochii* USNM 11962 | *Zygorhiza kochii* | Archaeocete | Basilosauridae | Eocene |

[Table on next page]

**Table S2.2.** 123 landmarks added to the entire surface of the skull. Landmarks highlighted in red were placed on the midline. Landmarks 1-66 (with 38, 40, 48, 49, 51, 54, 55, 56, 61 on the midline) were placed on the LHS, landmarks 67-123 were placed on the RHS.

| Landmark description | Number on LHS of the skull | Number on RHS of the skull |
|---|---|---|
| Nasal anterior | 1 | 120 |
| Left anterior lateral nasal | 2 | 67 |
| Posterior lateral corner of nasal | 3 | 68 |
| Posterior point of nasal | 4 | 121 |
| Tip of rostrum, anterior dorsal side, anterior midline of tooth row (usually premaxilla) | 5 | 69 |
| Anterior dorsal premaxilla | 6 | 70 |
| Posterior dorsal premaxilla | 7 | 71 |
| Anterior lateral ventral premaxilla | 8 | 72 |
| Anterior lateral ventral maxilla | 9 | 73 |
| Dorsal medial maxilla (suture with nasal and premaxilla) | 10 | 74 |
| Nasal-frontal-maxilla suture (posterior medial maxilla) | 11 | 75 |
| Dorsal posterior maxilla on orbit (including lacrimal - dorsal suture frontal) on orbit | 12 | 76 |
| Jugal maxilla orbit suture - front orbit lateral | 13 | 77 |
| Posterior ventral lateral most point of maxilla – tooth row - Jugal-maxilla ventral suture | 14 | 78 |
| Posterior tooth row lateral maxilla or lateral maxilla in species with no/negligible dentition | 15 | 79 |
| Jugal anterior dorsal | 16 | 80 |
| Jugal anterior ventral | 17 | 81 |
| Jugal posterior ventral | 18 | 82 |
| Anterior medial frontal | 19 | 122 |
| Posterior medial frontal | 20 | 123 |
| Lateral posterior frontal (posterior lateral parietal suture) | 21 | 83 |
| Postorbital process/bar tip (anterior on crest) | 22 | 84 |
| Anterior lateral frontal (on orbit) | 23 | 85 |
| Anterior dorsal corner of frontal (on orbit) | 24 | 86 |
| Anterior medial parietal | 25 | 87 |
| Posterior medial parietal | 26 | 88 |
| Posterior lateral parietal (squamosal/occipital suture) | 27 | 89 |
| Anterior lateral parietal (on vault) | 28 | 90 |
| Dorsal anterior lateral parietal (suture with frontal) | 29 | 91 |
| Dorsal anterior squamosal suture (with parietal, maybe alisphenoid/frontal) | 30 | 92 |
| Medial anterior zygomatic vault junction (squamosal) | 31 | 93 |
| Anterior dorsal jugal-squamosal suture | 32 | 94 |
| Posterior ventral jugal-squamosal suture, lateral | 33 | 95 |
| Anterior medial most point of the mandibular articular process. | 34 | 96 |
| Posterior lateral most point of the mandibular articular process | 35 | 97 |

| | | |
|---|---|---|
| Lateral posterior squamosal (occipital suture) | 36 | 98 |
| Posterior medial dorsal squamosal (parietal/occipital suture) | 37 | 99 |
| **MIDLINE:** posterior margin of skull roof | *38* | *38* |
| Medial anterior supraoccipital (parietal-occipital suture, usually) | 39 | 100 |
| **MIDLINE:** dorsal/superior margin of foramen magnum | *40* | *40* |
| Dorsal medial occipital condyle | 41 | 101 |
| Dorsal lateral occipital condyle | 42 | 102 |
| Tip of paraoccipital process - lateral tip | 43 | 103 |
| Lateral ventral occipital + process | 44 | 104 |
| Lateral dorsal occipital | 45 | 105 |
| Ventral medial occipital condyle | 46 | 106 |
| Ventral lateral occipital condyle | 47 | 107 |
| **MIDLINE:** ventral margin of foramen magnum | *48* | *48* |
| **MIDLINE:** anterior basioccipital | *49* | *49* |
| Lateral anterior basioccipital | 50 | 108 |
| **MIDLINE:** anterior most point of basisphenoid, just posterior to the pterygoids and palate | *51* | *51* |
| Lateral anterior basisphenoid | 52 | 109 |
| Lateral posterior basisphenoid | 53 | 110 |
| **MIDLINE:** Medial posterior basisphenoid | *54* | *54* |
| **MIDLINE:** Posterior ventral medial point of palate | *55* | *55* |
| **MIDLINE:** Palatine anterior midline ventral suture | *56* | *56* |
| Pal-pterygoid suture | 57 | 111 |
| Pal-max lateral posterior suture | 58 | 112 |
| Pterygoid posterior | 59 | 113 |
| Ventral posterior pterygoid | 60 | 114 |
| **MIDLINE:** Maxilla ventral midline posterior suture | *61* | *61* |
| Maxilla ventral midline anterior suture | 62 | 115 |
| Maxilla anterior lateral ventral | 63 | 116 |
| Premaxilla ventral midline posterior suture | 64 | 117 |
| **MIDLINE:** Anterior-most point of palatal surface immediately posterior to tooth row | 65 | 118 |
| Premaxilla posterior lateral ventral | 66 | 119 |

**Table S2.3.** Skulls scanned but excluded from analysis. Specimens were excluded for being too distorted, too heavily reconstructed or because of the unsure placement of them in the phylogeny.

| Species | Specimen number |
|---|---|
| Patriocetid or Waipatiid | CCNHM 1078 |
| *Pomatodelphis sp* | USNM 187414 |
| Waipatiid new gen | ChM PV7679 |
| *Xenorophus sp* | ChM PV7677 |



a.                                    b.                                    c.
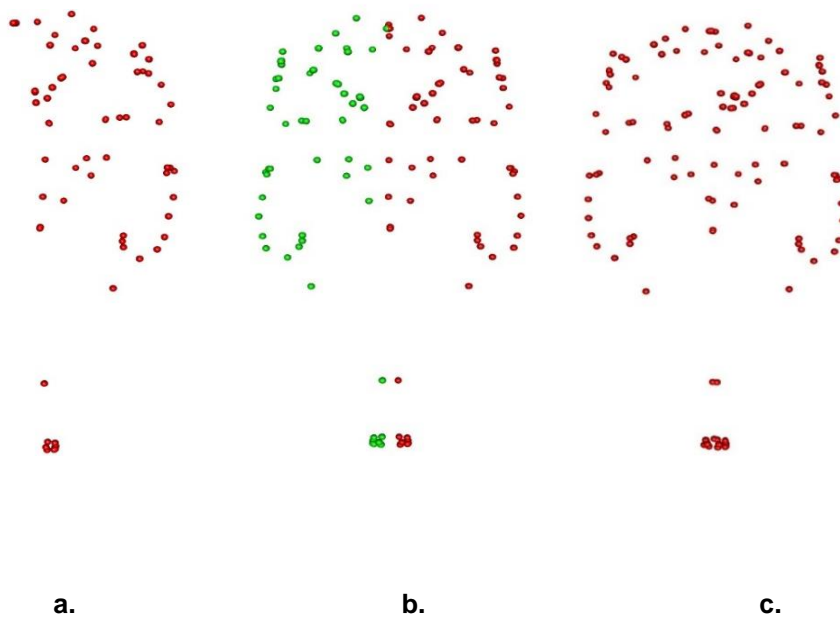
**Fig. S2.1.** The landmark configuration. (a) manually placed landmarks on half of the skull to be mirrored to the other half of the skull, (b) the inaccurate computer mirrored landmarks, and (c) the correct manually placed landmarks. Note the differences between the positioning of landmarks b. and c. Shown on the skull of *Delphinapterus leucas* USNM 305071.

a.                                              b.
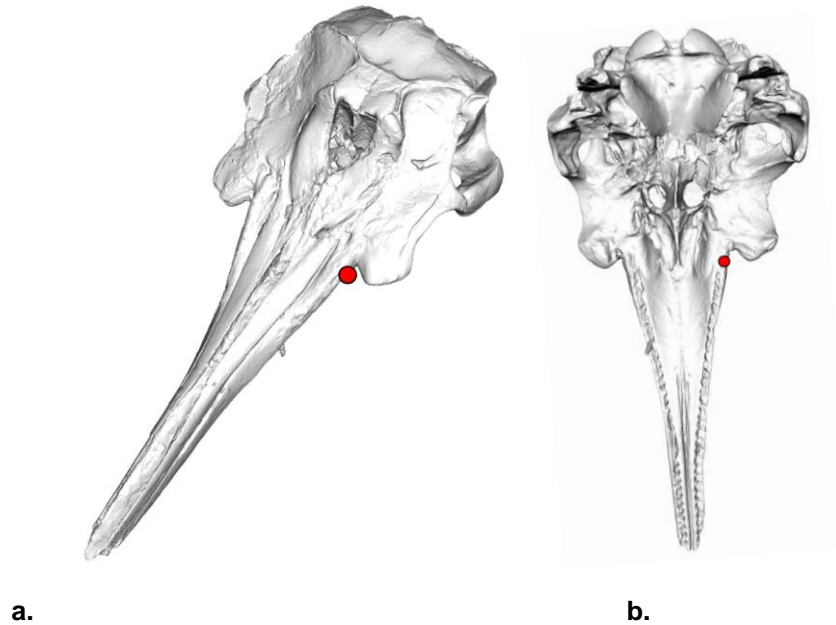
**Fig. S2.2.** The position of landmark 15. This landmark is mirrored as landmark 79: Posterior tooth row lateral maxilla or lateral maxilla in specimens with no/negligible dentition. This positioning is used for all specimens including those that lack a true tooth row with mandibular prognathism, absent, maxillary-only, or vestigial dentition (including Ziphiids, narwhals (*Monodon monoceros*) and sperm whales (*Physeter macrocephalus*)). Landmarks are shown on *Kentriodon pernix* (USNM 10670) (which has a visible tooth row) in an oblique (a) and ventral (b) view. Not to scale.

**Exclusion of the rostrum**

In the archaeocetes, 4 of the top 5 landmarks of variation are found in the rostrum. In the mysticetes, the rostrum, and landmarks on the anterior lateral ventral of the maxilla, and the premaxilla ventral midline posterior suture (both located on the rostrum) make up 6 of the 10 top highest landmarks of variation. In odontocetes, rostral landmarks accounted for 2 of the 10 highest landmarks of variation, and therefore removing them had the lowest impact for this group. These models were designed as sensitivity analyses to assess the impact of the rostrum on the overall skull asymmetry. Excluding the rostral landmarks had no effect on the ordering of the model fits), i.e., the ranking of the models by AIC weights **(Table S2.4b** - Akaike information criterion (AIC) rankings for each evolutionary model for asymmetry in the cetacean cranium) nor on the trait **(Fig. S2.3** - Asymmetry in the cetacean skull with

rostrum removed). Therefore, we ran all our remaining analyses on the whole data set with the rostrum included. Rostral landmarks were landmarks: 5, 6, 8, 9, 62, 63, 64, 65, 66, 69, 70, 72, 73, 115, 116, 117, 118, 119 (see **Table S2.2** -123 landmarks added to the entire surface of the skull) for details.

**Table S2.4.** Akaike information criterion (AIC) rankings for each evolutionary model for asymmetry in the cetacean cranium. The models were a classic Brownian Motion model (BM), a BM model with a selective regime (BMM), a BM model with a selective regime and an independent trend (BMMtr), a BM model with a selective regime which estimates separate phylogenetic means (BMMsm), a classic BM model with no selective regime and which estimates separate phylogenetic means (BMsm), a classic Ornstein-Ulenbeck (OU) model, and an OU model with a selective regime (OUM). a) with all landmarks b) with rostral landmarks removed c) with a phylogeny that includes only taxa that appear in a character matrix Lloyd and Slater (2020).

a)

| Model | Rank | AIC | Diff |
|---|---|---|---|
| OUM-regime | 1 | -448 | 0.00 |
| OUM-regime-split | 2 | -445 | 3.48 |
| OUM-echo-freq | 3 | -403 | 45.04 |
| OUM-ancestral | 4 | -379 | 69.66 |
| OUM-echo | 5 | -373 | 75.02 |
| BMM-echo | 6 | -372 | 75.99 |
| BMMtr-echo | 7 | -371 | 77.51 |
| BMMsm-echo | 8 | -367 | 81.08 |
| BMMsm-echo-freq | 9 | -343 | 105.82 |
| OU-ancestral | 10 | -342 | 106.55 |
| BMM-echo-freq | 11 | -323 | 124.96 |
| BMMtr-echo-freq | 12 | -322 | 126.13 |
| BMMsm-regime | 13 | -295 | 152.94 |
| BMMsm-regime-split | 14 | -294 | 154.17 |
| BMMtr-ancestral | 15 | -286 | 162.63 |
| BMM-ancestral | 16 | -285 | 163.57 |
| BMM-regime | 17 | -284 | 164.41 |
| BMM-regime-split | 18 | -283 | 165.55 |
| BMMtr-regime | 19 | -282 | 166.33 |
| BMMsm-ancestral | 20 | -282 | 166.71 |
| BMMtr-regime-split | 21 | -280 | 168.23 |
| BM-ancestral | 22 | -275 | 172.87 |
| BMtr-ancestral | 23 | -273 | 175.22 |
| BMsm-ancestral | 24 | -272 | 176.73 |

b)

| Model | Rank | AIC | Diff |
|---|---|---|---|
| OUM-regime | 1 | -498 | 0 |
| OUM-regime-split | 2 | -496 | 2.75 |
| OUM-echo-freq | 3 | -449 | 48.94 |
| OUM-ancestral | 4 | -424 | 74.7 |
| OUM-echo | 5 | -422 | 76.75 |
| BMM-echo | 6 | -402 | 96.02 |
| BMMtr-echo | 7 | -396 | 102.86 |
| BMMsm-echo | 8 | -394 | 104.47 |
| BMMsm-echo-freq | 9 | -391 | 107.78 |
| OU-ancestral | 10 | -390 | 108.08 |
| BMM-echo-freq | 11 | -380 | 117.99 |
| BMMtr-echo-freq | 12 | -379 | 119.26 |
| BMMsm-regime | 13 | -357 | 141.54 |
| BMMsm-regime-split | 14 | -356 | 142.39 |
| BMMtr-ancestral | 15 | -348 | 150.6 |
| BMM-ancestral | 16 | -346 | 151.89 |
| BMM-regime | 17 | -346 | 152.6 |
| BMM-regime-split | 18 | -345 | 153.8 |
| BMMtr-regime | 19 | -344 | 154.4 |
| BMMsm-ancestral | 20 | -344 | 154.81 |
| BMMtr-regime-split | 21 | -342 | 156.4 |
| BM-ancestral | 22 | -341 | 156.92 |
| BMtr-ancestral | 23 | -341 | 156.6 |
| BMsm-ancestral | 24 | -338 | 160.83 |

c)

| Model | Rank | AIC | diff |
|---|---|---|---|
| OUM-regime | 1 | -383 | 0 |
| OUM-regime-split | 2 | -380 | 3.41 |
| OUM-echo-freq | 3 | -354 | 29.07 |
| OUM-ancestral | 4 | -329 | 54.22 |
| OUM-echo | 5 | -323 | 60.2 |
| BMM-echo | 6 | -304 | 79 |
| BMMtr-echo | 7 | -302 | 80.72 |
| BMMsm-echo | 8 | -300 | 83.3 |
| OU-ancestral | 9 | -292 | 91.36 |
| BMM-echo-freq | 10 | -269 | 113.84 |
| BMMtr-echo-freq | 11 | -267 | 115.76 |
| BMMsm-echo-freq | 12 | -266 | 116.84 |
| BMMsm-echo-freq | 13 | -228 | 155.43 |
| BMMsm-regime | 14 | -227 | 156.07 |
| BMM-ancestral | 15 | -221 | 162.32 |
| BMMtr-ancestral | 16 | -219 | 164.03 |
| BMM-regime | 17 | -219 | 164.08 |
| BMMtr-regime | 18 | -217 | 165.92 |
| BMMsm-regime | 19 | -217 | 166 |
| BMM-regime-split | 20 | -217 | 166.57 |
| BMMtr-regime-split | 21 | -215 | 168.53 |
| BM-ancestral | 22 | -208 | 175.58 |
| BMtr-ancestral | 23 | -206 | 177.46 |
| BMsm-ancestral | 24 | -204 | 179.45 |

[Figure on previous page]

**Fig. S2.3.** Asymmetry in the cetacean skull with the rostrum removed. Time-calibrated phylogeny adapted from Lloyd and Slater (2020) for sampled cetacean species with branches showing the level of asymmetry ($\sum p_{spec}$) after rostral landmarks have been removed. The trait value is the sum of Euclidean distances between the computer mirrored landmark and the manually placed landmark. The larger the value for $\Sigma p_{spec}$, the more the landmarks have been displaced, indicating asymmetry between the two sides of the cranium.

[Figure on previous page]

**Fig. S2.4.** Reconstructed probability of shifts in cetacean cranial asymmetry ($\sum p_{spec}$) with the rostrum removed. Reconstructed probability along each branch of the phylogeny under the assumption of relaxed Brownian Motion with a Half-Cauchy distribution for the prior density of the rate scalar. Circles indicate a shift in the trait on either the branch or in the whole clade. The colour of the circle indicates the shift direction with red indicating forward shifts and blue indicating backwards shifts. The size of the circle indicates the probability of the shift occurring in that position in the clade with the largest circle (here, 0.875) indicating the highest probability of a shift occurring. The colour of the branch itself indicates posterior rates for that branch with red showing higher, increasing rates and blue showing lower, decreasing rates. The background rate is shown as grey. Phylogeny based on Lloyd and Slater (2020).
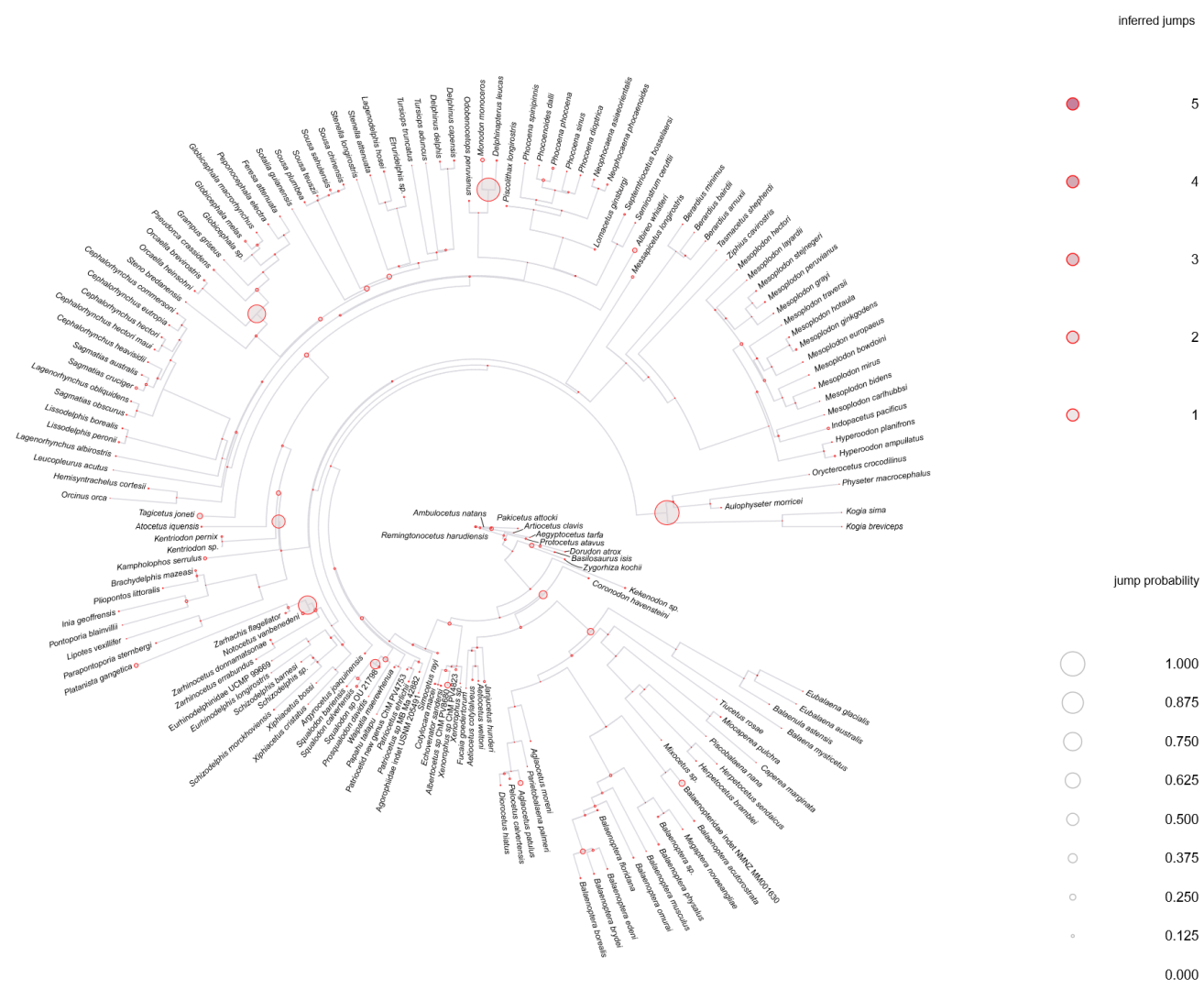
[Figure on previous page]

**Fig. S2.5.** Reconstructed jumps in the rate of cetacean cranial asymmetry ($\sum p_{spec}$) with the rostrum removed. The model also predicts the number of jumps which may have occurred. The size of the circle indicates the probability of the jump occurring there. The colour of the circle indicates the number of inferred jumps, where dark red = 5 and pale red = 1. Phylogeny based on Lloyd and Slater (2020).

**Fig. S2.6.** Asymmetry in the cetacean skull shown using a phylogeny that includes only taxa that appear in a character matrix. Adapted from Lloyd and Slater (2020). Phylogeny for sampled cetacean species with branches showing the level of asymmetry ($\sum p_{spec}$). The trait value is the sum of Euclidean distances between the computer mirrored landmark and the manually placed landmark. The larger the value for ($\sum p_{spec}$), the more the landmarks have been displaced, indicating asymmetry between the two sides of the cranium. The full complement of landmarks was used.

shift direction

1.00
0.80
0.50
0.20
0.00
−0.20
−0.50
−0.80
−1.00

posterior rates

0.00248
0.00120
0.00058
0.00028
0.00014
0.00007
0.00003
0.00002
0.00001

shift probability

1.000
0.875
0.750
0.625
0.500
0.375
0.250
0.125
0.000
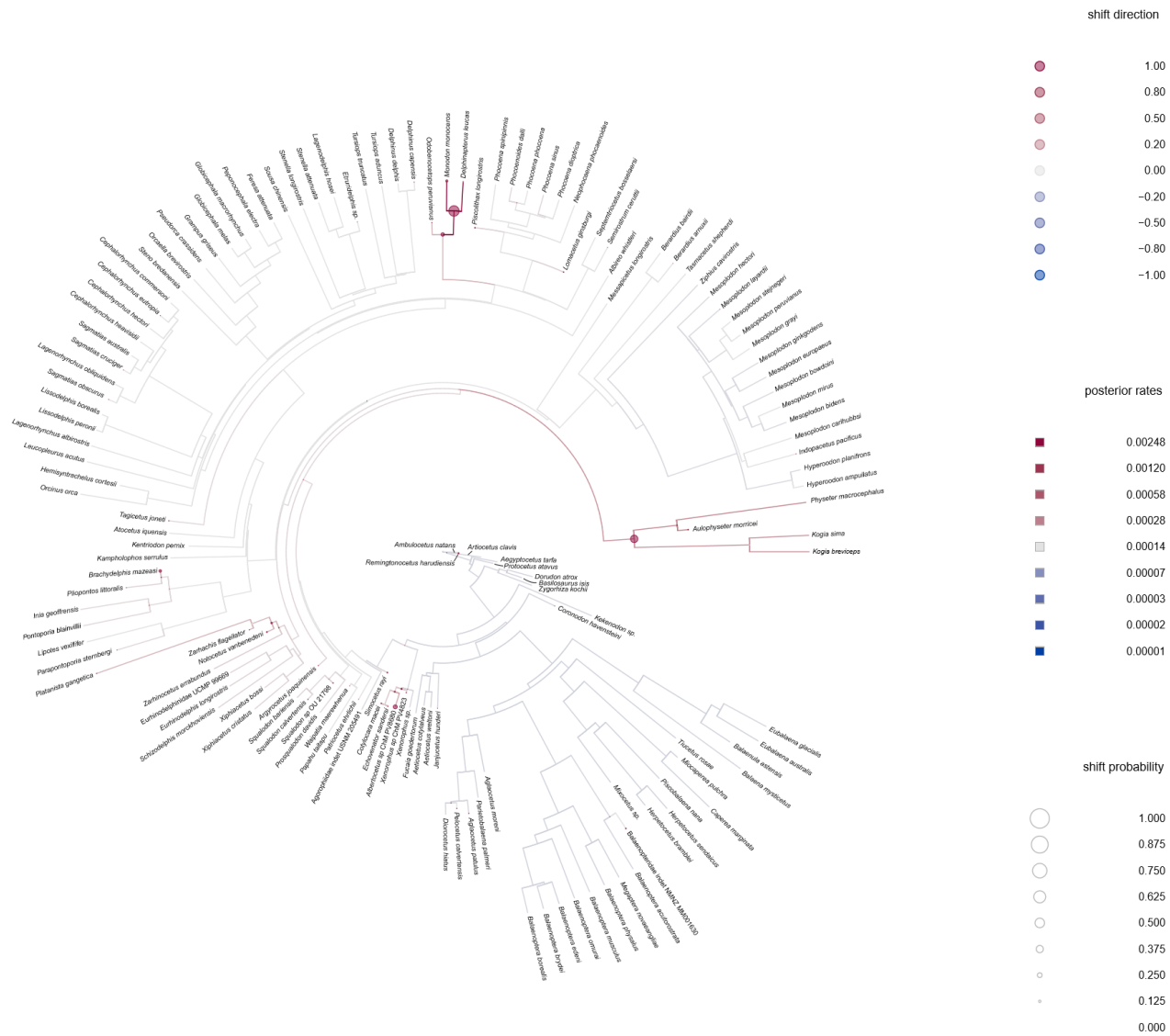
[Figure on previous page]

**Fig. S2.7**. Reconstructed probability of shifts in cetacean cranial asymmetry ($\sum p_{spec}$) using a phylogeny that includes only taxa that appear in a character matrix. Adapted from Lloyd and Slater (2020). Probability of shifts are shown along each branch of the phylogeny under the assumption of relaxed Brownian Motion with a Half-Cauchy distribution for the prior density of the rate scalar. Circles indicate a shift in the trait on either the branch or in the whole clade. The colour of the circle indicates the shift direction with red indicating forward shifts and blue indicating backwards shifts. The size of the circle indicates the probability of the shift occurring in that position in the clade with the largest circle (here, ~0.500) indicating the highest probability of a shift occurring. The colour of the branch itself indicates posterior rates for that branch with red showing higher, increasing rates and blue showing lower, decreasing rates. The background rate is shown as grey. Phylogeny based on Lloyd and Slater (2020). Full complement of landmarks used.
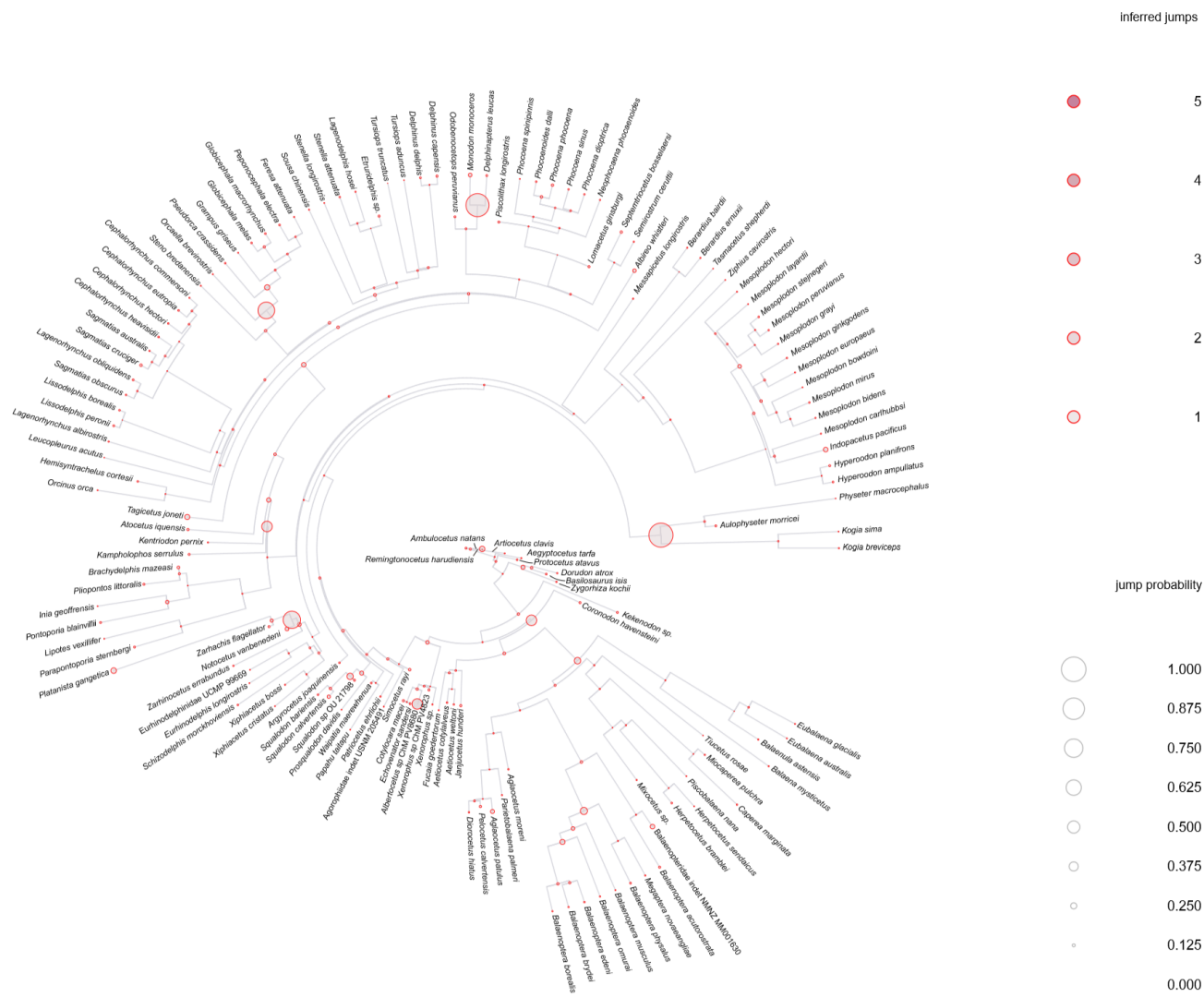
[Figure on previous page]

**Fig. S2.8.** Reconstructed jumps in the rate of cetacean cranial asymmetry ($\sum p_{\text{spec}}$) using a phylogeny that includes only taxa that appear in a character matrix. Adapted from Lloyd and Slater (2020). The model also predicts the number of jumps which may have occurred. The size of the circle indicates the probability of the jump occurring there. The colour of the circle indicates the number of inferred jumps, where dark red = 5 and pale red = 1. Full complement of landmarks used.

## Model diagnostics

We ran diagnostics on our two proposals to test their robustness. We assessed the trace of the variable (chain) for each of the models to ensure that burn-in had completed (we used the default value of 0.25 for the burn-in). The trace of the shifts (Fig.S2.9; S2.10) shows that the burn-in occurred long before 25% of the iterations had run, we therefore know that the default value is a safe assumption to use. We then assessed the trace to check that the MCMC sampler mixed well (i.e., it remains stationary after an initial burn-in) (Fig. S2.13). The same chain was obtained when the model was run with 5^6 iterations, and a sampling frequency of 5,000, as well as with different starting values. If the runs had not converged, longer MCMC chains would have been run. We also checked the effective sample size (ESS) using the 'coda' package in R (Plummer et al., 2006). This looks at the effective sample size for controlling the mean when the sample size has been adjusted for autocorrelation. Here the ES values for each model were all much higher than 100-200 (the generally accepted lower value of the standard error (SE), root, and likelihood value for each chain). See the supplemental information for the ES values of these two chains. We can also see the point (where the chains roughly converge) on the Gelman plot **(Fig. S2.13** - Gelman diagnostics for the two chains). We then used Gelman and Rubin's convergence diagnostics (Gelman and Rubin, 1992; Gelman, 2006) to get the scale reduction factor for each parameter. For these chains the point estimate for the potential scale reduction was 1, and the associated upper confidence limit was 1.01. Generally, values below 1.1 are accepted as a 'good' fit.
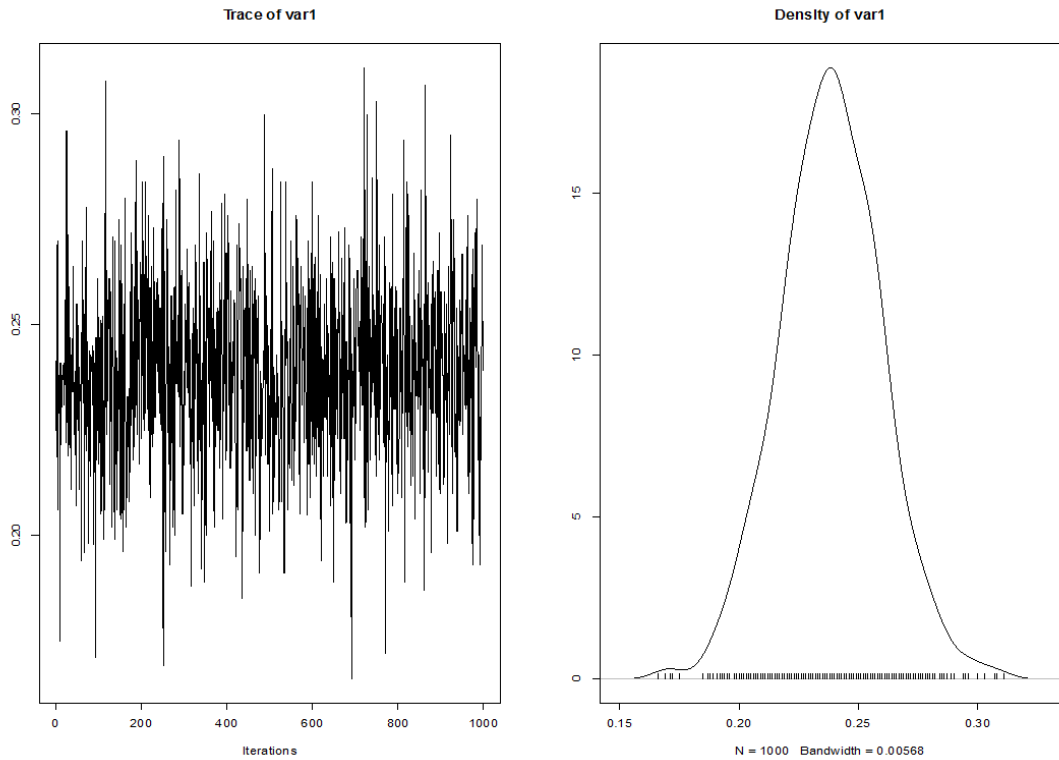
**Fig. S2.9.** Trace of the chain for model 1. The plot on the left, the trace plot shows the values the parameter took during the runtime of the chain (1000 iterations). The plot on the right, the density var plot (or marginal density plot) is the (smoothened) histogram of the values in the trace-plot, i.e., the distribution of the values of the parameter in the chain. Note the similarities between the models (Fig. S2.10 - Trace of the chain for model 2).
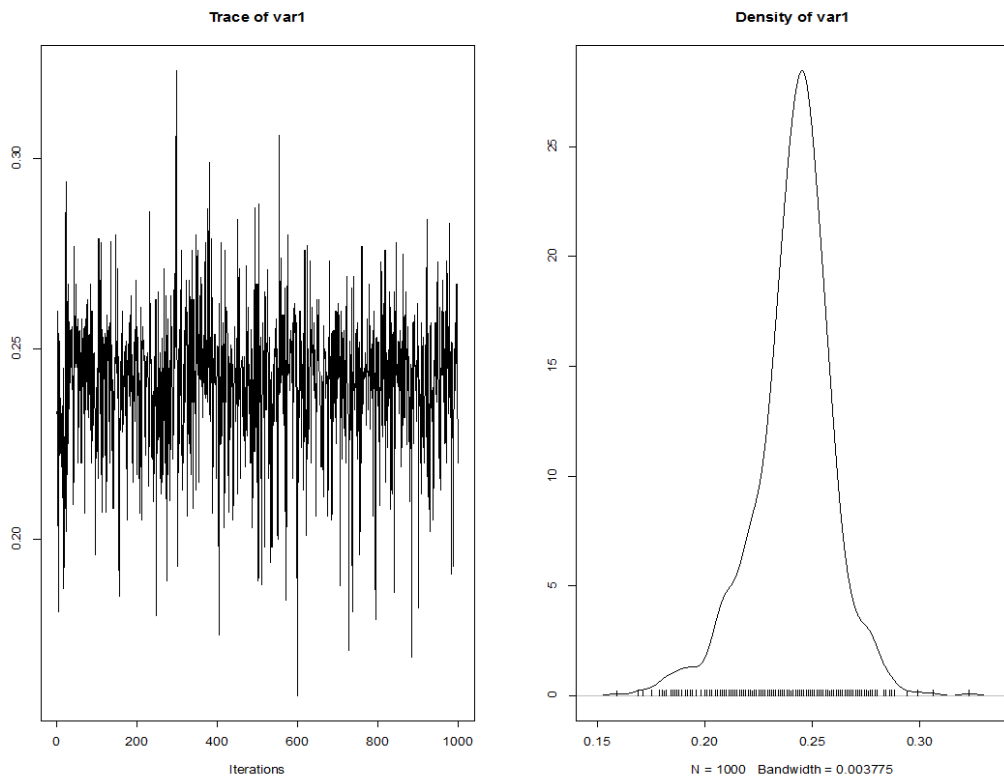
**Fig. S2.10.** Trace of the chain for model 2. The plot on the left, the trace plot shows the values the parameter took during the runtime of the chain (1000 iterations). The plot on the right, the density var plot (or marginal density plot) is the (smoothened) histogram of the values in the trace-plot, i.e., the distribution of the values of the parameter in the chain. Note the similarities between the models (Fig. S2.9 - Trace of the chain for model 1).

380

Trace of shifts

Density of shifts

Trace of jumps

Density of jumps

Trace of jumpvar

Density of jumpvar

Trace of min

Density of min

Trace of max

Density of max

Trace of median

Density of median
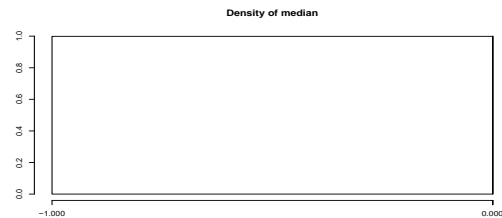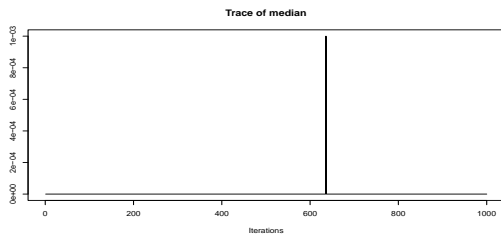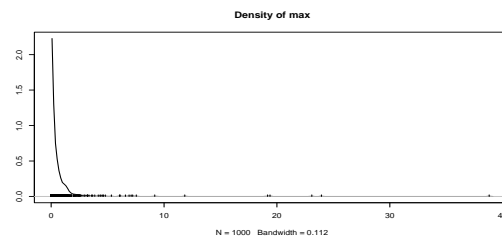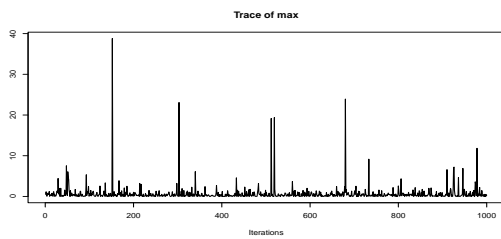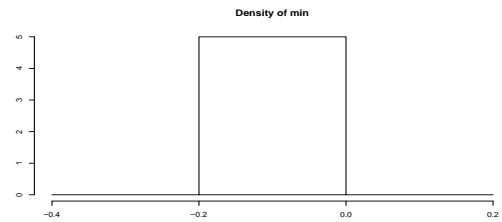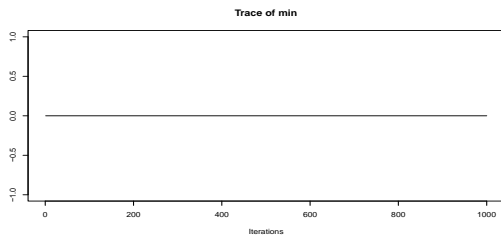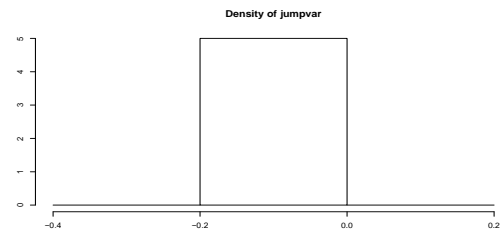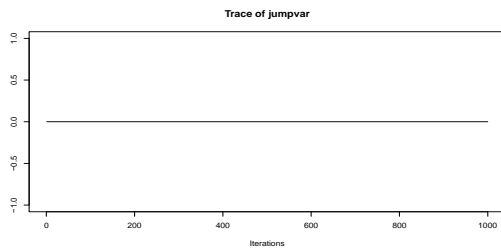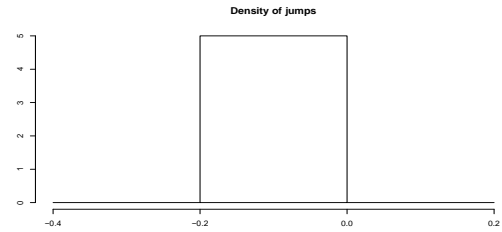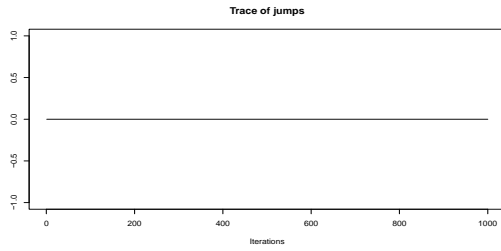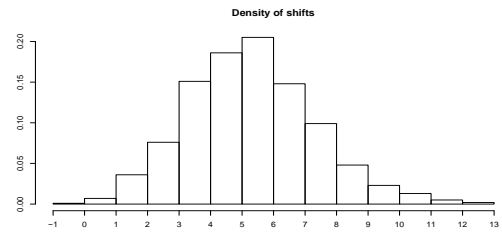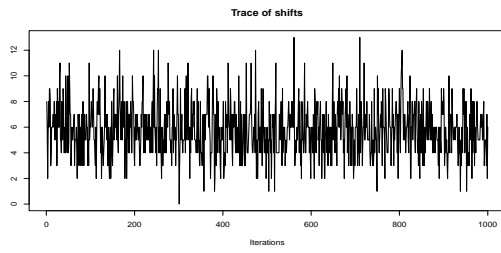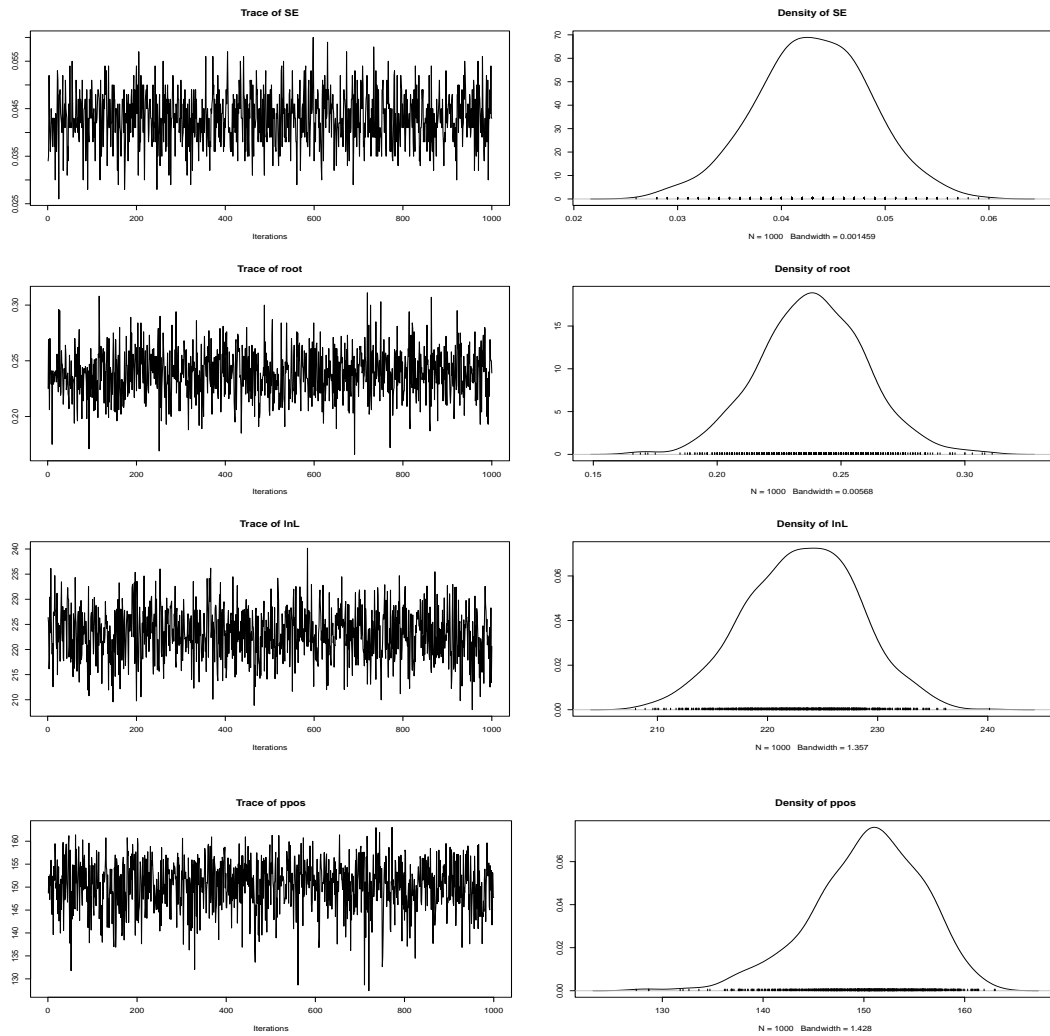
**Fig. S2.11.** Further model diagnostics for chain 1. Visualisation of results in Table S2.5 - Effective size (ES) for estimating the mean for each of the chains 1 and 2. The trace plots (left hand column) shows the values the parameter took during the runtime of the chain (1000 iterations). Note the early burn-in and then stabilisation of the chain before 250 iterations (25%). The density plots (right hand column) (or marginal density plots) are the (smoothened) histogram of the values in the trace-plot, i.e., the distribution of the values of the parameter in the chain.
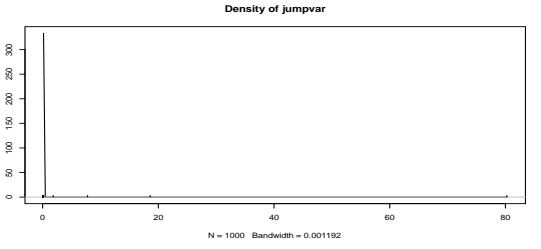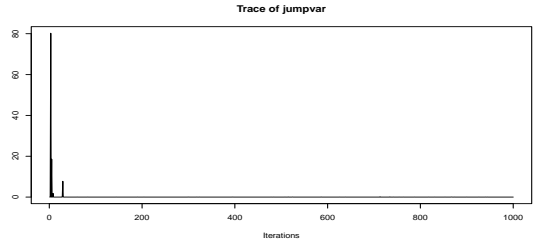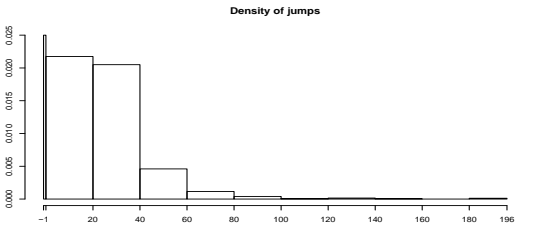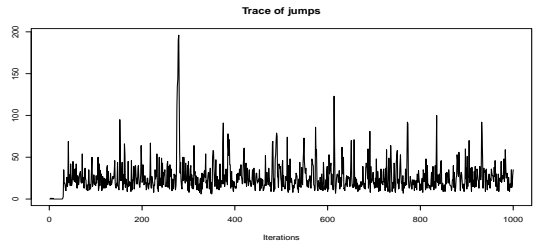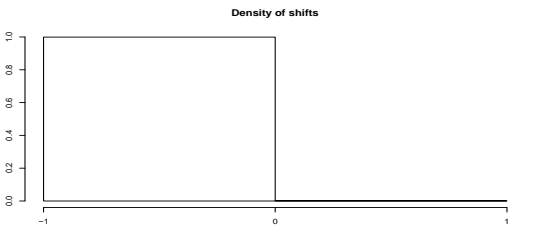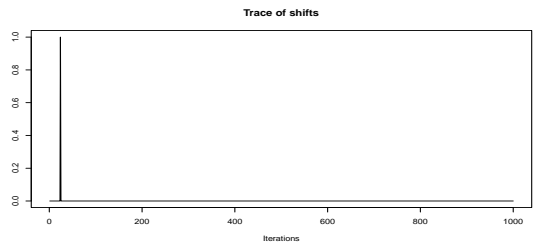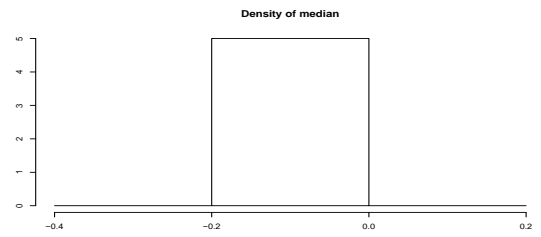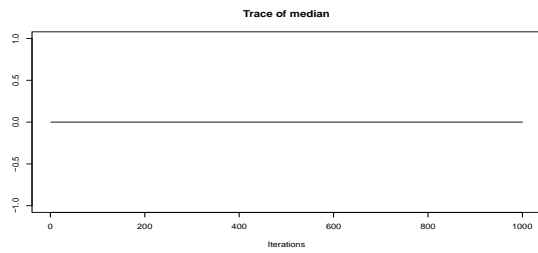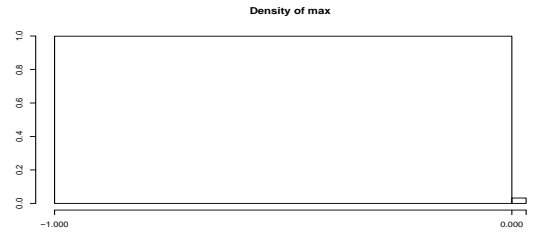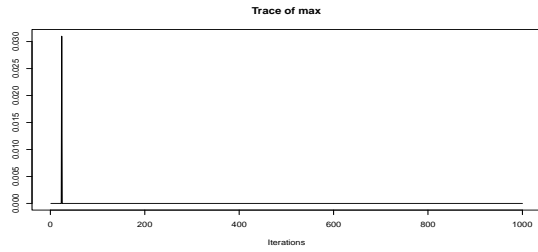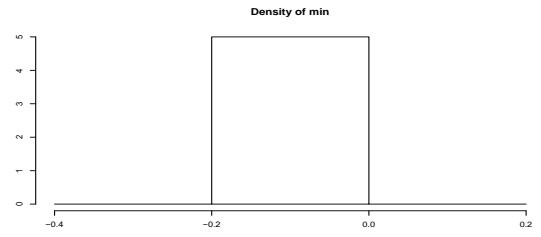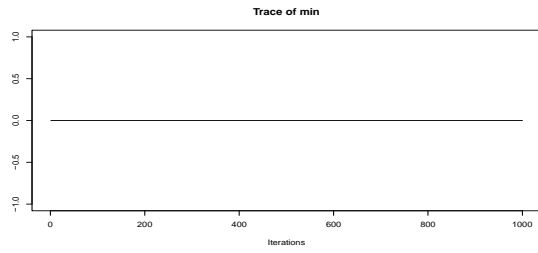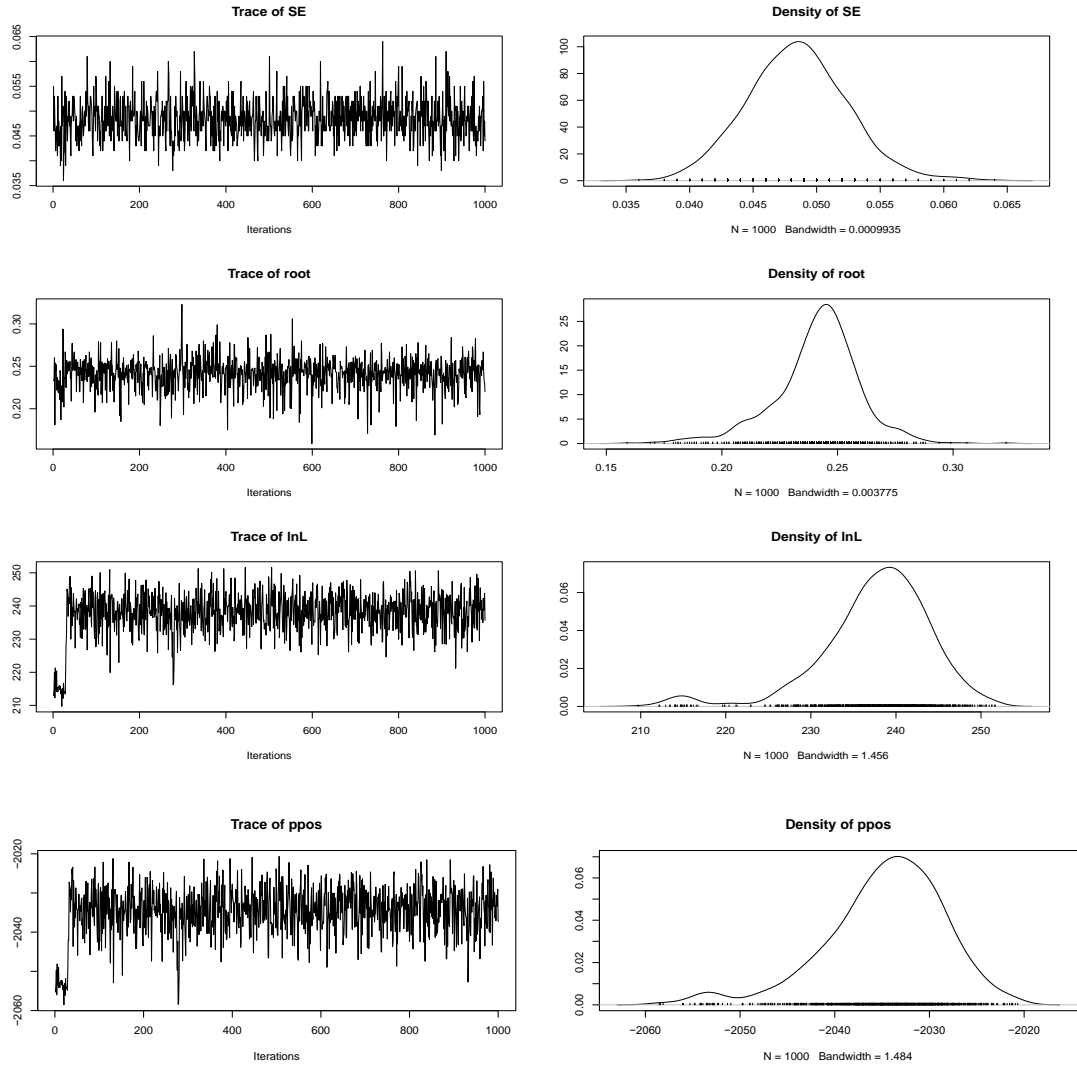
**Fig. S2.12.** Further model diagnostics for chain 2. Visualisation of results in Table S2.5 - Effective size (ES) for estimating the mean for each of the chains 1 and 2. The trace plots (left hand column) shows the values the parameter took during the runtime of the chain (1000 iterations). Note the early burn-in and then stabilisation of the chain before 250 iterations (25%). The density plots (right hand column) (or marginal density plots) are the (smoothened) histogram of the values in the trace-plot, i.e., the distribution of the values of the parameter in the chain.

**Table S2.5.** Effective size (ES) for estimating the mean for each of the chains 1 and 2. Chains used in our main model (model 1) and in an alternate model (named model 2, chain 2 here). Using the `effectiveSize` function in the R package 'coda' (Plummer et al., 2006) to look at the sample size adjusted for autocorrelation. Here the ES values for each model were all higher than 100-200 (the generally accepted lower value of the standard error (SE), root, and likelihood value for each chain). There are no jumps, and therefore `jumps.var` is zero in chain 1 (Model 1). Outputs are visualised in Fig. S2.9 - Trace of the chain for model 1 and Fig. S2.10 - Trace of the chain for model 2.

Chain 1

| min | max | median | shifts | jumps | jumpvar | SE | root | InL | ppos |
|---|---|---|---|---|---|---|---|---|---|
| 0.0000 | 1000.0000 | 1000.0000 | 760.4919 | 0.0000 | 0.0000 | 848.8171 | 1000.000 | 903.8943 | 1000.0000 |

Chain 2

| min | max | median | shifts | jumps | jumpvar | SE | root | InL | ppos |
|---|---|---|---|---|---|---|---|---|---|
| 0.0000 | 0.0000 | 0.0000 | 0.0000 | 298.48390 | 645.49524 | 863.92187 | 1000.00000 | 80.65584 | 125.28040 |

a)



b)
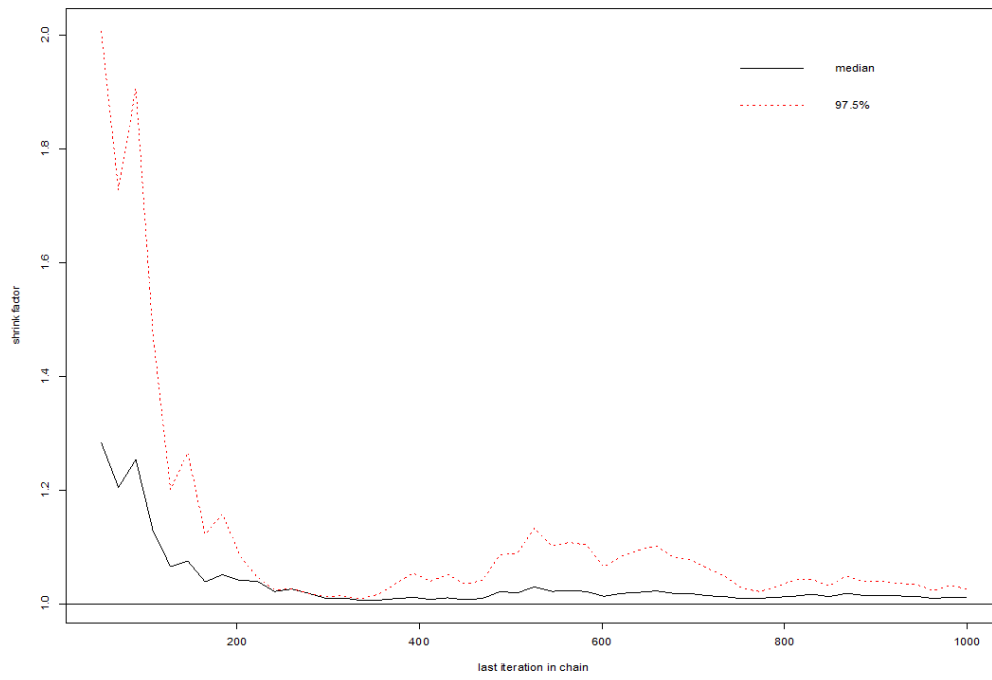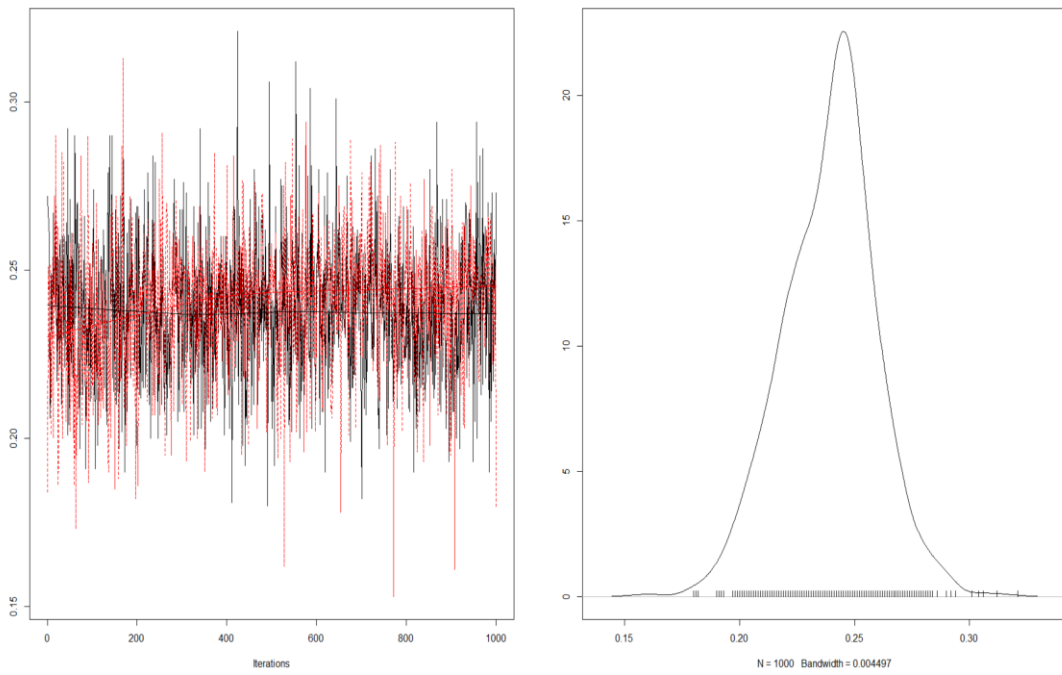
[Figure on previous page]

**Fig. S2.13.** Gelman diagnostics for the two chains. a) The evolution of the shrink factor (Gelman and Rubin, 1992; Gelman, 2006) as the number of iterations increases. The `gelman.diag` gives you the scale reduction factors for each parameter. Approximate convergence is diagnosed when the upper limit is close to 1. A factor of 1 means that between variance and within chain variance are equal. Larger values mean that there is still a notable difference between chains. A value of 1.1 or below is generally accepted. The confidence limits assume that the variable is normal. This plot was run as a diagnostic based on our chains which had 10^6 iterations. The plot shows the development of the scale-reduction over time (chain steps). This is useful because it allows you to see whether a low chain reduction is also stable. b) The convergence of the chains.


**Echolocation frequency categories - supporting paragraph**


This model was based on categorising by echolocation in the extant odontocetes, and sound production in the extant mysticetes.  Data on frequency specifics is not available for fossil data. The narrowband high-frequency (NBHF) cetaceans were designated as so according to Kastelein et al. (2002) and Morisaka et al. (2007), among others. The non-NBHF delphinids were assigned to broadband low frequency (BBLF) according to Jensen et al. (2013), and Ladegaard et al. (2015) among others. The sperm whale sits in its own category because the hypertrophied nasal structures and deep-diving behaviour produce a low-frequency multi-pulsed sound (Madsen et al., 2002) which does not fit into any of our categories. The beaked whales (Ziphiidae) did not fit in with any of the above categories so were put into their own category based on their acoustic repertoire of frequency-modulated buzz clicks (Johnson et al., 2008; Johnston et al., 2008; Baumann-Pickering et al., 2013a; Baumann-Pickering et al., 2013b; Moors-Murphy et al., 2015).  Mysticetes do not echolocate and were put into a separate category; low frequency mysticetes (LFM). The Monodontidae were separated into their own category based on their unique sound repertoire (narrowband structured; NBS) comprising pulses (Sjare and Smith, 1986; Turl, 1990; Racicot et al., 2018) ideal for projecting and receiving signals in shallow and cluttered, icy water (Turl, 1990) and further on the unique morphology of the inner ear which occupies a tightly constrained area showing clear separation from odontocetes which use NBHF echolocation (Racicot et al., 2018).

**Table S2.6.** Frequency categories used to group all extant cetaceans for the 'frequency echolocation' model. A description of the band width type, the taxa within that bandwidth, and supporting references are given.

| Band width (acronym) | Taxa | References |
|---|---|---|
| Unknown | All fossil taxa | NA |
| Broad band low frequency (BBLF) | All non-narrow-band high frequency (NBHF) delphinids | Turl and Penner, (1989); Jensen et al. (2013); Sugimatsu et al. (2014); Ladegaard et al. (2015); Galatius et al. 2019 |
| Frequency modulated buzz clicks (FMbuzz) | Ziphiids | Johnson et al. (2008); Johnston et al. (2008); Baumann-Pickering et al. (2013a); Baumann-Pickering et al. (2013b); Moors-Murphy et al. (2015) |
| Low frequency mysticetes (LFM) | All mysticetes | Clark (1990); Reidenberg and Laitman (2007) |
| Low frequency multi pulsed (LFMP) | *Physeter macrocephalus* | Madsen et al. (2002) |
| Narrow-band high frequency (NBHF) | Phocoenidae, *Inia*, *Pontoporia*, *Cephalorhynchus*, *Kogia*, *Lissodelphis* | Aguilar de Soto et al., (2008); Kastelein et al. (2002); Kyhn et al. (2009; 2013) |
| Narrow-band structured (NBS) | Monodontidae | Sjare and Smith (1986); Turl, 1990; Racicot et al. (2018) |

**Table S2.7.** Likelihood model results (AIC) for each potential scenario for asymmetry in the cetacean cranium. We used the 'fitDiscrete' function in 'geiger' v.1.3-1 (Harmon et al., 2008) to fit various likelihood models for discrete character evolution. These model arguments were an 'equal-rates' model (ER) where all transitions occur at equal rates, a 'symmetric transitions are equal' model (SYM), and 'all rates different model' (ARD) where each rate is a separate parameter (Yang, 2006).

| Model | Likelihood model | AIC | AICc | Rank |
|---|---|---|---|---|
| Ancestral | "ER" | 32.844513 | 32.869513 | 1 |
| Ancestral | "ARD" | 33.656537 | 34.198473 | 2 |
| Ancestral | "SYM" | 34.937848 | 35.089747 | 3 |
| Regime | "ER" | 64.520625 | 64.545625 | 1 |
| Regime | "SYM" | 68.892622 | 69.434558 | 2 |
| Regime | "ARD" | 73.136210 | 75.230170 | 3 |
| Regime split | "ER" | 69.724158 | 69.749158 | 1 |
| Regime split | "SYM" | 93.108987 | 96.396659 | 2 |
| Regime split | "ARD" | 115.719725 | 129.918198 | 3 |
| Echolocation | "ER" | 52.666484 | 52.691484 | 1 |
| Echolocation | "SYM" | 56.887372 | 57.429308 | 2 |
| Echolocation | "ARD" | 58.250569 | 60.344528 | 3 |
| Echolocation frequency | "ER" | 241.957102 | 241.982102 | 1 |
| Echolocation frequency | "SYM" | 247.316761 | 253.916761 | 2 |
| Echolocation frequency | "ARD" | 279.003293 | 309.356235 | 3 |

[Table on next page]

**Table S2.8.** ANOVA results for each potential scenario for asymmetry in the cetacean cranium. ANOVAs are run with Pagel's Lambda Correlation Structure (corPagel). Degrees of freedom (DF), p-value (p), F-value (F), and p-value adjusted using the Benjamini-Hochberg method for false discovery rate (Benjamini and Hochberg, 1995; Benjamini and Yekutieli, 2001) are shown.

| Model | Summary | ANOVA (corPagel) | | | |
|---|---|---|---|---|---|
| | | DF (degrees of freedom) | F | *p* | Adjusted *p* (Benjamini-Hochberg) |
| Geological age | Geological age of the species | 155 | 1.10 | 0.36 | 0.36 |
| Suborder | Split via suborder: archaeocete, mysticete, odontocete | 159 | 1.57 | 0.21 | 0.28 |
| Regime | Assumes selective evolutionary regimes for highly asymmetric taxa | 158 | 26.97 | < 0.001 | < 0.001 |
| Regime split | Each highly asymmetric group is evolving under its own separate selective regime | 156 | 15.78 | < 0.001 | < 0.01 |
| Echolocation | Presence or absence of the ability to echolocate | 158 | 1.44 | 0.23 | 0.28 |
| Echolocation frequency | The frequency at which a cetacean echolocates/produces sound | 155 | 5.83 | < 0.001 | < 0.001 |

**Removal of fossils**

The landmarks of highest variation change slightly when the fossils are removed. Firstly, in the mysticetes, the average amount of total cetacean cranial variation decreases to $\Sigma p = 0.142$ (with fossils: $\Sigma p = 0.191$) when only the extant mysticete skulls are analysed. This is likely because there is a higher amount of deformation in the rostrums of fossil mysticetes. When the fossils are removed there is a slight reordering in the landmarks of variation, including less asymmetry in the rostrum, and a low level of asymmetry in the orbit, squamosal, and parietal. In the odontocetes there is very little change in the top 10 landmarks of variation when the fossils are removed. The top landmarks of variation for all odontocetes combined are the nasal, frontal, posterior premaxilla, and maxilla. This does not change considerably when the fossils are removed. This is likely due to the odontocete signal being dominated by extant taxa. The average total skull variation in the extant odontocetes increased marginally when the fossils were removed: $\Sigma p = 0.292$ (with fossils $\Sigma p = 0.290$). This is probably due to fossil odontocetes having more symmetrical crania compared to extant odontocetes.

[Table on next page]

**Table S2.9.** All specimens ranked by sum radius ($\Sigma\rho_{spec}$). Odontocetes in green, mysticetes in blue, archaeocetes in orange, and terrestrial artiodactyls in yellow. Note how the top rankings are dominated by the odontocetes, and the bottom rankings by the mysticetes and terrestrial artiodactyls.

| Rank | Specimen | Family | Suborder | sum radius ($\Sigma\rho_{spec}$) |
|---|---|---|---|---|
| 1 | *Monodon monoceros* USNM 267959 | Monodontidae | odontocete | 0.546 |
| 2 | *Orycterocetus crocodilinus* USNM 22926 | Physeteridae | odontocete | 0.518 |
| 3 | *Aulophyseter morricei* UCMP 81661 | Physeteridae | odontocete | 0.489 |
| 4 | *Kogia breviceps* USNM 22015 | Kogiidae | odontocete | 0.462 |
| 5 | *Kogia simus* NHM.1952.8.28.1 | Kogiidae | odontocete | 0.457 |
| 6 | *Physeter macrocephalus* NHM 2007.1 | Physeteridae | odontocete | 0.456 |
| 7 | *Delphinapterus leucas* USNM 305071 | Monodontidae | odontocete | 0.453 |
| 8 | *Platanista gangetica* USNM 172409 | Platanistidae | odontocete | 0.449 |
| 9 | *Globicephala melas* NMNZ MM001946 | Delphinidae | odontocete | 0.410 |
| 10 | *Pseudorca crassidens* USNM 11320 | Delphinidae | odontocete | 0.408 |
| 11 | *Globicephala macrorhynchus* NHM 1912.10.27 | Delphinidae | odontocete | 0.407 |
| 12 | *Tagicetus joneti* IRSNB M. 1892 | Delphinida | odontocete | 0.406 |
| 13 | *Notocetus vanbenedeni* MLP 55 | Squalodelphinidae | odontocete | 0.404 |
| 14 | *Albertocetus* ChM PV8680 | Xenorophidae | odontocete | 0.394 |
| 15 | *Albireo whistleri* UCR 14589 | Albireonidae | odontocete | 0.393 |
| 16 | *Brachydelphis mazeasi* MNHN.F.PPI. 266 | Pontoporiidae | odontocete | 0.382 |
| 17 | *Septemtriocetus bosselaersi* IRSNB M.1928 | Phocoenidae | odontocete | 0.382 |
| 18 | *Orcaella brevirostris* NHM.1883.11.20.2 | Delphinidae | odontocete | 0.374 |
| 19 | *Squalodon calvertensis* NMNZ MM001996 | Squalodontidae | odontocete | 0.372 |
| 20 | *Feresa attenuata* USNM 504916 | Delphinidae | odontocete | 0.369 |
| 21 | *Lagenorhynchus cruciger* NHMUK 1960.8.24.1 (Sagmatias) | Delphinidae | odontocete | 0.368 |
| 22 | *Indopacetus pacificus* USNM 593534 | Ziphiidae | odontocete | 0.363 |
| 23 | *Kampholophus serrulus* UMCP 36045 | Kentriodontidae | odontocete | 0.357 |
| 24 | *Lagenorhynchus albirostris* AMNH 37162 | Delphinidae | odontocete | 0.355 |
| 25 | *Hemisyntrachelus cortesii* MBGPT NN | Delphinidae | odontocete | 0.354 |
| 26 | *Orcaella heinsohni* USNM 284430 | Delphinidae | odontocete | 0.350 |
| 27 | *Grampus griseus* USNM 571602 | Delphinidae | odontocete | 0.343 |
| 28 | Shark-toothed *squalodon* OU 21798 | Squalodontidae | odontocete | 0.340 |
| 29 | *Neophocaena phocaenoides* NHM 1903.9.12.3 | Phocoenidae | odontocete | 0.328 |
| 30 | *Lagenodelphis hosei* USNM 571619 | Delphinidae | odontocete | 0.328 |
| 31 | *Messapicetus longirostris* MSNUP NN | Ziphiidae | odontocete | 0.327 |
| 32 | *Zarhachis flagellator* USNM 10911 | Platanistidae | odontocete | 0.325 |
| 33 | *Globicephala* sp USNM 21867 | Delphinidae | odontocete | 0.324 |
| 34 | *Neophocaena asiaeorientalis* USNM 240001 | Phocoenidae | odontocete | 0.323 |
| 35 | *Peponocephala electra* USNM 504511 | Delphinidae | odontocete | 0.322 |
| 36 | *Lomacetus ginsburgi* MNHN.F.PPI.104 | Phocoenidae | odontocete | 0.322 |

| 37 | *Cephalorhynchus eutropia* NHM 1881.8.17.1 | Delphinidae | odontocete | 0.321 |
|----|---|---|---|---|
| 38 | *Kentriodon pernix* USNM 10670 | Kentriodontidae | odontocete | 0.320 |
| 39 | *Stenella longirostris* USNM 395270 | Delphinidae | odontocete | 0.320 |
| 40 | *Phocoena spinipinnis* NHM 1900.5.7.29 | Phocoenidae | odontocete | 0.320 |
| 41 | *Phocoena sinus* SDNHM 20697 | Phocoenidae | odontocete | 0.309 |
| 42 | *Lagenorhynchus australis* 1944.11.30.1 (Sagmatias) | Delphinidae | odontocete | 0.309 |
| 43 | *Hyperoodon ampullatus* NHM 1992.42 | Ziphiidae | odontocete | 0.308 |
| 44 | *Basilosaurus isis* SMNS 11787 | Basilosauridae | archaeocete | 0.308 |
| 45 | *Zygorhiza kochii* USNM 11962 | Basilosauridae | archaeocete | 0.306 |
| 46 | *Lissodelphis peronii* NMNZ MM002116 | Delphinidae | odontocete | 0.304 |
| 47 | Balaenopteridae NMNZ MM001630 | Balaenopteridae | mysticete | 0.300 |
| 48 | *Protocetus atavus* SMNS 11084 | Protocetidae | archaeocete | 0.298 |
| 49 | *Dorudon atrox* PV M 100149 | Basilosauridae | archaeocete | 0.298 |
| 50 | *Aglaocetus moreni* FMNH P13407 | Aglaocetidae | mysticete | 0.298 |
| 51 | *Janjucetus hunderi* NMV P216929 | Mammalodontidae | mysticete | 0.295 |
| 52 | *Cotylocara macei* CCNHM 101 | Xenorophidae | odontocete | 0.293 |
| 53 | *Kentriodon* sp NN | Kentriodontidae | odontocete | 0.293 |
| 54 | *Cephalorhynchus hectori maui* NMNZ MM002607 | Delphinidae | odontocete | 0.291 |
| 55 | *Squalodon bariensis* IRSNB 2372 | Squalodontidae | odontocete | 0.288 |
| 56 | *Berardius bairdii* NHM 1954.9.21.1 | Ziphiidae | odontocete | 0.285 |
| 57 | *Odobenocetops peruvianus* SMNK PAL 2491 | Odobenocetopsidae | odontocete | 0.284 |
| 58 | *Phocoena dioptrica* NHM 1939.9.30.1 | Phocoenidae | odontocete | 0.284 |
| 59 | *Orcinus orca* USNM 11980 | Delphinidae | odontocete | 0.284 |
| 60 | *Lagenorhynchus acutus* USNM 504196 (Leucopleurus) | Delphinidae | odontocete | 0.282 |
| 61 | *Sotalia guianensis* USNM 571558 | Delphinidae | odontocete | 0.281 |
| 62 | *Tursiops aduncus* NHM 1882.1.2.3 | Delphinidae | odontocete | 0.279 |
| 63 | *Cephalorhynchus hectori* NMNZ MM002288 | Delphinidae | odontocete | 0.279 |
| 64 | *Zarhinocetus donnamatsonae* UCMP 86139 | Allodelphinidae | odontocete | 0.279 |
| 65 | *Cephalorhynchus commersonii* USNM 252568 | Delphinidae | odontocete | 0.271 |
| 66 | *Xenorophus* new sp Yap CCNHM 168 | Xenorophidae | odontocete | 0.271 |
| 67 | *Hyperoodon planifrons* NHM 1952.9.30.1 | Ziphiidae | odontocete | 0.271 |
| 68 | *Mesoplodon peruvianus* USNM 571258 | Ziphiidae | odontocete | 0.269 |
| 69 | *Tursiops truncatus* SDNHM 23798 | Delphinidae | odontocete | 0.268 |
| 70 | *Phocoenoides dalli* USNM 276062 | Phocoenidae | odontocete | 0.268 |
| 71 | *Papahu taitapu* OU 22066 | Waipatiidae | odontocete | 0.267 |
| 72 | *Delphinus delphis* AMNH 75332 | Delphinidae | odontocete | 0.267 |
| 73 | *Ambulocetus natans* MSNUP I-16826 | Ambulocetidae | archaeocete | 0.266 |
| 74 | *Cephalorhynchus heavisidii* NHM 1948.7.27.1 | Delphinidae | odontocete | 0.266 |
| 75 | *Waipatia maerewhenua* OU 22095 | Waipatiidae | odontocete | 0.263 |

| 76 | *Prosqualodon davidis* USNM 467596 | Prosqualodontidae | odontocete | 0.260 |
|----|-----------------------------------|-------------------|------------|-------|
| 77 | Eurhinodelphinidae UCMP 99669 | Eurhinodelphinidae | odontocete | 0.257 |
| 78 | *Ziphius cavirostris* NHM 2006.15 | Ziphiidae | odontocete | 0.257 |
| 79 | *Aglaocetus patulus* USNM 23690 | Aglaocetidae | mysticete | 0.256 |
| 80 | *Lipotes vexillifer* AMNH 57333 | Lipotidae | odontocete | 0.255 |
| 81 | *Semirostrum cerutti* SDNHM 65276 | Phocoenidae | odontocete | 0.254 |
| 82 | *Berardius arnuxii* NHM 1935.10.23.1 | Ziphiidae | odontocete | 0.254 |
| 83 | *Lissodelphis borealis* USNM 550188 | Delphinidae | odontocete | 0.253 |
| 84 | *Mesoplodon hectori* NHM 1949.8.19.1 | Ziphiidae | odontocete | 0.252 |
| 85 | *Steno bredanensis* USNM 572789 | Delphinidae | odontocete | 0.250 |
| 86 | *Artiocetus clavis* GSP-UM 3458 | Protocetidae | archaeocete | 0.249 |
| 87 | *Balaenula astensis* MSNUP I-12555 | Balaenidae | mysticete | 0.249 |
| 88 | *Eurhinodelphis longirostris* USNM 244404 | Eurhinodelphinidae | odontocete | 0.249 |
| 89 | *Aegyptocetus tarfa* MSNTUP I-15459 | Protocetidae | archaeocete | 0.247 |
| 90 | *Lagenorhynchus obscurus* NHMUK 1846.3.11.8 (Sagmatias) | Delphinidae | odontocete | 0.247 |
| 91 | *Lagenorhynchus obliquidens* NHM 1992.83 | Delphinidae | odontocete | 0.245 |
| 92 | *Mesoplodon bowdoini* NMNZ MM001900 | Ziphiidae | odontocete | 0.244 |
| 93 | *Mesoplodon traversii* (juvenile) NMNZ TMP012996 | Ziphiidae | odontocete | 0.242 |
| 94 | Agorophiid USNM 205491 | Agorophiidae | odontocete | 0.242 |
| 95 | *Sousa teuszii* NHM 1992.138 | Delphinidae | odontocete | 0.241 |
| 96 | *Herpetocetus bramblei* UCMP 219111 | Cetotheriidae | mysticete | 0.241 |
| 97 | *Piscolithax longirostris* SAS 933 | Phocoenidae | odontocete | 0.240 |
| 98 | *Mesoplodon layardii* USNM 550150 | Ziphiidae | odontocete | 0.240 |
| 99 | *Pakicetus attocki* PV M 100148 | Pakicetidae | archaeocete | 0.238 |
| 100 | *Balaenoptera floridana* USNM 529244 | Balaenopteridae | mysticete | 0.238 |
| 101 | *Stenella attenuata* NHM 1966.11.18.5 | Delphinidae | odontocete | 0.238 |
| 102 | *Aetiocetus weltoni* UCMP 122900 | Aetiocetidae | mysticete | 0.236 |
| 103 | *Berardius minimus* USNM 276366 | Ziphiidae | odontocete | 0.234 |
| 104 | *Mesoplodon carlhubbsi* USNM 504128 | Ziphiidae | odontocete | 0.232 |
| 105 | *Zarhinocetus errabundus* LACM 149588 | Allodelphinidae | odontocete | 0.232 |
| 106 | *Sousa chinensis* NHM 1992.97 | Delphinidae | odontocete | 0.232 |
| 107 | *Sousa sahulensis* NHM 1992.92 | Delphinidae | odontocete | 0.231 |
| 108 | *Xiphiacetus cristatus* USNM 21363 | Eurhinodelphinidae | odontocete | 0.229 |
| 109 | *Chonecetus goedertorum* LACM 131146 (*Fucaia*) | Aetiocetidae | mysticete | 0.229 |
| 110 | *Schizodelphis* sp CCNHM 141 | Eurhinodelphinidae | odontocete | 0.229 |
| 111 | *Sousa plumbea* USNM 550941 | Delphinidae | odontocete | 0.228 |
| 112 | *Xiphiacetus bossi* USNM 8842 | Eurhinodelphinidae | odontocete | 0.226 |
| 113 | *Etruridelphis* sp MGPT PU 13884 | Delphinidae | odontocete | 0.226 |
| 114 | *Patriocetus ehrlichii* OL 1999-3 Cet. 4 | Patriocetidae | odontocete | 0.225 |

| 115 | *Herpetocetus sendaicus* NMNS-PV 19540 | Cetotheriidae | mysticete | 0.225 |
|---|---|---|---|---|
| 116 | *Tasmacetus shepherdi* USNM 484878 | Ziphiidae | odontocete | 0.224 |
| 117 | *Simocetus rayi* USNM 256517 | Simocetidae | odontocete | 0.223 |
| 118 | *Tiucetus rosae* MNHN.F. PPI261 | Cetotheriidae | mysticete | 0.222 |
| 119 | *Parietobalaena palmeri* USNM 24883 | Pelocetidae | mysticete | 0.216 |
| 120 | *Mesoplodon bidens* USNM 593438 | Ziphiidae | odontocete | 0.216 |
| 121 | *Phocoena phocoena* AMNH 212161 | Phocoenidae | odontocete | 0.214 |
| 122 | *Mesoplodon hotaula* USNM 593426 | Ziphiidae | odontocete | 0.213 |
| 123 | Patriocetid new genus ChM PV4753 | Patriocetidae | odontocete | 0.212 |
| 124 | *Delphinus capensis* NHM 1981.7.11 | Delphinidae | odontocete | 0.211 |
| 125 | *Mesoplodon europaeus* USNM 571665 | Ziphiidae | odontocete | 0.211 |
| 126 | *Echovenator sandersi* GSM 1098 | Xenorophidae | odontocete | 0.208 |
| 127 | *Mesoplodon grayi* USNM 49880 | Ziphiidae | odontocete | 0.207 |
| 128 | *Pliopontos littoralis* SAS 193 | Pontoporiidae | odontocete | 0.207 |
| 129 | *Capricornis sumatrensis* NHM 24.5.29.1 | Bovidae | terrestrial artiodactyl | 0.205 |
| 130 | *Argyrocetus joaquinensis* USNM 11996 | Unclear | odontocete | 0.205 |
| 131 | *Mesoplodon stejnegeri* USNM 504330 | Ziphiidae | odontocete | 0.204 |
| 132 | *Schizodelphis barnesi* MNHN AMN 19 | Eurhinodelphinidae | odontocete | 0.203 |
| 133 | *Mesoplodon mirus* USNM 504612 | Ziphiidae | odontocete | 0.202 |
| 134 | *Atocetus iquensis* MNHN.F.PPI. 113 | Delphinida | odontocete | 0.202 |
| 135 | *Balaenoptera* sp SDNHM 83695 | Balaenopteridae | mysticete | 0.201 |
| 136 | *Inia geoffrensis* AMNH 93415 | Iniidae | odontocete | 0.201 |
| 137 | *Diorocetus hiatus* USNM 16783 | Pelocetidae | mysticete | 0.200 |
| 138 | *Miocaperea pulchra* SMNS 46978 | Cetotheriidae | mysticete | 0.196 |
| 139 | *Bos* sp NHM 1981.984 | Bovidae | terrestrial artiodactyl | 0.195 |
| 140 | *Aetiocetus cotylalveus* USNM 25210 | Aetiocetidae | mysticete | 0.193 |
| 141 | *Mesoplodon ginkgodens* USNM 298237 | Ziphiidae | odontocete | 0.193 |
| 142 | *Choeropsis liberiensis* NHM 1967.3.20.1 | Hippopotamidae | terrestrial artiodactyl | 0.189 |
| 143 | *Parapontoporia sternbergi* SDNHM 75060 | Lipotidae | odontocete | 0.189 |
| 144 | *Patriocetus* sp MB Ma. 42882 | Patriocetidae | odontocete | 0.188 |
| 145 | *Tragulus kanchil* NHM 9.1.5.850 | Tragulidae | terrestrial artiodactyl | 0.187 |
| 146 | *Balaenoptera musculus* NHM 1892.3.1.1 | Balaenopteridae | mysticete | 0.184 |
| 147 | *Xenorophus* new sp ChM PV4823 | Xenorophidae | odontocete | 0.183 |
| 148 | *Schizodelphis morckhoviensis* USNM 13873 | Eurhinodelphinidae | odontocete | 0.183 |
| 149 | *Pontoporia blainvillei* USNM 482727 | Pontoporiidae | odontocete | 0.179 |
| 150 | *Cervus elaphus* NHM 2005.16 | Cervidae | terrestrial artiodactyl | 0.177 |
| 151 | *Saiga tatarica* NHM 1961.5.30.1 | Bovidae | terrestrial artiodactyl | 0.176 |
| 152 | *Piscobalaena nana* MNHN 1618 | Cetotheriidae | mysticete | 0.169 |
| 153 | *Eubalaena australis* NHM 1873.3.3 | Balaenidae | mysticete | 0.169 |

| | | | | |
|---|---|---|---|---|
| 154 | *Megaptera novaeangliae* GERM.792a (NHMUK) | Balaenopteridae | mysticete | 0.168 |
| 155 | *Eubalaena glacialis* MSNUP NN | Balaenidae | mysticete | 0.164 |
| 156 | *Mixocetus* sp LACM 143474 | Tranatocetidae | mysticete | 0.163 |
| 157 | *Kekenodon* OU 22294 | Kekenodontidae | archaeocete | 0.160 |
| 158 | *Coronodon havensteini* CCNHM 108 | Aetiocetidae | mysticete | 0.158 |
| 159 | *Hydropotes inemis* NHM 1551c | Cervidae | terrestrial artiodactyl | 0.157 |
| 160 | *Tayassu pecari labiatus* NHM 47.4.6.8 | Tayassuidae | terrestrial artiodactyl | 0.154 |
| 161 | *Giraffa camelopardalis* NHM NN | Giraffidae | terrestrial artiodactyl | 0.151 |
| 162 | *Caperea marginata* NHM 1876.2.16.1 | Cetotheriidae | mysticete | 0.145 |
| 163 | *Balaena mysticetus* 1986.1.16 | Balaenidae | mysticete | 0.143 |
| 164 | *Pelocetus calvertensis* USNM 11976 | Pelocetidae | mysticete | 0.137 |
| 165 | *Remingtonocetus harudiensis* USNM PAL 559313 | Remingtonocetidae | archaeocete | 0.135 |
| 166 | *Balaenoptera acutorostrata* NHM 1965.11.2.1 | Balaenopteridae | mysticete | 0.128 |
| 167 | *Balaenoptera omurai* NN | Balaenopteridae | mysticete | 0.124 |
| 168 | *Camelus dromedarius* NHM NN | Camelidae | terrestrial artiodactyl | 0.121 |
| 169 | *Balaenoptera edeni* NHM 1920.12.31.1 | Balaenopteridae | mysticete | 0.120 |
| 170 | *Balaenoptera borealis* NHM 1934.5.25.1 | Balaenopteridae | mysticete | 0.119 |
| 171 | *Balaenoptera physalus* NHM 1862.2.7.181 | Balaenopteridae | mysticete | 0.119 |
| 172 | *Balaenoptera brydei* USNM 572922 | Balaenopteridae | mysticete | 0.115 |

**Table S2.10.** Percentage of asymmetry in the rostrum – archaeocetes. The sum radii of the archaeocete skull, the sum radii of the archaeocete skull with the rostral landmarks removed, and the percentage (%) of the sum radii that is found in the rostrum of archaeocetes

| Species | Family | Sum radii with rostrum | Sum radii with rostrum removed | % of asymmetry in rostrum |
|---|---|---|---|---|
| *Aegyptocetus tarfa* MSNTUP I-15459 | Protocetidae | 0.247 | 0.213 | 13.8 |
| *Ambulocetus natans* MSNUP I-16826 | Ambulocetidae | 0.266 | 0.227 | 14.8 |
| *Artiocetus clavis* GSP-UM 3458 | Protocetidae | 0.249 | 0.171 | 31.3 |
| *Basilosaurus isis* SMNS 11787 | Basilosauridae | 0.308 | 0.257 | 16.4 |
| *Dorudon atrox* PV M 100149 | Basilosauridae | 0.298 | 0.244 | 18.1 |
| *Kekenodon sp* OU 22294 | Kekenodontidae | 0.160 | 0.137 | 14.5 |
| *Pakicetus attocki* PV M 100148 | Pakicetidae | 0.238 | 0.159 | 33.2 |
| *Protocetus atavus* SMNS 11084 | Protocetidae | 0.298 | 0.247 | 17.1 |
| *Remingtonocetus harudiensis* USNM PAL 559313 | Remingtonocetidae | 0.135 | 0.111 | 18.1 |
| *Zygorhiza kochii* USNM 11962 | Basilosauridae | 0.306 | 0.258 | 15.8 |

[Table on next page]

**Table S2.11.** Percentage of asymmetry in the rostrum – mysticetes. The sum radii of the mysticete skull, the sum radii of the mysticete skull with the rostral landmarks removed, and the percentage (%) of the sum radii that is found in the rostrum of mysticetes

| Species | Family | Sum radii with rostrum | Sum radii with rostrum removed | % of asymmetry in rostrum |
|---|---|---|---|---|
| *Aetiocetus cotylalveus* USNM 25210 | Aetiocetidae | 0.193 | 0.158 | 18.0 |
| *Aetiocetus weltoni* UCMP 122900 | Aetiocetidae | 0.236 | 0.215 | 8.7 |
| *Aglaocetus moreni* FMNH P13407 | Aglaocetidae | 0.298 | 0.262 | 11.8 |
| *Aglaocetus patulus* USNM 23690 | Aglaocetidae | 0.256 | 0.216 | 15.7 |
| *Balaena mysticetus* NHMUK 1986.1.16 | Balaenidae | 0.143 | 0.127 | 11.4 |
| *Balaenoptera acutorostrata* NHM 1965.11.2.1 | Balaenopteridae | 0.128 | 0.114 | 10.4 |
| *Balaenoptera borealis* NHMUK 1934.5.25.1 | Balaenopteridae | 0.119 | 0.103 | 13.8 |
| *Balaenoptera brydei* USNM 572922 | Balaenopteridae | 0.115 | 0.101 | 11.8 |
| *Balaenoptera sp* SDNHM 83695 | Balaenopteridae | 0.201 | 0.178 | 11.1 |
| *Balaenoptera edeni* NHMUK 1920.12.31.1 | Balaenopteridae | 0.120 | 0.104 | 14.0 |
| *Balaenoptera floridana* USNM 529244 | Balaenopteridae | 0.238 | 0.210 | 11.9 |
| *Balaenoptera musculus* NHMUK 1892.3.1.1 | Balaenopteridae | 0.184 | 0.159 | 13.8 |
| *Balaenoptera omurai* NN | Balaenopteridae | 0.124 | 0.108 | 12.6 |
| *Balaenoptera physalus* NHMUK 1862.2.7.181 | Balaenopteridae | 0.119 | 0.100 | 16.2 |
| Balaenopteridae NMNZ MM001630 | Balaenopteridae | 0.300 | 0.263 | 12.4 |
| *Balaenula astensis* MSNUP I-12555 | Balaenidae | 0.249 | 0.210 | 15.6 |
| *Caperea marginata* NHMUK 1876.2.16.1 | Cetotheriidae | 0.145 | 0.122 | 16.1 |
| *Chonecetus goedertorum* LACM 131146 (Fucaia) | Aetiocetidae | 0.229 | 0.189 | 17.6 |
| *Coronodon havensteini* CCNHM 108 | Aetiocetidae | 0.158 | 0.137 | 13.1 |
| *Diorocetus hiatus* USNM 16783 | Pelocetidae | 0.200 | 0.170 | 15.2 |
| *Eubalaena australis* NHM 1873.3.3 | Balaenidae | 0.169 | 0.147 | 13.0 |
| *Eubalaena glacialis* MSNUP NN | Balaenidae | 0.164 | 0.140 | 14.6 |
| *Herpetocetus bramblei* UCMP 219111 | Cetotheriidae | 0.241 | 0.183 | 24.3 |
| *Herpetocetus sendaicus* NMNS-PV 19540 | Cetotheriidae | 0.225 | 0.184 | 18.0 |
| *Janjucetus hunderi* NMV P216929 | Mammalodontidae | 0.295 | 0.252 | 14.8 |
| *Megaptera novaeangliae* GERM.792a (NHMUK) | Balaenopteridae | 0.168 | 0.146 | 13.2 |

| | | | | |
|---|---|---|---|---|
| *Miocaperea pulchra* SMNS 46978 | Cetotheriidae | 0.196 | 0.173 | 12.0 |
| *Mixocetus sp* LACM 143474 | Tranatocetidae | 0.163 | 0.140 | 14.2 |
| *Parietobalaena palmeri* USNM 24883 | Pelocetidae | 0.216 | 0.185 | 14.5 |
| *Pelocetus calvertensis* USNM 11976 | Pelocetidae | 0.137 | 0.118 | 13.5 |
| *Piscobalaena nana* MNHN 1618 | Cetotheriidae | 0.169 | 0.142 | 16.0 |
| *Tiucetus rosae* MNHN.F. PPI261 | Cetotheriidae | 0.222 | 0.187 | 16.1 |

**Table S2.12**. Percentage of asymmetry in the rostrum – odontocetes. The sum radii of the odontocete skull, the sum radii of the odontocete skull with the rostral landmarks removed, and the percentage (%) of the sum radii that is found in the rostrum of odontocetes.

| Species | Family | Sum radii with rostrum | Sum radii with rostrum removed | % of asymmetry in rostrum |
|---|---|---|---|---|
| Agorophiid USNM 205491 | Agorophiidae | 0.242 | 0.209 | 13.8 |
| *Albertocetus* ChM PV8680 | Xenorophidae | 0.394 | 0.304 | 22.7 |
| *Albireo whistleri* UCR 14589 | Albireonidae | 0.393 | 0.346 | 11.8 |
| *Argyrocetus joaquinensis* USNM 11996 | Unclear | 0.205 | 0.178 | 13.1 |
| *Atocetus iquensis* MNHN.F.PPI. 113 | Delphinida | 0.202 | 0.186 | 8.2 |
| *Aulophyseter morricei* UCMP 81661 | Physeteridae | 0.489 | 0.420 | 14.2 |
| *Berardius arnuxii* NHM 1935.10.23.1 | Ziphiidae | 0.254 | 0.198 | 22.0 |
| *Berardius bairdii* NHM 1954.9.21.1 | Ziphiidae | 0.285 | 0.231 | 19.0 |
| *Berardius minimus* USNM 276366 | Ziphiidae | 0.234 | 0.191 | 18.2 |
| *Brachydelphis mazeasi* MNHN.F.PPI. 266 | Pontoporiidae | 0.382 | 0.317 | 17.0 |
| *Cephalorhynchus commersonii* USNM 252568 | Delphinidae | 0.271 | 0.237 | 12.7 |
| *Cephalorhynchus eutropia* NHM 1881.8.17.1 | Delphinidae | 0.321 | 0.272 | 15.4 |
| *Cephalorhynchus heavisidii* NHM 1948.7.27.1 | Delphinidae | 0.266 | 0.233 | 12.3 |
| *Cephalorhynchus hectori maui* NMNZ MM002607 | Delphinidae | 0.291 | 0.253 | 13.1 |
| *Cephalorhynchus hectori* NMNZ MM002288 | Delphinidae | 0.279 | 0.243 | 12.9 |

| | | | | |
|---|---|---|---|---|
| *Cotylocara macei* CCNHM 101 | Xenorophidae | 0.293 | 0.237 | 19.1 |
| *Delphinapterus leucas* USNM 305071 | Monodontidae | 0.453 | 0.390 | 14.0 |
| *Delphinus capensis* NHM 1981.7.11 | Delphinidae | 0.211 | 0.180 | 14.8 |
| *Delphinus delphis* AMNH 75332 | Delphinidae | 0.267 | 0.222 | 16.9 |
| *Echovenator sandersi* GSM 1098 | Xenorophidae | 0.208 | 0.178 | 14.1 |
| *Etruridelphis* sp MGPT PU 13884 | Delphinidae | 0.226 | 0.207 | 8.5 |
| Eurhinodelphinidae UCMP 99669 | Eurhinodelphinidae | 0.257 | 0.231 | 10.1 |
| *Eurhinodelphis* longirostris USNM 244404 | Eurhinodelphinidae | 0.249 | 0.187 | 25.0 |
| *Feresa attenuata* USNM 504916 | Delphinidae | 0.369 | 0.318 | 13.9 |
| *Globicephala macrorhynchus* NHM 1912.10.27 | Delphinidae | 0.407 | 0.332 | 18.4 |
| *Globicephala melas* NMNZ MM001946 | Delphinidae | 0.410 | 0.370 | 9.7 |
| *Globicephala* sp USNM 21867 | Delphinidae | 0.324 | 0.274 | 15.5 |
| *Grampus griseus* USNM 571602 | Delphinidae | 0.343 | 0.298 | 13.3 |
| *Hemisyntrachelus cortesii* MBGPT NN | Delphinidae | 0.354 | 0.299 | 15.5 |
| *Hyperoodon ampullatus* NHM 1992.42 | Ziphiidae | 0.308 | 0.262 | 14.9 |
| *Hyperoodon planifrons* NHM 1952.9.30.1 | Ziphiidae | 0.271 | 0.228 | 15.9 |
| *Indopacetus pacificus* USNM 593534 | Ziphiidae | 0.363 | 0.288 | 20.6 |
| *Inia geoffrensis* AMNH 93415 | Iniidae | 0.201 | 0.168 | 16.2 |
| *Kampholophus serrulus* UMCP 36045 | Kentriodontidae | 0.357 | 0.312 | 12.6 |
| *Kentriodon pernix* USNM 10670 | Kentriodontidae | 0.320 | 0.275 | 14.3 |
| *Kentriodon* sp NN | Kentriodontidae | 0.293 | 0.227 | 22.5 |
| *Kogia breviceps* USNM 22015 | Kogiidae | 0.462 | 0.427 | 7.8 |
| *Kogia simus* NHM.1952.8.28.1 | Kogiidae | 0.457 | 0.416 | 9.0 |
| *Lagenodelphis hosei* USNM 571619 | Delphinidae | 0.328 | 0.280 | 14.5 |
| *Lagenorhynchus acutus* USNM 504196 (Leucopleurus) | Delphinidae | 0.282 | 0.232 | 17.5 |
| *Lagenorhynchus albirostris* AMNH 37162 | Delphinidae | 0.355 | 0.296 | 16.8 |
| *Lagenorhynchus australis* 1944.11.30.1 (Sagmatias) | Delphinidae | 0.309 | 0.278 | 10.0 |
| *Lagenorhynchus cruciger* NHMUK 1960.8.24.1 (Sagmatias) | Delphinidae | 0.368 | 0.316 | 14.1 |

| | | | | |
|---|---|---|---|---|
| *Lagenorhynchus obliquidens* NHM 1992.83 | Delphinidae | 0.245 | 0.220 | 10.1 |
| *Lagenorhynchus obscurus* NHMUK 1846.3.11.8 (Sagmatias) | Delphinidae | 0.247 | 0.217 | 12.0 |
| *Lipotes vexillifer* AMNH 57333 | Lipotidae | 0.255 | 0.211 | 17.3 |
| *Lissodelphis borealis* USNM 550188 | Delphinidae | 0.253 | 0.220 | 12.9 |
| *Lissodelphis peronii* NMNZ MM002116 | Delphinidae | 0.304 | 0.253 | 16.6 |
| *Lomacetus ginsburgi* MNHN.F.PPI.104 | Phocoenidae | 0.322 | 0.269 | 16.3 |
| *Mesoplodon bidens* USNM 593438 | Ziphiidae | 0.216 | 0.188 | 13.0 |
| *Mesoplodon bowdoini* NMNZ MM001900 | Ziphiidae | 0.244 | 0.200 | 18.2 |
| *Mesoplodon carlhubbsi* USNM 504128 | Ziphiidae | 0.232 | 0.197 | 15.2 |
| *Mesoplodon europaeus* USNM 571665 | Ziphiidae | 0.211 | 0.173 | 17.8 |
| *Mesoplodon ginkgodens* USNM 298237 | Ziphiidae | 0.193 | 0.161 | 16.6 |
| *Mesoplodon grayi* USNM 49880 | Ziphiidae | 0.207 | 0.172 | 17.0 |
| *Mesoplodon hectori* NHM 1949.8.19.1 | Ziphiidae | 0.252 | 0.211 | 16.4 |
| *Mesoplodon hotaula* USNM 593426 | Ziphiidae | 0.213 | 0.187 | 12.1 |
| *Mesoplodon layardii* USNM 550150 | Ziphiidae | 0.240 | 0.196 | 18.5 |
| *Mesoplodon mirus* USNM 504612 | Ziphiidae | 0.202 | 0.179 | 11.6 |
| *Mesoplodon peruvianus* USNM 571258 | Ziphiidae | 0.269 | 0.229 | 14.8 |
| *Mesoplodon stejnegeri* USNM 504330 | Ziphiidae | 0.204 | 0.174 | 14.6 |
| *Mesoplodon traversii* (juvenile) NMNZ TMP012996 | Ziphiidae | 0.242 | 0.192 | 20.6 |
| *Messapicetus longirostris* MSNUP NN | Ziphiidae | 0.327 | 0.298 | 9.0 |
| *Monodon monoceros* USNM 267959 | Monodontidae | 0.546 | 0.472 | 13.4 |
| *Neophocaena asiaeorientalis* USNM 240001 | Phocoenidae | 0.323 | 0.281 | 12.9 |
| *Neophocaena phocaenoides* NHM 1903.9.12.3 | Phocoenidae | 0.328 | 0.295 | 10.3 |
| *Notocetus vanbenedeni* MLP 55 | Squalodelphinidae | 0.404 | 0.338 | 16.4 |
| *Odobenocetops peruvianus* SMNK PAL 2491 | Odobenocetopsidae | 0.284 | 0.237 | 16.5 |
| *Orcaella brevirostris* NHM.1883.11.20.2 | Delphinidae | 0.374 | 0.321 | 14.3 |
| *Orcaella heinsohni* USNM 284430 | Delphinidae | 0.350 | 0.301 | 14.1 |
| *Orcinus orca* USNM 11980 | Delphinidae | 0.284 | 0.250 | 12.1 |

| | | | | |
|---|---|---|---|---|
| *Orycterocetus crocodilinus* USNM 22926 | Physeteridae | 0.518 | 0.456 | 11.9 |
| *Papahu taitapu* OU 22066 | Waipatiidae | 0.267 | 0.236 | 11.7 |
| *Parapontoporia sternbergi* SDNHM 75060 | Lipotidae | 0.189 | 0.156 | 17.5 |
| Patriocetid new genus ChM PV4753 | Patriocetidae | 0.212 | 0.192 | 9.3 |
| *Patriocetus ehrlichii* OL1999-3 Cet. 4 | Patriocetidae | 0.225 | 0.193 | 14.1 |
| *Patriocetus* sp MB Ma. 42882 | Patriocetidae | 0.188 | 0.166 | 12.0 |
| *Peponocephala electra* USNM 504511 | Delphinidae | 0.322 | 0.276 | 14.4 |
| *Phocoena dioptrica* NHM 1939.9.30.1 | Phocoenidae | 0.284 | 0.249 | 12.4 |
| *Phocoena phocoena* AMNH 212161 | Phocoenidae | 0.214 | 0.182 | 15.0 |
| *Phocoena sinus* SDNHM 20697 | Phocoenidae | 0.309 | 0.266 | 14.1 |
| *Phocoena spinipinnis* NHM 1900.5.7.29 | Phocoenidae | 0.320 | 0.278 | 12.9 |
| *Phocoenoides dalli* USNM 276062 | Phocoenidae | 0.268 | 0.221 | 17.6 |
| *Physeter macrocephalus* NHM 2007.1 | Physeteridae | 0.456 | 0.381 | 16.5 |
| *Piscolithax longirostris* SAS 933 | Phocoenidae | 0.240 | 0.192 | 20.3 |
| *Platanista gangetica* USNM 172409 | Platanistidae | 0.449 | 0.365 | 18.6 |
| *Pliopontos littoralis* SAS 193 | Pontoporiidae | 0.207 | 0.186 | 10.0 |
| *Pontoporia blainvillei* USNM 482727 | Pontoporiidae | 0.179 | 0.163 | 8.9 |
| *Prosqualodon davidis* USNM 467596 | Prosqualodontidae | 0.260 | 0.224 | 13.7 |
| *Pseudorca crassidens* USNM 11320 | Delphinidae | 0.408 | 0.357 | 12.6 |
| *Schizodelphis barnesi* MNHN AMN 19 | Eurhinodelphinidae | 0.203 | 0.184 | 9.5 |
| *Schizodelphis morckhoviensis* USNM 13873 | Eurhinodelphinidae | 0.183 | 0.150 | 18.0 |
| *Schizodelphis* sp CCNHM 141 | Eurhinodelphinidae | 0.229 | 0.194 | 15.0 |
| *Semirostrum cerutti* SDNHM 65276 | Phocoenidae | 0.254 | 0.230 | 9.3 |
| *Septemtriocetus bosselaersi* IRSNB M.1928 | Phocoenidae | 0.382 | 0.323 | 15.5 |
| Shark-toothed *squalodon* OU 21798 | Squalodontidae | 0.340 | 0.283 | 16.7 |
| *Simocetus rayi* USNM 256517 | Simocetidae | 0.223 | 0.180 | 19.4 |
| *Sotalia guianensis* USNM 571558 | Delphinidae | 0.281 | 0.237 | 15.6 |
| *Sousa chinensis* NHM 1992.97 | Delphinidae | 0.232 | 0.201 | 13.0 |
| *Sousa plumbea* USNM 550941 | Delphinidae | 0.228 | 0.204 | 10.6 |

| | | | | |
|---|---|---|---|---|
| *Sousa sahulensis* NHM 1992.92 | Delphinidae | 0.231 | 0.183 | 20.5 |
| *Sousa teuszii* NHM 1992.138 | Delphinidae | 0.241 | 0.208 | 13.7 |
| *Squalodon bariensis* IRSNB 2372 | Squalodontidae | 0.288 | 0.264 | 8.5 |
| *Squalodon calvertensis* NMNZ MM001996 | Squalodontidae | 0.372 | 0.307 | 17.4 |
| *Stenella attenuata* NHM 1966.11.18.5 | Delphinidae | 0.238 | 0.203 | 14.8 |
| *Stenella longirostris* USNM 395270 | Delphinidae | 0.320 | 0.272 | 15.1 |
| *Steno bredanensis* USNM 572789 | Delphinidae | 0.250 | 0.215 | 14.0 |
| *Tagicetus joneti* IRSNB M. 1892 | Delphinida | 0.406 | 0.344 | 15.4 |
| *Tasmacetus shepherdi* USNM 484878 | Ziphiidae | 0.224 | 0.199 | 10.9 |
| *Tursiops aduncus* NHM 1882.1.2.3 | Delphinidae | 0.279 | 0.231 | 17.3 |
| *Tursiops truncatus* SDNHM 23798 | Delphinidae | 0.268 | 0.227 | 15.1 |
| *Waipatia maerewhenua* OU 22095 | Waipatiidae | 0.263 | 0.204 | 22.5 |
| *Xenorophus* new sp ChM PV4823 | Xenorophidae | 0.183 | 0.153 | 16.4 |
| *Xenorophus* new sp Yap CCNHM 168 | Xenorophidae | 0.271 | 0.218 | 19.6 |
| *Xiphiacetus bossi* USNM 8842 | Eurhinodelphinidae | 0.226 | 0.201 | 10.9 |
| *Xiphiacetus cristatus* USNM 21363 | Eurhinodelphinidae | 0.229 | 0.201 | 12.2 |
| *Zarhachis flagellator* USNM 10911 | Platanistidae | 0.325 | 0.258 | 20.7 |
| *Zarhinocetus donnamatsonae* UCMP 86139 | Allodelphinidae | 0.279 | 0.247 | 11.3 |
| *Zarhinocetus errabundus* LACM 149588 | Allodelphinidae | 0.232 | 0.195 | 16.1 |
| *Ziphius cavirostris* NHM 2006.15 | Ziphiidae | 0.257 | 0.213 | 17.3 |
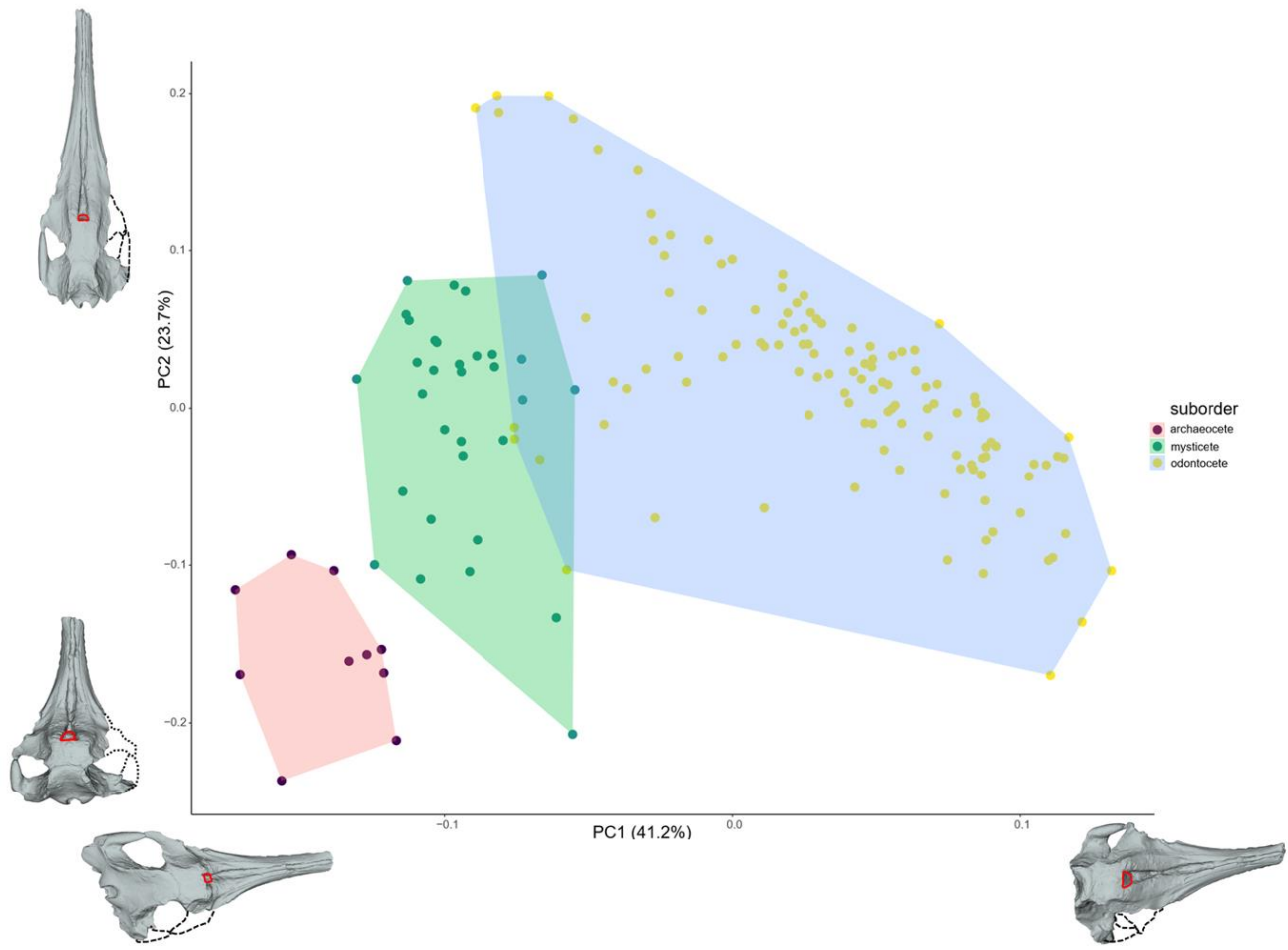
[Figure on previous page]

**Fig. S2.14.** Additional morphospace occupation of cetacean crania used in this study. Principal components (PC) 1 and 2 using 123 landmarks over the surface of the skull. PC1 (41.2%) shows variation in the positioning of the nares – the shift posteriorly on the skull from archaeocetes to extant cetaceans. PC2 (23.7%) shows variation in the length of the rostrum. Axes extremes indicated on a warped skull of a patriocetid. On the skulls, dotted lines show missing data, and the red outline indicates the position of the nares.  n = 162.
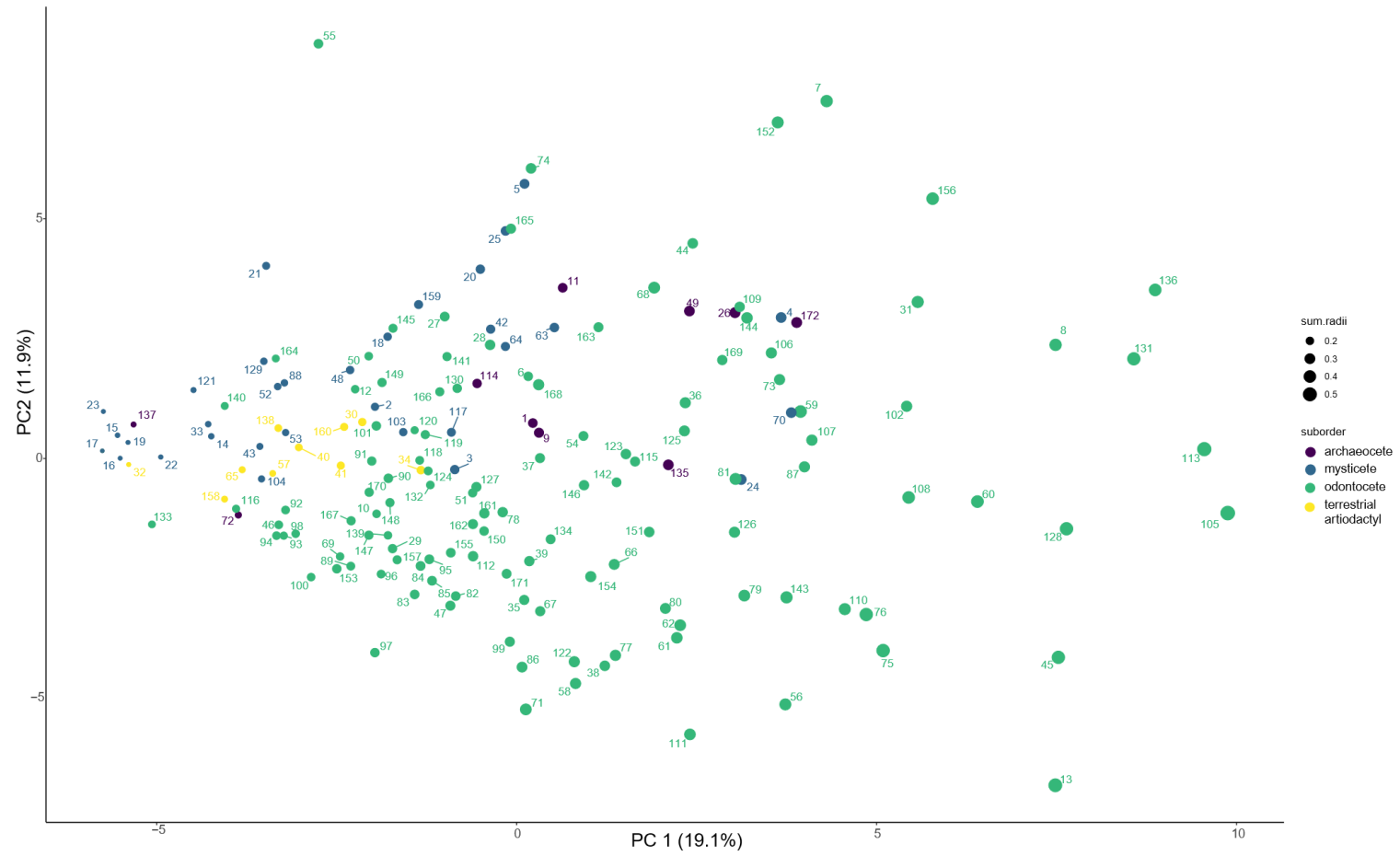
**Fig. S2.15.** Principal Components plot with PC1 and PC2 for each specimen in the study. The PC scores represent the sum radii ($\sum p_{spec}$) in the skull for each specimen. The larger the circle, the higher the $\sum p_{spec}$. Terrestrial artiodactyls are shown in yellow, archaeocetes in deep purple, mysticetes in blue, and odontocetes in green. For number corresponding to specimen see Table S2.1 - List of specimens used in the study. n = 172, including 10 terrestrial artiodactyls.
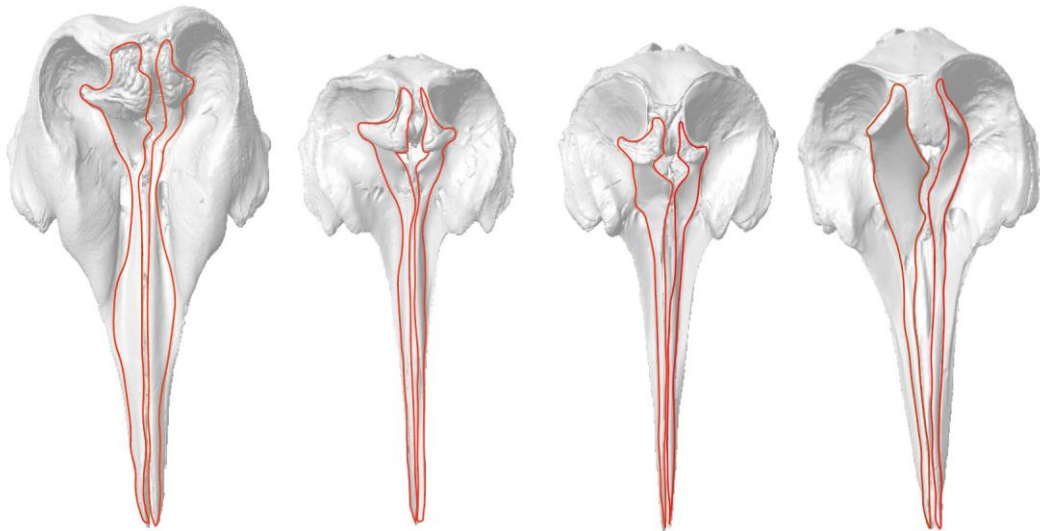


**Fig. S2.16.** Ziphiid skulls showing the marked asymmetry in the premaxillary crests. From left to right: *Hyperoodon planifrons* NHMUK 1952.9.30.1, *Mesoplodon carlhubbsi* USNM 504128, *Mesoplodon mirus* USNM 504612, *Ziphius cavirostris* NHMUK 2006.15. Crests outlined in red. Not to scale.

Appendix 3

# Chapter 3 Appendix

[Table on next page]

**Table S3.1.** Specimen list in alphabetical order. Additional details on family, suborder ('Archs' = archaeocetes, 'Mysts' = mysticetes, 'Odonts' = odontocetes), approximate age, dentition, diet, echolocation ability ('echo'), feeding method ('FM'), habitat, and additional references for ecological data.

| No. | Museum ID | Family | Suborder | Age | Dentition | Diet | Echo | FM | Habitat | Reference |
|---|---|---|---|---|---|---|---|---|---|---|
| 1 | *Aegytocetus tarfa* MSNTUP I-15459 | Protocetidae | Arch | Eocene | heterodont | benthic invertebrates + fish | band1 | biting | coastal | Bianucci, G. and Gingerich, P.D. 2011. *Aegyptocetus tarfa*, n. gen. et sp. (Mammalia, Cetacea), from the middle Eocene of Egypt: clinorhynchy, olfaction, and hearing in a protocetid whale. Journal of Vertebrate Paleontology, 31(6):1173-1188. |
| 2 | *Aetiocetus cotylalveus* USNM 25210 | Aetiocetidae | Myst | Oligocene | heterodont | zooplankton + fish | band1 | suction | coastal-pelagic | Deméré, T.A., and Berta, A. 2008. Skull anatomy of the Oligocene toothed mysticete *Aetiocetus weltoni* (Mammalia: Cetacea): implications for mysticete evolution and functional anatomy. Zoological Journal of the Linnean Society, 154: 308–52. D. Emlong. 1966. A new archaic cetacean from the Oligocene of Northwest Oregon. Bulletin of the Museum of Natural History, University of Oregon 3:1-51 |
| 3 | *Aetiocetus weltoni* UCMP 122900 | Aetiocetidae | Myst | Oligocene | heterodont | zooplankton + fish | band1 | suction | coastal-pelagic | Deméré, T.A., and Berta, A. 2008. Skull anatomy of the Oligocene toothed mysticete *Aetiocetus weltoni* (Mammalia: Cetacea): implications for mysticete evolution and functional anatomy. Zoological Journal of the Linnean Society, 154: 308–52. |
| 4 | *Aglaocetus moreni* FMNH P13407 | Aglaocetidae | Myst | Miocene | edentulous - baleen | zooplankton + fish | band1 | filter | coastal-pelagic | Kellogg, R. 1934. The Patagonian fossil whalebone whale, Cetotherium moreni (Lydekker). Carnegie Institution of Washington, 447:64-81. |
| 5 | *Aglaocetus patulus* USNM 23690 | Aglaocetidae | Myst | Miocene | edentulous - baleen | zooplankton + fish | band1 | filter | coastal-pelagic | Kellogg, R. 1934. The Patagonian fossil whalebone whale, Cetotherium moreni (Lydekker). Carnegie Institution of Washington, 447:64-81. R. Kellogg. 1968. A sharp-nosed cetothere from the Miocene Calvert. Proceedings of the United States National Museum 247(7):163-173 |
| 6 | *Agorophiid* USNM 205491 | Agorophiidae | Odont | Oligocene | heterodont | benthic invertebrates + fish | band2 | biting | pelagic | Fordyce, R.E.1981. Systematics of the odontocete whale *Agorophius pygmaeus* and the Family Agorophidae (Mammalia: Cetacea). Journal of Paleontology, 1028-1045. |
| 7 | *Albertocetus* ChM PV8680 | Xenorophidae | Odont | Oligocene | heterodont | benthic invertebrates + fish | band2 | biting | pelagic | Uhen, M.D. 2008. A new *Xenorophus*-like odontocete cetacean from the Oligocene of North Carolina. Journal of Systematic Paleontology, 6: 433-452. |
| 8 | *Albireo whistleri* UCR 14589 | Albireonidae | Odont | Miocene | homodont | cephalopods + fish | band2 | biting | coastal-pelagic | Barnes, L.G. 2008. Miocene and Pliocene Albireonidae (Ceatcea, Odontoceti), Rare and unusual fossil dolphins from the Eastern North Pacific Ocean. Natural History Musuem of Los Angeles County Science Series, 41:99-152. |
| 9 | *Ambulocetus natans* MSNUP I-16826 | Ambulocetidae | Arch | Eocene | heterodont | benthic invertebrates + fish | band1 | biting | coastal | Thewissen, J.G.M., Madar, S.I. and Hussain, S.T. 1996. *Ambulocetus natans*, and Eocene cetacean (Mammalia) from Pakistan. Courier Forschungsinstitut Senckenberg, 191:1-86. |
| 10 | *Ankylorhiza tiedemani* CCNHM 103 | incertae sedis | Odont | Oligocene | heterodont | tetrapods + fish | band2 | biting | pelagic | Boessenecker, Robert W.; Churchill, Morgan; Buchholtz, Emily A.; Beatty, Brian L.; Geisler, Jonathan H. 2020. Convergent Evolution of Swimming Adaptations in Modern Whales Revealed by a Large Macrophagous Dolphin from the Oligocene of South Carolina. Current Biology. |

| 11 | *Aprixokogia kelloggi* USNM 187015 | Kogiidae | Odont | Miocene | homodont | cephalopods + fish | band2 | suction | pelagic | Velez-Juarbe, J., Wood, A.R., De Gracia, C., Hendey, A.J.W. 2015. Evolutionary patterns among living and fossil kogiid sperm whales: evidence from the Neogene of Central America. PloS ONE, 10.4: e0123909. |
|----|----|----|----|----|----|----|----|----|----|----|
| 12 | *Argyrocetus joaquinensis* USNM 11996 | Delphinida | Odont | Miocene | homodont | fish | band2 | biting | coastal-pelagic | Kellogg, R. 1932. A Miocene long-beaked porpoise from California. Smithsonian Miscellaneous Collections, 87(2):1-11. R. Kellogg. 1932. A Miocene long-beaked porpoise from California. Smithsonian Miscellaneous Collections 87(2):1-11 |
| 13 | *Artiocetus clavis* GSP-UM 3458 | Protocetidae | Arch | Eocene | heterodont | benthic invertebrates + fish | band1 | biting | coastal | Gingerich, P.D., Haq, M., Zalmout, I.S., Khan, I.H., Malkani, M.S. 2001. Origin of whales from early artiodactyls: Hands and feet of Eocene Protocetidae from Pakistan. Science, 293:2239-2242. |
| 14 | *Atocetus iquensis* MNHN.F.PPI. 113 | Kentriodontidae | Odont | Miocene | homodont | cephalopods + fish | band2 | biting | pelagic | Muizon, C. 1988. Les vertebres fossiles de la Formation Pisco (Peru). Troisieme partie: Les Odontocetes (Cetacea, Mammalia) du Miocene. Editions Recherche sur les Civilisations (78)1-244 |
| 15 | *Aulophyseter morricei* UCMP 81661 | Physeteridae | Odont | Miocene | homodont | cephalopods + fish | band2 | suction | pelagic | Cope, E.D. 1895. Fourth contribution to the marine fauna of the Miocene Period of the United States. Proceedings of the American Philosophical Society 34: 135-155. J. Velez-Juarbe, A. R. Wood, C. Gracia and A. J. W. Hendy. 2015. Evolutionary patterns among living and fossil kogiid sperm whales: Evidence from the Neogene of Central America. PLoS One 10(4):e0123909 |
| 16 | *Balaena mysticetus* 1986.1.16 | Balaenidae | Myst | Extant | edentulous - baleen | zooplankton + fish | band1 | filter | pelagic | Berta, A., Lanzetti, A., Ekdale, E.G., and Deméré, T.A. 2016. Evolutionary innovations and ecology in mysticete cetaceans: transition from teeth to baleen and raptorial to bulk feeding. Integrative and Comparative Biology, 56:1271–1284. |
| 17 | *Balaenoptera acutorostrata* NHM 1965.11.2.1 | Balaenopteridae | Myst | Extant | edentulous - baleen | zooplankton + fish | band1 | filter | pelagic | Berta, A., Lanzetti, A., Ekdale, E.G., and Deméré, T.A. 2016. Evolutionary innovations and ecology in mysticete cetaceans: transition from teeth to baleen and raptorial to bulk feeding. Integrative and Comparative Biology, 56:1271–1284. |
| 18 | *Balaenoptera borealis* NHM 1934.5.25.1 | Balaenopteridae | Myst | Extant | edentulous - baleen | zooplankton + fish | band1 | filter | pelagic | Berta, A., Lanzetti, A., Ekdale, E.G., and Deméré, T.A. 2016. Evolutionary innovations and ecology in mysticete cetaceans: transition from teeth to baleen and raptorial to bulk feeding. Integrative and Comparative Biology, 56:1271–1284. |
| 19 | *Balaenoptera brydei* USNM 572922 | Balaenopteridae | Myst | Extant | edentulous - baleen | zooplankton + fish | band1 | filter | pelagic | Berta, A., Lanzetti, A., Ekdale, E.G., and Deméré, T.A. 2016. Evolutionary innovations and ecology in mysticete cetaceans: transition from teeth to baleen and raptorial to bulk feeding. Integrative and Comparative Biology, 56:1271–1284. |
| 20 | *Balaenoptera edeni* NHM 1920.12.31.1 | Balaenopteridae | Myst | Extant | edentulous - baleen | zooplankton + fish | band1 | filter | pelagic | Berta, A., Lanzetti, A., Ekdale, E.G., and Deméré, T.A. 2016. Evolutionary innovations and ecology in mysticete cetaceans: transition from teeth to baleen and raptorial to bulk feeding. Integrative and Comparative Biology, 56:1271–1284. |
| 21 | *Balaenoptera floridana* USNM 529244 | Balaenopteridae | Myst | Pliocene | edentulous - baleen | zooplankton + fish | band1 | filter | pelagic | Berta, A., Lanzetti, A., Ekdale, E.G., and Deméré, T.A. 2016. Evolutionary innovations and ecology in mysticete cetaceans: transition from teeth to baleen and raptorial to bulk feeding. Integrative and Comparative Biology, 56:1271–1284. |

| | | | | | | | | | |
|---|---|---|---|---|---|---|---|---|---|
| 22 | *Balaenoptera musculus* NHM 1892.3.1.1 | Balaenopteridae | Myst | Extant | edentulous - baleen | zooplankton + fish | band1 | filter | pelagic | Berta, A., Lanzetti, A., Ekdale, E.G., and Deméré, T.A. 2016. Evolutionary innovations and ecology in mysticete cetaceans: transition from teeth to baleen and raptorial to bulk feeding. Integrative and Comparative Biology, 56:1271–1284. |
| 23 | *Balaenoptera omurai* NN | Balaenopteridae | Myst | Extant | edentulous - baleen | zooplankton + fish | band1 | filter | pelagic | Berta, A., Lanzetti, A., Ekdale, E.G., and Deméré, T.A. 2016. Evolutionary innovations and ecology in mysticete cetaceans: transition from teeth to baleen and raptorial to bulk feeding. Integrative and Comparative Biology, 56:1271–1284. |
| 24 | *Balaenoptera physalus* NHM 1862.2.7.181 | Balaenopteridae | Myst | Extant | edentulous - baleen | zooplankton + fish | band1 | filter | pelagic | Berta, A., Lanzetti, A., Ekdale, E.G., and Deméré, T.A. 2016. Evolutionary innovations and ecology in mysticete cetaceans: transition from teeth to baleen and raptorial to bulk feeding. Integrative and Comparative Biology, 56:1271–1284. |
| 25 | *Balaenoptera* sp SDNHM 83695 | Balaenopteridae | Myst | Pliocene | edentulous - baleen | zooplankton + fish | band1 | filter | pelagic | Berta, A., Lanzetti, A., Ekdale, E.G., and Deméré, T.A. 2016. Evolutionary innovations and ecology in mysticete cetaceans: transition from teeth to baleen and raptorial to bulk feeding. Integrative and Comparative Biology, 56:1271–1284. |
| 26 | *Balaenopteridae* NMNZ MM001630 | Balaenopteridae | Myst | Miocene | edentulous - baleen | zooplankton + fish | band1 | filter | pelagic | Berta, A., Lanzetti, A., Ekdale, E.G., and Deméré, T.A. 2016. Evolutionary innovations and ecology in mysticete cetaceans: transition from teeth to baleen and raptorial to bulk feeding. Integrative and Comparative Biology, 56:1271–1284. |
| 27 | *Balaenula astensis* MSNUP I-12555 | Balaenidae | Myst | Pliocene | edentulous - baleen | zooplankton + fish | band1 | filter | coastal-pelagic | Bianucci, G. 1996. The Odontoceti (Mammalia, Cetacea) from Italian Pliocene systematics and phylogenesis of Delphinidae. Palaeontolographia Italia, 83:73-167. |
| 28 | *Basilosaurus isis* SMNS 11787 | Basilosauridae | Arch | Eocene | heterodont | tetrapods + fish | band1 | biting | coastal-pelagic | Uhen, M.D. 2013. A review of North American Basilosauridae. Alabama Museum of Natural History Bulletin, 31(2):1-45. |
| 29 | *Berardius arnuxii* NHM 1935.10.23.1 | Ziphiidae | Odont | Extant | reduced | cephalopods + fish | band2 | suction | pelagic | Balcomb III, K. C. 1989. Baird's beaked whale - *Berardius bairdii* Stejneger, 1883: Arnoux's beaked whale - *Berardius arnouxii* Duvernoy, 1851, p261–288 In Ridgway, S. H. and Harrison, R. (eds.), Handbook of Marine Mammals - Vol. 4: River dolphins and the Larger Toothed Whales. Academic Press. |
| 30 | *Berardius bairdii* NHM 1954.9.21.1 | Ziphiidae | Odont | Extant | reduced | cephalopods + fish | band2 | suction | pelagic | Balcomb III, K. C. 1989. Baird's beaked whale - *Berardius bairdii* Stejneger, 1883: Arnoux's beaked whale - *Berardius arnouxii* Duvernoy, 1851, p261–288 In Ridgway, S. H. and Harrison, R. (eds.), Handbook of Marine Mammals - Vol. 4: River dolphins and the Larger Toothed Whales. Academic Press. |
| 31 | *Berardius minimus* USNM 276375 | Ziphiidae | Odont | Extant | reduced | cephalopods + fish | band2 | suction | pelagic | Yamada, T.K., Kitamura, S., Abe, S. et al. 2019. Description of a new species of beaked whale (*Berardius*) found in the North Pacific. Sci Rep 9, 12723. |
| 32 | *Brachydelphis mazeazi* MUSM 564 | Pontoporiidae | Odont | Miocene | homodont | cephalopods + fish | band2 | biting | coastal-pelagic | Lambert, O. and Muizon, C. de. 2013. A new long-snouted species of the Miocene pontoporiid dolphin *Brachydelphis* and a review of the Mio-Pliocene marine mammal levels in the Sacaco Basin, Peru. Journal of Vertebrate Paleontology, 33(3):709-721. |
| 33 | *Caperea marginata* NHM 1876.2.16.1 | Cetotheriidae | Myst | Extant | edentulous - baleen | zooplankton + fish | band1 | filter | pelagic | Berta, A., Lanzetti, A., Ekdale, E.G., and Deméré, T.A. 2016. Evolutionary innovations and ecology in mysticete cetaceans: transition from teeth to baleen |

| | | | | | | | | | |
|---|---|---|---|---|---|---|---|---|---|
| | | | | | | | | | and raptorial to bulk feeding. Integrative and Comparative Biology, 56:1271–1284. |
| 34 | *Cephalorhynchus commersonii* NN | Delphinidae | Odont | Extant | homodont | cephalopods + fish | band2 | biting | coastal | Goodall, R.N.P. 1994. Commerson's dolphin - *Cephalorhynchus commersonii* (Lacepede, 1804), p. 241–268 In Ridgway, S.H. and Harrison, R. (eds.), Handbook of Marine Mammals - Vol. 5: The First Book of Dolphins. Academic Press. |
| 35 | *Cephalorhynchus eutropia* NHM 1881.8.17.1 | Delphinidae | Odont | Extant | homodont | cephalopods + fish | band2 | biting | coastal | Jefferson, T.A, Webber, M.A. Pitman, R.L. Marine Mammals of the World: a Comprehensive Guide to their Identification. Academic Press, San Diego (2015) |
| 36 | *Cephalorhynchus heavisidii* NHM 1948.7.27.1 | Delphinidae | Odont | Extant | homodont | cephalopods + fish | band2 | biting | coastal | Pauly, D., Trites, A.W., Capuli, E., and Christensen, V. 1998. Diet composition and trophic levels of marine mammals. ICES Journal of Marine Science, 55: 467–481. T.A. Jefferson, M.A. Webber, R.L. Pitman Marine Mammals of the World: a Comprehensive Guide to their Identification Academic Press, San Diego (2008) |
| 37 | *Cephalorhynchus hectori maui* NMNZ MM002607 | Delphinidae | Odont | Extant | homodont | cephalopods + fish | band2 | biting | coastal | Pauly, D., Trites, A.W., Capuli, E., and Christensen, V. 1998. Diet composition and trophic levels of marine mammals. ICES Journal of Marine Science, 55: 467–481. T.A. Jefferson, M.A. Webber, R.L. Pitman Marine Mammals of the World: a Comprehensive Guide to their Identification Academic Press, San Diego (2008) |
| 38 | *Cephalorhynchus hectori* NMNZ MM002288 | Delphinidae | Odont | Extant | homodont | cephalopods + fish | band2 | biting | coastal | Pauly, D., Trites, A.W., Capuli, E., and Christensen, V. 1998. Diet composition and trophic levels of marine mammals. ICES Journal of Marine Science, 55: 467–481. |
| 39 | *Cephalotropis coronatus* USNM 489194 | Cetotheriidae | Myst | Miocene | edentulous - baleen | zooplankton + fish | band1 | filter | pelagic | Marx, F.G. and Fordyce, R.E. 2015. Baleen boom and bust: a synthesis of mysticete phylogeny, diversity and disparity. Royal Society Open Science, 2, 140434. E. D. Cope. 1896. Sixth contribution to the knowledge of the marine Miocene fauna of North America. Proceedings of the American Philosophical Soceity 35(150):139-146 |
| 40 | *Chavinziphius maxillocristatus* MUSM 2538 | Ziphiidae | Odont | Miocene | homodont | cephalopods + fish | band2 | biting | pelagic | Bianucci G, Di Celma C, Urbina. M and Lambert. O. 2016. New beaked whales from the late Miocene of Peru and evidence for convergent evolution in stem and crown Ziphiidae (Cetacea, Odontoceti). PeerJ 4:e2479 |
| 41 | *Chilcacetus cavirhinus* MUSM 1401 | incertae sedis | Odont | Miocene | homodont | cephalopods + fish | band2 | biting | coastal-pelagic | Lambert, O., Muizon, C. de, and Bianucci, G. 2015. A new archaic homodont toothed cetacean (Mammalia, Cetacea, Odontoceti) from the early Miocene of Peru. Geodiversitas, 37(1):79-108. |
| 43 | *Coronodon havensteini* CCNHM 108 | Aetiocetidae | Myst | Oligocene | heterodont | zooplankton + fish | band1 | suction | coastal-pelagic | Geisler, J.H., Boessenecker, R.W., Brown, M., Beatty, B.L. 2017. The origin of filter feeding in whales. Current Biology, 27:1-7. |
| 44 | *Cotylocara macei* CCNHM 101 | Xenorophidae | Odont | Oligocene | heterodont | benthic invertebrates + fish | band2 | biting | coastal-pelagic | Geisler, J.H, Colbert M.W, and Carew J.L. 2014. A new fossil species supports an early origin for toothed whale echolocation. Nature |

413

| 45 | *Cynthiacetus peruvianus* MNHN.F. PRU10 | Basilosauridae | Arch | Eocene | heterodont | tetrapods + fish | band1 | biting | coastal-pelagic | Martinez-Cã¡ceres, M. and Muizon, C. de. 2011. A new basilosaurid (Cetacea, Pelagiceti) from the Priabonian to Rupelian Otuma Formation of Peru. Comptes Rendus Palevol, 10:517-526 |
|---|---|---|---|---|---|---|---|---|---|---|
| 46 | *Delphinapterus leucas* USNM 305071 | Monodontidae | Odont | Extant | homodont | cephalopods + fish | band2 | suction | coastal-pelagic | Stewart, B.E., and Stewart, R.E.A. 1989. *Delphinapterus leucas*. Mammalian Species, 336:1–8. |
| 47 | *Delphinodon dividum* USNM 7278 | Kentriodontidae | Odont | Miocene | homodont | cephalopods + fish | band2 | biting | coastal-pelagic | True, F.W. 1912. Description of a new fossil porpoise of the genus *Delphinodon* from the Miocene formation of Maryland. Journal of the Academy of Natural Sciences of Philadelphia, 2:165-194 |
| 48 | *Delphinus capensis* NHM 1981.7.11 | Delphinidae | Odont | Extant | homodont | cephalopods + fish | band2 | biting | coastal-pelagic | Heyning, J.E., and Perrin, W.F. 1994. Evidence for two species of common dolphins (genus *Delphinus*) from the eastern North Pacific. Contributions in Science, Natural History Musuem of Los Angeles County, 442:1–35 |
| 49 | *Delphinus delphis* AMNH 75332 | Delphinidae | Odont | Extant | homodont | cephalopods + fish | band2 | biting | coastal-pelagic | Heyning, J.E., and Perrin, W.F. 1994. Evidence for two species of common dolphins (genus *Delphinus*) from the eastern North Pacific. Contributions in Science, Natural History Musuem of Los Angeles County, 442:1–35. |
| 50 | *Dilophodelphis fordycei* USNM 214911 | Platanistidae | Odont | Miocene | homodont | cephalopods + fish | band2 | biting | coastal-pelagic | Boersma, A.T., McCurry, M.R. and Pyenson, N.D. 2017. A new fossil dolphin *Dilophodelphis fordycei* provides insight into the evolution of supraorbital crests in Platanistoidea (Mammalia, Cetacea). Royal Society Open Science, |
| 51 | *Diorocetus hiatus* USNM 16783 | Pelocetidae | Myst | Miocene | edentulous - baleen | zooplankton + fish | band1 | filter | coastal-pelagic | Dooley, A.C., Fraser, N.C. and Luo, Z. 2014. The earliest known member of the rorqual-gray whale clade (Mammalia, Cetacea). Journal of Vertebrate Paleontology, 24(2):453-463. |
| 52 | *Dorudon atrox* PV M 100149 | Basilosauridae | Arch | Eocene | heterodont | tetrapods + fish | band1 | biting | coastal-pelagic | Uhen, M.D. 2004. Form, function, and anatomy of *Dorudon atrox* (Mammalia, Cetacea): an archaeocete from the Middle to Late Eocene of Egypt. University of Michigan Papers in Paleontology, 34:1–222. |
| 53 | *Echovenator sandersi* GSM 1098 | Xenorophidae | Odont | Oligocene | heterodont | benthic invertebrates + fish | band2 | biting | coastal-pelagic | Churchill, M., Martinez-Caceres M; de Muizon, C; Mnieckowski, J; Geisler, JH (2016). "The Origin of High-Frequency Hearing in Whales". Current Biology. in press. doi: 10.1016/j.cub.2016.06.004. |
| 54 | *Ensidelphis riveroi* MUSM 3898 | incertae sedis | Odont | Miocene | homodont | cephalopods + fish | band2 | biting | coastal-pelagic | Bianucci, G, Muizon, C. De, Urbina, M. and Lambert, O. 2020. Extensive diversity and disparity of the early Miocene platanistoids (Cetacea, Odontoceti) in the southeastern Pacific (Chilcatay Formation, Peru). Life, 10, 27. |
| 55 | *Eschrichtius robustus* USNM 13803 | Eschrichtiidae | Myst | Extant | edentulous - baleen | benthic invertebrates + fish | band1 | suction | coastal-pelagic | Berta, A., Lanzetti, A., Ekdale, E.G., and Deméré, T.A. 2016. Evolutionary innovations and ecology in mysticete cetaceans: transition from teeth to baleen and raptorial to bulk feeding. Integrative and Comparative Biology, 56:1271–1284. |
| 56 | *Etruridelphis* PU 13884 | Delphinidae | Odont | Pliocene | homodont | cephalopods + fish | band2 | biting | coastal-pelagic | Bianucci, G., Vaiani, S.C. and Casati, S. 2009. A new delphinid record (Odontoceti, Cetacea) from the Zanclean of Tuscany (Central Italy): systematics and biostratigraphic considerations. Neus Jahrbuch fur Geologie und Palaontologie Abhandlungen, 254(3):275-292. |

| 57 | *Eubalaena australis* NHM 1873.3.3 | Balaenidae | Myst | Extant | edentulous - baleen | zooplankton + fish | band1 | filter | pelagic | Berta, A., Lanzetti, A., Ekdale, E.G., and Deméré, T.A. 2016. Evolutionary innovations and ecology in mysticete cetaceans: transition from teeth to baleen and raptorial to bulk feeding. Integrative and Comparative Biology, 56:1271–1284. |
|---|---|---|---|---|---|---|---|---|---|---|
| 58 | *Eubalaena glacialis* MSNUP | Balaenidae | Myst | Extant | edentulous - baleen | zooplankton + fish | band1 | filter | pelagic | Berta, A., Lanzetti, A., Ekdale, E.G., and Deméré, T.A. 2016. Evolutionary innovations and ecology in mysticete cetaceans: transition from teeth to baleen and raptorial to bulk feeding. Integrative and Comparative Biology, 56:1271–1284. |
| 59 | *Eurhinodelphid* UCMP 99669 | Eurhinodelphinidae | Odont | Miocene | homodont | fish | band2 | biting | coastal-pelagic | Benoit, J., Adnet, S., Welcomme, J.-L., and Fabre, P.-H. 2011. New skull of *Schizodelphis sulcatus* Gervais, 1861 (Mammalia, Odontoceti, Eurhinodelphinidae) from the Lower Miocene of Pignan (Hérault, France) and its implications for systematics of Eurhinodelphinidae. Geobios, 44(2011):323-334. |
| 60 | *Eurhinodelphinidae chilcocetus* MUSM | Eurhinodelphinidae | Odont | Miocene | homodont | fish | band2 | biting | coastal-pelagic | Benoit, J., Adnet, S., Welcomme, J.-L., and Fabre, P.-H. 2011. New skull of *Schizodelphis sulcatus* Gervais, 1861 (Mammalia, Odontoceti, Eurhinodelphinidae) from the Lower Miocene of Pignan (Hérault, France) and its implications for systematics of Eurhinodelphinidae. Geobios, 44(2011):323-334. |
| 61 | *Eurhinodelphis cocheteuxi* IRSNB | Eurhinodelphinidae | Odont | Miocene | homodont | fish | band2 | biting | coastal-pelagic | Lambert, O. 2005. Review of the Miocene long-snouted dolphin *Priscodelphinus cristatus* Du Bus, 1872 (Cetacea, Odontoceti) and phylogeny among eurhinodelphinids. Bulletin de L'Institute Royal des Sciences Naturelles de Belgique Sciences de la Terre, 75:211-235. O. Lambert. 2005. Phylogenetic affinities of the long-snouted dolphin *Eurhinodelphis* (Cetacea, Odontoceti) from the Miocene of Antwerp, Belgium. Palaeontology 48(3):653-679 |
| 62 | *Eurhinodelphis longirostris* USNM 244404 | Eurhinodelphinidae | Odont | Miocene | homodont | fish | band2 | biting | coastal-pelagic | Lambert, O. 2005. Review of the Miocene long-snouted dolphin *Priscodelphinus cristatus* Du Bus, 1872 (Cetacea, Odontoceti) and phylogeny among eurhinodelphinids. Bulletin de L'Institute Royal des Sciences Naturelles de Belgique Sciences de la Terre, 75:211-235. |
| 63 | *Feresa attenuata* USNM 504916 | Delphinidae | Odont | Extant | homodont | cephalopods + fish | band2 | biting | pelagic | Ross, J.B., and Leatherwood, S. 1994. Pigmy killer whale - *Feresa attenuata* Gray, 1874; pp. 387–404 In Ridgway, S.H. and Harrison, R. (eds.), Handbook of Marine Mammals - Vol. 5: The First Book of Dolphins. Academic Press. |
| 42 | *Fucaia goedertorum* LACM 131146 | Aetiocetidae | Myst | Oligocene | heterodont | zooplankton + fish | band1 | suction | coastal-pelagic | Marx, F. G., Tsai, C.-H. and Fordyce, R.E. 2015. A new Rupelian toothed baleen whale (Mysticeti: Aetiocetidae) from western North America: one of the oldest and the smallest. Royal Society Open Science, 2(12):150476. |
| 64 | *Globicephala macrorhynchus* NHM 1912.10.27 | Delphinidae | Odont | Extant | homodont | cephalopods + fish | band2 | suction | pelagic | Bernard, H.J., and Reilly, S.B. 1998. Pilot whales - *Globicephala*, 1828, p. 245–280 in Ridgway, S.H. and Harrison, R. (eds.), Handbook of Marine Mammals - Vol. 6: The second book of Dolphins and Porpoises. Elsevier Ltd. |
| 65 | *Globicephala melas* NMNZ MM001946 | Delphinidae | Odont | Extant | homodont | cephalopods + fish | band2 | suction | pelagic | Bernard, H.J., and Reilly, S.B. 1998. Pilot whales - *Globicephala*, 1828, p. 245–280 in Ridgway, S.H. and Harrison, R. (eds.), Handbook of Marine Mammals - Vol. 6: The second book of Dolphins and Porpoises. Elsevier Ltd. |

| 66 | *Globicephala* sp USNM 21867 | Delphinidae | Odont | Pleistocene | homodont | cephalopods + fish | band2 | suction | pelagic | Bernard, H.J., and Reilly, S.B. 1998. Pilot whales - *Globicephala*, 1828, p. 245–280 in Ridgway, S.H. and Harrison, R. (eds.), Handbook of Marine Mammals - Vol. 6: The second book of Dolphins and Porpoises. Elsevier Ltd. |
|---|---|---|---|---|---|---|---|---|---|---|
| 67 | *Goedertius oregonensis* LACM 123887 | Allodelphinidae | Odont | Miocene | homodont | fish | band2 | biting | coastal-pelagic | Kimura, T. and Barnes, L.G. 2016. New Miocene fossil Allodelphinidae (Cetacea, Odontoceti, Platanistoidea) from the North Pacific Ocean. Bulletin of the Gunma Museum of Natural History, 20:1-58. |
| 68 | *Grampus griseus* USNM 571602 | Delphinidae | Odont | Extant | homodont | cephalopods + fish | band2 | suction | pelagic | Bearzi, G., Reeves, R.R., Remonato, E., Pierantonio, N. and Airoldi, S. 2011. Risso's dolphin *Grampus griseus* in the Mediterranean Sea. Mammalian Biology, 76:385–400. |
| 69 | *Hemisyntrachelus cortesii* MBGPT NN | Delphinidae | Odont | Pliocene | homodont | cephalopods + fish | band2 | biting | coastal-pelagic | Bianucci, G. 1996. The Odontoceti (Mammalia, Cetacea) from Italian Pliocene systematics and phylogenesis of Delphinidae. Palaeontolographia Italia, 83:73-167. G. Pilleri and H. J. Siber. 1989. Neuer delphinid (Cetacea, Odontoceti) aus der Pisco-Formation Perus. Beitrage zur Palaontologie der cetaceen Perus 167-175 |
| 70 | *Hemisyntrachelus oligodon* SMNK-PAL 3841 | Delphinidae | Odont | Miocene | homodont | fish | band2 | biting | coastal-pelagic | Pilleri. G and Siber, H.J. 1989. Neuer delphinid (Cetacea, Odontoceti) aus der Pisco-Formation Perus. Beitrage zur Palaontologie der cetaceen Perus 167-175 |
| 71 | *Herpetocetus sendaicus* NMNS-PV 19540 | Cetotheriidae | Myst | Pliocene | edentulous - baleen | benthic invertebrates + fish | band1 | filter | coastal-pelagic | Boessenecker, R.W. 2011. Herpetocetine (Cetacea: Mysticeti) dentaries from the Upper Miocene Santa Margarita Sandstone of Central California. PaleoBios 30(1):1-12. El Adli, J.J., Deméré, T.A., and Boessenecker, R.W. 2014. *Herpetocetus morrowi* (Cetacea: Mysticeti), a new species of diminutive baleen whale from the upper Pliocene (Piacenzian) of California, USA, with observations on the evolution and relationships of the Cetotheriidae. Zoological Journal of the Linnean Society, 170:400–66. |
| 72 | *Huaridelphis raimondii* MUSM 1396 | Squalodelphinidae | Odont | Miocene | homodont | fish | band2 | biting | coastal-pelagic | Lambert, O., Bianucci, G. and Urbina, M. 2014. *Huaridelphis raimondii*, a new early Miocene Squalodelphinidae (Cetacea, Odontoceti) from the Chilcatay Formation, Peru. Journal of Vertebrate Paleontology, 34(5):987-1004. |
| 73 | *Hyperoodon ampullatus* NHM 1992.42 | Ziphiidae | Odont | Extant | reduced | cephalopods + fish | band2 | suction | pelagic | Boschma, H. 1951. Rows of Small Teeth in Ziphioid Whales. Zoologische Mededelingen, 31:139–148. T.A. Jefferson, M.A. Webber, R.L. Pitman Marine Mammals of the World: a Comprehensive Guide to their Identification Academic Press, San Diego (2015) |
| 74 | *Hyperoodon planifrons* NHM 1952.9.30.1 | Ziphiidae | Odont | Extant | reduced | cephalopods + fish | band2 | suction | pelagic | Boschma, H. 1951. Rows of Small Teeth in Ziphioid Whales. Zoologische Mededelingen, 31:139–148. Jefferson, T.A, Webber, M.A. Pitman, R.L. Marine Mammals of the World: a Comprehensive Guide to their Identification. Academic Press, San Diego (2015) |
| 75 | *Indopacetus pacificus* USNM 593534 | Ziphiidae | Odont | Extant | reduced | cephalopods + fish | band2 | suction | pelagic | Boschma, H. 1951. Rows of Small Teeth in Ziphioid Whales. Zoologische Mededelingen, 31:139–148. Jefferson, T.A, Webber, M.A. Pitman, R.L. Marine Mammals of the World: a Comprehensive Guide to their Identification. Academic Press, San Diego (2015) |

| | | | | | | | | | |
|---|---|---|---|---|---|---|---|---|---|
| 76 | *Inia geoffrensis* AMNH 93415 | Iniidae | Odont | Extant | homodont | fish | band2 | biting | riverine | Best, R.C., and Da Silva, V.M.F. 1993. *Inia geoffrensis*. Mammalian Species, 426:1–8. |
| 77 | *Janjucetus hunderi* NMV P216929 | Mammalodontidae | Myst | Oligocene | heterodont | benthic invertebrates + fish | band1 | biting | coastal-pelagic | Fitzgerald, E.M.G. 2006. A bizarre new toothed mysticete (Cetacea) from Australia and the early evolution of baleen whales. Proceedings of the Royal Society B; Fitzgerald, E.M.G. 2010. The morphology and systematics of *Mammalodon colliveri* (Cetacea: Mysticeti), a toothed mysticete from the Oligocene of Australia |
| 78 | *Kampholophus serrulus* UMCP 36045 | Kentriodontidae | Odont | Miocene | homodont | cephalopods + fish | band2 | biting | coastal-pelagic | Rensberger, J.M. 1969. A new iniid cetacean from the Miocene of California. University of California Publications in Geological Sciences, 82:1-34. |
| 79 | *Kekenodon* OU 22294 | Kekenodontidae | Arch | Oligocene | heterodont | zooplankton + fish | band1 | biting | coastal-pelagic | Clementz, M.T., Fordyce, E., Peek, S.L., and Fox, D.L. 2014. Ancient marine isoscapes and isotopic evidence of bulk-feeding by Oligocene cetaceans. Palaeogeography, Palaeoclimatology, Palaeoecology, 400:28-40. |
| 80 | *Kentriodon* NN | Kentriodontidae | Odont | Miocene | homodont | cephalopods + fish | band2 | biting | coastal-pelagic | Kellogg, R. 1927. *Kentriodon pernix*, a Miocene porpoise from Maryland. Proceedings of the United States National Museum, 69(19):1-14. |
| 81 | *Kentriodon pernix* USNM 10670 | Kentriodontidae | Odont | Miocene | homodont | cephalopods + fish | band2 | biting | coastal-pelagic | Kellogg, R. 1927. *Kentriodon pernix*, a Miocene porpoise from Maryland. Proceedings of the United States National Museum, 69(19):1-14. |
| 82 | *Kentriodon schneideri* USNM 323772 | Kentriodontidae | Odont | Miocene | homodont | cephalopods + fish | band2 | biting | coastal-pelagic | F. C. Whitmore and J. A. Kaltenbach. 2008. Neogene Cetacea of the Lee Creek Phosphate Mine, North Carolina. Virginia Museum of Natural History Special Publication 14:181-269. Kellogg, R. 1927. *Kentriodon pernix*, a Miocene porpoise from Maryland. Proceedings of the United States National Museum, 69(19):1-14. |
| 83 | *Kogia breviceps* USNM 22015 | Kogiidae | Odont | Extant | homodont | cephalopods + fish | band2 | suction | pelagic | Bloodworth, B.E., and Odell, D.K. 2008. *Kogia breviceps* (Cetacea: Kogiidae). Mammalian Species, 819:1–12. |
| 84 | *Kogia simus* NHM.1952.8.28.1 | Kogiidae | Odont | Extant | homodont | cephalopods + fish | band2 | suction | pelagic | Bloodworth, B.E., and Odell, D.K. 2008. *Kogia breviceps* (Cetacea: Kogiidae). Mammalian Species, 819:1–12. T.A. Jefferson, M.A. Webber, R.L. Pitman Marine Mammals of the World: a Comprehensive Guide to their Identification Academic Press, San Diego (2015) |
| 85 | *Koristocetus pescei* MUSM 888 | Kogiidae | Odont | Miocene | homodont | cephalopods + fish | band2 | suction | coastal-pelagic | Collareta, A., Lambert, O., Muizon, C. de, Urbina, M. and Bianucci, G. 2017. *Koristocetus pescei* gen. et sp. nov., a diminutive sperm whale (Cetacea: Odontoceti: Kogiidae) from the late Miocene of Peru. Fossil Record ,20:259-278. |
| 86 | *Lagenodelphis hosei* USNM 571619 | Delphinidae | Odont | Extant | homodont | cephalopods + fish | band2 | biting | pelagic | Jefferson, T. A., and S. Leatherwood. 1994. *Lagenodelphis hosei*. Mammalian Species, 470:1–5. |
| 87 | *Lagenorhynchus acutus* USNM 504196 | Delphinidae | Odont | Extant | homodont | cephalopods + fish | band2 | biting | coastal-pelagic | Berrow, S., and Cotton., D.C.F. 1990. White-sided dolphin *Lagenorhynchus acutus* (Gray). Irish Naturalists' Journal, 23:333–335. |

| | | | | | | | | | |
|---|---|---|---|---|---|---|---|---|---|
| 88 | *Lagenorhynchus albirostris* AMNH 37162 | Delphinidae | Odont | Extant | homodont | cephalopods + fish | band2 | biting | coastal-pelagic | Jefferson, T.A, Webber, M.A. Pitman, R.L. Marine Mammals of the World: a Comprehensive Guide to their Identification. Academic Press, San Diego (2015) |
| 89 | *Lagenorhynchus australis* 1944.11.30.1 | Delphinidae | Odont | Extant | homodont | cephalopods + fish | band2 | biting | coastal-pelagic | Jefferson, T.A, Webber, M.A. Pitman, R.L. Marine Mammals of the World: a Comprehensive Guide to their Identification. Academic Press, San Diego (2015) |
| 90 | *Lagenorhynchus cruciger* NHM 1960.8.24.1 | Delphinidae | Odont | Extant | homodont | cephalopods + fish | band2 | biting | coastal-pelagic | Jefferson, T.A, Webber, M.A. Pitman, R.L. Marine Mammals of the World: a Comprehensive Guide to their Identification. Academic Press, San Diego (2015) |
| 91 | *Lagenorhynchus obliquidens* NHM 1992.83 | Delphinidae | Odont | Extant | homodont | cephalopods + fish | band2 | biting | coastal-pelagic | Jefferson, T.A, Webber, M.A. Pitman, R.L. Marine Mammals of the World: a Comprehensive Guide to their Identification. Academic Press, San Diego (2015) |
| 92 | *Lagenorhynchus obscurus* NHM 1846.3.11.8 | Delphinidae | Odont | Extant | homodont | cephalopods + fish | band2 | biting | coastal-pelagic | Jefferson, T.A, Webber, M.A. Pitman, R.L. Marine Mammals of the World: a Comprehensive Guide to their Identification. Academic Press, San Diego (2015) |
| 93 | *Lamprolithax simulans* LACM 37858 | incertae sedis | Odont | Miocene | homodont | cephalopods + fish | band2 | biting | coastal-pelagic | Barnes, L.G. 1977. Outline of eastern North Pacific fossil cetacean assemblages. Systematic Zoology 25(4):321-343. R. Kellogg. 1931. Pelagic mammals of the Temblor Formation of the Kern River region, California. Proceedings of the California Academy of Science 19(12):217-397 |
| 94 | *Lipotes vexillifer* AMNH 57333 | Lipotidae | Odont | Extant | homodont | fish | band2 | biting | riverine | Brownell, R.L., and Herald, E.S. 1972. *Lipotes vexillifer*. Mammalian Species, 10:1–4. |
| 95 | *Lissodelphis borealis* USNM 550188 | Delphinidae | Odont | Extant | homodont | cephalopods + fish | band2 | biting | pelagic | Newcomer, M. W., Jefferson, T.A., Brownell, R.L. and Brownell Jr., R.L. 1996. *Lissodelphis peronii*. Mammalian Species, 531:1–5. T.A. Jefferson, M.A. Webber, R.L. Pitman. Marine Mammals of the World: a Comprehensive Guide to their Identification. Academic Press, San Diego (2015) |
| 96 | *Lissodelphis peronii* NMNZ MM002116 | Delphinidae | Odont | Extant | homodont | cephalopods + fish | band2 | biting | pelagic | Newcomer, M. W., Jefferson, T.A., Brownell, R.L. and Brownell Jr., R.L. 1996. *Lissodelphis peronii*. Mammalian Species, 531:1–5. |
| 97 | *Livyatan melvillei* MSNUP | incertae sedis | Odont | Miocene | homodont | tetrapods + fish | band2 | biting | pelagic | Lambert, O. Bianucci, G. Post, K. Muizon, C. de, Salas-Gismondi, R. Urbina, M and Reumer, J. 2010. Corrigendum: The giant bite of a new raptorial sperm whale from the Miocene epoch of Peru. Nature, 466:1134 |
| 98 | *Lomacetus ginsburgi* MNHN.F.PPI.104 | Phocoenidae | Odont | Miocene | homodont | cephalopods + fish | band2 | biting | coastal-pelagic | Muizon, C. de. 1986. Un nouveau Phocoenidae (Odontoceti, Mammalia) du Miocene superieur de la Formation Pisco (Perou). Comptes Rendus hebdomadaires des seances de l'Academie des Sciences, Serie II 303(16):1509-1512. |
| 99 | *Macrokentriodon* CMM V 15 | Kentriodontidae | Odont | Miocene | homodont | cephalopods + fish | band2 | biting | coastal-pelagic | Dawson, S.D. 1996. A description of the skull and postcrania of *Hadrodelphis calvertense* Kellogg 1966, and its position within the Kentriodontidae (Cetacea; Delphinoidea). Journal of Vertebrate Paleontology, 16(1):125-134. Dawson, S.D. 1996. A new kentriodontid dolphin (Cetacea; Delphinoidea) from the middle Miocene Choptank Formation, Maryland. Journal of Vertebrate Paleontology 16(1):135-140 |

| | | | | | | | | | | |
|---|---|---|---|---|---|---|---|---|---|---|
| 100 | *Macrosqualodelphis ukupachai* MUSM 2545 | Squalodelphinidae | Odont | Miocene | homodont | cephalopods + fish | band2 | biting | coastal-pelagic | Bianucci, G Bosio, G. Malinverno, E. Muizon, C. Villa, I.M, Urbina, M. and Lambert, O. 2018. A new large squalodelphinid (Cetacea, Odontoceti) from Peru sheds light on the Early Miocene platanistoid disparity and ecology. Royal Society Open Science 5(4):172302 |
| 101 | *Megaptera novaeangliae* GERM.792a | Balaenopteridae | Myst | Extant | edentulous - baleen | zooplankton + fish | band1 | filter | pelagic | Jefferson, T.A, Webber, M.A. Pitman, R.L. Marine Mammals of the World: a Comprehensive Guide to their Identification. Academic Press, San Diego (2015) |
| 102 | *Mesoplodon bidens* USNM 593438 | Ziphiidae | Odont | Extant | reduced | cephalopods + fish | band2 | suction | pelagic | Ellis, R., & Mead, J.G. (2017). Beaked Whales: A Complete Guide to Their Biology and Conservation. Baltimore: Johns Hopkins University Press. |
| 103 | *Mesoplodon bowdoini* NMNZ MM001900 | Ziphiidae | Odont | Extant | reduced | cephalopods + fish | band2 | suction | pelagic | Ellis, R., & Mead, J.G. (2017). Beaked Whales: A Complete Guide to Their Biology and Conservation. Baltimore: Johns Hopkins University Press. |
| 104 | *Mesoplodon carlhubbsi* USNM 504128 | Ziphiidae | Odont | Extant | reduced | cephalopods + fish | band2 | suction | pelagic | Ellis, R., & Mead, J.G. (2017). Beaked Whales: A Complete Guide to Their Biology and Conservation. Baltimore: Johns Hopkins University Press. |
| 105 | *Mesoplodon densirostris* NMV C 36362 | Ziphiidae | Odont | Extant | reduced | cephalopods + fish | band2 | suction | pelagic | Ellis, R., & Mead, J.G. (2017). Beaked Whales: A Complete Guide to Their Biology and Conservation. Baltimore: Johns Hopkins University Press. |
| 106 | *Mesoplodon europaeus* USNM 571665 | Ziphiidae | Odont | Extant | reduced | cephalopods + fish | band2 | suction | pelagic | Ellis, R., & Mead, J.G. (2017). Beaked Whales: A Complete Guide to Their Biology and Conservation. Baltimore: Johns Hopkins University Press. |
| 107 | *Mesoplodon ginkgodens* USNM 298237 | Ziphiidae | Odont | Extant | reduced | cephalopods + fish | band2 | suction | pelagic | Ellis, R., & Mead, J.G. (2017). Beaked Whales: A Complete Guide to Their Biology and Conservation. Baltimore: Johns Hopkins University Press. |
| 108 | *Mesoplodon grayi* USNM 49880 | Ziphiidae | Odont | Extant | reduced | cephalopods + fish | band2 | suction | pelagic | Ellis, R., & Mead, J.G. (2017). Beaked Whales: A Complete Guide to Their Biology and Conservation. Baltimore: Johns Hopkins University Press. |
| 109 | *Mesoplodon hectori* NHM 1949.8.19.1 | Ziphiidae | Odont | Extant | reduced | cephalopods + fish | band2 | suction | pelagic | Ellis, R., & Mead, J.G. (2017). Beaked Whales: A Complete Guide to Their Biology and Conservation. Baltimore: Johns Hopkins University Press. |
| 110 | *Mesoplodon hotaula* USNM 593426 | Ziphiidae | Odont | Extant | reduced | cephalopods + fish | band2 | suction | pelagic | Ellis, R., & Mead, J.G. (2017). Beaked Whales: A Complete Guide to Their Biology and Conservation. Baltimore: Johns Hopkins University Press. |
| 111 | *Mesoplodon layardii* USNM 550150 | Ziphiidae | Odont | Extant | reduced | cephalopods + fish | band2 | suction | pelagic | Ellis, R., & Mead, J.G. (2017). Beaked Whales: A Complete Guide to Their Biology and Conservation. Baltimore: Johns Hopkins University Press. |
| 112 | *Mesoplodon mirus* USNM 504612 | Ziphiidae | Odont | Extant | reduced | cephalopods + fish | band2 | suction | pelagic | Ellis, R., & Mead, J.G. (2017). Beaked Whales: A Complete Guide to Their Biology and Conservation. Baltimore: Johns Hopkins University Press. |
| 113 | *Mesoplodon perrini* LACM 97501 | Ziphiidae | Odont | Extant | reduced | cephalopods + fish | band2 | suction | pelagic | Ellis, R., & Mead, J.G. (2017). Beaked Whales: A Complete Guide to Their Biology and Conservation. Baltimore: Johns Hopkins University Press. |

| 114 | *Mesoplodon peruvianus* USNM 571258 | Ziphiidae | Odont | Extant | reduced | cephalopods + fish | band2 | suction | pelagic | Ellis, R., & Mead, J.G. (2017). Beaked Whales: A Complete Guide to Their Biology and Conservation. Baltimore: Johns Hopkins University Press. |
|---|---|---|---|---|---|---|---|---|---|---|
| 115 | *Mesoplodon stejnegeri* USNM 504330 | Ziphiidae | Odont | Extant | reduced | cephalopods + fish | band2 | suction | pelagic | Ellis, R., & Mead, J.G. (2017). Beaked Whales: A Complete Guide to Their Biology and Conservation. Baltimore: Johns Hopkins University Press. |
| 116 | *Mesoplodon traversii juv.* NMNZ TMP012996 | Ziphiidae | Odont | Extant | reduced | cephalopods + fish | band2 | suction | pelagic | Ellis, R., & Mead, J.G. (2017). Beaked Whales: A Complete Guide to Their Biology and Conservation. Baltimore: Johns Hopkins University Press. |
| 117 | *Messapicetus gregarius* MUSM 1481 | Ziphiidae | Odont | Miocene | reduced | cephalopods + fish | band2 | suction | pelagic | Ellis, R., & Mead, J.G. (2017). Beaked Whales: A Complete Guide to Their Biology and Conservation. Baltimore: Johns Hopkins University Press. |
| 118 | *Messapicetus longirostris* MSNUP | Ziphiidae | Odont | Miocene | reduced | cephalopods + fish | band2 | suction | pelagic | Ellis, R., & Mead, J.G. (2017). Beaked Whales: A Complete Guide to Their Biology and Conservation. Baltimore: Johns Hopkins University Press. |
| 119 | *Miocaperea pulchra* SMNS 46978 | Cetotheriidae | Myst | Miocene | edentulous - baleen | zooplankton + fish | band1 | filter | coastal-pelagic | Bisconti, M. 2012. Comparative osteology and phylogenetic relationships of *Miocaperea pulchra*, the first fossil pygmy right whale genus and species (Cetacea, Mysticeti, Neobalaenidae). Zoological Journal of the Linnean Society, 166:876-911. |
| 120 | *Mixocetus* LACM 143474 | Tranatocetidae | Myst | Miocene | edentulous - baleen | zooplankton + fish | band1 | filter | coastal-pelagic | Goldin, P. and Steeman, M. E. 2015. From problem taxa to problem solver: A new Miocene family, Tranatocetidae, brings perspective on baleen whale evolution. PLoS One 10(9):e0135500 |
| 121 | *Monodon monoceros* USNM 267959 | Monodontidae | Odont | Extant | reduced | cephalopods + fish | band2 | suction | coastal-pelagic | Reeves, R.R., and Tracey, S. 1980. *Monodon monoceros*. Mammalian Species, 127:1–7. |
| 122 | MUSM 563 | Kentriodontidae | Odont | Miocene | homodont | fish | band2 | biting | coastal-pelagic | Dawson, S.D. 1996. A description of the skull and postcrania of *Hadrodelphis calvertense* Kellogg 1966, and its position within the Kentriodontidae (Cetacea; Delphinoidea). Journal of Vertebrate Paleontology, 16(1):125-134. |
| 123 | MUSM 605 | Kentriodontidae | Odont | Miocene | homodont | fish | band2 | biting | coastal-pelagic | Dawson, S.D. 1996. A description of the skull and postcrania of *Hadrodelphis calvertense* Kellogg 1966, and its position within the Kentriodontidae (Cetacea; Delphinoidea). Journal of Vertebrate Paleontology, 16(1):125-134. |
| 124 | *Mystacodon selenensis* MUSM 1917 | Mystacodontidae | Myst | Eocene | heterodont | benthic invertebrates + fish | band1 | suction | coastal | Lambert O, Martínez-Cáeres, M, Bianucci G, Steurbaut E, Urbina M and Muizon C. 2017. Earliest Mysticete from the Late Eocene of Peru Sheds New Light on the Origin of Baleen Whales. Current Biology 27:17 |
| 125 | *Nazcacetus urbinai* MUSM 949 | Ziphiidae | Odont | Miocene | reduced | cephalopods + fish | band2 | suction | coastal-pelagic | Lambert, O. 2009. A new beaked whale (Odontoceti, Ziphiidae) from the middle Miocene of Peru. Journal of Vertebrate Paleontology, 29(3):910-922. |
| 126 | *Neophocaena asiaeorientalis* USNM 240001 | Phocoenidae | Odont | Extant | homodont | cephalopods + fish | band2 | biting | coastal | Jefferson, T.A, Webber, M.A. Pitman, R.L. Marine Mammals of the World: a Comprehensive Guide to their Identification. Academic Press, San Diego (2015) |

| | | | | | | | | | |
|---|---|---|---|---|---|---|---|---|---|
| 127 | *Neophocoena phocaenoides* NHM 1903.9.12.3 | Phocoenidae | Odont | Extant | homodont | cephalopods + fish | band2 | biting | coastal | Jefferson, T.A., and King, S.K. 2004. *Neophocaena phocaenoides*. Mammalian Species, 746:1–12. |
| 128 | *Notocetus vanbenedeni* MUSM 1395 | Squalodelphinidae | Odont | Miocene | homodont | cephalopods + fish | band2 | biting | coastal-pelagic | Dal Piaz, G. 1917. Gli Odontoceti del Miocene bellunese, Parte Terza. *Squalodelphis fabiannii*. Memorie dell' Instituto Geologico della R. Universita di Padova, 5(1):1-34. |
| 129 | *Odobenocetops peruvianus* SMNK PAL 2491 | Odobenocetopsidae | Odont | Pliocene | reduced | benthic invertebrates + fish | band1 | suction | coastal | Muizon, C. de, Domning, D.P. and Ketten, D.R. 2002. *Odobenocetops peruvianus*, the walrus-convergent delphinoid (Mammalia: Cetacea) from the Zanclean of Peru. Smithsonian Contributions to Paleobiology, 93:223-261. |
| 130 | *Orcaella brevirostris* NHM.1883.11.20.2 | Delphinidae | Odont | Extant | homodont | benthic invertebrates + fish | band2 | biting | coastal | Stacey, P.J., and Arnold, P.W. 1999. *Orcaella brevirostris*. Mammalian Species, 616:1–8. |
| 131 | *Orcaella heinsohni* USNM 284430 | Delphinidae | Odont | Extant | homodont | benthic invertebrates + fish | band2 | biting | coastal | Jefferson, T.A, Webber, M.A. Pitman, R.L. Marine Mammals of the World: a Comprehensive Guide to their Identification. Academic Press, San Diego (2015) |
| 132 | *Orcinus orca* USNM 11980 | Delphinidae | Odont | Extant | homodont | tetrapods + fish | band2 | biting | coastal-pelagic | Jefferson, T.A, Webber, M.A. Pitman, R.L. Marine Mammals of the World: a Comprehensive Guide to their Identification. Academic Press, San Diego (2015) |
| 133 | *Orycterocetus crocodilinus* USNM 22926 | Physeteridae | Odont | Miocene | homodont | fish | band2 | suction | coastal-pelagic | Bianucci, G., Landini, W. and Varola, A. 2004. First discovery of the Miocene northern Atlantic sperm whale *Orycterocetus* in the Mediterranean. Geobios, 37:569-573. |
| 134 | *Pakicetus attocki* PV M 100148 | Pakicetidae | Arch | Eocene | heterodont | benthic invertebrates + fish | band1 | biting | coastal | Gingerich, P.D. and Russell, D.E. 1981. *Pakicetus inachus*, a new archaeocete (Mammalia, Cetacea) from the early-middle Eocene Kuldana Formation of Kohat (Pakistan). Contributions from the Museum of Paleontology, University of Michigan, 25(11): 235-246. |
| 135 | *Papahu taitapu* OU 22066 | Waipatiidae | Odont | Miocene | homodont | fish | band2 | biting | coastal-pelagic | Aguirre-Fernández, G. and R. E. Fordyce. 2014. *Papahu taitapu*, gen. et sp. nov., an early Miocene stem odontocete (Cetacea) from New Zealand. Journal of Vertebrate Paleontology, 34(1):195-210. |
| 136 | *Parapontoporia sternbergi* SDNHM 75060 | Lipotidae | Odont | Pliocene | homodont | fish | band2 | biting | coastal | Barnes, L.G. 1985. Fossil pontoporiid dolphins (Mammalia: Cetacea) from the Pacific Coast of North America. Contributions in Science, Natural History Museum of Los Angeles County, 363:1-34. L. G. Barnes. 1984. Fossil odontocetes (Mammalia: Cetacea) from the Almejas Formation, Isla Cedros, Mexico. PaleoBios 42:1-46 |
| 137 | *Parietobalaena palmeri* USNM 24883 | Pelocetidae | Myst | Miocene | edentulous - baleen | zooplankton + fish | band1 | filter | coastal-pelagic | Bisconti, M., Lambert, O. and Bosselaers, M. 2013. Taxonomic revision of *Isocetus depauwi* (Mammalia, Cetacea, Mysticeti) and the phylogenetic relationships of archaic 'cetothere' mysticetes. Palaeontology, 56(1):95-127. |
| 138 | *Patriocetid* new genus ChM PV4753 | Patriocetidae | Odont | Oligocene | heterodont | benthic invertebrates + fish | band2 | biting | coastal-pelagic | Dubrovo, I. A. and Sanders,A. E. 2000. A new species of *Patriocetus* (Mamammalia, Cetacea) from the Chattian of Kazakstan. Journal of Vertebrate Paleontology, 20(3):577-590 |

| 139 | Patriocetid or Waipatiid new genus CCNHM 1078 | Patriocetidae | Odont | Oligocene | heterodont | benthic invertebrates + fish | band2 | biting | coastal-pelagic | Dubrovo, I. A. and Sanders,A. E. 2000. A new species of *Patriocetus* (Mamammalia, Cetacea) from the Chattian of Kazakstan. Journal of Vertebrate Paleontology, 20(3):577-590 |
|---|---|---|---|---|---|---|---|---|---|---|
| 140 | *Patriocetus ehrlichii* OL 1999-3 Cet. 4 | Patriocetidae | Odont | Oligocene | heterodont | benthic invertebrates + fish | band2 | biting | coastal-pelagic | Marx, F.G. 2011. The More the Merrier? A Large Cladistic Analysis of Mysticetes, and Comments on the Transition from Teeth to Baleen. Journal of Mammalian Evolution 18:77-100. Dubrovo,I. A. and Sanders,A. E. 2000. A new species of *Patriocetus* (Mamammalia, Cetacea) from the Chattian of Kazakstan. Journal of Vertebrate Paleontology, 20(3):577-590. |
| 141 | *Patriocetus* sp MB Ma. 42882 | Patriocetidae | Odont | Oligocene | heterodont | benthic invertebrates + fish | band2 | biting | coastal-pelagic | Dubrovo,I. A. and Sanders,A. E. 2000. A new species of Patriocetus (Mamammalia, Cetacea) from the Chattian of Kazakstan. Journal of Vertebrate Paleontology, 20(3):577-590 |
| 142 | *Pelocetus calvertensis* USNM 11976 | Pelocetidae | Myst | Miocene | edentulous - baleen | zooplankton + fish | band1 | filter | coastal-pelagic | Kellogg, R. 1965. A new whalebone whale from the Miocene Calvert Formation. Bulletin of the United States National Museum, 247(1):1-45. M. D. Uhen, R. E. Fordyce, and L. G. Barnes. 2008. Mysticeti. In C. M. Janis, K. M. Scott, and L. L. Jacobs (eds.), Evolution of Tertiary Mammals of North America II:607-628 |
| 143 | *Peponocephala electra* USNM 504511 | Delphinidae | Odont | Extant | homodont | cephalopods + fish | band2 | biting | pelagic | Jefferson, T.A., and Barros, N.B. 1997. *Peponocephala electra*. Mammalian Species, 553:1–6. |
| 144 | *Phocoena dioptrica* NHM 1939.9.30.1 | Phocoenidae | Odont | Extant | homodont | cephalopods + fish | band2 | biting | coastal-pelagic | Jefferson, T.A, Webber, M.A. Pitman, R.L. Marine Mammals of the World: a Comprehensive Guide to their Identification. Academic Press, San Diego (2015) |
| 145 | *Phocoena phocoena* AMNH 212161 | Phocoenidae | Odonts | Extant | homodont | cephalopods + fish | band2 | biting | coastal | Pauly, D., Trites, A.W., Capuli, E., and Christensen, V. 1998. Diet composition and trophic levels of marine mammals. ICES Journal of Marine Science, 55: 467–481. |
| 146 | *Phocoena sinus* SDNHM 20697 | Phocoenidae | Odont | Extant | homodont | cephalopods + fish | band2 | biting | coastal | Pauly, D., Trites, A.W., Capuli, E., and Christensen, V. 1998. Diet composition and trophic levels of marine mammals. ICES Journal of Marine Science, 55: 467–481. Brownell Jr., R.L. 1983. *Phocoena sinus*. Mammalian Species, 1. |
| 147 | *Phocoena spinipinnis* NHM 1900.5.7.29 | Phocoenidae | Odont | Extant | homodont | cephalopods + fish | band2 | biting | coastal-pelagic | Pauly, D., Trites, A.W., Capuli, E., and Christensen, V. 1998. Diet composition and trophic levels of marine mammals. ICES Journal of Marine Science, 55: 467–481. |
| 148 | *Phocoenoides dalli* USNM 276062 | Phocoenidae | Odont | Extant | homodont | cephalopods + fish | band2 | biting | coastal-pelagic | Pauly, D., Trites, A.W., Capuli, E., and Christensen, V. 1998. Diet composition and trophic levels of marine mammals. ICES Journal of Marine Science, 55: 467–481. |
| 149 | *Physeter macrocephalus* NHM 2007.1 | Physeteridae | Odont | Extant | homodont | cephalopods + fish | band2 | suction | coastal-pelagic | Jefferson, T.A, Webber, M.A. Pitman, R.L. Marine Mammals of the World: a Comprehensive Guide to their Identification. Academic Press, San Diego (2015) |
| 150 | *Piscobalaena nana* MNHN 1618 | Cetotheriidae | Myst | Miocene | edentulous - baleen | zooplankton + fish | band1 | filter | coastal-pelagic | Marx, F.G., Lambert, O., and Muizon, C. de. 2017. A new Miocene baleen whale from Peru deciphers |

| | | | | | | | | | |
|---|---|---|---|---|---|---|---|---|---|
| | | | | | | | | | the dawn of cetotheriids. Royal Society Open Science, 4:170560. |
| 151 | *Piscolithax longirostris* SAS 933 | Phocoenidae | Odont | Miocene | homodont | cephalopods + fish | band2 | biting | coastal-pelagic | Fajardo-Mellor, L. Berta, A. Brownell, R.L, Boy, C.C and Goodall, R. N. P. 2006. The phylogenetic relationships and biogeography of true porpoises (Mammalia: Phocoenidae) based on morphological data. Marine Mammal Science 22(4):910-932 |
| 152 | *Piscolithax tedfordi* UCMP 15972 | Phocoenidae | Odont | Miocene | homodont | cephalopods + fish | band2 | biting | coastal-pelagic | Fajardo-Mellor, L. Berta, A. Brownell, R.L, Boy, C.C and Goodall, R. N. P. 2006. The phylogenetic relationships and biogeography of true porpoises (Mammalia: Phocoenidae) based on morphological data. Marine Mammal Science 22(4):910-932 |
| 153 | *Platanista gangetica* USNM 172409 | Platanistidae | Odont | Extant | homodont | fish | band2 | biting | riverine | Reeves, R.R., and Brownell Jr., R.L. 1989. Susu - *Platanista gangetica* (Roxburgh, 1801) and *Platanista minor* Owen, 1853, pp. 69–100 In Ridgway, S.H. and Harrison, R. (eds.), Handbook of Marine Mammals - Vol. 4: River Dolphins and the Larger Toothed Whales. Academic Press. |
| 154 | *Pliopontos littoralis* SAS 193 | Pontoporiidae | Odont | Pliocene | homodont | cephalopods + fish | band2 | biting | coastal-pelagic | Muizon, C. de 1983. *Pliopontos littoralis* un nouveau Platanistidae Cetacea du Pliocene de la cote peruvienne. Comptes Rendus de l'Academie des Sciences Paris, Serie II, (296):1101-1104. |
| 155 | *Pomatodelphis* CMM V 3915 | Platanistidae | Odont | Miocene | homodont | fish | band2 | biting | coastal-pelagic | Kellogg, R. 1959. Description of the skull of *Pomatodelphis inaequalis*. Allen. Bulletin of the Museum of Comparative Zoology, 121(1):3-26 |
| 156 | *Pomatodelphis* USNM 187414 | Platanistidae | Odont | Miocene | homodont | fish | band2 | biting | coastal-pelagic | Kellogg, R. 1959. Description of the skull of *Pomatodelphis inaequalis*. Allen. Bulletin of the Museum of Comparative Zoology, 121(1):3-26 |
| 157 | *Pontoporia blainvillei* USNM 482727 | Pontoporiidae | Odont | Extant | homodont | cephalopods + fish | band2 | biting | coastal | Brownell Jr., R. L. 1989. Franciscana - *Pontorporia blainvillei* (Gervais and d'Orbigny, 1844), p. 45–68 in Ridgway, S.H. and Harrison, R. (eds.), Handbook of Marine Mammals - Vol. 4: River Dolphins and the Larger Toothed Whales. Academic Press. |
| 158 | *Prosqualodon davidis* USNM 467596 | Prosqualodontidae | Odont | Oligocene | heterodont | fish | band2 | biting | coastal-pelagic | True, F.W. 1909. A new genus of fossil cetaceans from the Santa Cruz Territory, Patagonia; and description of a mandible and vertebrae of Prosqualodon. Smithsonian Miscellaneous Collections, 52:441-455. |
| 159 | *Protocetus atavus* SMNS 11084 | Protocetidae | Arch | Eocene | heterodont | benthic invertebrates + fish | band1 | biting | coastal-pelagic | Fraas, E.1904. Neue Zeuglodonten aus dem unteren Mitteleocän vom Mokattam bei Cairo. Geologische und Paläontologische Abhandlungen. 6 (3): 199–220. M. Fornasiero and L. Del Vavero. 2014. I Cetacei fossili del Museo di Geologia e Paleontologia dell'Universita? di Padova. Museologia Scientifica Memorie 13:62-69 |
| 160 | *Pseudorca crassidens* USNM 11320 | Delphinidae | Odont | Extant | homodont | tetrapods + fish | band2 | biting | coastal-pelagic | Stacey, P.J., Leatherwood, S. and Baird, R.W. 1994. *Pseudorca crassidens*. Mammalian Species, 456:1–6. |
| 161 | *Remingtonocetus harudiensis* USNM PAL 559313 | Remingtonocetidae | Arch | Eocene | heterodont | benthic invertebrates + fish | band1 | biting | coastal | Cooper, L.N, Hieronymus. T.L, Vinyard, C.J, Bajpai. S and Thewissen, J.G.M. 2014. New Applications for Constrained Ordination: Reconstructing Feeding Behaviors in Fossil Remingtonocetinae (Cetacea: Mammalia). Topics in Geobiology 41:89-107 |
| 162 | *Scaphokogia totajpe* MUSM 973 | Kogiidae | Odont | Miocene | homodont | cephalopods + fish | band2 | suction | coastal-pelagic | Benites-Palomino, A. Vélez-Juarbe, J, Salas-Gismondi, R and Urbina, M. 2020. *Scaphokogia totajpe*, sp. nov., a new bulky-faced pygmy sperm whale (Kogiidae) from the late Miocene of Peru. Journal of Vertebrate Paleontology e1728538 |

| 163 | *Schizodelphis barnesi* MNHN AMN 19 | Eurhinodelphinidae | Odont | Miocene | homodont | fish | band2 | biting | coastal-pelagic | Benoit. J, Adnet. S, Welcomme. J-L and Fabre. P-H. 2011. New skull of *Schizodelphis sulcatus* Gervais, 1861 (Mammalia, Odontoceti, Eurhinodelphinidae) from the Lower Miocene of Pignan (Hérault, France) and its implications for systematics of Eurhinodelphinidae. Geobios 44(2011):323-334 |
|---|---|---|---|---|---|---|---|---|---|---|
| 164 | *Schizodelphis morckhoviensis* USNM 13873 | Eurhinodelphinidae | Odont | Miocene | homodont | fish | band2 | biting | coastal-pelagic | Benoit. J, Adnet. S, Welcomme. J-L and Fabre. P-H. 2011. New skull of *Schizodelphis sulcatus* Gervais, 1861 (Mammalia, Odontoceti, Eurhinodelphinidae) from the Lower Miocene of Pignan (Hérault, France) and its implications for systematics of Eurhinodelphinidae. Geobios 44(2011):323-334 |
| 165 | *Schizodelphis* sp CCNHM 141 | Eurhinodelphinidae | Odont | Miocene | homodont | fish | band2 | biting | coastal-pelagic | Benoit. J, Adnet. S, Welcomme. J-L and Fabre. P-H. 2011. New skull of *Schizodelphis sulcatus* Gervais, 1861 (Mammalia, Odontoceti, Eurhinodelphinidae) from the Lower Miocene of Pignan (Hérault, France) and its implications for systematics of Eurhinodelphinidae. Geobios 44(2011):323-334 |
| 166 | *Schizodelphis sulcatus* MGB | Eurhinodelphinidae | Odont | Miocene | homodont | fish | band2 | biting | coastal-pelagic | Benoit. J, Adnet. S, Welcomme. J-L and Fabre. P-H. 2011. New skull of *Schizodelphis sulcatus* Gervais, 1861 (Mammalia, Odontoceti, Eurhinodelphinidae) from the Lower Miocene of Pignan (Hérault, France) and its implications for systematics of Eurhinodelphinidae. Geobios 44(2011):323-334 |
| 167 | *Semirostrum cerutti* SDNHM 65276 | Phocoenidae | Odont | Pliocene | homodont | benthic invertebrates + fish | band2 | biting | coastal | Racicot, R.A., Deméré, T.A., Beatty, B.L. and Boessenecker, R.W. 2014. Unique feeding morphology in a new prognathous extinct porpoise from the Pliocene of California. Current Biology, 4: 774-779. |
| 168 | *Septemtriocetus bosselaersi* IRSNB M.1928 | Phocoenidae | Odont | Pliocene | homodont | benthic invertebrates + fish | band2 | biting | coastal | Lambert. O. 2008. A new porpoise (Cetacea, Odontoceti, Phocoenidae) from the Pliocene of the North Sea. Journal of Vertebrate Paleontology 28(3):863-872 |
| 169 | *Simocetus rayi* USNM 256517 | Simocetidae | Odont | Oligocene | heterodont | benthic invertebrates + fish | band2 | biting | coastal-pelagic | Fordyce, R.E. 2002. *Simocetus rayi* (Odontoceti, Simocetidae, new family); a bizarre new archaic Oligocene dolphin from the eastern North Pacific. Smithsonian Contributions to Paleobiology, 93:185-222. |
| 170 | *Sotalia guianensis* USNM 571558 | Delphinidae | Odont | Extant | homodont | fish | band2 | biting | coastal | Caballero, S., Trujillo, F., Vianna, J. a., Barrios-Garrido, H., Montiel, M. G., Beltrán-Pedreros, S., Marmontel, M., Santos, M.C., Rossi-Santos, M., Santos, F.R. and Baker, C.S. 2007. Taxonomic status of the genus *Sotalia*: species level ranking for "Tucuxi" (*Sotalia fluviatilis*) and "Costero" (*Sotalia guianensis*) dolphins. Marine Mammal Science, 23:358–386. |
| 171 | *Sousa chinensis* NHM 1992.97 | Delphinidae | Odont | Extant | homodont | fish | band2 | biting | coastal | Pauly, D., Trites, A.W., Capuli, E., and Christensen, V. 1998. Diet composition and trophic levels of marine mammals. ICES Journal of Marine Science, 55: 467–481. |
| 172 | *Sousa plumbea* USNM 550941 | Delphinidae | Odont | Extant | homodont | fish | band2 | biting | coastal | Pauly, D., Trites, A.W., Capuli, E., and Christensen, V. 1998. Diet composition and trophic levels of marine mammals. ICES Journal of Marine Science, 55: 467–481. |

| 173 | *Sousa sahulensis* NHM 1992.92 | Delphinidae | Odont | Extant | homodont | fish | band2 | biting | coastal | Pauly, D., Trites, A.W., Capuli, E., and Christensen, V. 1998. Diet composition and trophic levels of marine mammals. ICES Journal of Marine Science, 55: 467–481. |
|---|---|---|---|---|---|---|---|---|---|---|
| 174 | *Sousa teuszii* NHM 1992.138 | Delphinidae | Odont | Extant | homodont | fish | band2 | biting | coastal | Pauly, D., Trites, A.W., Capuli, E., and Christensen, V. 1998. Diet composition and trophic levels of marine mammals. ICES Journal of Marine Science, 55: 467–481. |
| 175 | *Squalodon bariensis* IRSNB 2372 | Squalodontidae | Odont | Miocene | heterodont | fish | band2 | biting | coastal-pelagic | Dal Piaz, G. 1916. *Squalodon*. Memoirie dell'Instituto geologico della R. Università di Padova, 4:1-94. |
| 176 | *Squalodon calvertensis* NMNZ MM001996 | Squalodontidae | Odont | Miocene | heterodont | fish | band2 | biting | coastal-pelagic | Dal Piaz, G. 1916. *Squalodon*. Memoirie dell'Instituto geologico della R. Università di Padova, 4:1-94. |
| 177 | *Squalodon* OU 21798 | Squalodontidae | Odont | Oligocene | heterodont | fish | band2 | biting | coastal-pelagic | Personal correspondence with Ewan Fordyce and Amber Coste |
| 178 | *Squalodon* OU 22126 | Squalodontidae | Odont | Oligocene | heterodont | fish | band2 | biting | coastal-pelagic | Personal correspondence with Ewan Fordyce and Amber Coste |
| 179 | *Squalodon* OU 22397 | Squalodontidae | Odont | Oligocene | heterodont | fish | band2 | biting | coastal-pelagic | Personal correspondence with Ewan Fordyce and Amber Coste. Dal Piaz, G. 1916. *Squalodon*. Memoirie dell'Instituto geologico della R. Università di Padova, 4:1-94. |
| 180 | *Stenella attenuata* NHM 1966.11.18.5 | Delphinidae | Odont | Extant | homodont | cephalopods + fish | band2 | biting | pelagic | Jefferson, T.A, Webber, M.A. Pitman, R.L. Marine Mammals of the World: a Comprehensive Guide to their Identification Academic Press, San Diego (2015) |
| 181 | *Stenella longirostris* USNM 395270 | Delphinidae | Odont | Extant | homodont | cephalopods + fish | band2 | biting | pelagic | Perrin, W. F. 1998. *Stenella longirostris*, Mammalian Species, 599:1–7. |
| 182 | *Steno bredanensis* USNM 572789 | Delphinidae | Odont | Extant | homodont | cephalopods + fish | band2 | biting | pelagic | West, K.L., Mead, J.G. and White, W. 2011. *Steno bredanensis* (Cetacea: Delphinidae). Mammalian Species, 43:177–189. |
| 183 | *Stenodelphininae* UCMP 125352 | Lipotidae | Odont | Miocene | homodont | fish | band2 | biting | coastal | Barnes, L.G. 1985. Fossil pontoporiid dolphins (Mammalia: Cetacea) from the Pacific Coast of North America. Contributions in Science, Natural History Museum of Los Angeles County, 363:1-34. |
| 184 | *Tagicetus joneti* IRSNB M. 1892 | Delphinida | Odont | Miocene | homodont | cephalopods + fish | band2 | biting | coastal-pelagic | Lambert, O., Estevens, M. and R. Smith, R. 2005. A new kentriodontine from the middle Miocene of Portugal. Acta Palaeontologica Polonica, 50(2):239-248. |
| 185 | *Tasmacetus shepherdi* USNM 484878 | Ziphiidae | Odont | Extant | reduced | cephalopods + fish | band2 | suction | pelagic | Ridgway, S.H. and Harrison, R. (eds.), Handbook of Marine Mammals - Vol. 4: River Dolphins and the Larger Toothed Whales. Academic Press. Ellis, R., & Mead, J.G. (2017). Beaked Whales: A Complete Guide to Their Biology and Conservation. Baltimore: Johns Hopkins University Press. |
| 186 | *Tursiops aduncus* NHM 1882.1.2.3 | Delphinidae | Odont | Extant | homodont | cephalopods + fish | band2 | biting | coastal-pelagic | Jefferson, T.A, Webber, M.A. Pitman, R.L. Marine Mammals of the World: a Comprehensive Guide to their Identification. Academic Press, San Diego (2015) |
| 187 | *Tursiops truncatus gilli* SDNHM 11102 | Delphinidae | Odont | Extant | homodont | cephalopods + fish | band2 | biting | coastal-pelagic | Jefferson, T.A, Webber, M.A. Pitman, R.L. Marine Mammals of the World: a Comprehensive Guide to their Identification. Academic Press, San Diego (2015) |

| 188 | *Tursiops truncatus* sp SDNHM 23798 | Delphinidae | Odont | Extant | homodont | cephalopods + fish | band2 | biting | coastal-pelagic | Jefferson, T.A, Webber, M.A. Pitman, R.L. Marine Mammals of the World: a Comprehensive Guide to their Identification.Academic Press, San Diego (2015) |
|---|---|---|---|---|---|---|---|---|---|---|
| 189 | *Waipatia maerwhenua* OU 22095 | Waipatiidae | Odont | Oligocene | heterodont | fish | band2 | biting | coastal-pelagic | Fordyce, R.E. 1994. *Waipatia maerewhenua*, New Genus and New Species, Waipatiidae, New Family, an archaic late Oligocene dolphin (Cetacea: Odontoceti: Platanistoidea) from New Zealand. Proceedings of the San Diego Society of Natural History 29:147-176 |
| 190 | *Waipatiid* CCNHM 567 | Waipatiidae | Odont | Oligocene | heterodont | fish | band2 | biting | coastal-pelagic | Fordyce, R.E. 1994. *Waipatia maerewhenua*, New Genus and New Species, Waipatiidae, New Family, an archaic late Oligocene dolphin (Cetacea: Odontoceti: Platanistoidea) from New Zealand. Proceedings of the San Diego Society of Natural History 29:147-176 |
| 191 | *Waipatiid* new gen ChM PV7679 | Waipatiidae | Odont | Oligocene | heterodont | fish | band2 | biting | coastal-pelagic | Fordyce, R.E. 1994. *Waipatia maerewhenua*, New Genus and New Species, Waipatiidae, New Family, an archaic late Oligocene dolphin (Cetacea: Odontoceti: Platanistoidea) from New Zealand. Proceedings of the San Diego Society of Natural History 29:147-176 |
| 192 | *Xenorophus* new sp ChM PV4823 | Xenorophidae | Odont | Oligocene | heterodont | benthic invertebrates + fish | band2 | biting | coastal-pelagic | Sanders, A.E. and Geisler, J. H. 2015. A new basal odontocete from the upper Rupelian of South Carolina, U.S.A., with contributions to the systematics of *Xenorophus* and Mirocetus (Mammalia, Cetacea). Journal of Vertebrate Paleontology, 35(1): e890107. |
| 193 | *Xenorophus* new sp Yap CCNHM 168 | Xenorophidae | Odont | Oligocene | heterodont | benthic invertebrates + fish | band2 | biting | coastal-pelagic | Sanders, A.E. and Geisler, J. H. 2015. A new basal odontocete from the upper Rupelian of South Carolina, U.S.A., with contributions to the systematics of *Xenorophus* and *Mirocetus* (Mammalia, Cetacea). Journal of Vertebrate Paleontology, 35(1): e890107. |
| 194 | *Xiphiacetus bossi* USNM 8842 | Eurhinodelphinidae | Odont | Miocene | homodont | fish | band2 | biting | coastal | Lambert. O. 2005. Review of the Miocene long-snouted dolphin *Priscodelphinus cristatus* Du Bus, 1872 (Cetacea, Odontoceti) and phylogeny among eurhinodelphinids. Bulletin de L'Institute Royal des Sciences Naturelles de Belgique Sciences de la Terre, 75:211-235. |
| 195 | *Xiphiacetus cristatus* USNM 21363 | Eurhinodelphinidae | Odont | Miocene | homodont | fish | band2 | biting | coastal | Lambert. O. 2005. Review of the Miocene long-snouted dolphin *Priscodelphinus cristatus* Du Bus, 1872 (Cetacea, Odontoceti) and phylogeny among eurhinodelphinids. Bulletin de L'Institute Royal des Sciences Naturelles de Belgique Sciences de la Terre, 75:211-235. |
| 196 | *Yaquinacetus* USNM 214705 | Squaloziphiidae | Odont | Miocene | heterodont | fish | band2 | biting | coastal-pelagic | Lambert, O. Godfrey, S.J. and Fitzgerald. E.M.G. 2019. *Yaquinacetus meadi*, a new latest Oligocene–early Miocene dolphin (Cetacea, Odontoceti, Squaloziphiidae, fam. nov.) from the Nye Mudstone (Oregon, U.S.A.). Journal of Vertebrate Paleontology e1559174. |
| 197 | *Zarhachis flagellator* USNM 10911 | Platanistidae | Odont | Miocene | homodont | fish | band2 | biting | coastal-pelagic | Cope, E.D. 1868. Second contribution to the history of the Vertebrata of the Miocene period of the United States. Proceedings of the Academy of Natural Sciences of Philadelphia 1868:184-194. Boersma. A and Pyenson N.D. 2016. *Arktocara yakataga*, a new fossil odontocete (Mammalia, |

| | | | | | | | | | |
|---|---|---|---|---|---|---|---|---|---|
| | | | | | | | | | Cetacea) from the Oligocene of Alaska and the antiquity of Platanistoidea. PeerJ 4:e2321 |
| 198 | *Zarhinocetus donnamatsonae* UCMP 86139 | Allodelphinidae | Odont | Miocene | homodont | fish | band2 | biting | coastal-pelagic | Kimura, T. and Barnes, L.G. 2016. New Miocene fossil Allodelphinidae (Cetacea, Odontoceti, Platanistoidea) from the North Pacific Ocean. Bulletin of the Gunma Museum of Natural History, 20:1-58. |
| 199 | *Zarhinocetus errabundus* LACM 149588 | Allodelphinidae | Odont | Miocene | homodont | fish | band2 | biting | coastal-pelagic | Kimura, T. and Barnes, L.G. 2016. New Miocene fossil Allodelphinidae (Cetacea, Odontoceti, Platanistoidea) from the North Pacific Ocean. Bulletin of the Gunma Museum of Natural History, 20:1-58. |
| 200 | *Ziphius cavirostris* NHM 2006.15 | Ziphiidae | Odont | Extant | reduced | cephalopods + fish | band2 | suction | pelagic | Heyning, J. E. 1989. Cuvier's beaked whale - *Ziphius cavirostris* Cuvier, 1823, p. 289–308 in Ridgway, S.H. and Harrison, R. (eds.), Handbook of Marine Mammals - Vol. 4: River Dolphins and the Larger Toothed Whales. Academic Press. |
| 201 | *Zygorhiza kochii* USNM 11962 | Basilosauridae | Arch | Eocene | heterodont | benthic invertebrates + fish | band1 | biting | coastal-pelagic | Daly, E. 1999. A middle Eocene *Zygorhiza* specimen from Mississippi (Cetacea, Archaeoceti). Mississippi Geology, 20(2):21-31. |

**Table S3.2.** Excluded specimens. Specimens that have been scanned and processed but not used in this study – the reason for their disqualification is given.

| Specimen ID | Reason for exclusion |
|---|---|
| *Aporotus dicyrtus* IRSNB 3808-M.541 | Incomplete |
| *Balaenoptera colcloughi* SDNHM 80102 | Incomplete/unsure of phylogenetic position |
| *Choneziphius planirostris* IRSNB M 1881 | Incomplete |
| *Dorudon osiris* SMNS 11786 | Incomplete |
| Emlong 204 Oligocene archaeocetid | Incomplete/unsure of phylogenetic position |
| *Eocetus schweinfurthi* SMNS 10986 | Incomplete |
| *Eosqualodon* n. species CCNHM 170.1 | Incomplete |
| *Hadrodelphis* CMM V 11 | Incomplete |
| *Herpetocetus bramblei* UCMP 219111 | Incomplete |
| *Herpetocetus morrowi* UCMP 124950 | Incomplete |
| *Inermorostrum xenops* CCNHM 171 | Incomplete |
| *Inticetus vertizi* MUSM 1980 | Incomplete |
| *Llanocetus denticrenatus* USNM 183022 | Incomplete |
| *Lophocetus calvetensis* USNM 16314 | Incomplete |
| *Lophocetus repenningi* USNM 23886 | Incomplete |
| *Macrokentriodon* USNM 241526 | Incomplete |
| *Maiacetus inuus* UMMP VP 118197 | Deformed |
| *Micromysticetus rothauseni* CCNHM 169.1 | Incomplete |
| Miocene mysticete SDNHM 141348 | Incomplete/unsure of phylogenetic position |
| *Monodontidae* SDNHM 26244 | Incomplete |
| *Neosqualodon* MBGPT | Incomplete |
| *Ninoziphius platyrostris* MNHN SAS 941 | Incomplete |
| *Otekaikea huata* OU 22125 | Incomplete |
| *Paradoxocetus* new Xenorophid gen Chm PV2758 | Incomplete/unsure of phylogenetic position |
| *Piscobalaena nana* MNHN 1617 | Duplicate fossil species |
| *Rodhocetus kasrani* UMMP VP 99969 | Incomplete |
| *Salumniphocoena stocktoni* UCMP 34576 | Incomplete |
| *Scaphokogia cochlearis* MUSM 1998 | Incomplete |
| *Tiocetus rosae* MNHN.F. PPI261 | Incomplete |
| *Tursiops capellinii* MGPT PU 13882 | Incomplete |
| Waipatiid new gen ChM PV4824 | Incomplete/unsure of phylogenetic position |

**Table S3.3.** Description of landmarks placed on each specimen. Includes a description and the number of the corresponding left-hand side (LHS) and right-hand side (RHS) landmarks. Midline landmarks are shown in red.

| Landmark description | Number on LHS of the skull | Number on RHS of the skull |
|---|---|---|
| Nasal anterior | 1 | 120 |
| Left anterior lateral nasal | 2 | 67 |
| Posterior lateral corner of nasal | 3 | 68 |
| Posterior point of nasal | 4 | 121 |
| Tip of rostrum, anterior dorsal side, anterior midline of tooth row (usually premaxilla) | 5 | 69 |
| Anterior dorsal premaxilla | 6 | 70 |
| Posterior dorsal premaxilla | 7 | 71 |
| Anterior lateral ventral premaxilla | 8 | 72 |
| Anterior lateral ventral maxilla | 9 | 73 |
| Dorsal medial maxilla (suture with nasal and premaxilla) | 10 | 74 |
| Nasal-frontal-maxilla suture (posterior medial maxilla) | 11 | 75 |
| Dorsal posterior maxilla on orbit (including lacrimal - dorsal suture frontal) on orbit | 12 | 76 |
| Jugal maxilla, orbit suture - front orbit lateral | 13 | 77 |
| Posterior ventral-lateral most point of maxilla – tooth row - Jugal-maxilla ventral suture | 14 | 78 |
| Posterior tooth row lateral maxilla or lateral maxilla in species with no/negligible dentition | 15 | 79 |
| Jugal anterior dorsal | 16 | 80 |
| Jugal anterior ventral | 17 | 81 |
| Jugal posterior ventral | 18 | 82 |
| Anterior medial frontal | 19 | 122 |
| Posterior medial frontal | 20 | 123 |
| Lateral posterior frontal (posterior lateral parietal suture) | 21 | 83 |
| Postorbital process/bar tip (anterior on crest) | 22 | 84 |
| Anterior lateral frontal (on orbit) | 23 | 85 |
| Anterior dorsal corner of frontal (on orbit) | 24 | 86 |
| Anterior medial parietal | 25 | 87 |
| Posterior medial parietal | 26 | 88 |

| | | |
|---|---|---|
| Posterior lateral parietal (squamosal/occipital suture) | 27 | 89 |
| Anterior lateral parietal (on vault) | 28 | 90 |
| Dorsal anterior lateral parietal (suture with frontal) | 29 | 91 |
| Dorsal anterior squamosal suture (with parietal, maybe alisphenoid/frontal) | 30 | 92 |
| Medial anterior zygomatic vault junction (squamosal) | 31 | 93 |
| Anterior dorsal jugal-squamosal suture | 32 | 94 |
| Posterior ventral jugal-squamosal suture, lateral | 33 | 95 |
| Anterior medial most point of the mandibular articular process. | 34 | 96 |
| Posterior lateral most point of the mandibular articular process | 35 | 97 |
| Lateral posterior squamosal (occipital suture) | 36 | 98 |
| Posterior medial dorsal squamosal (parietal/occipital suture) | 37 | 99 |
| **MIDLINE:** posterior margin of skull roof | *38* | *38* |
| Medial anterior supraoccipital (parietal-occipital suture, usually) | 39 | 100 |
| **MIDLINE:** dorsal/superior margin of foramen magnum | *40* | *40* |
| Dorsal medial occipital condyle | 41 | 101 |
| Dorsal lateral occipital condyle | 42 | 102 |
| Tip of paraoccipital process - lateral tip | 43 | 103 |
| Lateral ventral occipital + process | 44 | 104 |
| Lateral dorsal occipital | 45 | 105 |
| Ventral medial occipital condyle | 46 | 106 |
| Ventral lateral occipital condyle | 47 | 107 |
| **MIDLINE:** ventral margin of foramen magnum | *48* | *48* |
| **MIDLINE:** anterior basioccipital | *49* | *49* |
| Lateral anterior basioccipital | 50 | 108 |
| **MIDLINE:** anterior most point of basisphenoid, just posterior to the pterygoids and palate | *51* | *51* |
| Lateral anterior basisphenoid | 52 | 109 |
| Lateral posterior basisphenoid | 53 | 110 |
| **MIDLINE:** Medial posterior basisphenoid | *54* | *54* |
| **MIDLINE:** Posterior ventral medial point of palate | *55* | *55* |

| | | |
|---|---|---|
| **MIDLINE:** Palatine anterior midline ventral suture | *56* | *56* |
| Pal-pterygoid suture | 57 | 111 |
| Pal-max lateral posterior suture | 58 | 112 |
| Pterygoid posterior | 59 | 113 |
| Ventral posterior pterygoid | 60 | 114 |
| **MIDLINE:** Maxilla ventral midline posterior suture | *61* | *61* |
| Maxilla ventral midline anterior suture | 62 | 115 |
| Maxilla anterior lateral ventral | 63 | 116 |
| Premaxilla ventral midline posterior suture | 64 | 117 |
| **MIDLINE:** Anterior-most point of palatal surface immediately posterior to tooth row | 65 | 118 |
| Premaxilla posterior lateral ventral | 66 | 119 |

[Table on next page]

**Table S3.4.** Description of landmarks and curves placed on each specimen. Landmark anchors 1 and 2 are the landmarks between which semi-landmark curves are anchored. I subsampled the curve ('Resampled curve length') to ensure all curve points were equally spaced along curves. Midline curves and landmarks are shown in red. The coloured boxes show the following: blue = landmarks and curves placed on the left-hand side (LHS) of the specimens; green = manually placed landmarks on the right-hand side (RHS) of the archaeocetes and odontocetes. These (green) landmarks and curves were also placed on the mysticetes but were computer mirrored. Orange = computer mirrored landmarks and curves on archaeocetes, mysticetes, and odontocetes.

| Semi-landmark curve number | Semi-landmark curve description | Landmark anchor 1 | Landmark anchor 2 | Resampled curve length | Bone |
|---|---|---|---|---|---|
| 1 | Central nasal - anterior to posterior | 1 | 4 | 10 | nasal_l |
| 2 | Posterior nasal – medial to lateral | 4 | 3 | 5 | nasal_l |
| 3 | Lateral nasal – posterior to anterior | 3 | 2 | 10 | nasal_l |
| 4 | Anterior nasal – lateral to medial | 2 | 1 | 5 | nasal_l |
| 5 | Anterior, central, dorsal premaxilla | 5 | 6 | 5 | premax |
| 6 | Anterior to posterior central dorsal premaxilla | 6 | 7 | 35 | premax |
| 7 | Posterior to anterior lateral dorsal premaxilla | 7 | 8 | 35 | premax |
| 8 | Anterior most dorsal maxilla | 8 | 5 | 5 | premax |
| 9 | Medial dorsal maxilla | 9 | 10 | 35 | maxilla |
| 10 | Posterior dorsal maxilla | 10 | 11 | 10 | maxilla |
| 11 | Lateral maxilla over obit | 11 | 12 | 30 | maxilla |
| 12 | Dorsal posterior maxilla on orbit (including lacrimal - dorsal suture frontal) on orbit | 12 | 13 | 10 | maxilla |
| 13 | Jugal maxilla orbit suture - front orbit lateral | 13 | 14 | 10 | maxilla |
| 14 | Posterior ventral lateral most point of maxilla – tooth row - Jugal-maxilla ventral suture | 14 | 15 | 15 | maxilla |
| 15 | Posterior tooth row lateral maxilla or lateral maxilla in species with | 15 | 9 | 25 | maxilla |

| | | | | | |
|---|---|---|---|---|---|
| | no/negligible dentition | | | | |
| 16 | Anterior, medial frontal | 19 | 24 | 30 | frontal |
| 17 | Anterior lateral frontal (on orbit) | 24 | 23 | 10 | frontal |
| 18 | Posterior lateral frontal (on orbit) | 23 | 22 | 10 | frontal |
| 19 | Posterior lateral frontal | 22 | 21 | 15 | frontal |
| 20 | Posterior frontal | 21 | 20 | 20 | frontal |
| 21 | Medial frontal (would be midline in symmetrical taxa) | 20 | 19 | 5 | frontal |
| 22 | Medial dorsal parietal | 25 | 26 | 15 | parietal |
| 23 | Posterior parietal | 26 | 27 | 10 | parietal |
| 24 | Lateral parietal suture with squamosal | 27 | 28 | 15 | parietal |
| 25 | Anterior parietal | 28 | 29 | 15 | parietal |
| 26 | Anterior dorsal parietal | 29 | 25 | 10 | parietal |
| 27 | Anterior squamosal | 32 | 33 | 10 | squamosal |
| 28 | Lateral posterior dorsal squamosal - suture with parietal | 33 | 32 | 25 | squamosal |
| 29 | Medial dorsal zygomatic (with squamosal) – suture with parietal | 31 | 30 | 20 | squamosal |
| 30 | Dorsal posterior zygomatic (with squamosal) | 30 | 37 | 5 | squamosal |
| 31 | Posterior zygomatic (with squamosal) | 37 | 36 | 5 | squamosal |
| 32 | Dorsal medial zygomatic (with squamosal) | 36 | 31 | 20 | squamosal |

| 33 | Anterior ventral mandibular process | 34 | 35 | 15 | mandibular process |
|---|---|---|---|---|---|
| 34 | Posterior ventral mandibular process | 35 | 34 | 15 | mandibular process |
| *35* | *Midline – Medial supraoccipital* | *39* | *40* | *20* | *supraoccipital* |
| 36 | Supraoccipital suture with dorsal occipital condyle | 40 | 41 | 10 | supraoccipital |
| 37 | Supraoccipital suture with occipital condyle | 41 | 42 | 10 | supraoccipital |
| 38 | Ventral supraoccipital round to exoccipital | 42 | 43 | 15 | supraoccipital |
| 39 | Ventral exoccipital process of supraoccipital | 43 | 44 | 15 | supraoccipital |
| 40 | Dorsal supraoccipital – lateral to medial | 44 | 45 | 20 | supraoccipital |
| 41 | Dorsal medial supraoccipital | 45 | 39 | 10 | supraoccipital |
| 42 | Dorsal medial occipital condyle | 41 | 46 | 15 | occipital condyle |
| 43 | Ventral occipital condyle – medial to lateral | 46 | 47 | 10 | occipital condyle |
| 44 | Lateral occipital condyle | 47 | 41 | 10 | occipital condyle |
| *45* | *Midline – basioccipital medial from posterior to anterior* | *48* | *49* | *20* | *basioccipital* |
| 46 | Anterior basioccipital – medial to lateral | 49 | 50 | 15 | basioccipital |
| 47 | Lateral basioccipital anterior to posterior | 50 | 48 | 25 | basioccipital |

| | | | | | |
|---|---|---|---|---|---|
| *48* | *Midline – basisphenoid medial from posterior to anterior* | *54* | *51* | *15* | *basisphenoid* |
| 49 | Anterior basisphenoid medial to lateral | 51 | 52 | 15 | basisphenoid |
| 50 | Lateral basisphenoid – anterior to posterior | 52 | 53 | 15 | basisphenoid |
| 51 | Posterior basisphenoid – lateral to medial | 53 | 54 | 15 | basisphenoid |
| *52* | *Midline – palate posterior to anterior* | *55* | *56* | *20* | *palate* |
| 53 | Anterior palate round to lateral | 56 | 58 | 25 | palate |
| 54 | Posterior palate – lateral to medial | 58 | 57 | 25 | palate |
| 55 | Posterior medial palate – suture with pterygoid | 57 | 55 | 5 | palate |
| 56 | Dorsal posterior pterygoid | 57 | 59 | 10 | pterygoid |
| 57 | Dorsal posterior pterygoid | 59 | 60 | 10 | pterygoid |
| 58 | Anterior pterygoid, medial to lateral | 60 | 57 | 10 | pterygoid |
| 59 | Ventral medial maxilla – posterior to anterior | 61 | 62 | 25 | maxilla_vl |
| 60 | Very anterior lateral of ventral maxilla | 62 | 63 | 5 | maxilla_vl |
| 61 | Lateral maxilla anterior to posterior | 63 | 56 | 45 | maxilla_vl |
| 62 | Lateral ventral premaxilla posterior to anterior | 64 | 66 | 15 | premax |
| 63 | Anterior ventral premaxilla | 66 | 65 | 10 | premax |

| 64 | Medial ventral premaxilla anterior to posterior | 65 | 64 | 15 | premax |
|----|----|----|----|----|----|
| 65 | Central nasal - anterior to posterior | 69 | 70 | 10 | nasal_r |
| 66 | Posterior nasal – medial to lateral | 70 | 68 | 5 | nasal_r |
| 67 | Lateral nasal – posterior to anterior | 68 | 67 | 10 | nasal_r |
| 68 | Anterior nasal – lateral to medial | 67 | 69 | 5 | nasal_r |
| 69 | Anterior, central, dorsal premaxilla | 71 | 72 | 5 | premax |
| 70 | Anterior to posterior central dorsal premaxilla | 72 | 73 | 35 | premax |
| 71 | Posterior to anterior lateral dorsal premaxilla | 73 | 74 | 35 | premax |
| 72 | Anterior most dorsal maxilla | 74 | 71 | 5 | premax |
| 73 | Medial dorsal maxilla | 75 | 76 | 35 | maxilla |
| 74 | Posterior dorsal maxilla | 76 | 77 | 10 | maxilla |
| 75 | Lateral maxilla over obit | 77 | 78 | 30 | maxilla |
| 76 | Dorsal posterior maxilla on orbit (including lacrimal - dorsal suture frontal) on orbit | 78 | 79 | 10 | maxilla |
| 77 | Jugal maxilla orbit suture - front orbit lateral | 79 | 80 | 10 | maxilla |
| 78 | Posterior ventral-lateral most point of maxilla – tooth row - Jugal-maxilla ventral suture | 80 | 81 | 15 | maxilla |
| 79 | Posterior tooth row lateral maxilla or lateral maxilla in species with | 81 | 75 | 25 | maxilla |

|  |  |  |  |  |  |
|---|---|---|---|---|---|
|  | no/negligible dentition |  |  |  |  |
| 80 | Anterior, medial frontal | 89 | 88 | 30 | frontal |
| 81 | Anterior lateral frontal (on orbit) | 88 | 87 | 10 | frontal |
| 82 | Posterior lateral frontal (on orbit) | 87 | 86 | 10 | frontal |
| 83 | Posterior lateral frontal | 86 | 85 | 15 | frontal |
| 84 | Posterior frontal | 85 | 90 | 20 | frontal |
| 85 | Medial frontal (would be midline in symmetrical taxa) | 90 | 85 | 5 | frontal |
| 86 | Medial dorsal parietal | 91 | 92 | 15 | parietal |
| 87 | Posterior parietal | 92 | 93 | 10 | parietal |
| 88 | Lateral parietal suture with squamosal | 93 | 94 | 15 | parietal |
| 89 | Anterior parietal | 94 | 95 | 15 | parietal |
| 90 | Anterior dorsal parietal | 95 | 91 | 10 | parietal |
| 91 | Anterior squamosal | 33 | 32 | 25 | squamosal |
| 92 | Lateral posterior dorsal squamosal - suture with parietal | 31 | 30 | 20 | squamosal |
| 93 | Medial dorsal zygomatic (with squamosal) – suture with parietal | 30 | 37 | 5 | squamosal |
| 94 | Dorsal posterior zygomatic (with squamosal) | 37 | 36 | 5 | squamosal |
| 95 | Posterior zygomatic (with squamosal) | 36 | 31 | 20 | squamosal |
| 96 | Dorsal medial zygomatic (with squamosal) | 102 | 97 | 20 | squamosal |

| 97 | Anterior ventral mandibular process | 100 | 101 | 15 | mandibular process |
|----|------|-----|-----|----|------|
| 98 | Posterior ventral mandibular process | 101 | 100 | 15 | mandibular process |
| 99 | Supraoccipital suture with dorsal occipital condyle | 40 | 105 | 10 | supraoccipital |
| 100 | Supraoccipital suture with occipital condyle | 105 | 106 | 10 | supraoccipital |
| 101 | Ventral supraoccipital round to exoccipital | 106 | 107 | 15 | supraoccipital |
| 102 | Ventral exoccipital process of supraoccipital | 107 | 108 | 15 | supraoccipital |
| 103 | Dorsal supraoccipital – lateral to medial | 108 | 109 | 20 | supraoccipital |
| 104 | Dorsal medial supraoccipital | 109 | 104 | 10 | supraoccipital |
| 105 | Dorsal medial occipital condyle | 105 | 110 | 15 | occipital condyle |
| 106 | Ventral occipital condyle – medial to lateral | 110 | 111 | 10 | occipital condyle |
| 107 | Lateral occipital condyle | 111 | 105 | 10 | occipital condyle |
| 108 | Anterior basioccipital – medial to lateral | 49 | 112 | 15 | basioccipital |
| 109 | Lateral basioccipital anterior to posterior | 112 | 48 | 25 | basioccipital |
| 110 | Anterior basisphenoid medial to lateral | 51 | 113 | 15 | basisphenoid |
| 111 | Lateral basisphenoid – anterior to posterior | 113 | 114 | 15 | basisphenoid |

| 112 | Posterior basisphenoid – lateral to medial | 114 | 54 | 15 | basisphenoid |
|-----|---|-----|-----|-----|---|
| 113 | Anterior palate round to lateral | 56 | 116 | 25 | palate |
| 114 | Posterior palate – lateral to medial | 116 | 115 | 25 | palate |
| 115 | Posterior medial palate – suture with pterygoid | 115 | 55 | 5 | palate |
| 116 | Dorsal posterior pterygoid | 115 | 117 | 10 | pterygoid |
| 117 | Dorsal posterior pterygoid | 117 | 118 | 10 | pterygoid |
| 118 | Anterior pterygoid, medial to lateral | 118 | 115 | 10 | pterygoid |
| 119 | Ventral medial maxilla – posterior to anterior | 61 | 119 | 25 | maxilla_vl |
| 120 | Very anterior lateral of ventral maxilla | 119 | 120 | 5 | maxilla_vl |
| 121 | Lateral maxilla anterior to posterior | 120 | 56 | 45 | maxilla_vl |
| 122 | Lateral ventral premaxilla posterior to anterior | 121 | 123 | 15 | premax |
| 123 | Anterior ventral premaxilla | 123 | 122 | 10 | premax |
| 124 | Medial ventral premaxilla anterior to posterior | 122 | 121 | 15 | premax |
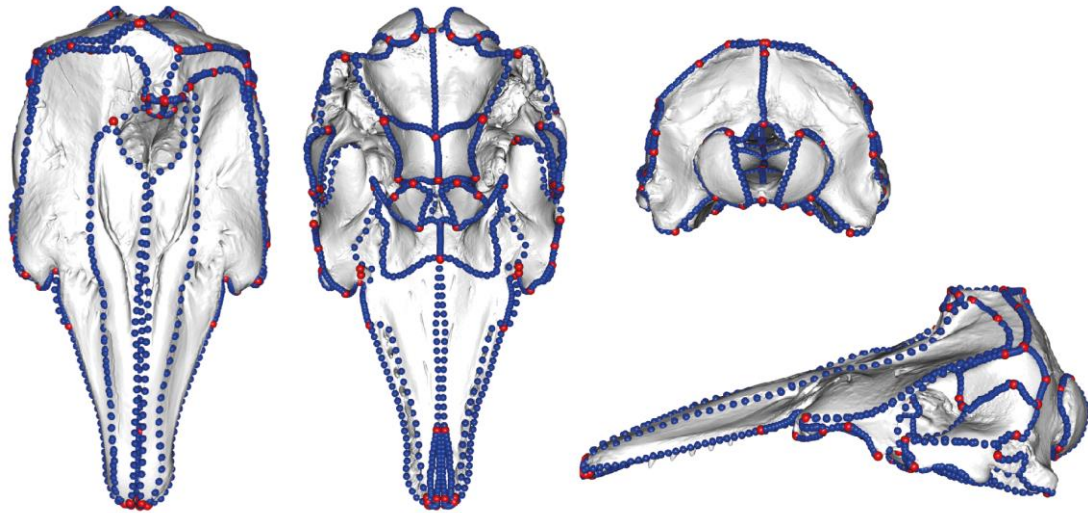
**Fig. S3.1.** Landmarks and curve sliding semi-landmark placement on a cetacean skull. From left to right, the skull is shown in dorsal, ventral, posterior (top) and lateral (bottom) view. The landmarks in red are type I and type II landmarks. The curves in blue define outlines and margins of bones. There are 123 landmarks and 124 curves on this specimen. Landmarks and curves shown on a beluga (*Delphinapterus leucas* USNM 305071) specimen.
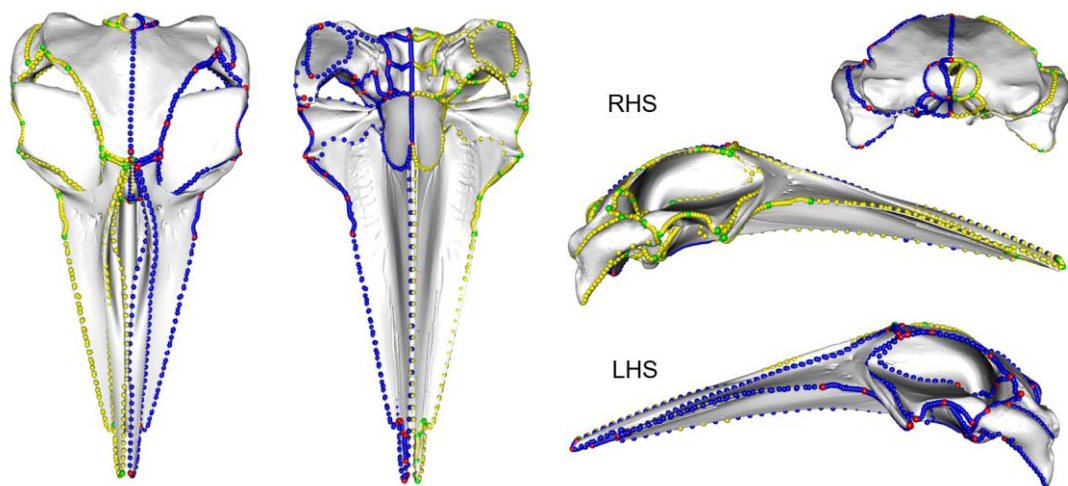


**Fig. S3.2.** Landmark configuration on a symmetric skull. Landmark protocol for the symmetric mysticete. Red = manually placed landmarks, green = computer mirrored landmarks, blue = manually placed curves (semi-landmarks), yellow = computer mirrored curves (semi-landmarks). Specimen is *Balaenoptera acutorostrata* (NHM 1965.11.2.1).
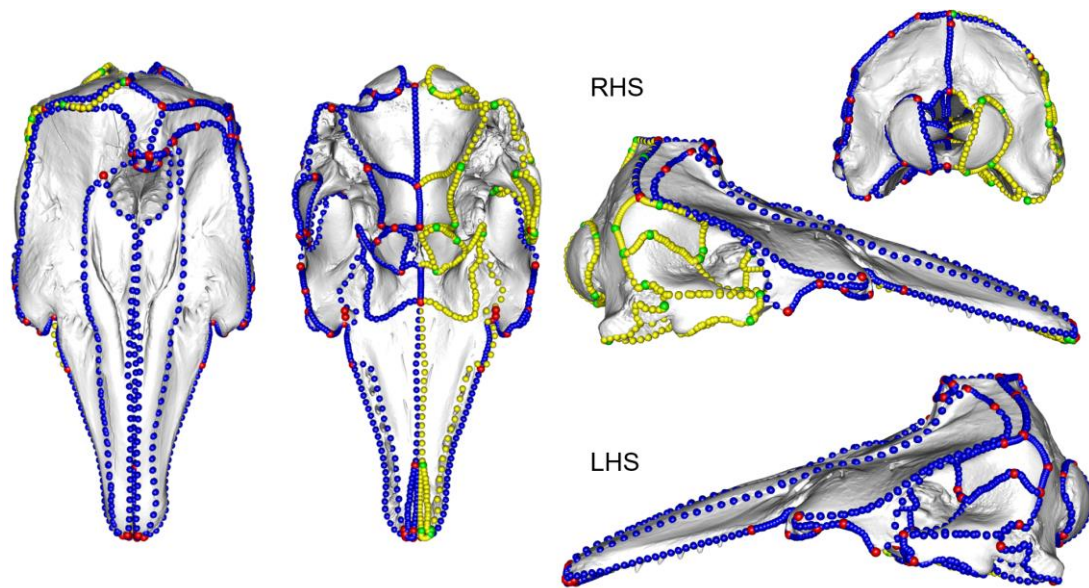
**Fig. S3.3.** Landmark configuration on an asymmetric skull. Landmark protocol for the asymmetric odontocetes and archaeocetes. Red = manually placed landmarks (on asymmetric bones), green = computer mirrored landmarks (on symmetric bones), blue = manually placed curves (semi-landmarks) on asymmetric bones, yellow = computer mirrored curves (semi-landmarks) on symmetric bones. Specimen is *Delphinapterus leucas* (USNM 305071).
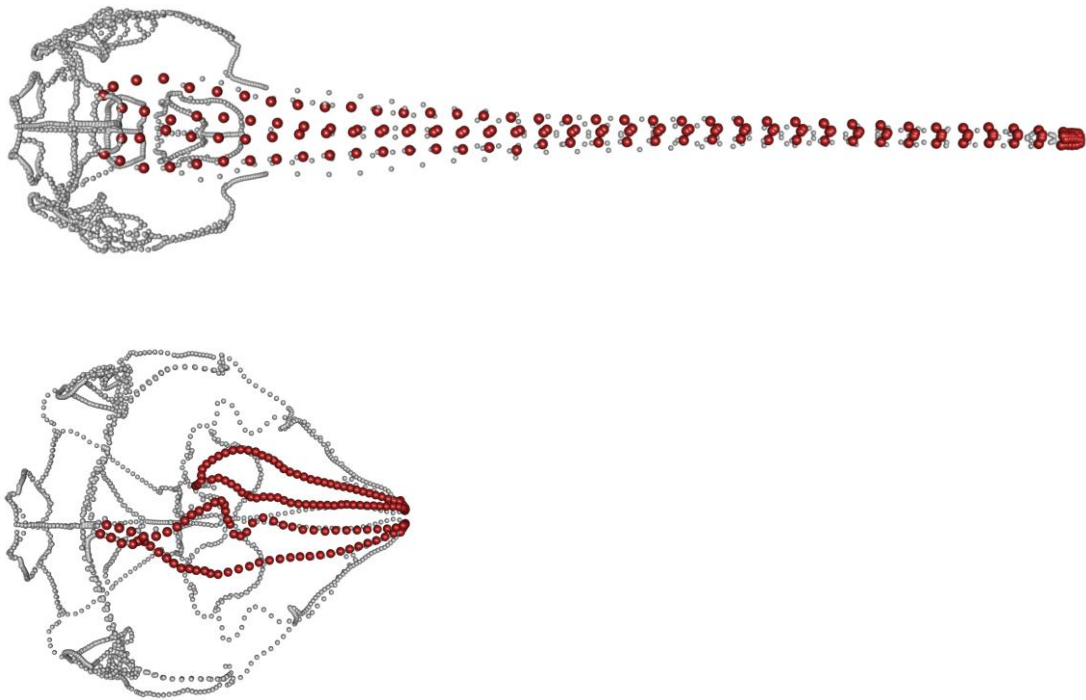
**Fig. S3.4.** An example of resampled curves. Curves shown on a dolichocephalic specimen (top: *Schizodelphis morckhoviensis* USNM 13873) and a brachycephalic specimen (bottom: *Kogia breviceps* USNM 22015). The premaxillae are highlighted in red (with points with a larger radius) on both specimens to illustrate that even once the curves are resampled, there is still a thorough coverage of landmarks along the length of the rostrum, even in the longest rostra.

[Figure on next page]

**Fig. S3.5.** Final phylogeny. Adapted phylogeny from Lloyd and Slater (2020) with all 201 specimens used in this study.

**Table S3.5.** Specimen list in order of centroid size (Csize) from largest to smallest. Note how the baleen whales occupy the top of the list and the porpoises occupy the bottom

| Specimen ID | Centroid size (Csize) |
|---|---|
| *Balaenoptera musculus* NHM 1892.3.1.1 | 77763.25295 |
| *Balaenoptera physalus* NHM 1862.2.7.181 | 54294.59958 |
| *Balaena mysticetus* 1986.1.16 | 49495.83696 |
| *Physeter macrocephalus* NHM 2007.1 | 47815.51933 |
| *Balaenoptera borealis* NHM 1934.5.25.1 | 45837.97629 |
| *Livyatan melvillei* MSNUP | 44912.99336 |
| *Eubalaena glacialis* MSNUP | 44911.55993 |
| *Balaenoptera edeni* NHM 1920.12.31.1 | 42453.74244 |
| *Eubalaena australis* NHM 1873.3.3 | 36134.21091 |
| *Balaenoptera brydei* USNM 572922 | 36078.53577 |
| *Megaptera novaeangliae* GERM.792a (NHMUK) | 35595.03802 |
| *Balaenoptera omurai* NN | 34950.26297 |
| *Eschrichtius robustus* USNM 13803 | 32139.23361 |
| *Mixocetus* sp. LACM 143474 | 26695.54071 |
| *Balaenoptera floridana* USNM 529244 | 26629.0807 |
| *Pelocetus calvertensis* USNM 11976 | 24768.42796 |
| *Balaenoptera* sp. SDNHM 83695 | 24523.55945 |
| *Hyperoodon ampullatus* NHM 1992.42 | 24444.67695 |
| *Aglaocetus moreni* FMNH P13407 | 23839.92412 |
| *Balaenula astensis* MSNUP I-12555 | 23262.93857 |
| *Balaenopteridae* NMNZ MM001630 | 22550.30914 |
| *Aglaocetus patulus* USNM 23690 | 21397.22059 |
| *Balaenoptera acutorostrata* NHM 1965.11.2.1 | 20911.59829 |
| *Berardius arnuxii* NHM 1935.10.23.1 | 18552.82928 |
| *Berardius bairdii* NHM 1954.9.21.1 | 18389.05234 |
| *Diorocetus hiatus* USNM 16783 | 17822.63727 |
| *Hyperoodon planifrons* NHM 1952.9.30.1 | 15595.1626 |
| *Xiphiacetus cristatus* USNM 21363 | 15370.06675 |
| *Tasmacetus shepherdi* USNM 484878 | 15290.05203 |
| *Basilosaurus isis* SMNS 11787 | 15247.89094 |
| *Miocaperea pulchra* SMNS 46978 | 14887.59651 |
| *Orcinus orca* USNM 11980 | 14696.79296 |
| *Caperea marginata* NHM 1876.2.16.1 | 14588.82886 |
| *Xiphiacetus bossi* USNM 8842 | 14165.33969 |
| *Pomatodelphis* sp. CMM V 3915 | 14124.05496 |
| *Eurhinodelphis cocheteuxi* IRSNB | 14056.28394 |
| *Piscobalaena nana* MNHN 1618 | 13844.20841 |
| *Schizodelphis barnesi* MNHN AMN 19 | 13842.17261 |
| *Cynthiacetus peruvianus* MNHN.F. PRU10 | 13836.29221 |
| *Berardius minimus* USNM 276375 | 13804.57187 |

| | |
|---|---|
| *Aulophyseter morricei* UCMP 81661 | 13575.0616 |
| *Parietobalaena palmeri* USNM 24883 | 13558.8355 |
| *Squalodon* sp. OU 21798 | 12984.26243 |
| *Herpetocetus sendaicus* NMNS-PV 19540 | 12916.25079 |
| *Zarhachis flagellator* USNM 10911 | 12908.66858 |
| *Cephalotropis coronatus* USNM 489194 | 12881.75029 |
| *Messapicetus gregarius* MUSM 1481 | 12871.98325 |
| *Mystacodon selenensis* MUSM 1917 | 12804.58007 |
| *Pomatodelphis* sp. USNM 187414 | 12490.42975 |
| *Mesoplodon layardii* USNM 550150 | 12481.5444 |
| *Messapicetus longirostris* MSNUP | 12480.78127 |
| *Coronodon havensteini* CCNHM 108 | 12452.32243 |
| *Ankylorhiza tiedemani* CCNHM 103 | 12109.94219 |
| *Schizodelphis* sp CCNHM 141 | 11844.07227 |
| *Schizodelphis morckhoviensis* USNM 13873 | 11687.91441 |
| *Macrokentriodon* sp. CMM V 15 | 11597.23874 |
| *Eurhinodelphis longirostris* USNM 244404 | 11589.14345 |
| *Ziphius cavirostris* NHM 2006.15 | 11548.2769 |
| *Ensidelphis riveroi* MUSM 3898 | 11523.34777 |
| *Mesoplodon carlhubbsi* USNM 504128 | 11463.52348 |
| *Dorudon atrox* PV M 100149 | 11357.968 |
| *Zarhinocetus errabundus* LACM 149588 | 11135.06531 |
| *Mesoplodon grayi* USNM 49880 | 11058.80126 |
| *Chilcacetus cavirhinus* MUSM 1401 | 11038.11956 |
| *Squalodon calvertensis* NMNZ MM001996 | 10961.13191 |
| *Patriocetus* sp. MB Ma. 42882 | 10834.67864 |
| *Orycterocetus crocodilinus* USNM 22926 | 10769.70367 |
| *Kekenodon* sp. OU 22294 | 10637.34362 |
| *Mesoplodon densirostris* NMV C 36362 | 10465.63395 |
| *Globicephala macrorhynchus* NHM 1912.10.27 | 10213.19715 |
| *Mesoplodon mirus* USNM 504612 | 10156.09478 |
| *Mesoplodon ginkgodens* USNM 298237 | 10113.44662 |
| *Zygorhiza kochii* USNM 11962 | 10086.26234 |
| *Ambulocetus natans* MSNUP I-16826 | 10064.00353 |
| *Eurhinodelphis chilcocetus* MUSM | 9986.347001 |
| *Mesoplodon bowdoini* NMNZ MM001900 | 9889.210264 |
| *Indopacetus pacificus* USNM 593534 | 9872.659259 |
| *Macrosqualodelphis ukupachai* MUSM 2545 | 9862.439478 |
| MUSM 563 | 9739.628674 |
| *Goedertius oregonensis* LACM 123887 | 9674.598742 |
| *Mesoplodon hotaula* USNM 593426 | 9621.684938 |
| *Eurhinodelphid* UCMP 99669 | 9619.225605 |
| *Squalodon bariensis* IRSNB 2372 | 9389.150598 |
| *Mesoplodon europaeus* USNM 571665 | 9375.398669 |
| *Xenorophus* sp. CCNHM 168 | 9284.109349 |
| *Mesoplodon stejnegeri* USNM 504330 | 9221.929857 |

| | |
|---|---|
| *Pseudorca crassidens* USNM 11320 | 9078.11429 |
| *Globicephala melas* NMNZ MM001946 | 8930.35961 |
| *Remingtonocetus harudiensis* USNM PAL 559313 | 8753.408806 |
| *Patriocetus ehrlichii* OL 1999-3 Cet. 4 | 8714.220498 |
| *Aegytocetus tarfa* MSNTUP I-15459 | 8652.265483 |
| *Chavinziphius maxillocristatus* MUSM 2538 | 8596.741227 |
| *Mesoplodon perrini* LACM 97501 | 8552.605379 |
| *Globicephala* sp. USNM 21867 | 8465.798939 |
| MUSM 605 | 8450.785273 |
| *Hemisyntrachelus oligodon* SMNK-PAL 3841 | 8388.371501 |
| *Monodon monoceros* USNM 267959 | 8221.699431 |
| *Xenorophus* new sp ChM PV4823 | 8184.763872 |
| *Hemisyntrachelus cortesii* MBGPT NN | 8110.768692 |
| *Aetiocetus cotylalveus* USNM 25210 | 8099.792693 |
| *Yaquinacetus* sp. USNM 214705 | 8010.484759 |
| *Notocetus vanbenedeni* MUSM 1395 | 7992.838913 |
| *Schizodelphis sulcatus* MGB | 7990.010389 |
| *Lipotes vexillifer* AMNH 57333 | 7876.501918 |
| *Kampholophus serrulus* UMCP 36045 | 7868.182297 |
| *Aetiocetus weltoni* UCMP 122900 | 7862.620663 |
| *Delphinapterus leucas* USNM 305071 | 7852.153104 |
| *Mesoplodon traversii juv.* NMNZ TMP012996 | 7733.077281 |
| *Mesoplodon hectori* NHM 1949.8.19.1 | 7698.311092 |
| *Cotylocara macei* CCNHM 101 | 7600.374316 |
| *Zarhinocetus donnamatsonae* UCMP 86139 | 7552.347504 |
| *Kogia breviceps* USNM 22015 | 7539.122454 |
| *Aprixokogia kelloggi* USNM 187015 | 7508.117448 |
| *Nazcacetus urbinai* MUSM 949 | 7500.041822 |
| *Artiocetus clavis* GSP-UM 3458 | 7282.12702 |
| *Prosqualodon davidis* USNM 467596 | 7242.619367 |
| *Grampus griseus* USNM 571602 | 7179.200789 |
| *Mesoplodon bidens* USNM 593438 | 7115.936164 |
| *Sousa plumbea* USNM 550941 | 7072.979499 |
| *Steno bredanensis* USNM 572789 | 7000.373949 |
| *Parapontoporia sternbergi* SDNHM 75060 | 6986.650303 |
| *Squalodon* sp. OU 22397 | 6959.528905 |
| *Waipatia* sp. CCNHM 567 | 6943.875997 |
| *Tursiops truncatus* SDNHM 23798 | 6934.658325 |
| *Inia geoffrensis* AMNH 93415 | 6933.424347 |
| *Waipatia maerwhenua* OU 22095 | 6882.920327 |
| *Etruridelphis* sp. PU 13884 | 6851.467504 |
| *Janjucetus hunderi* NMV P216929 | 6817.367686 |
| *Protocetus atavus* SMNS 11084 | 6780.263668 |
| *Patriocetus* sp. ChM PV4753 | 6646.258971 |
| *Tursiops truncatus gilli* SDNHM 11102 | 6578.609415 |
| *Huaridelphis raimondii* MUSM 1396 | 6576.073849 |

| | |
|---|---|
| *Sousa chinensis* NHM 1992.97 | 6573.613097 |
| *Delphinus capensis* NHM 1981.7.11 | 6432.448975 |
| *Albireo whistleri* UCR 14589 | 6402.317682 |
| *Peponocephala electra* USNM 504511 | 6365.401589 |
| *Patriocetus* sp. CCNHM 1078 | 6337.314683 |
| *Agorophius* sp. USNM 205491 | 6307.537971 |
| *Sousa sahulensis* NHM 1992.92 | 6155.372514 |
| *Delphinus delphis* AMNH 75332 | 6093.990268 |
| *Lagenorhynchus acutus* USNM 504196 | 6078.5911 |
| *Simocetus rayi* USNM 256517 | 6036.448199 |
| *Sousa teuszii* NHM 1992.138 | 6022.634852 |
| *Piscolithax longirostris* SAS 933 | 6009.020444 |
| *Tagicetus joneti* IRSNB M. 1892 | 5990.835713 |
| *Mesoplodon peruvianus* USNM 571258 | 5975.83785 |
| *Albertocetus* sp. ChM PV8680 | 5975.698111 |
| *Lissodelphis borealis* USNM 550188 | 5961.814375 |
| *Fucaia goedertorum* LACM 131146 | 5953.622665 |
| *Argyrocetus joaquinensis* USNM 11996 | 5952.815496 |
| *Lissodelphis peronii* NMNZ MM002116 | 5946.570878 |
| *Pontoporia blainvillei* USNM 482727 | 5896.878281 |
| *Dilophodelphis fordycei* USNM 214911 | 5882.441762 |
| *Odobenocetops peruvianus* SMNK PAL 2491 | 5847.114226 |
| *Scaphokogia totajpe* MUSM 973 | 5816.399052 |
| *Lagenodelphis hosei* USNM 571619 | 5752.72195 |
| *Lamprolithax simulans* LACM 37858 | 5737.505103 |
| *Kentriodon* sp. | 5690.342515 |
| *Squalodon* sp. OU 22126 | 5689.320955 |
| *Tursiops aduncus* NHM 1882.1.2.3 | 5670.492315 |
| *Echovenator sandersi* GSM 1098 | 5670.135086 |
| *Lagenorhynchus obliquidens* NHM 1992.83 | 5562.319634 |
| *Lagenorhynchus albirostris* AMNH 37162 | 5499.869421 |
| *Stenodelphin* sp. UCMP 125352 | 5366.222803 |
| *Lagenorhynchus cruciger* NHM 1960.8.24.1 | 5345.452762 |
| *Feresa attenuata* USNM 504916 | 5304.972746 |
| *Stenella attenuata* NHM 1966.11.18.5 | 5284.837181 |
| *Lagenorhynchus australis* 1944.11.30.1 | 5199.535683 |
| *Platanista gangetica* USNM 172409 | 5140.420799 |
| *Semirostrum cerutti* SDNHM 65276 | 5066.437061 |
| *Piscolithax tedfordi* UCMP 15972 | 5025.821164 |
| *Sotalia guianensis* USNM 571558 | 4986.196431 |
| *Lomacetus ginsburgi* MNHN.F.PPI.104 | 4978.678982 |
| *Lagenorhynchus obscurus* NHM 1846.3.11.8 | 4967.017878 |
| *Stenella longirostris* USNM 395270 | 4820.873936 |
| *Kentriodon schneideri* USNM 323772 | 4782.597845 |
| *Delphinodon dividum* USNM 7278 | 4781.821329 |
| *Atocetus iquensis* MNHN.F.PPI. 113 | 4759.468686 |

| | |
|---|---|
| *Koristocetus pescei* MUSM 888 | 4702.52087 |
| *Phocoenoides dalli* USNM 276062 | 4697.799111 |
| *Septemtriocetus bosselaersi* IRSNB M.1928 | 4641.267957 |
| *Pakicetus attocki* PV M 100148 | 4577.968908 |
| *Kogia simus* NHM.1952.8.28.1 | 4499.010619 |
| *Orcaella heinsohni* USNM 284430 | 4418.151942 |
| *Cephalorhynchus eutropia* NHM 1881.8.17.1 | 4398.195581 |
| *Orcaella brevirostris* NHM.1883.11.20.2 | 4379.85029 |
| *Cephalorhynchus hectori* NMNZ MM002288 | 4322.517214 |
| *Waipatia* sp. ChM PV7679 | 4239.360723 |
| *Papahu taitapu* OU 22066 | 4193.25279 |
| *Kentriodon pernix* USNM 10670 | 4167.149606 |
| *Cephalorhynchus commersonii* NN | 4102.784266 |
| *Phocoena dioptrica* NHM 1939.9.30.1 | 4088.75329 |
| *Cephalorhynchus heavisidii* NHM 1948.7.27.1 | 3956.239916 |
| *Cephalorhynchus hectori maui* NMNZ MM002607 | 3955.581917 |
| *Brachydelphis mazeasi* MUSM 564 | 3833.335755 |
| *Pliopontos littoralis* SAS 193 | 3569.729283 |
| *Phocoena phocoena* AMNH 212161 | 3419.587466 |
| *Phocoena spinipinnis* NHM 1900.5.7.29 | 3143.131876 |
| *Neophocaena asiaeorientalis* USNM 240001 | 3115.956626 |
| *Phocoena sinus* SDNHM 20697 | 2988.119118 |
| *Neophocoena phocaenoides* NHM 1903.9.12.3 | 2847.164267 |

**Table S3.6.** Summary of the PC axes for the full landmark and curve semi-landmark data set (all Cetacea). 39 of the PC axes were required to explain 95% of cranial shape variation.

| | Comp1 | Comp2 | Comp3 | Comp4 | Comp5 | Comp6 | Comp7 | Comp8 | Comp9 |
|---|---|---|---|---|---|---|---|---|---|
| Eigenvalues | 3.07E-03 | 2.47E-03 | 1.14E-03 | 9.31E-04 | 7.16E-04 | 4.76E-04 | 3.96E-04 | 2.42E-04 | 2.24E+06 |
| Proportion of Variance | 2.51E-01 | 2.02E-01 | 9.34E-02 | 7.61E-02 | 5.86E-02 | 3.89E-02 | 3.24E-02 | 1.98E-02 | 1.83E+08 |
| Cumulative Proportion | 2.51E-01 | 4.53E-01 | 5.47E-01 | 6.23E-01 | 6.82E-01 | 7.21E-01 | 7.53E-01 | 7.73E-01 | 9.10E+08 |
| | Comp10 | Comp11 | Comp12 | Comp13 | Comp14 | Comp15 | Comp16 | Comp17 | Comp18 |
| Eigenvalues | 2.09E-04 | 1.66E-04 | 1.52E-04 | 1.48E-04 | 1.26E-04 | 1.00E-04 | 8.70E-05 | 8.08E-05 | 7.54E-05 |
| Proportion of Variance | 1.71E-02 | 1.36E-02 | 1.25E-02 | 1.21E-02 | 1.03E-02 | 8.20E-03 | 7.11E-03 | 6.61E-03 | 6.16E-03 |
| Cumulative Proportion | 8.08E-01 | 8.22E-01 | 8.34E-01 | 8.46E-01 | 8.57E-01 | 0.864791 | 8.72E-01 | 8.79E-01 | 8.85E-01 |
| | Comp19 | Comp20 | Comp21 | Comp22 | Comp23 | Comp24 | Comp25 | Comp26 | Comp27 |
| Eigenvalues | 6.70E-05 | 6.50E-05 | 6.30E-05 | 5.26E-05 | 4.95E-05 | 4.77E-05 | 4.53E-05 | 4.31E-05 | 3.94E-05 |
| Proportion of Variance | 5.48E-03 | 5.32E-03 | 5.15E-03 | 4.30E-03 | 4.05E-03 | 3.90E-03 | 3.71E-03 | 3.52E-03 | 3.23E-03 |
| Cumulative Proportion | 8.90E-01 | 8.95E-01 | 9.01E-01 | 9.05E-01 | 9.09E-01 | 9.13E-01 | 9.17E-01 | 9.20E-01 | 9.23E-01 |
| | Comp28 | Comp29 | Comp30 | Comp31 | Comp32 | Comp33 | Comp34 | Comp35 | Comp36 |
| Eigenvalues | 3.67E-05 | 3.57E-05 | 3.34E-05 | 3.12E-05 | 3.00E-05 | 2.75E-05 | 2.70E-05 | 2.53E-05 | 2.40E-05 |
| Proportion of Variance | 3.00E-03 | 2.92E-03 | 2.73E-03 | 2.55E-03 | 2.45E-03 | 2.25E-03 | 2.21E-03 | 2.07E-03 | 1.96E-03 |
| Cumulative Proportion | 9.26E-01 | 9.29E-01 | 9.32E-01 | 9.35E-01 | 9.37E-01 | 9.39E-01 | 9.41E-01 | 9.44E-01 | 9.45E-01 |
| | Comp37 | Comp38 | Comp39 | Comp40 | Comp41 | Comp42 | Comp43 | Comp44 | Comp45 |
| Eigenvalues | 2.32E-05 | 2.22E-05 | 2.06E-05 | 1.98E-05 | 1.89E-05 | 1.82E-05 | 1.78E-05 | 1.77E-05 | 1.66E-05 |
| Proportion of Variance | 1.90E-03 | 1.81E-03 | 1.68E-03 | 1.62E-03 | 1.55E-03 | 1.49E-03 | 1.46E-03 | 1.45E-03 | 1.36E-03 |
| Cumulative Proportion | 9.47E-01 | 9.49E-01 | 9.51E-01 | 9.52E-01 | 9.54E-01 | 9.56E-01 | 9.57E-01 | 9.58E-01 | 9.60E-01 |
| | Comp46 | Comp47 | Comp48 | Comp49 | Comp50 | Comp51 | Comp52 | Comp53 | Comp54 |
| Eigenvalues | 1.61E-05 | 1.56E-05 | 1.5E-05 | 1.44E-05 | 1.41E-05 | 1.29E-05 | 1.26E-05 | 1.19E-05 | 1.18E-05 |
| Proportion of Variance | 1.32E-03 | 1.28E-03 | 1.22E-03 | 1.17E-03 | 1.15E-03 | 1.06E-03 | 1.03E-03 | 9.73E-04 | 9.66E-04 |
| Cumulative Proportion | 9.61E-01 | 9.62E-01 | 9.64E-01 | 9.65E-01 | 9.66E-01 | 9.67E-01 | 9.68E-01 | 9.69E-01 | 9.70E-01 |
| | Comp55 | Comp56 | Comp57 | Comp58 | Comp59 | Comp60 | Comp61 | Comp62 | Comp63 |
| Eigenvalues | 1.16E-05 | 1.07E-05 | 1.05E-05 | 1.03E-05 | 1.00E-05 | 9.45E-06 | 8.90E-06 | 8.66E-06 | 8.49E-06 |
| Proportion of Variance | 9.45E-04 | 8.75E-04 | 8.58E-04 | 8.42E-04 | 8.19E-04 | 7.73E-04 | 7.27E-04 | 7.08E-04 | 6.94E-04 |
| Cumulative Proportion | 9.71E-01 | 9.72E-01 | 0.972638 | 9.73E-01 | 9.74E-01 | 9.75E-01 | 9.76E-01 | 9.77E-01 | 9.77E-01 |
| | Comp64 | Comp65 | Comp66 | Comp67 | Comp68 | Comp69 | Comp70 | Comp71 | Comp72 |
| Eigenvalues | 8.35E-06 | 8.17E-06 | 7.91E-06 | 7.69E-06 | 7.65E-06 | 7.42E-06 | 6.75E-06 | 6.58E-06 | 6.48E-06 |
| Proportion of Variance | 6.82E-04 | 6.68E-04 | 6.47E-04 | 6.29E-04 | 6.25E-04 | 6.07E-04 | 5.52E-04 | 5.38E-04 | 5.30E-04 |
| Cumulative Proportion | 9.78E-01 | 9.79E-01 | 9.79E-01 | 9.80E-01 | 9.80E-01 | 9.81E-01 | 9.82E-01 | 9.82E-01 | 9.83E-01 |
| | Comp73 | Comp74 | Comp75 | Comp76 | Comp77 | Comp78 | Comp79 | Comp80 | Comp81 |
| Eigenvalues | 6.44E-06 | 6.20E-06 | 5.98E-06 | 5.88E-06 | 5.55E-06 | 5.28E-06 | 5.22E-06 | 4.92E-06 | 4.88E-06 |
| Proportion of Variance | 5.27E-04 | 5.07E-04 | 4.89E-04 | 4.81E-04 | 4.54E-04 | 4.32E-04 | 4.27E-04 | 4.03E-04 | 3.99E-04 |
| Cumulative Proportion | 9.83E-01 | 9.84E-01 | 9.84E-01 | 9.85E-01 | 9.85E-01 | 9.86E-01 | 9.86E-01 | 9.86E-01 | 9.87E-01 |
| | Comp82 | Comp83 | Comp84 | Comp85 | Comp86 | Comp87 | Comp88 | Comp89 | Comp90 |
| Eigenvalues | 4.74E-06 | 4.70E-06 | 4.47E-06 | 4.32E-06 | 4.20E-06 | 4.13E-06 | 4.06E-06 | 3.88E-06 | 3.82E-06 |

| | | | | | | | | | |
|---|---|---|---|---|---|---|---|---|---|
| **Proportion of Variance** | 3.88E-04 | 3.84E-04 | 3.66E-04 | 3.53E-04 | 3.44E-04 | 3.38E-04 | 3.32E-04 | 3.18E-04 | 3.12E-04 |
| **Cumulative Proportion** | 9.87E-01 | 9.88E-01 | 9.88E-01 | 9.88E-01 | 9.89E-01 | 9.89E-01 | 9.89E-01 | 9.90E-01 | 9.90E-01 |
| | **Comp91** | **Comp92** | **Comp93** | **Comp94** | **Comp95** | **Comp96** | **Comp97** | **Comp98** | **Comp99** |
| **Eigenvalues** | 3.74E-06 | 3.59E-06 | 3.51E-06 | 3.36E-06 | 3.33E-06 | 3.29E-06 | 3.12E-06 | 3.04E-06 | 2.98E-06 |
| **Proportion of Variance** | 3.06E-04 | 2.94E-04 | 2.87E-04 | 2.75E-04 | 2.73E-04 | 2.69E-04 | 2.55E-04 | 2.48E-04 | 2.43E-04 |
| **Cumulative Proportion** | 9.90E-01 | 9.91E-01 | 9.91E-01 | 9.91E-01 | 9.91E-01 | 9.92E-01 | 9.92E-01 | 9.92E-01 | 9.92E-01 |
| | **Comp100** | **Comp101** | **Comp102** | **Comp103** | **Comp104** | **Comp105** | **Comp106** | **Comp107** | **Comp108** |
| **Eigenvalues** | 2.80E-06 | 2.73E-06 | 2.69E-06 | 2.64E-06 | 2.52E-06 | 2.49E-06 | 2.32E-06 | 2.30E-06 | 2.25E-06 |
| **Proportion of Variance** | 2.29E-04 | 2.23E-04 | 2.20E-04 | 2.16E-04 | 2.06E-04 | 2.04E-04 | 1.89E-04 | 1.88E-04 | 1.84E-04 |
| **Cumulative Proportion** | 9.93E-01 | 9.93E-01 | 9.93E-01 | 9.93E-01 | 9.93E-01 | 9.94E-01 | 9.94E-01 | 9.94E-01 | 9.94E-01 |
| | **Comp109** | **Comp110** | **Comp111** | **Comp112** | **Comp113** | **Comp114** | **Comp115** | **Comp116** | **Comp117** |
| **Eigenvalues** | 2.19E-06 | 2.13E-06 | 2.08E-06 | 2.05E-06 | 1.92E-06 | 1.91E-06 | 1.87E-06 | 1.83E-06 | 1.79E-06 |
| **Proportion of Variance** | 1.79E-04 | 1.74E-04 | 1.70E-04 | 1.68E-04 | 1.57E-04 | 1.56E-04 | 1.53E-04 | 1.49E-04 | 1.46E-04 |
| **Cumulative Proportion** | 9.94E-01 | 9.95E-01 | 9.95E-01 | 9.95E-01 | 9.95E-01 | 9.95E-01 | 9.95E-01 | 9.96E-01 | 9.96E-01 |
| | **Comp118** | **Comp119** | **Comp120** | **Comp121** | **Comp122** | **Comp123** | **Comp124** | **Comp125** | **Comp126** |
| **Eigenvalues** | 1.69E-06 | 1.65E-06 | 1.60E-06 | 1.57E-06 | 1.52E-06 | 1.50E-06 | 1.47E-06 | 1.39E-06 | 1.35E-06 |
| **Proportion of Variance** | 1.38E-04 | 1.35E-04 | 1.31E-04 | 1.28E-04 | 1.25E-04 | 1.23E-04 | 1.20E-04 | 1.14E-04 | 1.11E-04 |
| **Cumulative Proportion** | 9.96E-01 | 9.96E-01 | 9.96E-01 | 9.96E-01 | 9.96E-01 | 9.96E-01 | 9.97E-01 | 9.97E-01 | 9.97E-01 |
| | **Comp127** | **Comp128** | **Comp129** | **Comp130** | **Comp131** | **Comp132** | **Comp133** | **Comp134** | **Comp135** |
| **Eigenvalues** | 1.34E-06 | 1.29E-06 | 1.27E-06 | 1.25E-06 | 1.25E-06 | 1.20E-06 | 1.17E-06 | 1.12E-06 | 1.10E-06 |
| **Proportion of Variance** | 1.09E-04 | 1.05E-04 | 1.04E-04 | 1.02E-04 | 1.02E-04 | 9.78E-05 | 9.56E-05 | 9.12E-05 | 8.98E-05 |
| **Cumulative Proportion** | 9.97E-01 | 9.97E-01 | 9.97E-01 | 9.97E-01 | 9.97E-01 | 9.97E-01 | 9.98E-01 | 9.98E-01 | 9.98E-01 |
| | **Comp136** | **Comp137** | **Comp138** | **Comp139** | **Comp140** | **Comp141** | **Comp142** | **Comp143** | **Comp144** |
| **Eigenvalues** | 1.04E-06 | 9.74E-07 | 9.56E-07 | 9.38E-07 | 8.95E-07 | 8.79E-07 | 8.54E-07 | 8.38E-07 | 8.17E-07 |
| **Proportion of Variance** | 8.54E-05 | 7.97E-05 | 7.82E-05 | 7.67E-05 | 7.32E-05 | 7.19E-05 | 6.98E-05 | 6.86E-05 | 6.68E-05 |
| **Cumulative Proportion** | 9.98E-01 | 9.98E-01 | 9.98E-01 | 9.98E-01 | 9.98E-01 | 9.98E-01 | 9.98E-01 | 9.98E-01 | 9.98E-01 |
| | **Comp145** | **Comp146** | **Comp147** | **Comp148** | **Comp149** | **Comp150** | **Comp151** | **Comp152** | **Comp153** |
| **Eigenvalues** | 7.80E-07 | 7.51E-07 | 7.43E-07 | 7.19E-07 | 7.01E-07 | 6.91E-07 | 6.71E-07 | 6.21E-07 | 6.06E-07 |
| **Proportion of Variance** | 6.38E-05 | 6.14E-05 | 6.07E-05 | 5.88E-05 | 5.73E-05 | 5.65E-05 | 5.49E-05 | 5.08E-05 | 4.96E-05 |
| **Cumulative Proportion** | 9.98E-01 | 9.99E-01 | 9.99E-01 | 9.99E-01 | 9.99E-01 | 9.99E-01 | 9.99E-01 | 9.99E-01 | 9.99E-01 |
| | **Comp154** | **Comp155** | **Comp156** | **Comp157** | **Comp158** | **Comp159** | **Comp160** | **Comp161** | **Comp162** |
| **Eigenvalues** | 6.03E-07 | 5.79E-07 | 5.63E-07 | 5.43E-07 | 5.29E-07 | 5.16E-07 | 5.02E-07 | 4.92E-07 | 4.71E-07 |
| **Proportion of Variance** | 4.93E-05 | 4.74E-05 | 4.61E-05 | 4.44E-05 | 4.33E-05 | 4.22E-05 | 4.10E-05 | 4.02E-05 | 3.85E-05 |
| **Cumulative Proportion** | 9.99E-01 | 9.99E-01 | 9.99E-01 | 9.99E-01 | 9.99E-01 | 9.99E-01 | 9.99E-01 | 9.99E-01 | 9.99E-01 |
| | **Comp163** | **Comp164** | **Comp165** | **Comp166** | **Comp167** | **Comp168** | **Comp169** | **Comp170** | **Comp171** |
| **Eigenvalues** | 4.69E-07 | 4.38E-07 | 4.06E-07 | 3.88E-07 | 3.70E-07 | 3.50E-07 | 3.47E-07 | 3.31E-07 | 3.23E-07 |
| **Proportion of Variance** | 3.83E-05 | 3.58E-05 | 3.32E-05 | 3.17E-05 | 3.03E-05 | 2.86E-05 | 2.84E-05 | 2.71E-05 | 2.64E-05 |
| **Cumulative Proportion** | 9.99E-01 | 9.99E-01 | 9.99E-01 | 9.99E-01 | 9.99E-01 | 9.99E-01 | 1.00E+00 | 1.00E+00 | 1.00E+00 |
| | **Comp172** | **Comp173** | **Comp174** | **Comp175** | **Comp176** | **Comp177** | **Comp178** | **Comp179** | **Comp180** |
| **Eigenvalues** | 3.15E-07 | 3.02E-07 | 2.97E-07 | 2.87E-07 | 2.65E-07 | 2.51E-07 | 2.45E-07 | 2.37E-07 | 2.27E-07 |
| **Proportion of Variance** | 2.57E-05 | 2.47E-05 | 2.43E-05 | 2.35E-05 | 2.17E-05 | 2.06E-05 | 2.00E-05 | 1.94E-05 | 1.85E-05 |
| **Cumulative Proportion** | 1.00E+00 | 1.00E+00 | 1.00E+00 | 1.00E+00 | 1.00E+00 | 1.00E+00 | 1.00E+00 | 1.00E+00 | 1.00E+00 |
| | **Comp181** | **Comp182** | **Comp183** | **Comp184** | **Comp185** | **Comp186** | **Comp187** | **Comp188** | **Comp189** |
| **Eigenvalues** | 2.08E-07 | 2.02E-07 | 1.90E-07 | 1.87E-07 | 1.82E-07 | 1.76E-07 | 1.71E-07 | 1.54E-07 | 1.48E-07 |

| | | | | | | | | |
|---|---|---|---|---|---|---|---|---|
| **Proportion of Variance** | 1.70E-05 | 1.65E-05 | 1.55E-05 | 1.53E-05 | 1.49E-05 | 1.44E-05 | 1.40E-05 | 1.26E-05 | 1.21E-05 |
| **Cumulative Proportion** | 1.00E+00 | 1.00E+00 | 1.00E+00 | 1.00E+00 | 1.00E+00 | 1.00E+00 | 1.00E+00 | 1.00E+00 | 1.00E+00 |
| | **Comp190** | **Comp191** | **Comp192** | **Comp193** | **Comp194** | **Comp195** | **Comp196** | **Comp197** | **Comp198** |
| **Eigenvalues** | 1.35E-07 | 1.33E-07 | 1.24E-07 | 1.16E-07 | 1.11E-07 | 1.05E-07 | 9.86E-08 | 9.27E-08 | 8.79E-08 |
| **Proportion of Variance** | 1.11E-05 | 1.08E-05 | 1.02E-05 | 9.46E-06 | 9.11E-06 | 8.61E-06 | 8.06E-06 | 7.58E-06 | 7.19E-06 |
| **Cumulative Proportion** | 1.00E+00 | 1.00E+00 | 1.00E+00 | 1.00E+00 | 1.00E+00 | 1.00E+00 | 1.00E+00 | 1.00E+00 | 1.00E+00 |
| | **Comp199** | **Comp200** | **Comp201** | | | | | | |
| **Eigenvalues** | 8.32E-08 | 7.45E-08 | 6.06E-34 | | | | | | |
| **Proportion of Variance** | 6.81E-06 | 6.10E-06 | 4.96E-32 | | | | | | |
| **Cumulative Proportion** | 1.00E+00 | 1.00E+00 | 1.00E+00 | | | | | | |

**Table S3.7.** Summary of the PC axes for the full landmark and curve semi-landmark data set for the archaeocetes. 8 of the PC axes were required to explain 95% of cranial shape variation.

| | Comp1 | Comp2 | Comp3 | Comp4 | Comp5 | Comp6 | Comp7 | Comp8 |
|---|---|---|---|---|---|---|---|---|
| **Eigenvalues** | 0.002445791 | 0.001326 | 0.000789 | 0.000428 | 0.000406 | 0.000352 | 0.000313 | 0.000216 |
| **Proportion of Variance** | 0.37620037 | 0.20397 | 0.121336 | 0.065766 | 0.062408 | 0.054124 | 0.048096 | 0.033203 |
| **Cumulative Proportion** | 0.37620037 | 0.58017 | 0.701507 | 0.767272 | 0.82968 | 0.883804 | 0.9319 | 0.965103 |
| | **Comp9** | **Comp10** | **Comp11** | | | | | |
| **Eigenvalues** | 0.000118182 | 0.000109 | 1.06E-32 | | | | | |
| **Proportion of Variance** | 0.018178202 | 0.016718 | 1.62E-30 | | | | | |
| **Cumulative Proportion** | 0.98328163 | 1 | 1.00E+00 | | | | | |

[Table on next page]

**Table S3.8.** Summary of the PC axes for the full landmark and curve semi-landmark data set for the mysticetes. 14 of the PC axes were required to explain 95% of cranial shape variation.

| | Comp1 | Comp2 | Comp3 | Comp4 | Comp5 | Comp6 | Comp7 | Comp8 |
|---|---|---|---|---|---|---|---|---|
| Eigenvalues | 0.002558947 | 0.001106 | 0.000611 | 0.000372 | 0.000282 | 0.000168 | 0.000125 | 0.000109 |
| Proportion of Variance | 0.425469985 | 0.183945 | 0.101596 | 0.061862 | 0.046939 | 0.02793 | 0.020859 | 0.018098 |
| Cumulative Proportion | 0.425469985 | 0.609415 | 0.71101 | 0.772872 | 0.819812 | 0.847742 | 0.8686 | 0.886698 |
| | Comp9 | Comp10 | Comp11 | Comp12 | Comp13 | Comp14 | Comp15 | Comp16 |
| Eigenvalues | 9.37E-05 | 7.88E-05 | 7.22E-05 | 6.55E-05 | 5.34E-05 | 4.50E-05 | 3.71E-05 | 3.35E-05 |
| Proportion of Variance | 1.56E-02 | 1.31E-02 | 1.20E-02 | 1.09E-02 | 8.88E-03 | 7.49E-03 | 6.17E-03 | 0.005567 |
| Cumulative Proportion | 9.02E-01 | 9.15E-01 | 9.27E-01 | 9.38E-01 | 9.47E-01 | 9.55E-01 | 9.61E-01 | 0.966355 |
| | Comp17 | Comp18 | Comp19 | Comp20 | Comp21 | Comp22 | Comp23 | Comp24 |
| Eigenvalues | 2.82E-05 | 2.65E-05 | 2.44E-05 | 2.05E-05 | 1.92E-05 | 1.34E-05 | 1.23E-05 | 1.10E-05 |
| Proportion | 4.69E-03 | 4.40E-03 | 4.05E-03 | 3.40E-03 | 0.003193 | 2.22E-03 | 2.05E-03 | 1.83E-03 |
| Cumulative Proportion | 9.71E-01 | 9.75E-01 | 9.79E-01 | 9.83E-01 | 0.986096 | 9.88E-01 | 9.90E-01 | 9.92E-01 |
| | Comp25 | Comp26 | Comp27 | Comp28 | Comp29 | Comp30 | Comp31 | Comp32 |
| Eigenvalues | 9.69E-06 | 8.76E-06 | 7.47E-06 | 6.05E-06 | 4.84E-06 | 4.05E-06 | 3.14E-06 | 2.91E-06 |
| Proportion of Variance | 1.61E-03 | 1.46E-03 | 1.24E-03 | 1.01E-03 | 8.05E-04 | 6.73E-04 | 5.22E-04 | 4.85E-04 |
| Cumulative Proportion | 9.94E-01 | 9.95E-01 | 9.97E-01 | 9.98E-01 | 9.98E-01 | 9.99E-01 | 1.00E+00 | 1.00E+00 |
| | Comp33 | | | | | | | |
| Eigenvalues | 5.50E-30 | | | | | | | |
| Proportion of Variance | 9.15E-28 | | | | | | | |
| Cumulative Proportion | 1.00E+00 | | | | | | | |

**Table S3.9.** Summary of the PC axes for the full landmark and curve semi-landmark data set for the odontocetes. 30 of the PC axes were required to explain 95% of cranial shape variation.

| | Comp1 | Comp2 | Comp3 | Comp4 | Comp5 | Comp6 | Comp7 | Comp8 |
|---|---|---|---|---|---|---|---|---|
| Eigenvalues | 0.003893 | 0.002952 | 0.001415 | 0.001102 | 0.000872 | 0.000578 | 0.000475 | 0.000274 |
| Proportion of Variance | 0.274115 | 0.207859 | 0.099628 | 0.077562 | 0.06137 | 0.040679 | 0.033442 | 0.019321 |
| Cumulative Proportion | 0.274115 | 0.481974 | 0.581601 | 0.659163 | 0.720533 | 0.761212 | 0.794654 | 0.813975 |
| | Comp9 | Comp10 | Comp11 | Comp12 | Comp13 | Comp14 | Comp15 | Comp16 |
| Eigenvalues | 0.000246 | 0.000202 | 0.00019 | 0.000158 | 0.000144 | 0.000111 | 9.92E-05 | 8.13E-05 |
| Proportion of Variance | 0.017324 | 0.014257 | 0.013387 | 0.01113 | 0.010125 | 0.007811 | 6.99E-03 | 5.72E-03 |
| Cumulative Proportion | 0.8313 | 0.845557 | 0.858944 | 0.870074 | 0.880199 | 0.88801 | 8.95E-01 | 9.01E-01 |
| | Comp17 | Comp18 | Comp19 | Comp20 | Comp21 | Comp22 | Comp23 | Comp24 |
| Eigenvalues | 7.96E-05 | 7.28E-05 | 6.57E-05 | 6.22E-05 | 5.80E-05 | 5.39E-05 | 5.09E-05 | 4.67E-05 |
| Proportion of Variance | 5.61E-03 | 5.13E-03 | 4.62E-03 | 4.38E-03 | 4.08E-03 | 3.79E-03 | 3.59E-03 | 3.29E-03 |
| Cumulative Proportion | 9.06E-01 | 9.11E-01 | 9.16E-01 | 9.20E-01 | 9.25E-01 | 9.28E-01 | 9.32E-01 | 9.35E-01 |
| | Comp25 | Comp26 | Comp27 | Comp28 | Comp29 | Comp30 | Comp31 | Comp32 |
| Eigenvalues | 4.31E-05 | 3.87E-05 | 3.77E-05 | 3.60E-05 | 3.37E-05 | 3.12E-05 | 3.08E-05 | 2.75E-05 |
| Proportion of Variance | 3.03E-03 | 0.002725 | 2.65E-03 | 2.54E-03 | 2.37E-03 | 2.20E-03 | 2.17E-03 | 1.94E-03 |

| | | | | | | | | |
|---|---|---|---|---|---|---|---|---|
| **Cumulative Proportion** | 9.38E-01 | 0.94096 | 9.44E-01 | 9.46E-01 | 9.49E-01 | 9.51E-01 | 9.53E-01 | 9.55E-01 |
| | **Comp33** | **Comp34** | **Comp35** | **Comp36** | **Comp37** | **Comp38** | **Comp39** | **Comp40** |
| **Eigenvalues** | 2.65E-05 | 2.55E-05 | 2.36E-05 | 2.26E-05 | 2.17E-05 | 2.09E-05 | 1.98E-05 | 1.91E-05 |
| **Proportion of Variance** | 1.86E-03 | 0.001793 | 1.66E-03 | 0.00159 | 1.53E-03 | 1.47E-03 | 1.39E-03 | 1.35E-03 |
| **Cumulative Proportion** | 9.57E-01 | 0.958483 | 9.60E-01 | 0.961735 | 9.63E-01 | 9.65E-01 | 9.66E-01 | 9.67E-01 |
| | **Comp41** | **Comp42** | **Comp43** | **Comp44** | **Comp45** | **Comp46** | **Comp47** | **Comp48** |
| **Eigenvalues** | 1.77E-05 | 1.75E-05 | 1.72E-05 | 1.55E-05 | 1.48E-05 | 1.44E-05 | 1.38E-05 | 1.35E-05 |
| **Proportion of Variance** | 1.25E-03 | 1.23E-03 | 1.21E-03 | 1.09E-03 | 1.04E-03 | 1.01E-03 | 9.73E-04 | 9.48E-04 |
| **Cumulative Proportion** | 9.69E-01 | 9.70E-01 | 9.71E-01 | 9.72E-01 | 9.73E-01 | 9.74E-01 | 9.75E-01 | 9.76E-01 |
| | **Comp49** | **Comp50** | **Comp51** | **Comp52** | **Comp53** | **Comp54** | **Comp55** | **Comp56** |
| **Eigenvalues** | 1.29E-05 | 1.22E-05 | 1.17E-05 | 1.13E-05 | 1.10E-05 | 1.08E-05 | 9.80E-06 | 9.62E-06 |
| **Proportion of Variance** | 9.11E-04 | 8.61E-04 | 0.000825 | 7.93E-04 | 7.76E-04 | 0.000758 | 6.90E-04 | 6.77E-04 |
| **Cumulative Proportion** | 9.77E-01 | 9.78E-01 | 0.978838 | 9.80E-01 | 9.80E-01 | 0.981164 | 9.82E-01 | 9.83E-01 |
| | **Comp57** | **Comp58** | **Comp59** | **Comp60** | **Comp61** | **Comp62** | **Comp63** | **Comp64** |
| **Eigenvalues** | 9.29E-06 | 8.83E-06 | 8.82E-06 | 8.28E-06 | 7.98E-06 | 7.50E-06 | 7.25E-06 | 7.20E-06 |
| **Proportion of Variance** | 6.54E-04 | 6.22E-04 | 6.21E-04 | 5.83E-04 | 5.62E-04 | 5.28E-04 | 5.11E-04 | 5.07E-04 |
| **Cumulative Proportion** | 9.83E-01 | 9.84E-01 | 9.84E-01 | 9.85E-01 | 9.86E-01 | 9.86E-01 | 9.87E-01 | 9.87E-01 |
| | **Comp65** | **Comp66** | **Comp67** | **Comp68** | **Comp69** | **Comp70** | **Comp71** | **Comp72** |
| **Eigenvalues** | 6.68E-06 | 6.52E-06 | 6.34E-06 | 5.90E-06 | 5.71E-06 | 5.61E-06 | 5.43E-06 | 5.28E-06 |
| **Proportion of Variance** | 4.70E-04 | 4.59E-04 | 4.46E-04 | 4.16E-04 | 4.02E-04 | 3.95E-04 | 3.82E-04 | 3.71E-04 |
| **Cumulative Proportion** | 9.88E-01 | 9.88E-01 | 9.88E-01 | 9.89E-01 | 9.89E-01 | 9.90E-01 | 9.90E-01 | 9.90E-01 |
| | **Comp73** | **Comp74** | **Comp75** | **Comp76** | **Comp77** | **Comp78** | **Comp79** | **Comp80** |
| **Eigenvalues** | 5.03E-06 | 4.95E-06 | 4.81E-06 | 4.73E-06 | 4.46E-06 | 4.29E-06 | 4.21E-06 | 4.10E-06 |
| **Proportion of Variance** | 3.54E-04 | 3.49E-04 | 3.39E-04 | 3.33E-04 | 3.14E-04 | 3.02E-04 | 2.97E-04 | 2.89E-04 |
| **Cumulative Proportion** | 9.91E-01 | 9.91E-01 | 9.92E-01 | 9.92E-01 | 9.92E-01 | 9.92E-01 | 9.93E-01 | 9.93E-01 |
| | **Comp81** | **Comp82** | **Comp83** | **Comp84** | **Comp85** | **Comp86** | **Comp87** | **Comp88** |
| **Eigenvalues** | 3.99E-06 | 3.88E-06 | 3.54E-06 | 3.48E-06 | 3.34E-06 | 3.12E-06 | 3.07E-06 | 2.95E-06 |
| **Proportion of Variance** | 2.81E-04 | 2.73E-04 | 2.49E-04 | 2.45E-04 | 2.35E-04 | 2.20E-04 | 2.16E-04 | 2.08E-04 |
| **Cumulative Proportion** | 9.93E-01 | 9.94E-01 | 9.94E-01 | 9.94E-01 | 9.94E-01 | 9.95E-01 | 9.95E-01 | 9.95E-01 |
| | **Comp89** | **Comp90** | **Comp91** | **Comp92** | **Comp93** | **Comp94** | **Comp95** | **Comp96** |
| **Eigenvalues** | 2.89E-06 | 2.78E-06 | 2.64E-06 | 2.60E-06 | 2.57E-06 | 2.47E-06 | 2.38E-06 | 2.33E-06 |
| **Proportion of Variance** | 2.03E-04 | 1.96E-04 | 1.86E-04 | 1.83E-04 | 1.81E-04 | 1.74E-04 | 1.68E-04 | 1.64E-04 |
| **Cumulative Proportion** | 9.95E-01 | 9.95E-01 | 9.96E-01 | 9.96E-01 | 9.96E-01 | 9.96E-01 | 9.96E-01 | 9.96E-01 |
| | **Comp97** | **Comp98** | **Comp99** | **Comp100** | **Comp101** | **Comp102** | **Comp103** | **Comp104** |
| **Eigenvalues** | 2.23E-06 | 2.19E-06 | 2.15E-06 | 2.02E-06 | 1.93E-06 | 1.87E-06 | 1.82E-06 | 1.80E-06 |
| **Proportion of Variance** | 1.57E-04 | 1.54E-04 | 1.52E-04 | 1.43E-04 | 1.36E-04 | 1.32E-04 | 1.28E-04 | 1.27E-04 |
| **Cumulative Proportion** | 9.97E-01 | 9.97E-01 | 9.97E-01 | 9.97E-01 | 9.97E-01 | 9.97E-01 | 9.97E-01 | 9.98E-01 |
| | **Comp105** | **Comp106** | **Comp107** | **Comp108** | **Comp109** | **Comp110** | **Comp111** | **Comp112** |
| **Eigenvalues** | 1.72E-06 | 1.62E-06 | 1.55E-06 | 1.49E-06 | 1.44E-06 | 1.33E-06 | 1.26E-06 | 1.21E-06 |
| **Proportion of Variance** | 0.000121 | 1.14E-04 | 1.09E-04 | 1.05E-04 | 1.02E-04 | 9.38E-05 | 8.88E-05 | 8.53E-05 |
| **Cumulative Proportion** | 0.997668 | 9.98E-01 | 9.98E-01 | 9.98E-01 | 9.98E-01 | 9.98E-01 | 9.98E-01 | 9.98E-01 |
| | **Comp113** | **Comp114** | **Comp115** | **Comp116** | **Comp117** | **Comp118** | **Comp119** | **Comp120** |
| **Eigenvalues** | 1.19E-06 | 1.15E-06 | 1.08E-06 | 1.04E-06 | 1.02E-06 | 9.66E-07 | 9.38E-07 | 9.21E-07 |

| | | | | | | | | |
|---|---|---|---|---|---|---|---|---|
| Proportion of Variance | 8.36E-05 | 8.08E-05 | 7.57E-05 | 7.30E-05 | 7.15E-05 | 6.80E-05 | 6.60E-05 | 6.49E-05 |
| Cumulative Proportion | 9.98E-01 | 9.99E-01 | 9.99E-01 | 9.99E-01 | 9.99E-01 | 9.99E-01 | 9.99E-01 | 9.99E-01 |
| | **Comp121** | **Comp122** | **Comp123** | **Comp124** | **Comp125** | **Comp126** | **Comp127** | **Comp128** |
| Eigenvalues | 9.06E-07 | 8.49E-07 | 7.86E-07 | 7.52E-07 | 7.35E-07 | 6.92E-07 | 6.51E-07 | 6.25E-07 |
| Proportion of Variance | 6.38E-05 | 5.98E-05 | 5.54E-05 | 5.29E-05 | 5.17E-05 | 4.87E-05 | 4.58E-05 | 4.40E-05 |
| Cumulative Proportion | 9.99E-01 | 9.99E-01 | 9.99E-01 | 9.99E-01 | 9.99E-01 | 9.99E-01 | 9.99E-01 | 9.99E-01 |
| | **Comp129** | **Comp130** | **Comp131** | **Comp132** | **Comp133** | **Comp134** | **Comp135** | **Comp136** |
| Eigenvalues | 6.00E-07 | 5.39E-07 | 5.23E-07 | 5.09E-07 | 4.91E-07 | 4.83E-07 | 4.53E-07 | 4.17E-07 |
| Proportion of Variance | 4.22E-05 | 3.80E-05 | 3.68E-05 | 3.58E-05 | 3.46E-05 | 3.40E-05 | 3.19E-05 | 2.94E-05 |
| Cumulative Proportion | 9.99E-01 | 9.99E-01 | 9.99E-01 | 1.00E+00 | 1.00E+00 | 1.00E+00 | 1.00E+00 | 1.00E+00 |
| | **Comp137** | **Comp138** | **Comp139** | **Comp140** | **Comp141** | **Comp142** | **Comp143** | **Comp144** |
| Eigenvalues | 3.92E-07 | 3.65E-07 | 3.55E-07 | 3.27E-07 | 3.21E-07 | 3.06E-07 | 3.00E-07 | 2.83E-07 |
| Proportion of Variance | 2.76E-05 | 2.57E-05 | 2.50E-05 | 2.30E-05 | 2.26E-05 | 2.15E-05 | 2.11E-05 | 1.99E-05 |
| Cumulative Proportion | 1.00E+00 | 1.00E+00 | 1.00E+00 | 1.00E+00 | 1.00E+00 | 1.00E+00 | 1.00E+00 | 1.00E+00 |
| | **Comp145** | **Comp146** | **Comp147** | **Comp148** | **Comp149** | **Comp150** | **Comp151** | **Comp152** |
| Eigenvalues | 2.75E-07 | 2.54E-07 | 2.26E-07 | 2.21E-07 | 1.99E-07 | 1.89E-07 | 1.78E-07 | 1.65E-07 |
| Proportion of Variance | 1.94E-05 | 1.79E-05 | 1.59E-05 | 1.56E-05 | 1.40E-05 | 1.33E-05 | 1.25E-05 | 1.16E-05 |
| Cumulative Proportion | 1.00E+00 | 1.00E+00 | 1.00E+00 | 1.00E+00 | 1.00E+00 | 1.00E+00 | 1.00E+00 | 1.00E+00 |
| | **Comp153** | **Comp154** | **Comp155** | **Comp156** | **Comp157** | | | |
| Eigenvalues | 1.54E-07 | 1.41E-07 | 1.37E-07 | 1.23E-07 | 3.13E-33 | | | |
| Proportion of Variance | 1.08E-05 | 9.91E-06 | 9.65E-06 | 8.67E-06 | 2.20E-31 | | | |
| Cumulative Proportion | 0.999972 | 1.00E+00 | 1.00E+00 | 1.00E+00 | 1.00E+00 | | | |

**Table S3.10.** Marginal likelihood results for each of the models run in Bayes Traits. BayesTraits: BayesTraitsV3 (http://www.evolution.rdg.ac.uk/). Lambda with variable rates had the highest marginal likelihood and the best model fit for the data. Results were obtained from BTprocessR (Ferguson-Gow, 2020).

| Model | Marginal Likelihood |
|---|---|
| Lambda_var | -32831 |
| Kappa_var | -32961 |
| BM_var | -33220 |
| OU_var | -33221 |
| Delta_var | -33238 |
| Lambda | -34843 |
| Delta | -36609 |
| Kappa | -38113 |
| BM | -42830 |
| OU | -42844 |

| | BM | BM_var | Delta | Delta_var | Kappa | Kappa_var | Lambda | Lambda_var | OU | OU_var |
|---|---|---|---|---|---|---|---|---|---|---|
| **BM** | | −19219.44 | −12442.98 | −19183.58 | −9433.94 | −19737.96 | −15973.72 | −19999.12 | 27.89 | −19219.22 |
| **BM_var** | 19219.44 | | 6776.46 | 35.86 | 9785.5 | −518.52 | 3245.72 | −779.68 | 19247.33 | 0.22 |
| **Delta** | 12442.98 | −6776.46 | | −6740.6 | 3009.04 | −7294.98 | −3530.74 | −7556.14 | 12470.87 | −6776.24 |
| **Delta_var** | 19183.58 | −35.86 | 6740.6 | | 9749.64 | −554.38 | 3209.86 | −815.54 | 19211.47 | −35.63 |
| **Kappa** | 9433.94 | −9785.5 | −3009.04 | −9749.64 | | −10304.02 | −6539.77 | −10565.18 | 9461.83 | −9785.27 |
| **Kappa_var** | 19737.96 | 518.52 | 7294.98 | 554.38 | 10304.02 | | 3764.25 | −261.16 | 19765.85 | 518.75 |
| **Lambda** | 15973.72 | −3245.72 | 3530.74 | −3209.86 | 6539.77 | −3764.25 | | −4025.4 | 16001.6 | −3245.5 |
| **Lambda_var** | 19999.12 | 779.68 | 7556.14 | 815.54 | 10565.18 | 261.16 | 4025.4 | | 20027.01 | 779.9 |
| **OU** | −27.89 | −19247.33 | −12470.87 | −19211.47 | −9461.83 | −19765.85 | −16001.6 | −20027.01 | | −19247.1 |
| **OU_var** | 19219.22 | −0.22 | 6776.24 | 35.63 | 9785.27 | −518.75 | 3245.5 | −779.9 | 19247.1 | |

Bayes factor
- <0
- 0–2
- 2–5
- 5–10
- >10
- NA

**Fig. S3.6.** Marginal likelihood results for each of the evolutionary modes models. Run in Bayes Traits using BayesTraitsV3 (http://www.evolution.rdg.ac.uk/). Lambda had the highest marginal likelihood and the best model fit for the data. Results were obtained from BTprocessR (Ferguson-Gow, 2020)

**Table S3.11.** Gelman-Rubin outputs – model convergence diagnostics. 'Point est.' is the points estimate, 'Upper C.I' is the upper confidence limit, 'multivariate psfr' is the point-estimate of the multivariate potential scale reduction factor. Generally, the closer the values, including the multivariate psrf, are to 1, the better the convergence of the chains. 8 chains were run and the combination of the two chains that had the best convergence were used in this study. The two chains are shown in the output here and in **Fig.S3.7**.

|  | Point est. | Upper C.I. |
|---|---|---|
| Lh | 1.01 | 1.07 |
| Lh...Prior | 1.03 | 1.11 |
| No.Pram | 1.04 | 1.18 |
| Alpha | 1.00 | 1.0 |
| Sigma.2 | 1.04 | 1.18 |
|  |  |  |
| Multivariate psrf |  | 1.20 |

[Figure on next page]

**Fig. S3.7.** Trace plots for checking parameter convergence for MCMC analyses. This example shows the final convergence of two chains run using the lambda model with variable rates, a burn-in of 20,000. The MCMC analyses were run 8 times with 200 million iterations. The outputs of the two runs (black and red lines) were compared visually to ensure both had converged on similar parameter values. 8 chains were run and the combination of the two chains that had the best convergence were used in this study. The two chains with the best convergence are shown here and inThe two chains with the best convergence are shown here and in **Table S3.11**.

Trace of Lh

Density of Lh

Trace of Lh...Prior

Density of Lh...Prior

Trace of No.Pram

Density of No.Pram

Trace of Alpha

Density of Alpha

Trace of Sigma.2

Density of Sigma.2
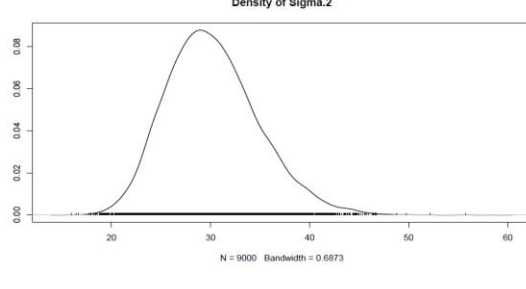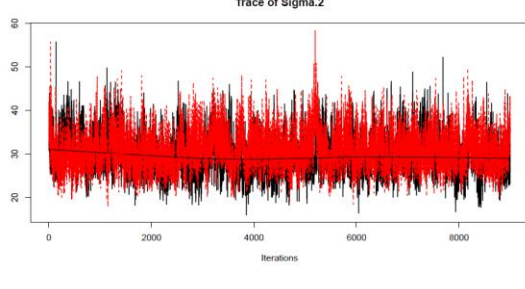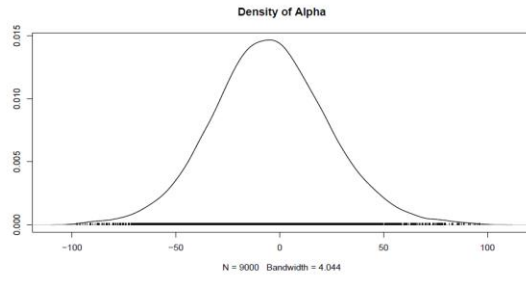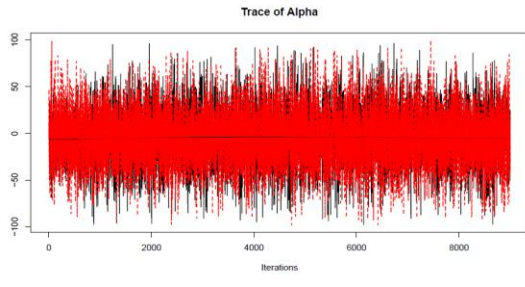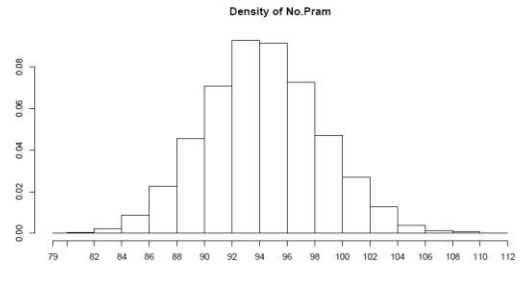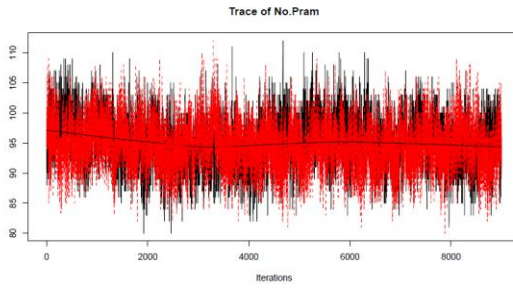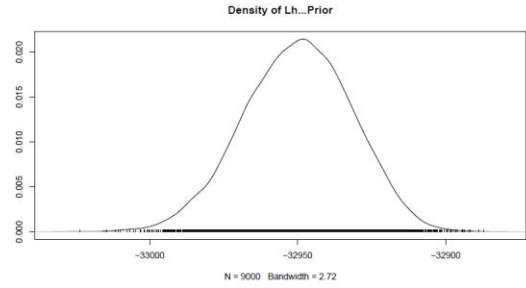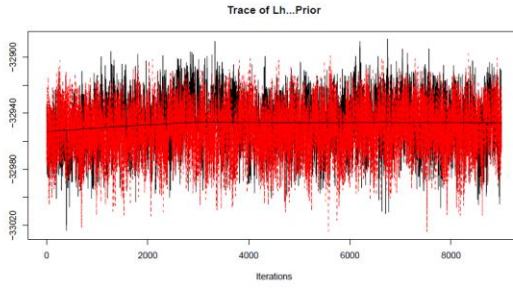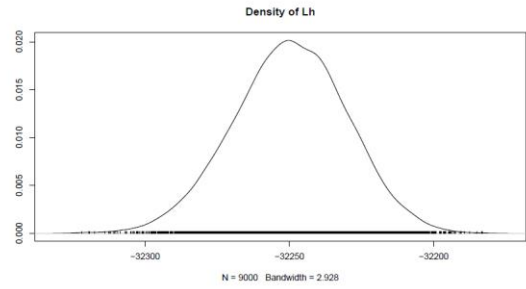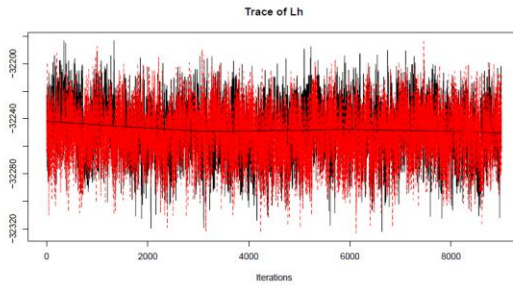
**Table S3.12.** Phylogenetic Principal Component (pPC) scores. These scores capture 95% of the variation for each bone in the cranium for the whole data set (all cetaceans), archaeocetes, mysticetes, and odontocetes. pPC scores were used in BayesTraits analyses (V3: http://www.evolution.rdg.ac.uk/) to model evolutionary rates through time.

| | All | Archaeocetes | Mysticetes | Odontocetes |
|---|---|---|---|---|
| Bone | pPC scores for 95% | pPC scores for 95% | pPC scores for 95% | pPC scores for 95% |
| **Whole skull** | **39** | **8** | **14** | **30** |
| Basioccipital | 7 | 6 | 6 | 7 |
| Basisphenoid | 4 | 5 | 6 | 4 |
| Frontal | 13 | 5 | 9 | 11 |
| Jugal | 5 | 4 | 5 | 5 |
| Mandibular process | 6 | 4 | 6 | 6 |
| Maxilla | 22 | 6 | 14 | 19 |
| Nasal | 5 | 4 | 3 | 5 |
| Occipital condyle | 7 | 4 | 4 | 6 |
| Palate | 9 | 5 | 8 | 8 |
| Parietal | 11 | 7 | 9 | 10 |
| Premaxilla | 14 | 5 | 9 | 13 |
| Pterygoid | 7 | 5 | 5 | 7 |
| Supraoccipital | 16 | 7 | 10 | 13 |
| Zygomatic (including squamosal) | 13 | 7 | 12 | 14 |
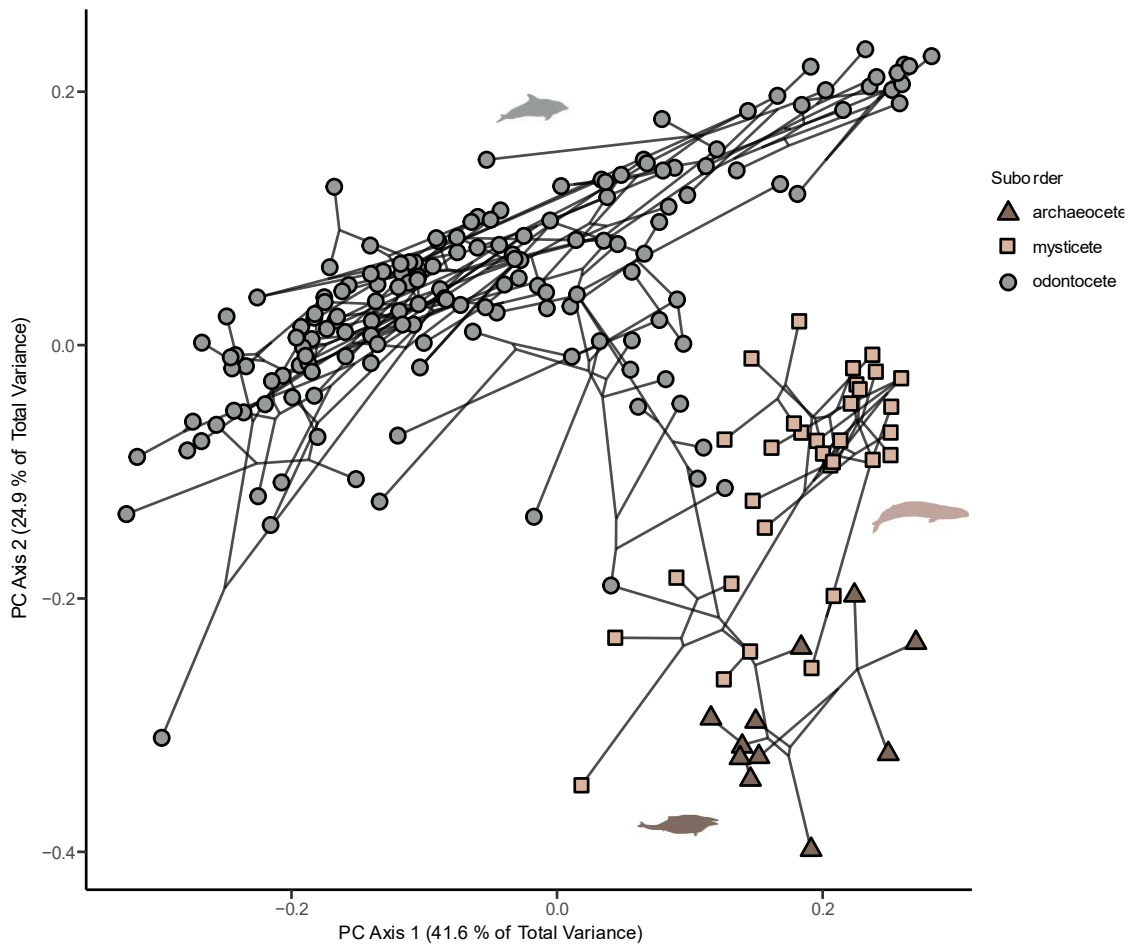
**Fig. S3.8.** Phylomorphospace of all 201 specimens using the entire landmark and curve semi-landmark data set. The black lines represent the phylogenetic relationships between the specimens. PC1 (41.6%) represents the elongation of the rostrum from left (brachycephalic) to right (dolichocephalic) and PC2 (24.9%) represents the positioning of the nares from bottom (anteriorly positioned) to top (posteriorly positioned).
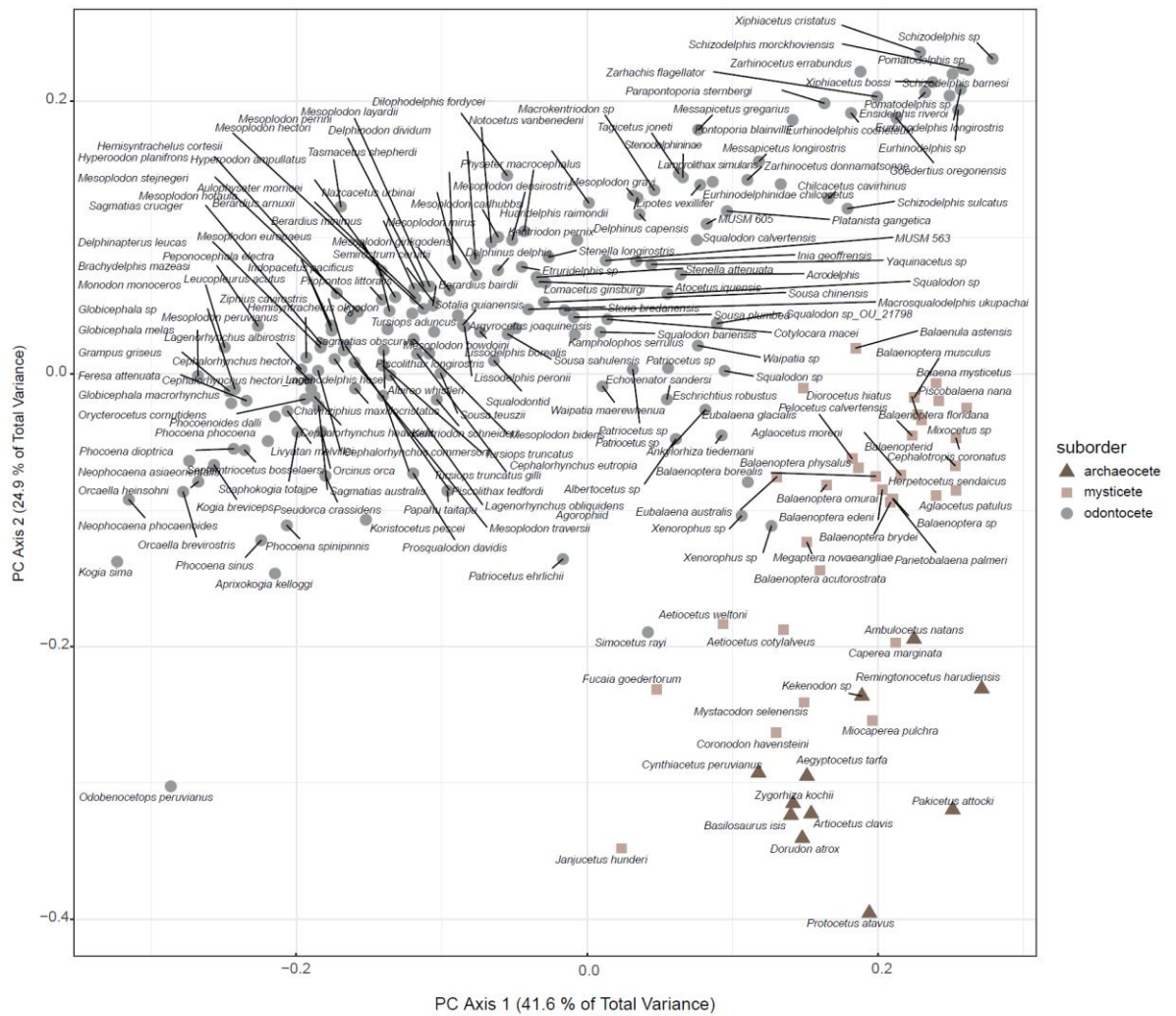
**Fig. S3.9.** Named morphospace of all 201 specimens. Shape captured using the entire landmark and curve semi-landmark data set. PC1 (41.6%) represents the elongation of the rostrum from left (brachycephalic) to right (dolichocephalic) and PC2 (24.9%) represents the positioning of the nares from bottom (anteriorly positioned) to top (posteriorly positioned). Due to the complexity and number of species in this morphospace the species names are added to the **approximate** location of the species
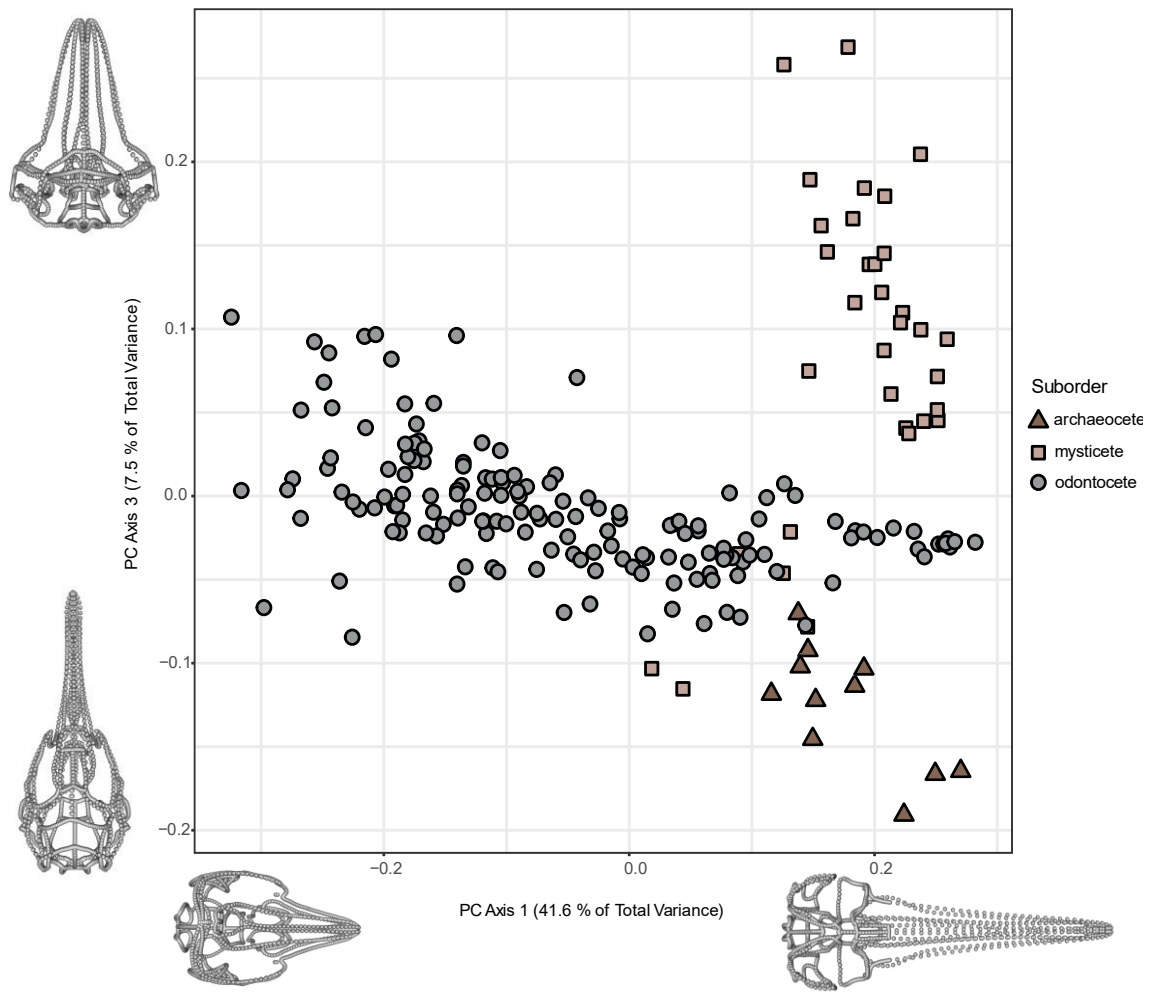
**Fig. S3.10.** PC1 and PC3 morphospace. Morphospace of all 201 specimens using the entire landmark and curve semi-landmark data set. Skull shapes represent the positive and negative extremes along PC1 (41.6%) and PC3 (7.5%). PC1 shows variation in the rostrum length (minimum = brachycephalic, maximum = dolichocephalic). PC3 shows variation in the width of the cranium (minimum = slim, maximum = broad).
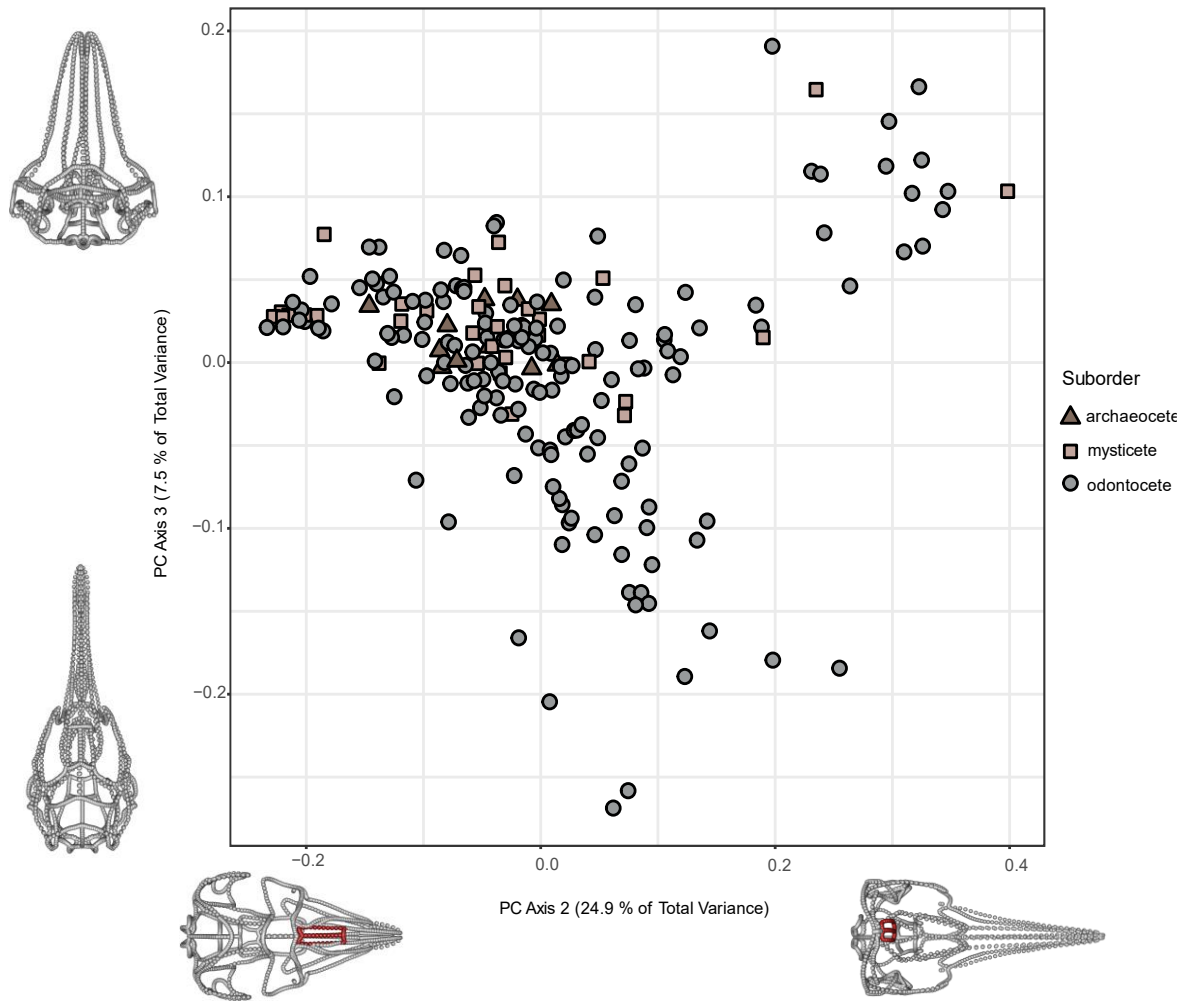
**Fig. S3.11.** PC2 and PC3 morphospace. Morphospace of all 201 specimens using the entire landmark and curve semi-landmark data set. Skull shapes represent the positive and negative extremes along PC2 (24.9%) and PC3 (7.5%). PC2 shows variation in the positioning of the nares (minimum = anteriorly, maximum= posteriorly). PC3 shows variation in the width of the cranium (minimum = slim, maximum = broad).
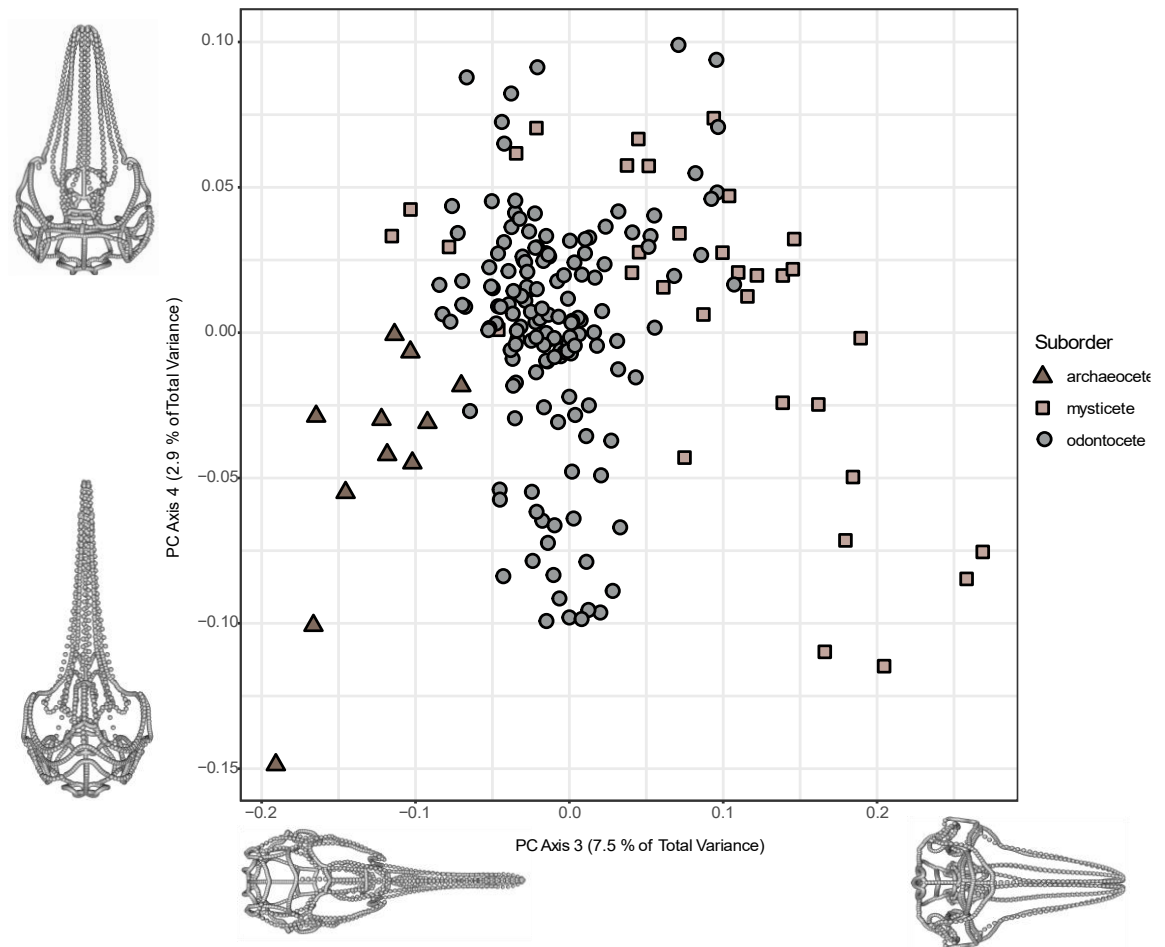
**Fig. S3.12.** PC3 and PC4 morphospace. Morphospace of all 201 specimens using the entire landmark and curve semi-landmark data set. Skull shapes represent the positive and negative extremes along PC3 (7.5%) and PC4 (2.9%). PC3 shows variation in the width of the cranium (minimum = slim, maximum = broad). PC4 shows variation in the width of the rostrum (minimum = slim, maximum = broad).

**Table. S3.13.** Specimen numbers in order of phylogeny. These numbers correspond to the numbers on specimens in Fig. S3.13-26 because each of the morphospaces were plotted using phylogenetic pPC scores which account for phylogeny, thus reordering the specimens.

| Number | Specimen | Number | Specimen | Number | Specimen | Number | Specimen | Number | Specimen | Number | Specimen | Number | Specimen |
|---|---|---|---|---|---|---|---|---|---|---|---|---|---|
| 1 | Livyatan melvillei | 31 | Berardius mimimus | 61 | Peponocephala electra | 91 | MUSM 605 | 121 | Eurhinodelphis chilcocetus | 151 | Aetiocetus weltoni | 181 | Mystacodon selenensis |
| 2 | Aprixokogia kelloggi | 32 | Chavinziphius maxillocristatu. | 62 | Globicephala sp | 92 | MUSM 563 | 122 | Xiphiacetus bossi | 152 | Janjucetus hunderi | 182 | Kekenodon sp |
| 3 | Kogia breviceps | 33 | Messapicetus gregarius | 63 | Globicephala macrorhynchus | 93 | Macrokentriodon sp | 123 | Xiphiacetus cristatus | 153 | Diorocetus hiatus | 183 | Zygorhiza kochii |
| 4 | Kogia simus | 34 | Messapicetus longirostris | 64 | Globicephala melas | 94 | Kampholophus serrulus | 124 | Yaquinacetus sp | 154 | Pelocetus calvertensis | 184 | Basilosaurus isis |
| 5 | Koristocetus pescei | 35 | Albireo whistleri | 65 | Grampus griseus | 95 | Brachydelphis mazeazi | 125 | Chilcacetus cavirhinus | 155 | Aglaocetus patulus | 185 | Dorudon atrox |
| 6 | Scaphokogia totajpe | 36 | Semirostrum cerutti | 66 | Pseudorca crassidens | 96 | Pliopontos littoralis | 126 | Argyrocetus joaquinensis | 156 | Parietobalaena palmeri | 186 | Cynthiacetus peruvianus |
| 7 | Aulophyseter morricei | 37 | Septemtriocetus bosselaersi | 67 | Orcaella brevirostris | 97 | Inia geoffrensis | 127 | Squalodon bariensis | 157 | Aglaocetus moreni | 187 | Protocetus atavus |
| 8 | Physeter macrocephalus | 38 | Lomacetus ginsburgi | 68 | Steno bredanensis | 98 | Pontoporia blainvillei | 128 | Squalodon calvertensis | 158 | Balaenoptera borealis | 188 | Aegytocetus tarfa |
| 9 | Orycterocetus crocodilinus | 39 | Neophocoena phocaenoides | 69 | Cephalorhynchus commerson. | 99 | Lipotes vexillifer | 129 | Squalodon sp | 159 | Balaenoptera floridana | 189 | Artiocetus clavis |
| 10 | Hyperoodon ampullatus | 40 | Phocoena dioptrica | 70 | Cephalorhynchus eutropia | 100 | Parapontoporia sternbergi | 130 | Squalodon sp | 160 | Balaenoptera brydei | 190 | Remingtonocetus harudiensis |
| 11 | Hyperoodon planifrons | 41 | Phocoena sinus | 71 | Cephalorhynchus hectori | 101 | Stenodelphin sp | 131 | Squalodon sp | 161 | Balaenoptera edeni | 191 | Ambulocetus natans |
| 12 | Indopacetus pacificus | 42 | Phocoena phocoena | 72 | Cephalorhynchus heavisidii | 102 | Dilophodelphis fordycei | 132 | Waipatiid sp2 | 162 | Balaenoptera omurai | 192 | Pakicetus attocki |
| 13 | Mesoplodon carlhubbsi | 43 | Phocoenoides dalli | 73 | Lagenorhynchus australis | 103 | Platanista gangetica | 133 | Prosqualodon davidis | 163 | Balaenoptera musculus | 193 | Neophocoena asiaeorientalis |
| 14 | Mesoplodon bidens | 44 | Phocoena spinipinnis | 74 | Lagenorhynchus cruciger | 104 | Pomatodelphis sp2 | 134 | Waipatiid sp | 164 | Eschrichtius robustus | 194 | Orcaella heinsohni |
| 15 | Mesoplodon mirus | 45 | Piscolithax longirostris | 75 | Lagenorhynchus obliquidens | 105 | Pomatodelphis sp | 135 | Waipatia maerwhenua | 165 | Balaenoptera physalus | 195 | Tursiops truncatus gilli |
| 16 | Mesoplodon bowdoini | 46 | Piscolithax tedfordi | 76 | Lagenorhynchus obscurus | 106 | Zarhachis flagellator | 136 | Papahu taitapu | 166 | Balaenoptera sp | 196 | Berardius bairdii |
| 17 | Mesoplodon europaeus | 47 | Delphinapterus leucas | 77 | Lissodelphis borealis | 107 | Huaridelphis raimondii | 137 | Patriocetid new genus | 167 | Megaptera novaeangliae | 197 | Cephalorhynchus hectori maui |
| 18 | Mesoplodon ginkgodens | 48 | Monodon monoceros | 78 | Lissodelphis peronii | 108 | Notocetus vanbenedeni | 138 | Patriocetus ehrlichii | 168 | Balaenoptera acutorostrata | 198 | Mesoplodon hotaula |
| 19 | Mesoplodon traversii juv. | 49 | Odobenocetops peruvianus | 79 | Lagenorhynchus albirostris | 109 | Macrosqualodelphis ukupachai | 139 | Patriocetid or Waipatiid new genus | 169 | Balaenoptera sp2 | 199 | Sousa plumbea |
| 20 | Mesoplodon densirostris | 50 | Delphinus capensis | 80 | Lagenorhynchus acutus | 110 | Goedertius oregonensis | 140 | Patriocetus sp | 170 | Mixocetus sp | 200 | Sousa teuszii |
| 21 | Mesoplodon grayi | 51 | Delphinus delphis | 81 | Hemisyntrachelus cortesii | 111 | Ensidelphis riveroi | 141 | Ankylorhiza tiedemani | 171 | Herpetocetus sendaicus | 201 | Sousa sahulensis |
| 22 | Mesoplodon perrini | 52 | Tursiops aduncus | 82 | Hemisyntrachelus oligodon | 112 | Zarhinocetus donnamatsonae | 142 | Agorophiid sp | 172 | Piscobalaena nana | | |
| 23 | Mesoplodon peruvianus | 53 | Tursiops truncatus | 83 | Orcinus orca | 113 | Zarhinocetus errabundus | 143 | Simocetus rayi | 173 | Caperea marginata | | |
| 24 | Mesoplodon stejnegeri | 54 | Etruridelphis sp | 84 | Tagicetus joneti | 114 | Eurhinodelphis cocheteuxi | 144 | Cotylocara macei | 174 | Miocaperea pulchra | | |
| 25 | Mesoplodon layardii | 55 | Lagenodelphis hosei | 85 | Atocetus iquensis | 115 | Eurhinodelphis longirostris | 145 | Echovenator sandersi | 175 | Cephalotropis coronatus | | |
| 26 | Mesoplodon hectori | 56 | Stenella attenuata | 86 | Delphinodon dividum | 116 | Schizodelphis barnesi | 146 | Albertocetus sp | 176 | Balaena mysticetus | | |
| 27 | Ziphius cavirostris | 57 | Stenella longirostris | 87 | Lamprolithax simulans | 117 | Xenorophiid sp | 147 | Xenorophiid sp2 | 177 | Balaenula astensis | | |
| 28 | Nazcacetus urbinai | 58 | Sousa chinensis | 88 | Kentriodon pernix | 118 | Schizodelphis sp | 148 | Xenorophiid sp | 178 | Eubalaena australis | | |
| 29 | Tasmacetus shepherdi | 59 | Sotalia guianensis | 89 | Kentriodon sp | 119 | Schizodelphis morckhoviensis | 149 | Chonecetus goedertorum | 179 | Eubalaena glacialis | | |
| 30 | Berardius arnuxii | 60 | Feresa attenuata | 90 | Kentriodon schneideri | 120 | Schizodelphis sulcatus | 150 | Aetiocetus cotylalveus | 180 | Coronodon havensteini | | |

**Figs. S3.13 - S.26.** Morphospace and extreme shapes of each bone.

BASIOCCIPITAL
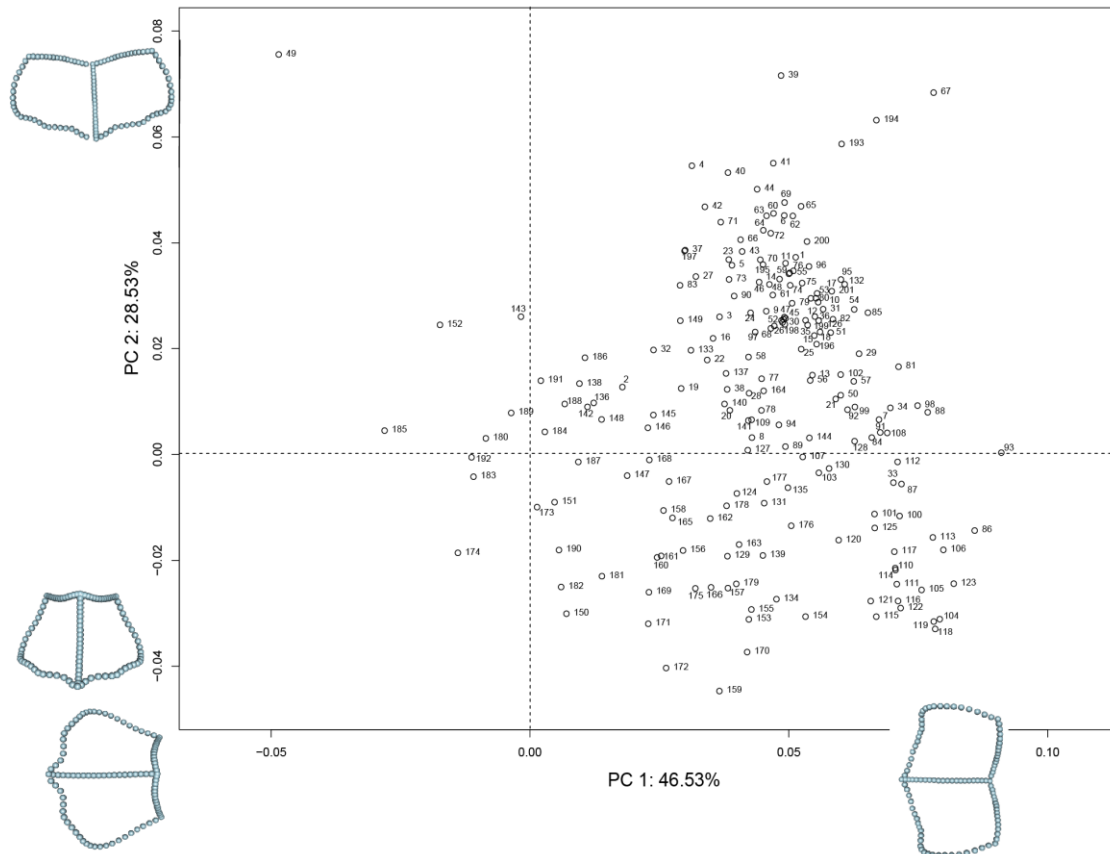


**Fig. S3.13.** Morphospace of the basioccipital for all specimens. The morphospace was generated from a PCA of the individual bone, so axes may not align with those of the entire data set. Positive and negative shape extremes for PC1 and PC2 are displayed in ventral view. A list of specimen names (attributed to the numbers in the plot) are given in **Table S3.13**.
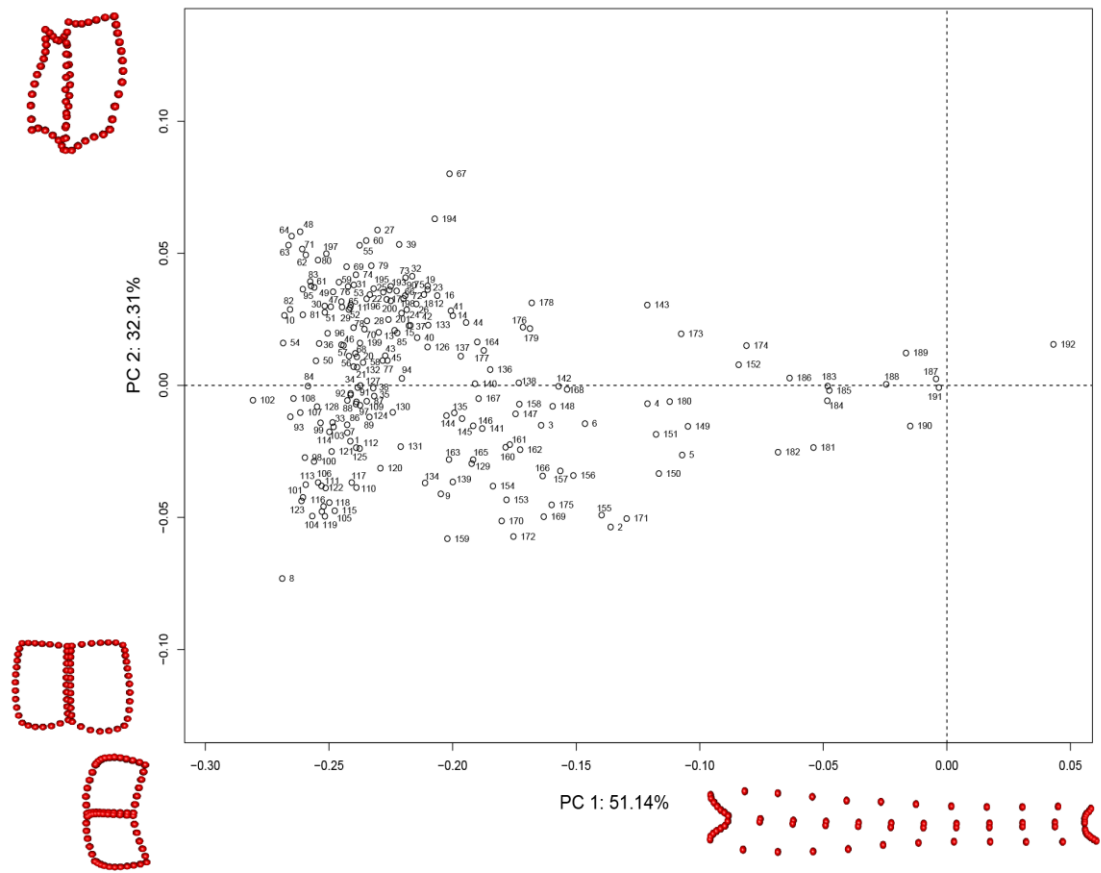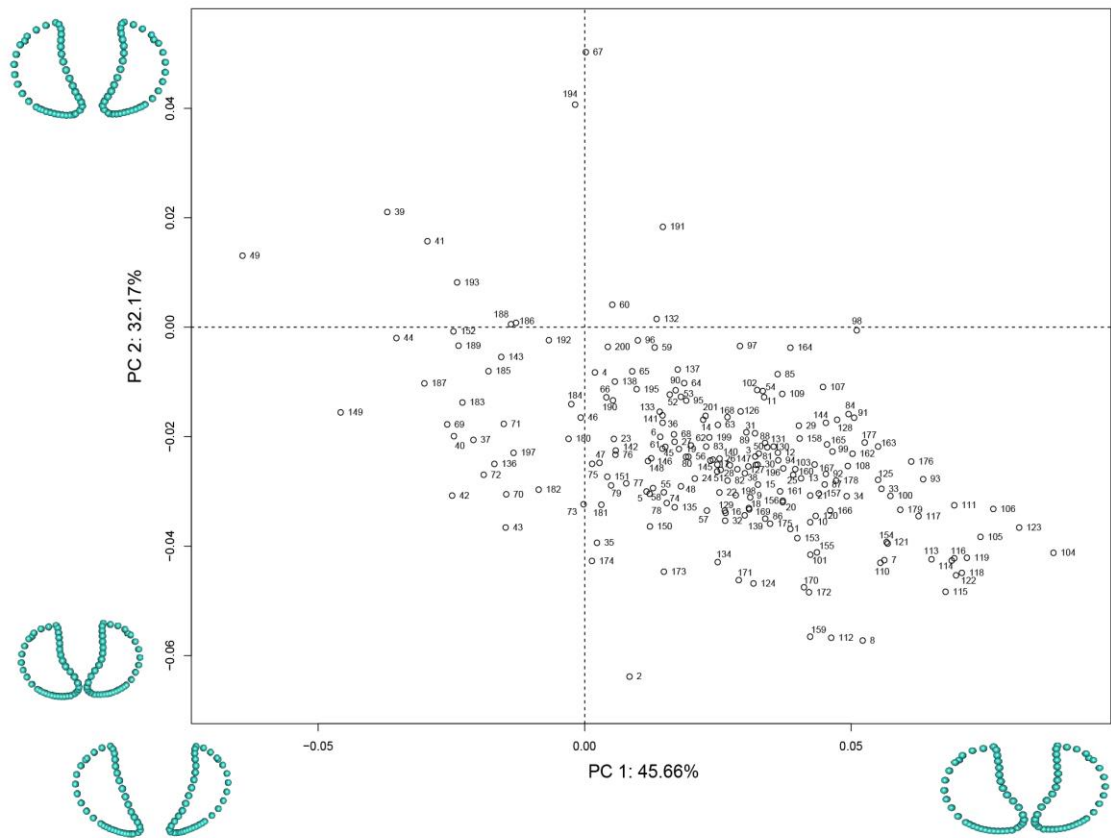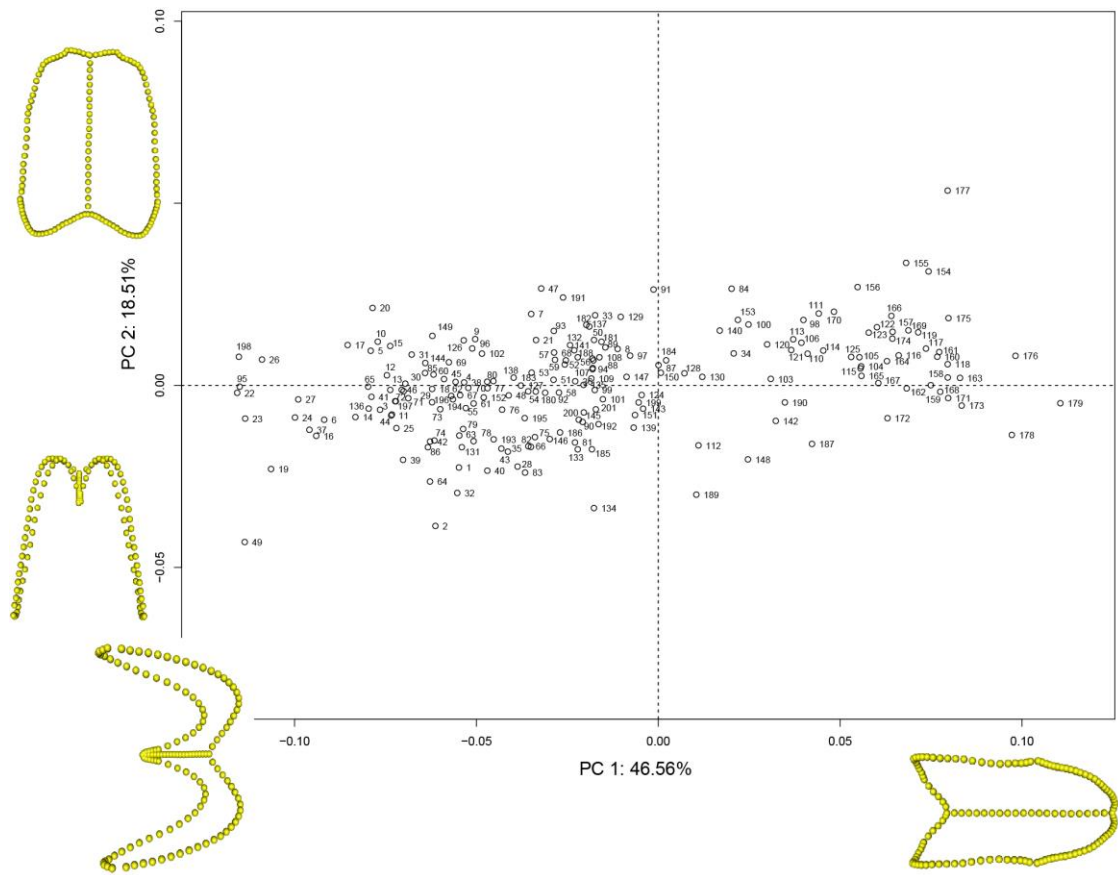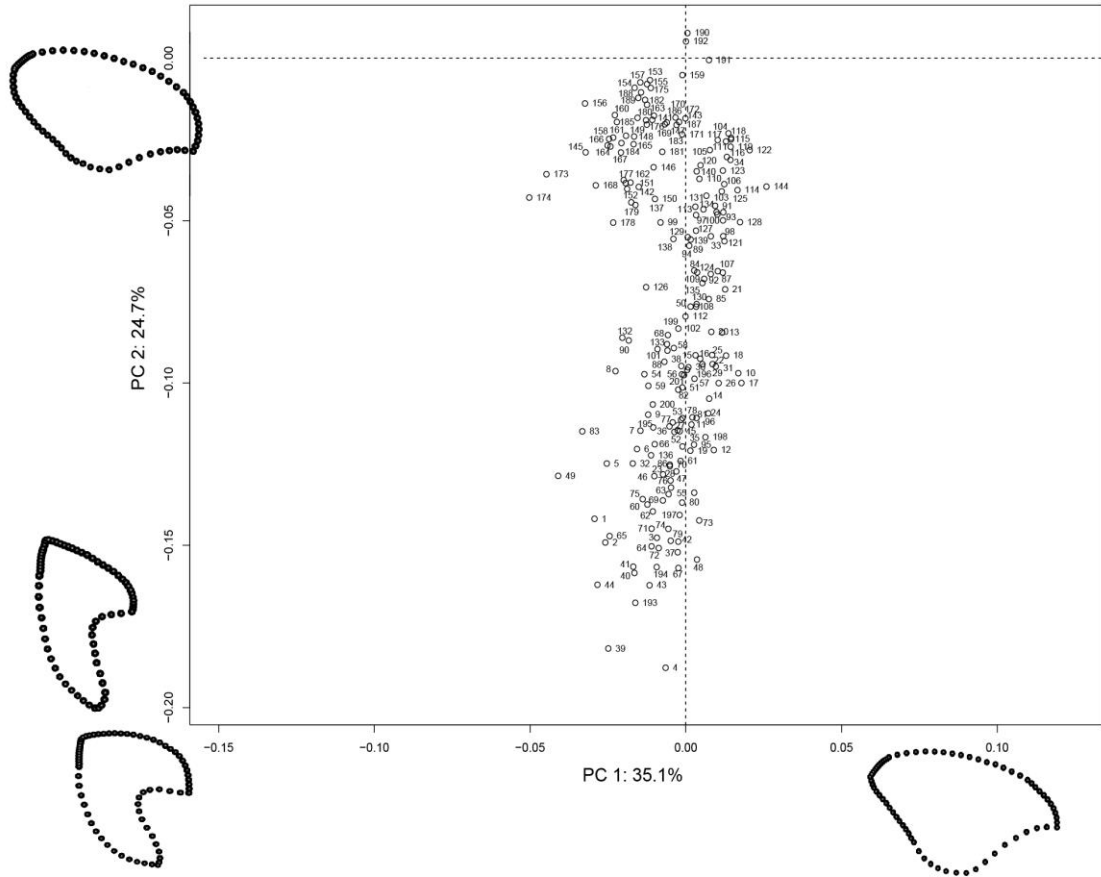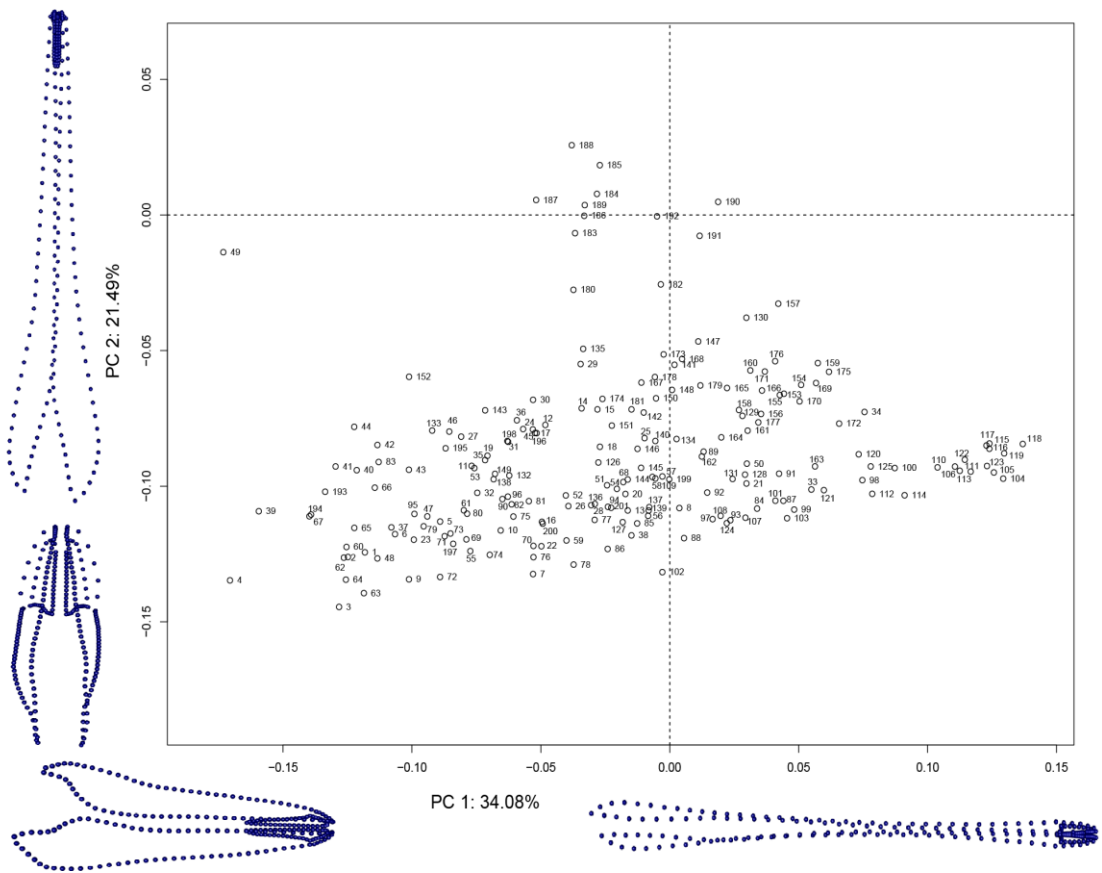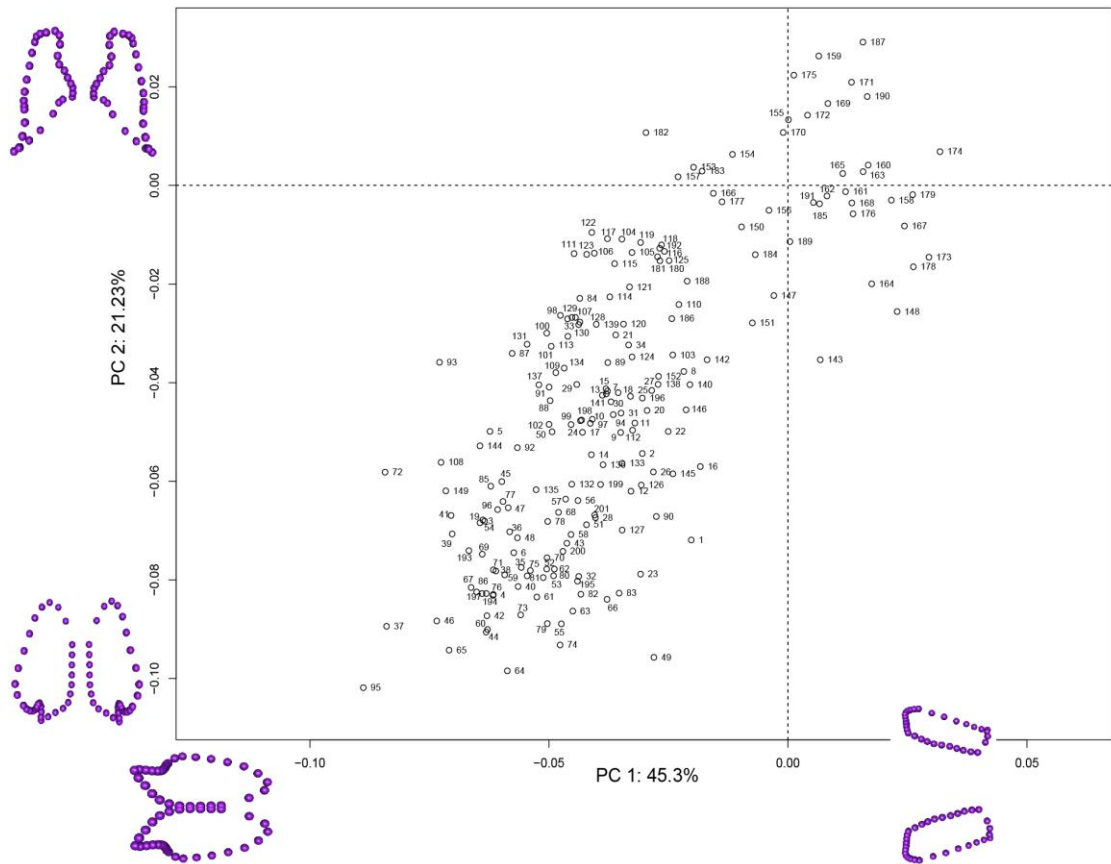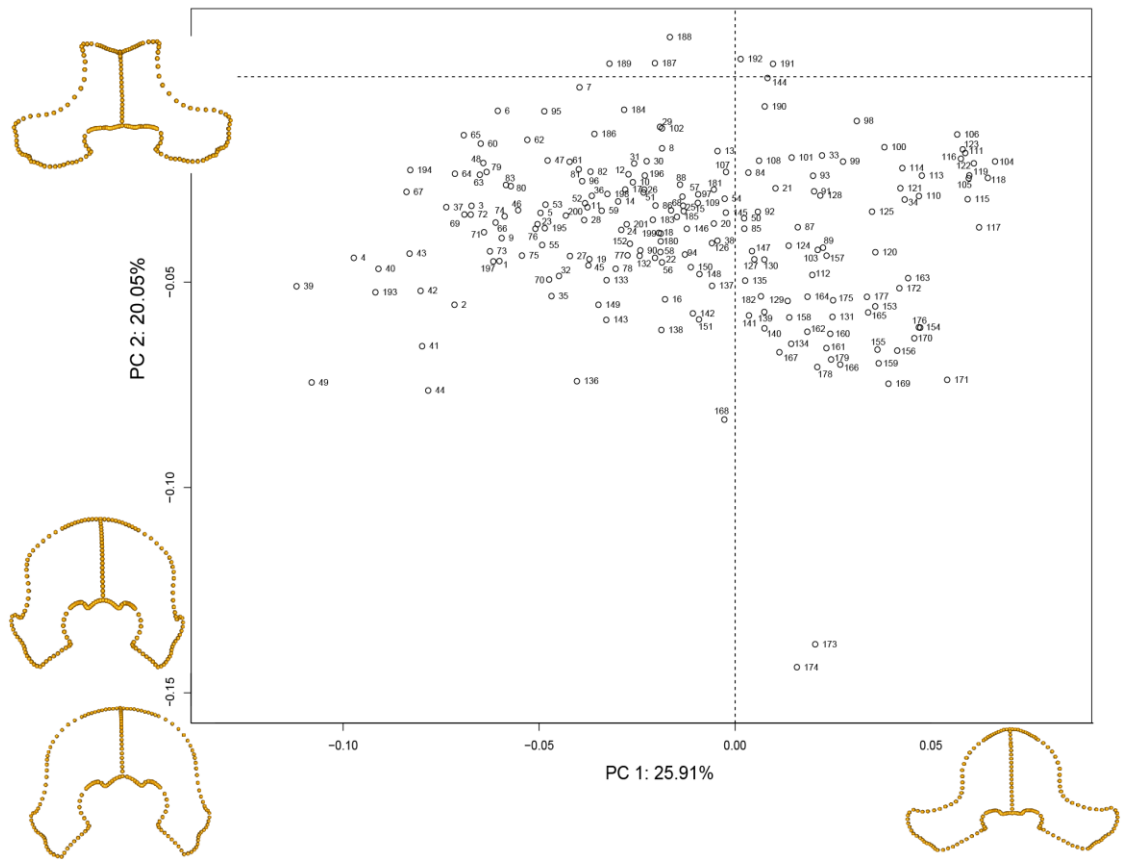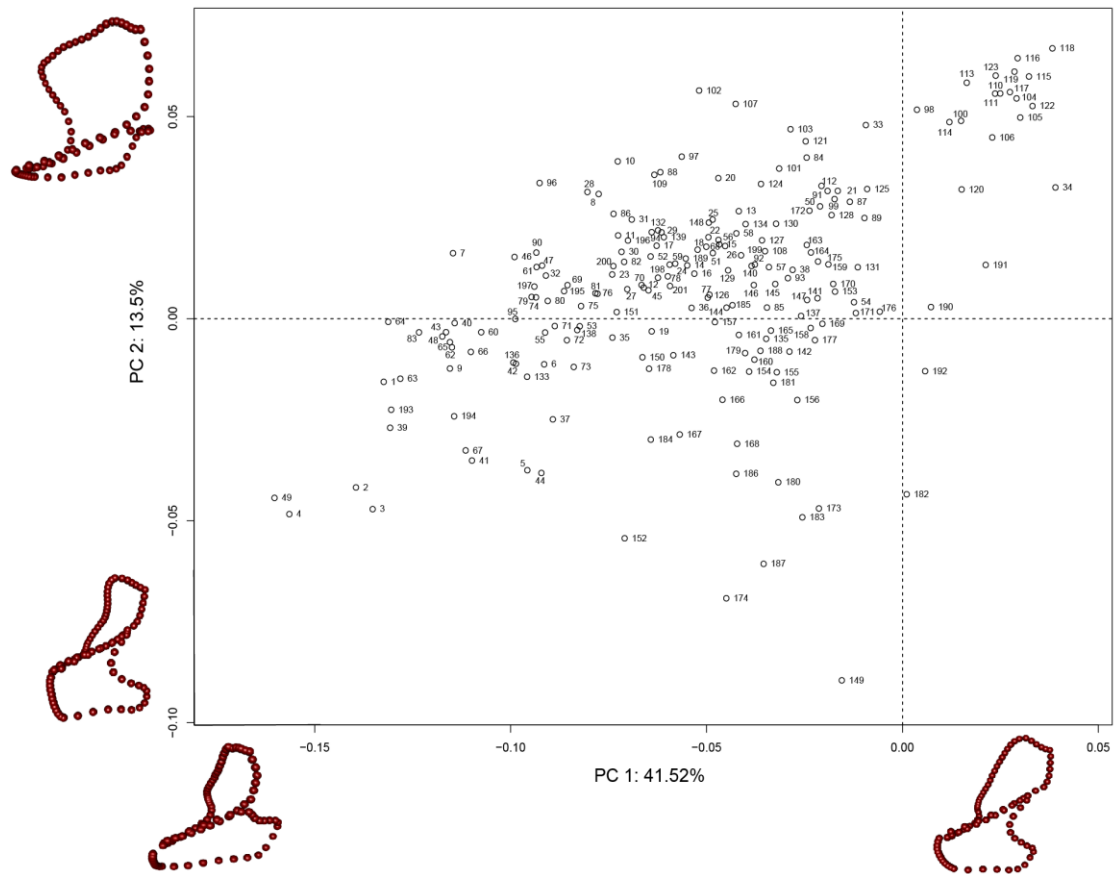
BASISPHENOID
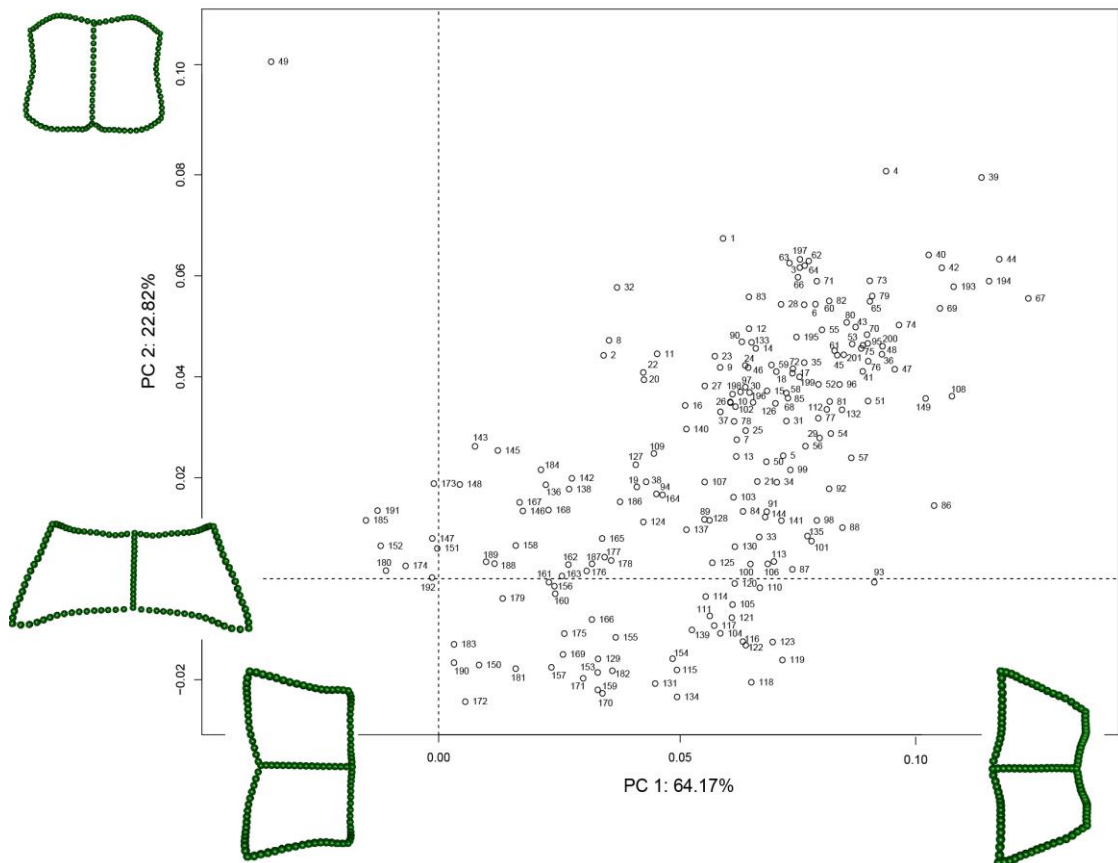


**Fig. S3.14.** Morphospace of the basisphenoid for all specimens. The morphospace was generated from a PCA of the individual bones, so axes may not align with those of the entire data set. Positive and negative shape extremes for PC1 and PC2 are displayed in ventral view. A list of specimen names (attributed to the numbers in the plot) are given in **Table S3.13**.
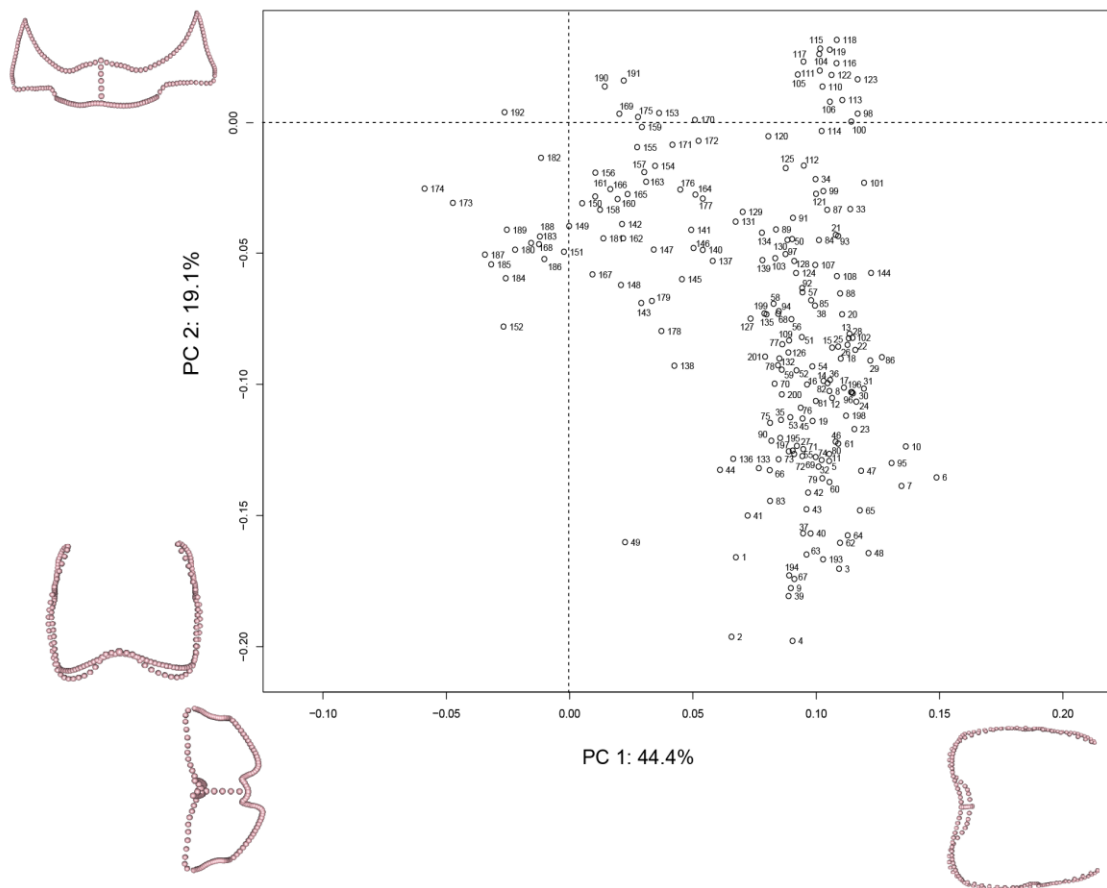
**Fig. S3.15**. Morphospace of the frontal for all specimens. The morphospace was generated from a PCA of the individual bone, so axes may not align with those of the entire data set. Positive and negative shape extremes for PC1 and PC2 are displayed in dorsal view. A list of specimen names (attributed to the numbers in the plot) are given in **Table S3.13**.
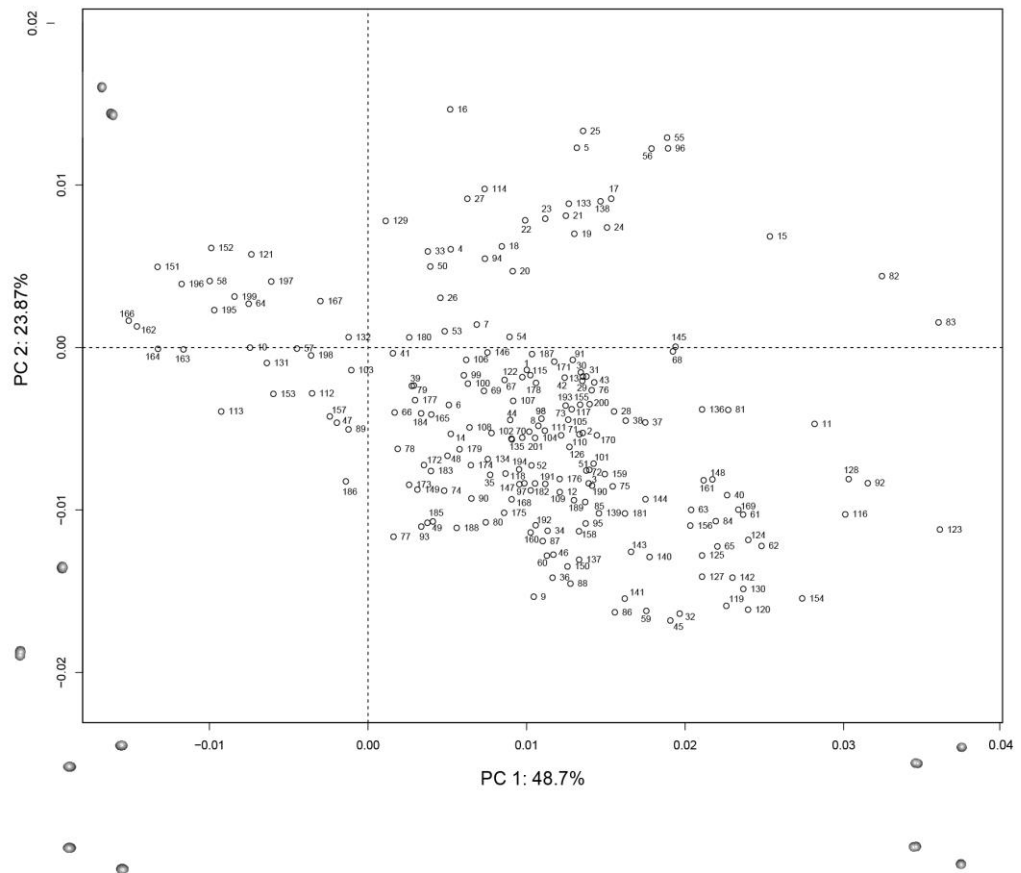
**Fig. S3.16**. Morphospace of the jugal for all specimens. The morphospace was generated from a PCA of the individual bone, so axes may not align with those of the entire data set. Positive and negative shape extremes for PC1 and PC2 are displayed in ventral view. A list of specimen names (attributed to the numbers in the plot) are given in **Table S3.13**. As the jugal was broken in most specimens, landmarks were placed at the anterior and posterior ends of the bone. No curves were added.
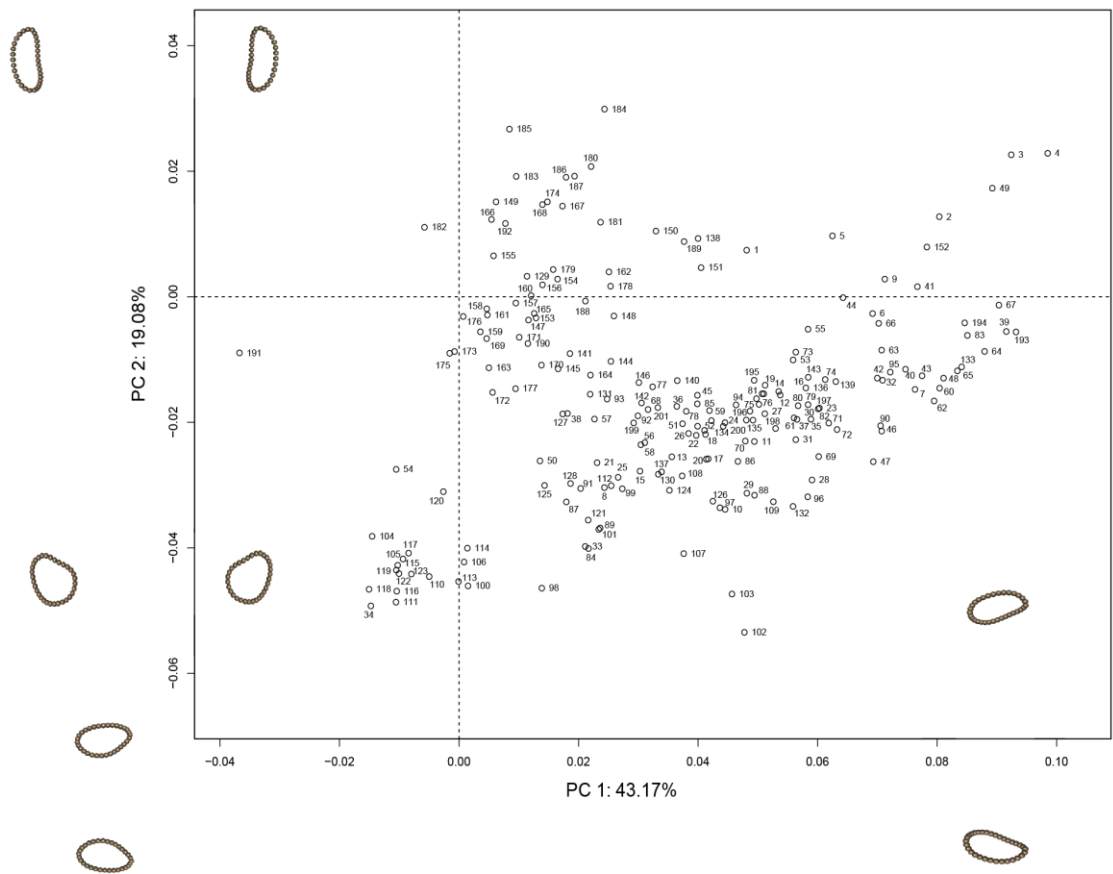
**Fig. S3.17.** Morphospace of the mandibular process for all specimens. The morphospace was generated from a PCA of the individual bone, so axes may not align with those of the entire data set. Positive and negative shape extremes for PC1 and PC2 are displayed in ventral view. A list of specimen names (attributed to the numbers in the plot) are given in **Table S3.13**.
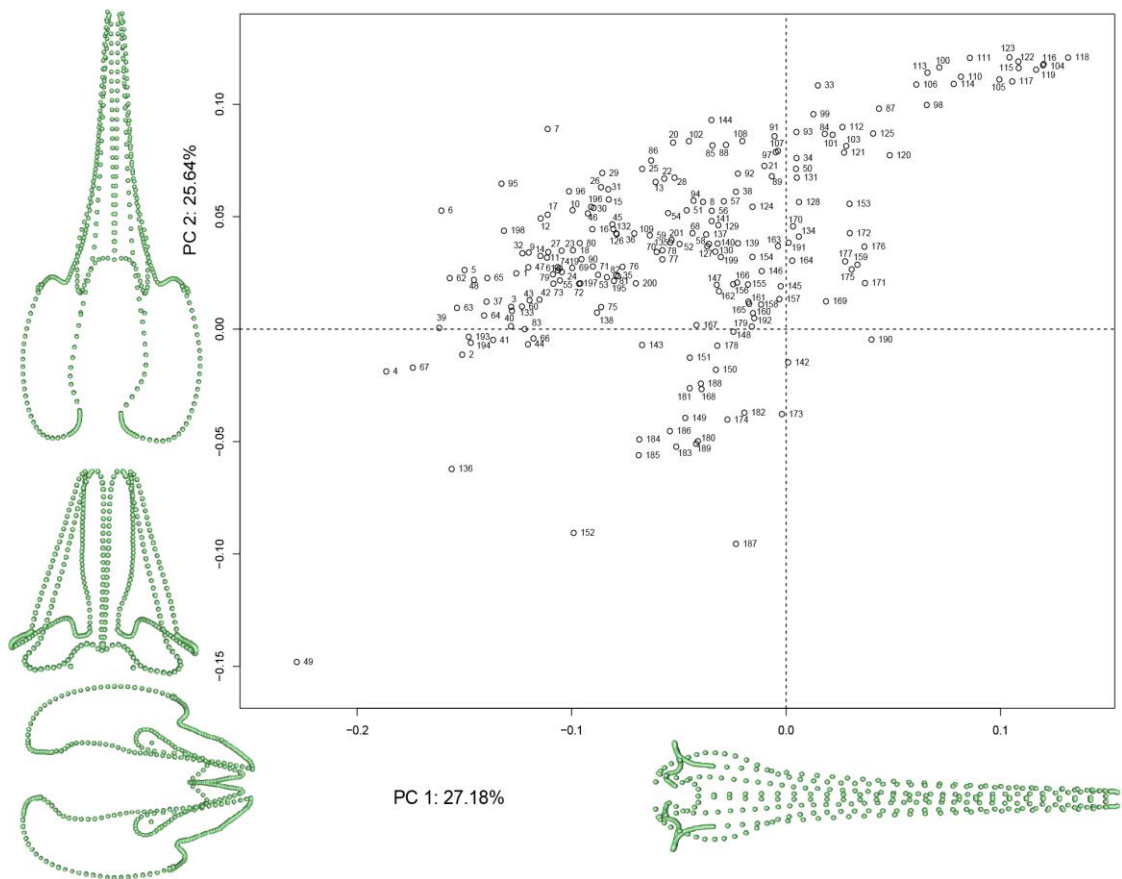
**Fig. S3.18**. Morphospace of the dorsal and ventral maxilla for all specimens. The morphospace was generated from a PCA of the individual bone, so axes may not align with those of the entire data set. Positive and negative shape extremes for PC1 and PC2 are displayed in dorsal view. A list of specimen names (attributed to the numbers in the plot) are given in **Table S3.13**.

**Fig. S3.19**. Morphospace of the nasals for all specimens. The morphospace was generated from a PCA of the individual bone, so axes may not align with those of the entire data set. Positive and negative shape extremes for PC1 and PC2 are displayed in dorsal view. A list of specimen names (attributed to the numbers in the plot) are given in **Table S3.13**.

**Fig. S3.20**. Morphospace of the occipital condyles for all specimens. The morphospace was generated from a PCA of the individual bones, so axes may not align with those of the entire data set. Positive and negative shape extremes for PC1 and PC2 are displayed in posterior view. A list of specimen names (attributed to the numbers in the plot) are given in **Table S3.13**.

**Fig. S3.21**. Morphospace of the palate for all specimens. The morphospace was generated from a PCA of the individual bones, so axes may not align with those of the entire data set. Positive and negative shape extremes for PC1 and PC2 are displayed in ventral view. A list of specimen names (attributed to the numbers in the plot) are given in **Table S3.13**.

**Fig. S3.22**. Morphospace of the parietal for all specimens. The morphospace was generated from a PCA of the individual bones, so axes may not align with those of the entire data set. Positive and negative shape extremes for PC1 and PC2 are displayed in lateral view. A list of specimen names (attributed to the numbers in the plot) are given in **Table S3.13**.

**Fig. S3.23.** Morphospace of the dorsal and ventral premaxilla for all specimens. The morphospace was generated from a PCA of the individual bones, so axes may not align with those of the entire data set. Positive and negative shape extremes for PC1 and PC2 are displayed in dorsal view. A list of specimen names (attributed to the numbers in the plot) are given in **Table S3.13**.

**Fig. S3.24**. Morphospace of the pterygoid for all specimens. The morphospace was generated from a PCA of the individual bones, so axes may not align with those of the entire data set. Positive and negative shape extremes for PC1 and PC2 are displayed in ventral view. A list of specimen names (attributed to the numbers in the plot) are given in **Table S3.13**.

**Fig. S3.25.** Morphospace of the supraoccipital for all specimens. The morphospace was generated from a PCA of the individual bones, so axes may not align with those of the entire data set. Positive and negative shape extremes for PC1 and PC2 are displayed in posterior view. A list of specimen names (attributed to the numbers in the plot) are given in **Table S3.13**.

**Fig. S3.26.** Morphospace of the squamosal (including the zygomatic) for all specimens. The morphospace was generated from a PCA of the individual bones, so axes may not align with those of the entire data set. Positive and negative shape extremes for PC1 and PC2 are displayed in lateral view. A list of specimen names (attributed to the numbers in the plot) are given in **Table S3.13**.

**Table. S3.14.** Evolutionary rates per bone per suborder.

| bone | archaeocete | odontocete | mysticete |
|---|---|---|---|
| basioccipital | 7.445453 | 4.707233 | 0.621531 |
| basisphenoid | 15.20879 | 7.410418 | 0.807622 |
| frontal | 30.75606 | 10.31533 | 7.861886 |
| jugal | 7.478693 | 0.981096 | 1.673759 |
| mandibular process | 12.53936 | 5.17473 | 7.858969 |
| maxilla | 53.64476 | 11.36442 | 14.6093 |
| nasal | 52.444 | 16.14446 | 8.308556 |
| occipital | 5.279348 | 3.431033 | 0.781651 |
| palate | 28.61059 | 7.368608 | 6.584204 |
| parietal | 23.50142 | 4.876422 | 7.342303 |
| premaxilla | 22.96796 | 12.2608 | 5.513355 |
| pterygoid | 12.28178 | 4.627707 | 1.707664 |
| supraoccipital | 8.528619 | 4.796202 | 4.876253 |
| zygo-squamosal | 34.98247 | 3.211202 | 8.923168 |

**Table. S3.15.** Disparity per bone per suborder.

| bone | archaeocete | mysticete | odontocete |
|---|---|---|---|
| basioccipital | 0.00055 | 0.001417 | 0.001667 |
| basisphenoid | 0.000678 | 0.001412 | 0.001965 |
| frontal | 0.001875 | 0.005956 | 0.008494 |
| jugal | 4.85E-05 | 1.88E-04 | 2.01E-04 |
| mandibular process | 0.00049 | 0.001552 | 0.001869 |
| maxilla | 0.003279 | 0.01365 | 0.016022 |
| nasal | 0.0008 | 0.005257 | 0.005224 |
| occipital | 0.000382 | 0.001135 | 0.001138 |
| palate | 0.001272 | 0.003391 | 0.004645 |
| parietal | 0.001131 | 0.003552 | 0.005079 |
| premaxilla | 0.002645 | 0.010676 | 0.009518 |
| pterygoid | 0.000722 | 0.001871 | 0.002415 |
| supraoccipital | 0.001577 | 0.004265 | 0.004814 |
| zygo-squamosal | 0.001427 | 0.004117 | 0.004498 |

## Section 1: Cranial rates, binned by ecological categories

Rates of cranial evolution calculated for the whole skull across the full cetacean dataset, with species binned by five ecological categories.

| Dentition: | edentulous - baleen | heterodont | homodont | reduced |
|---|---|---|---|---|
| Rate: | 9.845391 | 109.950088 | 16.493512 | 12.863828 |

| Diet: | fish | benthic invertebrates + fish | cephalopods + fish | tetrapods + fish | zooplankton + fish |
|---|---|---|---|---|---|
| Rate: | 15.36672 | 131.9809 | 15.47147 | 18.72396 | 11.82144 |

| Echolocation band: | band1 | band2 |
|---|---|---|
| Rate: | 35.69735 | 15.77866 |

| Feeding method: | biting | filter | suction |
|---|---|---|---|
| Rate: | 16.780530 | 9.962307 | 44.149075 |

| Habitat: | coastal | coastal-pelagic | pelagic | riverine |
|---|---|---|---|---|
| Rate: | 29.7376031 | 27.7888914 | 6.7045051 | 0.4856411 |

**Table. S3.16.** Evolutionary rates per bone per dentition category.

| bone | heterodont | homodont | reduced | edentulous - baleen |
|---|---|---|---|---|
| basioccipital | 12.62977 | 4.992727 | 2.576441 | 0.250954 |
| basisphenoid | 25.09691 | 6.267331 | 3.485315 | 0.361959 |
| frontal | 37.26691 | 9.23564 | 5.354896 | 5.68833 |
| jugal | 4.197901 | 1.186233 | 0.272021 | 1.511817 |
| mandibular process | 22.69156 | 4.33568 | 3.686968 | 6.383626 |
| maxilla | 43.09787 | 9.510881 | 11.70895 | 13.0361 |
| nasal | 58.8022 | 13.67759 | 6.205102 | 9.695312 |
| occipital | 6.785284 | 4.204339 | 1.100768 | 0.397391 |
| palate | 19.39223 | 6.123783 | 9.254684 | 5.927491 |
| parietal | 30.31801 | 4.504333 | 1.174494 | 4.997242 |
| premaxilla | 19.35508 | 11.75824 | 12.01866 | 5.072534 |
| pterygoid | 12.53483 | 2.969989 | 12.12408 | 0.464452 |
| supraoccipital | 11.35414 | 5.061116 | 2.257432 | 3.628305 |
| zygo-squamosal | 27.86139 | 3.406051 | 1.212069 | 5.776563 |

**Table. S3.17.** Evolutionary rates per bone per diet category.

| bone | fish | tetrapods + fish | benthic inverts + fish | cephalopods + fish | zooplankton + fish |
|---|---|---|---|---|---|
| basioccipital | 3.72E+00 | 1.44E-05 | 2.15E+01 | 3.391895 | 0.585206 |
| basisphenoid | 4.90131 | 13.24926 | 38.33475 | 4.584607 | 0.805647 |
| frontal | 17.85342 | 5.139171 | 40.33284 | 5.732375 | 6.249922 |
| jugal | 2.026739 | 1.632615 | 1.384014 | 0.537066 | 1.671214 |
| mandibular process | 10.83018 | 6.203132 | 18.56186 | 2.254824 | 6.869568 |
| maxilla | 19.6455 | 18.29702 | 42.97812 | 5.944009 | 12.68879 |
| nasal | 21.63668 | 50.82366 | 53.39971 | 7.905337 | 9.509058 |
| occipital | 2.326677 | 3.917646 | 11.81853 | 3.042298 | 0.706376 |
| palate | 7.962197 | 8.736314 | 13.41759 | 6.413355 | 6.59182 |
| parietal | 5.916898 | 21.83766 | 51.17176 | 2.396161 | 8.292214 |
| premaxilla | 11.95403 | 18.28115 | 45.69811 | 9.501989 | 5.364746 |
| pterygoid | 3.244616 | 1.059586 | 11.45299 | 4.720636 | 1.050093 |
| supraoccipital | 5.108097 | 8.119693 | 18.65363 | 3.448619 | 4.951364 |
| zygo-squamosal | 7.31822 | 11.40055 | 16.171 | 1.497778 | 8.518574 |

**Table. S3.18.** Evolutionary rates per bone per echolocation category.

| bone | band1 | band2 |
|---|---|---|
| basioccipital | 1.959412 | 4.653983 |
| basisphenoid | 3.041067 | 6.959155 |
| frontal | 9.808044 | 11.95567 |
| jugal | 2.761968 | 0.94678 |
| mandibular process | 10.20563 | 5.109197 |
| maxilla | 22.42829 | 10.29504 |
| nasal | 20.24838 | 16.51266 |
| occipital | 1.731391 | 3.442961 |
| palate | 9.181349 | 7.033148 |
| parietal | 11.99176 | 4.865515 |
| premaxilla | 10.39378 | 11.94182 |
| pterygoid | 3.570432 | 4.231128 |
| supraoccipital | 6.286832 | 4.745466 |
| zygo-squamosal | 16.64911 | 3.227591 |

**Table. S3.19.** Evolutionary rates per bone per feeding method category.

| bone | biting | suction | filter |
|---|---|---|---|
| basioccipital | 5.14612 | 8.610379 | 0.251741 |
| basisphenoid | 7.103368 | 18.15163 | 0.447425 |
| frontal | 10.53196 | 13.60436 | 5.818743 |
| jugal | 1.220818 | 0.845164 | 1.296101 |
| mandibular process | 5.47051 | 7.180111 | 5.3452 |
| maxilla | 9.566825 | 24.88999 | 12.63487 |
| nasal | 19.5758 | 18.94311 | 7.3461 |
| occipital | 4.393888 | 2.461672 | 0.472681 |
| palate | 6.985273 | 9.496801 | 5.897925 |
| parietal | 6.803151 | 4.198299 | 5.061153 |
| premaxilla | 8.969135 | 37.21095 | 5.629064 |
| pterygoid | 4.275032 | 8.81851 | 0.769403 |
| supraoccipital | 5.077433 | 6.453811 | 3.571623 |
| zygo-squamosal | 4.461005 | 3.890105 | 4.710061 |

**Table. S3.20.** Evolutionary rates per bone per habitat category.

| bone | coastal | coastal-pelagic | pelagic | riverine |
|---|---|---|---|---|
| basioccipital | 9.884939 | 5.217458 | 1.200829 | 0.000107 |
| basisphenoid | 8.878749 | 5.017459 | 2.266869 | 0.001144 |
| frontal | 21.67519 | 12.84686 | 3.445953 | 10.52972 |
| jugal | 10.12211 | 9.936798 | 6.607661 | 6.650997 |
| mandibular process | 3.585317 | 8.305969 | 1.956101 | 1.086843 |
| maxilla | 14.17811 | 15.9341 | 7.903505 | 7.650947 |
| nasal | 31.63972 | 20.3359 | 5.811904 | 4.660696 |
| occipital | 8.89E+00 | 3.54E+00 | 5.23E-01 | 4.09E-05 |
| palate | 7.08144 | 8.079356 | 6.375029 | 5.179024 |
| parietal | 8.716307 | 9.112755 | 1.481695 | 3.631947 |
| premaxilla | 12.05957 | 17.25873 | 4.854011 | 0.00022 |
| pterygoid | 6.08142 | 8.779371 | 5.375055 | 5.2279 |
| supraoccipital | 7.552172 | 6.87622 | 1.638774 | 1.613572 |
| zygo-squamosal | 6.596727 | 5.904236 | 1.919916 | 6.950247 |

## Section 2: Cranial disparity, binned by ecological categories

Cranial disparity calculated for the whole skull across the full cetacean dataset, with species binned by five ecological categories.

| Dentition: | edentulous - baleen | heterodont | homodont | reduced |
|---|---|---|---|---|
| **Disparity:** | 0.06093224 | 0.05205697 | 0.05840106 | 0.06012313 |

| Diet: | fish | benthic invertebrates + fish | cephalopods + fish | tetrapods + fish | zooplankton + fish |
|---|---|---|---|---|---|
| **Disparity:** | 0.072224 | 0.043584 | 0.054437 | 0.064807 | 0.058487 |

| Echolocation band: | band1 | band2 |
|---|---|---|
| **Disparity:** | 0.05164977 | 0.06521561 |

| Feeding method: | edentulous - baleen | heterodont | homodont | reduced |
|---|---|---|---|---|
| **Disparity:** | 0.06093224 | 0.05205697 | 0.05840106 | 0.06012313 |

| Habitat: | coastal | coastal-pelagic | pelagic | riverine |
|---|---|---|---|---|
| Disparity: | 0.05944374 | 0.05726554 | 0.05919639 | 0.02739572 |

**Table. S3.21.** Disparity per bone per dentition category.

| bone | edentulous baleen | heterodont | homodont | reduced |
|---|---|---|---|---|
| basioccipital | 0.001426 | 0.001478 | 0.001649 | 0.001349 |
| basisphenoid | 0.0015 | 0.001628 | 0.001958 | 0.001459 |
| frontal | 0.006229 | 0.006355 | 0.007765 | 0.009372 |
| jugal | 0.000174 | 0.000174 | 0.000187 | 0.000202 |
| mandibular process | 0.001502 | 0.001399 | 0.001784 | 0.002103 |
| maxilla | 0.013624 | 0.012862 | 0.015112 | 0.015829 |
| nasal | 0.005938 | 0.003981 | 0.004656 | 0.006365 |
| occipital | 0.00105 | 0.001268 | 0.001045 | 0.000981 |
| palate | 0.003416 | 0.002852 | 0.0042 | 0.005395 |
| parietal | 0.003719 | 0.003873 | 0.004769 | 0.0047 |
| premaxilla | 0.008669 | 0.008107 | 0.009252 | 0.010974 |
| pterygoid | 0.002056 | 0.001503 | 0.002262 | 0.002233 |
| supraoccipital | 0.004413 | 0.004302 | 0.004377 | 0.005244 |
| zygo-squamosal | 0.004025 | 0.003844 | 0.004448 | 0.004287 |

**Table. S3.22.** Disparity per bone per diet category.

| bone | fish | benthic inverts + fish | cephalopods + fish | tetrapods + fish | zooplankton + fish |
|---|---|---|---|---|---|
| basioccipital | 0.001909 | 0.001355 | 0.001474 | 0.00166 | 0.001351 |
| basisphenoid | 0.002171 | 0.00153 | 0.001715 | 0.002003 | 0.001435 |
| frontal | 0.008819 | 0.004933 | 0.008282 | 0.007314 | 0.005889 |
| jugal | 0.000228 | 0.000131 | 0.000194 | 0.000232 | 0.000174 |
| mandibular process | 0.001997 | 0.001148 | 0.001833 | 0.00167 | 0.001489 |
| maxilla | 0.018404 | 0.009538 | 0.015216 | 0.012701 | 0.013081 |
| nasal | 0.005598 | 0.002127 | 0.005088 | 0.007668 | 0.005444 |
| occipital | 0.001317 | 0.001227 | 0.000945 | 0.001031 | 0.001044 |
| palate | 0.003918 | 0.003015 | 0.004993 | 0.002259 | 0.003254 |
| parietal | 0.004527 | 0.003732 | 0.004872 | 0.005291 | 0.003587 |
| premaxilla | 0.011341 | 0.007193 | 0.008361 | 0.011207 | 0.010362 |
| pterygoid | 0.001993 | 0.001807 | 0.002514 | 0.001101 | 0.001891 |
| supraoccipital | 0.005134 | 0.003823 | 0.004397 | 0.005513 | 0.004186 |
| zygo-squamosal | 0.005088 | 0.003163 | 0.004211 | 0.004631 | 0.003992 |

**Table. S3.23.** Disparity per bone per echolocation category.

| bone | band1 | band2 |
|---|---|---|
| basioccipital | 0.001188 | 0.001674 |
| basisphenoid | 0.001223 | 0.001975 |
| frontal | 0.011196 | 0.016046 |
| jugal | 1.55E-04 | 2.01E-04 |
| mandibular process | 0.001327 | 0.00186 |
| maxilla | 0.011196 | 0.016046 |
| nasal | 0.004228 | 0.005216 |
| occipital | 0.000937 | 0.001142 |
| palate | 0.002966 | 0.004665 |
| parietal | 0.003012 | 0.005094 |
| premaxilla | 0.008891 | 0.009527 |
| pterygoid | 0.001613 | 0.002426 |
| supraoccipital | 0.003604 | 0.004831 |
| zygo-squamosal | 0.003527 | 0.00449 |

**Table. S3.24.** Disparity per bone per feeding method category.

| bone | biting | filter | suction |
|---|---|---|---|
| basioccipital | 0.001621 | 0.001368 | 0.001433 |
| basisphenoid | 0.001891 | 0.001488 | 0.001617 |
| frontal | 0.007371 | 0.006097 | 0.00874 |
| jugal | 0.000183 | 0.000163 | 0.000224 |
| mandibular process | 0.001667 | 0.001436 | 0.002128 |
| maxilla | 0.014607 | 0.012988 | 0.015865 |
| nasal | 0.004603 | 0.005996 | 0.005535 |
| occipital | 0.001154 | 0.000982 | 0.00094 |
| palate | 0.003865 | 0.003266 | 0.004864 |
| parietal | 0.004551 | 0.003706 | 0.004649 |
| premaxilla | 0.009042 | 0.008932 | 0.010619 |
| pterygoid | 0.002098 | 0.00206 | 0.002295 |
| supraoccipital | 0.004475 | 0.004302 | 0.004633 |
| zygo-squamosal | 0.004289 | 0.003882 | 0.004513 |

**Table. S3.25.** Disparity per bone per habitat category.

| bone | coastal | coastal-pelagic | pelagic | riverine |
|---|---|---|---|---|
| basioccipital | 0.00183 | 0.001494 | 0.001605 | 0.000168 |
| basisphenoid | 0.002147 | 0.001705 | 0.001868 | 0.000172 |
| frontal | 0.006569 | 0.00735 | 0.009054 | 0.000816 |
| jugal | 1.36E-04 | 1.83E-04 | 2.46E-04 | 3.55E-05 |
| mandibular process | 0.001545 | 0.001685 | 0.002043 | 0.0002 |
| maxilla | 0.015313 | 0.014009 | 0.016559 | 0.003213 |
| nasal | 0.003884 | 0.005232 | 0.0054 | 0.000378 |
| occipital | 0.001205 | 0.001055 | 0.001134 | 0.000151 |
| palate | 0.004167 | 0.003378 | 0.00542 | 0.000858 |
| parietal | 0.004 | 0.004571 | 0.005037 | 0.000359 |
| premaxilla | 0.009895 | 0.009104 | 0.009643 | 0.001521 |
| pterygoid | 0.002352 | 0.001863 | 0.002742 | 0.000275 |
| supraoccipital | 0.004061 | 0.004445 | 0.005123 | 0.000484 |
| zygo-squamosal | 0.003831 | 0.004221 | 0.004871 | 0.000482 |

Appendix 4

# Chapter 4 Appendix

[Table on next page]

**Table S4.1.** Models fitted to cetacean evolutionary rates data - landmarks only. 31 models, a combination of standard evolutionary models (Brownian Motion, (BM), Early-Burst (EB), and accelerating rates (AC)) and climate models were run using 3 different climate/productivity proxies. These are then ranked. The cells are coloured according to which of the climate data sets was used: $\delta^{18}O_{Cr}$ results are shown in grey, $\delta^{18}O_W$ in blue, and $\delta^{13}C_W$ in green, and the combined model ($\delta^{18}O_W$/ $\delta^{13}C_W$) in orange. Cells coloured white are standard evolutionary models. Model is the type of model fitted to the evolutionary rates data (Chapter 4, Table 4.1); rank is the model rank according to the GIC (generalised information criterion) score. Log-likelihood is is a measure of goodness of fit for the model.

| Rank | Model | GIC | Log-likelihood |
|------|-------|-----|----------------|
| 1 | Clim7 | -690892 | 354064 |
| 2 | Clim8 | -690884 | 354061.7 |
| 3 | Clim5 | -690396 | 353797.8 |
| 4 | Clim2 | -690394 | 353795.1 |
| 5 | Clim3 | -690371 | 353785.1 |
| 6 | Clim8 | -690307 | 353751.6 |
| 7 | Clim7 | -690303 | 353748.4 |
| 8 | Clim7 | -690287 | 353739.5 |
| 9 | Clim8 | -690282 | 353737.7 |
| 10 | Clim4 | -690266 | 353729.3 |
| 11 | Clim2 | -690262 | 353722.7 |
| 12 | Clim2 | -690257 | 353722.3 |
| 13 | Clim5 | -690250 | 353719.7 |
| 14 | Clim4 | -690249 | 353716.1 |
| 15 | Clim3 | -690247 | 353717.6 |
| 16 | Clim4 | -690246 | 353717.8 |
| 17 | Clim3 | -690240 | 353710.7 |
| 18 | Clim5 | -690240 | 353712 |
| 19 | AC | -690178 | 353678.2 |
| 20 | EB | -690175 | 353676.5 |
| 21 | Clim1 | -689338 | 353209.5 |
| 22 | Clim_combined | -689149 | 353099.8 |
| 23 | Clim1 | -688358 | 352674.8 |
| 24 | Clim9 | -687527 | 352172.4 |
| 25 | Clim9 | -687484 | 352170.4 |
| 26 | Clim1 | -686700 | 351734.2 |
| 27 | Clim9 | -686464 | 351595.5 |
| 28 | Clim6 | -686460 | 351594.9 |
| 29 | BM | -686416 | 351565 |
| 30 | Clim6 | -686380 | 351550.7 |
| 31 | Clim6 | -686323 | 351518.3 |
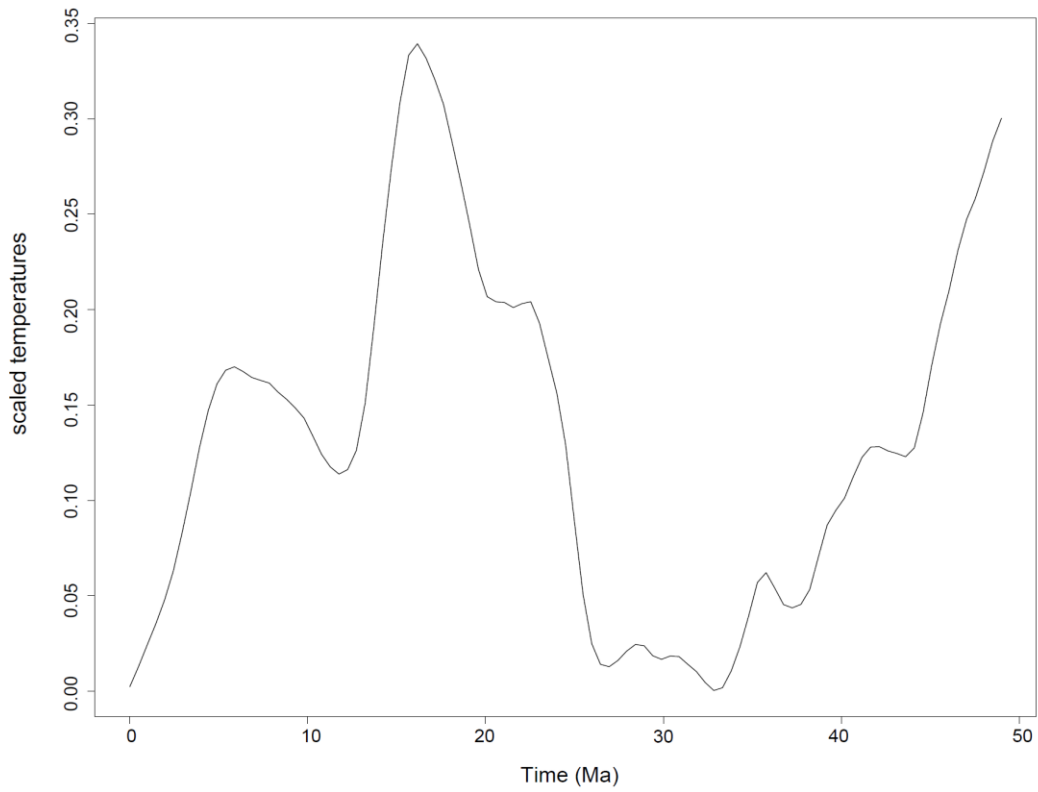
**Fig. S4.1.** Detrended temperature curve of Cramer et al. (2020) δ¹⁸O data. Used in the models outlined in Table 4.1.
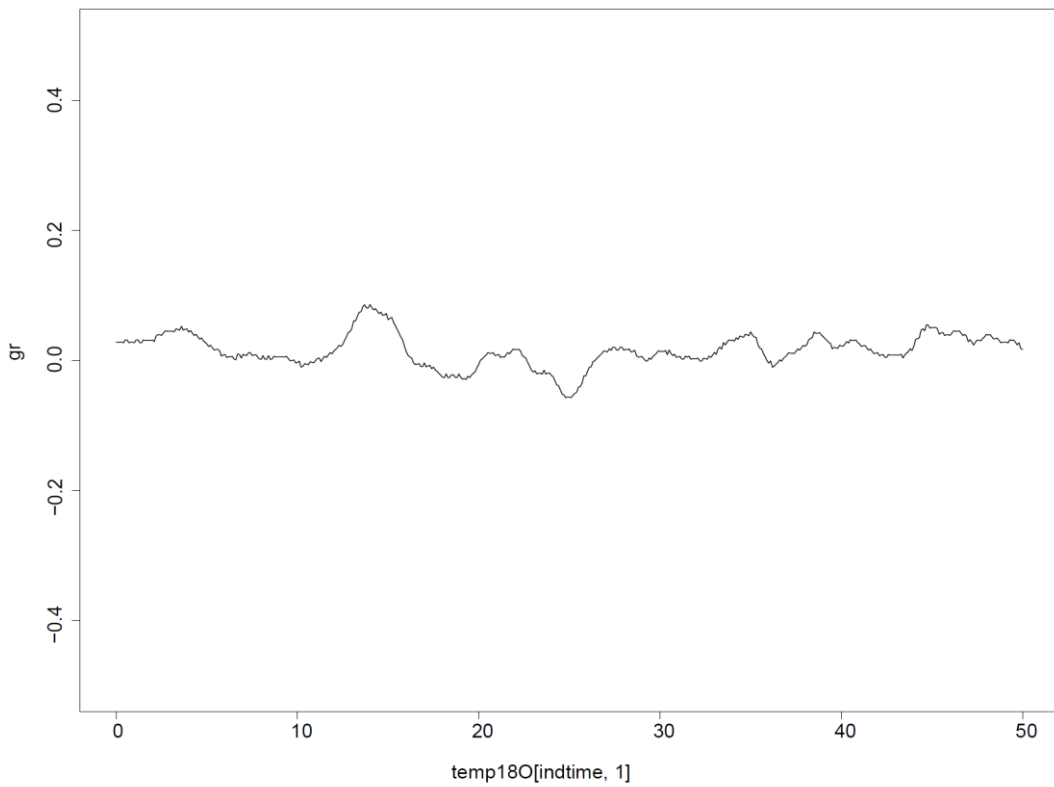


**Fig. S4.2.** Derivative temperature curve of Cramer et al. (2011) δ¹⁸O data. Used in models outlined in Table 4.1
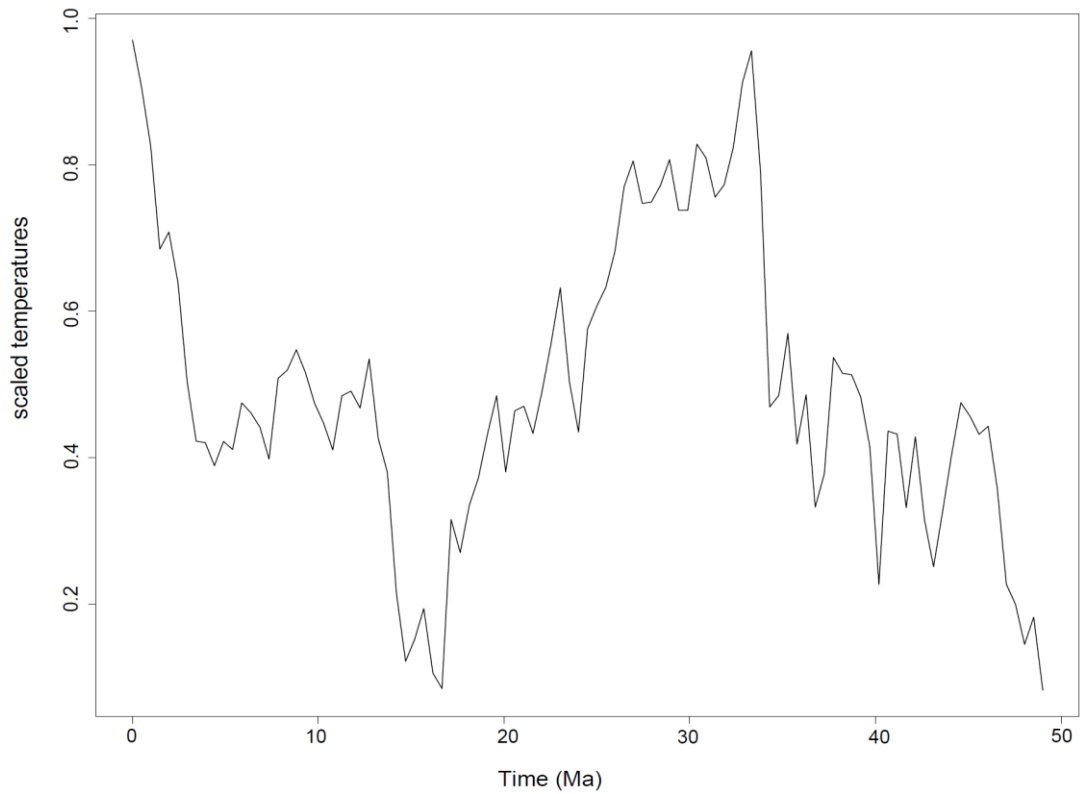
**Fig. S4.3.** Detrended temperature curve of Westerhold et al. (2020) $\delta^{18}O$ data. Used in models outlined in Table 4.1.
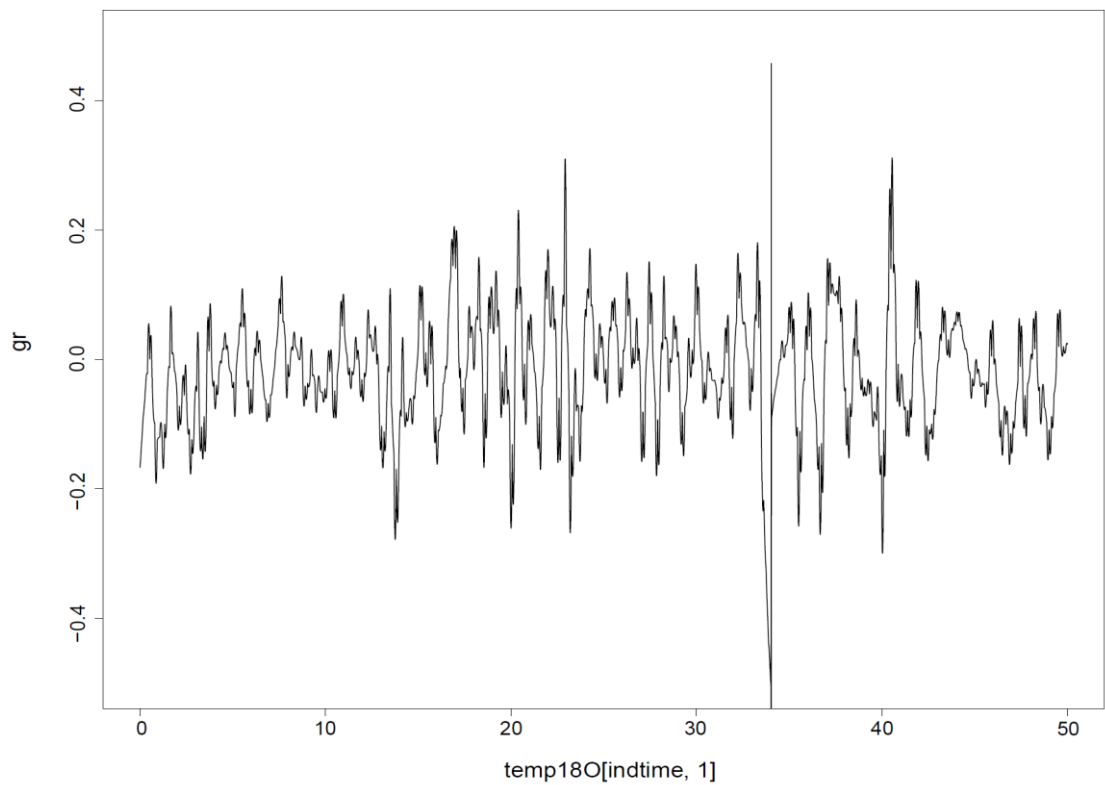


**Fig. S4.4.** Deriative temperature curve of Westerhold et al. (2020) $\delta^{18}O$. Used in models outlined in Table 4.1.
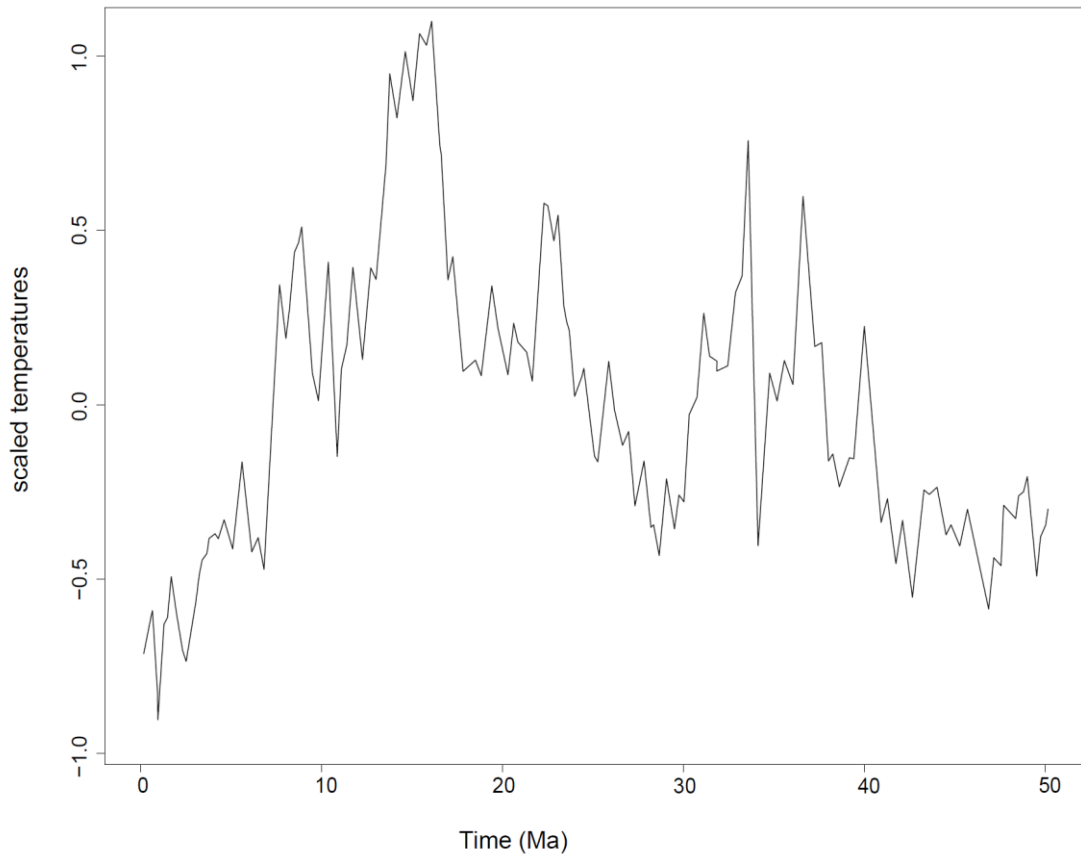
**Fig. S4.5.** Detrended temperature curve of Westerhold et al. (2020) $\delta^{13}C$ data. Used in models outlined in Table 4.1.
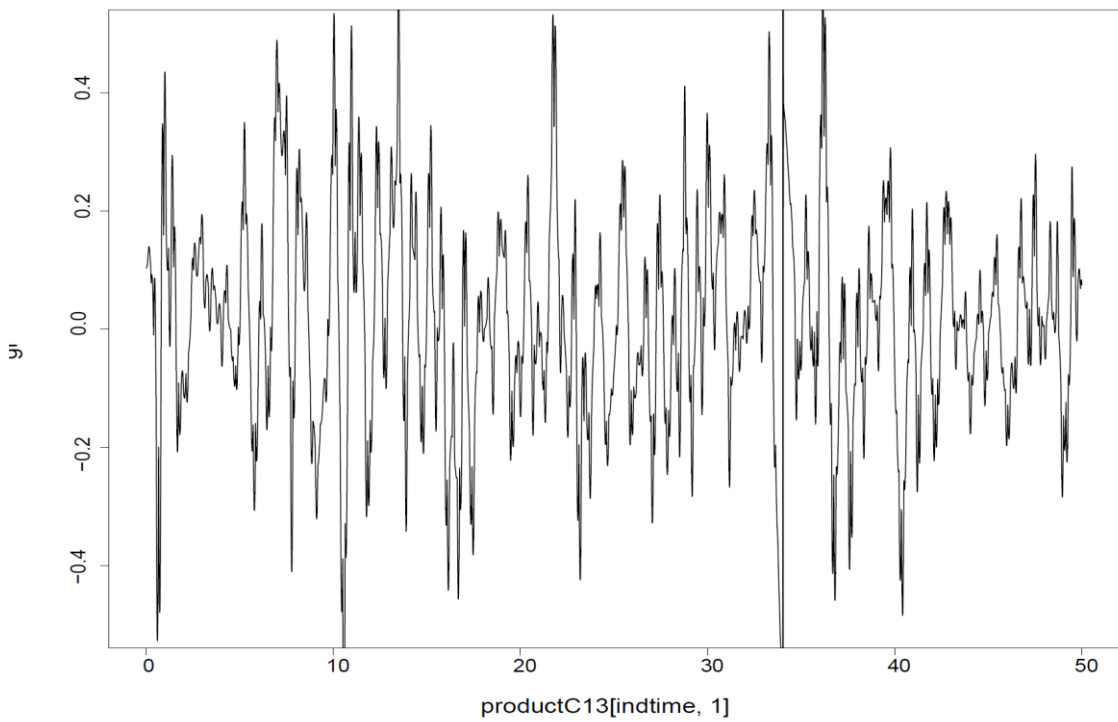


**Fig. S4.6.** Derivative temperature curve of Westerhold et al. (2020) $\delta^{13}C$ data. Used in models outlined in Table 4.1.

[Table on next page]

**Table S4.2.** All raw results for models fitted to cetacean evolutionary rates data. I ran 31 models, a combination of standard evolutionary models (Brownian Motion, (BM), Early-Burst (EB), and accelerating rates (AC)) and climate models using 3 different climate/productivity proxies. The cells are coloured according to which of the climate data sets was used: $\delta^{18}O_{Cr}$ results are shown in grey, $\delta^{18}O_W$ in blue, and $\delta^{13}C_W$ in green, the combined model ($\delta^{18}O_W$ / $\delta^{13}C_W$) in orange. Cells coloured white are standard evolutionary models. Model is the type of model fitted to the evolutionary rates data (Chapter 4, Table 4.1); rank is the model rank according to the GIC (generalised information criterion) score. Log-likelihood is is a measure of goodness of fit for the model. 'Clim_comb' is the combined climate model.

| Cetacea | | | | Archaeocetes | | | | Mysticetes | | | | Odontocetes | | | |
|---|---|---|---|---|---|---|---|---|---|---|---|---|---|---|---|
| Model | Rank | GIC | LL | Model | Rank | GIC | LL | Model | Rank | GIC | LL | Model | Rank | GIC | LL |
| Clim2 | 1 | 65800.37 | -32351.3 | Clim2 | 1 | 908.84 | -444.759 | Clim2 | 1 | 5300.38 | -2598.81 | Clim7 | 1 | 40394.02 | -19852.83 |
| Clim3 | 2 | 65801.34 | -32351.3 | Clim3 | 2 | 908.93 | -444.199 | Clim3 | 2 | 5302.42 | -2598.75 | Clim8 | 2 | 40394.48 | -19852.37 |
| Clim5 | 3 | 65802.39 | -32351.3 | EB | 3 | 909.63 | -445.813 | Clim4 | 3 | 5302.47 | -2598.87 | Clim7 | 3 | 40395.22 | -19853.48 |
| Clim7 | 4 | 65802.6 | -32350.9 | Clim7 | 4 | 909.68 | -444.055 | Clim2 | 4 | 5302.54 | -2602.15 | Clim2 | 4 | 40395.78 | -19856.8 |
| Clim4 | 5 | 65802.77 | -32351.5 | Clim3 | 5 | 910.47 | -444.518 | Clim5 | 5 | 5302.95 | -2598.98 | Clim4 | 5 | 40395.81 | -19856.81 |
| Clim8 | 6 | 65803.86 | -32349 | Clim7 | 6 | 910.80 | -444.673 | Clim7 | 6 | 5302.98 | -2599.00 | Clim8 | 6 | 40396.37 | -19853.03 |
| Clim3 | 7 | 65812.25 | -32357.6 | Clim5 | 7 | 910.84 | -444.759 | Clim5 | 7 | 5303.07 | -2601.60 | Clim5 | 7 | 40397.75 | -19856.78 |
| Clim7 | 8 | 65812.26 | -32364.91 | Clim4 | 8 | 910.85 | -444.79 | Clim7 | 8 | 5304.49 | -2602.13 | Clim3 | 8 | 40401.39 | -19859.05 |
| Clim8 | 9 | 65817.23 | -32364.11 | Clim2 | 9 | 911.13 | -445.39 | Clim4 | 9 | 5304.50 | -2602.12 | Clim2 | 9 | 40402.23 | -19860.06 |
| Clim2 | 10 | 65821.19 | -32360.98 | Clim2 | 10 | 911.63 | -445.63 | Clim8 | 10 | 5304.98 | -2599.01 | Clim3 | 10 | 40403.13 | -19859.08 |
| Clim7 | 11 | 65821.88 | -32359.11 | AC | 11 | 911.65 | -445.81 | Clim8 | 11 | 5305.04 | -2601.59 | Clim4 | 11 | 40404.2 | -19860 |
| Clim5 | 12 | 65823.18 | -32360.96 | Clim9 | 12 | 912.46 | -445.63 | Clim3 | 12 | 5305.33 | -2602.50 | Clim5 | 12 | 40404.24 | -19860.07 |
| Clim4 | 13 | 65823.24 | -32361 | Clim3 | 13 | 912.61 | -445.25 | Clim2 | 13 | 5307.32 | -2605.40 | Clim7 | 13 | 40405.14 | -19860.78 |
| Clim8 | 14 | 65823.85 | -32359.06 | Clim_comb | 14 | 912.72 | -445.82 | Clim3 | 14 | 5308.69 | -2605.00 | Clim8 | 14 | 40405.8 | -19860.2 |
| Clim2 | 15 | 65832.3 | -32376.4 | Clim8 | 15 | 912.75 | -444.65 | Clim7 | 15 | 5308.89 | -2605.35 | EB | 15 | 40406.42 | -19863.72 |

| | | | | | | | | | | | | | | | |
|---|---|---|---|---|---|---|---|---|---|---|---|---|---|---|---|
| EB | 16 | 65836.59 | -32374.81 | Clim4 | 16 | 912.78 | -445.35 | Clim5 | 16 | 5309.14 | -2605.64 | AC | 16 | 40409.41 | -19863.71 |
| AC | 17 | 65836.66 | -32374.9 | Clim8 | 17 | 913.05 | -444.37 | Clim4 | 17 | 5309.30 | -2605.38 | Clim3 | 17 | 40409.57 | -19863.04 |
| Clim5 | 18 | 65844.22 | -32376.31 | Clim5 | 18 | 913.12 | -445.39 | AC | 18 | 5309.32 | -2607.66 | Clim2 | 18 | 40412.88 | -19864.67 |
| Clim4 | 19 | 65844.35 | -32376.47 | Clim7 | 19 | 913.19 | -445.41 | Clim_comb | 19 | 5310.06 | -2606.50 | Clim9 | 19 | 40413.04 | -19862.12 |
| Clim3 | 20 | 65846.47 | -32376.74 | Clim4 | 20 | 913.63 | -445.63 | Clim8 | 20 | 5310.72 | -2605.18 | Clim4 | 20 | 40413.88 | -19864.29 |
| Clim_comb | 21 | 65976.05 | -32440.19 | Clim5 | 21 | 913.64 | -445.63 | Clim9 | 21 | 5358.59 | -2633.23 | Clim5 | 21 | 40413.9 | -19864.31 |
| Clim1 | 22 | 65994.68 | -32450.62 | Clim1 | 22 | 914.58 | -446.62 | Clim9 | 22 | 5429.50 | -2661.57 | Clim9 | 22 | 40416.01 | -19861.42 |
| Clim1 | 23 | 66053.98 | -32479.51 | Clim8 | 23 | 915.19 | -445.42 | Clim1 | 23 | 5432.90 | -2667.48 | Clim6 | 23 | 40430.84 | -19870.69 |
| Clim9 | 24 | 66113.34 | 32483.83 | Clim1 | 24 | 915.65 | -446.93 | EB | 24 | 5443.44 | -2668.91 | Clim_comb | 24 | 40436.81 | -19875.85 |
| Clim9 | 25 | 66239.51 | -32542.71 | Clim9 | 25 | 916.04 | -446.17 | Clim9 | 25 | 5453.50 | -2674.43 | Clim1 | 25 | 40474.68 | -19898.52 |
| Clim9 | 26 | 66302.65 | 32572.1 | Clim6 | 26 | 917.60 | -448.51 | Clim1 | 26 | 5457.36 | -2678.04 | Clim6 | 26 | 40480.1 | -19898.78 |
| Clim1 | 27 | 66367.56 | -32618.8 | BM | 27 | 917.60 | -449.14 | Clim1 | 27 | 5460.96 | -2678.97 | Clim1 | 27 | 40490.92 | -19906.2 |
| Clim6 | 28 | 66368.65 | -32614.04 | Clim6 | 28 | 918.62 | -448.29 | Clim6 | 28 | 5462.32 | -2679.45 | Clim1 | 28 | 40519.88 | -19920.92 |
| Clim6 | 29 | 66397.67 | -32626.19 | Clim1 | 29 | 919.21 | -448.75 | BM | 29 | 5463.24 | -2680.62 | Clim6 | 29 | 40529.85 | -19922.79 |
| Clim6 | 30 | 66417.58 | -32635.16 | Clim6 | 30 | 919.48 | -448.94 | Clim6 | 30 | 5465.34 | -2680.22 | Clim9 | 30 | 40533.79 | -19923.15 |
| BM | 31 | 66452.14 | -32655.34 | Clim9 | 31 | 922.11 | -448.10 | Clim6 | 31 | 5467.79 | -2682.63 | BM | 31 | 40542.44 | -19930.87 |
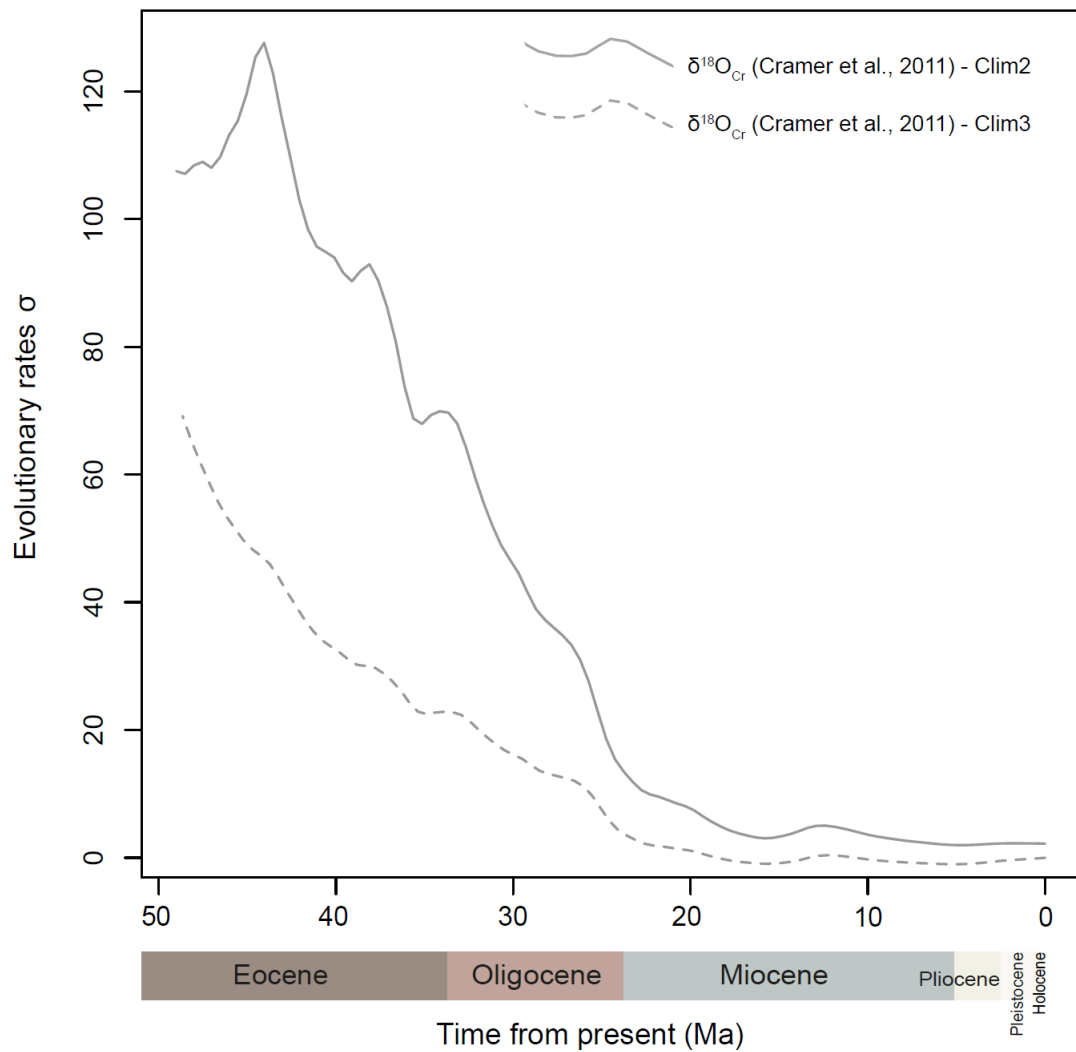
**Fig. S4.7.** Reconstructed evolutionary rates for Cetacea under the 'Clim2' and 'Clim3'. Rates modelled using deep sea $\delta^{18}O_{Cr}$ reconstructed ocean temperatures. Scale on the y-axis is arbitrary (see Chapter 4, Methods 4.3).
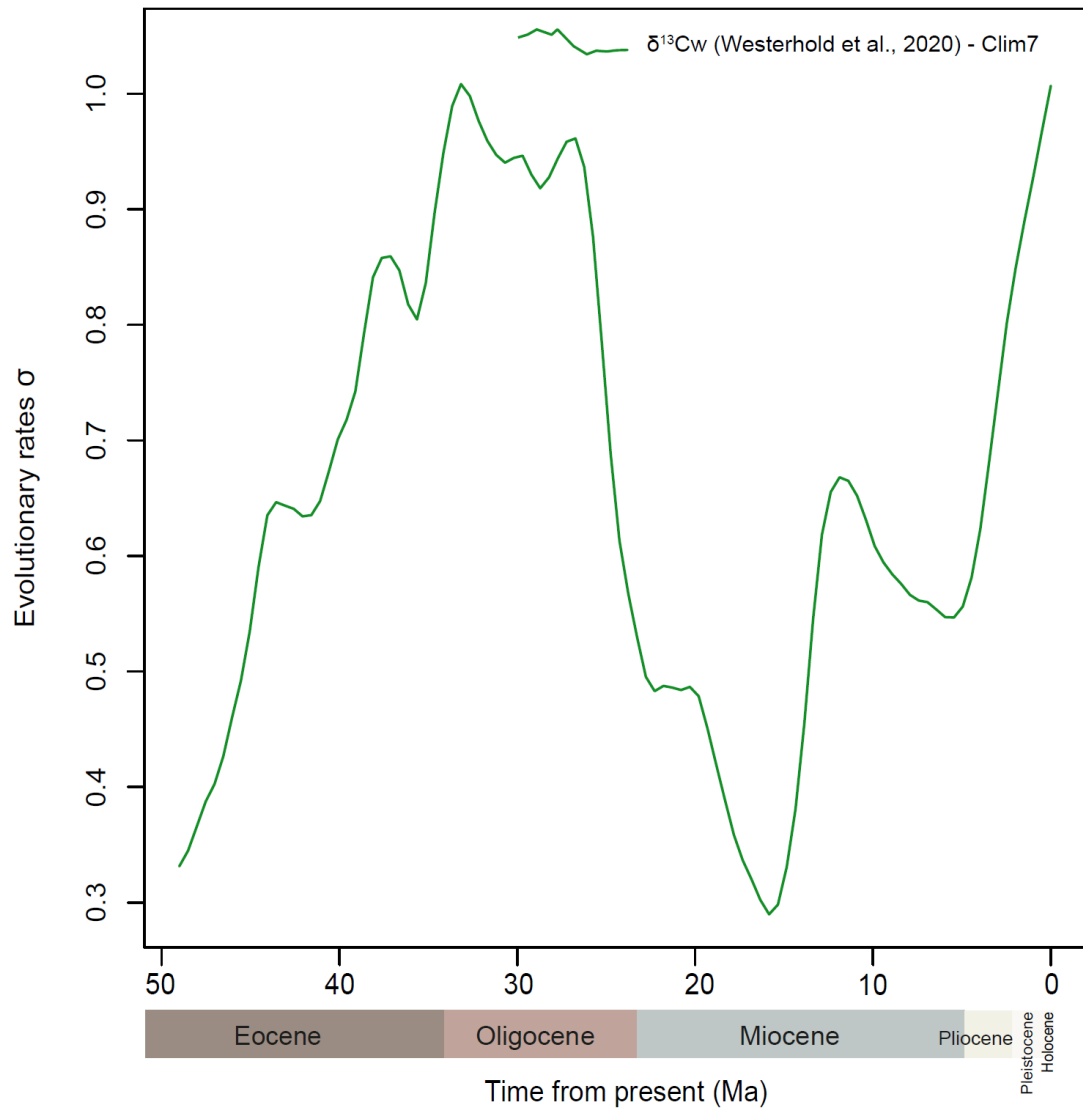
**Fig S4.8.** Reconstructed evolutionary rates for Cetacea under the 'Clim7' model. Rates modelled using deep sea $\delta^{13}C_W$ reconstructed ocean productivity. Scale on the y-axis is arbitrary (see Chapter 4, Methods 4.3).
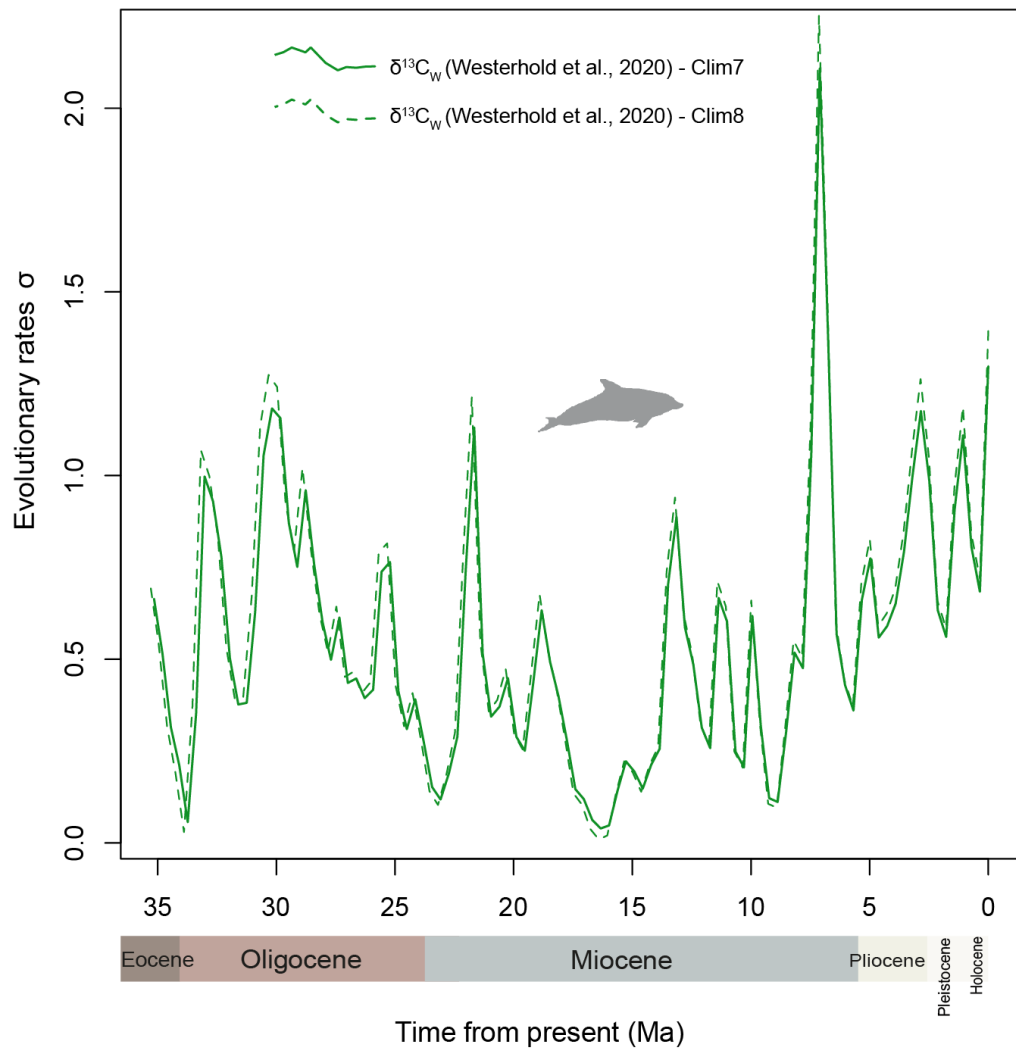
**Fig. S4.9.** Reconstructed evolutionary rates for odontocetes under the 'Clim7' and 'Clim8' models. Rates modelled using deep sea $\delta^{13}C_W$ reconstructed ocean productivity. Scale on the y-axis is arbitrary (see Chapter 4, Methods 4.3)

Appendix 5

# Chapter 5 Appendix

All code to reproduce the analyses is available at
https://github.com/EllenJCoombs/cetacean-strandings-project All data are available
at https://doi.org/10.5519/0090038 and https://doi.org/10.5519/0028204

**Data collection**

**Identification and removal of rare cetacean species**

Before analyses we removed rare cetacean species from the strandings data. We identified these by looking at occurrence data for each of the species from the OBIS-SEAMAP (Halpin et al., 2009) and the Joint Cetacean Protocol (Reid et al., 2003). We gave a score of 1-5 (Table S5.1) for each of the species depending on their occurrence data from the OBIS-SEAMAP, Reid et al. (2003) and the stranding data. If the species was scored as one and was recorded in the stranding data set on three or fewer occasions, it was removed from the data set. This was because it was likely to be a misidentification (especially in the historical data), or it was a one-off event (i.e., a single, disorientated animal) that would not contribute to general patterns for that species.

**Table S5.1.** Descriptions of how frequently species were seen in the stranding data set. With score assigned to each description. Species were removed if they received a score of '1' (i.e., which were seen in the stranding records 3 times or fewer). This is because these were likely to be cases where species had been misidentified (especially in the historical data) or were rare events that would not contribute to general patterns for that species.

| Description | Score |
| --- | --- |
| Very rarely seen in UK waters (i.e., 1-3 records) | 1 |
| Infrequent visitor to UK waters (i.e., 3+ total records) | 2 |
| Frequent visitor to UK waters (i.e., seen several times every decade) | 3 |
| Regular and frequent visitor to UK waters (i.e., yearly records) | 4 |
| Regular and frequent year-round UK resident (i.e., monthly records) | 5 |

[Table on next page]

**Table S5.2** Scientific and common names of all 28 species that have stranded in the cetacean stranding data set (1913-2015). The data set contains records from the Natural History Museum, London (NHM), the Cetacean Stranding Investigation Programme (CSIP), and the Irish Whale and Dolphin group (IWDG). A score from 1-5 was given for each of the species based on the descriptions in **Table S5.1**. This score was given for species occurrence data from the OBIS-SEAMAP, distribution and relative abundance maps from Reid et al. (2003), and range maps from Carwardine (2016). These scores were compared to the score given for how frequently cetaceans have been recorded in the stranding data set. Species were removed if they received an average score of '1', i.e., **very rarely seen in UK waters (1-3 records)**. First, last, and total number of strandings are shown for each species. Removed species are highlighted in orange.

| Scientific name | Suborder | Habitat* | Range OBIS* | Range JCP** | Stranding data set | Additional source*** | Remove from data set? | First record | Last record | Total strandings |
|---|---|---|---|---|---|---|---|---|---|---|
| *Balaenoptera acutorostrata* | mysticete | both | 5 | 5 | 5 | 5 | N | 1913 | 2015 | 621 |
| *Balaenoptera borealis* | mysticete | oceanic | 2 | 2 | 2 | 2 | N | 1913 | 2013 | 20 |
| *Balaenoptera musculus* | mysticete | oceanic | 1 | 1 | 1 | 2 | N | 1916 | 1957 | 5 |
| *Balaenoptera physalus* | mysticete | oceanic | 3 | 3 | 3 | 2 | N | 1913 | 2015 | 115 |
| *Delphinapterus leucas* | odontocete | coastal | 2 | NA | 1 | 1 | Y | 1932 | 2014 | 2 |
| *Delphinus delphis* | odontocete | both | 5 | 5 | 5 | 5 | N | 1913 | 2015 | 3110 |
| *Globicephala melas* | odontocete | oceanic | 5 | 5 | 5 | 5 | N | 1913 | 2015 | 1606 |
| *Grampus griseus* | odontocete | oceanic | 4 | 4 | 4 | 4 | N | 1913 | 2015 | 402 |
| *Hyperoodon ampullatus* | odontocete | oceanic | 4 | 4 | 4 | 4 | N | 1913 | 2014 | 173 |
| *Kogia breviceps* | odontocete | oceanic | 2 | 2 | 2 | 3 | N | 1966 | 2015 | 24 |
| *Kogia sima* | odontocete | oceanic | 2 | NA | 1 | 1 | Y | 2011 | 2011 | 1 |
| *Lagenodelphis hosei* | odontocete | both | 1 | NA | 1 | 1 | Y | 1986 | 1996 | 2 |
| *Lagenorhynchus acutus* | odontocete | coastal | 4 | 4 | 4 | 4 | N | 1913 | 2015 | 565 |
| *Lagenorhynchus albirostris* | odontocete | coastal | 4 | 4 | 4 | 4 | N | 1913 | 2015 | 539 |
| *Megaptera novaeangliae* | mysticete | both | 2 | 2 | 2 | 3 | N | 1982 | 2015 | 25 |
| *Mesoplodon bidens* | odontocete | oceanic | 3 | 1 | 3 | 3 | N | 1914 | 2015 | 127 |
| *Mesoplodon densirostris* | odontocete | oceanic | 1 | 2 | 1 | 1 | Y | 1993 | 2013 | 2 |
| *Mesoplodon europaeus* | odontocete | oceanic | 1 | 2 | 1 | 1 | Y | 1989 | 1989 | 1 |

| | | | | | | | | | | |
|---|---|---|---|---|---|---|---|---|---|---|
| *Mesoplodon mirus* | odontocete | oceanic | 1 | 2 | 1 | 1 | N | 1917 | 2013 | 12 |
| *Monodon monoceros* | odontocete | coastal | 2 | NA | 1 | 1 | Y | 1949 | 1949 | 2 |
| *Orcinus orca* | odontocete | both | 3 | 3 | 3 | 4 | N | 1916 | 2015 | 106 |
| *Peponocephala electra* | odontocete | oceanic | 2 | NA | 1 | 1 | Y | 1949 | 1949 | 1 |
| *Phocoena phocoena* | odontocete | coastal | 5 | 5 | 5 | 5 | N | 1913 | 2015 | 8265 |
| *Physeter macrocephalus* | odontocete | oceanic | 3 | 3 | 3 | 3 | N | 1913 | 2015 | 285 |
| *Pseudorca crassidens* | odontocete | oceanic | 2 | 1 | 1 | 3 | N | 1927 | 1976 | 254 |
| *Stenella coeruleoalba* | odontocete | oceanic | 3 | 2 | 3 | 3 | N | 1923 | 2015 | 487 |
| *Tursiops truncatus* | odontocete | both | 5 | 4 | 5 | 5 | N | 1914 | 2015 | 595 |
| *Ziphius cavirostris* | odontocete | oceanic | 3 | 2 | 3 | 3 | N | 1913 | 2015 | 155 |

* Halpin, P.N., A.J. Read, E. Fujioka, B.D. Best, B. Donnelly, L.J. Hazen, C. Kot, K. Urian, E. LaBrecque, A. Dimatteo, J. Cleary, C. Good, L.B. Crowder, and K.D. Hyrenbach. 2009. OBIS-SEAMAP: The world data center for marine mammal, sea bird, and sea turtle distributions. Oceanography 22(2):104-115

** Reid, J.B., Evans, P.G.H., & Northridge, S.P., (2003) Atlas of Cetacean distribution in north-west European waters. Joint Nature Conservation Committee, Peterborough.

*** Carwardine. M (2016) Mark Carwardine's Guide To Whale Watching In Britain And Europe: Second Edition. Bloomsbury Natural History: 2nd Revised ed

**Geomagnetic data (K-index)**

**Data source:** British Geographical Survey (BGS)

**Data access:**
http://www.geomag.bgs.ac.uk/data_service/data/magnetic_indices/k_indices.html

**Date accessed:** 30th August 2017

Raw data files were obtained from the British Geological Survey
(http://www.bgs.ac.uk/) on 30th August 2017. The raw data files are available here:
http://www.geomag.bgs.ac.uk/data_service/data/magnetic_indices/k_indices.html
and extra information can be obtained by contacting: enquires@bgs.ac.uk

These data are geomagnetic values (K-index) taken from five magnetic observatories from around the UK. At present, Lerwick (LER) in Shetland, Eskdalemuir (ESK) in Dumfries and Galloway, and Hartland (HAD) in Devon are operational. Historic readings were gathered from Greenwich (GRW) and Abinger (ABN). These observatories constantly monitor changes in the Earth's magnetic field, giving three-hourly K-index readings. The K-index has a scale from 0-9, with 1 being calm and 5 or more indicating a geomagnetic storm (for further details see: http://www.geomag.bgs.ac.uk/education/current_activity.html).

**Data availability from each station**

The data file for Hartland contains data from both the Greenwich observatory, Greenwich (1868-1925) and the Abinger observatory (1926-1956). This is because in 1924 geomagnetic observations were moved away from Greenwich (London) to Abinger (Surrey) because of magnetic interference from trams. Geomagnetic data were collected from the site in Abinger from 1926 to 1957 when the observatory had to be moved to Hartland, Devon because of magnetic interference from the electrification of local railways. Data are available from Hartland from 1957-present and from Lerwick and Eskdalemuir from 1940-present.

**Data extraction from each station**

K-index values were recorded every three hours at stations during their operating years. This means that there were eight readings for every 24-hour period. We took the maximum daily K-index from these hourly records. From this, we then took the maximum yearly reading from that station.

When only one station reading was available for a certain year or period, e.g., Greenwich 1913-1925, we took the maximum yearly reading from that station only. When readings were available from multiple stations for a certain year or period, e.g., Hartland, Lerwick and Eskdalemuir (1957-2015), we calculated a mean of the maximum yearly readings from all the available stations. This worked as follows:

**1913 – 1925**

Greenwich: Maximum yearly K-index was used from this station only for this time period.

**1926 – 1939**

Abinger: Maximum yearly K-index was used from this station only for this time period.

**1940 – 1956**

Abinger, Lerwick and Eskdalemuir: Mean maximum yearly K-index was calculated from these three stations for this time period.

**1957 – 2015**

Hartland, Lerwick and Eskdalemuir:  Mean maximum yearly K-index was calculated from these three stations for this time period.

**Geomagnetic data:** A general cyclical rise and fall in the maximum mean k-index from 1913 -2015. 2009 saw the lowest recorded mean maximum k-index of around 5. The UK experienced an unusually cold winter in 2009 - 2010. The Met Office reported that this coincided with low solar activity (Lockwood et al., 2010) and with an exceptionally negative phase of the NAO.

**Sea surface temperature (SST) data**

**Data source:** Met Office HadISST

**Data access:** https://www.metoffice.gov.uk/hadobs/hadisst/

**Date accessed:** 23rd July 2017

These data consist of monthly SST ($^o$C) readings for the most easterly, westerly, northerly, and southerly points of the UK and Ireland, and then NW, NE, SW, SE + additional locations from 1913-2015 (Table S5.3). We took the yearly maximum SST reading for each location, and then calculated the yearly mean maximum SST from all 14 locations. This was used in our models.

**Table S5.3.** Locations of sea surface temperature data. The latitude and longitudes of 14 locations from around the UK and Ireland from which monthly sea surface temperatures (SST) for 1913 - 2015 were taken

| Location | Latitude (°) | Longitude (°) |
|---|---|---|
| Ballyhillin, UK | 55.34 | -7.4 |
| Barrow, UK | 54.11 | -3.22 |
| Dover, UK | 51.13 | 1.34 |
| Gore Cliff, UK | 50.58 | -1.31 |
| Holyhead, UK | 53.31 | -4.65 |
| John O' Groats, UK | 58.64 | -3.07 |
| Lands' End, UK | 50.06 | -5.712 |
| Lindisfarne, UK | 55.68 | -1.8 |
| Lowerstoft, UK | 52.48 | 1.75 |
| Mull, UK | 56.44 | -6 |
| Shetland, UK | 60.86 | -1.23 |
| Browhead, Ireland | 51.44 | -9.7 |
| Cleggan, Ireland | 53.56 | -10.11 |
| Wicklow, Ireland | 52.98 | -6.04 |
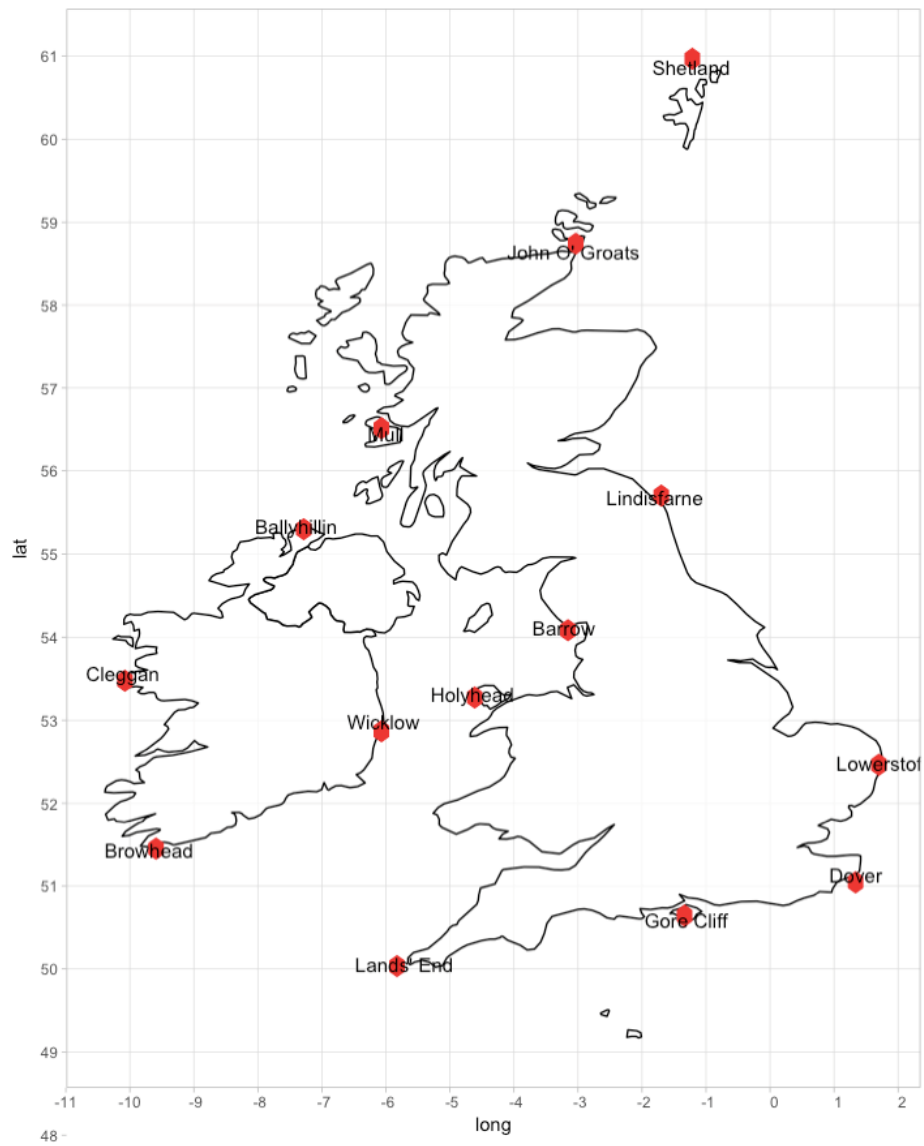
**Fig. S5.1.** Map of locations of sea surface temperature data. Map with the latitude and longitudes of 14 locations from around the UK and Ireland from which monthly sea surface temperatures (SST) for 1913 - 2015 were taken.
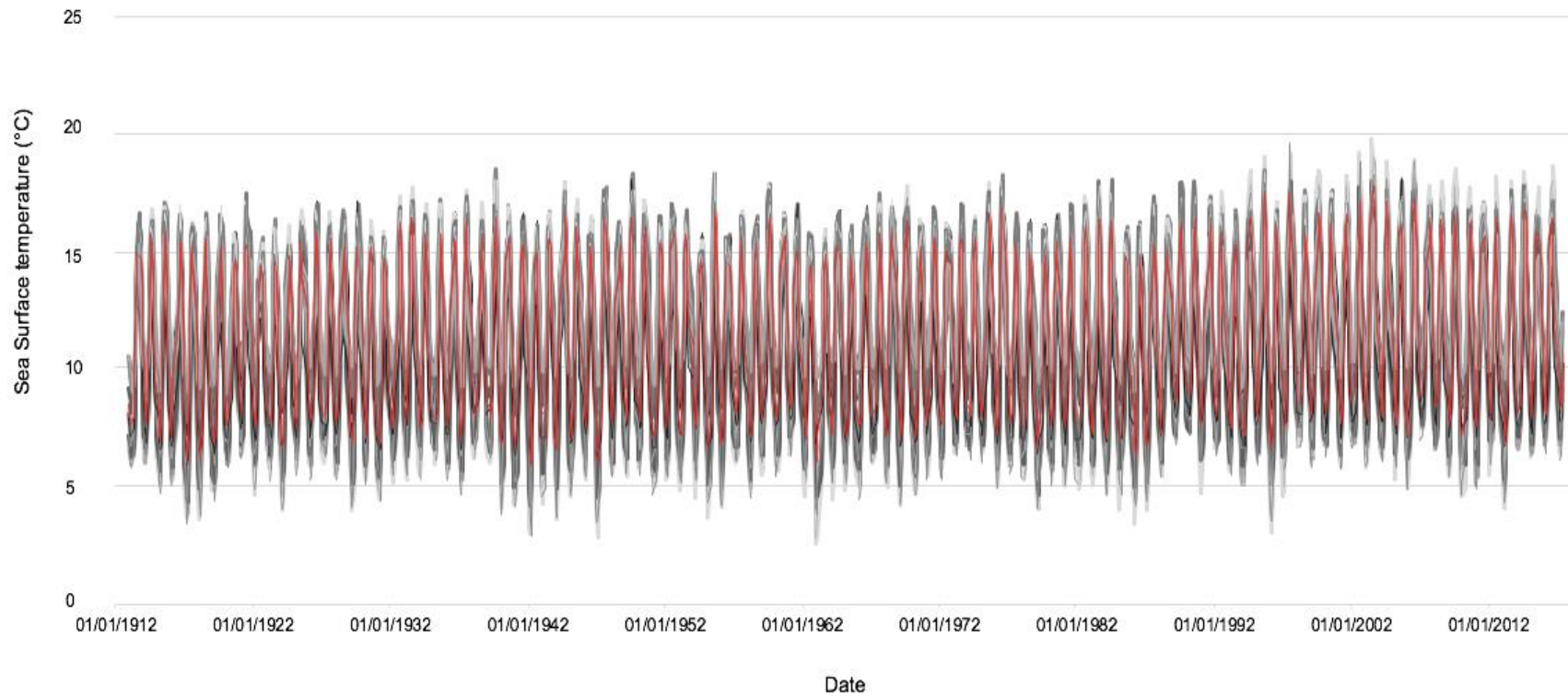
**Fig. S5.2.** Monthly sea surface temperatures (°C) from all 14 UK and Irish locations. Data from 1913 - 2015 (shown in greys). The mean monthly sea surface temperature which was used in the main analysis is shown in red.

**Sea surface temperature:** There has been an increase in SST over the past century from 1913 - 2015. The lowest maximum mean SST was 14.3° C in 1922. The highest maximum mean SST was 17.7° C in 2003


**Storm counts**

**Data source:** Lamb and Frydendahl (1991), the Met Office, and Met Éireann

**Data access:** https://github.com/EllenJCoombs/cetacean-strandings-project

**Date collected:** September 2017

These data are yearly counts of storms that occurred in the UK and Ireland from 1913-2015. For this study, a 'storm' is defined as a weather event with winds having an average speed of over 47 knots (88 km/h) and includes specific hurricane events which have recorded surface winds of 64 knots, (or 74 mph) or greater (NOAA, 2017). In this study, both storms and hurricanes are labelled as 'storms'. Where possible information on maximum wind speed (mph), the largest area affected, and the duration of the event were given to help define historical weather events as storms or not, as in Lamb and Frydendahl (1991).

We collected data from Lamb and Frydendahl (1991) for storms before 1991 and collected data from the Met Office (https://www.metoffice.gov.uk/) and the Met Éireann (http://www.met.ie/default.asp) for storms after 1991. See raw data for more details (https://github.com/EllenJCoombs/cetacean-strandings-project)

**Storm count:** Generally cyclic and seasonal with more storms recorded from October to January. A slight increase in the number of storms recorded throughout the century, perhaps due to an increase in meteorological knowledge, storm detection, and monitoring effort.

**North Atlantic Oscillations (NAO) data**

**Data source:** University Corporation for Atmospheric Research

**Data access:**
https://climatedataguide.ucar.edu/sites/default/files/nao_station_annual.txt

**Date accessed:** Downloaded on 28th October 2017

This data set shows yearly North Atlantic Oscillation (NAO) records from 1865-2016. We extracted yearly readings for 1913-2015 only. The NAO is based on the difference of normalized sea level pressure (SLP) between Stykkisholmur/Reykjavik, Iceland, and Lisbon, Portugal and is given as a yearly reading here.

**North Atlantic Oscillation:** A general cyclical rise and fall in the index throughout the century from 1913-2015. The coldest winter in 30 years (2009-2010) likely coincided with an exceptionally negative phase of the NAO (Osborn, 2011).

**Fisheries data**

**Data source:** International Council for the Exploration of the Sea (ICES)

**Data access:** http://www.ices.dk/marine-data/dataset-collections/Pages/Fish-catch-and-stock-assessment.aspx?fbclid=IwAR0_iCS2vBEZ0Hoc9Z9mYyzZDRo2HuAOFHBsklWXWN5mkbNSgeuyAVodg9A

**Date accessed:** Downloaded on 11th November 2018

The data set was compiled from 3 separate ICES data sets:

ICES Historical Landings: 1903 – 1949

Historical Nominal Catches: 1950 – 2010

Official Nominal Catches: 2006 – 2016

The country codes were used as follows (from the ICES country notes)

| GBE | UK England and Wales |
|-----|----------------------|
| | From 1928 - 1939 (and possibly other years) the England & Wales data may include Scottish landings in foreign ports. |
| | |
| | Reports of data for Division "XIV, XV" are thought to be for Division XV (the NW Atlantic) and are thus omitted from this table. |
| | |
| | Data for 1903-1949 |
| | |
| | No shellfish data until 1918 |
| GBS | UK Scotland |
| | Scottish landings in foreign ports are included in the data for England and Wales. |
| | |
| | Data for 1903-1949 |
| | No shellfish data until 1911 |
| GBU | UK England and Wales and Northern Ireland |
| | Data in these worksheets are primarily derived from the corresponding volume of ICES Bulletin Statistique.  However, in some cases corrections to the earlier data published in later volumes of the Bulletin have been included as have other data from the ICES archives. |
| IRL | Ireland |
| | From 1930 onwards, data for Ireland excludes data for Northern Ireland which will be found in the file GBU_23_49 |
| | |
| | Data in these worksheets are primarily derived from the corresponding volume of ICES Bulletin Statistique.  However, in some cases corrections to the earlier data published in later volumes of the Bulletin have been included as have other data from the ICES archives. |

**Fishing data:** There were two key drops in fishing catch (1000 tonnes per year) during WWI (1914-1918) and WWII (1939-1945). Fishing catches increased from the 1950s to the 1970s. There has been a steady decline in fish catches this century.  Landings have stabilised since 2009 and are at the lowest levels of any years outside the two world wars (Parliament, House of Commons, 2017).

**Human population data**

**Data source:** Office of National Statistics

**Data access:** https://www.ons.gov.uk/

**Date accessed:** Downloaded August 2017

This data set shows yearly human population (in millions) for the UK from 1913-2015.

No clean-up of these data was required before modelling.

**Human population:** This has seen an overall increase from 1913-2015 with one or two notable dips such as during 1918 when an influenza outbreak, as well as human losses from WWI saw the UK population fall.

## Data analysis
Correlates of strandings through time

## Environmental variables
We considered that some environmental variables may be highly correlated/collinear with one another or could be used as a proxy for one another. For example, storm events, and fluctuations in sea surface temperature (SST) are both associated with changes in the North Atlantic Oscillation (NAO) (Hurrell, 1995; Alexander et al., 2005). However, they may also occur independently (i.e., unrelated to NAO fluctuations). Long-term fluctuations in the NAO have caused a significant increase in severe storm events in the UK, but there is a non-significant relationship between the NAO and severe storms in the months October to December (Alexander et al., 2005). To explore this uncertainty, we performed linear regressions of NAO index as a function of storms, and NAO index as a function of SST. We found that there was no significant relationship between NAO and storms (slope = $0.462 \pm 0.023$, t = 20.1, df = 2161, adj $r^2 = 0.157$) and no significant relationship between NAO and SST (slope = $- 0.045 \pm 0.056$, t = -0.798, df = 2162, adj $r^2 = < 0.001$). We therefore modelled storm events, NAO fluctuations, and max SST as separate environmental variables
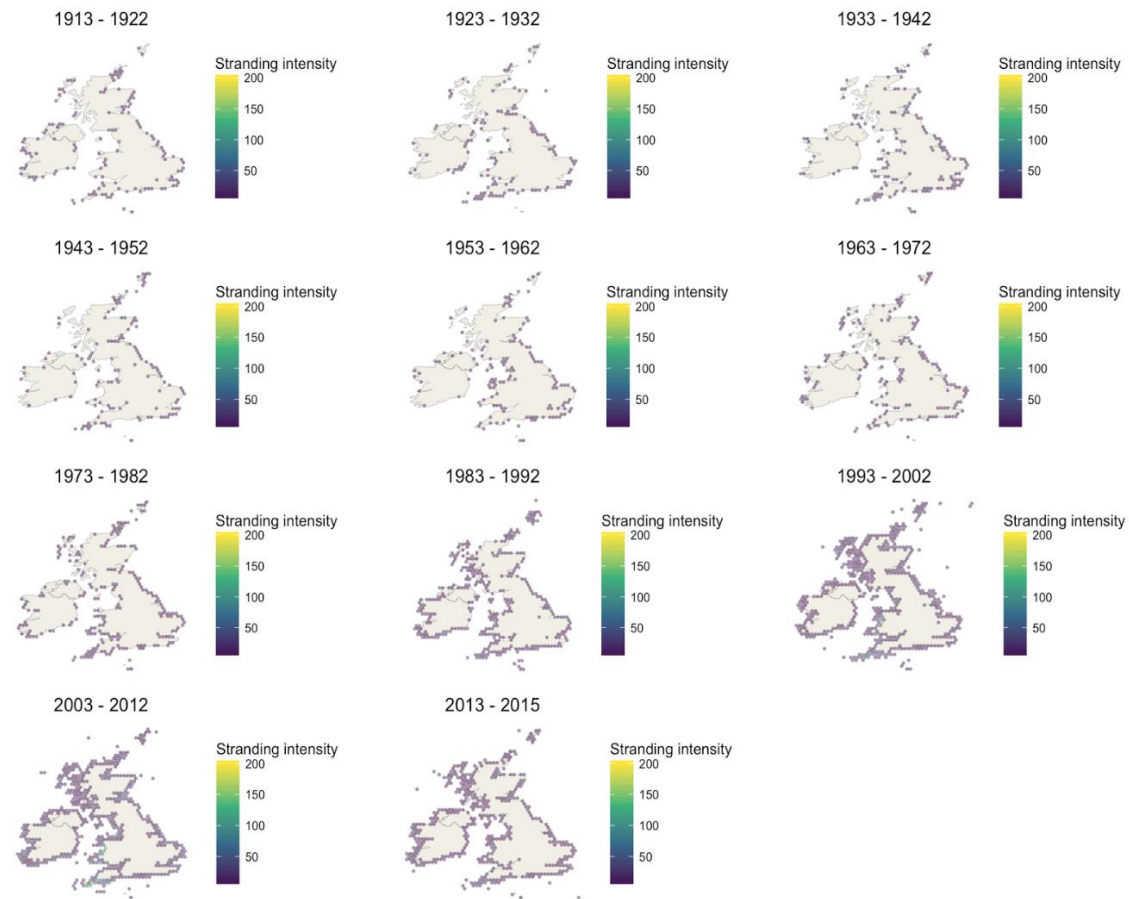
**Fig. S5.3.** Decadal maps of cetacean strandings around the UK and Ireland: 1913-2015. Stranding intensity is the number of cetaceans stranded within a decade within each hexagonal grid cell.
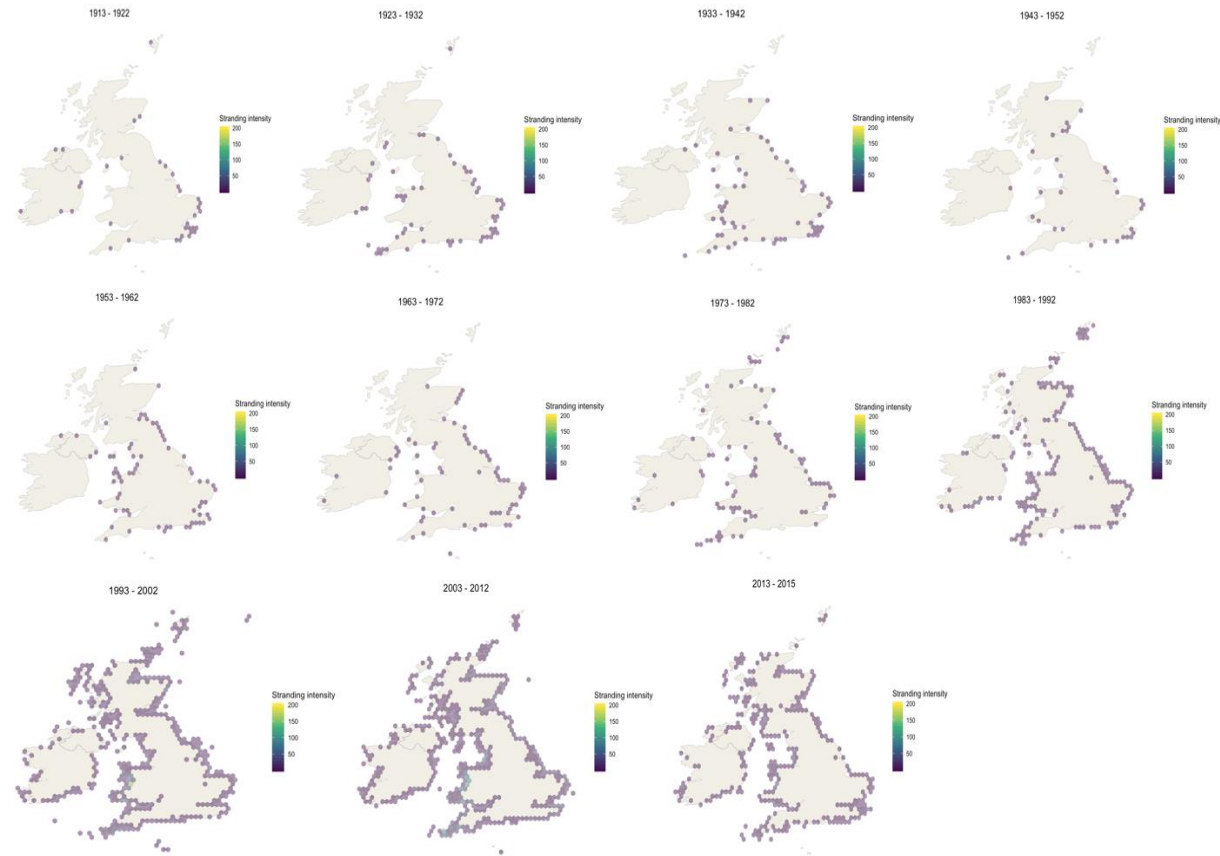
**Fig. S5.4.** Decadal maps of harbour porpoises (*Phocoena phocoena*) strandings around the UK and Ireland: 1913-2015. Stranding intensity is the number of cetacean strandings within a decade, shown within each hexagonal grid cell.
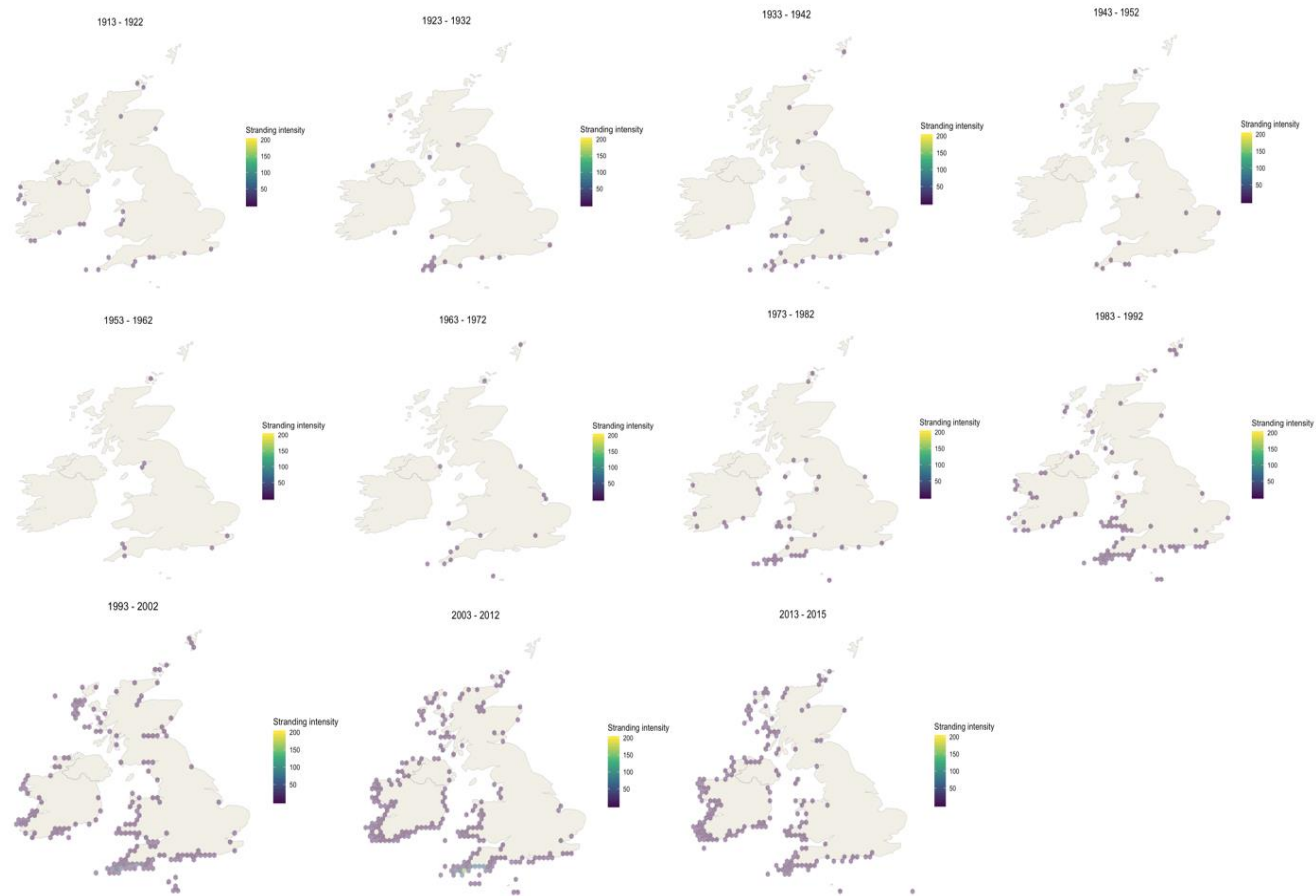
**Fig. S5.5.** Decadal maps of common dolphins (*Delphinus delphis*) strandings around the UK and Ireland: 1913-2015. Stranding intensity is the number of cetacean strandings within a decade, shown within each hexagonal grid cell.
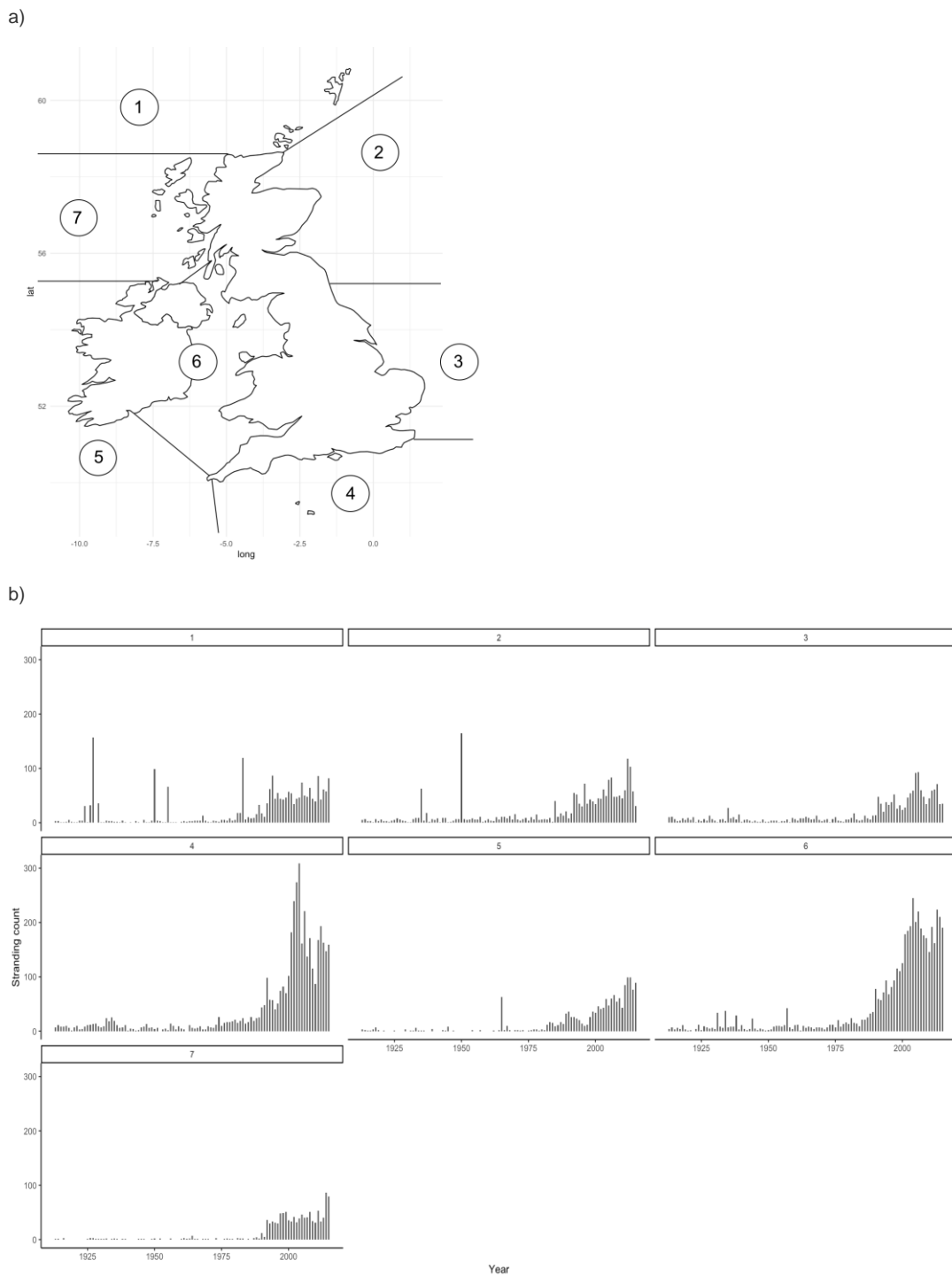
**Fig. S5.6.** Regional cetacean stranding counts from 1913 – 2015. **a)** A map of the UK and Ireland split into 7 regional zones as in MacLeod et al., 2004. Zones are as follows: 1) North Atlantic coasts, $n$ = 2150; 2) Northern North Sea coasts, $n$ = 2101; 3) Southern North Sea coasts, $n$ = 1663, 4) English Channel coasts, $n$ = 4231; 5) Southern Atlantic coast, $n$ = 1514; 6) Irish Sea coasts, $n$ = 4613; 7) Mid-Atlantic coasts, $n$ = 1118, NA = 101. **b)** Yearly stranding counts from 1913 - 2015 for each of the 7 regions.

**GAM candidate response distributions**

There are several possible candidate response distributions for the GAMs we fitted, therefore we repeated the models using negative binomial, Poisson, quasi-Poisson and Tweedie candidate response distributions. Below are the model diagnostic plots for each distribution (Fig. S1; S4). The negative binomial gave the best model diagnostics (Fig. S1) and was therefore used in the models reported in the paper.
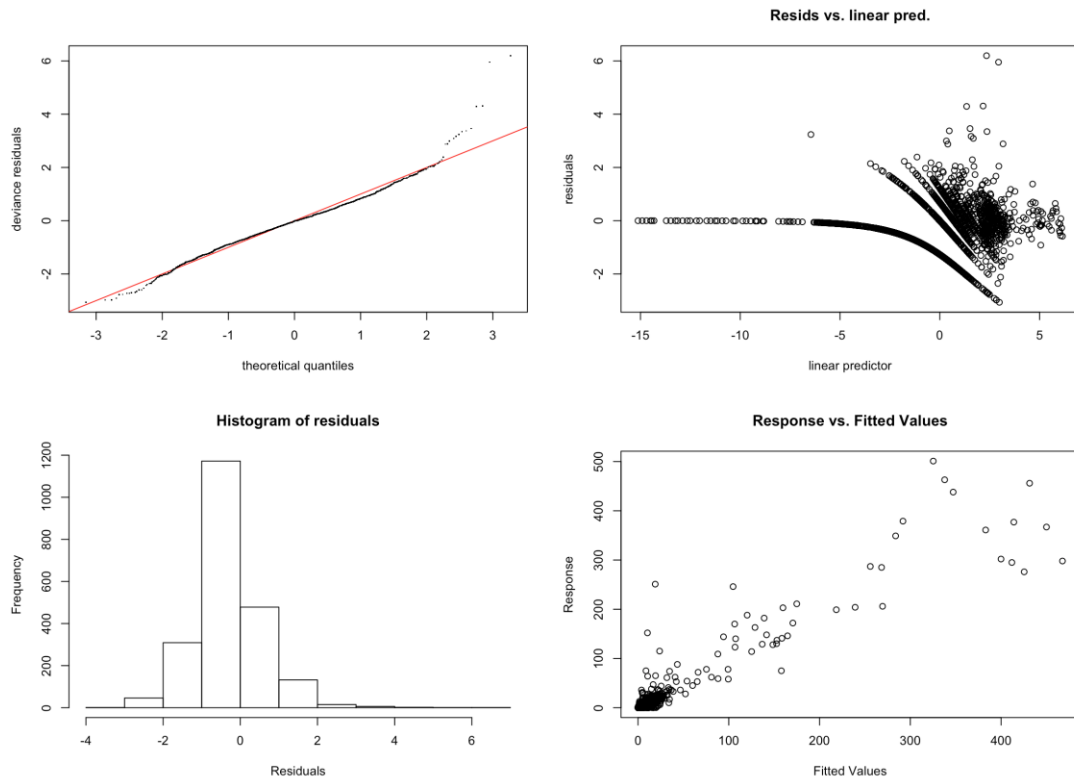


**Fig. S5.7.** Generalised additive model (GAM) check plots for all strandings using negative binomial response count distribution. The Q-Q plot (top left) shows the closest fit to a y=x line, here this shows a good model fit. The histogram of residuals (bottom left) also shows a normal distribution, suggesting that most of the residuals fall around the mean. The residuals vs. linear predictors plot (top right) shows that there is some heteroscedasticity in the data set i.e., there is an increase in the residuals with increasing values of the linear predictor. The response vs. fitted values show a normal distribution (bottom right). The residuals were smallest when modelled using a negative binomial response distribution suggesting the best model fit.
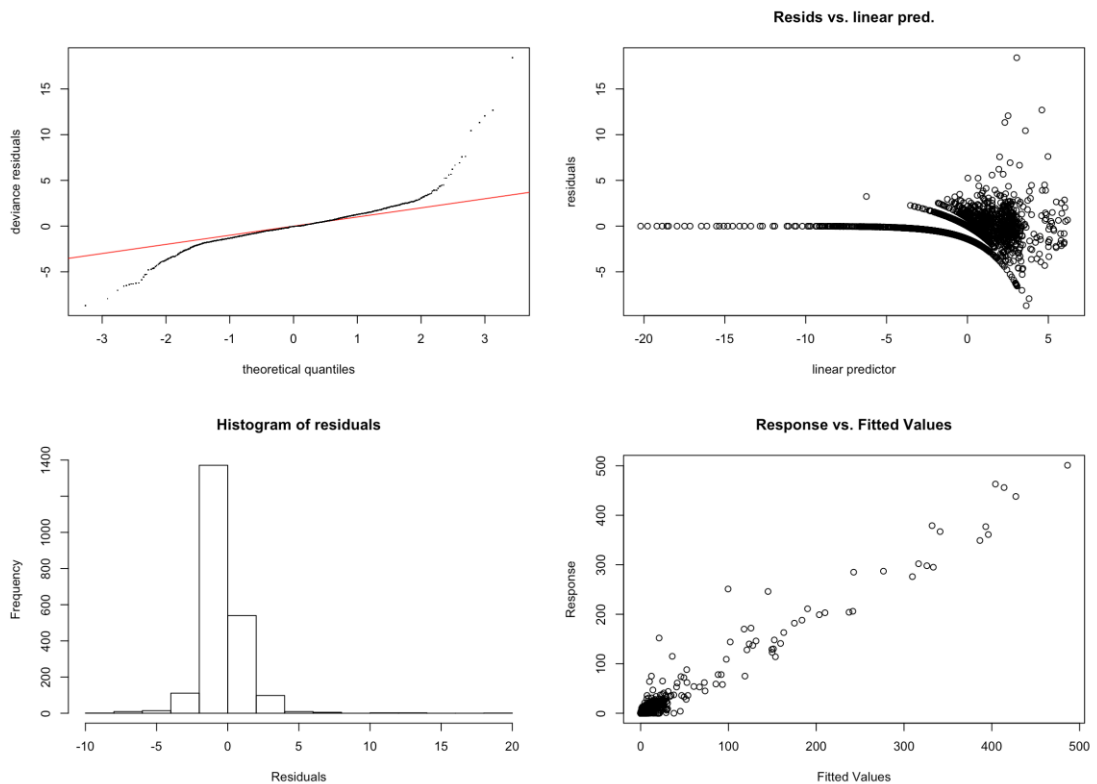
**Fig. S5.8.** Generalised additive model (GAM) check plots for all strandings using a Poisson response count distribution. The Q-Q plot (top left) shows the closest fit to a y=x line, here this shows a poorer model fit when compared to the negative binomial response distribution (**Fig. S5.7**). The histogram of residuals (bottom left) shows a normal distribution, suggesting that most of the residuals fall around the mean. The residuals vs. linear predictors plot (top right) shows that there is some heteroscedasticity in the data set. The residuals are much higher than when fitting the model with a negative binomial response distribution. The response vs. fitted values show a normal distribution (bottom right). The larger residuals and poor Q-Q plot meant that the Poisson response distribution was not used in our model.
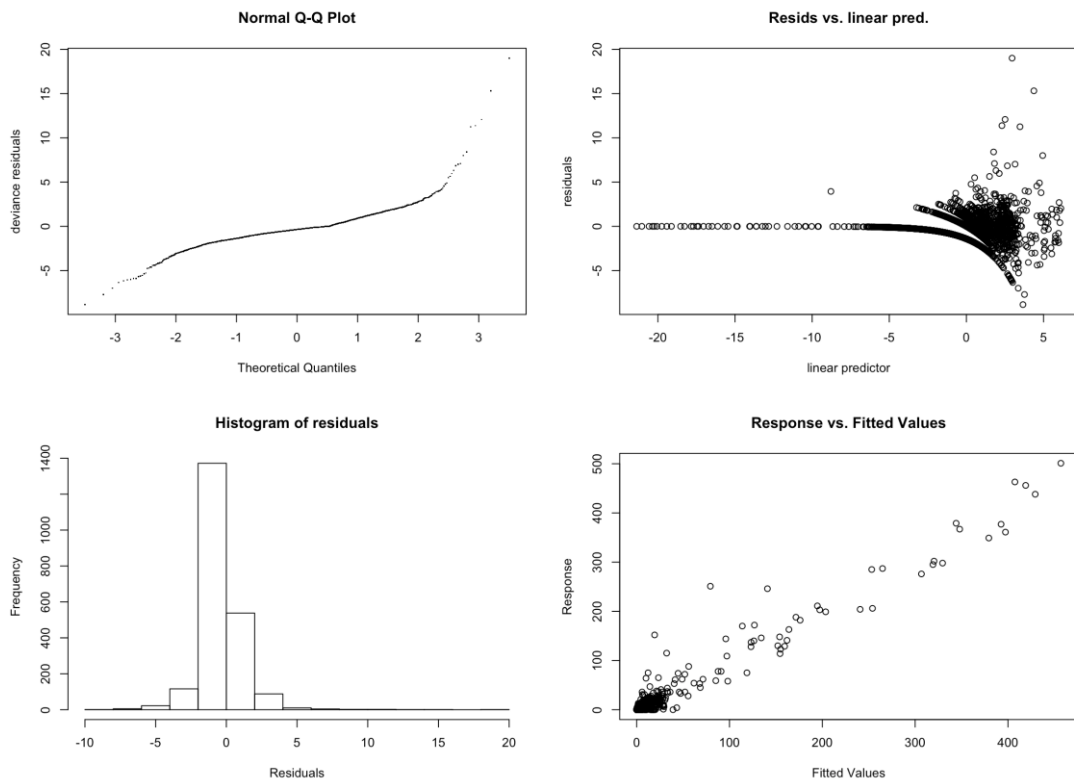
**Fig. S5.9.** Generalised additive model (GAM) check plots for all strandings using a quasi-Poisson response count distribution. The Q-Q plot (top left) shows the closest fit to a y=x line, here this shows a poor model fit, particularly when compared to the negative binomial response distribution (**Fig. S5.7**). The histogram of residuals (bottom left) shows a normal distribution, suggesting that most of the residuals fall around the mean. The residuals vs. linear predictors plot (top right) shows that there is some heteroscedasticity in the data set. The residuals are much higher than when fitting the model with a negative binomial response distribution. The response vs. fitted values show a normal distribution (bottom right). The larger residuals and poor Q-Q plot meant that the quasi-Poisson response distribution was not used in our model.
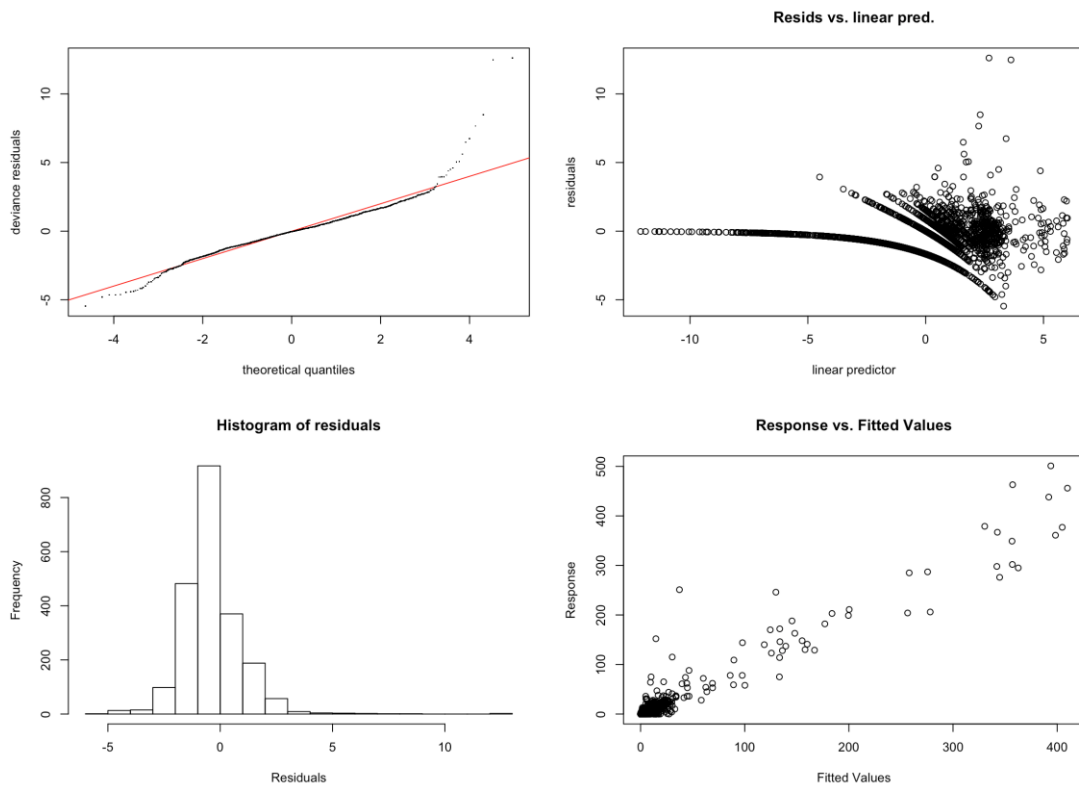
**Fig. S5.10.** Generalised additive model (GAM) check plots for all strandings using a Tweedie response count distribution. The Q-Q plot (top left) shows the closest fit to a y=x line, here this shows a reasonable fit. The histogram of residuals (bottom left) shows a normal distribution, suggesting that most of the residuals fall around the mean. The residuals vs. linear predictors plot (top right) shows that there is some heteroscedasticity in the data set. The residuals are much higher than those obtained when fitting the model with a negative binomial response distribution (Fig. S5.7). The response vs. fitted values show a normal distribution (bottom right). The larger residuals meant that the Tweedie response distribution was not used in our model.

**GAM model checking**

GAMs are flexible and can provide a good fit in the presence of noise in the predictor variables, or for nonlinear relationships. However, caution must be taken to not over fit the data and it is important to obtain diagnostic information about the fitting procedure and model fit. We fitted our models using several response distributions (see section above). Standard GAM checks showed that a negative binomial response distribution had the best model fit (Fig. S1). Residual checking can be done in much the same way as for GLMs and assumes basic assumptions such as normality of residuals and equality of variance. The negative binomial response distribution was used in our model. The GAM checks (Fig. S1) assessed data normality via a Q-Q plot and histogram. The Q-Q plot for negative binomial shows the closest fit to a 1:1 line, this shows a good model fit. The histogram of residuals also shows a normal distribution, suggesting that most of the residuals fall around the mean. The residuals vs. linear predictors plot shows that there is some heteroscedasticity in the data set i.e., there is an increase in the residuals with increasing values of the linear predictor. The response vs. fitted values show a normal distribution. The residuals were smallest in the negative binomial plot, suggesting a better model fit.

**Setting the k parameter**

In a GAM, k is the maximum complexity of the basis used to represent the smooth term. When a value for k is not specified, the model uses basic specific default values. If the k value is high enough, we can be sure that there is enough flexibility in the model. If this is not high enough, we can specify the complexity for the smooth term by manually setting the k parameter if needed. We can find out if k is high enough by increasing the k value and refitting the original model. These statistical changes can be checked by examining the *P*-values, k' and estimated degrees of freedom (EDF) values in the basis dimension of the standard GAM output. If there are no statistically important changes after doing this, then k is large enough. The EDF can be interpreted as how much of the variable is smoothed. A higher EDF implies that the splines are more complex.

**Residuals by covariate**

As part of the model validation process, we made additional checks for model fit that looked at the per-covariate residuals. This validation was made for the final model that looked at all strandings and used a negative binomial response count distribution. Checking the covariate residuals allows us to see whether the spread in the data varies between bins of residuals and can highlight important model deficiencies. Variation within each box plot should be consistent (homoscedastic) if the model is a good fit. 'Whiskers' represent highest and lowest values that are not outliers (open circles) (Fig. S5). Low variation in the covariate residuals suggests that the model is a good fit (Fig. S5).

**a. SST**

**b. Storms**

**c. Geomagnetic**

**d. NAO**

**e. Fishing catch**
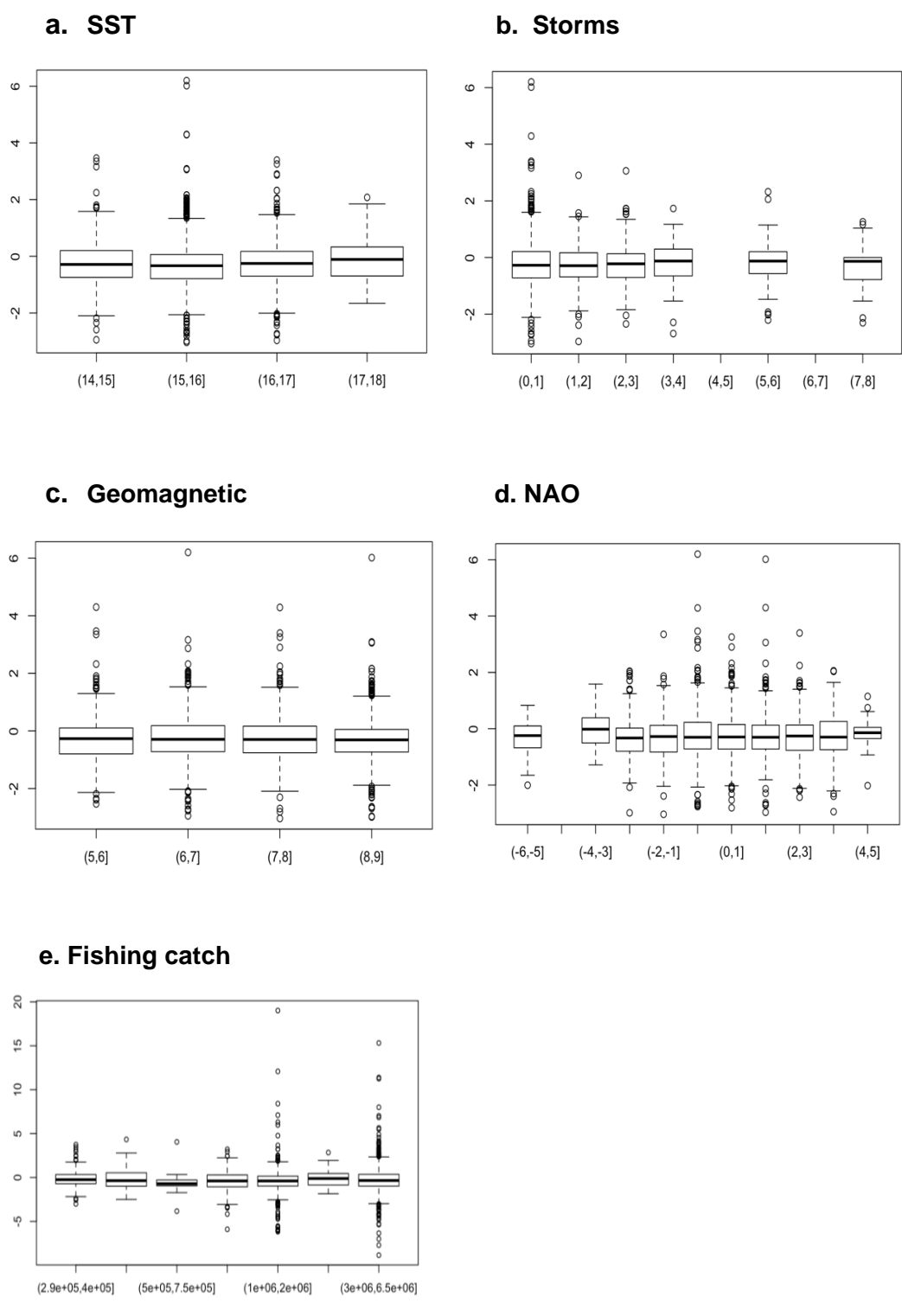
**Fig. S5.11.** Residuals by covariate to confirm the goodness of our model fit. These residuals were taken from the final model, which was modelled using a negative binomial response count distribution. **a.** Sea surface temperature (SST) residuals, **b.** Storm count residuals, **c.** Geomagnetic K-index residuals, **d.** North Atlantic Oscillation

(NAO) residuals, **e.** Fishing catch residuals.   Low variation in these covariate residuals suggest that the model is a good fit.

## Removing *Phocoena phocoena* from the data set

47% of the data set is made up of harbour porpoise (*Phocoena phocoena)* records, as these small cetaceans are very common off the UK and Ireland. To ensure that our results were not merely reflecting signal in the harbour porpoise data we repeated our analyses removing these species records, and then for harbour porpoises separately.
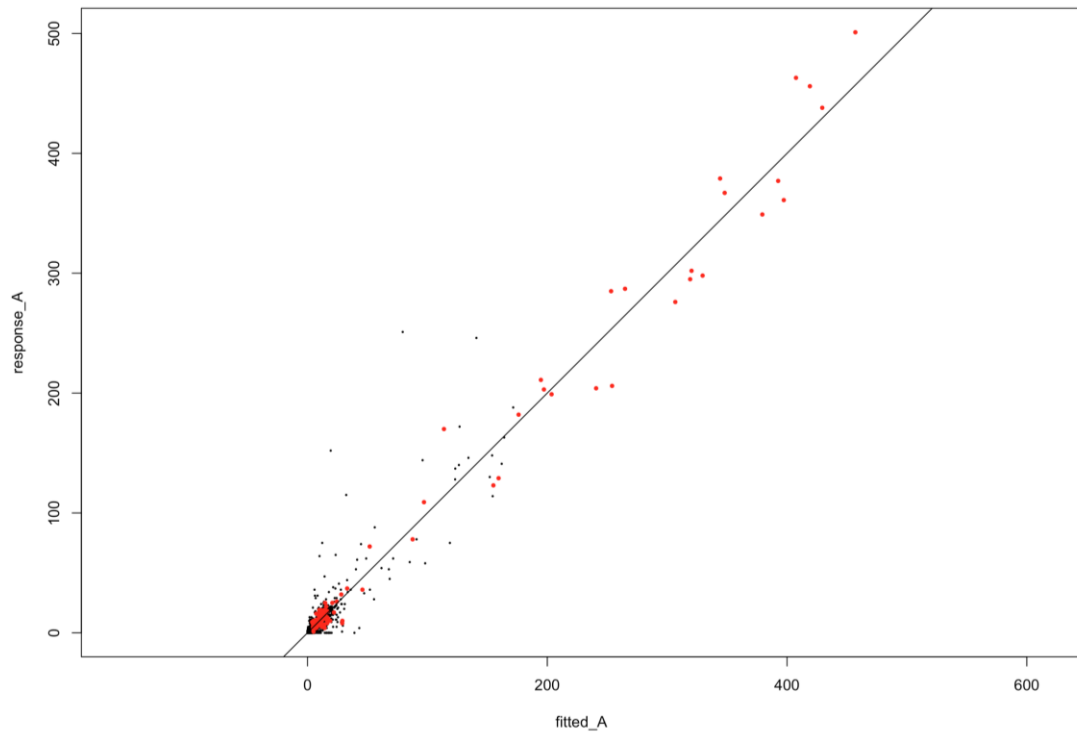


**Fig. S5.12.** All strandings plotted with their response. Here the y axis shows the response of all strandings as fitted in the final Generalised additive model (with negative binomial response distribution), and the x axis shows the fitted values from the same model. Harbour porpoises (*Phocoena phocoena*) are highlighted in red, showing their response distribution compared to other species (shown in black). Code for running this analysis and identifying specific responses is available at https://github.com/EllenJCoombs/cetacean-strandings-project
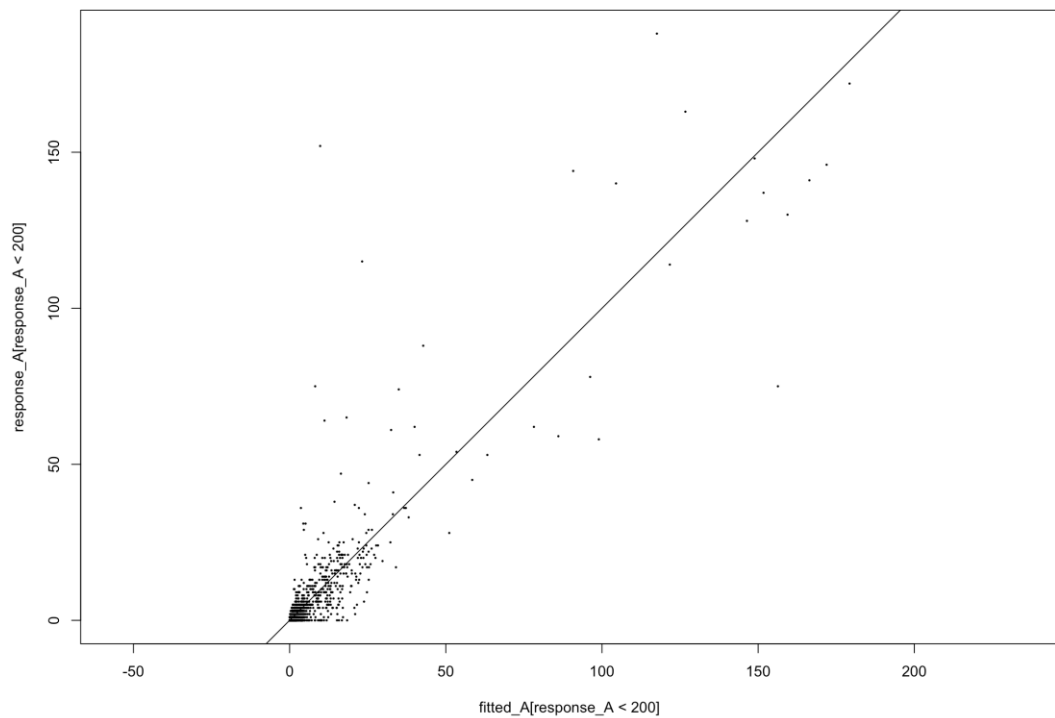
**Fig. S5.13.** Strandings plotted with harbour porpoises (*Phocoena phocoena*) removed. Here the y axis shows the response of strandings as fitted in the Generalised additive model (with negative binomial response distribution), and the x axis shows the fitted values from the same model with harbour porpoises removed. Harbour porpoises (*Phocoena phocoena*) are highlighted in red, showing their response distribution compared to other species (shown in black). Code for running this analysis and identifying specific responses is available at https://github.com/EllenJCoombs/cetacean-strandings-project

**Supplemental results**

**Correlates of strandings through time for all species**

[Figure on next page]

e.

f.
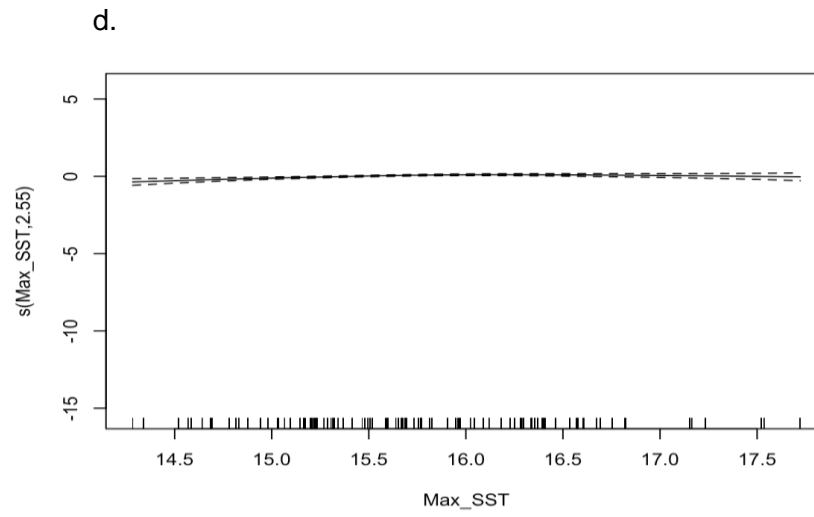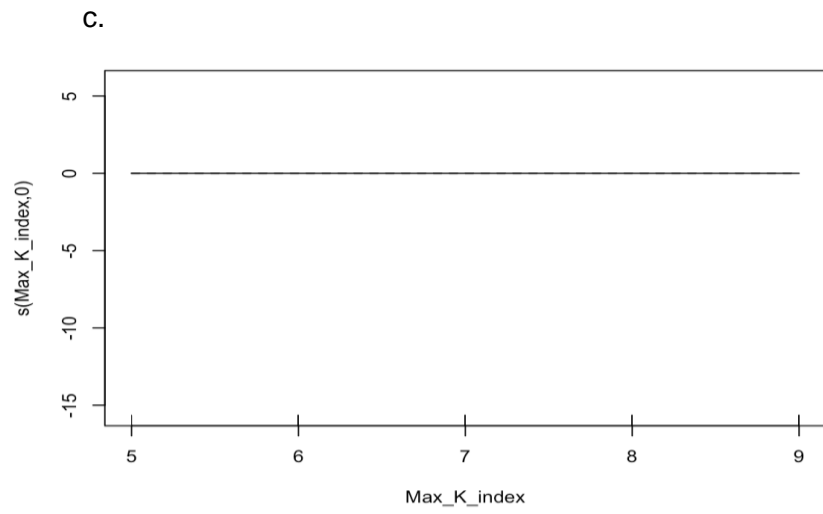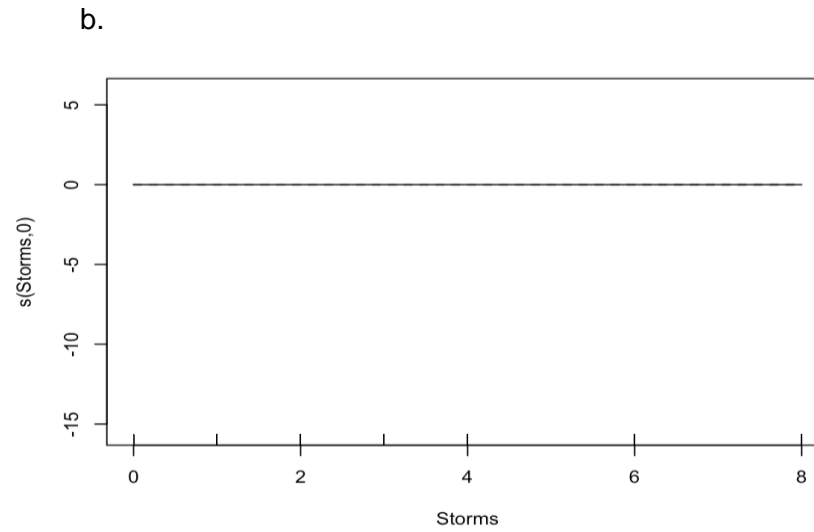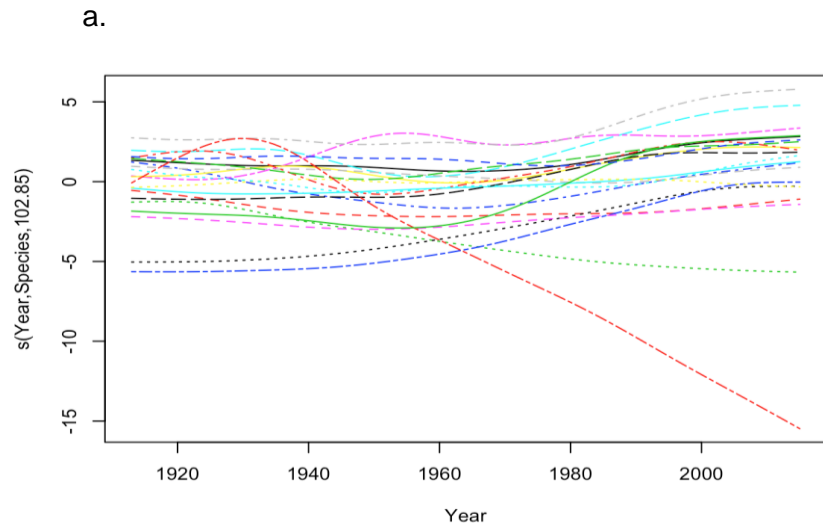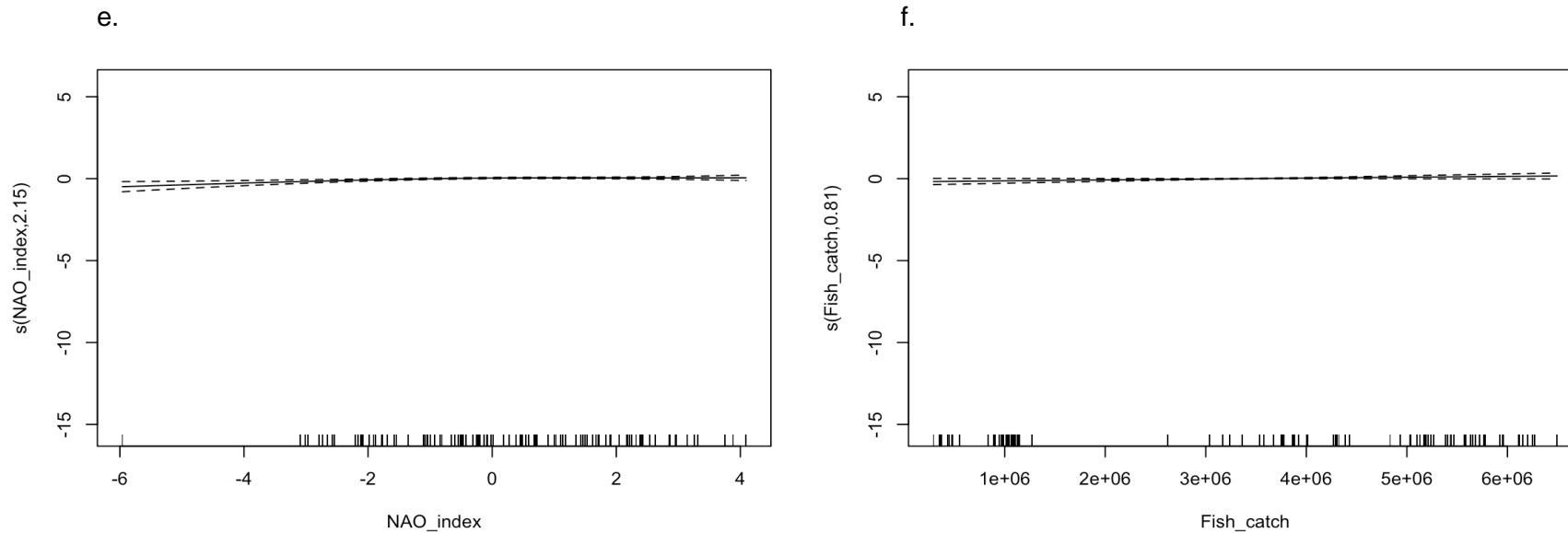


[Figures on this and previous page]

**Fig. S5.14.** GAM summary plots for variables included in the final model of correlates of cetacean strandings: **a.** Factor-smooth interaction between year of stranding and species, **b.** Storm events, **c.** Geomagnetic fluctuations, **d.** Maximum sea surface temperatures, **e.** North Atlantic Oscillation index, **f.** Annual fishing catch. Modelled using the negative binomial response count distribution. The model with all strandings had a deviance explained of 84.5%, $n = 2163$.

**Correlates of strandings through time with all rare and 'unknown' records included**



a.

b.

c.

d.

527

e.

f.
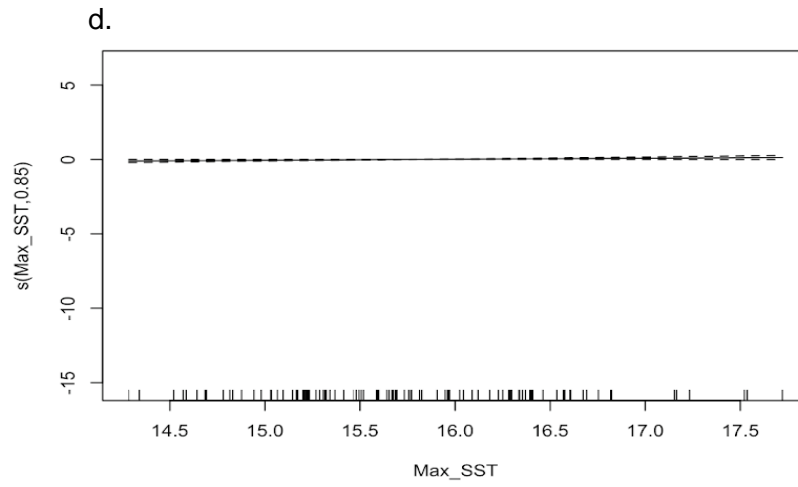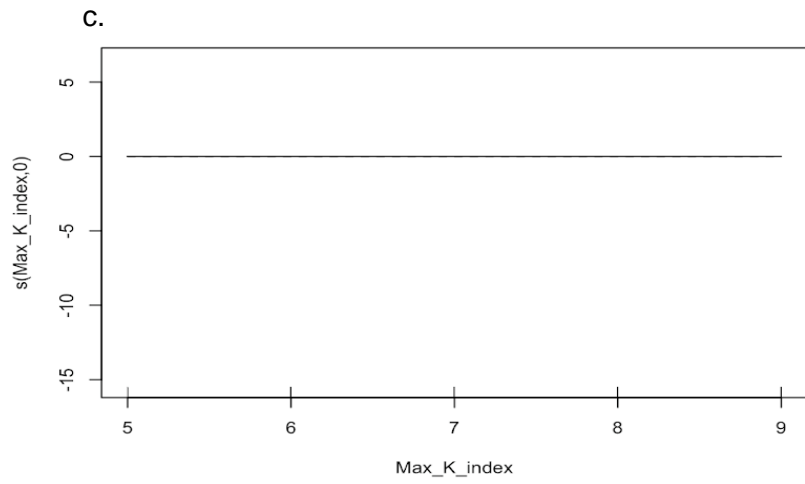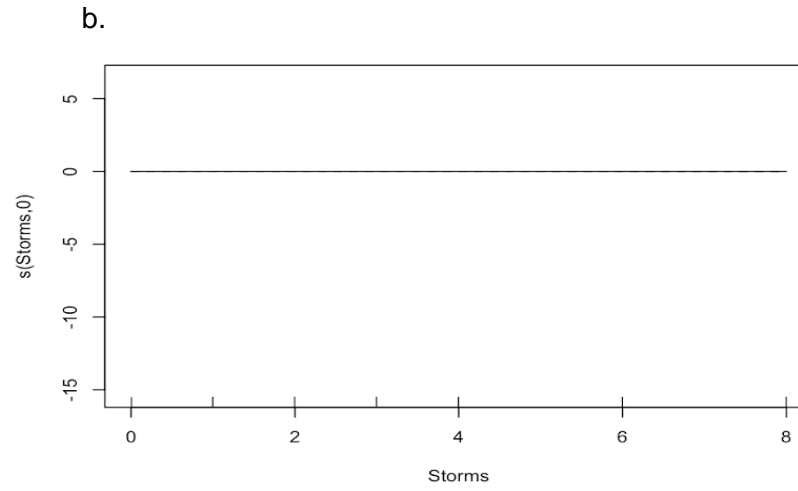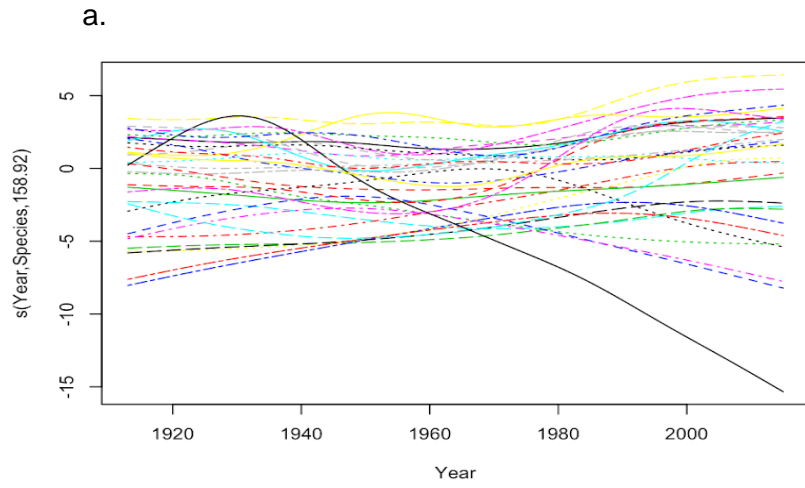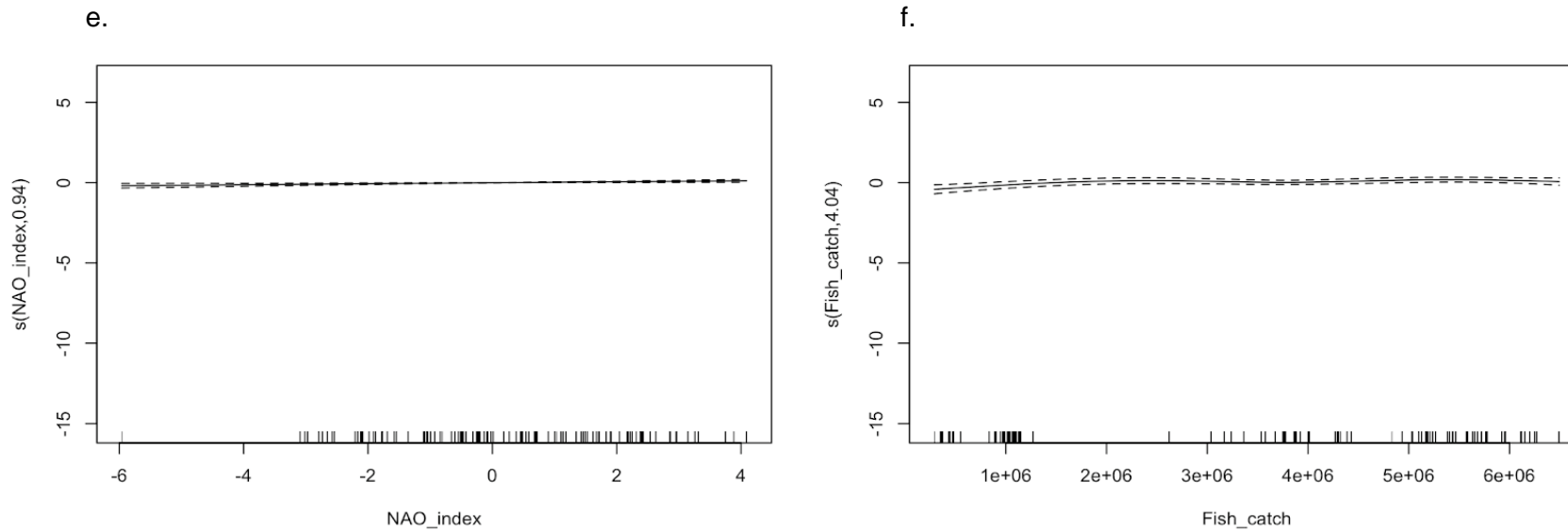
[Figures on this and previous page]

**Fig. S5.15.** GAM summary plots for model which contains all species, including 'rare' and 'unknown' identifications. **a.** Factor-smooth interaction between year of stranding and species, **b.** Storm events**, c.** Geomagnetic fluctuations, **d.** Maximum sea surface temperatures**, e.** North Atlantic Oscillation index, f. Annual fishing catch. Modelled using the negative binomial response count distribution. The model with all strandings had a deviance explained of 88%, n = 3502.

**Table S5.4.** Correlates of strandings GAM output with 'rare' and 'unknown' records included. s() are smooths of the explanatory variables. 'Storms' is storm count, 'Max_K_index' is the geomagnetic K-index, 'Max_SST' is the maximum yearly sea surface temperature, 'NAO_index' is the North Atlantic Oscillation, 'Fish_catch' is annual fish catch. EDF shows the estimated degrees of freedom (EDF) for each of the different predictor variables. The P-values shows whether the smooth of that variable is significantly different from "no effect", i.e., if we estimated the "smooth" as a flat line at zero. k shows the maximum basis complexity.

| Correlates as modelled | EDF | *P*-value | k |
|---|---|---|---|
| s(Storms) | < 0.005 | 0.56 | 6.00 |
| s(Max_K_index) | < 0.005 | 0.57 | 3.00 |
| s(Max_SST) | 0.85 | 0.02 | 9.00 |
| s(NAO_index) | 0.94 | < 0.005 | 9.00 |
| s(Fish_catch) | 4.04 | < 0.001 | 9.00 |
| s(Year, Species) | 158 | < 0.001 | 210 |

**Correlates of strandings through time – strandings at genus-level**
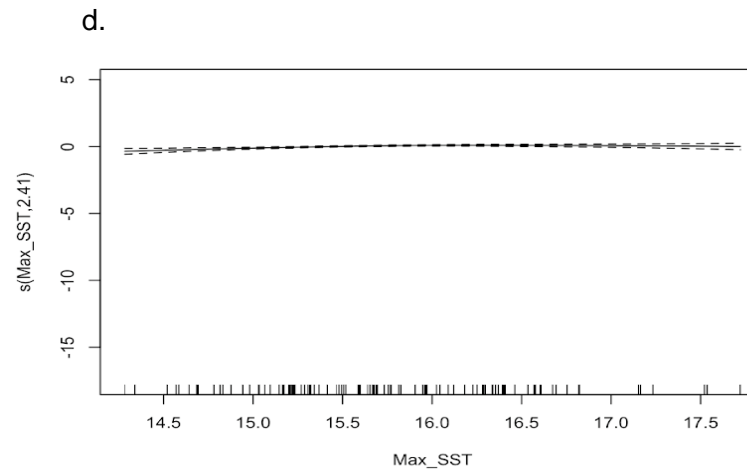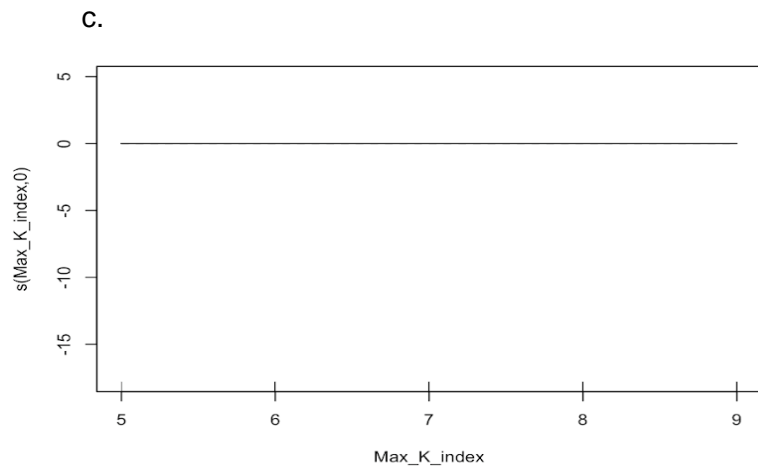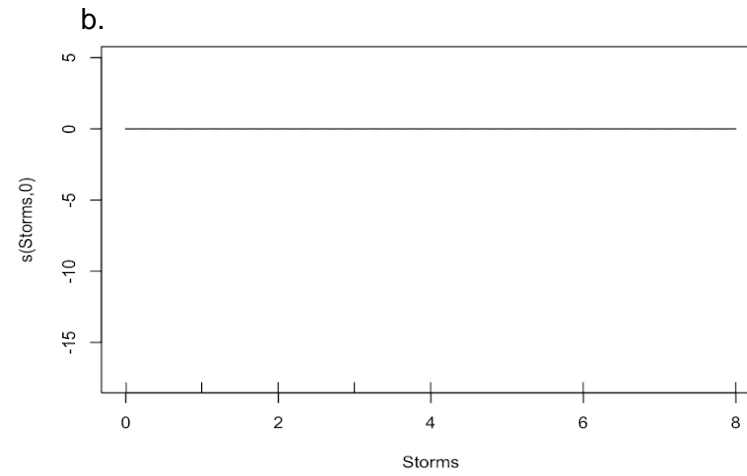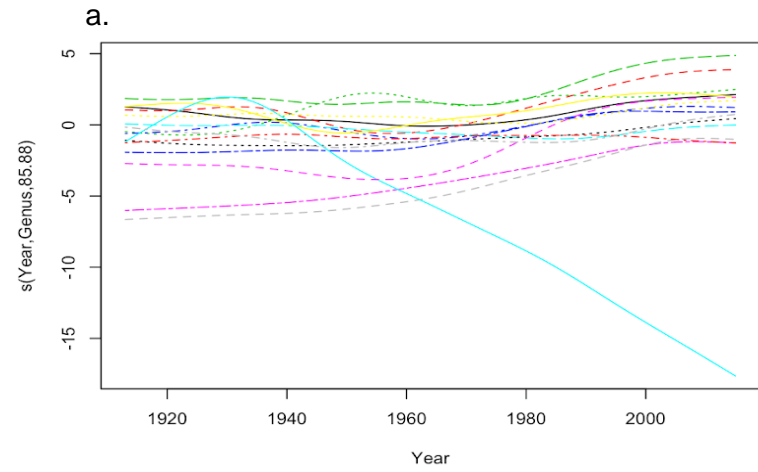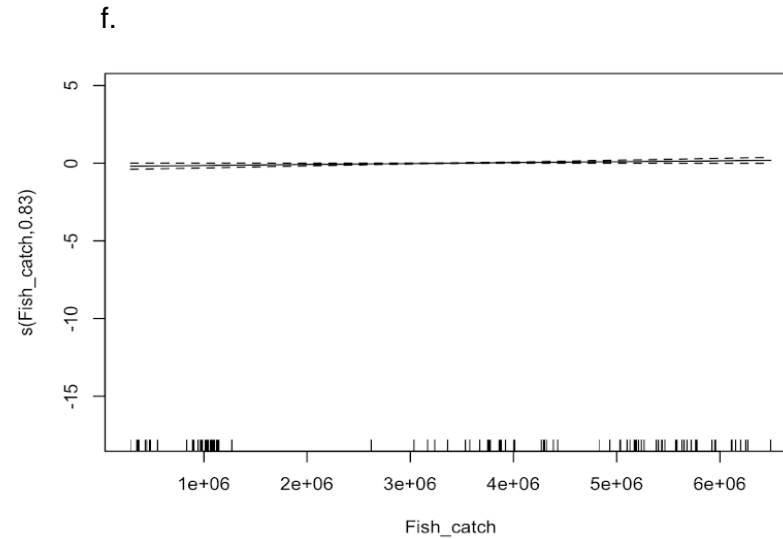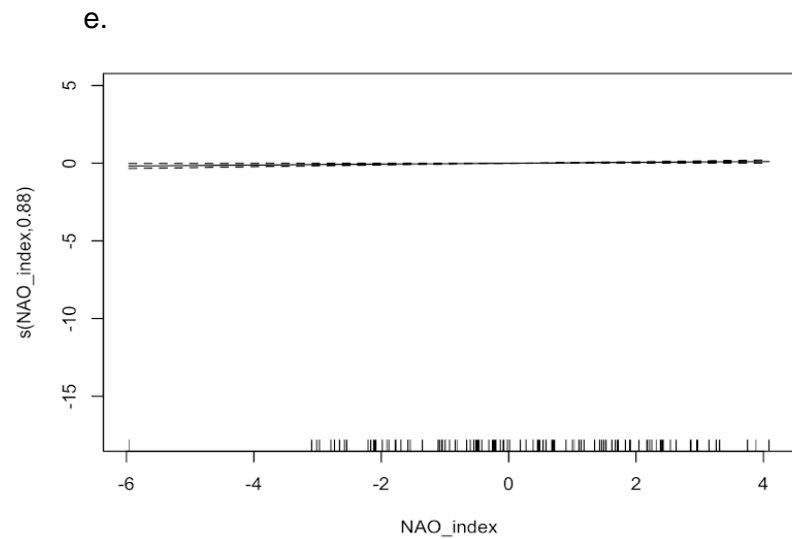
[Figures on this and previous page]

**Fig. S5.16**. GAM summary plots for model which contains all strandings at the genus level. **a.** Factor-smooth interaction between year of stranding and species, **b.** Storm events, **c.** Geomagnetic fluctuations, **d.** Maximum sea surface temperatures, **e.** North Atlantic Oscillation index, **f.** Annual fishing catch. Modelled using the negative binomial response count distribution. The model with all strandings had a deviance explained of 84.2%, $n = 1648$.

**Table S5.5.** Correlates of strandings GAM output with records at the genus-level. s() are smooths of the explanatory variables. 'Storms' is storm count, 'Max_K_index' is the geomagnetic K-index, 'Max_SST' is the maximum yearly sea surface temperature, 'NAO_index' is the North Atlantic Oscillation, 'Fish_catch' is annual fish catch. EDF shows the estimated degrees of freedom (EDF) for each of the different predictor variables. The P-values shows whether the smooth of that variable is significantly different from "no effect", i.e., if we estimated the "smooth" as a flat line at zero. k shows the maximum basis complexity.

| Correlates as modelled | EDF | *P-value* | k |
|---|---|---|---|
| s(Storms) | < 0.001 | 0.88 | 6.00 |
| s(Max_K_index) | < 0.001 | 0.71 | 3.00 |
| s(Max_SST) | 2.41 | < 0.001 | 9.00 |
| s(NAO_index) | 0.88 | 0.01 | 9.00 |
| s(Fish_catch) | 0.83 | 0.01 | 9.00 |
| s(Year, Genus) | 85.9 | < 0.001 | 210 |

**Correlates of strandings through time using only CSIP & IWDG stranding data (1990 – 2015)**

e.

f.

g.
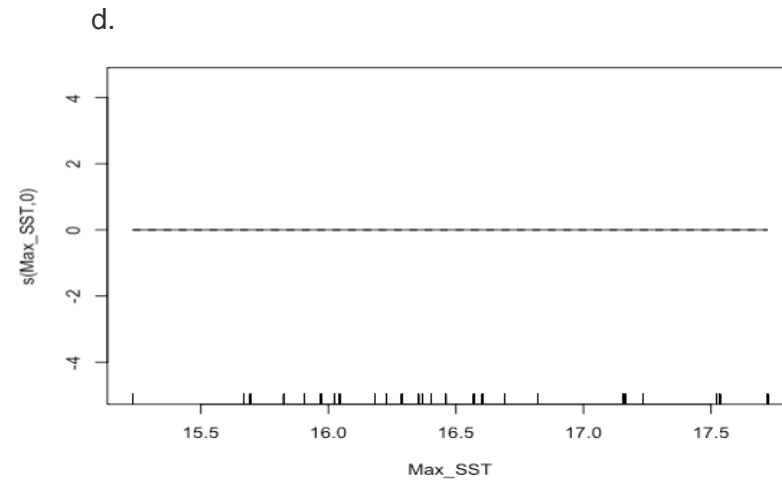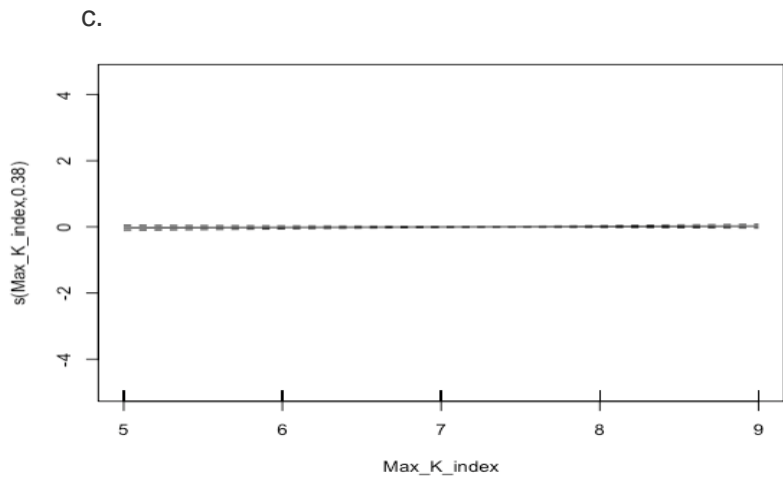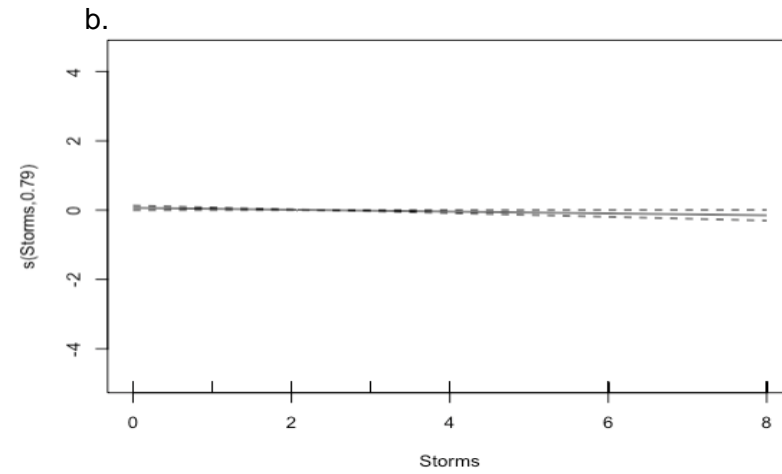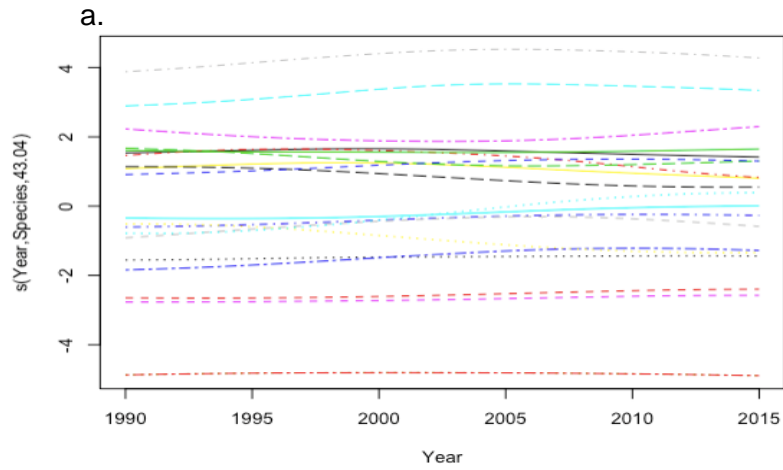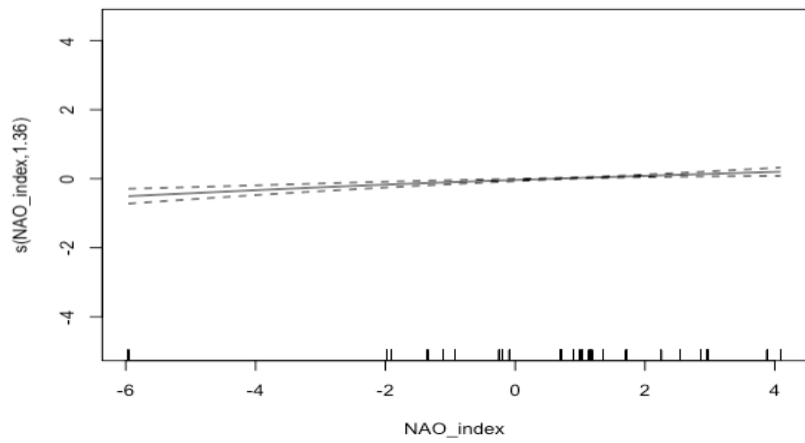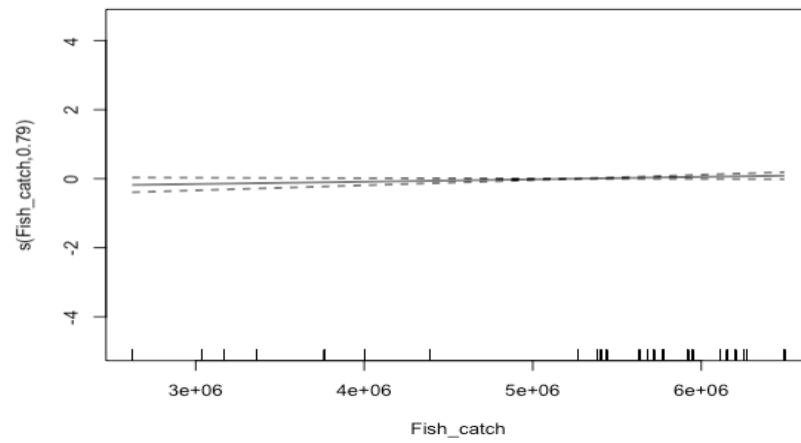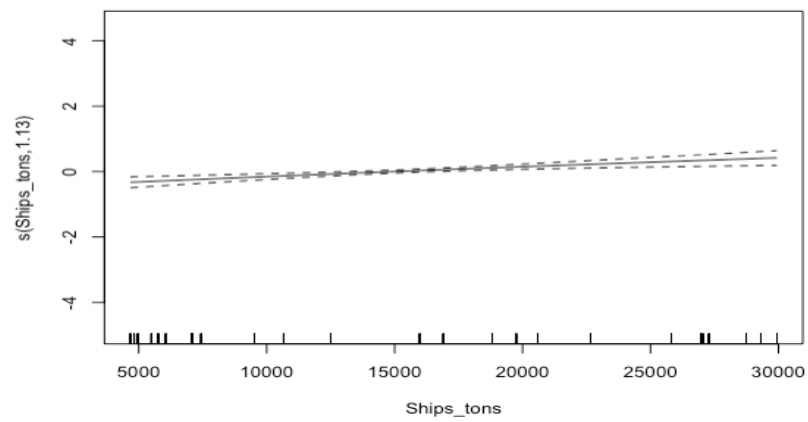
**Fig. S5.17.** GAM summary plots for model which contains CSIP and IWDG strandings only (1990-2015). **a.** Factor-smooth interaction between year of stranding and species, **b.** Storm events, **c.** Geomagnetic fluctuations, **d.** Maximum sea surface temperatures, **e.** North Atlantic Oscillation index, **f.** Annual fishing catch, **g.** Shipping traffic. Modelled using the negative binomial response count distribution. The model with CSIP and IWDG strandings had a deviance explained of 94.4%, $n = 546$.

**Table S5.6.** Correlates of strandings GAM output with CSIP and IWDG strandings only. s() are smooths of the explanatory variables. 'Storms' is storm count, 'Max_K_index' is the geomagnetic K-index, 'Max_SST' is the maximum yearly sea surface temperature, 'NAO_index' is the North Atlantic Oscillation, 'Fish_catch' is annual fish catch, 'Ship_tons' is a proxy for shipping traffic. EDF shows the estimated degrees of freedom (EDF) for each of the different predictor variables. The P-values shows whether the smooth of that variable is significantly different from "no effect", i.e., if we estimated the "smooth" as a flat line at zero. k shows the maximum basis complexity.

| Correlates as modelled | EDF | *P*-value | k |
|---|---|---|---|
| s(Storms) | 0.79 | 0.02 | 6.00 |
| s(Max_K_index) | 0.38 | 0.18 | 3.00 |
| s(Max_SST) | < 0.001 | 0.92 | 9.00 |
| s(NAO_index) | 1.36 | < 0.001 | 9.00 |
| s(Fish_catch) | 0.79 | 0.02 | 9.00 |
| s(Ships_tons) | 1.13 | < 0.001 | 9.00 |
| s(Year, Species) | 43.0 | < 0.001 | 210 |

**Correlates of strandings through time with *Phocoena phocoena* removed**



a.

b.

c.

d.
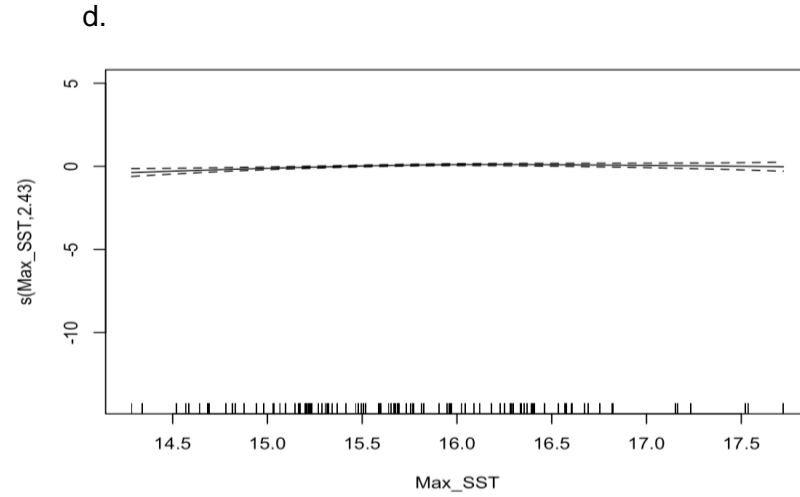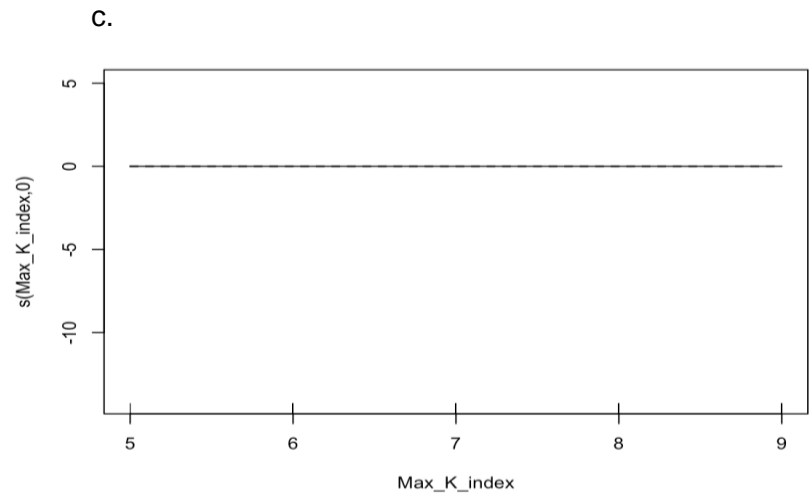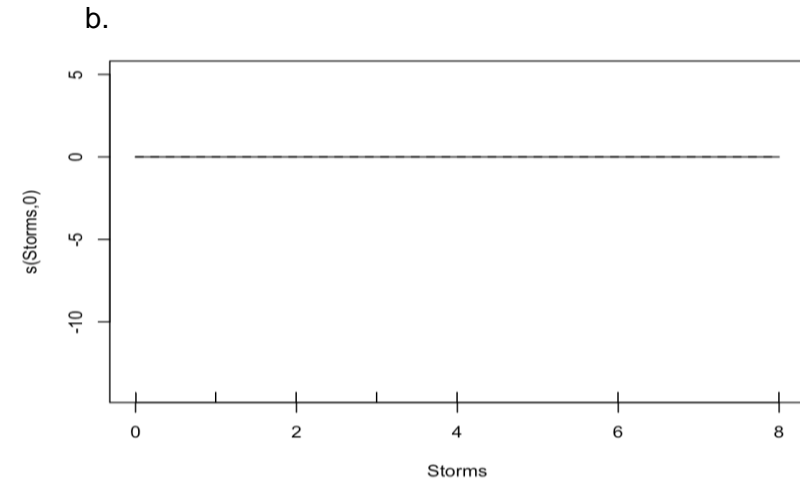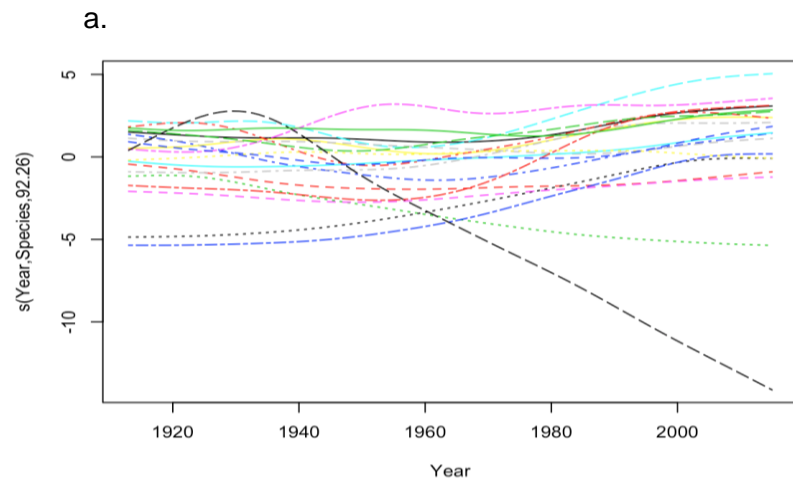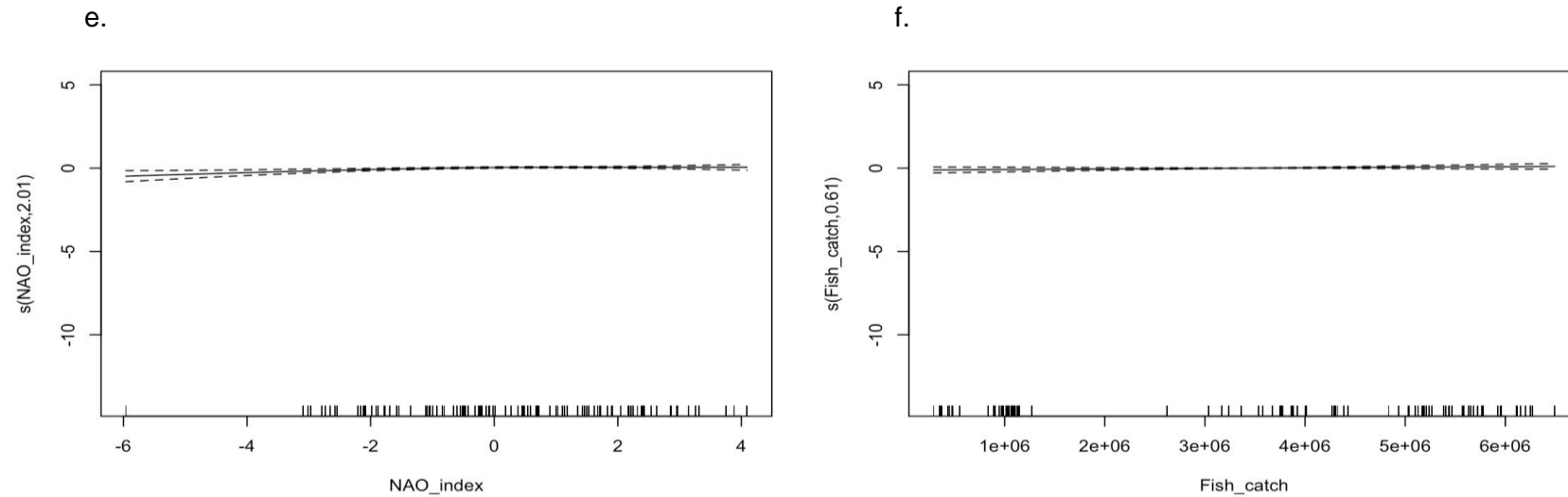
[Figures on this and previous page]

**Fig. S5.18.** GAM summary plots for variables included in the final model of correlates of cetacean strandings with harbour porpoises (*Phocoena phocoena*) removed: **a.** Factor-smooth interaction between year of stranding and species, **b.** Storm events, **c.** Geomagnetic fluctuations, **d.** Maximum sea surface temperatures, **e.** North Atlantic Oscillation index, f. Annual fishing catch. Modelled using the negative binomial response count distribution. The model without harbour porpoise had a deviance explained of 77.4%, *n* = 2060.

**Table S5.7.** Correlates of strandings GAM output, with harbour porpoises removed. s() are smooths of the explanatory variables. 'Storms' is storm count, 'Max_K_index' is the geomagnetic K-index, 'Max_SST' is the maximum yearly sea surface temperature, 'NAO_index' is the North Atlantic Oscillation, 'Fish_catch' is annual fish catch. EDF shows the estimated degrees of freedom (EDF) for each of the different predictor variables. The P-values shows whether the smooth of that variable is significantly different from "no effect", i.e., if we estimated the "smooth" as a flat line at zero. k shows the maximum basis complexity.

| Correlates as modelled | EDF | *P*-value | k |
|---|---|---|---|
| s(Storms) | < 0.001 | 0.86 | 6.00 |
| s(Max_K_index) | < 0.001 | 0.69 | 3.00 |
| s(Max_SST) | 2.43 | < 0.001 | 9.00 |
| s(NAO_index) | 2.01 | 0.001 | 9.00 |
| s(Fish_catch) | 0.61 | 0.07 | 9.00 |
| s(Year, Species) | 92.3 | < 0.001 | 200 |

**Correlates of harbour porpoise (*Phocoena phocoena*) strandings through time**
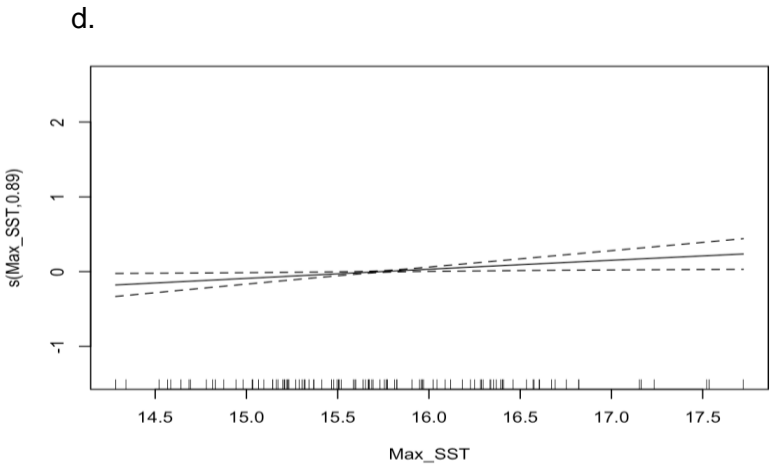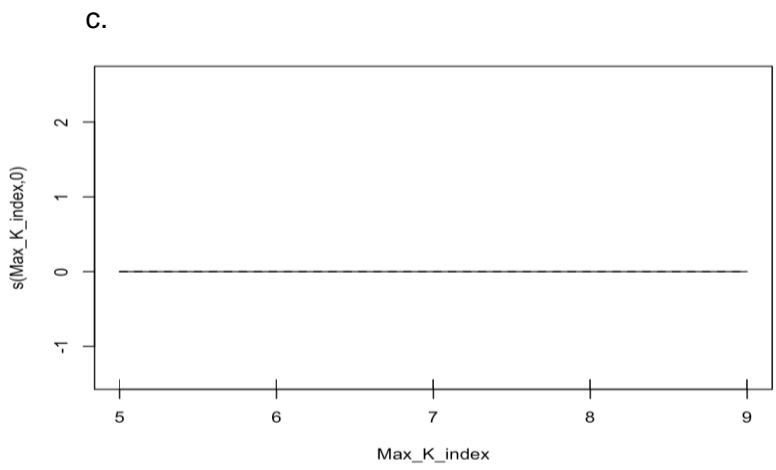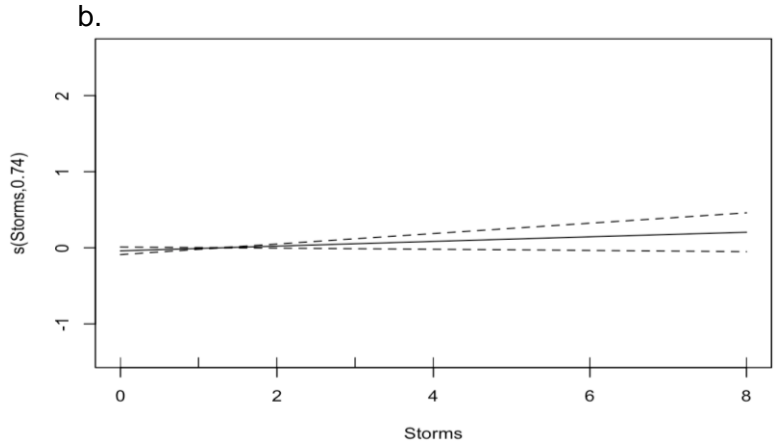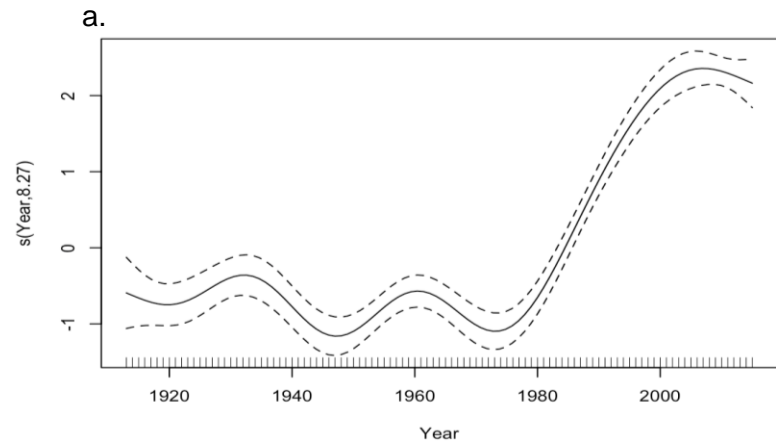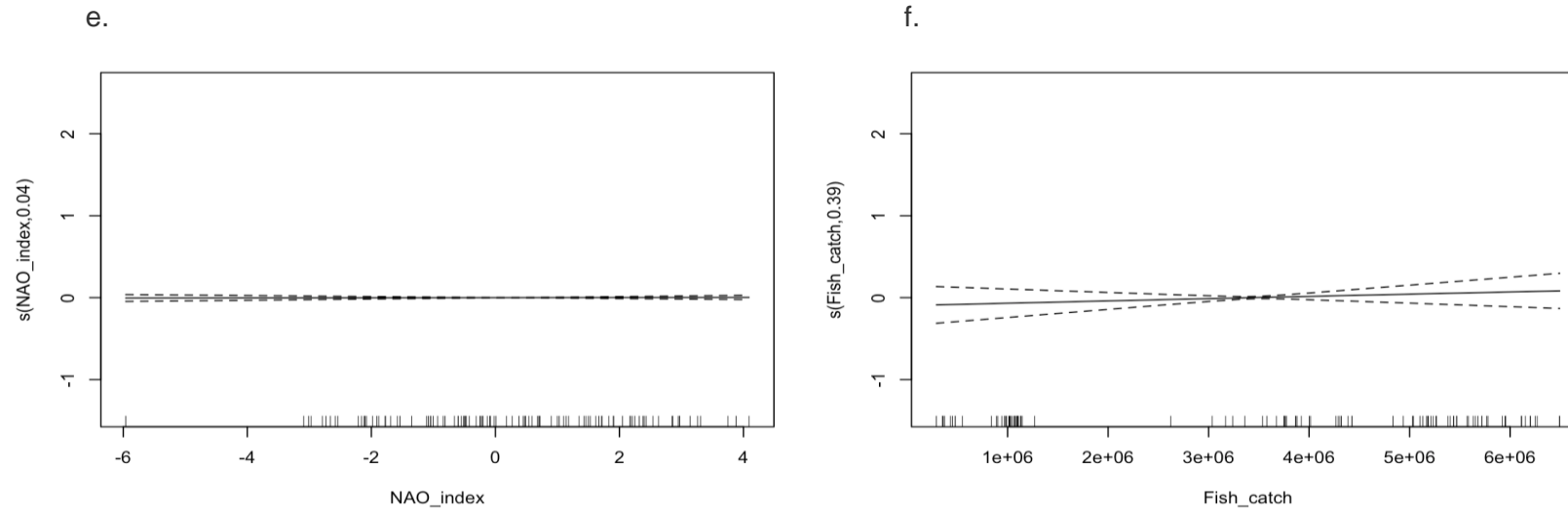
[Figures on this and previous page]

**Fig. S5.19**. GAM summary plots for variables included in the final model of correlates of cetacean strandings with harbour porpoises (*Phocoena phocoena*) only: **a.** Factor-smooth interaction between year of stranding and species, **b.** Storm events, **c.** Geomagnetic fluctuations, **d.** Maximum sea surface temperatures, **e.** North Atlantic Oscillation index, **f.** Annual fishing catch. Modelled using the negative binomial response count distribution. Correlates of stranding through time with harbour porpoises only. Note that no species smooth was given as harbour porpoises were the sole species in this model. Deviance explained = 96.9%, *n* = 103.

**Table S5.8.** Correlates of strandings GAM output, with harbour porpoises only. s() are smooths of the explanatory variables. 'Storms' is storm count, 'Max_K_index' is the geomagnetic K-index, 'Max_SST' is the maximum yearly sea surface temperature, 'NAO_index' is the North Atlantic Oscillation, 'Fish_catch' is annual fishing catch. EDF shows the estimated degrees of freedom (EDF) for each of the different predictor variables. The *P*-values shows whether the smooth of that variable is significantly different from "no effect", i.e., if we estimated the "smooth" as a flat line at zero. k shows the maximum basis complexity.

| Correlates as modelled | EDF | *P*-value | k |
|---|---|---|---|
| s(Storms) | 0.74 | 0.06 | 4.00 |
| s(Max_K_index) | < 0.001 | 0.67 | 3.00 |
| s(Max_SST) | 0.89 | < 0.01 | 9.00 |
| s(NAO_index) | 0.04 | 0.31 | 9.00 |
| s(Fish_catch) | 0.39 | < 0.19 | 9.00 |
| s(Year) | 8.27 | < 0.001 | 9.00 |

# Shipping model

## Shipping data

**Data source:** Gov.uk

**Data access:** https://www.gov.uk/government/statistical-data-sets

**Date accessed:** 8th November 2018

## Shipping fleet statistics: data tables (FLE)

These data consist of the yearly combined weight (tons) of all UK owned vessels (over 500 tons) from 1950 - 2015. This is the best historical, yearly data we could find that gave a comparable unit per year measure. This is only a proxy for shipping traffic. We were unable to find yearly, historical statistics on vessels of 100 tons, or on private vessels, or on international vessels entering UK and Irish waters.

**Correlates of strandings through time (1950 – 2015) with a proxy for shipping traffic included**

a.



b.



c.



d.



544
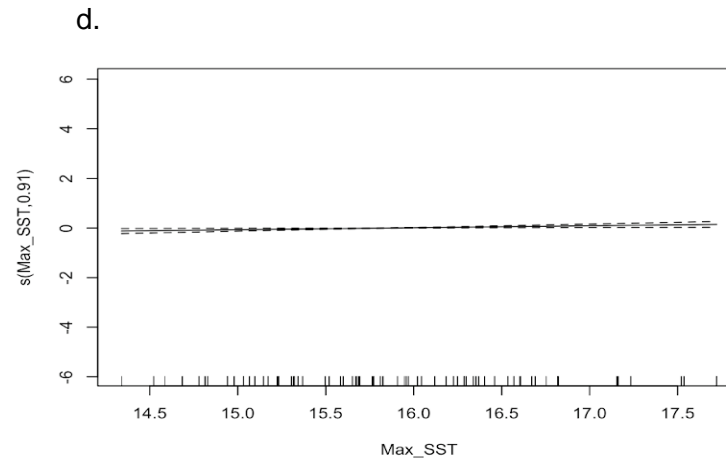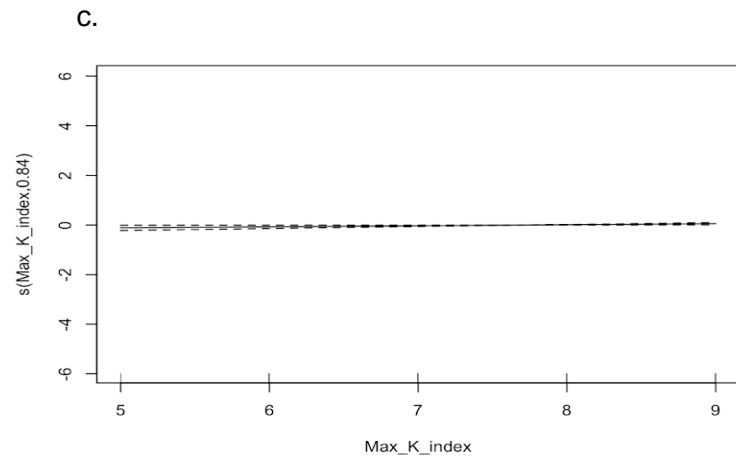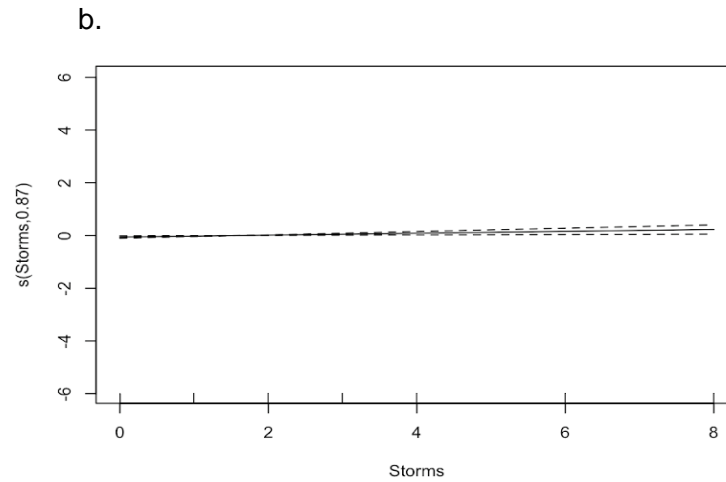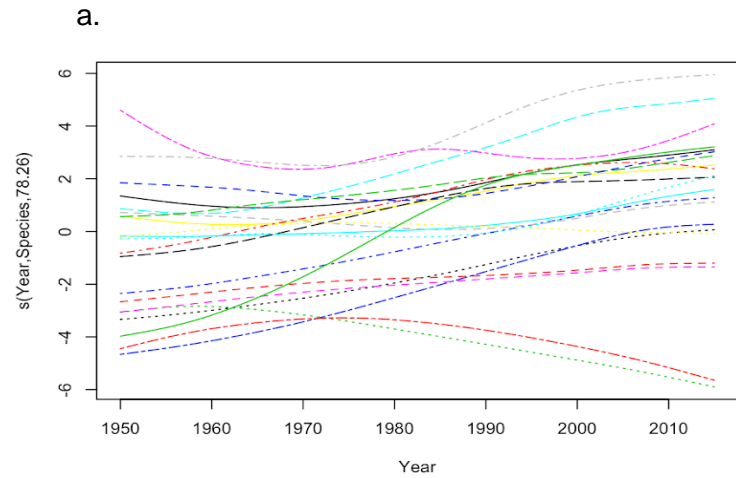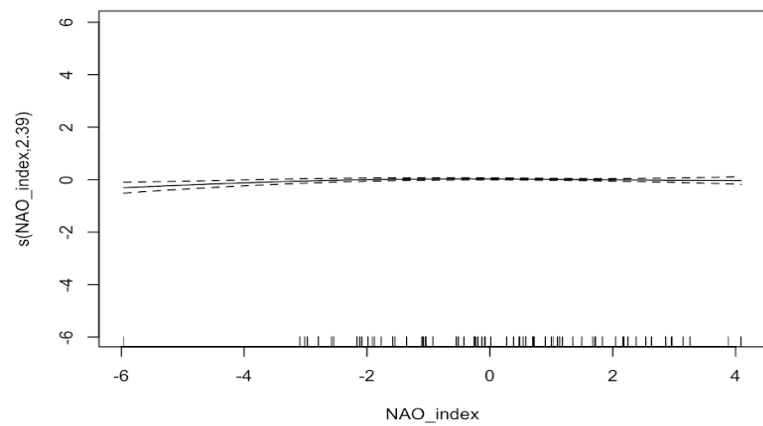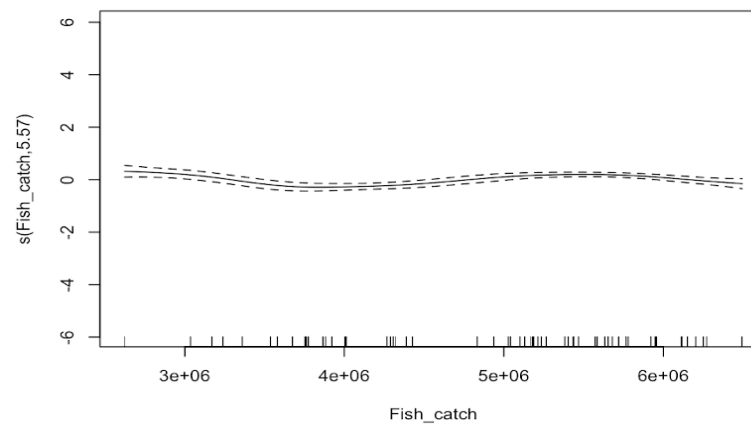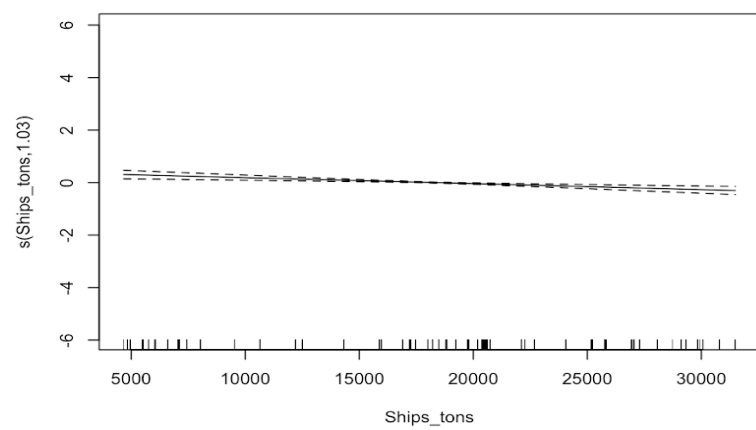
[Figure on previous page]

**Fig. S5.20.** GAM summary plots for correlates of cetacean strandings with a proxy for shipping (1950-2015) a. Factor-smooth interaction between year of stranding and species, b. Storm events, c. Geomagnetic fluctuations, d. Maximum sea surface temperatures, e. North Atlantic Oscillation index, f. Annual fishing catch, g. Shipping traffic. Modelled using the Tweedie response count distribution. Correlates of stranding through time with a proxy for shipping traffic. Deviance explained = 93%%, *n* = 1386.

**Table S5.9.** Correlates of strandings GAM output, with a proxy for shipping traffic. s() are smooths of the explanatory variables. 'Storms' is storm count, 'Max_K_index' is the geomagnetic K-index, 'Max_SST' is the maximum yearly sea surface temperature, 'NAO_index' is the North Atlantic Oscillation, Fish_catch' is annual fish catch, 'Ship_tons' is a proxy for shipping traffic. EDF shows the estimated degrees of freedom (EDF) for each of the different predictor variables. The P-values shows whether the smooth of that variable is significantly different from "no effect", i.e., if we estimated the "smooth" as a flat line at zero. k shows the maximum basis complexity.

| Correlates as modelled | EDF | *P*-value | k |
|---|---|---|---|
| s(Storms) | 0.87 | < 0.005 | 6.00 |
| s(Max_K_index) | 0.84 | < 0.01 | 3.00 |
| s(Max_SST) | 0.91 | < 0.01 | 9.00 |
| s(NAO_index) | 2.39 | < 0.01 | 9.00 |
| s(Fish_catch) | 5.57 | < 0.001 | 9.00 |
| s(Ships_tons) | 1.03 | < 0.001 | 9.00 |
| s(Year, Species) | 78.26 | < 0.001 | 210 |

**Correlates of strandings through time – stranding events**

a.



b.



c.



d.
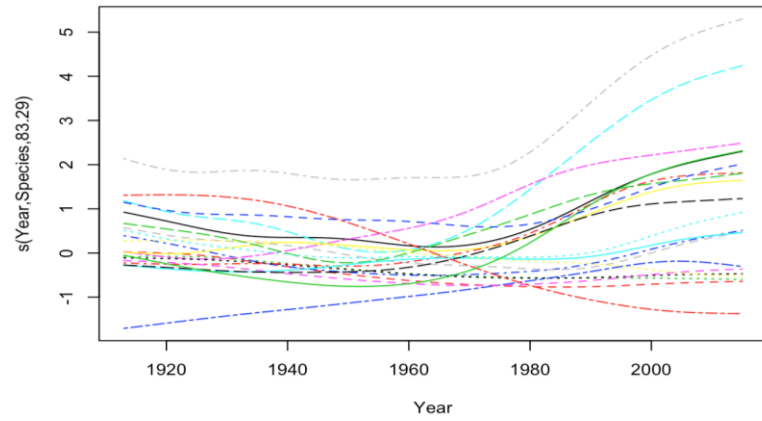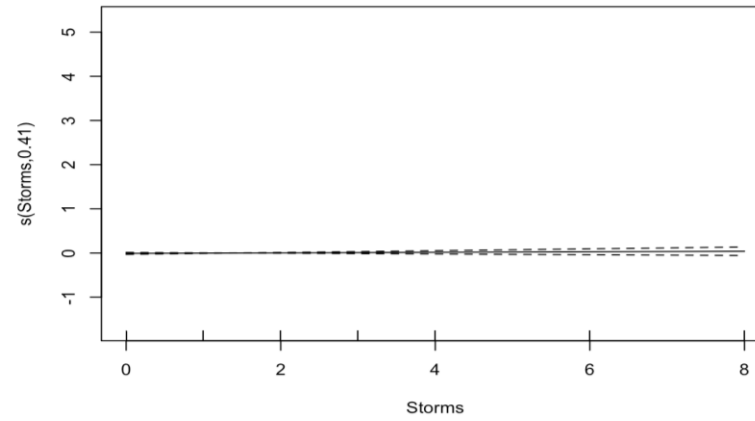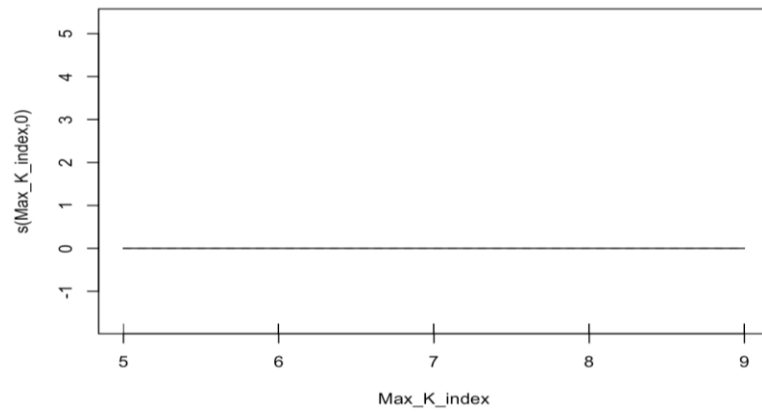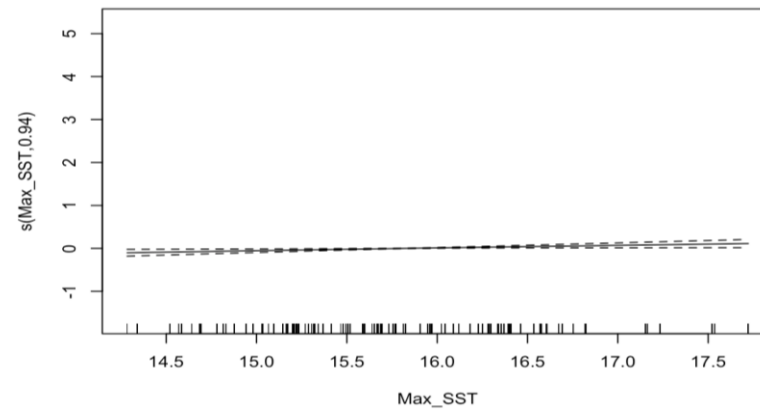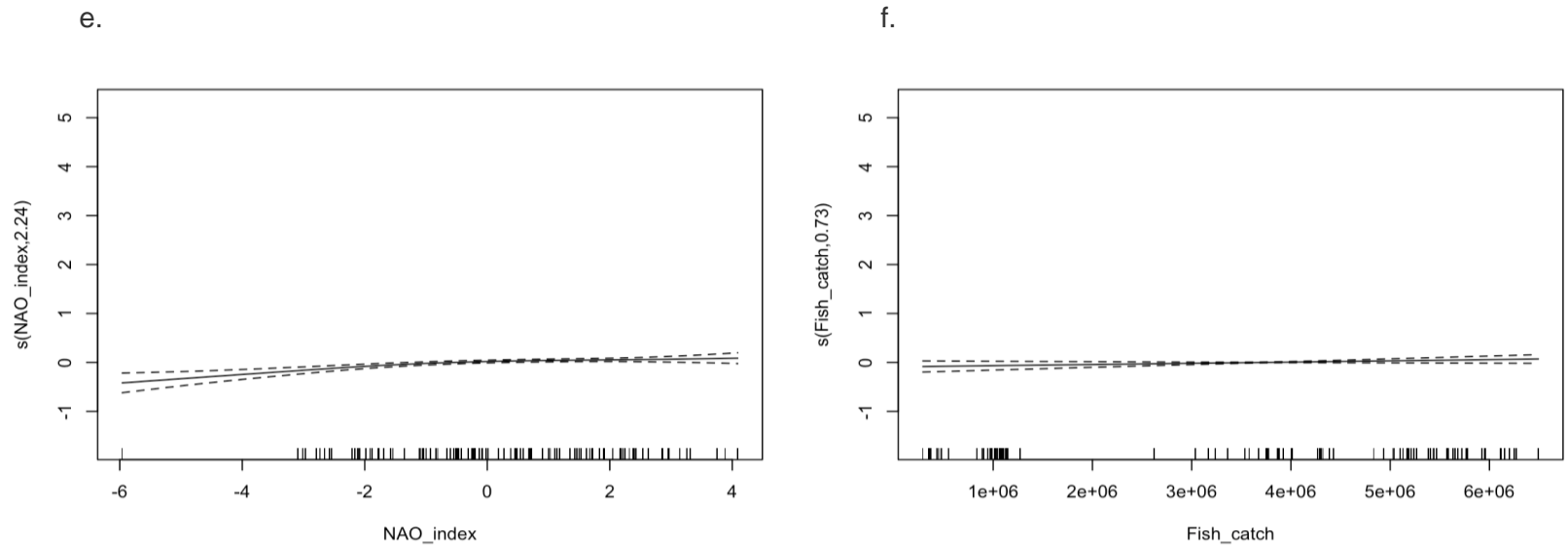
[Figures on this and previous page]

**Fig. S5.21.** GAM summary plots for correlates of cetacean strandings with mass strandings modelled as a single event. **a.** Factor-smooth interaction between year of stranding and species, **b.** Storm events, **c.** Geomagnetic fluctuations, **d.** Maximum sea surface temperatures, **e.** North Atlantic Oscillation index, **f.** Annual fishing catch. Modelled using the Tweedie response count distribution. Correlates of stranding through time with mass stranding events modelled as a single event. Deviance explained = 89.5%, $n$ = 1158.

**Table S5.10.** Correlates of strandings GAM output, with mass strandings modelled as a single event. All mass strandings were recorded as one event. s() are smooths of the explanatory variables. 'Storms' is storm count, 'Max_K_index' is the geomagnetic K-index, 'Max_SST' is the maximum yearly sea surface temperature, 'NAO_index' is the North Atlantic Oscillation, Fish_catch' is annual fish catch. EDF shows the estimated degrees of freedom (EDF) for each of the different predictor variables. The *P*-values shows whether the smooth of that variable is significantly different from "no effect", i.e., if we estimated the "smooth" as a flat line at zero. k shows the maximum basis complexity.

| Correlates as modelled | EDF | *P*-value | k |
|---|---|---|---|
| s(Storms) | 0.41 | 0.46 | 6.00 |
| s(Max_K_index) | < 0.001 | 0.70 | 3.00 |
| s(Max_SST) | 0.94 | 0.005 | 9.00 |
| s(NAO_index) | 2.32 | < 0.001 | 9.00 |
| s(Fish_catch) | 0.73 | 0.04 | 9.00 |
| s(Year, Species) | 83.29 | < 0.001 | 210 |

**Correlates of strandings through time by suborder**



a.

b.

c.

d.
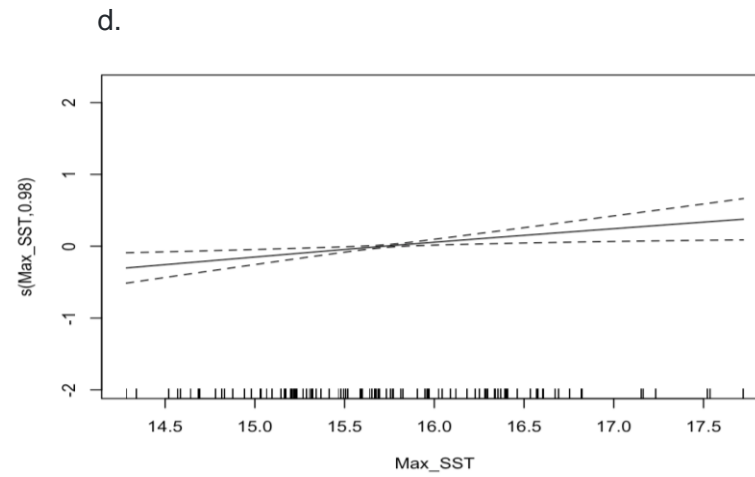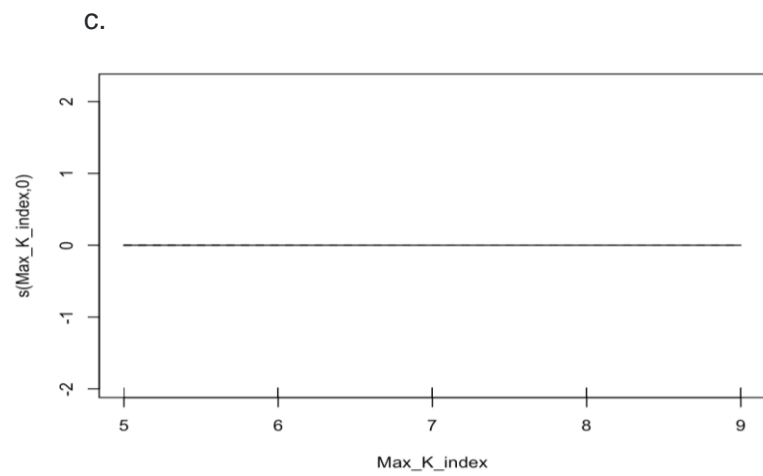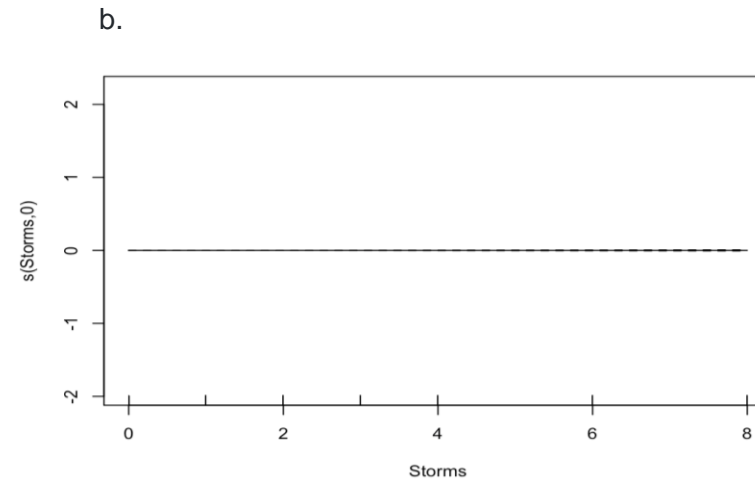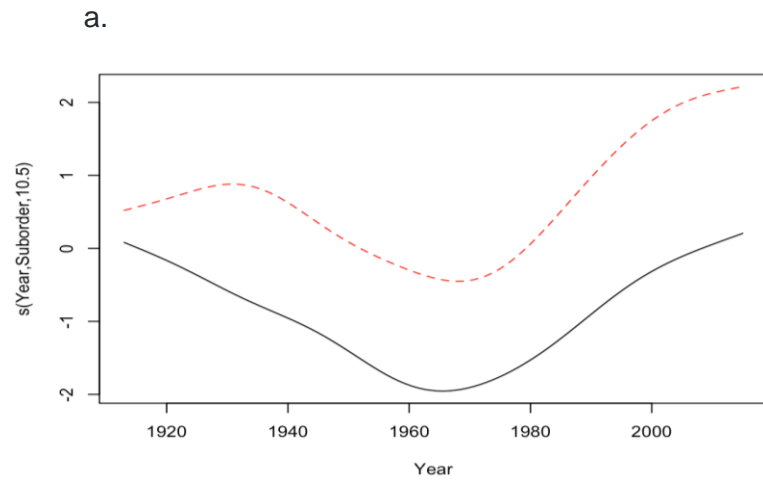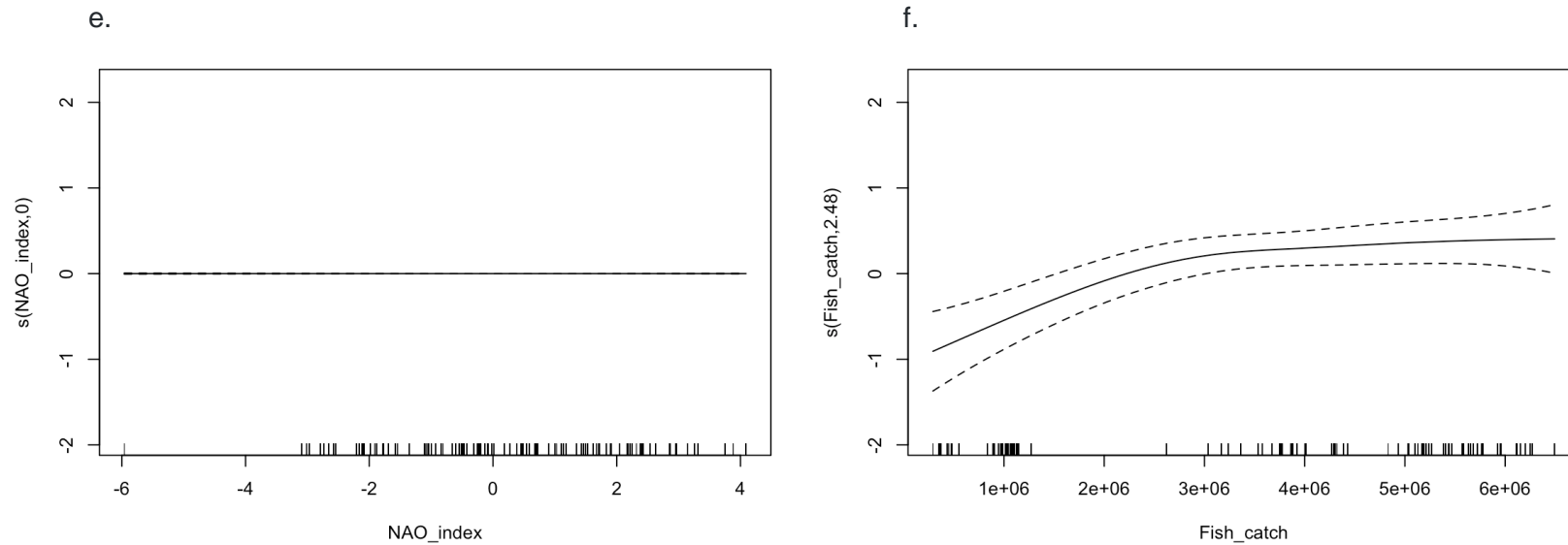
[Figure on this and previous page]

**Fig. S5.22.** GAM summary plots for variables included in a model looking correlates of strandings with a smooth of suborder; mysticetes and odontocetes.   **a.** Factor-smooth interaction between year of stranding and suborder, **b.** Storm events, **c.** Geomagnetic fluctuations, **d.** Maximum sea surface temperatures, **e.** North Atlantic Oscillation index, **f.** Fish_catch' is annual fishing catch. Modelled using the negative binomial response count distribution. Correlates of stranding through time with a smooth of suborder. Deviance explained = 31.8%, *n* = 2163.

**Table S5.11.** Correlates of strandings GAM output, with a smooth of suborder; mysticetes and odontocetes. s() are smooths of the explanatory variables. 'Storms' is storm count, 'Max_K_index' is the geomagnetic K-index, 'Max_SST' is the maximum yearly sea surface temperature, 'NAO_index' is the North Atlantic Oscillation, Fish_catch' is annual fish catch. EDF shows the estimated degrees of freedom (EDF) for each of the different predictor variables. The *P*-values shows whether the smooth of that variable is significantly different from "no effect", i.e., if we estimated the "smooth" as a flat line at zero. k shows the maximum basis complexity.

| Correlates as modelled | EDF | *P*-value | k |
|---|---|---|---|
| s(Storms) | < 0.001 | 0.47 | 4.00 |
| s(Max_K_index) | < 0.001 | 0.91 | 3.00 |
| s(Max_SST) | 0.98 | < 0.005 | 9.00 |
| s(NAO_index) | < 0.005 | 0.57 | 9.00 |
| s(Fish_catch) | 2.48 | < 0.001 | 9.00 |
| s(Year, Suborder) | 10.5 | < 0.001 | 200 |

**Correlates of strandings through time by habitat**

553
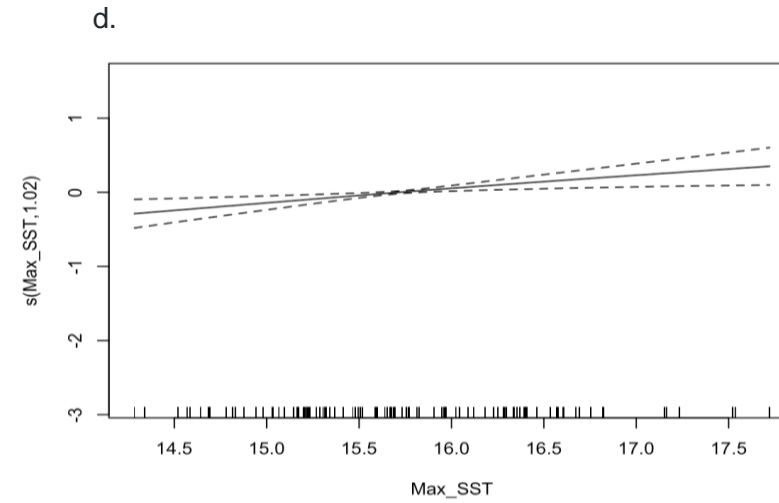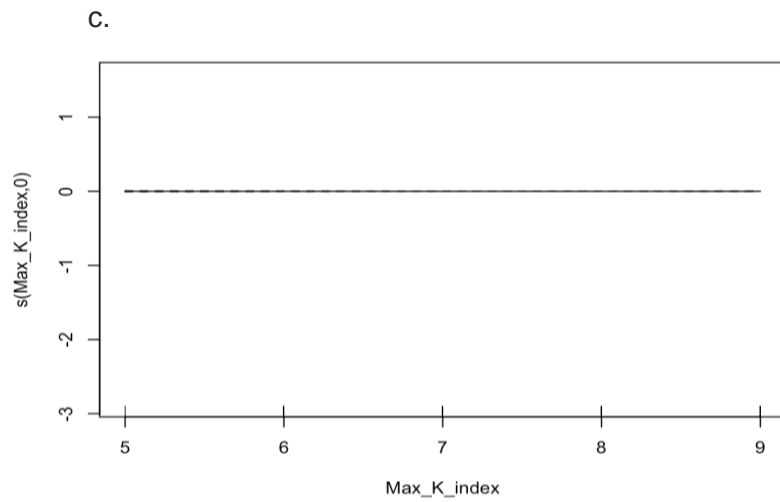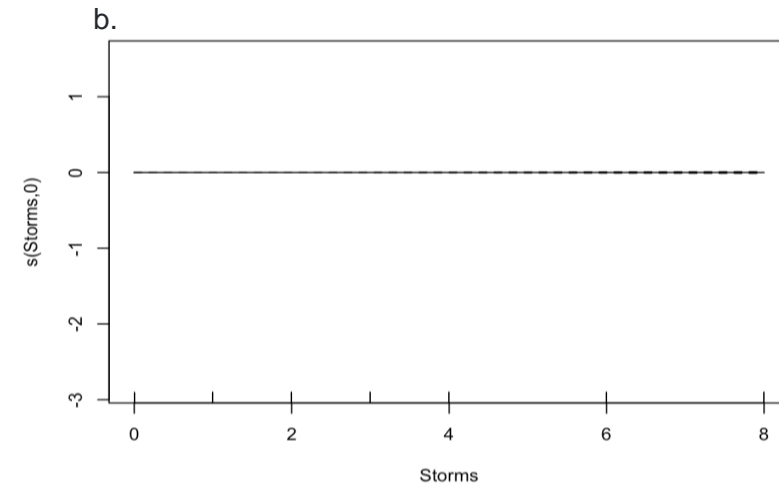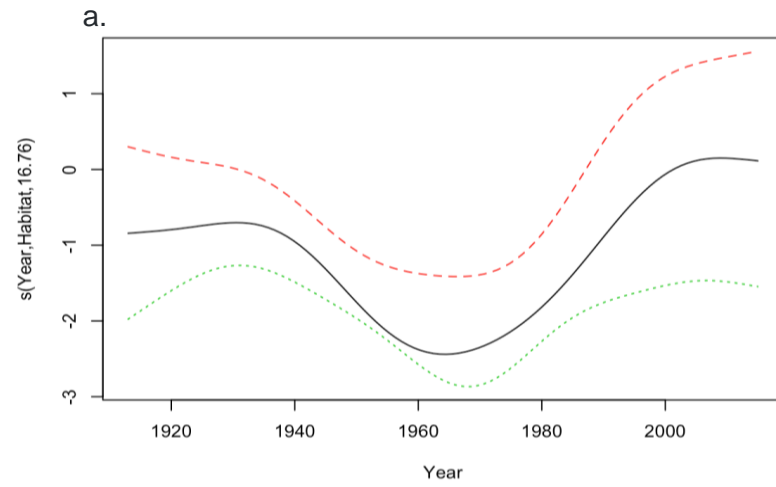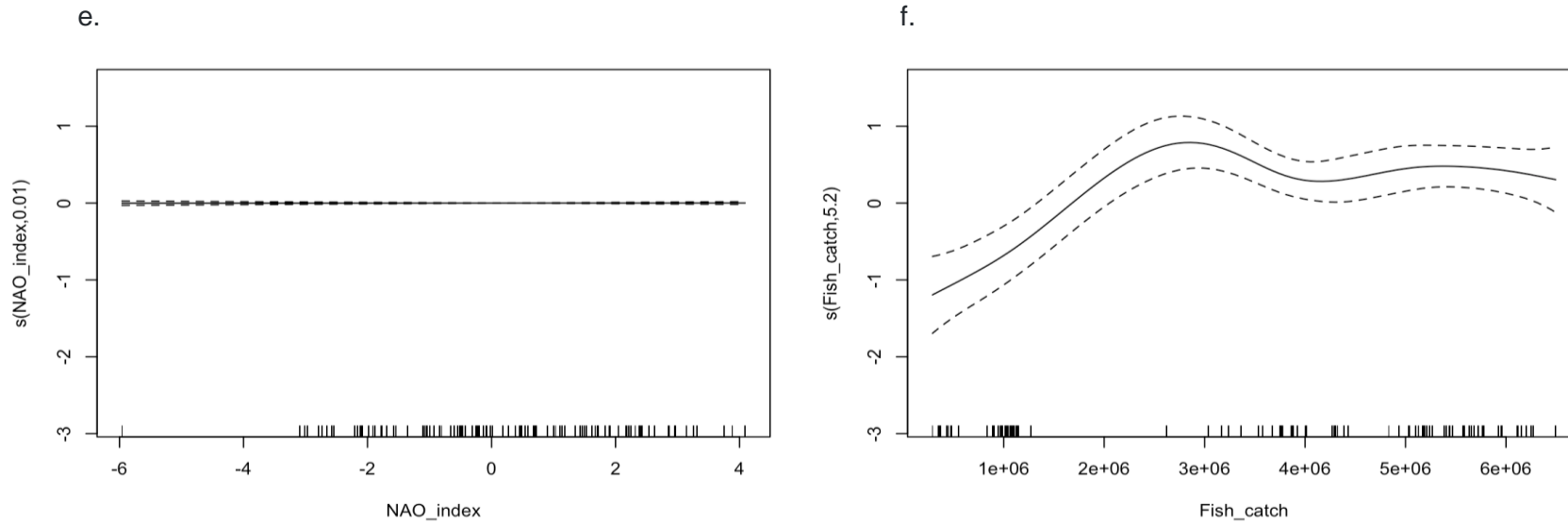
[Figure on this and previous page]

**Fig. S5.23.** GAM summary plots for variables included in a model looking at correlates of strandings with a smooth of habitat; coastal, oceanic, or both.   a. Factor-smooth interaction between year of stranding and suborder, b. Storm events, c. Geomagnetic fluctuations, d. Maximum sea surface temperatures, e. North Atlantic Oscillation index, f. Fish_catch' is annual fish catch.   Modelled using the Tweedie response count distribution. Correlates of stranding through time with a smooth of 'habitat'. Deviance explained = 43.9%, $n$ = 2163

**Table S5.12.** Correlates of strandings GAM output, with a smooth of habitat; coastal, oceanic, or both. s() are smooths of the explanatory variables. 'Storms' is storm count, 'Max_K_index' is the geomagnetic K-index, 'Max_SST' is the maximum yearly sea surface temperature, 'NAO_index' is the North Atlantic Oscillation, Fish_catch' is annual fish catch**.** EDF shows the estimated degrees of freedom (EDF) for each of the different predictor variables. The P-values shows whether the smooth of that variable is significantly different from "no effect", i.e., if we estimated the "smooth" as a flat line at zero. k shows the maximum basis complexity. Habitat information was taken from Reid et al., 2003.

| Correlates as modelled | EDF | *P*-value | k |
|---|---|---|---|
| s(Storms) | < 0.001 | 0.40 | 4.00 |
| s(Max_K_index) | < 0.001 | 0.90 | 3.00 |
| s(Max_SST) | 1.02 | 0.001 | 9.00 |
| s(NAO_index) | 0.01 | 0.36 | 9.00 |
| s(Fish_catch) | 5.20 | < 0.001 | 9.00 |
| s(Year, Habitat) | 16.8 | < 0.001 | 30.0 |

**Regional model 1: South west UK**


**Regional model 1**: South west UK (England): High human population, and high incidences of stranding records. This model uses the population of Cornwall, Devon, Somerset, and Dorset combined as the proxy for observer effort. These data were only available for 1991-2015, which constrained the model accordingly. This model was based on the fact that the human population (and thus observer effort) has increased in this area year on year since 1991. These counties were chosen because they have a shoreline and had yearly county population data available for 1991-2015. The total area of this regional study is ~17,093 km$^2$.
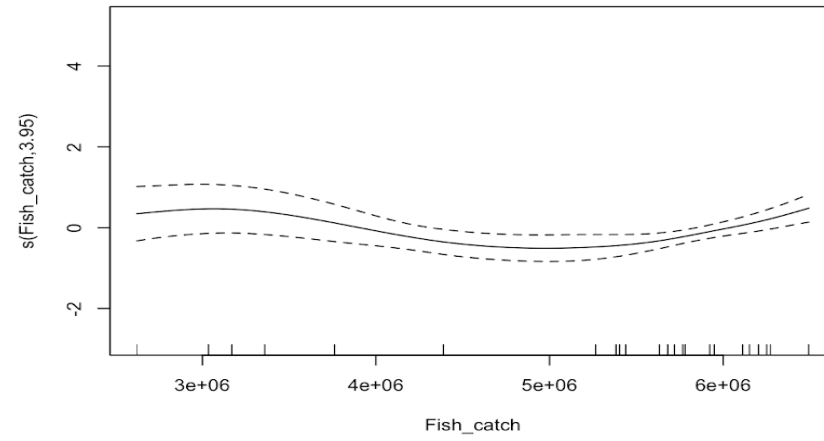
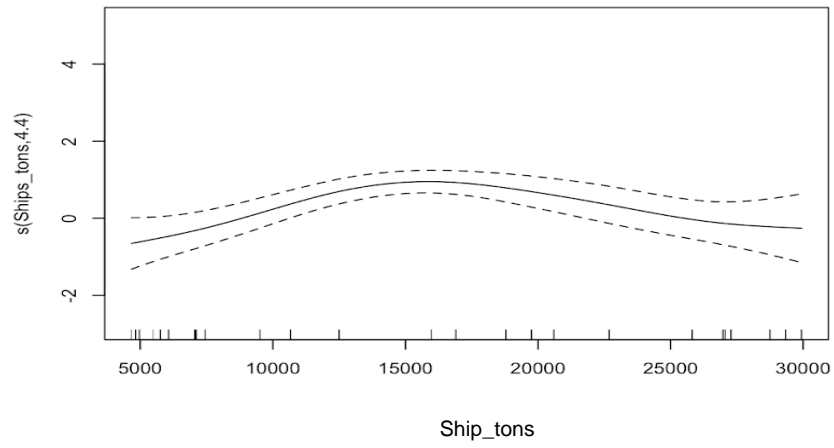**Correlates of strandings in the south west UK**
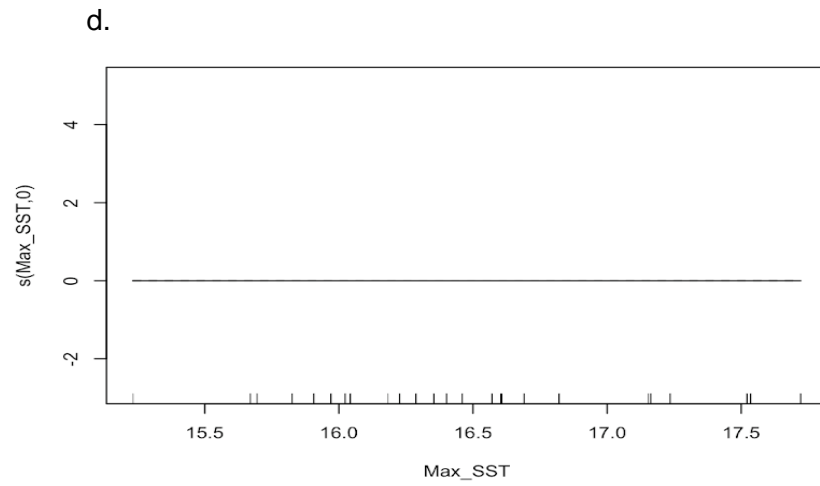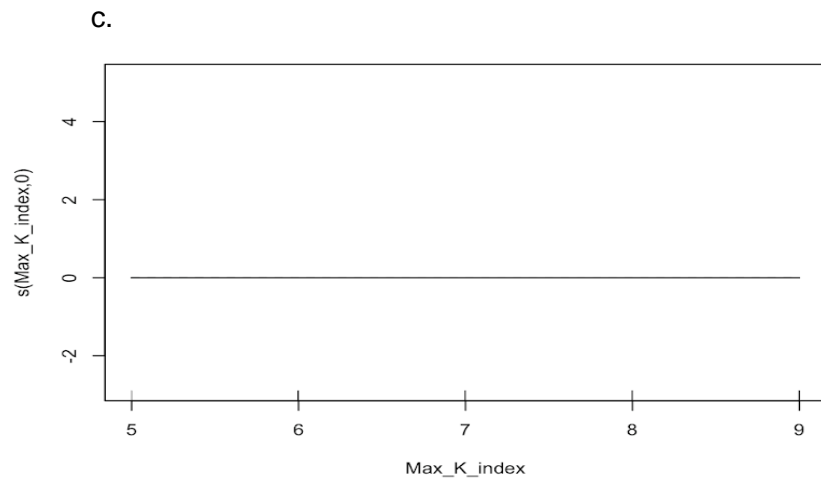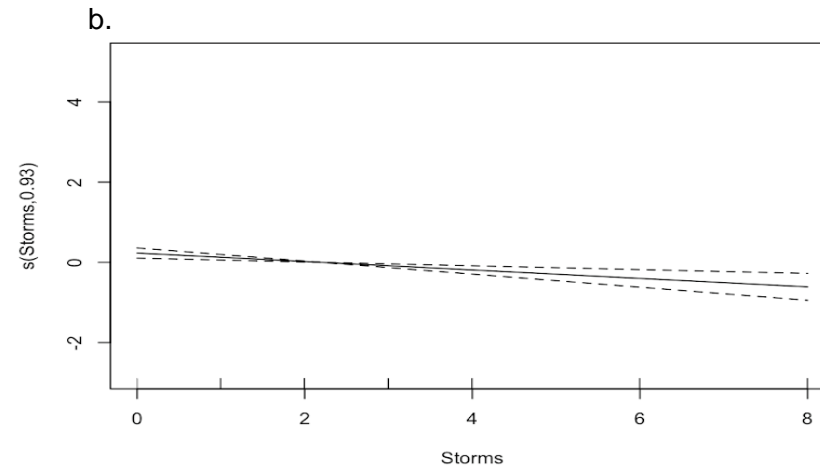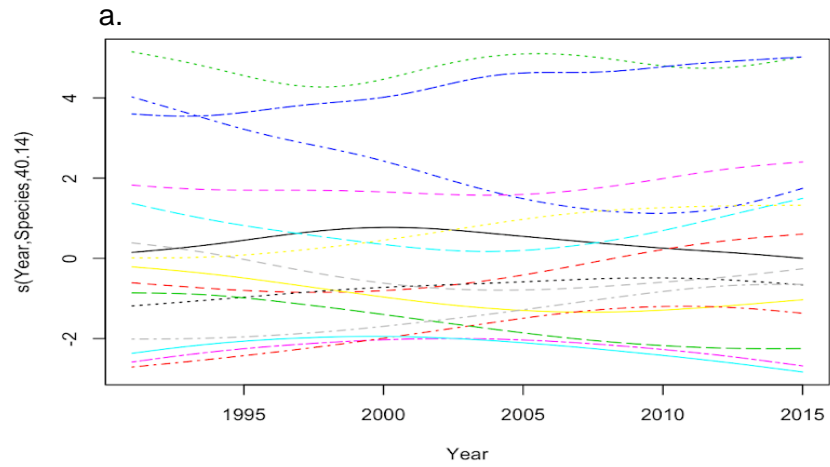
e.
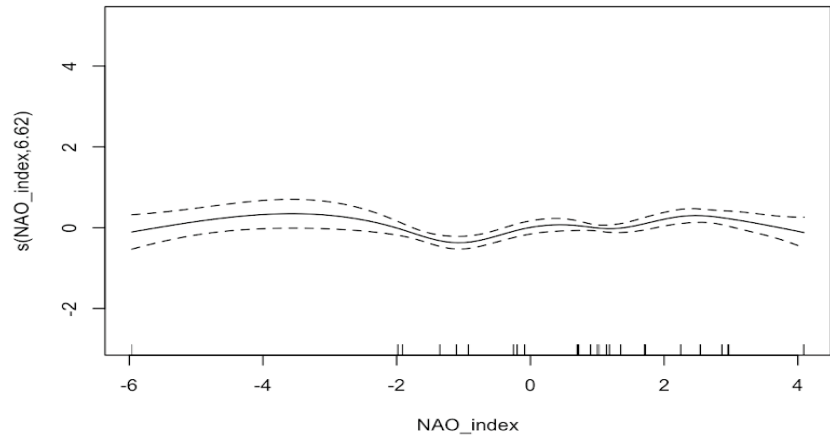


f.



g.

[Figure on previous page]

**Fig. S5.24.** GAM summary plots for variables included in a model looking at correlates of strandings in the south west of the UK (England) (Regional study 1).   **a.** Factor-smooth interaction between year of stranding and suborder, **b.** Storm events, **c.** Geomagnetic fluctuations, **d.** Maximum sea surface temperatures, **e.** North Atlantic Oscillation index, **f.** Fish_catch' is annual fish catch, **g.** Shipping traffic.   Modelled using the Poisson response count distribution. Correlates of stranding through time in the south west of the UK (Scotland) with a smooth of 'species'. Deviance explained = 96.5%, *n* = 400

**Table S5.13.** Correlates of strandings GAM output for the south west UK, with a smooth of 'species'. s() are smooths of the explanatory variables. 'Storms' is storm count, 'Max_K_index' is the geomagnetic K-index, 'Max_SST' is the maximum yearly sea surface temperature, 'NAO_index' is the North Atlantic Oscillation, 'Fish_catch' is annual fish catch, 'Ships_tons' is a proxy for shipping traffic. EDF shows the estimated degrees of freedom (EDF) for each of the different predictor variables. The P-values shows whether the smooth of that variable is significantly different from "no effect", i.e., if we estimated the "smooth" as a flat line at zero. k shows the maximum basis complexity.

| Correlates as modelled | EDF | *P*-value | k |
|---|---|---|---|
| s(Storms) | 0.93 | < 0.001 | 4.00 |
| s(Max_K_index) | < 0.001 | 0.25 | 3.00 |
| s(Max_SST) | < 0.001 | 0.75 | 9.00 |
| s(NAO_index) | 6.62 | < 0.001 | 9.00 |
| s(Fish_catch) | 3.95 | < 0.001 | 9.00 |
| s(Ships_tons) | 4.40 | < 0.001 | 9.00 |
| s(Year, Species) | 40.1 | < 0.001 | 160 |

**Regional model 2: South west UK**

**Regional study 2:** North west UK (Scotland): Low human population, high incidences of strandings. This model uses the population of Argyll, Inverclyde, Ayrshire, and Western Isles combined as the proxy for observer effort. These data were only available for 1991-2015, which constrained the model accordingly. This model was based on the fact that the human population (and thus observer effort) has decreased in this area year on year since 1991. These counties were chosen because they have a shoreline and had yearly county population data available for 1991-2015. The total area of this regional study is ~16,781 km$^2$.
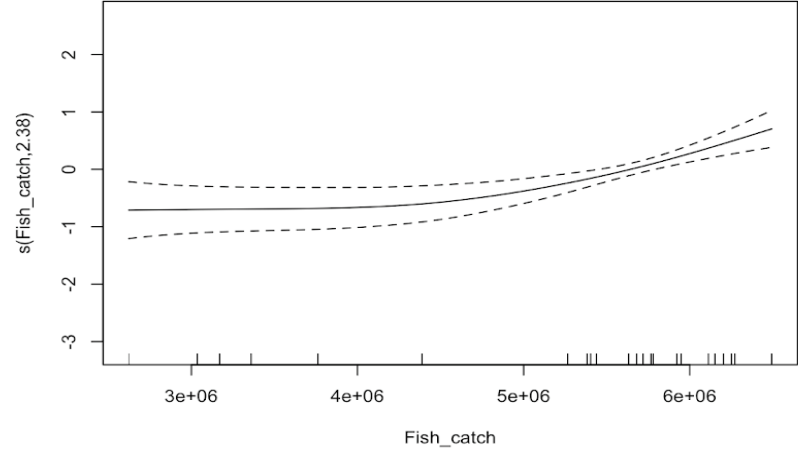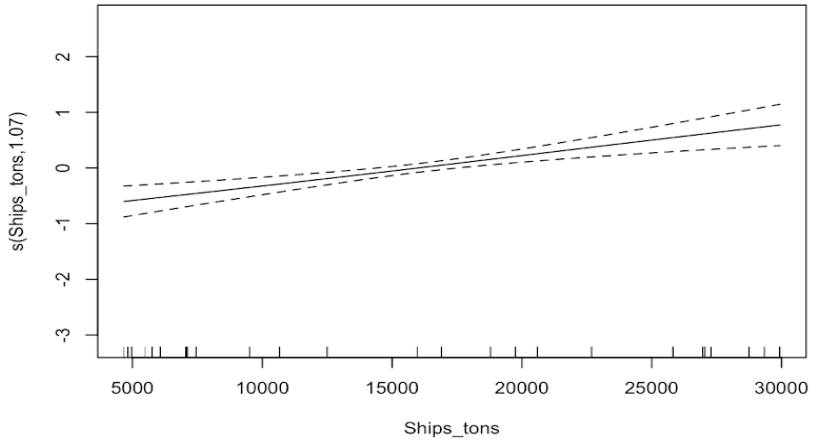
# Correlates of strandings in the north west UK

a.



b.



c.



d.

e.

f.

g.

562
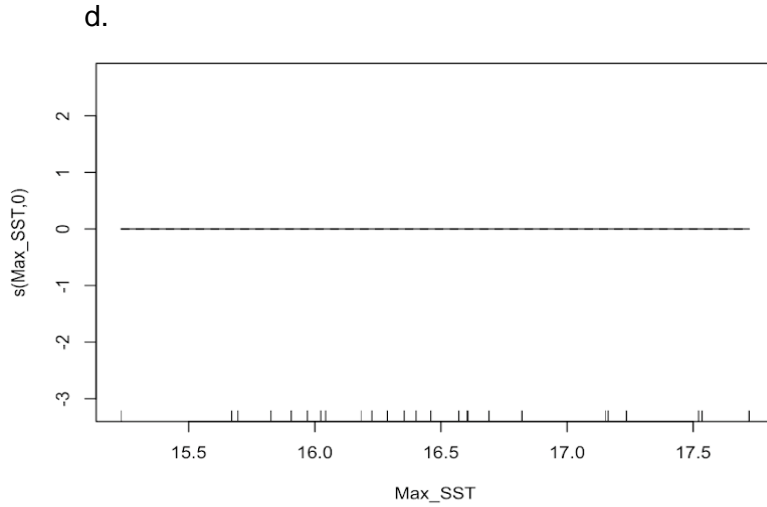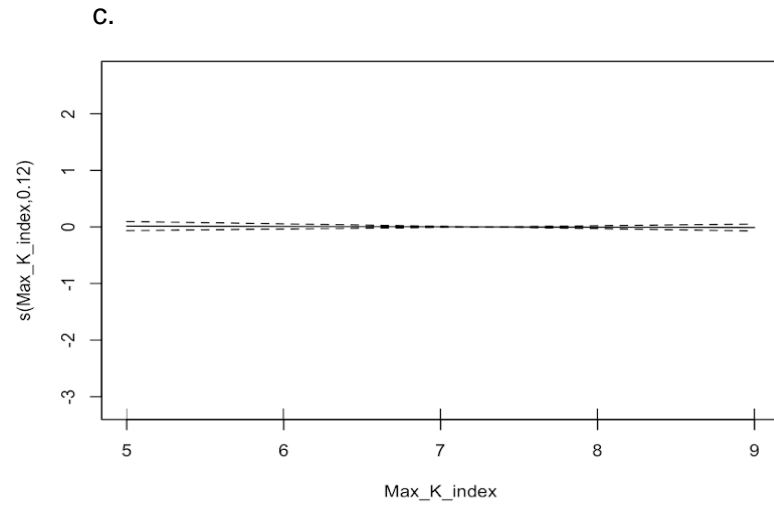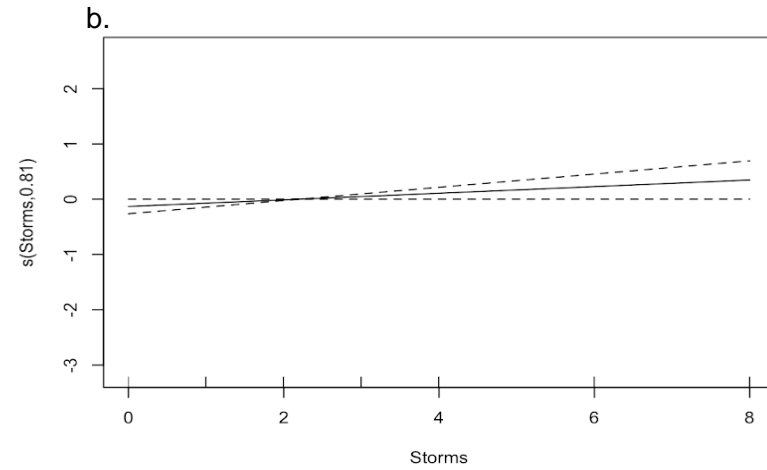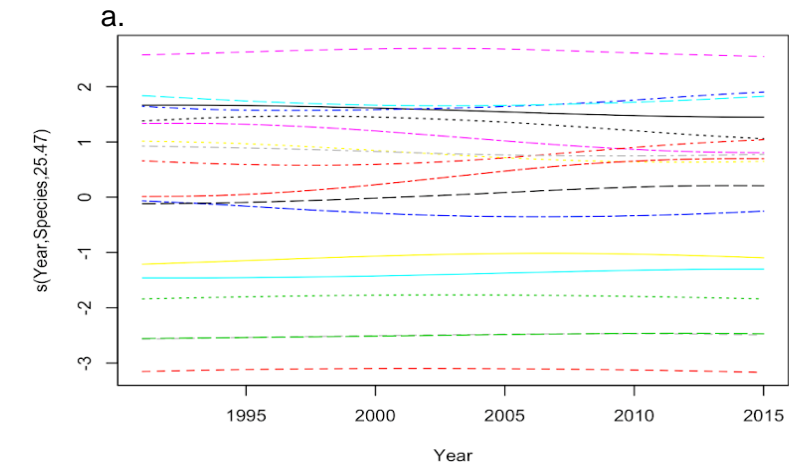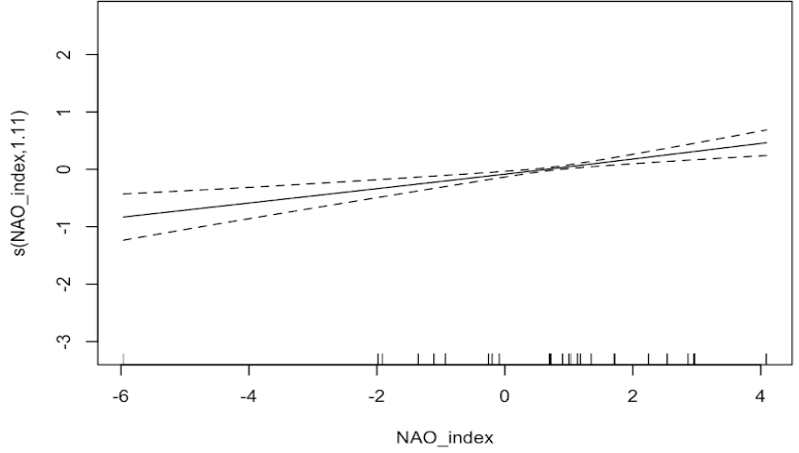
[Figure on previous page]

**Fig. S5.25.** GAM summary plots for variables included in a model looking at correlates of strandings in the north west of the UK (Scotland) (Regional study 2). **a.** Factor-smooth interaction between year of stranding and suborder, **b.** Storm events, **c.** Geomagnetic fluctuations, **d.** Maximum sea surface temperatures, **e.** North Atlantic Oscillation index, **f.** Fish_catch' is annual fish catch, **g.** Shipping traffic.  Modelled using the negative binomial response count distribution. Correlates of stranding through time in the north west UK (Scotland) with a smooth of 'species'. Deviance explained = 71.5%, *n* = 450.

**Table S5.14.** Correlates of strandings GAM output for the north west UK, with a smooth of 'species' s() are smooths of the explanatory variables. 'Storms' is storm count, 'Max_K_index' is the geomagnetic K-index, 'Max_SST' is the maximum yearly sea surface temperature, 'NAO_index' is the North Atlantic Oscillation, 'Fish_catch' is annual fish catch, 'Ships_tons' is a proxy for shipping traffic. EDF shows the estimated degrees of freedom (EDF) for each of the different predictor variables. The P-values shows whether the smooth of that variable is significantly different from "no effect", i.e., if we estimated the "smooth" as a flat line at zero. k shows the maximum basis complexity.

| Correlates as modelled | EDF | *P*-value | k |
|---|---|---|---|
| s(Storms) | 0.81 | 0.02 | 4.00 |
| s(Max_K_index) | 0.12 | 0.27 | 3.00 |
| s(Max_SST) | < 0.001 | 1.00 | 9.00 |
| s(NAO_index) | 1.11 | < 0.001 | 9.00 |
| s(Fish_catch) | 2.38 | < 0.001 | 9.00 |
| s(Ships_tons) | 1.07 | < 0.001 | 9.00 |
| s(Year, Species) | 25.5 | < 0.001 | 180 |

**Outputs for all supplementary models**

| Correlates as modelled | Unknowns + rares | Genus-level | *Phocoena* removed | *Phocoena* only | Shipping | Stranding events | Suborder smooth | Habitat smooth |
|---|---|---|---|---|---|---|---|---|
| s(Storms) | < 0.005 | < 0.001 | < 0.001 | 0.74 | 0.87** | 0.41 | < 0.001 | < 0.001 |
| s(Max_K_index) | < 0.005 | < 0.001 | < 0.001 | < 0.001 | 0.84** | < 0.001 | < 0.001 | < 0.001 |
| s(Max_SST) | 0.85* | 2.41** | 2.43** | 0.89** | 0.91** | 0.94** | 0.98** | 1.02** |
| s(NAO_index) | 0.94** | 0.88* | 2.01** | 0.04 | 2.39** | 2.32** | < 0.005 | 0.01 |
| s(Fish_catch) | 4.04** | 0.83* | 0.61* | 0.39 | 5.57** | 0.73* | 2.48** | 5.20** |
| s(Ships_tons) | - | - | - | - | 1.03** | - | - | - |
| s(Year, Species) | 158** | 85.9** | 92.3** | 8.27** | 78.26** | 83.29** | 10.5** | 16.8** |

*$P < 0.05$, **$P < 0.01$

[Table on previous page]

**Table S5.15.** Correlates of strandings Generalised additive Model (GAM) output for additional models. 'Unknowns + rares' is correlates of stranding GAM including all 'rare' and unknown records. 'Genus-level' is correlates of stranding GAM using with records grouped at the genus-level. 'Phocoena removed' is correlates of stranding GAM with harbour porpoises removed. 'Phocoena only' is correlates of stranding GAM with harbour porpoises only. 'Shipping' is correlates of stranding GAM with a proxy for shipping traffic (1950-2015). 'Stranding events' is correlates of stranding GAM with mass strandings listed as a single event. 'Suborder smooth' is correlates of stranding GAM with a smooth for suborder (i.e., mysticete and odontocete). 'Habitat smooth' is the correlates of stranding GAM with a smooth for habitat (coastal, oceanic, both). Explanatory variables consist of data for the UK and Ireland, from 1913-2015. 'Storms' refer to the storm count per year, 'Max_K_Index' is the geomagnetic reading (where the K-index is used to characterize the magnitude of geomagnetic storms), 'Max_SST' is the yearly maximum sea surface temperature (°C), 'NAO_index' is the North Atlantic Oscillation which is the difference of normalized sea level pressure (SLP) between Stykkisholmur/Reykjavik, Iceland, and Lisbon, Portugal, 'Fish_catch' is annual fish catch (1000 tonnes) for the UK and Ireland, 'Year' is the years 1913-2015, 'Species' are the cetacean species that make up the strandings data set. This table shows the estimated degrees of freedom (EDF) for each of the different variables that had a $P < 0.05$ (indicated by *) or $P < 0.01$ (indicated by **). The $P$-values show whether the smooth of that variable is significantly different from "no effect", i.e., if we estimated the smooth as a flat line at zero.

# Appendix references

Aguilar de Soto N, Johnson M, Madsen P, Díaz F, Domínguez I, Brito A, Tyack P (2008) Cheetahs of the deep sea: deep foraging sprints in short-finned pilot whales off Tenerife (Canary Islands). *J Anim Ecol.* 77:936–47.

Alexander L, Tett S, and Jonsson T (2005). Recent observed changes in severe storms over the United Kingdom and Iceland. *Geophysical Research Letters.* 32, 13.

Baumann-Pickering S (2013b) Baird's beaked whale echolocation signals. *J Acoust Soc Am.* 133(6):4321–31.

Baumann-Pickering S, Simonis A, Wiggins S (2013a) Aleutian Islands beaked whale echolocation signals. *Mar Mamm Sci.* 29(1):221–7

Benjamini Y and Hochberg Y (1995) Controlling the false discovery rate: a practical and powerful approach to multiple testing. *J R Stat Soc Ser B Methodol.* 57(1):289–300.

Benjamini Y and Yekutieli D (2001) The control of the false discovery rate in multiple testing under dependency. *Ann Stat.* 29(4):1165–88.

Clark C (1990) Acoustic behavior of Mysticete whales. In: *Sensory abilities of Cetaceans.* US: Springer: 571–83.

Galatius A, Olsen M, Steeman M, Racicot R and Bradshaw C (2019) Raising your voice: evolution of narrow-band high-frequency signals in toothed whales (Odontoceti). *Biol J Linn Soc.*126(2):213–24.

Gelman A (2006) Prior distributions for variance parameters in hierarchical models. *Bayesian Anal.* 1(3):515–33.

Gelman A and Rubin D (1992) Inference from iterative simulation using multiple sequences. *Stati Sci Inst Math Stat.* 7(4):457–72.

Halpin P, Read A, Fujioka E, Best B, Donnelly B, Hazen L, Kot C, Urian K, LaBrecque E, Dimatteo A, Cleary J. Good C, Crowder L and Hyrenbach K (2009) OBIS-SEAMAP: The world data center for marine mammal, sea bird, and sea turtle distributions. *Oceanography* 22(2):104-115.

Harmon L, Weir J, Brock C, Glor R and Challenger W (2008) GEIGER: investigating evolutionary radiations. *Bioinformatics.* 24(1):129–31.

Hurrell J (1995) Decadal Trends in the North Atlantic Oscillation: Regional Temperatures and Precipitation. *Science 269,* 5224, 676-679

Jensen F, Rocco A, Mansur R, Smith B, Janik V and Madsen P (2013) Clicking in shallow rivers: short-range echolocation of Irrawaddy and Ganges River dolphins in a shallow, acoustically complex habitat. *PLoS One.* 8(4): e59284.

Johnson M, Hickmott L, Aguilar Soto N, Madsen P (2008) Echolocation behaviour adapted to prey in foraging Blainville's beaked whale (*Mesoplodon densirostris*). *Proc R Soc B Biol Sci.* 275(1631):133–9.

Johnston D, McDonald M, Polovina J, Domokos R, Wiggins S and Hildebrand J (2008) Temporal patterns in the acoustic signals of beaked whales at Cross Seamount. *Biol Lett*. 4(2):208–11.

Kastelein R, Bunskoek P, Hagedoorn M, Au W and de Haan D (2002) Audiogram of a harbor porpoise (*Phocoena phocoena*) measured with narrow-band frequency-modulated signals. *J Acoust Soc Am*. 112(1):334–44.

Kyhn L, Tougaard J, Beedholm K, Jensen F, Ashe E, Williams R and Madsen P (2013) Clicking in a killer whale habitat: narrow-band, high-frequency biosonar clicks of harbour porpoise (*Phocoena phocoena*) and Dall's porpoise (*Phocoenoides dalli*). *PLoS One.* 8(5): e63763.

Kyhn L, Tougaard J, Jensen F and Wahlberg M (2009) Feeding at a high pitch: source parameters of narrow band, high-frequency clicks from echolocating off-shore hourglass dolphins and coastal Hector's dolphins. *J Acoust Soc Am*. 125(3):1783–91.

Ladegaard M, Jensen F, de Freitas M, da Silva V and Madsen P (2015) Amazon river dolphins (*Inia geoffrensis*) use a high-frequency short-range biosonar. *J Exp Biol*. 218(19):3091–101.

Lamb H and Frydendahl K (1991) *Historic storms of the North Sea, British Isles and Northwest Europe*. (1st edn) Cambridge University Press

Lloyd G and Slater G (in prep). A Total-Group Phylogenetic Metatree for Cetacea and the Importance of Fossil Data in Diversification Analyses. *bioRxiv* 169078.

Lockwood M, Harrison R, Woollings T and Solanki S (2010) Are cold winters in Europe associated with low solar activity? *Environmental Research Letters* 5 (2): 024001.

MacLeod C, Pierce G, and Begoña Santos M (2004) Geographic and temporal variations in strandings of beaked whales (Ziphiidae) on the coasts of the UK and the Republic of Ireland from 1800-2002. *Journal of Cetacean Research and Management*. 6(1):79–86.

Madsen P, Payne R, Kristiansen N and Wahlberg M (2002) Sperm whale sound production studied with ultrasound time/depth-recording tags. *J Exp Biol*. 205:1899–906.

Moors-Murphy H (2015) Patterning in northern bottlenose whale (*Hyperoodon ampullatus*) click trains. *Can Acoust*. 43(3):1–2.

Morisaka T and Connor R (2007) Predation by killer whales (*Orcinus orca*) and the evolution of whistle loss and narrow-band high frequency clicks in odontocetes. *J Evol Biol*. 20(4):1439–58.

NOAA. (2017). http://www.opc.ncep.noaa.gov/product_description/keyterm.shtml - [Accessed 4th September 2017].

Osborn T (2011) Winter 2009/2010 temperatures and a record-breaking North Atlantic Oscillation index. *Weather*.

Parliament House of Commons (2017) UK Sea Fisheries Statistics (Number 2788). London: *The Stationery Office*.

Plummer M, Best N, Cowles K and Vines K (2006) CODA: convergence diagnosis and output analysis for MCMC. *R News.* 6:7–1.

Racicot R, Darroch S and Kohno N (2018) Neuroanatomy and inner ear labyrinths of the narwhal, *Monodon monoceros*, and beluga, *Delphinapterus leucas* (Cetacea: Monodontidae). *J Anat.* 233:421–39.

Reid J, Evans P and Northridge S (2003) Atlas of cetacean distribution on north-west European waters. *Joint Nature Conservation Committee* (JNCC). Available at: https://data.jncc.gov.uk/data/a5a51895-50a1-4cd8-8f9d-8e2512345adf/atlas-cetacean-distribution-web.pdf.

Reidenberg J and Laitman J (2007) Discovery of a low frequency sound source in mysticeti (baleen whales): anatomical establishment of a vocal fold homolog. *Anat Rec.* 290(6):745–59.

Sjare B and Smith T (1986) The vocal repertoire of white whales, *Delphinapterus leucas*, summering in the Cunningham Inlet, Northwest Territories. *Can J Zool.* 64:407–15.

Sugimatsu H, Kojima J, Tamaki U and Bahl R (2014) Advanced technique for automatic detection and discrimination of a click train with short interclick intervals from the clicks of Ganges river dolphins (*Platanista gangetica*) recorded by a passive acoustic monitoring system using hydrophone arrays. *Mar Technol Soc* J. 48(3):167–81.

Turl C (1990) Echolocation abilities of the beluga, a review and comparison with the bottlenose dolphin Tursiops truncatus. In: Smith TG, St. Aubin DJ, Geraci JR, editors. *Advances in research of the Beluga whale, Delphinapterus leucas*, 24: 119–28.

Turl C and Penner R (1989) Differences in echolocation click patterns of the beluga (*Delphinapterus leucas*) and the bottlenose dolphin (*Tursiops truncatus*). *J Acoust Soc Am.* 86(2):497–502.

Yang Z (2006) *Computational molecular evolution.* Oxford: Oxford University Press.